CONTENTS

SESSION I – Applications

Chairman: Prof. Joop Sloot

SESSION II – Technology, Design, Manufacturing, Standards, Testing

Chairman: Prof. A.D. Stokes

SESSION III – Fundamental processes

Chairman: Dr. R. Wilkins

1.	Bussière William, Rochette David and Pellet René	Influence of the Filling Material Properties on Pressure in HBC Fuse. Comparison Between Experimental Results and Simulation
2.	Bussière William, Rochette David and André Pascal	Study of the SiO_2 Plasma Physical Parameters: Temperature, Electron Density, Pressure, Radiation
3.	Jean-Louis Gelet	Thermal Fatigue Damage of Ultra-Fast Fuses
4.	E. Maira, S. Arai	Electric Behavior of Capillary Arcs Ignited at High Current Density Levels in Copper Vapor
5.	Michael J Taylor	Current Diversion Around a Fragmenting Wire During the Voltage Spike Associated With Exploding Wires
6.	Martin Bizjak, Mitja Koprivšek and Franc Pikl	Breaking by Melting Fuse at Anomalous M-Effect
7.	R. E. Brown, P. M. McEwan	A Bifurcated Beam Opto-Electronic Camera For Investigation of Phenomena Associated With Fast Rising Arc Voltage.
8.	J. Gärtner, M. Krins, E. Gockenbach, H. Borsi	Partial Discharge (Pd) Behavior of High Voltage Fuses With Modified Filler
9.	Józef Czucha	Arc ignition process in short fuse elements
10.	G. Hoffmann and U. Kaltenborn	Thermal Modeling of High Voltage H. R. C. Fuses and Simulation of Tripping Characteristic
11.	K. Jakubiuk, W. Aftyka	Heating of Fuse-Elements in Transient and Steady-State
12.	Rochette David, Clain Stéphane and Bussière William	Mathematical Model Using Macroscopic and Microscopic Scales of An Electrical Arc Discharge Through a Porous Medium in Hbc Fuses
13.	G. A. Cividjian	Current Distribution in Variable Section Fuses
14.	Adrian Pleşca	Thermal Simulations of Fast Fuses For Power Semiconductor Devices Protection

SESSION IV – Hazard and environmental aspects

Chairman: G. Newberry

1.	Claus Deußer	- Protecting Our Environment - Environmentally Compatible Recycling of High Performance Fuse Links
2.	Gerd Fink	Development of Legislation in the Area of Environmental Protection in Europe and Effects To Be Expected Onto the Fuse Industry
3.	A. D. Stokes and D. K. Sweeting	Electric Arcing Burn Hazards
4.	R. Wilkins, M. Allison and M. Lang	Time-Domain Analysis of 3-Phase Arc Flash Hazard
5.	J.G.J. Sloot and R.J. Ritsma	Protection Against Fault Arcs in Low Voltage Distribution Boards

FOREWORD

This year, the Seventh International Conference on Electric Fuses and Their Applications is held in historic Gdańsk, the town known for events important for many European countries. It is organized by the Gdańsk University of Technology in co-operation with the Polish Association of Electric Engineers on the eve of the 100th anniversary of the beginning of higher technical education in Gdańsk, (which began with the building of the Technische Hochschule Danzig), and the 60th anniversary of GUT, founded by the Polish after the World War II.

It is important to recall that the organisation of periodic meetings of ICEFA is closely associated with the Fuse Club founded many years ago by a group of young visionaries, outstanding fuse people. The Fuse Club is concerned with the international co-ordination of activity leading to the development of theory and application of electric fuses, and the quality of ICEFA. Regretfully, two of its founders i.e. Lipski and Turner have recently fulfilled their missions forever. We pay tribute to the knowledge, dedication and ever-ready helpful hands of these two great colleagues.

The seventh ICEFA meeting sums up the past 27-year period of development of electric fuses. Over that time ICEFA has contributed to a better understanding of physical phenomena associated with the operation of fuses, the development of many valuable ideas concerning new technologies and fuse designs, the elaboration of many fuse standards and improvement of fuse applications and maintenance. Conference discussions has stimulated many brains with ideas, generating new research and new approaches to the application and maintenance of fuses.

The 27-year old history of ICEFA emphasises changes and trends in the development of the protection of power systems, helps in a better understanding of the effect of broad introduction of power semiconductor devices, the processing of numerical data, the consideration of environmental problems and the quality of energy. All these factors have affected in some way the attitude to fuse applications and their development. They close some fields where frequent automatic operation is welcome, and open new horizons, as fault currents limitation becomes more important, protection of high power converters looks indispensable, and reduction of hazards is necessary. In order to promote fuse applications and facilitate understanding their features, a couple of years ago the ProFuse International organisation was created. This year, for the first time ICEFA hosts its President, to encourage broad discussion on actual problems of manufacturing and application of fuses. The presentations on environmental and hazard topics are also important new topics for ICEFA'2003.

In the enlarged European Union standardisation will become more important than ever. Therefore the second invited paper is dedicated to that theme. The first one, will give a vision of the future.

The bulk of papers submitted by the authors taking part in ICEFA’2003 focus on the phenomena associated with the fuse operation. New ideas and technologies, measurements, applications, standardisation are also to be found in the program.

The dynamics of the world economy influences significantly the allocation of funds for fuse manufacturing and research. Asian centres are strengthening and the European ones, especially those in post-communist countries are losing their importance. One notices with regret that publications from previously “ever-present” Russian and Ukrainian teams fail to appear at ICEFA’2003. Although Romanian colleagues submitted a few theoretical papers, they enounced problems with the participation in conference meetings. On the other hand some interest of African countries and Turkey is noted with pleasure. The application of a Chinese group for the organisation of the next meeting of ICEFA indicates that for the first time the centre of inertia of activity in electrical fuses may be moving to Asia.

The ICEFA’2003 Organising Committee believes that the conference meetings and discussions will be interesting, generate new ideas and bring much satisfaction for all participants.

Andrzej Wolny
Chairman
Scientific Committee

Electric Behavior of Capillary Arcs Ignited at High Current Density Levels in Copper Vapor

E. Maira, S. Arai

Tokyo Denki University 2-2 Kandanishiki-cho, Chiyoda-ku, Tokyo 101-8457 JAPAN
arai@e.dendai.ac.jp

Abstracts: In order to understand the mechanism of the high arc voltage generation of the current limiting fuses, the experimental studies were made by the capillary arc ignited in copper vapor at high current density. The experimental sample consists of a Pyrex glass capillary, a copper wire element and copper electrodes.

The line spectral radiation intensity of copper atom decreases, the continuous component of spectral radiation intensity increases and the mean arc voltage builds up as the inner diameter of capillary is becoming smaller.

During the arcing time in the breaking of high current density, the dynamical movement and geometrical construction of copper medium in the capillary are conjectured by the observation of spectral radiation. The temperature of arc column is estimated by the measured copper spectral lines of 521.8 nm and 510.6 nm in wavelength for the glass tube of 3.5 mm in diameter. The temperature of arc column in this experimental conditions obtained change from 4500 to 19000 K roughly.

Keywords: current limiting fuses, capillary arc, high arc voltage, line spectrum, continuous spectrum, cluster

1. Introduction

The purpose of this research is to understand the phenomenon of high arc voltage generation of current limiting fuses in the breaking heavy current. The sample piece is mainly consisted of a Pyrex glass capillary, a copper wire element and copper electrodes. Two kinds of copper wires with different diameter were used as fuse elements.

It is supposed that the discharge space is axial symmetry and the arc column is surrounded by the layer of copper vapor and clusters after the developing the multi arcing process and fully growing the single arc. Due to the continuous spectral intensity distribution observed in capillaries of the smallest diameter, it is supposed that the layer is at least consisted of two zones. One is the high temperature and optical dense inside zone of layer including copper vapor and clusters closely surrounding the arc column. The other is the low temperature outside zone of layer including vapor and clusters of copper and sodium on the wall of glass tube. These zone construction of layer will be affected by the ratio of arc energy injected until the instant to the mass of copper element.

The inside zone of layer heated high temperature radiates the radiation like blackbody, which is selectively absorbed by the outside zone of layer including the vapor and clusters of copper and sodium. The temperature of inside zone was estimated by considering the continuous spectral intensity distribution observed for the glass tube of 1 mm in diameter as the black body radiation. [1]

The transmissivity of the white light through the sample which was stained by the copper thin film on the inner wall of glass tube for the experiment was measured to investigate the selective spectral absorbing

phenomena.

The radiation temperature of arc column was estimated by measuring the two copper spectral lines of 521.8 nm and 510.6 nm in wavelength for the glass tube of 3.5 mm in diameter. The temperature just after ignited arc is from 5000 to 8000 K, then after passing through the minimum temperature about 4500 K, the arc temperature monotonously increases to about 15000 to 19000 K.

2. Experimental equipments and method

2.1. The experimental circuit and apparatus

Fig.1 shows the experimental circuit. A current breaking experiment is carried as follows. The charged capacitor bank C of 0.136 F discharges through the reactor L of 1.96 mH and breaker B interrupts the current of CL loop to disconnect the capacitor bank near the maximum current. Thereafter the current is commutated to flow in the LR discharge circuit which consists of reactor L, the experimental apparatus and current shunt Sh.

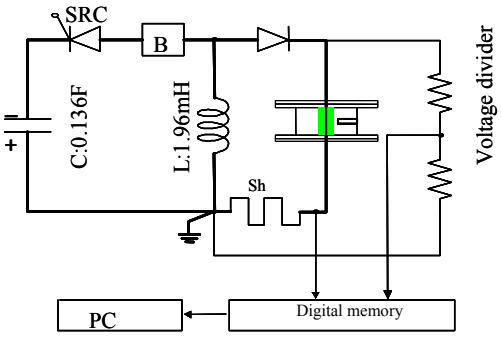

Fig.1 Experimental circuit

The experimental apparatus mainly consists of a pressure container and an experimental sample. The pressure container is constituted with the top and bottom stainless steel circular disks of 15 mm in thickness and a insulation cylinder of 58 mm in length and 80 mm in outer diameter. The experimental sample consists of a copper wire element, a Pyrex glass tube and electrodes which serve to hold elements and to seal the arc burning space of capillary. The dimension of a copper wire is 50 mm in length, 0.18 and 0.26 mm in diameter and the dimension of Pyrex glass tube is 50 mm in length and 1 to 3.5 mm in inner diameter every 0.5 mm.

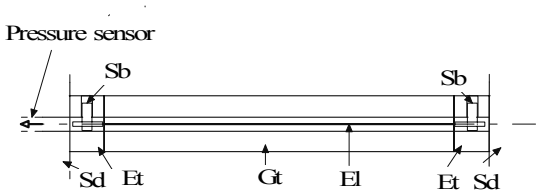

El: Copper wire element, Gt: Glass tube,
Et: Copper electrode, Sb: Screw bolt,
Sd: Stainless steel disc.

Fig.2 The experimental sample

2.2. Spectral measurement systems

The 2 spectral measurement systems were used to make measurement of the radiation spectrum from the inside of glass tube. One called PMA (Photonic Multichannel Analyzer) consists of the multichannel spectral equipment and the controller of optical system. The PMA measures simultaneously the spectral intensity of time integral during 25 msec in the range of 300 to 800 nm in wavelength. The other measures 2 line spectral intensities with time. The radiation conducted by the single optical fiber is equally divided on the way of optical channel and then each divided radiation is conducted to a monochromatic spectrometer.

3. Experimental Results

3.1. Spectrum in the glass tube of 1 mm in inner diameter

The experiment was made to obtain arc current and voltage, line spectral intensities of 510.6 nm and 521.8 nm to time and spectral intensity distribution to spectral wavelength using experimental samples. The samples made up by a copper wire element of 0.18 mm or 0.26 mm in diameter and a Pyrex glass tube of 1 mm in inner diameter. The breaking current was same in pre-arcing time.

Fig.3 shows current and voltage in Fig.3(a),

spectrum intensities of 521.8 nm and 510.6 nm in wavelength observed by the 2 spectrometer system in Fig.3(b), and spectral intensity distribution obtained by PMA in Fig.3(c) for the copper wire element of 0.18 mm in diameter.

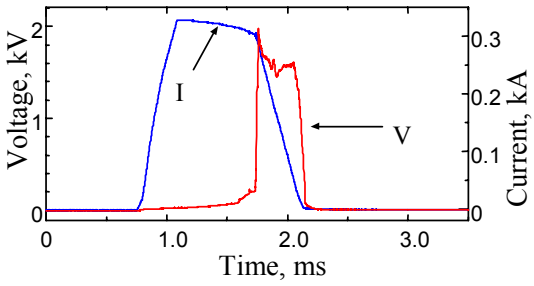

(a) Current and voltage

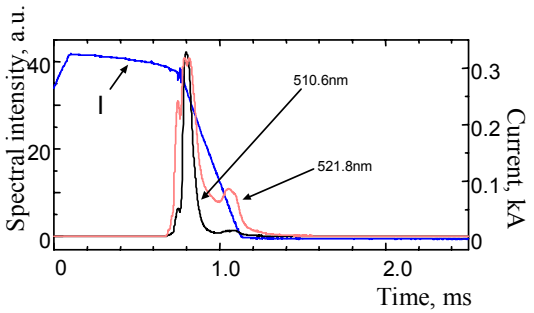

(b) Current and spectral intensities of 521.8 nm and 510.6 nm in wavelength to time

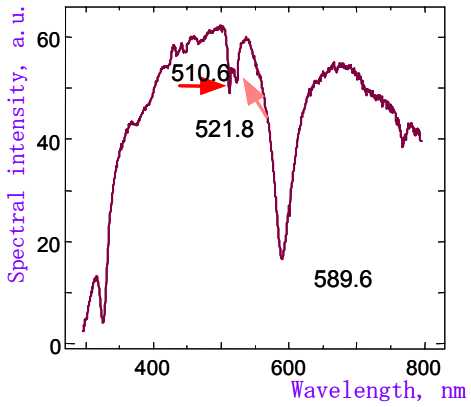

(c) Spectral intensity to spectral wavelength

Fig.3 Current, voltage, line spectral intensities and spectral intensity distribution for the element diameter of 0.18 mm and the glass tube inner diameter of 1.0 mm

Fig.4 shows current and voltage, line spectral intensities to time and the spectral intensity distribution to spectral wavelength obtained for copper wire elements of 0.26 mm in diameter, and Pyrex glass tubes of 1 mm in inner diameter.

As seen in Fig.3(a) the current wave form is roughly rectangular during prearcing time of 1.0 ms. An arc voltage builds up rapidly to the maximum voltage of 2.0 kV just after arc initiation and decreases 1.55 kV.

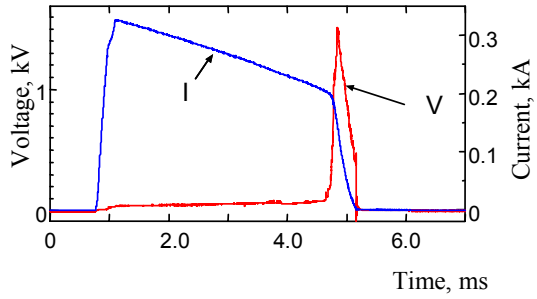

(a) Current and voltage

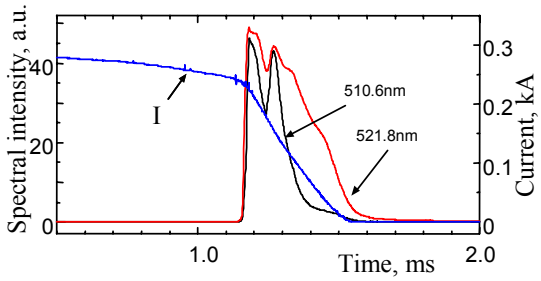

(b) Current and spectral intensities of 521.8 nm and 510.6 nm to time

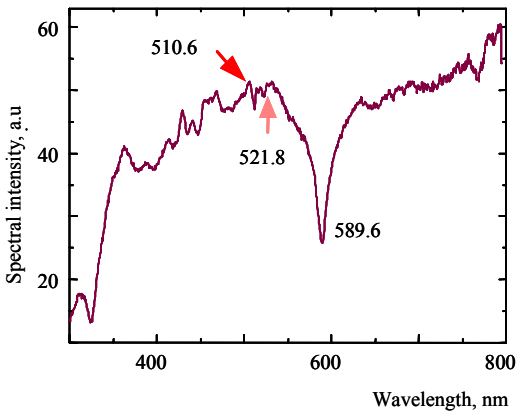

(c) Spectral intensity to spectral wavelength

Fig.4 Current and voltage, line spectral intensities and spectral intensity distribution for the element diameter of 0.26 mm and the glass tube inner diameter of 1.0 mm

As seen in Fig.4(a) the current during the pre-arcing time is same wave form as that in Fig.3(a), but the pre-arcing time of 4.1 ms is longer because of the larger diameter of element. According to the lower arc ignition current, the arc voltage decreases linearly from the maximum of 1.5 kV at arc initiation to the minimum of 0.4 kV just before an arc current zero and instantly rises 0.5 kV at the current zero.

Fig.3(b) shows the line spectral radiation intensities of 521.8 and 510.6 nm in spectral wavelength for copper atoms. Both intensities very quickly increase after the ignition of arc, the intensity of 521.8 nm is larger than that of 510.6 nm for 115 μ s before the maximum intensity, and the intensities inverse each other around the maximum intensity, that is, the intensity of 510.6 nm is larger than that of 521.8 nm. And the intensities again inverse each other and decrease with time, the intensity of 521.8 nm swells before arc current zero.

Fig.4(b) shows the same behavior of line spectral intensities as Fig.3(b). Both intensities very quickly increase after the ignition of arc, the intensity of 521.8 nm is larger than that of 510.6nm for 47 μ s before the maximum intensity. Both intensities have a deep dent around the maximum intensity. Then both intensities decrease with time, and the intensity of 521.8 nm is kept over and decreases slower than that of 510.6 nm until arc current zero.

As seen in Fig.3(c) and Fig.4(c), the spectral intensity distribution to the spectral wavelength is roughly continuous and strong spectral absorption is clearly recognized at two portions around 325 to 327 nm and 590 nm of wavelength for the glass tube of 1 mm in inner diameter. It is supposed that the spectral absorption around 325 to 327 nm is brought on the copper clusters and vapor, absorption around 590 nm is brought on sodium clusters and vapor.

3.2. Spectrum in the glass tube of 3.5 mm in inner diameter

The same experiment as the section 3.1. was made except using Pyrex glass tubes of 3.5 mm in inner diameter as parts of experimental samples. The breaking current was same in prearcing time.

Fig.5 shows current and arc voltage, line spectral intensities and spectrum distributions obtained by a experimental sample made of a copper wire of 0.18 mm in diameter as the element.

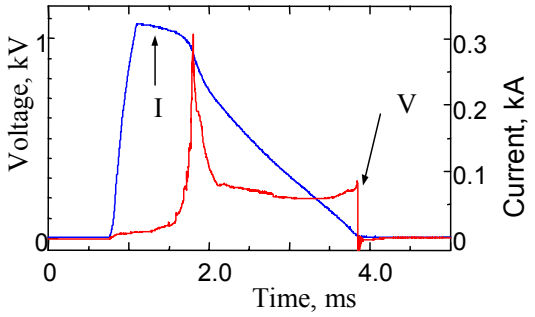

(a) Current and voltage

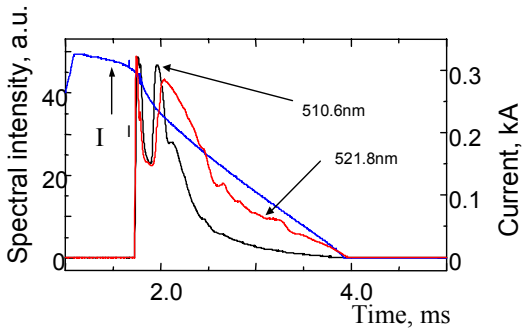

(b) Current and spectral intensities of 521.8 nm and 510.6 nm to time

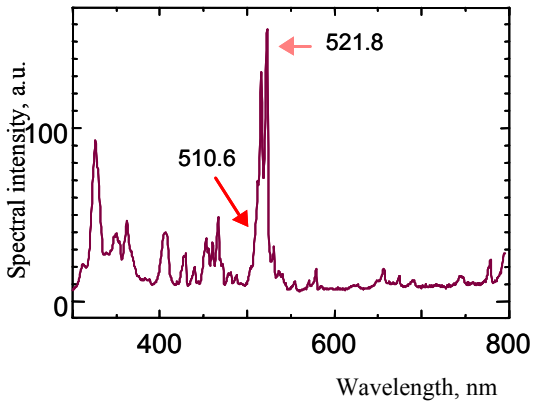

(c) Spectral intensity to spectral wavelength

Fig.5 Current and voltage, line spectral intensities to time and spectral intensity distribution to spectral wavelength for the element diameter of 0.18 mm and the glass tube inner diameter of 3.5 mm.

Fig.6 shows current and arc voltage, spectral intensities to time and spectral intensity distribution to wavelength obtained by a experimental sample made of a copper wire of 0.26 mm in diameter as elements.

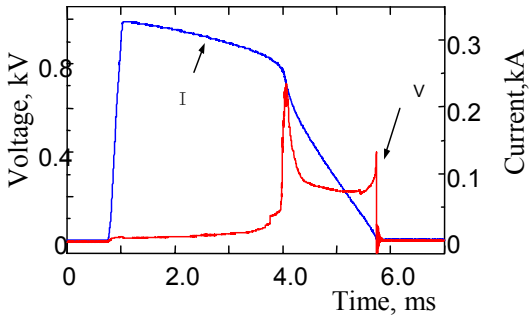

(a) Current and voltage

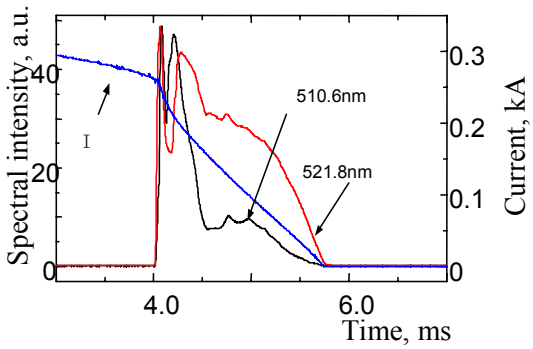

(b) Current and spectral intensities of 521.8 nm and 510.6 nm to time

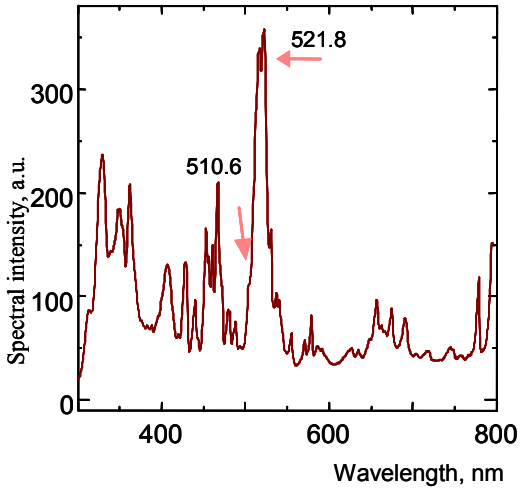

(c) Spectral intensity distribution to spectral wavelength

Fig.6 Current and voltage, line spectral intensities to time and spectral intensity distribution to spectral wavelength for the element diameter of 0.26 mm and the glass tube inner diameter of 3.5 mm.

As seen in Fig.5(a) the current wave form is roughly rectangular during prearcing time of 0.85 ms. An arc voltage builds up rapidly to the maximum voltage of 1.0 kV after arc initiation and decreases 0.25 kV for 0.3 ms and is kept from 0.2 to 0.25 kV.

As seen in Fig.6(a) the current is the same wave form as that of Fig.5(a) except for pre-arcing time of 3.3 ms. Since the arc ignition current is lower than that of Fig.5(a), the arc voltage decreases linearly from the maximum of 0.7 kV at arc initiation to 0.35 kV and the minimum of 0.2 kV just before an arc current zero and quickly rises the peak voltage of 0.4 kV at the current zero.

Fig.5(b) and Fig.6(b) show the distribution of line spectral radiation intensities of copper atom for the glass tube of 3.5 mm in inner diameter.

The both line spectral intensities on each figure from the arc discharge space suddenly build up at the same time of arc ignition and reach the peak values in a few micro seconds. After reaching the peak intensity, the both spectra collapse and return in 0.2 to 0.3 msec. The spectral intensity of 510.6 nm in wavelength is larger than that of 521.8 nm for this duration.

Thereafter both spectral intensities change each other, that is, the spectral intensities of 521.8 nm is larger than that of 510.6 nm and the spectral intensity of 510.6 nm collapses more quickly than that of 521.8 nm. Both spectral intensities mostly disappear at the same time near arc current extinction.

Fig.5(c) and Fig.6(c) show the spectral intensity distribution to the spectral wavelength for the glass tube of 3.5 mm in inner diameter. The spectral intensity distribution is mostly line spectrum.

The spectral radiation intensity in the glass tube of 3.5 mm in inner diameter is about 7 times larger than that of 1 mm for the values around 515 to 520 nm of spectral wavelength.

The remarkable difference for the distribution of spectral intensity to the wavelength is observed for the inner diameter difference of glass tube. The continuous spectral intensity distribution was observed by PMA for the glass tube of narrow inner diameter and the line spectral intensity distribution was observed on the large inner diameter of glass tube. The result suggests that the higher density of copper layer surrounding arc is as the diameter of glass tube is smaller, the weaker spectral intensity pass out through the glass tube.

4. Consideration and investigation

4.1. Optical state of copper vapor surrounding arc column estimated by spectral radiation intensity distribution

Using the PMA, the distributions of continuous spectral and line spectral intensity are observed by the measurement of spectrum emitted through the glass tube during arcing time. It is supposed that the different distribution of spectral intensity emitted through the glass tube during arcing time depends on the state of medium generated from the dispersed and decomposed wire element and surrounding the arc discharged space.

As previously reported about the continuous distribution of spectral intensity, [1] it is estimated that the arc column is surrounded by the layer of optical dense medium, this layer absorbs the some spectral radiation from the arc depending on the optical density. The medium includes copper vapor, copper clusters which consist of many kinds of assembly of copper atoms and radiate the continuous spectra.[2]

On the other hand, the medium surrounding arc column becomes optically thinner and the line spectral radiation intensity through the glass tube is stronger as inner diameter of glass tube is larger.

4.2. The arc column temperature estimated by the line spectral radiation measurement

It is supposed that the line spectral radiation through the glass tube of larger inner diameter is directly emitted from the arc column. If the local area thermal equilibrium is maintained in an arc column, the temperature of arc column is estimated by the ratio of 2 line spectral intensities as given by the following equation for copper atoms.[3]

$$T = \frac{11975}{2.05 - ln\frac{I_{521.8}}{I_{510.6}}} \quad [K] \qquad (1)$$

where T is the absolute temperature of arc column, $I_{521.8}$ and $I_{510.6}$ are the spectral intensities of 521.8 nm and 510.6 nm in wavelength respectively.

The temperature of arc column was calculated by the equation (1) about the data of line spectral intensities shown in Fig.5(b) and Fig.6(b). The calculated results are shown in Fig.7 and Fig.8.

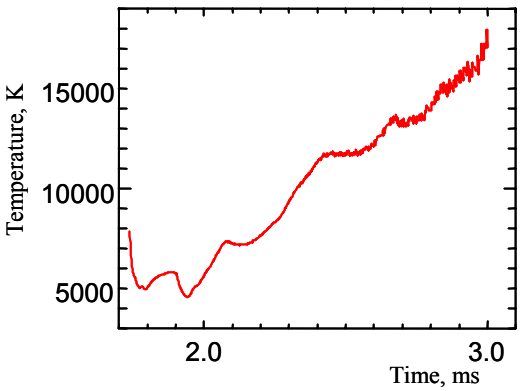

Fig.7 the temperature of arc column obtained from the data of Fig.5(b) for the sample made of the element of

0.18mm in diameter and the glass tube of 3.5mm in inner diameter

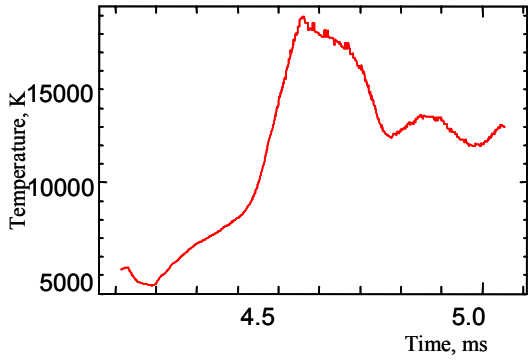

Fig.8 the temperature of arc column obtained from the data of Fig.6(b) for the sample made of the element of 0.26mm in diameter and the glass tube of 3.5mm in inner diameter

The change of arc temperature is shown in Fig.7 obtained for the sample made of the element of 0.18mm in diameter and the glass tube of 3.5mm in inner diameter. The temperature is 8000 K at the arc ignition, and decreases to the minimum value of 4950 K, and then increases monotonously to 18000 K for 1 msec.

Fig.8 shows the change of arc temperature obtained by using the sample made of the element of 0.26mm in diameter and the glass tube of 3.5mm in inner diameter. The temperature is 5500 K at the arc ignition, and decreases to the minimum value of 4950 K, and then increases monotonously for 0.35 msec to the maximum value of 19000 K, and again decreases to the mean value of 13000 K.

4.3. Development of medium surrounding the arc column

In the breaking current level of the experimental circuit adapted for this research,[4] just a little before the arc ignition, the element changes from a cylindrical liquid of uniform cross section to one of variable cross section constricted at many points along the length of element. The constrictions in the cross section of element develop at many points along the length of wire element as the result of current pinch effect. It is estimated that the temperature of element at that instant may be slightly higher than the melting temperature by the value of specific Joule integral.

At last the multi-arc starts along the length of element following the development of constriction of element cross section in very short time. Each arc burns back and joins together, and single arc is formed in very short time duration.

For the short duration after the ignition of multi-arc, the energy flowing into the experimental sample increases abruptly according to the generation of high arc voltage, but most energy may concentrate into the zones of arc burning points, so that a smaller amount of energy supplies to a layer of decomposed copper wire element diffused outside the arc burning space. Therefore a copper layer outside the arc space may consist of copper vapor and clusters mixed up various sizes.

4.4. Line and continuous spectral radiations depending on the glass tube diameter

In early arcing time, the arc discharge space is surrounded by the layer consisting of copper vapor and various size clusters. The spectra emitted from the arc discharge space may be affected by the density of layer which depends on the inner diameter of glass tube.

The lower density of layer surrounding arc discharge space is and also the thinner optical thickness of the layer is, the larger inner diameter of glass tube is. The absorption of emission from arc discharge space decreases and the line spectral intensity observed outside the glass tube is stronger as the inner diameter of glass tube is larger. It is supposed that the line spectral intensity observed outside the glass tube of larger inner diameter may directly come through from the arc discharge space.

The density of layer surrounding arc discharge space is denser and the optical thickness of the layer is also thicker as the inner diameter of glass tube is smaller. The absorption of emission from the arc discharge space by the layer increases and the line spectral intensity attenuates and at last the only continuous

spectral distribution observes outside the glass tube as the inner diameter of glass tube is furthermore smaller. The mechanism of continuous spectral radiation observed in the smallest inner diameter of glass tube is supposed as follows. The clusters which absorb the emission from arc discharge space radiate the continuous spectrum within the longest limited wavelength depending on the size of cluster.

5. Conclusions

Using samples stretched a copper wire element in the capillary of glass tube, and in the region of current limiting level for the prearcing time of a few milli-seconds order, the formation of medium distribution in the arc discharging space was considered by the spectral radiation during arcing time. And the temperature of arc column was observed by two lines spectral intensities emitted from the copper atom in an arc column.

After the multi arcs ignite along the wire element at the start of arcing time, the single arc is formed by each arc burning back for the duration of quite short time.

The line spectral distribution was observed in the glass tube of larger inner diameter, the continuous spectral distribution was observed in glass tubes of the smallest diameter.

The process of distribution of arc space media of the element material in relatively short arcing time is supposed from the spectral observation as follows. Each arc is surrounded by the vapor and clusters of the element material in the duration of multi arc, multi arcs grow up into the single arc between the electrodes, the arc column is surrounded by the layer of copper vapor and clusters.

On the observation of line spectral distribution in the glass tube of larger inner diameter, spectral radiation of arc column directly comes through the glass tube because of the thin density of clusters in the layer. On the continuous spectral distribution in the smallest inner diameter, the spectral radiation of arc column is absorbed by the inside zone of optical dense layer and then the continuous radiation form the dense cluster zone in the layer comes out through the glass tube because of thick density of clusters in the layer.

The continuous radiation emitted by the inside zone of the layer of high temperature is absorbed the outside zone of the layer including copper and sodium clusters. The sodium may be supplied by the ablation of inside wall surface of Pyrex glass tube.

It was made certain that the thin membrane of copper adhered to the glass tube wall after experiment absorved selectively little line spectral radiation.

The line spectra of arc column directly come out through the glass tube, so that the temperature of arc column is obtained by the two line spectra of copper atom assuming the local area thermal equilibrium. The temperature of arc column changes from 4500K to 19000K.

References

[1] S. Arai: Geometrical Model of Discharge Space in the State of the High Arc Voltage Generation of Capillary Arcs, Proc. ICEFA, pp119～124, (1999)

[2] B. Weber and R. Scholl: A Noble Type of Light Source: Continuous Radiation from Small Clusters in Microwave Exited Discharges, J. of IES, Summer, pp93～97 (1992)

[3] Miyaji, Kito, Okada: (Japanese), J of IEEJ

Vol.87, p1227 (1967)
[4] S. Arai: Deformation and Disruption of Silver Wires, Proc. ICEFA, pp50～58, (1976)

RESPONSE OF A MEDIUM VOLTAGE CURRENT LIMITING FUSE OF SMALL SIZE TESTED AS GENERAL PURPOSE AND FULL-RANGE TYPE.

Alfonso Avila Ramírez.

Corporativo Arian, S.A. de C.V., Hidalgo 26 Santa Ana Tlacotenco, Milpa Alta D.F., México C.P. 12900
www.arian.com.mx, arian@arian.com.mx

Abstract: This paper describes laboratory investigations on a distribution current-limiting fuse of relatively reduced dimensions applied in an enclosure with restricted air flow surrounding it, tested as general purpose and full-range types respectively. The most important differences found in both cases are closely related with the application of the minimum interrupting current I_3 which was determined following the criteria established in the IEEE STD C37.41-2000 [1]. There is not a great difference between their magnitudes but its thermal effect is determinant for the satisfactory performance of them. However as we have found, if only the fuse body material is changed it is quite possible to have in only one model both types of fuses taking into account that all the others components of it have been chosen and designed in the best possible way.

Keywords: FEP_S Fuse Enclosure Packages

1. Introduction

The IEEE std C37.41-2000 specifies design test requirements for high-voltage fuses amongst which are included the distribution and power class current-limiting type fuses.

The distribution type current-limiting fuse described here, was designed to be used in an enclosure with relatively free air circulation within the enclosure trying to satisfy the corresponding interrupting test series 1, 2 and 3 indicated in the paragraph 6.6.

In particular the test series 3 was carried out following carefully the criteria indicated in the paragraphs 6.6.2, 6.6.3 and 6.7. Paragraph 6.6.2 describes an alternate test method for series 3 using a low-voltage source for the first part of the test and a high-voltage source for the second part of the test

6.6.3 describes the method for series 3 tests on full-range current-limiting fuses.

6.7 gives a description of interrupting tests for FEP´s using current-limiting type indoor distribution and power class fuses.

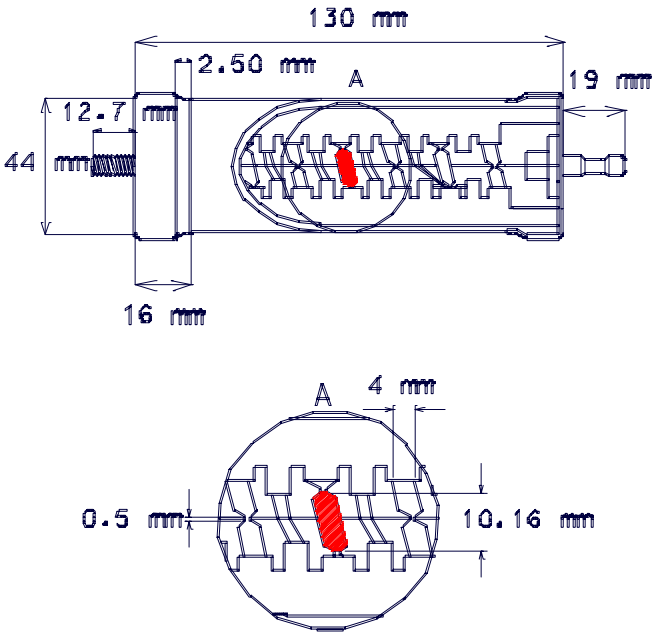

Figure1: Medium Voltage Current-Limiting Fuse

2. Construction.

The current-limiting fuse described in this paper has been designed for nominal current and voltage ratings of the 30 A and 8.3 kV A.C. respectively.

Because of its small size, Fig 1, it has only one silver ribbon wound with M-spot made of eutectic tin alloy located on its middle, Fig 2.

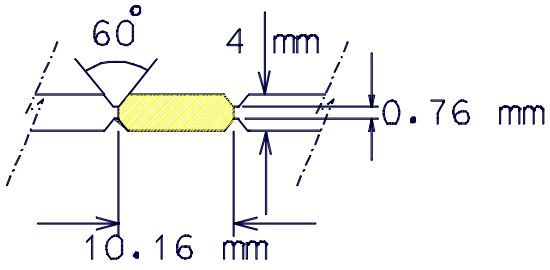

Fig 2. Silver Ribbon wound with M-spot .

Also and connected in parallel with it are two auxiliary elements made of silver wire for controlling the arcing in more than one point [2]. The element support is made of mica (aluminosilicate-mineral) of optimized design for continuous operating temperature of 500°C and dielectric strength of 13 kV/mm at 400 °C.

The fuse body is made of glass epoxy tubing NEMA G-11 for a continuous operating temperature of 150 °C and 205 °C for short time. In order to have a good mechanical strength and a maximum heat dissipation by conduction to the end terminals, the end cylindrical caps are made of cooper.

The core (spider) has the right concentricity with the cylindrical body. This condition added to an adequate compactness of the quartz sand [3] of an average size of 0.45mm, improves the behavior of the fuse under steady-state operating conditions, distributing uniformly the axial and radial dissipation mainly and under short-circuit conditions, facing satisfactorily its thermal, dielectrical and mechanical effects.

As these type of fuses are applied in underground circuits to protect pad-mounted transformers, its fuse-body has an external semi-conducting wrap that provides a fully shielded system.

Also we have avoided to use the polluting agents like the flux for soldering metallic components located inside the cylindrical body after assembly due to its disastrous effects.

3. Heating Process

For the purpose of our experimental study directed basically to the response of the fuse to the small overcurrents comprised between the minimum breaking current I_3 and the minimum melting current, we consider the heating process a steady state thermal phenomenon, so the heat generated within the fuse, is dissipated to the surroundings by conduction and convection due to the enclosure (FEP) used under normal application operating conditions and also during all the tests made in our investigation.

The equation developed by Verdet in 1872 for the temperature in an element section [4] heated by electric current is:

$$Ks\ \frac{d^2T}{dx^2} - \frac{T}{g} + \frac{I^2\ \rho o\ (1+\alpha\ T)}{s} = 0 \qquad (1)$$

Axial heat conduction loss — Heat loss from surface — Internal heat generation

In this ordinary differential equation:
K= thermal conductivity of the element metal
$_S$= cross-sectional area of the fuse element
T= temperature rise above ambient
g= thermal resistance per unit length
ρ_o= resistivity at ambient temperature.
α= temperature coefficient of resistivity

In the above referenced paper [4] are described the solutions of the differential equation (1) that in the case of low currents the temperature distribution is governed by hyperbolic functions and also are shown the calculations of:

- Heat transfer by conduction to the ends of the section taking into account that the whole element is formed by a combination in series of a given number of such sections.
- The radial thermal resistance.
- Effect of field distortion.
- Heat generated in the caps, and
- Heat lost to end assemblies.

In order to determine the more convenient I_3 current magnitudes, we made a series of melting tests in the long-time zone of operation of the time-current characteristics previously defined by experimentation (Figure 3). Making some changes in an orderly way and with only one change each time on the central design parameters.

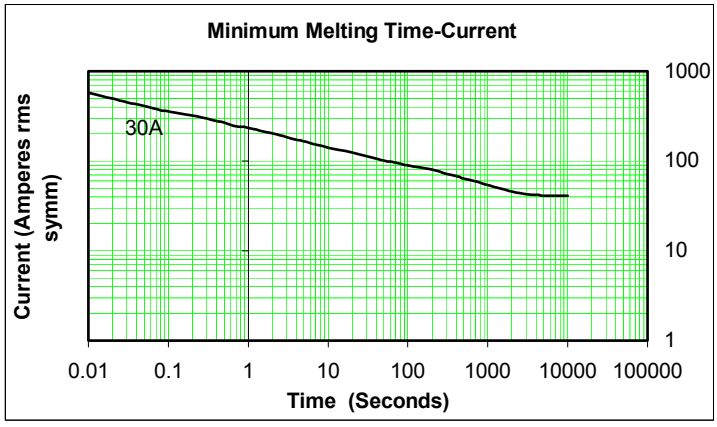

Figure 3 Melting time-current curve

The most relevant changes and results were:

Variation of the neck cross-section and the ratio between the width (b) of the neck and the width of the strip (B) looking for a ratio of five in order to reduce additionally the arcing energy

$$\int Va\ ia\ dt$$

generated [5] during the short-circuit tests.
In tables 1 and 2 are presented some significative variations attained.

Cross section (mm^2)	Maximum temperature rise (°C)	Melting time (minutes)
0.11375	73.12	33
0.16912	146.70	67

Table 1 Testing current = 43 A.

Ratio $\frac{B}{b}$	Maximum temperature rise (°C)	Melting time (minutes)
8	131.87	142
5.333	112.5	123

Table 2 Testing current = 41 A.

Average grain size of the quartz sand and its influence on the magnitude of melting time, maximum temperature generated and the behavior of the fuse link when is tested with I_3 at rated voltage [6], [7], [8] See table 3

Average Ø of quartz sand (mm)	Maximum temperature rise (°C)	Melting time (minutes)
0.70	141.87	871
0.45	119.83	715

Table 3. Results attained applying increases of melting current of 5% with a final magnitude of 30A

The quantity of alloy chosen for the M-spot [9] and its influence on the melting time and temperature-rise. See table 4

Weight of the alloy added (p.u.)	Maximum temperature rise (°C)	Melting time (minutes)
1	66.36	72
0.36	101.98	71

Table 4. Testing Current = 41A

4. Operating temperature within the enclosure and I_3 current magnitudes

The rated maximum application temperature chosen for the fuse link within the enclosure was 77 °C.

In the case of fuse links considered as general purpose type and applying the established criteria in the paragraphs 6.6.2.2, 6.7.2.1 (FEP type 1C) and 6.7.4 of the IEEE std. Referenced in [1], starting with a melting current of 41 A, taken from the melting time-current curve, the I_3 current obtained a final magnitude of 32.5 A approx.

The derating factor recommended in [10] was:

$$0.4\% / °C$$

$$\text{percentage reduction factor} = (77\text{-}25)\ 0.4 = 20.8\%$$

$$\Rightarrow\ I_3 = 41\ (1\text{-}0.208) \approx 32.5\ A$$

When the fuse was considered as full-range type the increases of current steps from a given value until its final value when the fuse link melted, was applied the method described in 6.6.3.1 of the above indicated std.

In both cases the minimum number of test made with the final model was at least five.

The results of the test for each case are shown in table 6 and 7.

I_3 current magnitude (A)	Maximum temperature rise (°C)	Melting time (minutes)
32.5	160.24	199

Table 6. General Purpose type fuse (initial temperature = (77°C)

Current steps (A)	Maximum * temperature rise (°C)	Melting time (minutes)
21	88.78	-----
22.5	93.40	-----
24	98.08	-----
25.5	101.98	-----
27	108.16	-----
28.5	113.30	-----
30	120.38	-----
31.5	142.44	-----
33	143.12	1115

Table 7. Full range type fuse (initial temperature = 77°C)

*For each current step, the temperature was considered stable when the temperature rise above ambient did not exceed 2% per hour.

Table 6 shows the final current magnitude I_3 applied to the general purpose type fuse and table 7 shows the current step values with its corresponding stabilized temperatures together with the final current and melting time determined for the full-range type fuse.

The highest current that a total of five fuses carried without melting was 31.5 A so:

$$I_3 = 0.9\ (31.5) = 28.35\ \text{A and we use}$$

$$I_3 \approx 28.5\ \text{A}.$$

5. Breaking Tests and Results

The test series 1 2 and 3 were performed applying the methods described in 6.6 and 6.7 of the referenced IEEE std. The results were:

Test series 1

Test current: 50 kA rms symmetrical
Test voltage: 8.31 kV
Ambient Temperature: 30°C
Oscillogram of one test

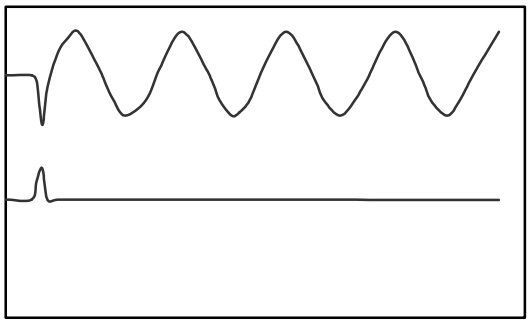

Figure 4. peak current:5485 A
peak voltage: 16.354 kV

Test series 2

Test current: 16.56 kA rms symmetrical
Test voltage: 8.31 kV
Temperature within the enclosure: 77°C

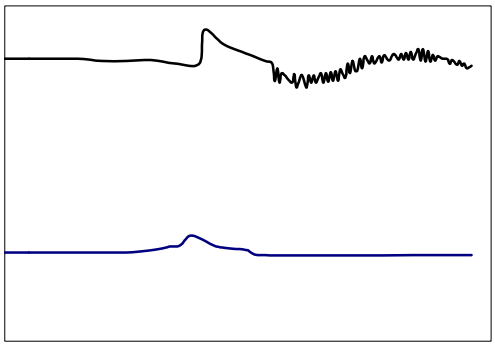

Figure 5 Peak current:4.86 kA
Peak voltage: 27 kV

Duration of recovery voltage after interruption = 60 seconds.

Test series 3

Considering The fuse as general purpose-type

Test current at low voltage { 32.5 A during 60 minutes; 37.4 A during 9 minutes }

Test voltage applied after 69 minutes: 8.33 kV
Temperature within the enclosure: 77°C
The following oscillogram shows only the part of test made a 8.33 kV

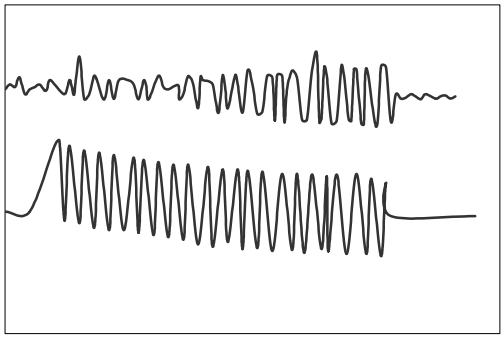

Figure 6 Peak voltage: 11.78 kV
Melting time: 69 minutes
Duration of recovery voltage after interruption: 10 minutes
Number of tests : 2

Fuse link considered as full-range type

Test current at low voltage { 28.5 A during 60 minutes; 32.7 A during 30 minutes }

Test voltage applied after 90 minutes: 8.33 kV
Temperature within the enclosure: 77°C

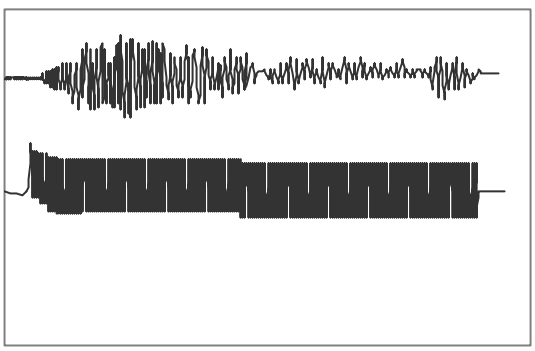

Figure 6

The fuse failed to open the medium voltage circuit after applying 28.5 and 32.7 A in the low voltage circuit

The tube of the fuse-body presented several burns without an intense carbonization on its inner wall.

By reasons of economy this was the only test made under the above described conditions.

Note: All the interrupting tests were carried out at the High Power Laboratory LAPEM of the Comisión Federal de Electricidad.

6. Conclusions

After all tests made, until now we conclude that our final model of fuse link failed to interrupt the I_3 testing current when it was considered as full-range type, it is possible to improve its response taking into account these remarks:

- To change the material for the tubing of the fuse-body. For instance to use NEMA Grade G-7 material.
- In order to assure the success of an optimized model it is necessary to avoid in its construction the use of polluting agents like: flakes of mica, iron oxide, and flux for soldering any metallic component located within the fuse body.
- The more convenient I_3 current magnitude for testing full range fuses requires the use of increases of current steps as small as possible although this condition spend more time

References.

[1] IEEE std C37.41-2000, "IEEE Standard Design Tests for High-Voltage Fuses, Distribution Enclosed Single-pole Air Switches, Fuse Disconnecting Switches, and Accessories"

[2] H.W. Mikulecky, "Current-Limiting Fuse with Full-Range clearing Ability", IEEE Transactions on Power Apparatus and Systems, Vol PAS-84 No 12, pp 1107-1112, December 1965

[3] Chen Su Tsing, "Research on the technique of Filling Quartz sand in Fuses", Third International Conference on electrical fuses and Their applications, Eindhoren, The Netherlands, pp 93-98, May 11-13 1987.

[4] R Willkins, "Simulation of Fuse link Temperature-Rise Tests", International Conference on Electric Fuses and their applications, pp 24-32, Tronheim 1984

[5] V. Narancic, M Braubonic, A-C Westrom, "The composite fuse- A new Technology for Current Limiting Fuses", 7th. IEEE/PES, Transmission and Distribution Conference and Exposition, pp 462-470 April 1-6 1979

[6] Sei-Hyun Lee et al, "The test method to acquire the optimal parameter for CL-Fuse" International Conference on Electric Fuses and their applications, pp 265-270, Torino Italy, September 20-22 1999

[7] H.V. Turner and C. Turner, "Phenomena occurring during the extinction of arc fuses", Electrical Research Association, pp 253-256, Leatherhed, England

[8] Aslak Ofte and W Rondeel, "Test procedures and Arcing phenomena in H.V. Fuse links Near the minimum breaking current", International conference on electric Fuses and their applications, pp 190-199, Trondheim, Norway June 13-15 1984

[9] M. Hofmann and Lindmayer, "Pre-calculation of time/current characteristics of "M"-effect fuse elements", Third International Conference on Electrical Fuses and Their applications, pp 30-38, Eindhoven, The Netherlands, May 11-13 1987.

[10] IEEE std C37.48-1997, "IEEE Guide for the application Operation, and Maintenance of High Voltage Fuses, distribution Enclosed Single-Pole Air Switches, and Accessories".

THE FUTURE OF FUSES

Herbert Bessei
EFEN GmbH, Germany

1. Introduction

Fuses belong to the first devices of commercial electricity and they still use the same physical principle since their invention much more than a hundred years ago. In fact, many fuses don't appear to have changed in design over decades. Just the fact of an extremely long product history in a rapidly developing technical environment seems to be reason enough for people of different interests to question the future of fuses.-

- Customers, driven by the desire of a perfect convenient protective device
- C.b. manufacturers, wishfully thinking of ousting a nuisant competitive device
- Fuse manufacturers, being concerned about future business

The author intends to discard his admittedly positive attitude to fuses and to develop an unbiased scenario of fuses and applications that may enable the fuses to survive in a growingly competitive environment. Three methods of prognostication are used.-

- Chart technique
- Technical facts
- Market psychology

2. Chart technique

One very common attempt to predict the future development of markets is the extrapolation of past figures. In conjunction with an estimation of future development in technology this may give a reasonable prediction of the future of fuses as well. Looking at the demand of electronic fuses in Fig. 1 it can be seen that there has been an approximately linear growth of about 6 % per year until now. There is not too much prophetic skill necessary to predict a similar growth rate for the years to come as the major fields of application are still to be seen in growing markets like computer hardware, cellular phones and consumer electronics. Unfortunately the sales value cannot be expected to grow in line with the number of fuses as significant price erosion has to be expected.

A second field of growing fuse application can be seen in the automotive market. Even if the number of new cars produced would not increase, the number of fuses used in cars has been increasing with each new model and can still be expected to grow further on. Fig. 2 shows how the number of fuses (not including electronic fuses) has increased in one popular compact size European car. Similar graphs can be drawn for almost every model of car.

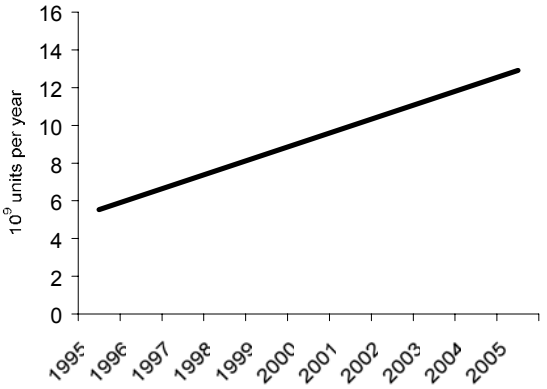

Fig. 1: Demand of electronic fuses

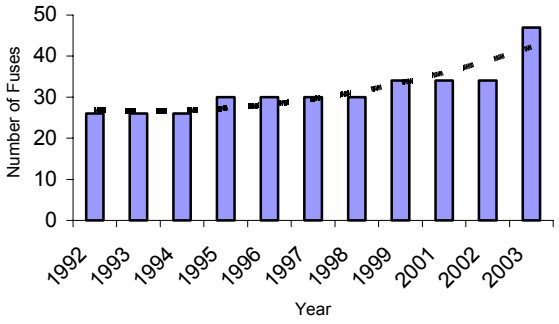

Fig. 2: Fuses in cars

Unfortunately, the author could not find any solid numbers on low voltage and high voltage power fuses but with increasing worldwide electric power consumption and huge future demand for electric power in developing countries, the number of power fuses can also be expected to grow with a remarkable pace.

Increasing power consumption and still growing markets for electronic devices and electric appliances means a growing number of electric circuits that need to be protected. While there is no doubt that the market for circuit protection devices will still be growing, there is no guarantee that future circuit protection will necessarily raise the need for electric fuses.

There are however, competitive devices using different technologies that have to be taken into

account and carefully watched. Fuses will only maintain or increase their share in circuit protection if they offer significant technical advantages and benefits over other protective devices.

3. Technical facts

Fuses exhibit a number of very positive attributes that make them technically superior to other protective devices. The current-limiting fuse provides complete protection against the effects of overcurrent by protecting both electric circuits and their components. Fuses offer a combination of exceptional features, for example:

a) High breaking capacity (current interrupting rating)
b) No need for complex short-circuit calculations
c) Easy and inexpensive system expansion involving increased fault currents
d) Mandatory fault elimination before resetting:- Unlike other short-circuit protective devices (SCPD), fuses cannot be reset, thus forcing the user to identify and correct the overcurrent condition before re-energizing the circuit.
e) Reliability
No moving parts to wear out or become contaminated by dust, oil or corrosion. Fuse replacement ensures protection is restored to its original state of integrity.
f) Cost effective protection
Compact size offers low cost overcurrent protection at high short-circuit levels.
g) No damage for type 2 protection according to IEC 60947-4-1
By limiting short-circuit energy and peak currents to extremely low levels, fuses are particularly suitable for type 2 protection without damage to components in motor circuits. This type of protection may be achieved without installing a fuse with a smaller ampere rating.
h) Safe, silent operation
No emission of gas, flames, arcs or other materials when clearing the highest levels of short-circuit currents. In addition, the speed of operation at high short-circuit currents significantly limits the arc flash hazard at the fault location.
i) Easy coordination
Standardized fuse characteristics and a high degree of current limitation ensure effective coordination between fuses and other devices.
j) Standardized performance
Fuse-links according to IEC 60269 ensure availability of replacements with standardized characteristics throughout the world.
k) Improved power supply quality
Current-limiting fuses interrupt high fault currents in a few milliseconds, minimizing dips in system supply voltage.
l) Tamperproof
Once installed, fuses cannot be modified or adjusted in order to change their level of performance, and thus malfunction is avoided.

There are, however, some weaknesses to be considered before adding up the fuse benefits to an unsurpassed product that would not need to fear any competition.

a) Fuses are single-action devices that need replacement after operation.
b) Replacement fuses may not always be at hand.
c) Too many different and incompatible fuse systems laid down in national and international standards round the world can be rather confusing to the customer and make fuse selection complicated (see fig. 3).
d) A lack of information on fuse application may cause misapplication and consequently malfunction

Fig. 3: Confusing utilisation categories

Malfunction of fuses is very rare and usually a consequence of lacking information and understanding of how fuses work. This applies to both, design engineers who have to select the proper fuses according to the equipment to be protected and even more to field operators who need to replace operated fuse-links.

Depending on the qualification of the user and the nature of the job performed when using fuses, the judgment of fuses as protective devices may vary from unsurpassed cost efficient safety device to a nuisant pain in the neck.

4. Market psychology

Commercial success or failure of a product is not only based on technical data and operational performance of a product as manufacturers and even more development engineers may believe.

Commercial success depends to a great deal on market psychology i.e., on what benefits the customer believes to enjoy when using a product. In the contrary even excellent technical solutions may fail if

potential users fear the product may be inconvenient or potentially dangerous to use. In this respect it is unimportant whether real danger or inconvenience exists or the benefits can be measured in currency. What counts is what the user believes or better to say the image of fuses that develops in the user's mind.

4.1 The image of fuses

Fuses are among the best known electrical devices to people around the world. Unfortunately, most people may have become aware that fuses exist after fuse operation and consequent power outage. The image of fuses is therefore widely dominated by the personal experience of the search for replacement fuses in literally dark moments of life.

These moments usually do not generate a lot of sympathy for fuses but trigger a deep desire for more convenient protective devices and more advanced (preferably electronic) devices replacing these dinosaurs of electricity. The long history of fuses and their wide spread use has also developed a not very sophisticated even martial language to describe the effect of fuses which associates a number of negative feelings to the use of fuses.-

- Danger: Fuse blows!
- Heat and fire: Fuse burns out!
- Nuisance defects: Fuse fails, fuse is defective.

Depending on local language and habits, you will find similar discriminative expressions describing fuses and their operation round the world. Even fuse experts use these expressions and laid them down in national and international standards.

The poor reputation of fuses and the need for replacement necessarily implies low value (throw-away product) and consequently low prices. Price pressure sometimes has got its impact on quality and operational reliability which again confirms and enhances a biased image of fuses. This way it seems the reputation of fuses is washed down the drain in a vicious circle of self fulfilling prophecy.

Strange to see that just competitive devices are called "fuses" e.g., "automatic fuses" for m.c.b., "resettable fuses" for PTC overcurrent protectors or "fuse board" for breaker panels. That means, the term "fuse" has become synonymous for "protective device" which is to be seen an extremely valuable asset fuses and fuse manufacturers can build their future upon.

4.2 Customer benefits

The benefits of fuses as listed above will only be honoured by the customer if he is fully aware of. This requires:-

- Availability of information
- Clarity of information
- Availability of suitable fuses and
- Positive field experience.

While service men and ordinary unskilled persons would usually suffer from a lack of suitable replacement fuses in case of line or equipment defects, laboratory engineers have to deal with the selection of the optimum fuse for their application out of a seemingly uncountable variety of fuses available in the market.

Without viable information and preferably professional technical assistance both are very likely to run into the vicious circle of misapplication and product failure that necessarily ends up in frustration, a poor esteem of fuses and search for believed to be better protective devices. These development and application engineers who know how to use fuses will usually experience positive results and likely continue using fuses whenever possible.

5. The future of fuses

5.1 Improving the image

The future of fuses will very much depend on their positive image among design engineers and users alike. There is a good chance to build upon the widespread awareness that "fuse" stands for "safety" and "protection". But to eliminate also existing prejudice and alleged weaknesses of fuses, the fuse industry will have to work hard making fuse application a common art to the technical community rather than preserving the "mystery of I^2t".

Significant effort has already been spent to work out an application guide for fuses, recently published as Technical Report IEC TR 61818.

The European fuse manufacturers founded "Pro Fuse International", an organization to promote the knowledge of fuses and fuse application.

The German fuse manufacturers established a recycling system (NH/HH Recycling e.V.) for fuses that have fulfilled their duty.

All activities of this nature that are not only thought to promote a single manufacturer's product but to promote the acceptance and improve the image of fuses are suited to sustain future fuse application.

5.2 Future fuse applications

5.2.1 Overload protection

The question about the future of fuses can only be answered based on knowledge or projections of their future applications. Most likely fuses will be replaced by other protective devices in applications where the weaknesses prevail and strengths do not offer enough benefits to the user. This happened widely in l.v. a.c. distribution systems up to 63 A rated current and up to about 6 kA prospective short-circuit current i.e., mainly cable and line overload protection.

Overload protection means that the protected electric circuit or equipment is still operational but the fuse-link needs to be replaced. A situation that may be troublesome and annoying suited to trigger a deep desire for resettable protective devices.

Fuses will therefore be most vulnerable in overload protection applications. Whenever resettable devices e.g., circuit-breakers, PTC or electronic controls fulfill the requirements of time-current characteristics and breaking capacity they will very likely be preferred.

5.2.2 Short-circuit protection

In fact, fuses cannot prevent short-circuits as they can prevent dangerous overloads, but they limit the effects of short-circuit currents very efficiently to the faulted circuit and prevent potentially catastrophic results of high faults and disturbing arcs.

As mentioned above, fuses show their strengths in high breaking capacity and by limiting short-circuit energy and peak currents to extremely low levels. They offer these benefits at an extremely compact physical size and unbeatable low costs.

A faulted circuit or equipment anyhow needs to be repaired before fuses are replaced. It may therefore even be a valuable benefit that fuses cannot be reset. I.e., if fuses are used to protect adjacent circuits or components from the effects of a faulty component, the need for replacement does no longer appear to be a disadvantage.

Short-circuit protection or more precisely "fault containment", specifically at high fault levels, does therefore seem to offer chances for future fuse application.

5.2.3 Semiconductor and c.b. protection

Semiconductor equipment is usually well protected against overload by electronic controls. The protection of semiconductors can therefore be seen as a specific type of short-circuit protection. Because of the fast and reliable response to short-circuit currents, no other devices can be seen to replace fuses in the near future.

Fuses backing up electro-mechanical switching devices e.g., circuit-breakers or motor starters can make a very cost efficient solution as they upgrade the fault current levels up to which these devices can be used. Increasing performance of these devices may however cannibalize the use of accompanying fuses.

5.3 Future fuse design

5.3.1 Integrated back-up fuses

Future fuses shall exhibit all strengths as listed above and not show any apparent weaknesses to the user. What appears to be utopian is in fact nothing unusual as it depends more on the application than on the design. Many of today's fuses are not intended to protect the equipment they are assigned to but to operate after the equipment has failed and to contain the fault i.e., to protect the adjacent circuits and other devices as well as the environment from further damage. Consequently, these fuses could be integral part of the assigned equipment and replaced during equipment repair or discarded with the demolished equipment.

Fig. 4 shows m.v. back-up fuses installed under oil in a distribution type transformer. The fuses are selected to operate in case of internal transformer faults only. No on site replacement does therefore need to be considered. For overload protection, fuses or circuit-breakers are installed on the l.v. transformer side.

Fig. 5 shows the integration of a custom designed cylindrical back-up fuse to protect the adjacent overvoltage protector enclosed in the same device.

Fig. 4: Under-oil m.v. back-up fuses in a transformer tank

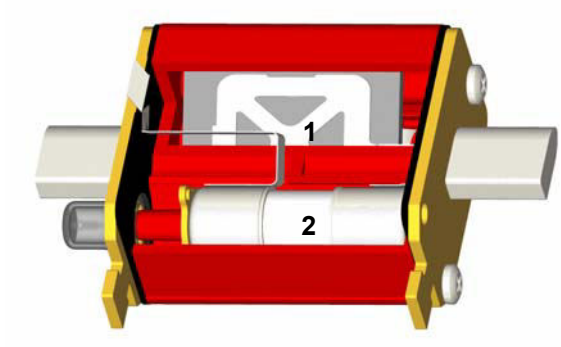

Fig 5: Back-up fuse (1) and overvoltage protector (2) integrated in NH fuse casing

Back-up fuses designed to application are ideal for devices with integrated protection. Integrated back-up protection seems to be the fuse application offering a maximum of benefits and a minimum of disadvantages in application.-

- fuse selection by design engineers, preferably assisted by manufacturer's application engineers, reduces the risk of misapplication
- no trouble with fuse replacement
- compact and cost efficient fuse design
- low power dissipation

5.3.2 Miniature dimensions

Following the general trend for more compact dimensions of electrical equipment, fuses will

continue to adopt smaller dimensions in the future. This is especially true with electronic fuses where miniaturization was a major development task in the past and will certainly be in the future (see figs. 6 and 7). This trend will also affect the future development of power fuses that are integral part of electrical equipment. By coincidence, back-up fuses allow for the most compact dimensions.

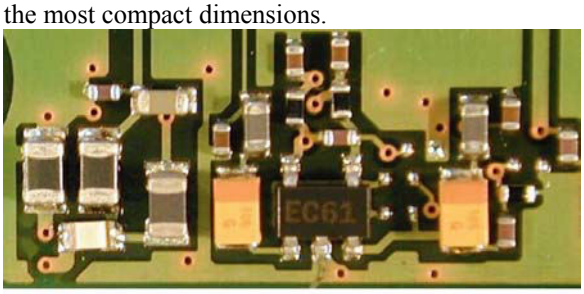

Fig. 6 –PCB with chip fuse (lower left corner)

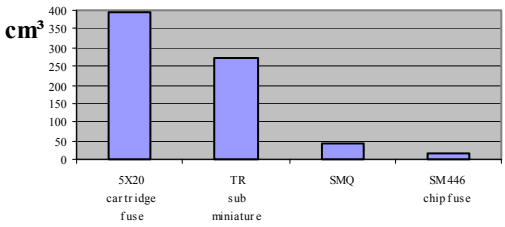

Fig. 7: Miniaturization of fuse dimensions

5.3.3 Intelligent fuses with additional functions

Fuses are simple technical devices that operate at a given current after a defined period of time. Fuses cannot be adjusted nor discriminate fault currents from operating currents. I.e., fuses will not always interrupt high impedance arc faults that may cause fire.

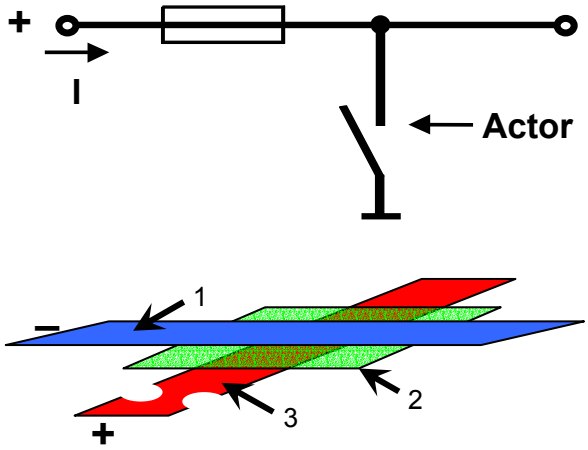

Fig. 8: Actor fuse
1 - Frame potential 2 - Actor layer 3 - Voltage plus

Ordinary fuses cannot transmit or receive signals or information i.e., fuses are all but intelligent.

Some types of fuses are equipped with strikers to indicate fuse operation and trigger switch releases or microswitch for remote indication including electronic fuse monitoring. It is also possible to integrate more functions in a fuse than just current dependent operation. Microchips applied to the melting element may be used to sense current and temperature for energy control and fault current or overload sensing.

No fuses have however been found to receive external signals and operate accordingly. Studies show that the characteristics of fuses can be adjusted within a broad range even below the rated current by the application of compact sized heaters to the melting elements (see fig.8).

This type of fuse can be externally triggered e.g., by a crash sensor and interrupt low fault currents to avoid fire after a car crash. In a further step, several fuses connected to a busbar can be combined to a distribution fuse-board including sensors for currents and temperatures as well as actors for external triggering of fuse operation. Fig. 9 shows a working prototype of such a complex device.

Fig. 9: Distribution board with sensor-actor fuses

Whether and when such protection systems will be included in cars is still uncertain and will finally depend on market needs.

6. Conclusions

A positive image will be necessary but not sufficient to ensure a prosperous future of fuses. Fuse benefits exceeding the advantages of competitive devices will be major key to success.

It seems that the features and advantages of fuses are somewhat difficult to communicate to users whose major subjects are others than fuses. In the contrary, the draw backs are deeply rooted in peoples mind. Consequently, successful fuses shall have eliminated all the weaknesses listed above, i.e. future fuses will be

- integrated in equipment
- designed to application
- invisible to users
- never replaced

BREAKING BY MELTING FUSE AT ANOMALOUS M-EFFECT

Martin Bizjak, Mitja Koprivšek and Franc Pikl

ETI d. d. Izlake, Obrezija 5, SI-1411 Izlake, Slovenia, bizjakm@email.si, mitja.koprivsek@eti.si, franc.pikl@eti.si

Abstract: At breaking of moderate overcurrent by melting fuse the M-effect is prevalent process. Sometimes heat dissipation at M-effect is so intensive, that the temperature rise on surface of ceramic fuse link attains extremely high value. On the other hand at normal M-effect the temperature rise is quite moderate. In order to investigate the phenomena of *anomalous* M-effect the variation of voltage drop on fuse link terminals during breaking process was measured. After that the optical microscopy of interrupting sites of fuse element, the metallographic and SEM examinations with EDX microprobe analysis were conducted. A comparison with characteristics of *regular* M-effect was performed. The substantial differences in the course of voltage drop and material state were found out between both types. At the *anomalous* type a broad interrupting zone of an alloy with high melting temperature was formed on fuse element, while at *regular* type the interruption sites are located on notches of fuse element, where an alloy with low melting temperature was formed. Initially the both type of M-effect followed the same characteristics, which deviate from each other just before the interruption.

Keywords: fuse element, M-effect, heating up period, melting period, voltage drop, Cu-solder alloy

1. Introduction

When the melting fuse is used for the protection of circuit against overcurrent, the duration of breaking process depends on the current to be broken. This relationship should follow the required time/current characteristics, given by relevant standards [1]. At overcurrent slightly greater than rated current the time to break is in the order of magnitude 1000 s, but when it attains a value of 10 times rated current or more, a fuse blows in a few ms. The fuse element is properly designed in order to meet the required operating characteristics. Regarding current ratings of the fuse it is made either of thin Ag or Cu wire or strip. Strip is perforated (Fig. 1) in order to form special pattern of nodes, where current lines are constricted due to controlled heating of fuse element [2].

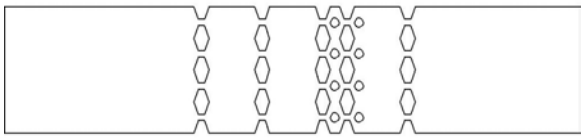

Fig. 1: Node patterns of fuse element

At the inrush of high overcurrent the heat dissipated in fuse element for few ms causes almost adiabatic heating of nodes resulting in melting and boiling. At low overcurrents more moderate process takes place in the time scale of 100 or even 1000 s. Dissipated heat is conducted away from the fuse element through the filling sand toward the outer surface of ceramic cartridge of fuse link as a semi stationary thermal process. In the moment of break it can results in a considerable temperature rise of the fuse link, which should be kept in limits regarding thermal withstand ability of parts in its vicinity.

In order to investigate thermal effects of break on fuse links gL 63A, a standard time/current test was conducted at load current 100 A. During testing the test pieces achieved surface temperature of cartridge below 300°C, but some of them were found to be heated up to the red glow. Therefore the additional measurements and examination of test pieces were accomplished in order to investigate this anomaly.

2. Measuring and analytical methods

Each test piece gL 63A was inserted into standard terminal socket and loaded by test current 100 A from stabilized DC current source. The temporal variation of voltage drop u between terminals was recorded from the onset of load current to the moment of blow of the tested fuse link. Results were sampled with the frequency of 1 s and digitally processed by the grating of 16 mV. They were stored in computer for further analyses.

Some typical results of voltage drop versus time obtained by measurements at the described test conditions were shown graphically on Fig. 2, where each plotted curve corresponds to particular test sample. A typical course of voltage drop curve $u(t)$ is evident for particular test, which starts from the initial low value (some 200 mV), proceeds with slow increase until after certain time it exhibits the final steep increase over 500 mV and even up to 1400 mV at the moment of current interruption.

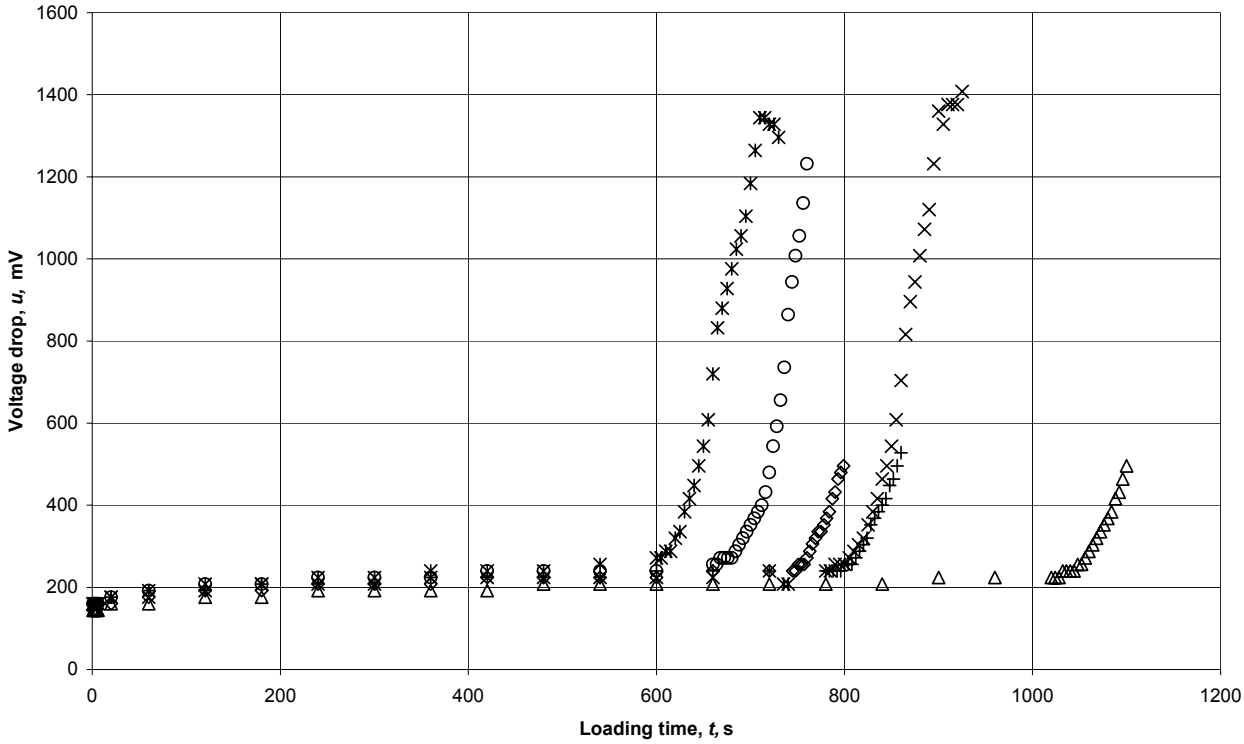

.
Fig. 2: Temporal variation of terminal voltage drop under load current measured on several test pieces

Slowly increasing part of each curve shown in Fig. 2 reflects the heating-up of fuse element at constant current. A physical approach to this effect leads to an analytical expression for this part of curve, which can be written in general form as follows:

$$u_{\text{heat}}(t) = A + B\left[1 - \exp\left(-\frac{t}{\tau}\right)\right] \qquad (1)$$

The *heating-up phase* is followed by the period of fast increase of voltage drop, which is attributed to the transitions of the material state of fuse element. Regarding the design of fuse element, where some of the nodes are coated by solder in order to facilitate their melting, the break of overcurrent by fuse element takes place particularly by melting of soldered nodes. Therefore this period is called *melting phase*.

Test results obtained by measurement of the voltage drop versus loading time (see examples in Fig. 2) were correlated with measurements of temperature of fuse links and physical state of fuse element after break in order to explain breaking phenomena. For this purpose optical microscopy was applied at the investigations of fuse element after blow as well as metallographic methods and electron microprobe analysis.

3. Analysis of measured results

Two clearly evident types of voltage drop/time curves can be distinguished: the type with short duration of M-effect having peak value at break at some 500 mV, and the type with longer M-effect and peak value somewhere between 1200 mV and 1400 mV. Therefore the first type is called *regular* and the second type *anomalous* melting phase.

The surface temperature of fuse link measured on each particular test piece during break test was in close correlation with the type of melting phase. At break by *regular* type it never exceeds 300°C, while at *anomalous* type a red glow on cartridge surface was observed, which was assessed to be at least 600°C.

No correlations between parameters which would facilitate anomalous M-effect were found. Therefore an analysis of voltage/time variations in melting period was conducted. Measured voltage drop resulted from the contributions of partial voltage drops on fuse terminals, end caps, terminating ends of fuse element strip and nodes in series. In the melting period the essential variation of voltage drop took place on the nodes of the interrupting sites, so all other contributions to them were disturbing. They were eliminated by extrapolation of heating-up voltage curve and subtraction from actual voltage drop. An example of best fit approximation is shown in Fig. 3.

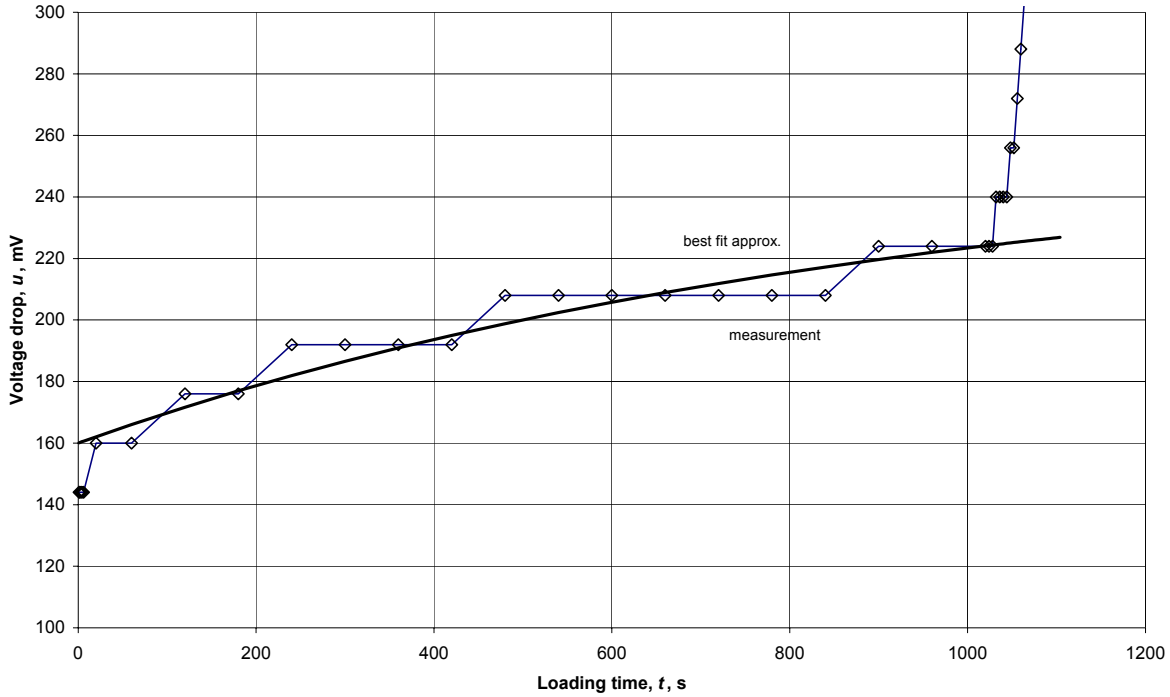

Fig. 3: Best fit approximation of heating up curve and extrapolation into the area of melting voltage drop.

In order to obtain best fit curve the relation (1) was used by fitting parameters *A, B* and τ. The value τ was chosen such that (1) fitted better the results in the interval $t > 10$ s. By subtraction of best fit curve from measured data the voltage drop on melted parts of fuse element, $u_M(t)$, was calculated with certain inaccuracy:

$$u_M(t) = u(t) - u_{heat}(t) \qquad (2)$$

By applying (2) on measuring results of each tested fuse link a "melting voltage" curves $u_M(t)$ were obtained.

As it was confirmed that the duration of heating-up period does not influence the melting process a shift of time scale was made into the moment of melting onset. In order to compare temporal variation of melting voltage for individual test pieces, a shifted time axis t_M were used in order to follow the development of melting for various test pieces. So the relation of melting voltage/time, $u_M(t_M)$, was applied for further analysis. The origin of t_M - axis determined from the set of measured results corresponding to several test pieces implies certain inaccuracy arising from the estimation of moment, when the transition from heating-up into melting occurred. As the result a set of calculated curves $u_M(t_M)$ which describe the variation of melting voltage starting from the onset of melting was shown in Fig. 4 for several fuse elements under discussion.

Curves of Fig. 4 are plotted on the semi-logarithmic graph due to better presentation. The melting curves for both *regular* and *anomalous* melting phase are shown. Regardless of several sources of inaccuracy a substantial overlap of curves is noticeable. It indicates that similar physical processes presumably took place in tested fuse links. Moreover the curves corresponding to regular (symbols Δ, ◊ and O) and anomalous type (symbols +, × and ∗) overlap each other. In the moment of interruption u_M attains characteristic peak value U_M at 250 mV < U_M < 280 mV for regular type of M-effect and at 1000 mV < U_M < 1100 mV for anomalous type. Particularly for anomalous type u_M attains its maximum by voltage leveling, which is characteristic for e.g. transitions from solid state into melt, well known as the phenomenon of contact spot [3]. The temperature rise on contact spot is directly proportional to the contact voltage drop. Terms such as "softening voltage" or "melting voltage" are commonly used in contact physics. Although quantitative analogy between fuse element and contact spot can not be drawn, the essential elements are analogous. So it can be presumed that the interruption of fuse element at the anomalous M-effect takes place at substantially higher (melting) temperature than for regular one.

4. Methods of examination

Test pieces were subjected to the examination of its state after break. The residue of blown fuse element was carefully extracted from its cartridge. Prior to examination it was carefully cleaned from the loose grains of sand.

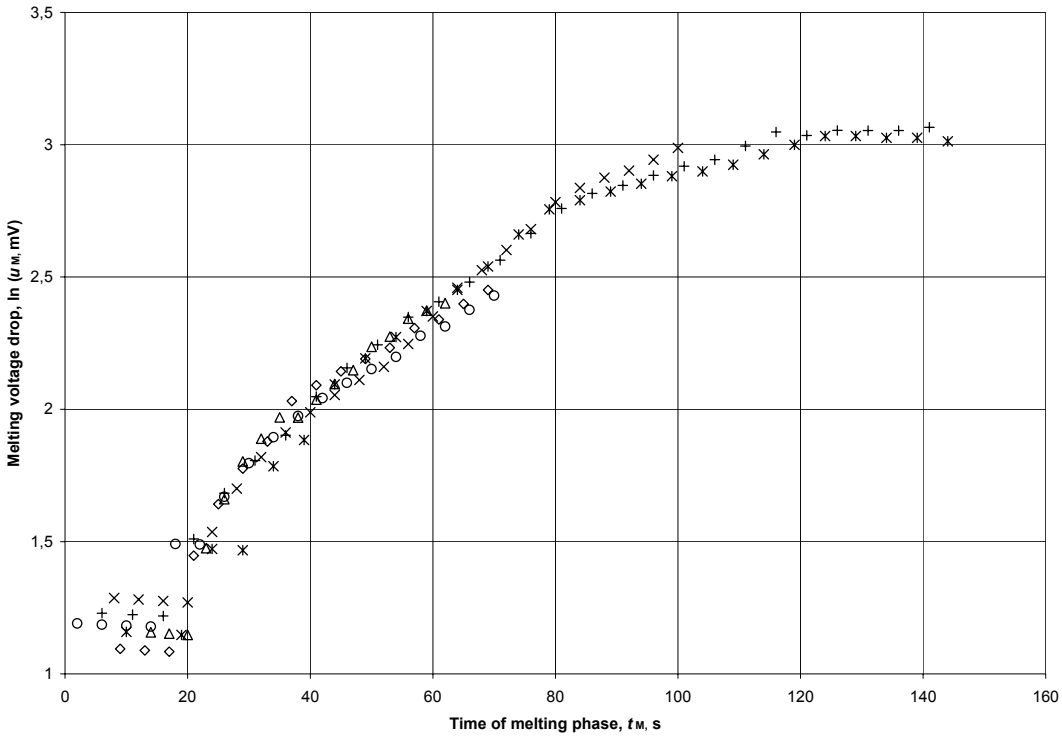

Fig. 4: Curves of melting voltage drop for fuse links having *regular* and *anomalous* type of M-effect.

At first the interrupting sites of blown fuse element were examined by optical stereo microscope at lower magnification. A close correlation between the appearance of blown piece and the type of M-effect taken place was established. While on the one hand the interrupting sites of regularly blown fuse element were located in the small area around notches (as shown in Fig. 5), on the other hand the interrupting sites of fuse element blown by anomalous melting phase were spread along the broad area of perforation and were covered by thick layer of vitrified filling sand (see Fig. 6).

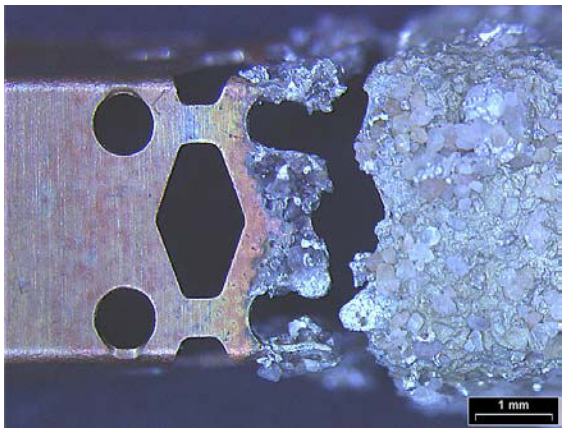

Fig. 5: Interrupting area of regularly blown fuse element with solder layer on the right side.

Interrupting sites shown in Fig. 5 were dissolved by melted solder (seen on the right side of photos with embedded grains of filling sand) which is spread over the adjacent notches.

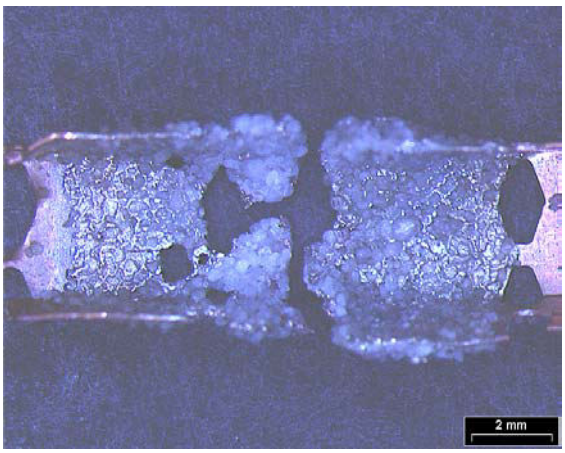

Fig. 6: Interrupting area of fuse element after the break by anomalous M-effect spread along more than two segments of perforation, where melting is indicated.

The metallographic structure of the interrupting site on fuse element, shown in Fig. 5, is illustrated in Fig. 7, where the metallographic cross-section of this part in presented at larger magnification. At the left side to the bottom the remnant of partially dissolved Cu-strip of fuse element is shown, which is covered by a thick layer of solder alloy. Dark irregularly shaped "islands" at the top of photo belongs to the embedded sand grains. The metallographic structure

of solder shown in Fig. 7, although uniform across the solder layer, does not show the original structure of solder coating.

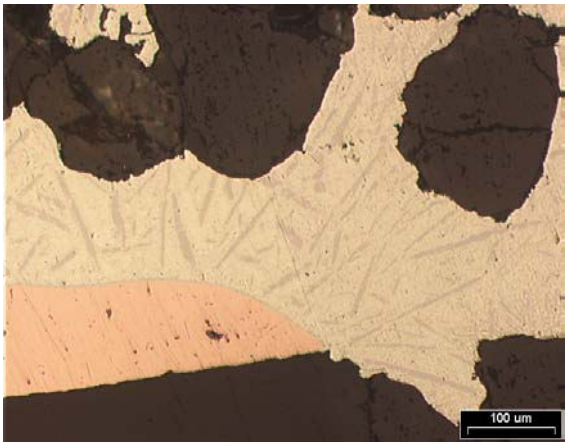

Fig. 7: Cross-section of interrupting site on fuse element for regular type of melting.

Scanning electron microscopy (SEM) was also conducted on several cross-sections similar to that shown in Fig. 7. SEM image of solder layer under discussion obtained by emitted secondary electrons was shown in Fig. 8.

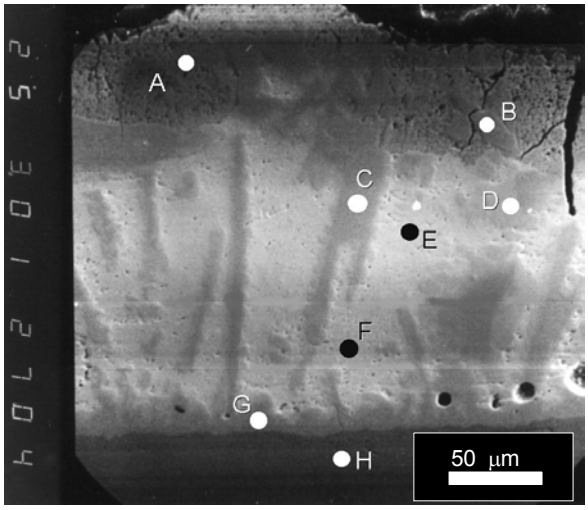

Fig. 8: SEM secondary electron image of cross-section of solder layer after blow of fuse element by regular melting phase.

The deviation of chemical composition is qualitatively indicated from the darkness of particular area proportional to the average atomic number on the observed site [4]. The darkest area at the bottom of Fig. 7 belongs to Cu-strip, while the central area of microphotography obviously corresponds to the alloy of lighter elements. In order to identify chemical composition of particular metallographic phases a microprobe EDX spectroscopy [5] was conducted on the sites of labeled in Fig. 8 by letters from A to H. In the needle-like phase of this alloy (indicated in Fig. 7 and 8) elements Cu and Sn were detected with the amount of Cu > 50 wt % (site C in Fig. 8). The lighter phase, indicated by letters E and F is composed of Cu, Sn and Cd, where the amount of Cu does not exceed 20 wt %. The described alloy structure was found to be characteristic for process of regular M-effect.

The cross-section of fuse element blown by anomalous melting phase, as illustrated in Fig. 6, is shown magnified in Fig. 9.

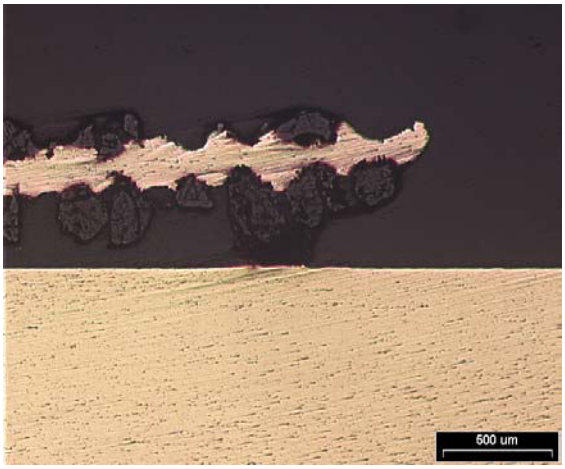

Fig. 9: Cross-section of interrupting area at anomalous type of M-effect.

Microphotography shows the cross-section along the interrupting area of semi-melted fuse element with embedded sand particles on both sides of its strip. At larger magnification it was observed, that in the interrupting zone the metallographic structure of the strip material is more homogenous in contrast to the structure shown in Fig. 7, where regular M-effect was active. The transition region from melting zone into the rest of the intact Cu-strip is shown in Fig. 10.

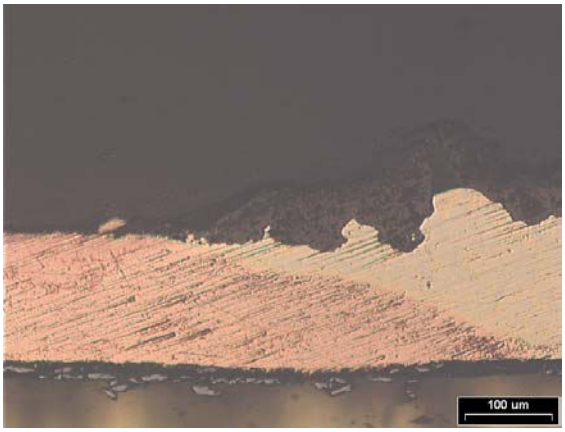

Fig. 10: The transition region between "melting" zone and the rest of fuse element strip.

No remnants of the solder layer can be observed on this cross-section. On the left side of photo the rest of Cu-strip is visible, while on the right side the "melted" part of strip is shown. No more than two metallurgical phases are discernible in the zone of interruption (not distinguishable in Fig. 10) even on the boundary between pure Cu and the alloy of "melted" region.

5. Discussion

The metallographic examinations of interrupting sites or melting zone indicated the formation of the alloy with a variety of metallurgical phases at the *regular* type of melting process and the formation of two-phase alloy at the *anomalous* type. Phases with high content of Sn and Cd were found by EDX analysis on the interrupting sites in the case of *regular* type of M-effect, while in the case of *anomalous* type of M-effect only two metallurgical phases were found in the alloy even at the boundary to Cu. The conditions at which particular phases of alloys are able to exist could be considered to a great extent from a diagrams of metallurgical states for involved elements. In fact a ternary diagram of states would be used in order to discuss the alloy of Cu, Sn and Cd. But in the literature only binary diagrams of states having Cu, Sn and Cd are available [6]. The role of Cd in the formation of alloy Cu-solder seems to be minor concerning microprobe EDXA. So for the qualitative assessment of "melting" process of M-effect of both types the binary Cu-Sn diagram as shown in Fig. 11 is considered sufficient.

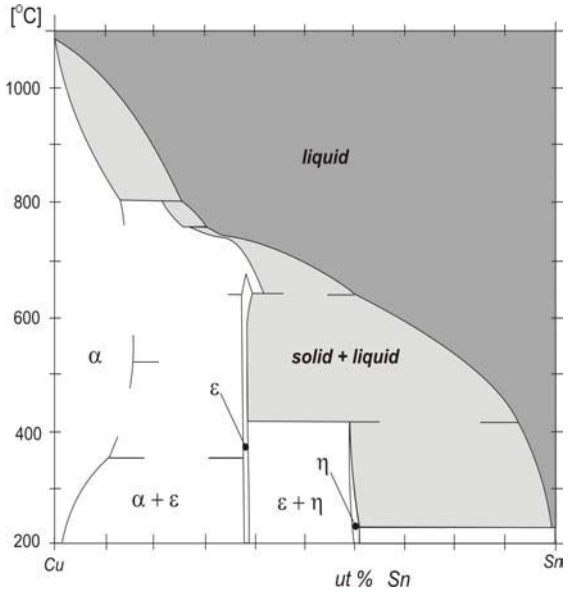

Fig. 11: Binary diagram of states for Cu-Sn alloys

In the diagram various solid metallurgical phases for Cu-Sn alloy can be found depending on the content of Sn (or Cu) given in the weight percent. The boundary of solidification at given Cu-Sn composition as well as the boundary of melt is shown as the curve of temperature versus wt % of alloying component. The region of melt is shown in Fig 11 as dark shadowed area while the region of solid-liquid mixture as light shadowed area. As it can be seen from the diagram the melting temperature of the alloy increases with the increasing content of Cu, as well as the temperature of solidification. Concerning the metallographic structure of the alloy as observed by optical metalography (Fig. 7) and in the SEM image (Fig. 8) in connection with EDX analyses, the needle-like forms presumably belongs to ε phase of Cu-Sn alloy, which is stable below 700°C. Its grains are surrounded by the thin layer likely of η phase, which is stable below 415°C. At the content of Cu up to 37 wt %, only the mixture of α and ε phase exists at low temperature, at which the metallographic preparation and observations of the structure was actually accomplished.

Following the above considerations some estimations of interrupting temperature could be established. During the interruption of fuse element by *regular* M-effect probably some 50% of Cu was dissolved in the melt with solder. The interrupting temperature of the notch presumably reached a value below 600°C but over 415°C, the limit of the existence of η phase. As the process was far from stationarity, the layer of η phase around the grains of ε phase was formed in the cooling period of interruption. In the interrupting zone of *anomalous* M-effect the alloy of only two metallurgical phases, having the highest possible content of Cu, was found. It is presumably the alloy of α and ε phase in approximately equal content, as were indicated by optical metallography. Concerning Cu-Sn binary diagram the Cu strip of the fuse element comprised some 20 wt % of Sn dissolved in in the "melting" zone. The temperature of solidification of such alloy is 798°C, which means that the interruption by *anomalous* M-effect could not be accomplished below 800°C.

The above consideration was confirmed qualitatively by taking into account values of "melting" voltage u_M at the moment of interruption (see plotted curves in Fig. 4 of Section 4). They are concentrated around two characteristic values, so that an apparent distinction between *regular* and *anomalous* M-effect can be established over the interrupting values U_M. Lower values of *regular* type indicate lower breaking temperatures of interrupting site and vice versa for the interrupting zone of *anomalous* type.

6. Conclusions

Due to possible detrimental consequences of *anomalous* M-effect in the application of fuse links for circuit protection the answers on the two principal questions should be given in the conclusion: a) what is the source of effects, which consequences are assigned to the *anomalous* M-effect, and b) how to avoid the possibility of *anomalous* melting effect to appear. Both answers are interesting primarily for the manufacturer of melting fuses in order to ensure high reliability of protection against all kinds of overcurrent.

As already mentioned the detrimental consequence of *anomalous* M-effect is a risk of thermal defects in the vicinity of fuse link due to its extremely high surface temperature rise. It is shown in the preceding Sections, that in the case of *anomalous* M-effect the "melting" period lasts more than 100 s and the temperature of the great region of fuse element presumably exceeds 800°C. Due to the good thermal conductivity of sand filler and ceramic cartridge the surface temperature at these conditions consequently attains "red glow" value. In the contrary at *regular* M-effect the "melting" period is significantly shorter (up to 70 s) and only a very small area of notches attains temperature not greater than some 600°C. So the heat dissipated in the fuse element is significantly smaller and the temperature rise of fuse link cartridge is within the safe limit.

From the temporal variations of melting voltage it is apparent, that regardless of how the melting and dissolution process proceeds, the phenomena taking place in the initial period of *regular* as well as in *anomalous* M-effect are common. The deviation from common course (as it can be indicated from Fig. 4) can be observed just before the termination of *regular* type. Obviously a gradual deviation from the conditions, which lead the phenomena toward the *regular* melting process causes the M-effect to proceed into the *anomalous* one. A competitive effects between the dissolution of notches and spreading of melted solder along the fuse element could be due to the slight deviations of conditions sometimes in favor of *anomalous* M-effect instead of *regular* one and vice versa. But they can be controlled by conditions determined by the design of fuse element.

References

[1] IEC 60269-1 (1998-12), IEC 60269-3-1 (2001-06)

[2] H. Johann: Elektrische Schmelzsicherungen fur Niederspannung, Springer-Verlag, Berlin Heidelberg New York, 1982

[3] P. G. Slade: Electrical Contacts, Marcel Dekker, 1999

[4] J. I. Goldstein, H. Jakowitz: Practical Scanning Microscopy, Plenum Press, New York 1975

[5] S. J. B. Reed: Electron Microprobe Analysis, Cambridge University Press, Cambridge, 1993

[6] C. J. Smithells: Metals Reference Book, Volume II, Butherworths, 1967

A Bifurcated Beam Opto-electronic Camera for Investigation of Phenomena Associated with Fast Rising Arc Voltage.

R. E. Brown, P. M. McEwan,

R E Brown
8 Oak Grove
Thurcroft
ROTHERHAM
South Yorkshire S66 9EZ
Email: bob.brown@bun.com

P M McEwan,
Department of Design,
Faculty of Technology and Information Systems
Brunel University
Egham, Surrey, UK.
TW20 0JZ
Email: pmcewan@iee.org

Abstract

Recent technical advances in sensitive opto-electronic sensors have enabled the development of optical instruments for investigating arcing ignition and other phenomena related to fast-rising arc voltage transients, typically occurring during disintegration of fuse wire elements carrying short circuit fault currents. This paper presents the design, testing and performance attributes of an experimental 'black box' slit aperture camera, based on such a sensor, which is able to operate at approximately 30000 frames/second (f/s) in bifurcated beam, two-sensor quadrature mode. Also presented are evaluations of the camera images compared with other forms of transient and historical data captured during the disintegration of high breaking capacity (HBC) wire fuse elements, which indicate good cross-correlation and acuity of arc ignition phenomena. The evaluations of the data indicate that the camera is capable of distinguishing the intensity, position and dimensions of arc ignition and elongation during disintegration of wire elements within a 10 μs time frame, which are validated by cross-correlation with the attributes of extant fulgurites obtained using a fast-acting synchronized 'crowbar' switched test circuit.

1. Introduction

Visual observation of arcs in motion, invariably, provides better understanding of arcing behaviour. Observation of arc formation and motion within hermetic enclosures, such as compacted sand-filled high breaking capacity (hbc) fuse types, pose special problems because of the speed (typically <10μs) of individual arc ignitions; the hazards of measurements and the invasiveness of arc data capture techniques. Consequently, the phenomena of fuse element disintegration and the effect of confinement on this process remain largely unresolved according to Wolny [1], and hence are still a principal focus of research which may be supported by the bifurcated beam opto-electronic camera and data capture methodology presented and discussed here.

Accordingly, novel very fast measurement techniques have been devised to capture arc ignition data to represent the various parameters of the current interruption process in hbc experimental fuse arrangements, which, broadly, divide into invasive and non-invasive 'transient voltage/current' and 'fossil' data capture techniques.

The principal exponents of the invasive fuse arc data capturing techniques are Kleen [2], and Daalder & Schreues [3] who, independently, used multiple voltage probes inserted through the walls of fuse cartridges. The probes were distributed along fuse elements such that the probes became immersed, at some stage, in the extended arcs.

Non-invasive flash x-ray photography techniques, developed by Arai [4], were used to provide images of the break-up of wire fuse elements. Non-invasive measures of arc light emissions have also been captured during element disintegration by Gomez [5] Barrow and Howe [6] and Cheim [7] using several optical fibres in close proximity to elements. Additionally, images of fuse element disintegration and arcing in wires suspended in air have been captured by Baxter [8] using a fast 'cine' camera, Vermij [9] using a streak

camera and Brown [10] using a fast (2000f/s) video camera.

The principal 'fossil' arc investigation techniques, primarily, involve obtaining data from sintered sand-element arc track remnants extant within hbc fuse filler after arcing has been terminated by natural or forced current-commutation of the fuse current. The remnants, referred to as fulgurites, permit measures of arc length, arc energy, the rate of element erosion [11] and arc elongation [12].

The principal design requirement for the proposed opto-electronic camera was to capture individual arc ignitions and cross-correlate arc light emission, arc voltage/current transients and fossil attributes of progressive arc ignitions and extended arc burning in hbc fuse wire and notched element types during current interruption periods, corresponding to short-circuit test duties for fast-acting hbc fuses, such as exhibited by thick metal conductive film substrate fuse types.

2. Opto-electronic Camera Design and Data Capture Techniques.

The proposed opto-electronic camera was designed specifically for light image capture of multiple arc ignitions occurring along wires and hbc fuse elements within a time period 10μs~150μs and to be able to capture extended arcing within periods in excess of 5ms.

The camera's optical system comprises a planar convex lens, a beam splitter and two light sensors; optically aligned within an opaque black box, figure 1. The arc light source converges onto the two light sensors after passing through a slit aperture and beam splitter. The beam splitter enables two light image captures per integration cycle and a doubling of the capture speed of the camera.

The camera's design was based on the Texas Instruments 8 pin DIL optical sensor device TSL 1401, comprising 128 'pixels' with individual photo diode; associated charge amplifier and pixel data hold circuitry. Photo current from a pixel diode, when integrated, outputs a voltage indicator of the light energy falling onto the pixel in a predefined integration period. The sensor's pixel data hold function, additionally, provides simultaneous start and stop time instances for all pixels.

Figure 2 shows a simplified block diagram of the camera and the interconnections between the fuse test facility, optical system, camera control electronics and two oscilloscopes for capturing the image attributes of the bifurcated arc light source.

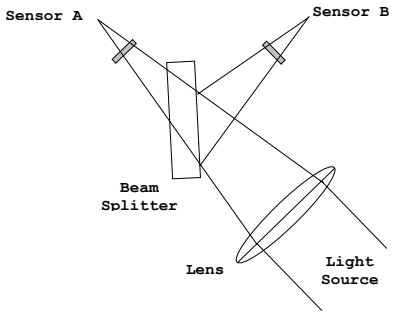

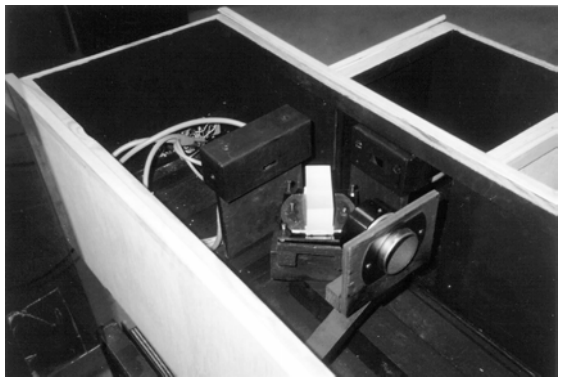

Fig 1. Opto-electronic camera optical system.

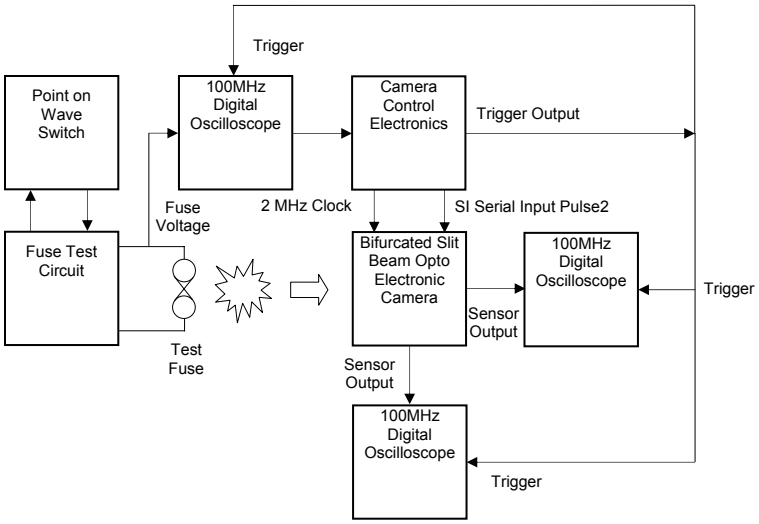

Fig. 2. Schematic diagram of opto-electronic camera control, optical system and fuse test circuit.

At the beginning of the integration period, a pre-discharged (sampling) capacitor connects to each of the integrators through an analogue switch. The output and reset of the pixel integrators are controlled by a 128-bit shift register and reset logic. The sensor output sequences are initiated by the application of the (SI) serial input pulses. These signals are derived from a comparator, set to latch at the onset of disintegration of the fuse element, which is then inputted to the time delay circuit of each beam image trigger circuit to give time shifted SI series for each beam by manual pre-set adjustment. This dual delay configuration enables capture of two pre-settable time-differentiated image attributes by the camera, with reference to a pre-settable test circuit time-phase reference as indicted in the pulse timing diagram of figure 3. Each oscilloscope displays both temporal and light intensity attributes of arc ignition at separate pre-settable intervals in the range 1μs~64μs. A thyristor 'crow bar' switch is configured so that it is able to divert the test circuit current from the fuse test sample within 5μs of the instant of an image capture to permit momentary capture of fulgurites [12].

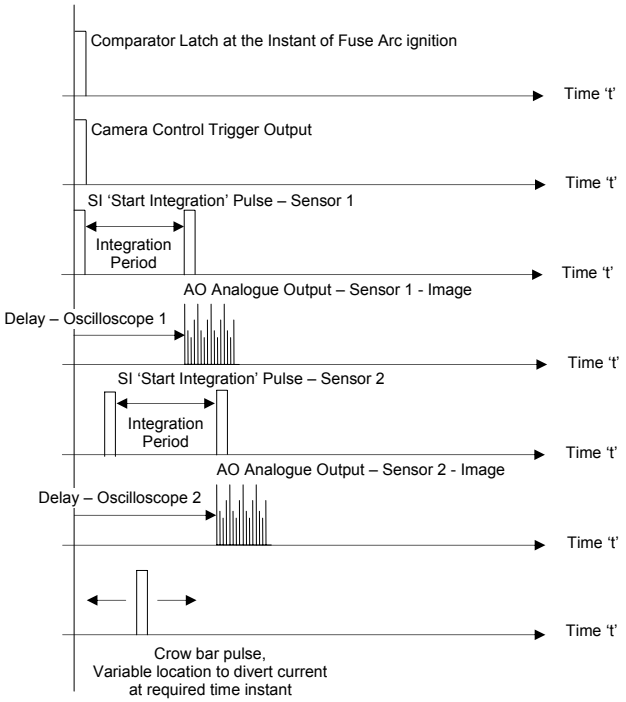

Figure 3 Diagram indicating control pulse (SI) and camera image (AO) capture instances

3. Experimental arrangement for image capture of arc ignitions in wire and notched element hbc fuses

Special robust experimental enclosures were devised to detect arc ignitions in fuse elements within compacted silica filler to ensure good acuity of arc light emission and protection of the camera lens from expulsed arc products. The wire and notched fuse element samples were bonded to glass slides as shown in figure 4, hence the glass slides acted as a window, arc shield and fuse substrate base. The elements were pressed against the glass substrate by the filler, which was compacted by vigorous mechanical vibration.

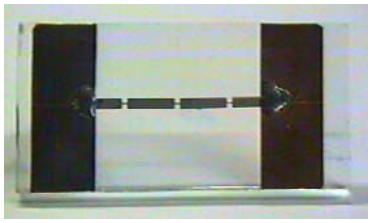

Fig 4i Examples of the wire and a notched fuse element window/substrate test samples used in experimental investigations.

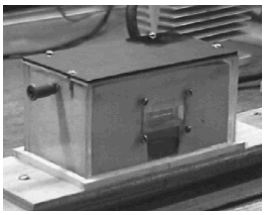

Fig 4ii Fuse test samples and test enclosure showing glass substrate-mounted fuse wire and elements with and without filler

4. Camera calibration methods and techniques

Special camera calibration procedures and hardware were devised to validate the camera attributes. Testing procedures were also developed to validate the transient performance of the camera.

The calibration and testing set-up consisted of a homogenous light source comprising a columnar light box with a 650W white light source and a small hole on one side of the box, figure 5., which was positioned on the same horizontal axis to the light aperture of the camera such that the light radiating through the hole entered the camera through a 25mm (l) × 0.2mm (w) slit and focused onto the two light sensors. The alignments of each sensor were calibrated relative to the horizontal axis of the optical system by capturing the sensor outputs when triggered using ramp voltage latch techniques and were monitored until the responses of all pixel outputs were within a range of ±0.1 volts (3% nominal full scale deflection). The results from testing confirmed that the pixel voltage output-integration time relationship was linear.

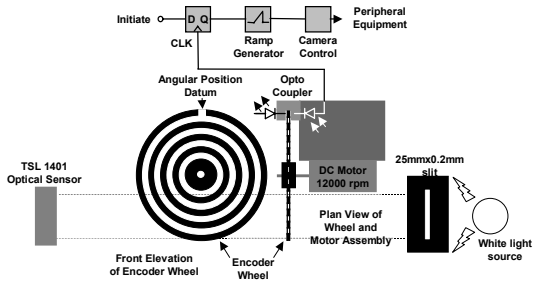

Fig. 5. Patterned encoded wheel and simplified block diagram of camera timing test arrangements.

Validation of the transient response necessitated devising a series of patterned encoded wheels, figure 6i. These wheels were positioned against the camera aperture and rotated at 12000 rpm with the horizontal axes of the wheel and the optical system aligned. The wheels were pattern encoded with 25 alternating transparent and opaque rings, where the centre ring of a wheel is aligned with the vertical axis of the optical system. The angular position datum is referenced on each wheel by a transparent window in the opaque outer ring, which, when detected by an opto-coupler, initiates camera data capture. An example of the normalized output of the sensors is shown in figure 6ii.

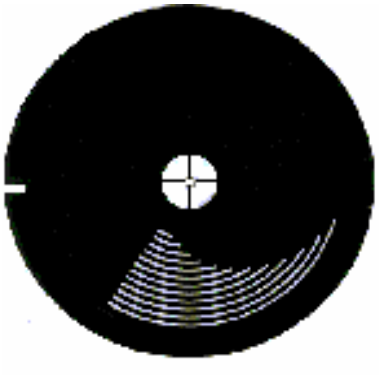

Fig. 6i Patterned-encoded wheel, typical of sequential arc ignition

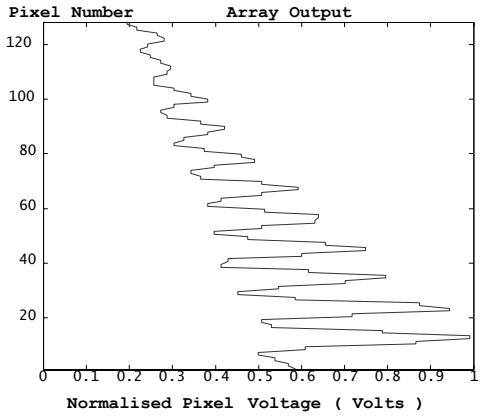

Fig. 6ii Normalised sensor output with integration time = 1.5ms

Figs 6 Example of a simulated sequential arc ignition pattern-encoded wheel and corresponding sensor output

5. Camera commissioning

Commission tests included setting the range of the sensor output (0~2volts) within the range of the maximum light intensity radiated from the fuse element to determine the camera's noise limitations and the degree of image lag, i.e. the amount of trapped data in successive camera images.

6. Time correlation and fuse current commutation techniques

Time correlation of data representing arc ignition phenomena in fuse elements was achieved by synchronizing the capture of transient data relative to a single time event instant, the 'event' being the latching of the opto-electronic camera comparator whereby all cross-correlation data from each source was verified.

7. Results of Temporal and spatial correlation of arc ignition measurements

Figure 7 shows the time-correlated attributes of two-beam mode camera operation over one integration cycle for a single test of a copper wire sample. The corresponding sensor data sets are captured on two oscilloscopes; 20μs after the arc voltage is detected by the first oscilloscope and after an interval of 10μs by the second, figure 6i. Figure 7ii indicates the instant of 'crow-barring' the circuit current after a further interval of 5μs, resulting in a 35us time frame for the arc voltage and extant fulgurite attribute, immediately following current commutation. The results, figure 7, show that the pixel data correlates the positions, intensities and widths of arcs which is evidenced in the size and positions of sintered remnants in the corresponding fulgurite. The arc voltage attribute indicates the instances the arc voltages appear and contribute to the instantaneous value. Furthermore, correlated analysis of multiple arc ignitions and momentary fulgurite attributes can be achieved by repetitive testing of identical fuse samples at different 'crowbar' switch time settings [13].

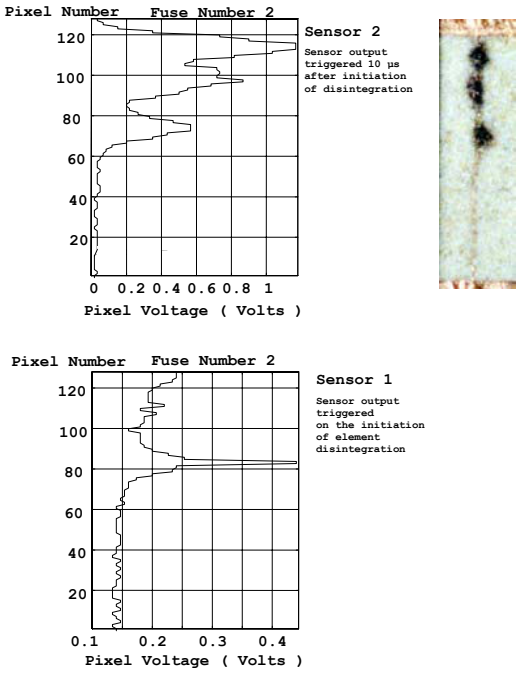

Fig 7i Sensor outputs delayed by 10μs and fuse fulgurite

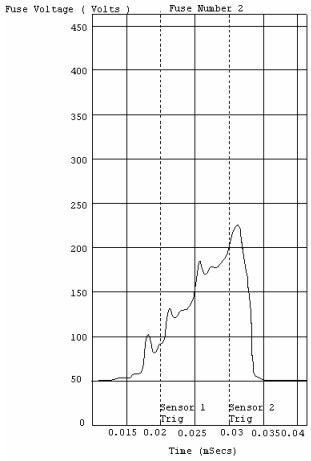

Fig. 7ii Fuse voltage oscillogram – with current 'crow-barred' 5μs after Sensor 2 triggered

Fig. 7 Two-beam mode (10μs sensor-delayed) opto-electronic camera image & fuse fulgurite attributes and arc voltage oscillogram for single test on fuses wires.

8. Conclusions

The presented results demonstrate that current opto-electronic pixel array chip technology is sufficiently advanced to enable the design of accurate and responsive optical systems that are fast enough to enable investigation and data capture of fuse element break up, arc ignition and arc extension phenomena in hbc fuse wires and notched type elements in both the spatial and temporal domains.

The presented black box slit aperture camera design, together with the proposed data capture and test techniques, demonstrate good data cross-correlation of the camera arc light source attributes with respective conventional circuit temporal and spatial arc disposition attributes.

Use of the camera in conjunction with a p.o.w switch demonstrated good camera image acuity for individual arcs of 10μs durations and that good acuity of ignition attributes in the 1μs domain is feasible.

The results show that the camera operates at approximately 30,000 f/p in two-beam repetitive frame data-capture mode and at 15,000 f/s in corresponding single-beam mode and, that in single-shot mode, the camera has an equivalent speed, for a 10μs duration data capture sets, of 100,000 f/s and 1000,000 f/p for 1μs duration data sets.

Finally, the hbc fuse data capture results, Fig. 7, show that the camera data sets, clearly, distinguish the intensity, position and dimensions and incidence of individual, successive, arc ignitions, which correlate precisely to the attributes of respective fulgurite remnants. The proposed camera, therefore, provides new insights into fundamental fuse element disintegration phenomena and is considered to be a useful tool for determining the fuse element design constraints of arc formation for varying fuse short-circuit fault conditions, element shape and surrounding fuse media.

9. References

[1] WOLNY, A., 'Effect of Fuse Element Confinement on the Rate of Rise of Fuse Arc Ignition Voltage', 6th International Conference on Electrical Fuses and their Applications, September 1999, Torino, Italy, pp 135-139.

[2] KLEEN, W., 'Uber den durchgang der elektrizitat durch matallishe Haardrahte', *Ann.Phys*., 1931, **11** (5), pp579 - 605.

[3] DAALDER, J.E., SCHREURS, E.F., 'Arcing phenomena in high voltage fuses.' EUT Report 83-E-137, Department of Electrical Engineering, Eindhoven University of Technology, 1983.

[4] ARAI, S., 'Deformation and disruption of silver wires', International Conference on Electrical Fuses and their Applications, April 1976, Liverpool, U.K., pp50-58.

[5] GOMEZ, J. C., 'HBC fuse models based on fundamental arcing mechanisms', Ph.D. Thesis, Sheffield Hallam University, UK, September 1994.

[6] BARROW, D.R., HOWE, A.F., 'The use of Optical Spectroscopy in the Analysis of Electrical Fuse Arcing', 4th International Conference on Electrical Fuses and their Applications, September 1991, Nottingham, U.K., pp 221-225.

[7] CHEIM, L.A.V., HOWE, A.F., 'Spectroscopic Observations of High Breaking Capacity Fuse Arcs'. *IEE Proc.-Sci*. Meas. *Technol*., 1994, **141** (2), pp 123-128.

[8] BAXTER H.W., Electric Fuses, ERA Report GT/224, ERA Technology Limited, Cleeve Road, Leatherhead, Surrey. KT22 75A

[9] VERMIJ, L., 'The voltage across a fuse during the current interruption process', *IEEE Transactions on Plasma Science*, Dec. 1980, **PS-8** (4), pp460-468.

[10] BROWN, R. E., 'Investigation of Disintegration and Arcing in Electric Fuses', Ph.D. Thesis, Sheffield Hallam University, UK, January 2000.

[11] GNANALINGHAM, S., WILKINS, R., **'**Digital Simulation of Fuse Breaking Tests'. *I.E.E. Proc*. **127 C** (6), November 1980.

[12] DOLEGOWSKI, M., **'**Calculation of the Course of the Current and Voltage of a Current Limiting Fuse'. International Conference on Electric Fuses and their Applications, April 1976, Liverpool U.K., pp218.

[13] BROWN, R. E., MCEWAN, P.M., 'Opto-electronic camera for non-invasive investigation of arcing in short-circuit current-carrying conductors and HBC fuse elements', *IEE Proc.-Sci*. Meas. *Technol*., Accepted for publication Feb. 2003.

INFLUENCE OF THE FILLING MATERIAL PROPERTIES ON PRESSURE IN HBC FUSE. COMPARISON BETWEEN EXPERIMENTAL RESULTS AND SIMULATION

Bussière William[(1)], Rochette David[(2)] and Pellet René[(3)]

LAEPT CNRS UMR 6069 [(1)], Phys. Bât. 5 – 24, Av. des Landais – F63177 AUBIERE CEDEX FRANCE,
william.BUSSIERE@laept.univ-bpclermont.fr
LAEPT CNRS UMR 6069 [(2,3)], Phys. Bât. 5 – 24, Av. des Landais – F63177 AUBIERE CEDEX FRANCE,
david.ROCHETTE@laept.univ-bpclermont.fr [(2)], rene.PELLET@laept.univ-bpclermont.fr [(3)]

Abstract: By varying the mean granulometry and the packing density of the arc quenching material (silica sand), we show the influence of the silica sand morphometric properties on the pressure evolution during the HBC fuse working. Pressure measurements are made using piezoelectric transducers inserted at various lengths taken from the fuse strip plane. The measurements are compared with the results get from the simulation of the energy withdraw within a granular material. Both types of results show that the pressure evolution is strongly correlated with the electric power evolution and the morphometric properties.

Keywords: H.B.C. fuse, pressure, packing density, mean granulometry, porosity, Darcy's law and Forchheimer's law.

1. Introduction

High Breaking Capacity (H.B.C.) fuses are classically made of four main elements: an insulating cartridge, two metal electrodes, a fuse strip (silver), and the arc quenching material, granular silica sand in our case. The morphometric properties of the silica sand, namely the mean granulometry, the packing density, the form factor, play an important role during the prearcing and arcing times, depending on the fault current value.

Silica sand is widely used in H.B.C. fuses [1-2] because of its ability to withdraw the energy brought by the fault current from the arc column. To quantify more precisely the influence of the silica sand properties, we give experimental and simulated results concerning three main points.

- The dependence between the mean granulometry and the maximum packing density.
- The influence of the these two properties on the electrical parameters and pressure evolution.
- The correlation with the mechanical forces.

In Section 2. we give the experimental results concerning the morphometric properties and the pressure measurements. In Section 3. we give the results obtained with the simulation. The results are discussed in Section 4.

2. Experiment

2.1. Experimental device

The fuse used in the tests is designed so as to reproduce the breaking phenomenon as in an industrial fuse. The main discrepancy is that the energy is delivered by means of a capacitor bank discharge (C = 16.5 mF, L = 145 µH, R = 270 mΩ). The shape of the current waveform is due to the (R,L,C) value of the capacitor bank. The prearcing plus arcing time is about 4 ms. The prearcing time is about 0.85 ms. The maximum of the electric power is observed in the time interval from ~ 1.7 ms to ~ 2.2 ms.

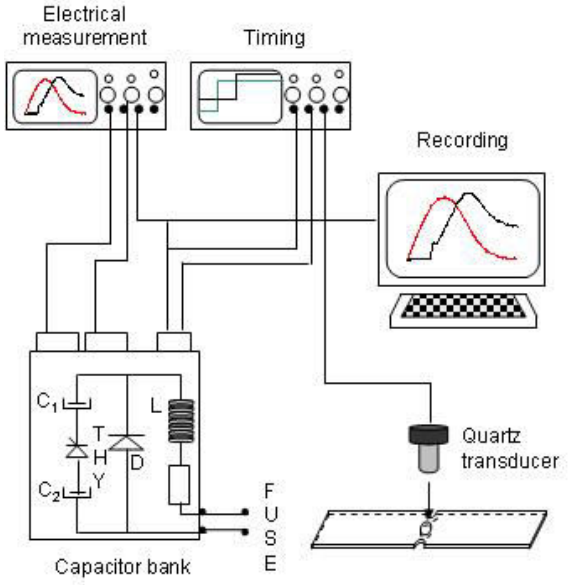

Fig. 1: Schematic diagram of the test set-up. The pressure sensor is directly above one of the fuse element constriction.

To measure the pressure, we have designed a specific set-up taking into consideration the fulgurite growth, especially at right angles to the fuse strip

notches. The cartridge is made of Polyoxymethylene and is chosen cylindrical. The beginning of the discharge ($di/dt > 0$) is set as the zero value for the time scale.

Two TEK TDS 224 oscilloscopes are used do display the current through and the voltage across the fuse, and the pressure inside the granular filler. The pressure is measured using a piezoelectric pressure transducer whose frequency response is 150 kHz (Kistler quartz high pressure sensor 601A).

2.2. Silica sand

The silica sand used in the tests is the same as the industrial one. It is high purity quartz sand (99.80 %) whose mean granulometry and packing density are checked carefully in each experiment.

Table 1. Characterization of the silica sand. Each of the granulometric intervals is 50 µm wide. Each of the packing density letter represents 0.04 g.cm^{-3}.

Parameter	Value
Real density (g.cm^{-3})	2.65
Apparent density (g.cm^{-3})	1.50
Granulometry (µm)	A, B, C, D, E, F, G
Packing density (g.cm^{-3})	a, b, c, d, e, f

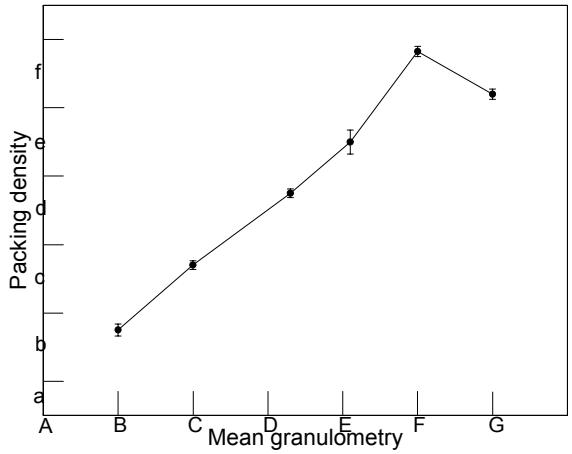

Fig. 2: Packing density of the silica sand versus the mean granulometry. The upper limit of the mean granulometry is inferior to 1000 µm. The upper limit of the packing density is inferior to 2 g.cm^{-3}.

For each mean granulometry in Fig. 3, we give the highest packing density value which we obtain using a specific mechanical device. The error bars represent the statistical deviations around this highest mean value calculated using at least five experiments. For the mean granulometric interval studied (A .. G), the packing density varies linearly with the mean granulometry, excepted for the interval symbolyzed G for which we obtain a reproducible value.

2.3. Fulgurite

Many publications have pointed out the role of the arc quenching material on the breaking phenomenon in a fuse [1-2]. A direct observation using fast imagery clearly shows the spreading of the fluid from the centre of the arc channel towards the surroundings [3].

Due to the fusion and the vaporization of the fuse element and the very near layer of silica sand, the pressure inside the arc channel gradually increases, at the condition that the energy brought by the fault current is sufficient enough. This implies the increase of the fulgurite thickness (Fig. 4).

Thus, as a first approximation, we can suppose that the fulgurite thickness is both the result of the maximum pressure and the fluid spreading in the interstices of the granular fuse filler.

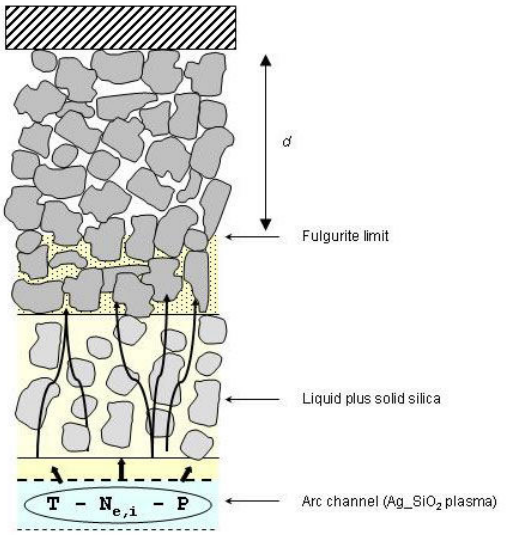

Fig. 3: Various locations of the pressure transducer (d) defined taking into consideration the growth of the fulgurite thickness.

Moreover, to avoid a direct contact between the pressure sensor and the hot surroundings of the fulgurite, we have used the results concerning the evolution of the fulgurite thickness versus the mean granulometry [4]. From these results, we can roughly estimate the minimum length d for the pressure measurement for each mean granulometry.

2.4. Pressure measurement

All the tests have been performed with the same configuration given in Table 2. The short circuit current is about 3.2 kA; the di/dt is about 2.1×10^{6} A.s^{-1}.

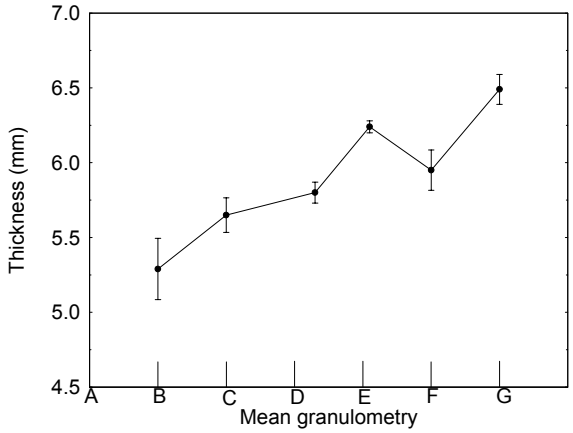

Fig. 4: Evolution of the thickness of the fulgurite versus the mean granulometry.

Table 2. Configuration of the tests. U, stored voltage ; E, total dissipated energy ; I².t, total value of $\int i^2(t).dt$; $t_{PREARCING}$, prearcing time ; t_{TOTAL}, prearcing plus arcing time ; d, length between the pressure sensor and the fuse strip.

Parameter	**Value**
U (V)	460
E (J)	~ 1100
I².t (A².s)	~ 7000 to 9000
$t_{PREARCING}$ (ms)	~ 0.85
t_{TOTAL} (ms)	4.00
d (mm)	7 – 9.5 – 12 – 17
Mean granulometry	B – D – F

For each value of *d* (Fig. 3), at least three experiments were done with the same morphometric conditions (mean granulometry and packing density). A typical set of electrical measurements is given in Fig. 5 in the case of a 460 V- stored voltage. The prospective fault current is about 3.2 kA. The pressure evolution is showed in Fig. 6.

We do not attempt to measure the pressure inside the arc channel by means of the quartz pressure sensor. In fact, the sensor should be damaged due to the very high temperature of the fuse plasma. Thus we measure the pressure of the sand grains on the sensor. This mechanical strength is directly due to the pressure propagation from the plasma to the surroundings, successively through the liquid layer immediately after the plasma, the fused plus solid silica layer, and then the solid sand grains.

The pressure evolution can be divided in three intervals.

- At the beginning of the arcing time: the over pressure due to the arc ignition is the result of the fusion and vaporization of the silver fuse strip. The pressure increase is clearly observed for the smaller *d* values.

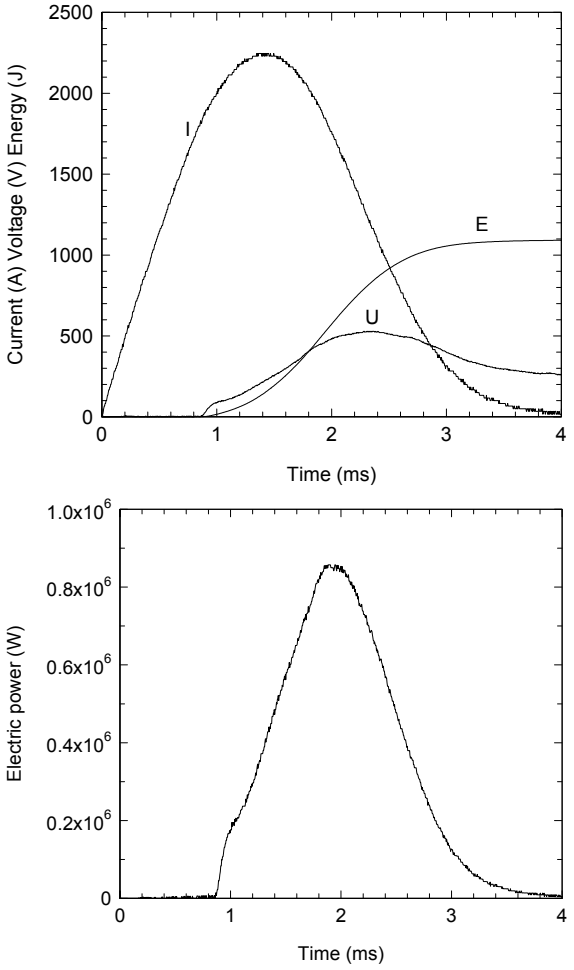

Fig. 5: Evolution of the electric current through and the voltage across the fuse, the total dissipated energy, and the electric power.

- Once the plasma is initiated, the fuse strip and the very near sand grains are gradually melted and vaporized. Thus the pressure increases continuously until the maximum pressure.
- Once the maximum pressure is obtained, the pressure decreases down to values around the atmospheric pressure. This pressure decrease is linked to the dissipated energy rate which is due to the capacitor bank characteristics.

The observed values are inferior to $17\ 10^5$ Pa whatever the test configuration. These values are clearly less than those measured in [5]: $50\ 10^5$ Pa for the maximum. We can suppose that the discrepancy is due to the fact that we measure the mechanical strength due to the sand grains, whereas in [5], the measured pressure is the result of the shock wave due to the plasma pressure transmitted to the sensor. Thus we can approximate that the maximum true value is in the interval [17-50] 10^5 Pa.

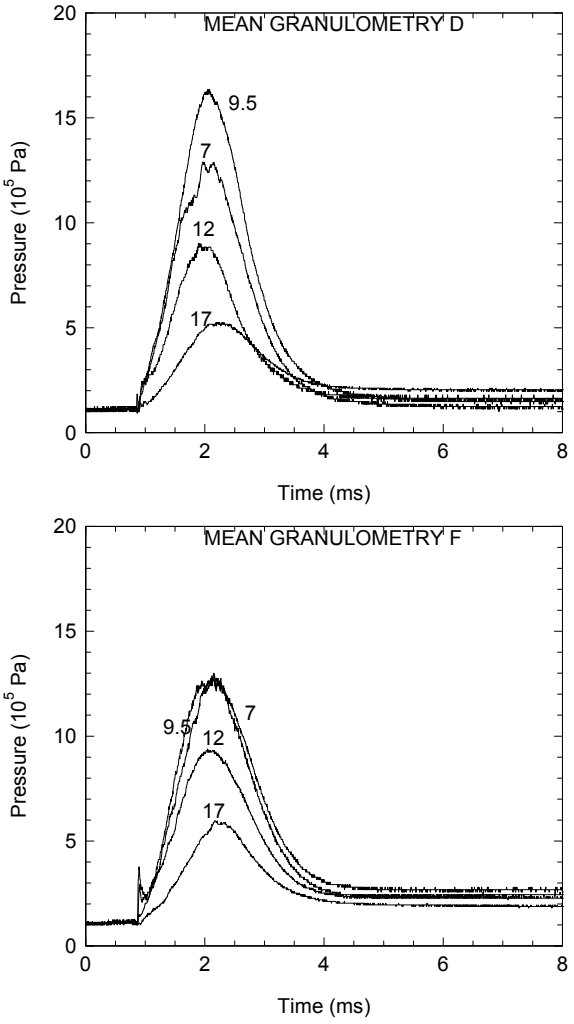

Fig. 6: Evolution of the absolute pressure versus time for the three mean granulometries symbolized B, D, F. The numbers represent the length *d* in mm.

3. Modeling

We present an one-dimensional model to describe the fluid flow and the heat transfer in HBC fuse. The model is based on the compressible Euler equations for perfect gas coupled with a porous media model taking into account the mechanical interaction between the fluid and the silica sand and the heat transfer between hot fluid and cold silica sand [6-7]. In addition to describe the solid temperature evolution, we introduce the heat equation for the solid in porous media [8]. The governing equations are discretized following a finite volume scheme coupled with a fractional step technique and the fluxes are evaluated using the Roe solver [9].

3.1. Mathematical model

The one-dimensional governing equations for single-phase fluid flow in an isotropic, homogeneous porous medium based on the Darcy-Forchheimer model [8] can be written in the following form:

$$\frac{\partial(\rho_f \phi)}{\partial t} + \frac{\partial(\rho_f \phi u)}{\partial x} = r \qquad (1)$$

$$\frac{\partial(\rho_f \phi u)}{\partial t} + \frac{\partial(\rho_f \phi u^2 + \phi p)}{\partial x} = p\frac{\partial \phi}{\partial x} - \phi^2 \frac{\mu}{k} u - \phi^3 \beta \rho_f |u| u \qquad (2)$$

$$\frac{\partial(E\phi)}{\partial t} + \frac{\partial[(E+p)\phi u]}{\partial x} = pu\frac{\partial \phi}{\partial x} + S - h_{sf} A_0 (T_f - T_s) \qquad (3)$$

The physical parameters are ρ_f the fluid density, u the interstitial velocity, p the pressure, E the total energy, T_f , T_s the fluid and solid temperature and ϕ the porosity.

In Eq.(1), the quantity r represents the material source due to the vaporization of the material. In Eq.(2), the expression $\phi^2 \frac{\mu}{k} u$ represents the viscous friction between fluid and grains silica sand where μ is the dynamic viscosity, k is the medium permeability and the term $\phi^3 \beta \rho_f |u| u$ is the Forchheimer flow resistance where β is the Forchheimer coefficient. In Eq.(3), S represents the electrical energy injected in the fuse (Fig.5) and the quantity $h_{sf} A_0 (T_f - T_s)$ is the thermal dispersion representing heat exchanges between fluid and silica sand.

In addition to close the system, we use the ideal gas equation of state:

$p = (\gamma - 1)\rho_f e$ with γ>1,

where γ is the ratio of specific heat and e is the specific internal energy.

To model the heat transfer processes with a thermal non-equilibrium between the fluid and solid phases, we introduce the classical heat equation with longitudinal thermal conduction in the solid phase to evaluate the solid temperature T_s :

$$\rho_s c_{vs} \frac{\partial T_s}{\partial t} - \frac{k_{eff}}{(1-\phi)} \frac{\partial^2 T_s}{\partial x^2} = \frac{h_{sf} A_0}{(1-\phi)} (T_f - T_s) \qquad (4)$$

where ρ_s denotes the solid density, c_{vs} is the solid specific heat and k_{eff} is the porous media conductivity.

3.2. Source terms

An excess current generates heat at the silver fuse element constrictions and leads to the fusion and vaporization of the silver at the beginning, and vaporization of the silica sand later. In a first approximation, we assume that the rate of vaporized mass is proportional to the electrical power injected in the fuse. The mass source term is given by:

$$r = \delta \frac{S}{H_{vap}}$$

where $\delta \in [0,1]$ represents the percentage of electrical power responsible for silica vaporization. The value of δ is chosen in order to obtain a coherent fluid temperature with the experimental value.

The energy source term has contributions from electrical power and thermal dissipation. The injected energy is characterized by a power density function representing the energy quantity per unit volume and time based on Fig.5.

An great part of the energy injected in the fuse is dissipated by transfer between the hot fluid and the cold silica sand. Following [10] the modelling of the heat transfer is given by:

$$Q = h_{sf} A_0 \left(T_f - T_s\right)$$

where A_0 is the specific surface area and h_{sf} represents the interfacial convection heat transfer coefficient which depends on the fluid nature, the fluid flow regime, the morphology and roughly of silica sand grains.

3.3. Numerical method

In order to obtain an approximate solution of the gas flow model in porous media, we use a fractional step technique [9]: on the one hand we solve separately during a small time step Δt the homogeneous conservative system, and on the other hand the right-hand side terms. Let ρ^n be an approximation of $\rho(t^n)$ at time t^n. In order to obtain an approximation of $\rho(t^{n+1})$ at time $t^{n+1}=t^n+\Delta t$, we first determine an approximate solution of the homogeneous problem using the finite volume scheme of the form:

$$\tilde{\rho}_i^{n+1} = \rho_i^n - \frac{\Delta t}{\Delta x}\left(F_{i+1/2}^n - F_{i-1/2}^n\right)$$

where $F_{i+1/2}^n$ and $F_{i-1/2}^n$ represent respectively the numerical fluxes calculated at the interface cells $x = x_{i+1/2}$ and $x = x_{i-1/2}$ using Roe method. Assumed now that $\tilde{\rho}^{n+1}$ is the approximated solution value at $t = t^{n+1}$ of the previous homogeneous problem, we solve the ordinary differential equation. Numerically, we add the right hand side contribution using a fourth-order explicite Runge-Kutta method.

To compute the solid temperature T_s we use an explicit finite volume method given by:

$$\rho_s c_{vs} T_{i,s}^{n+1} = \rho_s c_{vs} T_{i,s}^n + \frac{\Delta t}{\Delta x}\left(G_{i+1/2}^n - G_{i-1/2}^n\right) - \Delta t \frac{h_{i,sf}^n A_0}{1-\phi}\left(T_{i,s}^n - T_{i,g}^n\right)$$

where central differences are used to determine the fluxes $G_{i+1/2}^n$ and $G_{i+1/2}^n$.

3.4. Numerical results

We present a simulation of an electrical arc discharge through the porous medium using realistic physical parameters. To compare with the measurements, we use the three silica sand granulometries symbolized B, D, F. In steady state, we have determined experimentally the friction coefficients used in the mechanical interaction laws for each granulometry (Table 3).

Table 3. Configuration of the tests. k permeability; β Forchheimer coefficient.

Granulometry	k (m^2)	β (m^{-1})
B	9.3×10^{-12}	1.54×10^{5}
D	1.5×10^{-11}	1.35×10^{5}
F	2.6×10^{-11}	1.2×10^{5}

Computations have been performed using the C++ finite volume library OFELI [11] on a 200 elements mesh composed of two uniform meshes where 100 cells correspond to the first area $x \in [0,2]mm$ and 100 cells to the second area $x \in [2,20]mm$. At the initial time, the system is at rest, the fluid present in the silica sand interstices is at atmospheric pressure and ambient temperature.

We present the plasma pressure evolution during the fuse operation for the three granulometries in Fig. 7. The pressure increases up gradually to the maximum value which falls nearly on the same time of the maximum electric power. The maximum pressure is higher for the smallest granulometry B. The maximum pressure values are in the range from ~ 19 10^5 Pa to ~ 24 10^5 Pa. At the decrease of the electric power, the pressure decreases. The atmospheric pressure is obtained a little less than ~ 10 ms after the start of the current waveform. The results of the simulation confirm the experiments in so far as: first, a small granulometry implies a more efficient overpressure linked to the voltage increase due to the fuse ; second, considering only the mechanical point of view, the results show that the pressure wave propagation is directly influenced by the grain size and the interstices volume.

The pressure wave propagation in the silica sand during the fuse operation is given in Fig. 8 for the three granulometries.

- Whatever the position in the fuse domain, the pressure increases with decreasing granulometry. The values in Table 4. are consistent with the measurements.
- The comparison of the experiment with the simulation shows that the maximum values are different. This can be due to: first, the pressure wave propagation can imply the rearrangement of the sand grains, and consequently, the

measurement is more or less reproducible ; second, neither the condensation of the vapours in the surroundings of the plasma and the thermal flow in the sand grains are considered in this modeling: the pressure at the surroundings is thus overestimated.

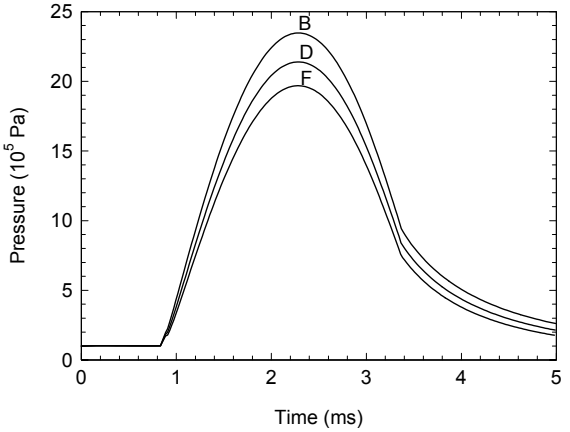

Fig. 7: Evolution of the plasma pressure versus time for three mean granulometry values symbolized B, D, F.

To compare the experimental and simulated evolutions, we give the evolution of the normalized pressure versus time for the granulometry B in Fig. 9. For each type of results, the normalization is realized by dividing the curves by the maximum pressure observed for d = 7 mm. The evolutions are similar for d = 7 mm and d = 9.5 mm. For higher values of d, we observe a significant discrepancy mainly due to two main reasons. First, the modeling restrictions. Second, the observed pressure is obtained for a given d ; due to the presence of the sand grains, the measurement is not unidirectional ; thus, the pressure waveforms responsible for the mechanical strength on the sensor come from different areas in the filler ; this can lead to an overestimation, especially for d = 12 mm and d = 17 mm.

The Fig. 10 represents the velocity and the friction forces evaluated at the plasma periphery for the three mean granulometries. The velocities are higher for the biggest granulometry which is consistent with the simulated and experimental pressures. For the small granulometry, the interstices volume is reduced compared to the upper granulometries. Moreover, for the velocity range calculated, we remark that the Forchheimer term is prominent. The Darcy term is clearly less and nearly constant during the arcing time.

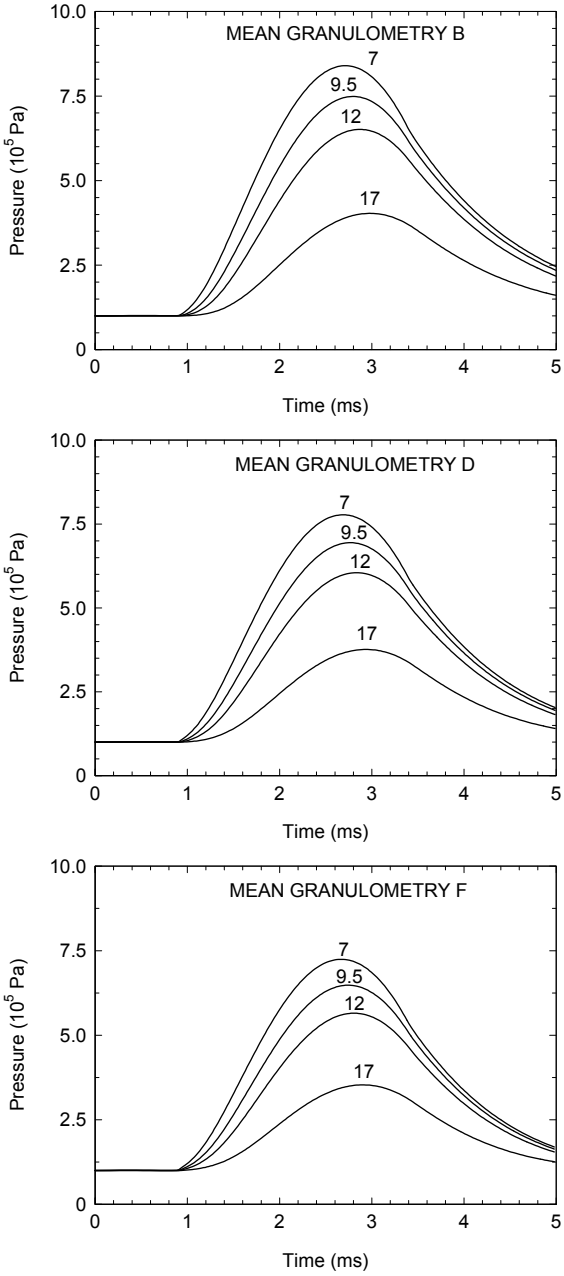

Fig. 8: Evolution of the fluid pressure versus time for the three mean granulometry values symbolized B, D, F. The numbers represent the position in the fuse domain (in mm).

Table 4. Maximum pressure observed for the three granulometries at various positions (d) in the fuse domain.

Granulometry	***d (mm)***			
	7	***9.5***	***12***	***17***
B	$8.4\ 10^5$	$7.5\ 10^5$	$6.5\ 10^5$	$4.0\ 10^5$
D	$7.8\ 10^5$	$6.9\ 10^5$	$6.1\ 10^5$	$3.8\ 10^5$
F	$7.2\ 10^5$	$6.5\ 10^5$	$5.7\ 10^5$	$3.5\ 10^5$

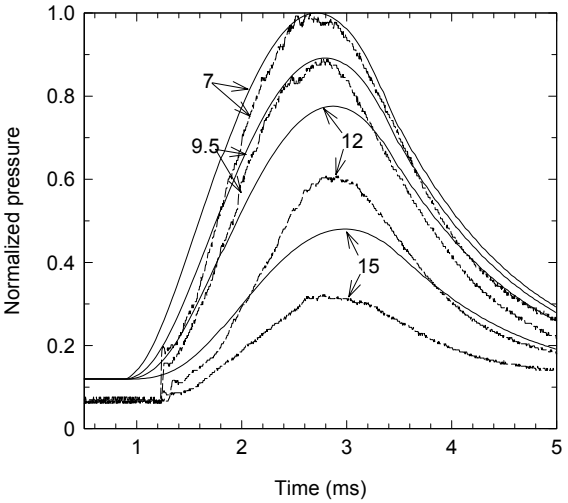

Fig. 9: Evolution of the normalized pressures versus time for the granulometry B. The numbers represent the position in the fuse domain (in mm). The full curves correspond to the simulation, the dash curves correspond to the experiment.

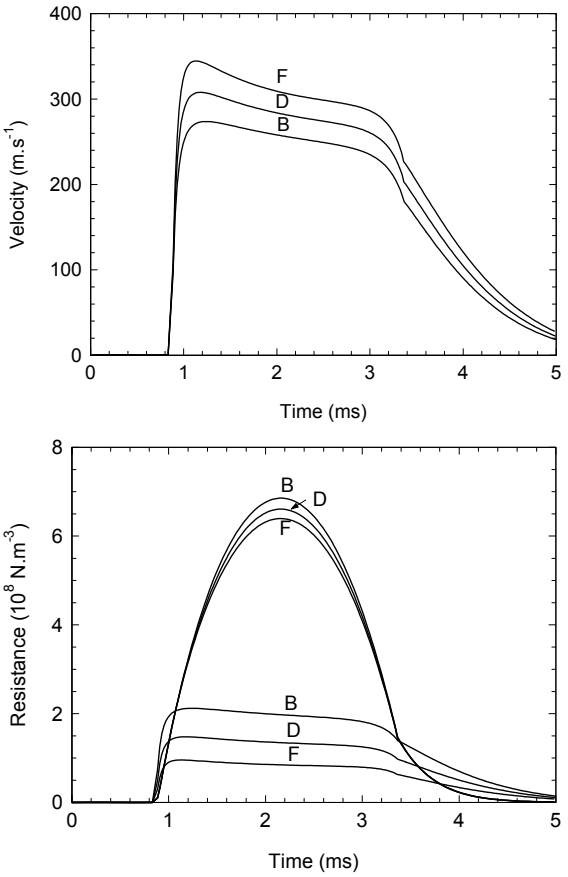

Fig.10: Evolution of the velocity and friction forces versus time for the three mean granulometry at the plasma periphery.

4. Conclusion

Due to the difficulty to access to the plasma pressure by a direct measurement, we have observed the pressure generated by the sand grains. The measurements are compared with a modeling based on the mechanical interaction between the fluid and the sand grains.

The two types of results are similar in so far as the studied area in the filler is not far from the plasma. For further areas, the modeling and the measurement show specific limitations. Especially, in the modeling, we attempt to consider the influence of the vapour recondensation, which should imply smaller pressures. At the present time, such calculations are helpful to test the influence of various morphometric property values on the H.B.C. fuse working.

Acknowledgements

We thank, both for their financial support and their help through many discussions, M. S. Melquiond and T. Godechot from Alstom, M. Vérité from E.D.F, M. T. Rambaud and J.L. Gelet from Ferraz-Shawmut, and M. C. Fiévet and F. Gentils from Schneider Electric.

References

[1] Saquib M.A., Stokes A.D., "Characteristics of fuse arcing in different fillers". *ICEFA* Turin 1999, p. 275.

[2] Sei-Hyun L., In-Sung K., Sang-Ok H., "The test method to acquire the optimal parameter for CL-fuse". *ICEFA* Turin 1999, p.265.

[3] Bussière W., "Estimation of the burn-back rate in high breaking capacity fuses using fast imagery", J. Phys. D: Appl.Phys., 34, pp 1007-1016, 2001.

[4] Bussière W., "Influence of sand granulometry on electrical characteristics, temperature and electron density during high-voltage fuse arc extinction", J. Phys. D: Appl.Phys., 34, pp 925-935, 2001.

[5] Saquib M.A., Stokes A.D., Seebacher P.J., "Pressure inside the arc channel of a high-voltage fuse". *ICEFA* Turin 1999, p.83.

[6] Rochette D., Clain S., "Numerical simulation of Darcy and Forchheimer force distribution in a H.B.C. fuse", Transport in Porous Media, 53, pp. 25-37, 2003.

[7] Rochette D, "Modélisation et simulation de la décharge d'arc electrique dans un fusible moyenne tension", Ph.D Thesis (in french), Blaise Pascal University.

[8] Jiang P.X., Ren Z.P. : Numerical investigation of forced convection heat transfer in porous media using a thermal non-equilibrium model,

International Journal of Heat and Fluid Flow, 22, 102-110, 2001.

[9] Toro E.F.: Riemann Solvers and Numerical Methods for Fluid Dynamics, Springer-Verlag, Berlin.

[10] RoHSENOW W.M., Hartnett J.P., Cho Y.I.: Handbook of Heat Transfer, McGraw-Hill Hanbooks, New York.

[11] Touzani R. : Object Finit Element Library Copyright © 1998-2001.

STUDY OF THE SiO_2 PLASMA PHYSICAL PARAMETERS: TEMPERATURE, ELECTRON DENSITY, PRESSURE, RADIATION

Bussière William[(1)], **Rochette David**[(2)] and **André Pascal**[(3)]

LAEPT CNRS UMR 6069 [(1)], Phys. Bât. 5 – 24, Av. des Landais – F63177 AUBIERE CEDEX FRANCE,
william.BUSSIERE@laept.univ-bpclermont.fr
LAEPT CNRS UMR 6069 [(2,3)], Phys. Bât. 5 – 24, Av. des Landais – F63177 AUBIERE CEDEX FRANCE,
david.ROCHETTE@laept.univ-bpclermont.fr [(2)], pascal.ANDRE@laept.univ-bpclermont.fr [(3)]

Abstract: During the fault current breaking process in a fuse, the energy brought by the electric current implies the fusion and the vaporization of the fuse element and the filler (usually silica sand). Consequently a plasma is created. The plasma consists of metallic and silicon. We use the radiation escaped from the plasma to measure the plasma temperature and the electron density. The results are given for different mean granulometry and packing density, and compared with other experimental results obtained from the literature. Moreover, for modelling purpose, the measurements are compared with theoretical calculation (thermodynamic properties) to deduce the valid assumptions.

Keywords: Plasma, atomic spectroscopy, Stark broadening, Helmoltz free energy minimisation, composition, electron density, pressure.

1. Introduction

Within the framework of research areas concerning fault current breaking devices, especially H.B.C. fuse, researchers are interested with the evolutions of the physical parameters of the plasma, namely the plasma temperature (T) [1-2], the electron density (n_e) [3-5], the pressure (P) [6]. These properties are linked to fundamental parameters, such as the electrical conductivity, the thermal conductivity, the transport coefficients which are necessary to establish realistic modelling.

Once the fuse plasma is initiated, the dissipated energy is responsible for the fuse element and silica sand fusion and vaporization. Thus the plasma volume varies according to the energy brought by the electric current and the ability of the filler to withdraw the energy from the plasma to the surroundings. In Section 2, we give a quick depiction of the experimental set-up used to collect the radiation escaped from the plasma, and the n_e/T characteristics measured for different morphometric properties of the silica sand. In Section 3, we briefly recall the hypothesis, the physical formulation and the calculation method concerning electron density, pressure and spectral line intensity. In Section 4, the two types of results are compared.

2. Temperature and electron density measurement

2.1. Test fuse and test circuit

The test fuse is designed to reproduce the breaking phenomenon of an industrial fuse. We use a single silver fuse element with two notches. The front side of the test fuse consist of a quartz window designed to collect the light issued from the plasma. The fuse strip is set in such a way that only the section of the fuse strip is in contact with the quartz window. Thus the interaction between the plasma and the window is reduced, and the fulgurite obtained after the fuse working is similar to those obtained in an industrial fuse. The cavity is filled with silica sand grains. The mean granulometry and packing density are controlled before the test.

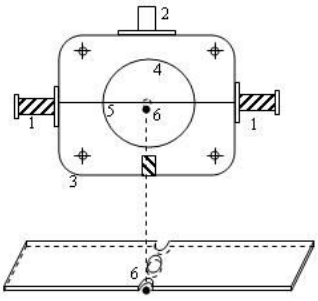

Fig. 1: Test fuse. 1, metal electrodes ; 2, cavity obturator ; 3, cartridge ; 4, filling cavity ; 5, fuse strip ; 6, observation point.

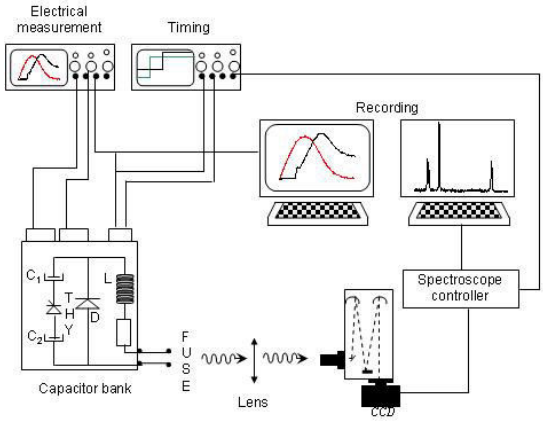

Fig. 2: Schematic diagram of the test set-up.

The energy is delivered by means of a capacitor bank discharge: the short-circuit prospective current is 3.2 kA, and the stored voltage is 460 V. The frequency of the waveforms of the current through and the voltage across the fuse is about 50 Hz. A 416 $A.V^{-1}$ current shunt and 100 $V.V^{-1}$ voltage shunt are used to measure the current through and the voltage across the fuse. The start of the capacitor bank discharge is synchronized with the emission of the radiation escaped from the plasma. Typical electrical measurements can be found in [7].

The fuse filler is silica sand of high purity (99.80%). Various mean granulometry and packing densities are used (Table 1).

Table 1. Characterization of the silica sand. Each of the granulometric intervals is 50 µm wide. Each of the packing density letter represents 0.04 $g.cm^{-3}$. The first letter represents the smallest value for the two parameters.

Parameter	Value
Real density ($g.cm^{-3}$)	2.65
Apparent density ($g.cm^{-3}$)	1.50
Granulometric intervals	A, B, C, D, E, F, G
Packing density	a, b, c, d, e, f

2.2. Collection of the plasma radiation

The radiation issued from the plasma is collected via an optic fibre plus lens system and focussed to the entrance slit of the spectroscope. The used spectroscope is a Chromex 500 IS, 500 mm-focal length. We use two diffraction gratings, a 1200-$gr.mm^{-1}$ and 1800-$gr.mm^{-1}$ grating, which correspond to the respective spectral range ~ 45 nm and ~ 25 nm. The spectrum is recorded by means of a CCD matrix (size in pixel: 1242×1152) used in a kinetic mode which allows to obtain many tracks equally distributed throughout the whole duration of the plasma radiation emission. A viewing of the maximum and minimum intensity of each track is given in Fig. 3 together with the electric power evolution during the fuse working. The radiation intensity depends directly to the electric power level: immediately after the arc ignition corresponding to the voltage drop (~ 0.9 ms), the radiation intensity quickly increases such as the electric power. At the decrease of the electric power, the radiation intensity gradually decreases until 4 ms. Once the electric power is zero, the radiation can not be used any more.

Two spectral intervals are studied in order to evaluate the temperature and the electron density. For both evaluations, we used the ionized silicon lines whose spectroscopic properties are in given in Table 2.

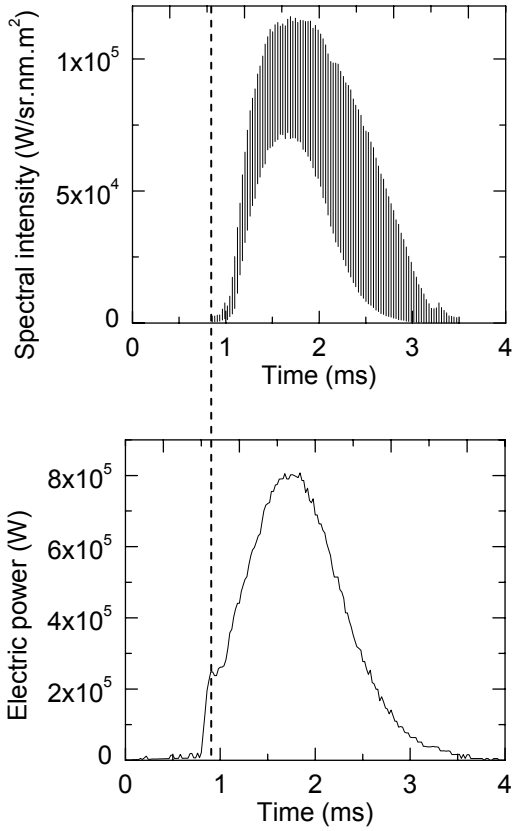

Fig.3: Evolution of the radiation profile for the spectral interval focussed on 635 nm and the electric power for the prearcing plus arcing time.

Table 2. Configurations of the two kinetic modes used for the study of the plasma radiation.

Total duration of a track (ms)	0.038	0.022
Number of tracks	94	143
Total time (ms)	~ 3.6	~ 3.1

2.3. Temperature measurement

The temperature is obtained from the ratio of two spectral line intensities issued from the same ion species, assuming that the Boltzmann distribution of the energy levels is valid. The temperature is given by:

$$T = \frac{E_{u1} - E_{u2}}{k_B} \times \frac{1}{\log\left(\frac{\lambda_{ul,2} g_{u1} A_{ul,1}}{\lambda_{ul,1} g_{u,2} A_{ul,2}} \times \frac{J_2}{J_1} \right)}$$

where the subscript 1 and 2 correspond to the two spectral lines, λ_{ul} is the central wavelength, g_u is the statistical weight of the upper energy level E_u,

Table 2. Spectroscopic properties of the ionized silicon lines used for the evaluation of the temperature and the electron density [8].

Multiplet	Theoretical wavelength (nm)	Upper energy level (eV)	Statistical weight	Transition probability (10^8 s^{-1})	Theoretical intensity ratio within multiplets (LS coupling) [9]
1	385.602	10.073883	4	0.25	1.78
	386.259	10.066447	2	0.28	
2	634.711	10.073883	4	0.70	2.00
	637.137	10.066447	2	0.69	
3	413.089	12.839316	8	1.32	1.43
	412.805	12.839332	6	1.42	

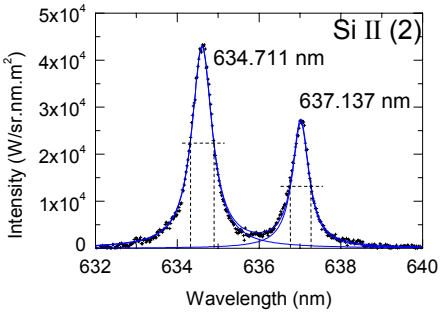

Fig. 4: Fit of the experimental Si II (2) multiplet line profiles (+). The full curves represent the fitted profile from which the HWHMs are deduced. This spectrum is observed at the end of the fuse working (~ 3.5 ms).

A_{ul} is the transition probability, and J is the total area of the spectral line. The difference in energy between the upper energy levels of the two lines must be 2 eV at least. To reduce the possible errors in the intensity calibration, we choose two ionized silicon lines visible in the same spectral interval. The total areas J are fitted for each of the tracks, and for the four lines corresponding to the multiplets 1 and 3. Thus we express four temperature values for each track. We use the total area rather than the maximal intensity because the corresponding line profile is due to some broadening processes resulting from the plasma parameters (density, temperature, pressure). We have to notice that the light escaped from the plasma is integrated on an unknown thickness. Thus the resulting temperature is not a local value.

2.4. Electron density measurement

Many processes can be responsible for the broadening of the spectral line. We can distinguish the broadening due to the collisions of the radiating species with neutral particles (natural, Doppler, Van der Waals broadenings), and the broadening due to the collisions with charged particles (Stark effect mainly). The first type of broadening is not significant in the case of the fuse plasma. The resulting Half Width at Half Maximum (HWHM) is clearly less than one nanometre. On the contrary, the local electric strength in the fuse plasma implies the splitting of the radiating energy level, and thus the broadening of the spectral line profile. The resulting HWHM can be several nanometres. The ionized silicon Half HWHM due to the Stark effect is tabulated in the literature for various temperature and electron density values [10]. Considering that the electron impact HWHM varies linearly with the electron density (the dependence with the temperature is weak) we can deduce the electron density in the fuse plasma from the experimental HWHM. This processing is valid as long as the lines are isolated, such as the Si II (3) lines. But in the fuse, the plasma core is surrounded by cold layers responsible for the radiation absorption. This implies a supplementary broadening which can not be differentiated from the Stark broadening. Consequently, the electron density deduced from the Si II (3) HWHM can be overestimated.

2.5. Electron density versus temperature characteristics for different morphometric properties

In order to compare the measurements with the calculations, we represent the electron density versus temperature for various values of the granulometry and packing density of the silica sand. The results are given in Fig. 5 for six consecutive granulometric intervals, each of them being 50 µm-wide.

The number of measurements is linked to the granulometry. Smaller the granulometry, smaller the number of valid spectrums can be observed. On the full temperature range investigated, it is not possible to fit the experimental profiles for temperature higher than 17 000 K. The measurements corresponding to this temperature range show a decreasing electron density with increasing temperature. From the experimental point of view, it may be explained by the absorption of the radiation escaped from the

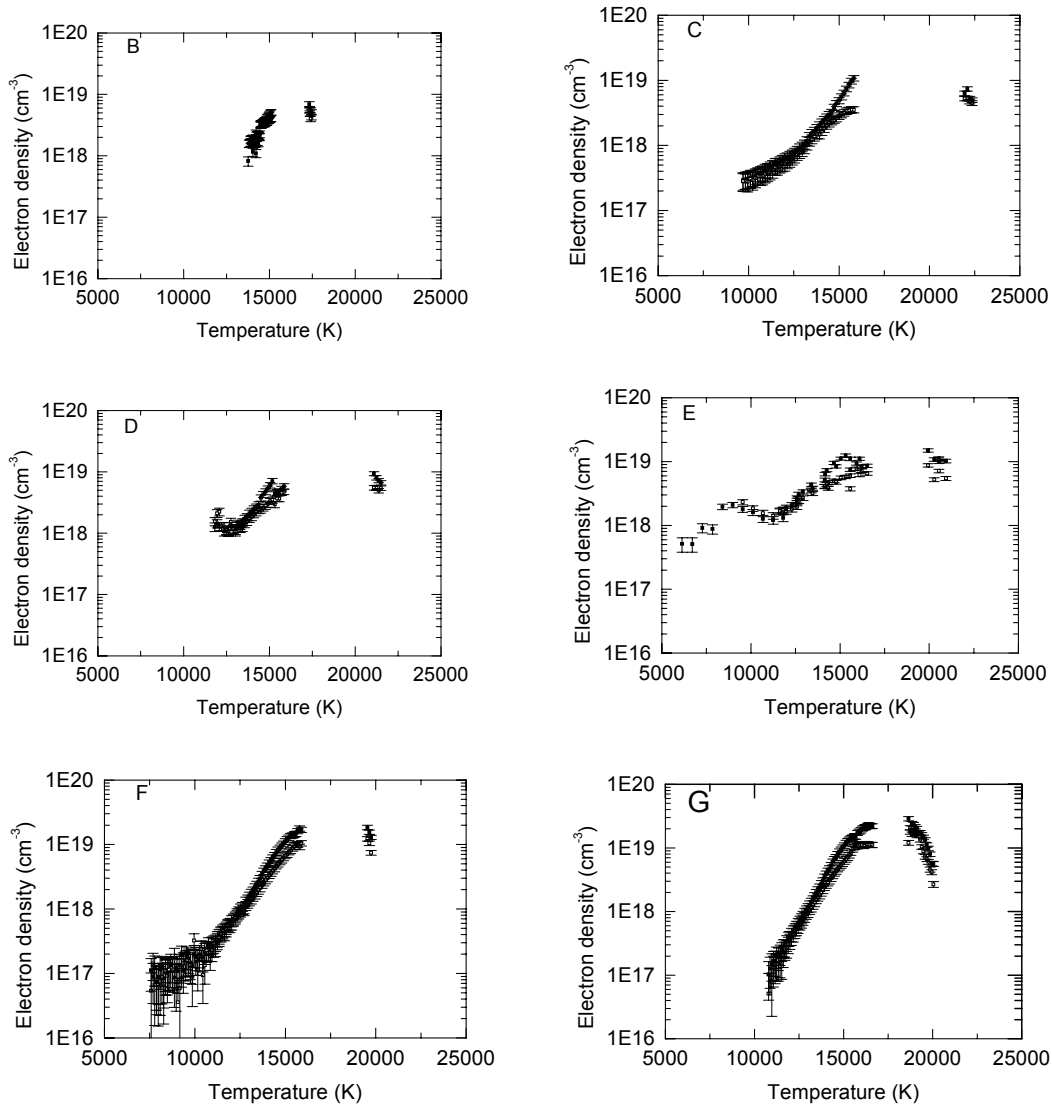

Fig. 5: Electron density versus temperature for the increasing 50 µm-granulometric intervals B, C, D, E, F, G.

inner part of the plasma by the cooler surrounding layers. Thus, the ionized silicon line profile is broadened by absorption, and the fitted HWHM is the combination of the two broadening processes, Stark broadening and absorption broadening. From This is linked to the dissipated energy, the $I^2.t$, the electric power which vary in function of the morphometric properties. Whatever the parameter, the variation is significant: the temperature varies between 22 000 K and 10 000 K, and the electron density varies between 10^{16} cm^{-3} and 10^{19} cm^{-3}. To measure the temperature and the electron density, we observe the plasma radiation in two different spectral domains that can not be studied simultaneously with a single acquisition. Thus, in Fig. 5, the temperature is the value deduced from the acquisition realized in a different spectral domain than those observed for the electron density measurement.

the electron density versus temperature characteristics, there is no significant discrepancy between the different granulometries, except for the smallest temperatures.

3. Calculation applied in the case of a SiO_2 plasma

In a purpose to determine theoretically the electronic density number, the pressure and the intensity of monatomic spectral lines versus temperature and for various densities, we have made a calculation code. This calculation code is based on the minimisation of Helmoltz free energy that allows us to determine the plasma composition versus temperature for a fix plasma density. With the Dalton law we calculate the pressure versus temperature. Then for the interesting chemical species (Si^+), by assuming a Boltzmann distribution on excitation

level we calculate the spectral line intensities versus temperature [11].

In our calculation code, we take the following chemical species into account: e^-, O, O^-, O^+, O^{++}, O^{+++}, Si, Si^-, Si^+, Si^{++}, Si^{+++}, O_2, O_2^-, O_2^+, Si_2, SiO, O_3, Si_3, SiO_2.

We have to notice that the calculation is made only with silica. As a matter of fact since the comparison is made after the creation of plasma between the two silver electrodes and since the thermal conductivity of liquid and solid silver is higher than for the silica. The diffusion of heat is made quicker for silver than for silica. So, the vaporisation is higher for silica than for silver [12] and consequently in a simplification purpose we consider a plasma formed in silica vapours in our calculation.

4. Discussion

As a first step, we compare the intensity of the ionized silicon lines versus temperature in so far as these lines are used in the diagnostic (Fig. 6). Second, we compare the profiles of the pressure measured inside the filler with the profiles obtained from the simulation and the calculation (Fig. 7). Third, we compare the electron density versus temperature characteristics (Fig. 8).

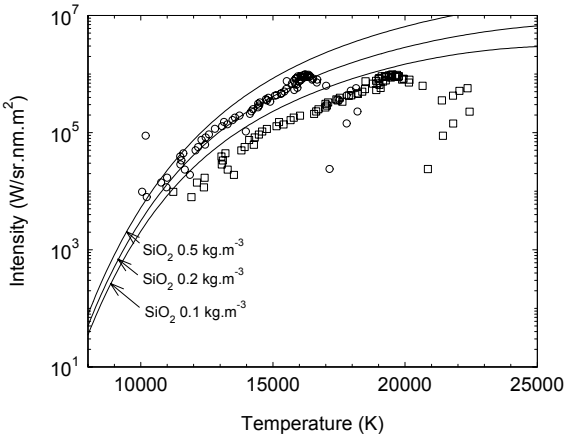

Fig. 6: Comparison of the observed intensity of the Si II (1) 385.602 nm line with the calculation at constant volume for three initial densities of silica. ○, temperature scale 1 ; □, temperature scale 2.

The evolution of the Si II (1) 385.602 nm line versus temperature is given in Fig. 6 for two experimental temperature scales. These temperature scales are deduced from the Si II (1) and Si II (3) lines areas. For each track, four values are fitted from which we express two mean trends, symbolized 1 and 2 in Fig. 6. We observe that the experimental points follow the calculated curves for a given SiO_2 initial density. For the higher temperatures, the experimental points clearly deviate from the calculated curves. Two main reasons can justify this discrepancies.

- First, at the beginning of the arcing time, the plasma is made of silver and silicon. The relative proportion of the two species is very difficult to determine. But a few percentage of silver can strongly influences the silicon lines intensity.
- Second, the radiation absorption due to the cold surroundings can strongly affects the spectral line area. Moreover, the radiation absorption depends on the wavelength and it can be different for the Si II (1) and Si II (3) multiplets.

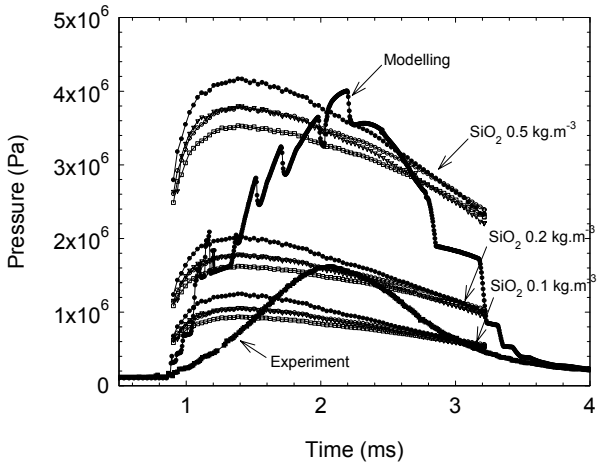

Fig. 7: Evolution of the pressure versus time. We report the SiO_2 plasma pressure calculated at constant volume for three initial densities, the pressure in the arc core obtained with modelling [13], and the pressure measured inside the filler at the immediate vicinity of the fulgurite.

Taking into consideration the evolution of the Si II (1) and Si II (3) lines intensity on one side, and the calculation on the other side, we can deduce the corresponding plasma pressure for a given density and temperature. Then, the plasma pressure is expressed as a function of time. The deduced pressure is compared in Fig. 7 with the pressure obtained from modelling and with the pressure measured in the filler, at the vicinity of the fulgurite. The experimental pressure can be interpreted as the low limit of the plasma core pressure. Three results can be expressed.

- First, the experiment and the modelling give coherent results ; the curves are similar for the increase and the decrease of the pressure. The maximum is different: ~ 40.10^5 Pa for modelling, ~ 16.10^5 Pa for experiment ; this discrepancy is logical in so far as we compare the plasma pressure with the pressure inside the filler. The plasma pressure is transmitted to the granular filler via the surroundings of the fuse plasma. These surroundings consist of different layers, mainly liquid and eroded sand grain

resulting from the flow of vapour from the plasma core [14].

- Second, the two maximums are nearly observed simultaneously, and they correspond to the maximum of the electric power. On the whole duration of the fuse working, the evolution of the pressure is nearly the same as the evolution of the electric power.
- Third, the pressure deduced from the Si II spectral lines intensity and the calculation do not show a logical evolution versus time. In fact, the calculation is performed for a given density ; due to the closeness of the plasma with the sand grains, we can suppose that some silicon vapours are produced while the energy is sufficient. If the energy decreases, the density of the plasma should decrease too. Thus the plasma pressure has to be calculated using different initial densities to describe the whole duration of the fuse working.

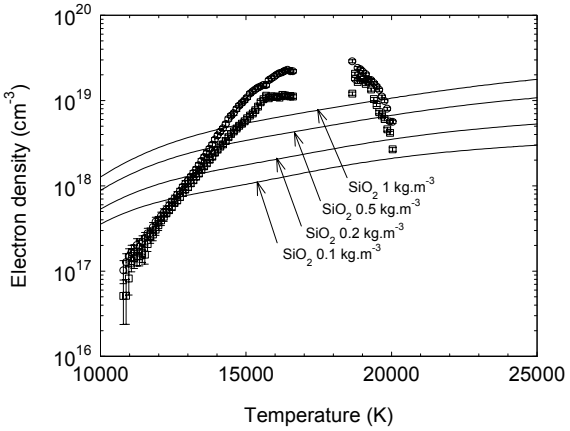

Fig. 8: Comparison between the experimental electron density and the calculation at constant volume for various initial densities.

The electron density number deduced from the Si II (2) multiplet HWHMs is given versus temperature in Fig. 8 together with the calculated evolution with corresponding initial density.

- The electron density number logically increases for the temperature range from ~ 10 000 K to ~ 17 000 K. This trend is similar to the calculated curves. For the temperature range from ~ 17 000 K to ~ 19 000 K, the Si II (2) multiplet line profile can not be fitted any more. The spectral lines are broadened by absorption, and the continuum (Bound-free and free-free radiation) becomes more intense than the discrete radiation. For the temperature range from ~ 19 000 K to ~ 22 000 K, the electron density number decreases. This is opposite to the calculation. This error can be due to the absorption: first the absorption implies a broadening of the Si II (2) multiplet line profile ; second, the temperature deduced from the Si II (1) and Si II (3) multiplets can be overestimated.
- The experimental points can not be described by a calculation with a single initial density. The experimental curve corresponds successively to different plasma states resulting from increasing initial density. Thus, the difficulty is to define the duration of one state defined by a given density.

5. Conclusion

The physical and thermodynamic properties of the H.B.C. fuse plasma are studied using experiment and theoretical calculations. The two approaches are necessary to give an estimation of the parameters used in the modelling.

By studying the plasma radiation, we estimate the *ne/T* characteristics. These trends are compared with the calculations assuming a constant volume and a given initial density in the case of a SiO_2 plasma. The comparison of the experimental and calculated Si II lines intensity allows the estimation of the initial density. The corresponding calculated pressure is more difficult to interpret ; it seems obvious that, due to the electrical energy injection on one side, and the plasma energy withdraw linked to the sand properties on the other side, the calculation can not be performed for a single value of the initial density. The evolution of the density used in the calculation has to be determined in the future to give the necessary information for the modelling.

Acknowledgements

We thank, both for their financial support and their help through many discussions, M. S. Melquiond and T. Godechot from Alstom, M. Vérité from E.D.F, M. T. Rambaud and J.L. Gelet from Ferraz-Shawmut, and M. C. Fiévet and F. Gentils from Schneider Electric.

References

[1] Saquib M.A., Stokes A.D., James B.W., Falconner I.S., “Arc temperature measurement in a high-voltage fuse”, ICEFA Turin 1999, p.107.

[2] Bussière W, Bezborodko P., “Measurement of time-resolved spectra of fuse arcs using a new experimental arrangement”, J. Phys. D: Appl. Phys., 32, pp. 1693-1701.

[3] Saquib M.A., Stokes A.D., James B.W., Falconner I.S., “Measurement of electron density in a high-voltage fuse arc”, ICEFA Turin 1999, p.129.

[4] Chikata T., Ueda Y., Murai Y., Miyamoto T., “Spectroscopic observations of arcs in current limiting fuse through sand”, ICEFA Liverpool 1976, p. 114.

[5] Bussière W., “Influence of sand granulometry granulometry on electrical characteristics, temperature and electron density during high-voltage fuse arc extinction”, J. Phys. D: Appl. Phys., 34, pp. 935-935.

[6] Saquib M.A., Stokes A.D., Seebacher P.J., “Pressure inside the arc channel of a high-voltage fuse”, ICEFA Turin 1999, p.83.

[7] Bussière W., Rochette D., Pellet R., “Influence of the filling material properties on pressure. Comparison between experimental results and simulation”, ICEFA Gdansk, 2003.

[8] NIST Database 61, Database for Atomic Spectroscopy (DAS) 1995 National Institute of Standards and Technology, http:// aeldata.phy.nist.gov/archive/el.html.

[9] Lesage A., Rathore R.A., Lakicevic I.S., Puric J., “Stark widths and shifts of singly ionized silicon spectral lines”, Phys. Rev. A, 28, pp. 2264-2268.

[10] Griem H.R., “Spectral line broadening by plasmas”, New York: Academic Press, 1974.

[11] Bussière W., André P., “Evaluation of the composition, the pressure, the thermodynamic properties and the monoatomic spectral lines at fixed volume for a SiO2-Ag plasma in the temperature range 5000-25000 K”, J. Phys. D: Appl. Phys., **34**, pp 1657-1664, 2001.

[12] Lefort A., Abbaoui M., André P., Private communication.

[13] Rochette D., Clain S., “Numerical simulation of Darcy and Forchheimer force distribution in a H.B.C. fuse”, Transport in Porous Media, 53, pp. 25-37, 2003.

[14] S. Gnanalingam, R. Wilkins, “Digital simulation of fuse breaking tests”, IEE Proc., Vol. 127, Pt. C, N°6, November 1980.

CURRENT DISTRIBUTION IN VARIABLE SECTION FUSES

G. A. Cividjian

University of Craiova
Bd. Decebal, 107, RO-1100 CRAIOVA, Romania, E-mail: gcividjian@elth.ucv.ro

Abstract: The thermal and electro-dynamic effects of the current in the fuse depend essentially on the local value of the current density. Using the conformal mappings, the constriction resistance, the current distribution in variable section flat fuses is studied. In particular, the current distribution in arbitrary angle corner and the corresponding resistance is evaluated. Transitory parameters of monophase line with rectangular bar conductors are determined.

Keywords: Current distribution. Transitory parameters. Corner resistance. Constriction resistance.

1. Introduction

The fuses elements for low voltage and large rating currents have in general large cross-section and irregular shapes. This is why the common simplification used for filiform circuits are not more applicable in this case: the current distribution cannot be considered uniform in corners or in regions with sharp cross-section modification and the electromagnetic field in conductor is not established instantaneous when a current step is applied. In the paper some such situations are analyzed and the effects on the element parameters are evaluated.

2. Constriction resistance of bandwidth reduction

The analytical function

$$z(t)=\frac{a}{\pi}\left[\begin{array}{l}\operatorname{Arch}\dfrac{2t-x^2-1}{x^2-1}\\ -\dfrac{1}{x}\operatorname{Arch}\dfrac{(x^2+1)t-2x^2}{(x^2-1)t}\end{array}\right];\ x=\frac{a}{b} \qquad (1)$$

maps the upper half plane t into the shaded domain from fig. 1 a (fig. 1b) [1].

The "constriction resistance" is defined as a difference between the real resistance of the constricted from a to b band and the sum of the resistances of the two segments, for the case $\overline{PN}\to\infty$, $\overline{MQ}\to\infty$:

$$R_s\left(\frac{a}{b}\right)=\frac{1}{\sigma d}\lim_{\substack{r\to 0\\ R\to\infty}}\left[\frac{1}{\pi}\ln\frac{R}{r}-\frac{\overline{PN}}{a}-\frac{\overline{MQ}}{b}\right] \qquad (2)$$

where d is the (constant) thickness of the band and σ the material conductivity.

After the computations, similar to given in annex of [4], the following formula was obtained for the constriction resistance of the d thickness band (fig. 2):

$$R_s(x)=\frac{x}{\sigma\pi d}\left[\left(1+\frac{1}{x^2}\right)\ln\frac{x+1}{x-1}+\frac{2}{x}\ln\frac{x^2-1}{4x}\right];\ [\Omega] \qquad (3)$$

The resistance of the shaded band from fig. 1 a) is equal to the sum of the resistances of two segments (with uniform distributed current) plus R_s.

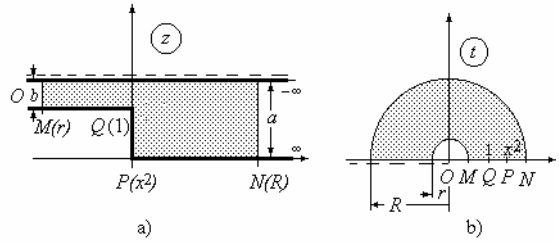

Fig. 1: Domain of the map for "constriction resistance"

The complex potential of the current density field δ in t-plane will be:

$$W=-i\frac{I}{\pi d}\operatorname{Ln}t;\quad t=\rho e^{i\theta}$$
$$\delta=-i\overline{W'}=\frac{I}{\pi\rho d}e^{i\theta} \qquad (4)$$

where I [A] is the current and the complex conjugate of current density in z-plane is

$$\bar{\delta} = i\frac{\mathrm{d}W}{\mathrm{d}z} = i\frac{\mathrm{d}W}{\mathrm{d}t}\frac{\mathrm{d}t}{\mathrm{d}z} = \frac{I}{a\,d}\sqrt{\frac{t-x^2}{t-1}} \qquad (5)$$

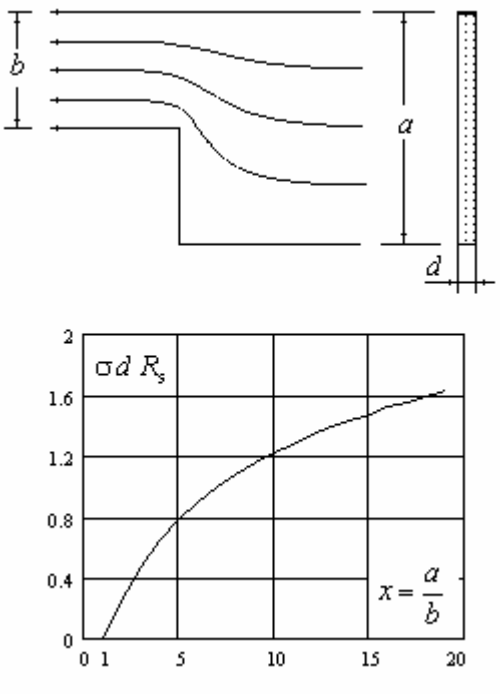

Fig. 2: Constriction resistance of bandwidth reduction

3. "Corner resistance"

A supplementary resistance, which we will call "corner resistance", must be considered in the case of the slab having the shape shown in fig. 3.

The analytical function

$$z(t) = \frac{b}{\pi}\int_t^1 \left(\frac{1-t}{1+t}\right)^{\beta}\frac{\mathrm{d}t}{t};\quad t = \rho\, e^{i\theta}$$
$$z = x + iy;\quad \beta = 1-\alpha/\pi \qquad (6)$$

maps the shaded domain between the two angles equals to α from the *z*- plane (Fig. 3) into the upper half-plane *t* [1].

The corner resistance can be defined as a limit:

$$R_c(\alpha) = \frac{-2}{\sigma\,\pi\,d}\lim_{\substack{\rho_0\to 0\\ z_0\to\infty}}\left[\ln\rho_0 + \frac{\pi}{b}z_0\right]$$
$$\frac{\pi}{b}z_0 = \int_{\rho_0}^1\left(\frac{1-r}{1+r}\right)^{\beta}\frac{\mathrm{d}r}{r} \qquad (7)$$

The values of corner resistance are given in fig. 4 and can be approximated with the formula:

$$R_c = \frac{1}{\sigma\,d}\left(0.882 - 0.324\frac{\alpha}{90°}\right)\ [\Omega] \qquad (8)$$

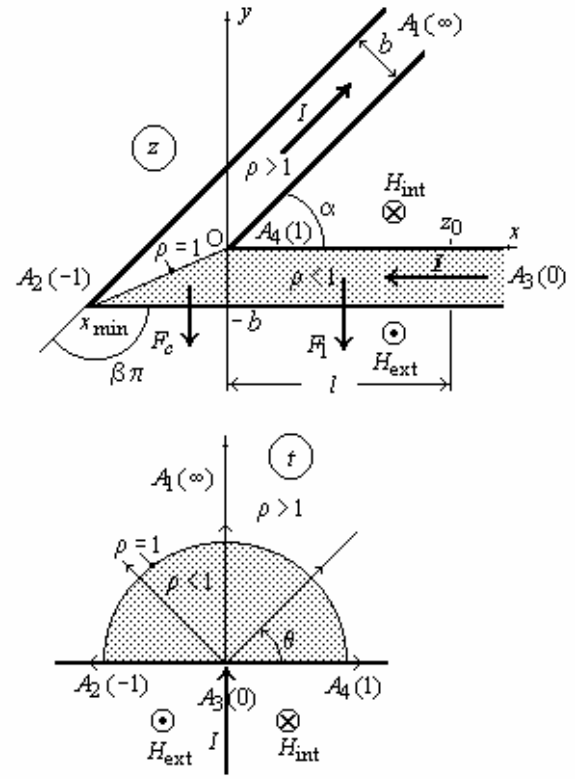

Fig. 3: Domain of the map for "corner resistance"

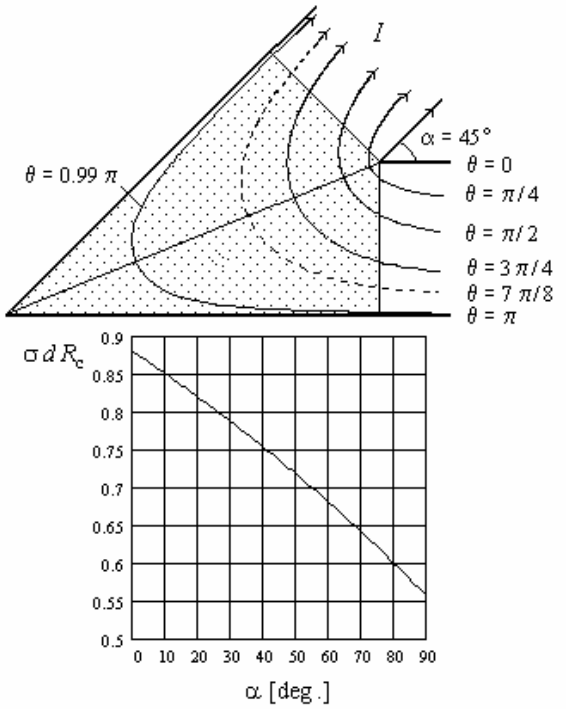

Fig. 4: Corner resistance

The complex conjugate of current density in *z*-plane (fig. 3 and 4) is:

$$\overline{\delta} = i\frac{\mathrm{d}W}{\mathrm{d}z} = i\frac{\mathrm{d}W}{\mathrm{d}t}\frac{\mathrm{d}t}{\mathrm{d}z} = -\frac{I}{b}\left(\frac{1+t}{1-t}\right)^{\beta} \qquad (9)$$

4. Transitory parameters of rectangular bus bars

4.1. Magnetic field of singular bar

The transitory parameters of two identical very high and close disposed rectangular bars, when the external magnetic field can be neglected, are determined in [3], where a complete smart solution is given for transitory electromagnetic field in such a line. In the paper, the external magnetic field H_B is approximately considered. Assuming the bars enough high to neglect the horizontal component of magnetic field, and consequently the magnetic field constant along the vertical direction, the problem is solved in function of the ratio η between the magnetic fields on the two sides of the bar. The obtained results, for $\eta = 0$ coincide with the given in [3].

4.2. Magnetic field of two rectangular bars

The vertical component of magnetic field of a solitary rectangular bar, with uniform distributed current density δ, issued from the Biot-Savart law, is given in [1] and can be written as follows:

$$H_y(x,y) = \frac{\delta}{2\pi}\left[\begin{array}{l}(x+a_1)(\theta_2-\theta_3)- \\ (x-a_1)(\theta_1-\theta_4)+ \\ (y+b_1)\ln\dfrac{r_2}{r_1}- \\ (y-b_1)\ln\dfrac{r_3}{r_4}\end{array}\right] \qquad (10)$$

For a vertical infinite-length current sheet *I*, a very thin bar, with $a_1 \to 0$, can be considered and the vertical component of the magnetic field (10) becomes:

$$H_y(x,y) = \frac{I}{4\pi b_1}\varphi \qquad (11)$$

where φ is the angle at which the sheet cross-section is seen from the point (*x, y*).

In the case of two parallel rectangular bars we will denote by η the ratio of the magnetic fields H_B / H_A for stabilized direct current and by η_0 the same ratio for the beginning of the process of current vertical infinitely thin sheets.

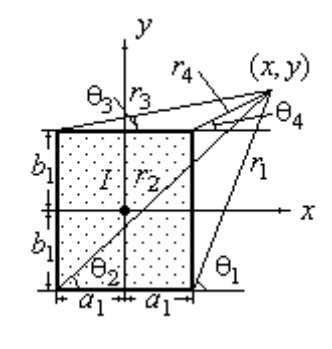

Fig. 5: Rectangular bar

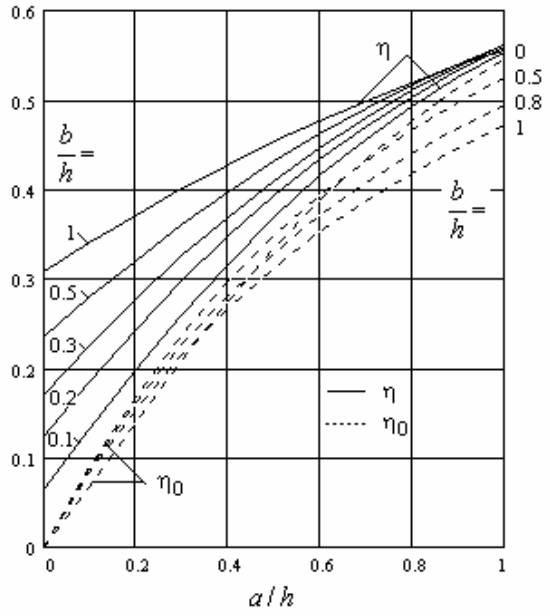

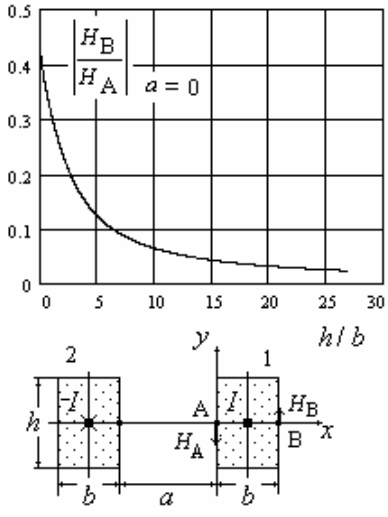

Fig. 6: Ratio of the magnetic field on the external side of the bar to the magnetic field on the internal side, for superficial and uniform distributed currents in two parallel rectangular bars, as function of *a/h* and *b/h*

We will assume a constant current density in each vertical sheet.

Using the function:

$$f(x)=\frac{2x}{h}\arctan\left(\frac{h}{2x}\right)+\ln\sqrt{1+\left(\frac{2x}{h}\right)^2} \tag{12}$$

the two ratio can be written as follows:

$$\eta=\frac{f(a+b)+f(b)-f(a+2b)}{f(a+b)+f(b)-f(a)}$$

$$\eta_0=\frac{\arctan\frac{h}{b}-\arctan\frac{h}{2a+b}}{\arctan\frac{h}{b}+\arctan\frac{h}{2a+3b}} \tag{13}$$

From the fig. 6 we can observe a small variation of the ratio of the magnetic fields on the two sides from the beginning to the end of current step injection.

4.3. Electromagnetic field in the conductor at current step injection

In the case of current step injection, the Laplace transforms of electric and magnetic field in central part of conductor satisfy the Maxwell equations:

$$\begin{cases}\dfrac{\mathrm{d}E}{\mathrm{d}x}=p\,\mu\,H\\[2ex]\dfrac{\mathrm{d}H}{\mathrm{d}x}=\sigma E\end{cases}\Rightarrow\begin{cases}\dfrac{\mathrm{d}^2E}{\mathrm{d}x^2}=p\,\mu\,\sigma\,E\\[2ex]\dfrac{\mathrm{d}^2H}{\mathrm{d}x^2}=p\,\mu\,\sigma\,H\end{cases} \tag{14}$$

In the case of thin bars, considering the ratio η of magnetic fields determined above, the magnetic field on the two lateral sides of the bar could be approximated as follows:

$$H_\mathrm{A}\approx\frac{I}{(1+\eta)h};\quad H_\mathrm{B}=\eta H_\mathrm{A}$$
$$E_0=\frac{I}{\sigma b h}\approx\frac{1+\eta}{\sigma b}H_\mathrm{A};\quad b\ll h \tag{15}$$

At the beginning of the process, when the current flows only on the surface of the conductors, the ratio η_0 must replace η in above equations.

Using the notations:

$$\nu=\sqrt{p\,\tau};\quad \xi=\frac{x}{b};\quad \tau=\mu\,\sigma\,b^2 \tag{16}$$

the solution of the equations (12) in conductor will be:

$$H(\xi,p)=\frac{H_\mathrm{A}}{p}\frac{\eta\sinh\nu\,\xi-\sinh\nu(1-\xi)}{\sinh\nu};$$
$$E(\xi,p)=\frac{H_\mathrm{A}}{\sigma b}\cdot\frac{\nu}{p}\cdot\frac{\eta\cosh\nu\,\xi+\cosh\nu(1-\xi)}{\sinh\nu} \tag{17}$$

Using the steady state electric field in conductor E_0, the Laplace transform of the transitory electric field will be:

$$E(\xi,p)=\frac{E_0}{1+\eta}\cdot\frac{\sqrt{\tau}}{\sqrt{p}}\cdot\frac{\eta\cosh\nu\,\xi+\cosh\nu(1-\xi)}{\sinh\nu} \tag{18}$$

The induction law applied to short-circuited in origin end line, gives the Laplace transform of the other end voltage:

$$U(z,p)=z\left[2\,E(0,p)+a\,\mu_0\;p\,H(0,p)\right] \tag{19}$$

where z is the length of the line.

The time constant τ of transitory electromagnetic field in 1 mm thickness copper or silver at 25 °C is ~ 75 μs.

4.4. Transitory parameters

The operational impedance of the bars at distance z from the short-circuited end results from (15)- (17):

$$Z(p)=\frac{1}{1+\eta}\left[r_\mathrm{s}\,\nu\frac{\eta+\cosh\nu}{\sinh\nu}+p\,l_\mathrm{e}\right] \tag{20}$$

where r_s is the direct current resistance of the bars and

$$r_s=\frac{2z}{\sigma b h};\quad \theta=\frac{t}{\tau};\quad l_\mathrm{e}=\mu_0\frac{a\,z}{h} \tag{21}$$

The Laplace transforms of the transitory resistance and inductance are defined as [2], [3]:

$$R(p)=\frac{Z(p)}{p}-l(0+)$$
$$L(p)=\frac{Z(p)-r_\mathrm{s}}{p^2} \tag{22}$$

From limit theorem of the Laplace transform it results

$$l(0+)=\lim_{p\to\infty}\left(p\,L(p)\right)=\frac{l_\mathrm{e}}{1+\eta} \tag{23}$$

Replacing (20) in (22) we obtain the Laplace transforms of the parameters:

$$R(p)=\frac{1}{1+\eta}\frac{r_\mathrm{s}}{p}\frac{\eta+\cosh\nu}{\sinh\nu}\nu \tag{24}$$

$$L(p)=$$

$$\frac{1}{1+\eta}\left[\frac{l_e}{p}+\frac{r_s}{p}\,\frac{\eta+\cosh\nu-(1+\eta)\dfrac{\sinh\nu}{\nu}}{p\dfrac{\sinh\nu}{\nu}}\right] \qquad (25)$$

The poles of the meromorphic function are the solution of the equation:

$$\sinh\nu=0\Rightarrow\nu_k=i\,k\,\pi\Rightarrow p_k=-\frac{(k\,\pi)^2}{\tau} \qquad (26)$$

Applying the inversion theorem, it results for the transitory resistance of the line in Ω:

$$r(\theta)=r_s\left[1+\frac{2}{1+\eta}\sum_{k=1}^{\infty}\left(1+(-1)^k\,\eta\right)e^{-(k\,\pi)^2\theta}\right] \qquad (27)$$

and for the transitory inductance in H:

$$l(\theta)=$$

$$\frac{1}{1+\eta}\left[l_e+\tau\,r_s\left(\frac{2-\eta}{6}-\frac{2}{\pi^2}\cdot\sum_{k=1}^{\infty}\frac{1+(-1)^k\,\eta}{k^2}\,e^{-(k\,\pi)^2\theta}\right)\right] \qquad (28)$$

Taking into account (2) and that

$$r_s\,\tau=2\,z\,\mu\,\frac{b}{h} \qquad (29)$$

The inductance of z – length short-circuited end line in Henry become:

$$l(\theta)=$$

$$\frac{\mu_0\,z}{(1+\eta)\,h}\left[a+2\,\mu_r\,b\left(\frac{2-\eta}{6}-\frac{2}{\pi^2}\cdot\sum_{k=1}^{\infty}\frac{1+(-1)^k\,\eta}{k^2}\,e^{-(k\,\pi)^2\theta}\right)\right] \qquad (30)$$

The inductance in direct current (at $t\to\infty$) is

$$l(\infty)=\frac{\mu_0\,z}{(1+\eta)\,h}\left[a+\mu_r\,b\,\frac{2-\eta}{3}\right]\ \text{[H]} \qquad (31)$$

We will use the following functions (fig.7):

$$\Psi(\theta)=\frac{1}{\pi^2}\sum_{k=1}^{\infty}\frac{1}{k^2}\,e^{-(k\,\pi)^2\theta}$$

$$\Psi_1(\theta)=\frac{-1}{\pi^2}\sum_{k=1}^{\infty}\frac{(-1)^k}{k^2}\,e^{-(k\,\pi)^2\theta} \qquad (32)$$

The relative values of transitory parameters,

$$\rho(\theta)=\frac{r(t)}{r_s};\qquad \lambda(\theta)=\frac{l(\theta)}{l(\infty)} \qquad (33)$$

can be written as

$$\rho(\theta)=\frac{r(t)}{r_s}=1-\frac{2}{1+\eta}\left[\Psi'(\theta)-\eta\,\Psi_1'(\theta)\right]$$

$$\lambda(\theta)=1-\frac{4\,\mu\,b\,z}{(1+\eta)\,h\,l(\infty)}\left[\Psi(\theta)-\eta\,\Psi_1(\theta)\right] \qquad (34)$$

$$\lambda(\theta)=1-\frac{4}{\dfrac{a}{\mu_r b}+\dfrac{2-\eta}{3}}\left[\Psi(\theta)-\eta\,\Psi_1(\theta)\right]$$

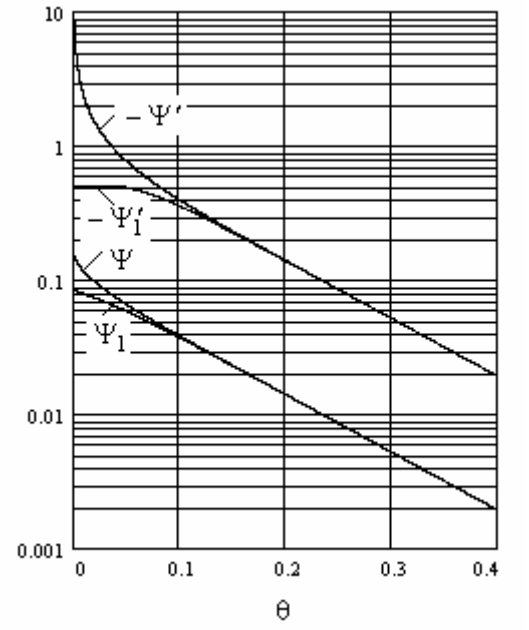

Fig. 7: Functions Ψ, Ψ_1 and its derivatives versus θ

The two transitory parameters satisfy the differential equation:

$$\rho(\theta)=1+K\,\frac{\mathrm{d}\lambda}{\mathrm{d}\theta};$$

$$K=\frac{1}{2\,(1+\eta)}\left[\frac{a}{\mu_r b}+\frac{2-\eta}{3}\right] \qquad (35)$$

The line resistance is infinity at the beginning of current injection and become equal to the direct current resistance of the conductors at infinite time. The inductance is equal to external inductance at the beginning of the connection process (the magnetic field in conductor is zero) and increase to the final value (31), equal to the sum of external and internal inductance.

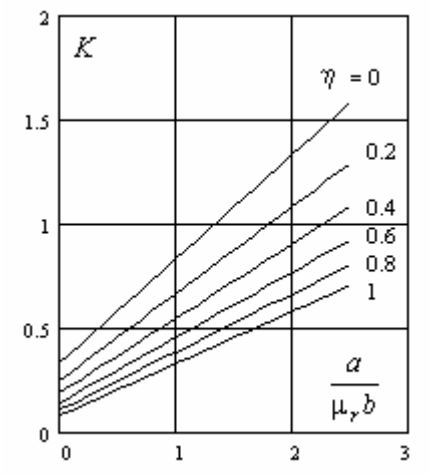

Fig. 8: Parameter *K* from differential eq. (33)

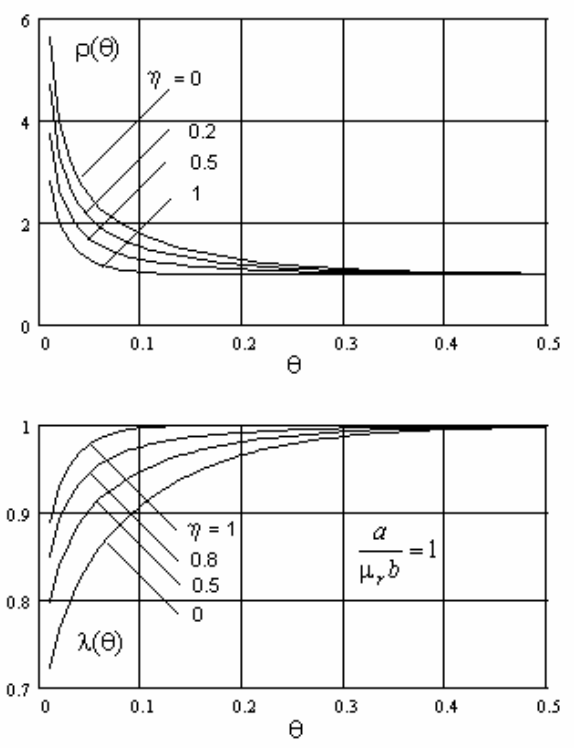

Fig. 9: Time variation of transitory parameters

From the previous figure we can see that in reality (in the case of finite height of the bars), due to the external magnetic field, the transitory parameters reach their stationary values faster than in the case of infinity high bars, when the external magnetic field is zero.

The inductance variation in fig 9 is given only for $a = \mu_r b$, for other values the last formula (34) must be used.

The equation (35) shows that the variation of the inductance is equivalent to a conductor resistance.

Conclusions

1. The design of the electrical fuse elements and their supports must take into consideration several effects, usually neglected as secondary, like the real distribution of the current in massive and large cross-section conductors. The conductor parameters and the thermal effects depends on the square power of the local current density and the dynamic effects depend also on the magnetic field distribution, which if function of the position of the back current conductors, in the vicinity of the fuse.
2. When the resistance of the variable section band is evaluated, the constriction resistance (3) must be added for each cross-section changing.
3. In the case of bent conductors or zigzag tapes the corner resistance (8) and the fig 4 has to be considered.
4. The electrodynamic forces acting on the fuse element depends on current density and the magnetic field. The local current densities for the mentioned cases can be determined using the equations (5) for the constriction or enlargement and (9) for the corners. The local magnetic field depends essentially on the position of the back current conductors, sometimes far away from the fuse.
5. The large cross-section conductors cannot be considered filiforms if the time constant τ is of the same order with the time constant of the considered processes. The real behavior of such conductors can be characterized by the transitory parameters, defined for step current injection or voltage step application. These parameters can be calculated using the equations (31), (34), (35) or evaluated from the fig. 9.

References

[1] K.J. Binns, P.J. Lawrenson, *Analysis and computation of electric and magnetic field problems*, Pergamon Press, Oxford, 1963

[2] R. Răduleț, A. Tmotin, A. Țugulea, Introduction of transitory parameters in linear electric circuits with non filiform elements and supplementary losses, Rev. Roum. Sci. tech. – Electrotechn. Energ. 16, no. 4, pp. 857-929, Bucharest, 1966.

[3] A.Țugulea, Transitory electromagnetic field in massive bus bars. Transitory parameters, (In Rumanian) *St. cerc. Energ. Electr.,* tom 22, nr. 1, pp. 67-93, Bucharest, 1972.

[4] G. A. Cividjian, A.G. Cividjian, N.G. Silvis-Cividjian, Some formulas for two-dimensional permeances, IEEE Trans. on Magnetics, vol. 36, no. 5, pp. 3754-3758, Sept. 2000.

High-voltage thin-layer fuses

Ćwidak K. [1], **Sulikowski J.** [2] and **Gregorczyk W.**[3]

Electrotechnical Institute Gdańsk Branch, Narwicka 1, 80-557 Gdańsk Poland, krzysztof.cwidak@iel.gda.pl [1],
Gdansk University of Technology, ul. Własna Strzecha 18A, 80-952 Gdańsk Poland,
and Electrotechnical Institute Gdańsk Branch, jsulik@ely.pg.gda.pl [2],
Telecommunications Research Institute, ul. Poligonowa 30, 00-991 Warszawa Poland, wojgreg@pit.edu.pl[3]

Abstract: A new design and technology of high-voltage fuses is presented in this paper. The microelectronic technology was applied to form the fuse-element shape. The arc extinguishing process in high-voltage thin-layer fuses takes place in a narrow slot between insulating plates.
The making of the fuse-element in the form of the metal layer deposited on the insulating substrate, diminishing the fuse-element sensibility to damage and improving fuse-element cooling. The arc extinction in a slot between two insulating plates makes it possible to diminish the fuse-element length and operating I^2t.

Keywords: high-voltage fuse, thin-layer fuse, fuse-link, fuse-element, characteristics

1. Introduction

The hitherto existing kinds of high-voltage fuses based on classical technologies have a number of flaws. The most important of them is the relatively long fuse-element necessary for efficient interruption of overloads and short-circuit currents. The long fuse-element increases the fuse dimensions and the power dissipation of fuses. In the case of classical fuses for small rated currents, the substantial difficulty is to obtain repeatable dimensions of a fuse-element and difficult process of assembling. Very delicate notches in the fuse-elements, often of cross-sections smaller then 0,05 mm^2, are easy to break. Thus, if the fuse-element is made in the form of a metal layer durably deposited on the insulating substrate, the fuse-element sensitivity to damage is radically diminished. As a consequence the reliability of fuse-links is improved and the width of the band of time-current characteristics is diminished. The width of the band of time-current characteristics is also diminished due to the better repeatability of cross-section of the constrictions. Using the available technologies it is possible to make the constrictions of a cross-section smaller than 0.0001 mm^2 with a tolerance of ± 3%.

It is possible to make the thin-layer fuses with ultra-quick and quick characteristics. The dimensions of such the fuse-links may be considerably smaller than the fuse-links used till now. However, to ensure compatibility with the present used fuse-bases, the authors assumed that the first manufactured fuse-links should have the external shape and dimensions of hitherto existing fuse-links.

Previously the investigations on the miniature thin-layer fuses with the fuse-element deposited on insulating substrate have been carried out in the Electrotechnical Institute Gdańsk Branch [1-3].

2. Thin-layer fuses for rated voltages above 1 kV

The main problem in high-voltage thin-layer fuse designing is to define the influence of the fuse-element shape (the number of constrictions, the distance between the constrictions, the number of parallel modules and the distance between the modules) on the breaking capacity of the fuses. Using the vacuum deposition technology for fuse-element manufacturing gives the designer freedom in the fuse-element forming. Nevertheless a very important design restriction is related to the dimensions of the glass-crystal insulating plate, on which the fuse-element metal layers are deposited. According to the manufacturer information it is not possible to make plates longer than 60 mm. This means that one plate is sufficient for a fuse-element for a voltage of up to 2.5 kV. By serial connection of the fuse-elements it is possible to obtain fuses for higher voltages, for example for 5 kV, 7,5 kV etc, i.e. a multiplicity of 2.5 kV.

In the case of d.c. fuses this level of working voltages is satisfactory because it makes possible to use these fuses in the railway traction at 1.5 kV d.c. and 3.0 kV d.c. rated voltages.

In the case of a.c. fuses it is very interesting to use thin-layer fuses of small rated currents (smaller then 1 A) for the protection of voltage transformers for rated voltages up to 6 kV.

The investigations of high-voltage thin-layer fuse models show new problems, which are not found in the classical fuses and which are related to the new unconventional fuse design. For example, the cracking of glass-crystal insulating plates during small over-currents is observed. The reason of cracking is not only the difference between the thermal expansion coefficients of epoxy resin (fuse body) and the glass-crystal plate, on which the fuse-

element is deposited, but also the resin contraction owing to the cure process (a few percent).

To increase the fuse breaking capacity of overloads currents, the classic method of partitioning of the fuse element for parallel modules (strips) was used. For working voltages higher then 2.5 kV, the fuse construction should consist of two or even three serially connected glass-crystal plates with the deposited fuse-elements. To overcome interruption problems of low overcurrents the single modules shall be connected in series which is important in the case of interrupting the overloads. The bridging of the modules at the single plate terminal makes it impossible the correct switching of the arc between the modules in the area of the whole fuse-link. This is confirmed during the breaking capacity tests.

3. Fuse design

It was assumed that due to the assembly reasons, a fuse-link should not contain more then three plates with deposited fuse-elements connected in series.

The construction of the fuse-link was extended using the additional cover-plates (Fig. 1), which considerably diminish the influence of temperature stresses on the fuse-element. These stresses are generated by thermal shrinkage of the epoxy resin during air-tight sealing process. The efficient way to prevent cracking of the plates is by separation of the resin layer from the glass-crystal plate using another insulating plates also made from glass-crystal material.

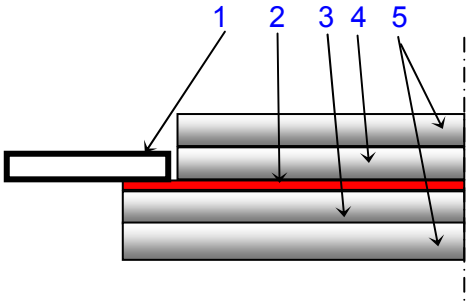

Fig. 1: The sketch of a traction thin-layer fuse after the introduction of the additional insulating cover plates – before air-tight sealing.
1 – termination, 2 – fuse-element,
3 – insulating substrate, 4 – cover plate,
5 – additional cover plates

After joining of three modules of the fuse-element (Fig.2) and solder the terminations, the fuse-element and cover plates are sealed with the epoxy resin air-tight sealing (fluidization method) (Fig.3).

The kind of shape of fuse-link was ensured by the inserting the fuse-element in the classical boron-silicate glass tube (Fig. 4).

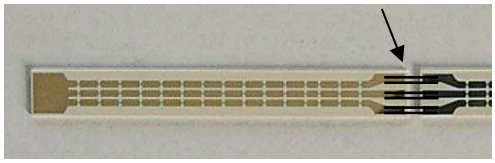

Fig.2: The insulating plate with the deposited fuse-element. The manner of joining of three modules of the fuse-element is indicated by the arrow.

Fig.3: Fuse-element of thin-layer fuse after epoxy resin air-tight sealing.

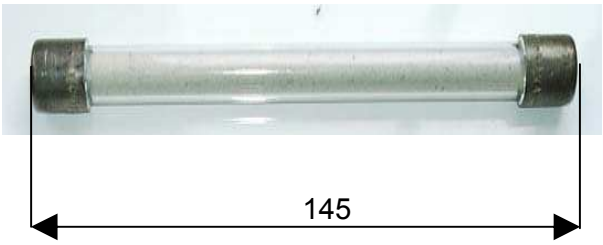

Fig.4: The traction fuse-link for the rated voltage of 3 kV d.c. and the rated current of 1.25 A.

4. Test procedure

The tests have been carried out on fuses, which were made using the new design and technology and designed for the rated voltage of 3 kV d.c. The test procedure included heating tests, breaking capacity tests, time-current characteristic tests and endurance tests.

4.1 . Heating tests

The heating tests were carried out according to the standards [4, 5]. These tests were used to estimate the rated currents, to verification of the contacts temperature rises and to evaluate the power dissipation of the thin-layer fuse-links. All test were positive. The measured power dissipations (from 2 to 6 W) were of about tens percent smaller then those presented in the catalogues of classical fuse-links.

4.2. Breaking capacity tests

The tests of high-voltage d.c. thin-layer fuses were carried out according to the Polish Standard [4], which is in principle based on the international standards for low-voltage and high-voltage fuses. These tests consist of:

- Rated breaking capacity test at the current I_1 of about 40 kA and the time constant of 9,9 ms;
- breaking capacity tests at the prospective current I_2 (critical current);
- Minimum breaking capacity test at the current I_3.

All the tested fuse-links (of a rated currents from 1.25 A to 3.15 A) correctly interrupted the I_1 and I_2 currents. The overvoltages did not exceed 13.4 kV. Fig. 5 shows the example of the records of interrupting of the prospective current I_1 by the traction thin-layer fuse.

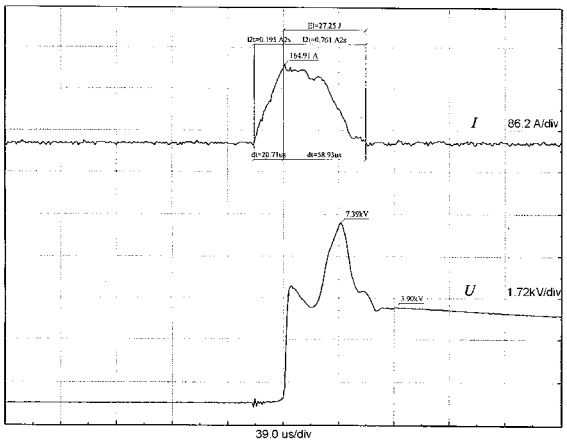

Fig.5: Records of interrupting of the prospective current I_1 of ab. 40 kA, 3.9 kV d.c., time constant 9.9 ms by the traction thin-layer fuse of the rated current of 3.15 A.

The results of the minimum breaking capacity tests were positive in a range of currents no smaller then 2.5 I_n.

4.3. Time current characteristics

There are no special requirements of the standards [4, 5] regarding the shape of the time-current characteristics for high-voltage fuses. There are only recommendations relating to it verification and plotting.

The time-current characteristics of d.c. thin-layer fuses are presented in Fig. 6. The broken lines mark the parts of the time-current characteristics, in which the fuses fait to break the current.

The difference between the rate of rise of a time-current characteristics of the fuse-links for rated current of 1.25 A and the fuse-links for all other rated currents is due to the fuse-element design.

4.4. Endurance test

There are no endurance tests listed in the standards [4, 5] for high-voltage fuses. However, with regard to the used unconventional fuse-link in new traction fuses it seems necessary to carry out the endurance test to repeated overloads. The endurance test according to IEC 60127-1 [6] and 60127-2 [7] was used as a base, because this test seems to be the one of the hardest endurance tests of the fuse-link. In this test the current of 1.2 I_n is passed through the fuse-link for a period of 1 h. The current is then switched off for a period of 15 min. This cycle is repeated 100 times. Finally the fuse-link is loaded with the current of 1.5 I_n for 1 h and the power dissipation is measured.

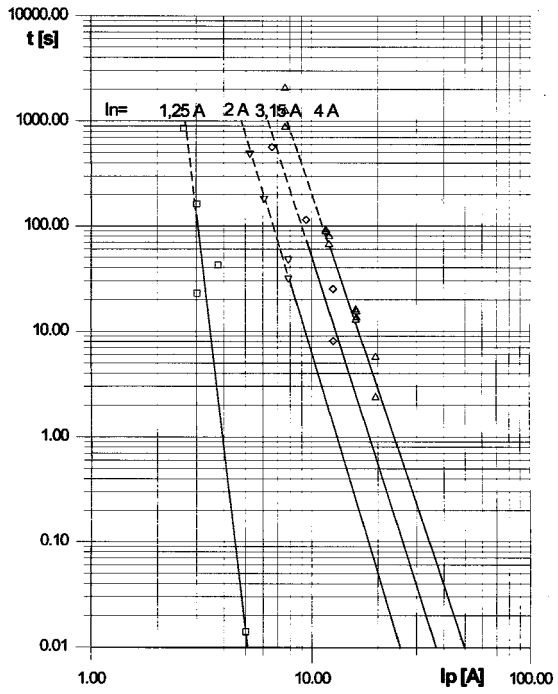

Fig.6: Example of the time-current characteristics of d.c. high-voltage thin-layer fuses.

The endurance test was performed only on the fuse-links of the highest rated current because these fuse-links are exposed to the highest temperature rises. During the cycles the condition of fuse-element was monitored by the measurement of the power dissipation before the end of same overload periods. Any ageing of fuse-element was noticed during the load current of 1.2 I_n. It was observed that the power dissipation diminish during endurance tests, which means diminishing of the fuse–element resistance. It was probably due to recrystallization of vacuum deposited metal layers of the fuse-element. After finishing the overload cycles the resistance of the fuse-links was measured again and the control test was performed on one of the tested fuse-links. This fuse-link was loaded with conventional non-fusing current of 1.5 I_n for 1 h and next with conventional fusing current of 1.9 I_n. The tested fuse-link did not operate during conventional non-fusing current and the pre-arcing time measured during conventional fusing current was no shorter then the pre-arcing time

of fuse-links which were not subjected to the endurance test.

As there was no noticed any ageing of the fuse-element, the endurance test was continued with the current raised to 1.5 I_n. Next 100 overload cycles were performed. After finishing the overload cycles test the resistance of the fuse-link was measured and the control test was performed. This fuse-link was loaded with the conventional fusing current of 1.9 I_n. The pre-arcing time measured for the conventional fusing current was insignificantly shorter than that of fuse-links which were not subjected to the endurance test. This means the possibility of initiation of ageing process.

As a summary of the endurance tests one can say that it is possible to state that the fuse-links with thin-layer fuse-elements are resistant to ageing process when loaded with the rated current and small overcurrents.

5. Conclusions

The design of high-voltage thin-layer fuses radically differs from that of existing fuses. The new technology makes it possible not only to improve technical parameters of the fuse-link but also to diminish fuse dimensions.

The essential limitation for high-voltage thin-layer fuses is the rated voltage, which should no exceed 3 kV d.c. and 6 kV a.c. Also the rated currents should not be higher then 3.15 A. The design of the thin-layer fuses for the rated voltages exceeding 3 kV d.c. and 6 kV a.c. causes essential assembling difficulty which considerably enlarge costs of production. On the other hand the design of the thin-layer fuses for rated currents exceeding a few amps makes it necessary to deposit the fuse-element layer exceeding 1.5 μm in the thickness. The tests show that in this case the benefits from arc quenching in narrow slot between glass-crystal plates are lost. The enhanced quantity of silver vapour created during the arc quenching process is not absorbed by the structure of glass-crystal material. It is possible to design thin-layer fuses for very small rated currents (considerably smaller then 1 A), which is very difficult in the case of classical fuses.

The thin-layer fuses may be manufactured as fuses of ultra-quick and quick time-current characteristics. As the thin-layer fuses have very small I^2t (Joule's integral) it is possible to use them for the protection of semiconductor devices. Due to the very fast recovery of electric strength, the thin-layer fuses could be particularly useful in d.c. circuits.

Acknowledgements

The work has been carried out in frames of the research project 8T10A 02620 financed by the Committee of Scientific Research in Poland.

References

[1] Sulikowski J., Ćwidak K. and Ossowicki J.:"Miniature layer fuses of high breaking capacity", *ICEFA* Turin 1999, p.289.
[2] Sulikowski J. and Ćwidak K.:"New method of overload currents quenching in miniature layer fuses". SAP Łódź 2001, p. 296.
[3] Sulikowski J., Ćwidak K. and Gregorczyk W.: "New miniature layer fuses of quick and ultra-quick time-current characteristic". *XXVI Int. Conf. of International Microelectronic and Packaging Society*, Warsaw 2002, p. 198.
[4] PN-E-06172:1999 "Bezpieczniki topikowe trakcyjne prądu stałego na znamionowe napięcia od 1000 do 3000 V. Bezpieczniki ograniczające prąd. Wymagania i badania" (D.C. electric fuses for traction purposes for voltage ratings 1000 ÷ 3000 volts – Current-limiting fuses – Requirements and tests).
[5] IEC 60282-1 "High-voltage fuses – Part 1: Current-limiting fuses".
[6] IEC 60127-1 "Miniature fuses – Part 1: Definitions for miniature fuses and general requirements for miniature fuse-links".
[7] IEC 60127-2 "Miniature fuses – Part 2: Cartridge fuse-links".

ARC IGNITION PROCESS IN SHORT FUSE ELEMENTS

Jozef CZUCHA

Gdansk University of Technology, 80-952 Gdansk, ul. G.Narutowicza 11/12, Poland,
jczucha@ely.pg.gda.pl

***Abstract**:* Research on short fuse elements, approx. 1 mm in length, allows for analysis of the disintegration process at the stage of of single elementary gaps in the fuse element. Examinations were performed at a current density of 4...150 kA/mm^2. It was shown that arc voltage at a single gap, during arc ignition, does not exceed 30 V. Higher values observed are a resultant value of arc ignition voltages at a larger number of very short (0,04 .. 0,12 mm) segments of arcs between fragments of the fuse element material, connected in series. These examinations confirm the two-stage character of fuse element disintegration. The first stage, with a considerably shorter module of disintegration is caused by an electro-thermo-hydro-dynamic mechanism. Next, longer channels of electrical arc discharge are formed after neighbouring segments of elementary short arcs from the first stage of fuse element disintegration join together one by one. The average module of fuse element disintegration becomes longer, while the unitary voltage of a segment of the fuse element's current circuit decreases. Results of examinations allow us to modify some earlier hypotheses on fuse element disintegtration and contribute new numerical data characterising these phenomena.

Keywords: electric fuse, arc ignition voltage

1. Introduction

The active area of operation of a fuse includes current values above fusing current, which corresponds to the current value at which curcuit – fuse element continuity is lost. The fuse element is most often made from conductive materials: copper or silver. Many research works were made to explain the mechanism of fuse element disintegration at current flow above fusing current value. It was noted [1, 2,] that the mechanism of fuse element disintegration depends mainly on the intensity of the energy accumulation process, i.e. the power P_F of energy transformations in the fuse element's environment. The power P_F depends on the intensity of the current I_F flowing through the fuse element, and on the physical properties and dimensions of the fuse element. To determine the properties of fuse element disintegration, we most often use the parameter of current density j_F of the fuse element. With high dynamics of current density increase in the fuse element, dynamic energy transformations take place in the fuse element material. Phase transformations, as well as movements of the fuse element material can take place, leading to deformation of its original shape. This forces a dynamic change of the elastic thermal and electromagnetic field of the circuit segment. These are effects mutually dependent in the area and they can lead to instability of particular states. A characteristic symptom of this instability is disintegration of the fuse element.

The droplets disintegration mechanism in the fuse element, taking place at small current overloads has been well examined, while striated and chaotic disintegration mechanism, which take place at large overcurrents, have been extensively described in literature, but are not yet been fully known.

In recent times, two large state of research works have been published, treating this issue. Wolny [3] cites many results from his own and other scientists' research, around 300 bibliographic items, explaining the process of current cut-off, including that in fuses. This literature treats mainly effects taking place in the macroscopic scale, e.g. a long fuse element of various short-circuit conditions corresponding to electrical power circuits of AC 50 (60) Hz or DC with typical values of the time constant for short-circuit currents (7,5 ...30 ms). The second research work, by Jakubiuk [4], is a very deep study of the physical effects taking place in a fragment of the current circuit in which there is an extremely high concentration of energy connected with flowing current. In these conditions, the physical segment of the circuit simply explodes.

Table 1 shows conventional current values, marked I_p and I_{SSS}, respectively, in several types of circuits, which correspond to assumed rates of current increase. The I_p current is the value of (RMS) expected short-circuit current, while the I_{SSS} current is the conventional maximum switching current value for a Solid State Switch in a power electronics converter. In classical electric circuits, rates of current increase do not exceed approx. 20 ... 50 A/μs. Physical effects taking place in a disintegrating fuse element in these conditions, are usually assessed on the basis of an analysis of oscillograms of the voltage at the fuse element (usually long) and on the basis of the condition of the fuse element after the current has been cut off.

Prospective short circuit current: I_p- in an AC (f - frequency), or DC (T - time constant) and I_{SSS} – for Solid-State-Switches (SSS) in power electronic converters ($T/2$-half period time for free oscillations circuits, t_r – SSS switching on time) for the rate of the current di/dt

di/dt *[A/[μs]*		0,5	1	2	5	10	20	50	100	200	500	1000
		I_p *[kA]*										
f *[Hz]*	50	1,13	2,26	4,52	11,3	22,6	45,2	113	225			
	60	0,93	1,87	3,74	9,95	18,7	37,4	93,5	187			
T *[ms]*	30	15	30	60								
	15	7,5	15	30	75							
	7,5	3,75	7,5	1`5	37,5	75						
		I_{SSS} *[kA]*										
T/2*[ms]*	1	0,16	0,32	0,64	1,6	3,2	6,4					
t_r *[μs]*	5	0,0025	0,005	0,01	0,025	0,05	0,1	0,25	0,5	1,0	2,5	5
	1	0,0005	0,001	0,002	0,005	0,01	0,02	0,05	0,1	0,2	0,5	1

Works – dating from 1960-1970, by Lipski [1], Hibner [5], Nasiłowski [2] and other scientists examining X-ray photos of fuse elements after the current was cut off, and by Arai [6], Fansler, Shear [7], and others, who took X-ray pictures of particular phases of fuse element disintegration – are commonly known. The image of the fuse element in the pictures was proof of a particular type of fuse element disintegration. The full mechanism of disintegration during large overcurrents was not, however, assessed. Lipski [8] was the author of the hypothesis, that during the initial phase, the fuse element breaks up into a larger number of segments than can be seen in the final form of the use element, after the current has been cut off. Jakubiuk [4,9,10] gave the theoretical bases for the fuse element's initial and secondary disintegration at high current densities.
Presented below are selected results of examinations during the initial phase of arc ignition in a fuse element, at a high rate of current increase.

2. Research

As was mentioned above, numerous authors examined the characteristics of fuses, which had a (high) ability to limit and cut-off fault currents in a cicuit with a rated voltage U_e, of e.g. 500 V, 3 kV and more. In such conditions, voltage in the fuse reflects the sum of voltages of a dynamically changing number of arcings in the elementary gaps of a long segment of a fuse element.
Fig.1 gives an example of current trace $i_F(t)$ and of the voltage $u_F(t)$ in the fuse element in a circuit with a rated voltage U_e = 4 kV DC and with a current increase rate $di_F/dt \approx 5$ A/μs. If we use oscillogram descriptions of voltage at the fuse during current cut-off as criteria, the voltage trace $u_F(t)$ in fig.1 has the following description: line segment 0 - 1 – increase of voltage in the heating fuse element; line segment 1 - 2 – 3 – arc ignition voltage, line segment 3 - 4 – arc voltage. Assessment of the voltage trace $u_F(t)$ in details regarding the arc ignition mechanism in individual gaps in this oscillogram is impossible.

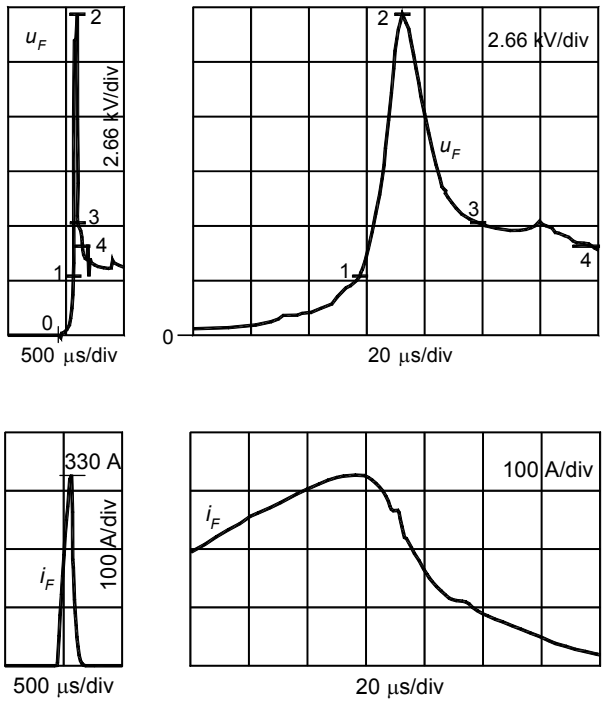

Fig.1: Example of voltage u_F and current i_F
3 kV DC / 3 A fuse in 4 kV, 40 kA / 25 ms short circuit test

E.g. a certain type of fuse, for a voltage U_e = 4 kV DC had an element with a total length $l_F \approx 600$ mm, while the length of an elementary segment of conducting plasma λ_e between particular segments of the disintegrating fuse element was $\lambda_e \leq 0{,}15$ mm, and the number n_e of such stochastically distributed and dynamically variable elementary arcing segments exceeded $n_e \geq 500$. The dynamic voltage characteristic $u_F(t)$ of the fuse element conduction during operation results not only from a time-variable balance of the energy that is delivered to the fuse element, and from the conditions (cooling, generally), but is also determined by the "lifetime" dynamics – the appearance and disappearance – of particular segments of short arcs.

If the fuse element length is large, compared to the module of fuse element disintegration in a given sample, then the mechanism of its disintegration does not depend on its length. Therefore, when conducting research on a short fuse element, it is possible to image the physical effects taking place in the elementary fuse element segments with much higher resolution. The dynamics of current changes in electrical circuits (table 1) are relatively small, compared to the dynamics with which particular gaps appear (single μs), therefore, in research on short fuse elements, the rate of increase of the expected short-circuit current should be kept the same as for examinations of long fuse elements. Since the examinations regard a very short interval of time for the appearance of a particular gap in the fuse element, it can be assumed [3,4], that the environment surrounding the fuse element does not have a large influence on the arcing process.

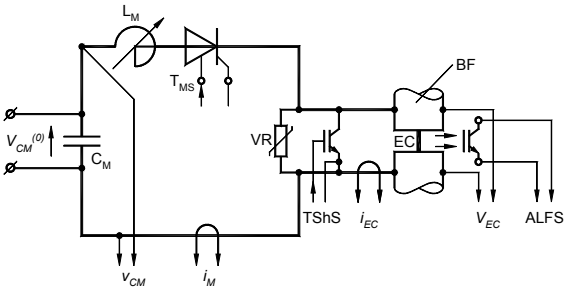

Fig.2. Test circuit diagram. C_M- capacitive source of energy, T_{MS}- thyristor making switch, EC – exploding short fuse element, TShS – transistor shunting switch, VR – ZnO varistor, ALFS – arc light flux sensor, BF – fuse base

Fig.2 shows an equivalent circuit diagram of a test circuit for examining the properties of disintegration of a short fuse element. This is a circuit with a capacitive source of electric energy C_M with adjusted initial voltage $U_{CM}^{(o)}$. Current increase rate in the circuit was set by inductor L_M. The short circuit making switch *TMS* was a thyristor switch. The examined segment of the short fuse element *EC* l_{EC} = 1 mm was placed in the fuse base BF. Parallel to the fuse element *EC* , a very fast transistor shunting switch *TShS* was connected, that could be used at any moment t_1, with an accuracy of +/- 1 μs, to force current commutation from the *EC* branch to the *TShS* . Current commutation from *EC* to *TSh*S allowed for a controlled stopping of energy flow to the fuse element *EC*. Assessment of the results of the current flow through the fuse element was possible until the instant t_1. After the the transistor switch *TrSh* was cut off, current i_M commuted to the branch witih the varistor *VR*. In this way, it was possible to shape the transient recovery voltage $u_{EC(TRV)}$ at the fuse element gap.

Fig. 3 shows examples of oscillograms of short fuse element examinations in a test circuit similar to that in Fig .2. Similarly to the oscillograms on the left side of fig. 3, there is no visible any difference in the voltage trace. However, if we stretch the time scale - the oscillograms on the right hand side, we see the differences. Table 2 gives a detailed description of the oscillogram in Fig. 3.b.

An original result of these examinations is documentation of the voltage increase in the fuse element in certain conditions caused by practically a single fuse element disintegration. In this research, details regarding the influences of the fuse element material, current density, current variability or other factors on the arc ignition mechanism during disintegration were not analised.

a)

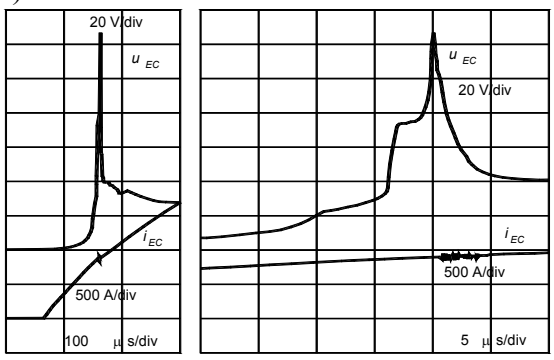

b)

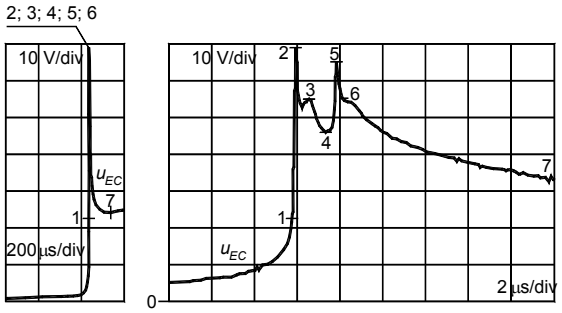

Fig.3. Short fuse elements, l_F = 1 mm, test results: a) – Φ 0,1 mm Cu, di/dt ≈ 100 A/μs; b) – 0,1 x 1 mm Ag, di/dt ≈ 25 A/μs – details in tabl.2.

Table.2. A description of physical effects taking place in the current circuit of a fuse element during dynamic current increase i_{EC} (oscillogram in Fig.3b)

Instant/ time interval	Description	Characteristic features	Result in the current circuit EC	Number of gaps n_e
0	current switched on (TMS making)	di_{EC} / dt = 4A/μs dj_{EC} / dt = 40 A/mm^2 μs	increase of temperature, resistance, deformation of shape and cross-section of the EC circuit,	0
0 – 1	voltage increase in the heating fuse element			
1	rapid increase of voltage increase rate	du_{EC} / dt = 450 V/μs	loss of EC circuit continuity – first EC disintegration – a plasma conductivity channel forms	
1 – 2 (0,15 μs)	increase of voltage decrease rate in the EC curcuit	$\Delta u_{EC\,(1-2)}$ = 46 V two (serial) gaps appear	electro-thermo-hydro-dynamic deformation of the EC, appearance of local constrictions of the material, weakening of atomic bonds, increase of internal pressure of the EC matter	2
2	change of voltage increase trend	u_{EC} voltage drops rapidly	as a result of electro-thermo-hydro-dynamic forces, one gap "sticks" back together	1
2 – 3 (0,1 μs)		$\Delta u_{EC\,(2-3)}$ = 20 V; du_{EC} / dt = 200 V/μs		
3		„quasi-oscillatory" variation of voltage	„quasi-oscillatory" character of electro-thermo-hydro-dynamic forces causes the appearance / closure of two neighboring gaps, further deformation of the fuse element material	1 → 2 → 1
3 – 4 (0,45 μs)				
4	rapid increase of voltage	steep increase of voltage $\Delta u_{EC\,(2-3)}$ = 23 V; du_{EC} / dt = 200 V / μs	a „new" gap appears	2
4 – 5 (0,12 μs)				
5 – 6 (0,18 μs)	change of voltage increase trend voltage decreases	u_{EC} voltage drops rapidly $\Delta u_{EC\,(2-3)}$ = 14 V; du_{EC} / dt = 130 V/μs	as a result of electro-thermo-hydro-dynamic forces, one gap "sticks" back together	1
6		instability of voltage decrease tendency	instability of EC conductivity: oscillation of matter between successive gaps (?)	1 → 2 → 1
6 – 7 (≥ 30 μs)	slow decrease of voltage to "quasi-steady" state	arc voltage „stabilizes" $u_{EC\,(7)}$ = 24 V;	the electrode bases of the arc come close to the terminals, "constant" arc cooling conditions	1

On the basis of many measurements, it was noted that elementary increase of voltage at a single gap of the disintegrating Cu or Ag fuse element, with fuse element current density j_{EC} within the examined 4 ... 150 kA / mm^2 interval, was approx. $u_{EC}^{(n)}$ = 20...30 V. On the basis of an analysis of the balance of electrical energy delivered to the examined fuse elements and the given physical properties of the fuse element materials, the amount of exploding matter Δm_e, was calculated and converted to a linear measure of the length of a single elementary gap λ_e in the fuse element material, called metallic plasma, or, more often, an arcing discharge. Results were obtained, indicating that the length of an elementary gap during fuse element disintegration at current densities j_{EC} within the examined 4 .. 150 kA / mm^2 interval and fuse element cross-section area s_{EC} = (0,008 ... 0,1 mm^2) equals λ_e = 0,04 ... 0,12 ... mm.

Fig.4 shows examples of an analysis of phase transformations of the mass m_x of a fuse element EC at successive instants t_x during disintegration of a Cu Φ 0,1 mm l_{EC} = 1 mm fuse element, oscillogram in Fig.3.a. This is a considerably smaller value than the one given by Hibner [5], Nasiłowski [2], Vermij [11] and others. On the basis of the high value of voltage during the initial phase of current cut-off and the number of fuse element gaps observed after current

cut-off, the value of arc ignition voltage was given for a single elementary gap – as over 50 ..200 V. This was explained, mistakenly – in the author's opinion – by "overvoltages at the inductance of the short-circuit".

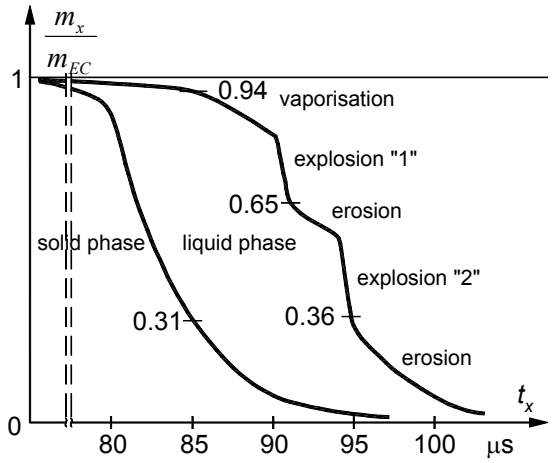

Fig.4 Phase transformation of mass m_x of a fuse element l_F = 1 mm, Φ 0,1 mm Cu at successive instants t_x

Very interesting results, with photos of a disintegrating fuse element, made at mocrosecond time intervals, together with an oscillogram of voltage and current, was presented in [7]. The number of fuse element disintegrations calculated for this oscillogram, corresponding to the instant of maximum voltage in the fuse element, n_a equalled approx. 480, the length of the module of elementary arcing discharges, λ_e = 0,04 mm (at voltage of the n-th gap $\Delta u_{EC}^{(n)}$ = 30 V). Due to the high rate of voltage increase, fuse element disintegration was almost simultaneous along its entire length, which is why such high rates of increase of voltage were observed during the initial phase of disintegration of fuse element EC. Some authors call this chaotic disintegration. In the author's opinion, low resolution of X-ray photography does not allow for observation of such short (regular!) gaps along the fuse element.

The above-mentioned hypothesis of Lipski and the results of the theoretical analysis of the more complex mechanism of fuse element disintegration by Jakubiuk have not – so far - been unequivocally confirmed experimentally.

Selected characteristic results of examinations and calculations regarding the fuse element and test circuit are given in Table 3. Results with the index *R* (***R****eference)* treat calculations made in accordance with principles given in literature, while those with the index *T* (***T****est)* treat results obtained by the author in the course of his own research.

It is worth noting, that while analysing the example oscillogram in Fig.3.a, the result of appearing of successive fuse element disintegrations at two successive instants, marked *2* and *5*, and approx. 1,9 µs away from each other, can be also be seen in the form of voltage increase by around 50 V. each. The value of this voltage increase indicates the simultaneous appearance of two microdisintegrations. The appearance, as well as the disappearance of particular gaps is the result of the balance of energy transformations in the fuse element current circuit. Hence, their dynamics are similar – rate of voltage increase during the appearance and during the disappearance of a gap have a similar value.

Table 3. Test (T) and calculation (R) results for the EC tested

Type of EC			Φ 0,1 mm, Cu		0,1 x 1 mm, Ag
$I_{EC(1expl)}$	A	*T*	840	1320	2030
$j_{EC(1expl)}$	kA/mm^2		107	170	22,7
di_{EC} / dt	A/µs		10	43	2,5
dj_{EC} / dt	A/µs.mm^2		1,25	4,3	40
$s^2_{EC}.K$	A^{2}s	*R*	6,08		583
$I^2t_{(0-1expl)}$	A^{2}s	*T*	23,1	22,8	2690
$W_{(0-1expl)}$	Ws		0,33	0,363	1,38
$\Delta W_{(n\ expl)} / n_{expl}$	Ws		0,12 / 2 = 0,06	0,118 / 2 = 0.059	0,202 / 2 = 0,101
λ_e @:s_{EC} = const; h_{gb} = const	mm	*T+R*	0,15	0,145	0,05

s^2_{EC}.K- (square) EC cross section times Mayer's constant; $I^2t_{(0-1expl)}$ parameter value for the time to the first explosion of EC take place; $\Delta W_{(n\ expl)} / n_{expl}$ - only n - explosions energy; λ_e – average length of n-th arcing (disruption); h_{gb} – specific enthalpy of the gaseous phase in boiling temperature

4. Conclusions

An analysis of short fuse element voltage and current allows for observation of single fuse element disintegrations during high density current flow.
Elementary, very rapid increases of voltage can be observed in the fuse element, with a repetitive (in the sense of measured current densities of approx. 5 ...150 kA/mm^2 at the instant of disintegration) $\Delta u_{EC}^{(n)} = 20...30$ V values with a rate of increase of a single gap approx. $du_{EC}^{(n)} / dt = 30 ... 50$ V/μs.
The number of elementary segments n_e of the fuse element with an ignited arc, whose measure is the instantaneous voltage value u_{EC}, is variable in time. Increase of voltage (the number of gaps) is proof of the appearance of further disintegrations while electrical energy is delivered to the fuse element area. Decrease of voltage (the number of gaps) is a result of axial thermo-hydro-elastic forces on the elementary fragments of matter (in solid and/or liquid state) causing short circuiting of neighboring segments. This is a dynamic process, dependent on the parameters of the electrical energy and properties of the fuse element.
The voltage observed at the terminals of the real fuse base is the sum of decreases of voltages on a dynamically changing number of elementary arc segments characteristic for the fuse element material and the flowing current, whose number, in an extreme case, may come down to $n_e = 1$. Then, the arc characteristic determines the voltage in the fuse in a given specific solution of the fuse element cooling conditions.
In the time interval of dynamic changes of voltage, a model of a fuse should be built, based on a circuit diagram consisting of a number (variable in time) n_e of voltage sources with the voltage value of one gap, in conditions similar to those in the research, $\Delta u_{EC}^{(n))} = 20 ... 30$ V.
It is necessary to perform further research in order to determine the parameters of fuse element disintegration in other conditions: the fuse element material, current density and the material directly adjacent to the exploding fuse element.

References

[1]. Lipski T.: Low voltage electric fuses. (in polish) Warszawa, WNT, 1968

[2]. Nasilowski J.: Unduloids and striated disintegration of wires. Exploding Wires, vol.3. New York, Plenum Press, 1964, p.295

[3]. Wolny A.: Current breaking through commutation. Technical Univ. of Gdansk Publishing, Poland, 2001

[4]. Jakubiuk K.: Electrical explosion and implosion of conductors. Technical Univ. of Gdansk Publishing, Poland, 2000.

[5]. Hibner J.: The number of arcs initiated during striated disintegration of uniform strip h.b.c. fuse elements at A.C. short-circuit current interruption. Int. Confer. On Electric Fuses and their Applications, Trondheim (Norway),1984.

[6] Arai S.: Deformation and disruption of silver wires. . Int. Confer. On Electric Fuses and their Applications, Liverpool (UK),1984

[7]. Fansler K.S., Shear D.D.: Correlated X-ray and optical streak photographs of exploding wires. Exploding Wires,vol.4. New York, Plenum Press, 1968,p.185

[8]. Lipski T.: On the theory of the striated fuse-wire disintegration. Trans.IEEE, vol. PS-10, No.4, 1982.

[9]. Jakubiuk K.: Striated disintegration of exploding wires (in polish; Mechanizm rozpadu prążkowego eksplodujących przewodów). Zesz. Nauk. Politechn. Gdańskiej, Elektryka, No.75, Gdańsk, 1994.

[10]. Jakubiuk K.: Secondary stritation during fuse-elements disintegration. . Int. Confer. On Electric Fuses and their Applications, Torino, (Italy), 1999

[11]. Vermij L.: Electrical behavior of fuse elements. Doct. Thesis, Technical Univ. of Eindhoven, (Netherlands), 1969.

NH/HH-Recycling

Verein zur Förderung des umweltgerechten Recycling von abgeschalteten NH/HH-Sicherungseinsätzen e.V.

- Protecting our environment -
Environmentally compatible recycling of high performance fuse links

Claus Deußer
NH/HH-Recycling
Germany

Everyone knows how important the environment is to us all and how we must all do whatever we can to help protect it. Industry too has an important role to play, not only by employing manufacturing processes that cause as little harm as possible to the environment in the first place but also by ensuring that when its products come to the end of their lives they can be disposed of safely and efficiently.

The task of the Verein zur Förderung des umweltgerechten Recycling von abgeschalteten NH/HH-Sicherungseinsätzen e.V., a non-profit association established by German fuse manufacturers, is to process the various materials of which fuse links are made so that they can be returned to the cycle of manufacture for further use. In 2002, for example, the association collected and recycled more than 160 tonnes of materials. It is currently estimated that, in Germany alone, this figure could be increased to around 1400 tonnes. Other manufacturers and users are being encouraged to participate in the project.

The practice of simply disposing of old products at the refuse tip without a moment's thought for their recycling potential is not only frowned upon these days from the point of view of social responsibility for future generations but, in many cases, it is actually illegal too.

The law demands environmentally-compatible recycling and disposal

Article 1 § 22 of the German legislation on environmentally-compatible recycling and waste disposal states that products must be designed in a way which, at the end of their service life, allows the materials which they are made of to be recycled and any waste disposed of in an environmentally-compatible manner. Another requirement of the legislation is that products must be returnable and any recyclable waste must be used again.

Since most products are made of a very wide variety of different materials it is no easy task to take them apart and recycle each raw material separately. Plastics, for example, are often joined by thermowelding processes whereas other parts are either screwed, bolted, soldered, welded or bonded. This means, of course, that disassembly is very labor-intensive and therefore costly. In addition, the process of disassembly also has its dangerous side, such as when asbestos gaskets, glass-fiber-reinforced plastic parts, solders containing harmful substances, etc. have been used in the original items.

Recycling symbols clarify matters for users

Environmental protection and waste disposal do not come free-of-charge so a thorough fundamental analysis must be carried out first in order to determine whether recycling, disposal or separation is the most appropriate course of action as far as the environment and safety are concerned. For example, if the process of recycling consumes more energy than the manufacture of a new product it is obvious that an alternative solution will have to be found. Also, the environmental legislation in Western Europe is stricter than elsewhere so inevitably it becomes a factor in the commercial market-place involving, say, our competitors in Asia. This means that it is important for the customer to be made aware

of the reason for any higher price that might be involved. Consequently, it is necessary to identify the products as having been manufactured by environmentally-compatible processes and being suitable for disposal by environmentally-compatible means - "recycling symbols" are used.

As far as the electrical industry is concerned, a ground-breaking initiative has been taken by the German manufacturers of low-voltage and high-voltage high-breaking-capacity fuse links. Even before the most recent German legislation on recycling came into force customers had begun asking the manufacturers of fuse links if they could set up a methodical system which would allow used fuse links to be returned for environmentally-compatible disposal. As a result, several fuse manufacturers began offering and charging for a disposal service for used fuse links. Then, in 1995, with the aim of putting the subject of environmentally-compatible disposal on a regular footing, a number of the manufacturers involved (Fritz Driescher KG, EFEN GmbH, Lindner GmbH, Jean Müller GmbH, M. Schneider-Annaberg GmbH, Siba GmbH and Siemens AG) joined forces with the ZVEI (Zentralverband Elektrotechnik- und Elektronik-industrie) and, through an initial working party, established the non-profit-making "Verein zur Förderung des umweltgerechten Recycling von abgeschalteten NH/HH-Sicherungseinsätzen", otherwise known as "NH/HH-Recycling", registered in Regensburg and with its Head Office in Frankfurt.

Recycling the products and materials of 20 years ago

For many applications, fuse links represent a relatively cheap and safe way of providing protection for electrical systems and equipment. L.v. h.b.c. (NH) fuse links (low-voltage high-breaking-capacity) are used in low-voltage installations and h.v. h.b.c. (HH) (high-voltage high-breaking-capacity) fuse links in medium-voltage installations. The volume of the l.v. h.b.c. fuses varies between 45 and 900 cm^3 (5 to 15 cm long and 3 to 10 cm wide). The h.v. h.b.c. fuses, on the other hand, are substantially larger: 20 to 65 cm long and 5 to 8.5 cm in diameter. The service life of these fuses, provided they are not called upon to blow, is approximately 20 years, which is well above the average life of most other types of electrical equipment. This means that, with these long-life products, recyclers are having to deal with materials that were in common use 20 years ago. In "old" fuse links, for example, asbestos was still being used as a jointing material. Fig. 1 shows a cross section through an l.v. h.b.c. fuse link and lists the other materials used in its construction; similarly Fig. 2 illustrates an h.v. h.b.c. fuse link.

Structure of an LV HRC fuse link

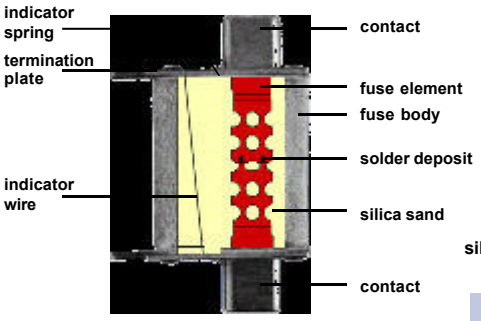

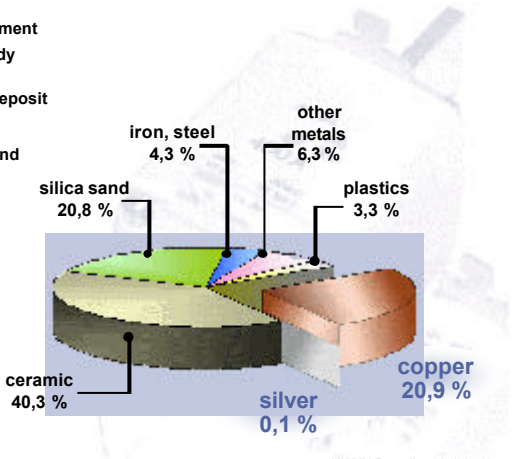

- Values averaged over all sizes and types
- Depending on the year of construction and type, there may be slight amounts of cadmium (solder) and asbestos (seal)

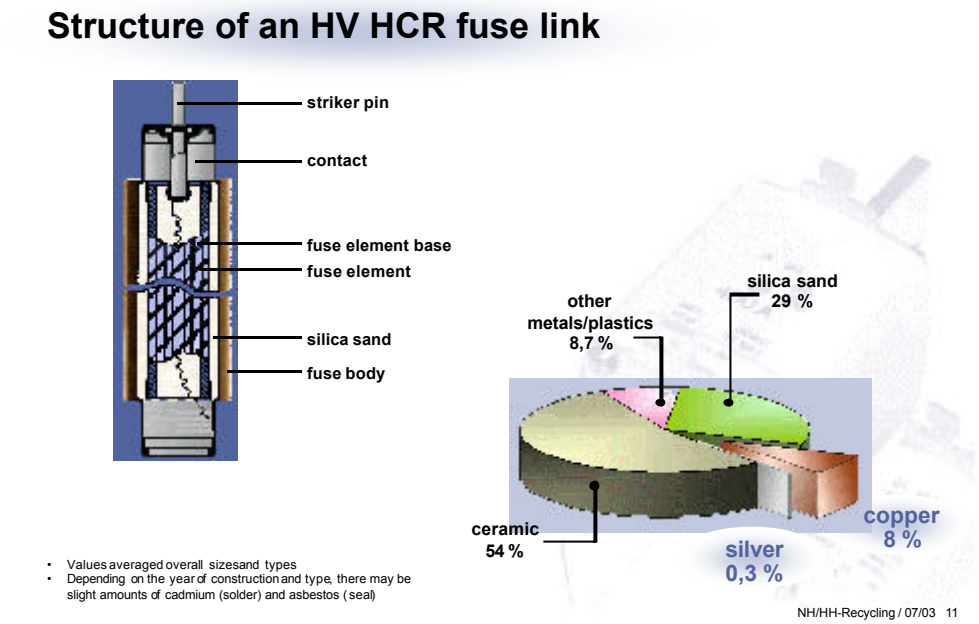

The result: copper, silver and materials for the building trade and the chemical industry

The percentages of different materials also listed in Fig. 1 show that the recycling and re-use of copper and silver is thoroughly worthwhile and, as ”valuables”, do not deserve to be included amongst the residual waste or dumped on the refuse tip. The classic alternatives of disassembly or shredding offer the possible means by which the materials can be recovered.

Although disassembling these fuse links is a labor-intensive process, some successful projects have been set up, e.g. with power utilities and disabled people’s organizations working together, in which the fuses are disassembled and the valuable materials they contain recovered so that they can be returned to the manufacturing cycle. The actual cost of disassembly is not covered by the profit obtained from the raw materials so the disabled people’s organizations have to make a small charge for each fuse. The asbestos joint gaskets mentioned previously also cause some problems with disassembly.

The strict rules that apply when working with asbestos make disassembly a complex and costly process - as also is shredding or processing by pan grinder (a crushing process producing coarser results than a shredder) with subsequent melting down in the blast furnace. This situation has led to further tests being carried out in conjunction with a copper smeltery which have demonstrated that fuse links can be processed directly in a converter without any pre-processing at all. Under normal circumstances it is necessary to add quartz sand during the process in order to produce slag and promote the precipitation of iron. Since the fuse links that are being melted down already contain around 30% quartz sand, however, this ”waste product” actually helps in the process.

Following an inquiry among various copper smelters and recycling companies throughout the country, the Norddeutsche Affinerie in Hamburg was eventually chosen because of its capacity and environmental capabilities. As a second waste handler the NH/HH-Recycling entered into a contract with the copper smelter Brixlegg, Austria.

For direct processing in copper converters the fuse links must normally satisfy the following specification:

- Plastics content less than 3.5%
- Asbestos content less than 0.05%
- Cadmium content less than 0.005%

The plastics are utilized to produce heat with continuous monitoring of the flue gas. During the melting, any zinc that originates from, say, brass contact blades is converted into zinc dust and collects in the plant filters. However, this is not a problem provided the total amount of zinc remains below 50 tonnes per annum - as it will given the total amount of recycling anticipated. The ceramic body of the fuses and the quartz sand are converted to slag that can be used again for road building and in the concrete industry. Another end-product, sulfuric acid, can be re-utilized by the chemical industry. The asbestos is rendered harmless by being incorporated into the slag.

Research benefits from the profits

Most of the l.v. and h.v. h.b.c. fuse links come from the country's power utilities and general industry. They are usually collected in "egg box" pallets placed at specified collecting points. The various sales organizations, which also function as collecting points, provide information for smaller users, such as electrical contractors and installers, on the recycling facilities that are available. Danzas, with branches all over Germany, has been awarded the contract for collecting the egg-box pallets when they are full and transporting them to the company's own buffer store. When a collecting point has full pallets to be collected it notifies the transport company by fax and the pallets are then collected within three days and replaced with new empty pallets.

When a sufficient quantity of fuse links has accumulated in the buffer store, the haulier delivers them to the copper smeltery and invoices "NH/HH-Recycling" for its work. There are no charges to users for any aspect of the logistics involved or the recycling process.

After deduction of the costs for logistics, recycling and advertising etc., in accordance with the statutes of the association, the revenue is donated to a research agency to promote research in the area of fuse link technology and environmental compatibility. The agency is asked to publish results in appropriate manner.

Spreading throughout Europe

In 2001, approximately 116 tonnes of used l.v. and h.v. h.b.c. fuse links were collected and recycled; in 2002, by the end of December, the collected total had already reached 166 tonnes. For Germany alone the estimated annual figure of used fuse links is approximately 1400 tonnes so it can be seen that the potential of recycling is very considerable indeed (Fig. 3).

"NH/HH-Recycling" intends to also enable foreign customers of the member companies to have their old fuse links disposed of by environmentally-compatible means. The organization's trade-marks have already been registered in approximately 30 countries and inquiries about the concept of the recycling process have been received from Austria, Sweden and recently England.

Memorandum on the European activities of NH/HH Recycling (members' meeting resolution of 17.05.00)

1. The main tasks of NH/HH Recycling involve recycling fuse links that are manufactured or distributed either by members of the Association or by companies which use its sign. If these fuse links can be collected from foreign customers or at foreign production locations, they may also be included in the recycling concept.
2. Based on a legal assessment by ZVEI (German electrical industry), there are unlikely to be any benefits from operating NH/HH Recycling as a European association.
3. As a German nonprofit making association, it is not a primary objective of NH/HH Recycling to extend the system beyond Germany's borders.

4. The legal opportunities of a German nonprofit making association are limited outside Germany.
5. It is part of NH/HH Recycling's basic philosophy to offer startup assistance for recycling systems in other countries under these countries' own leadership.

Claus Deußer (53)
Vice President of NH/HH Recycling and Purchasing
Logistic Manager at EFEN GmbH, Eltville
(Germany).

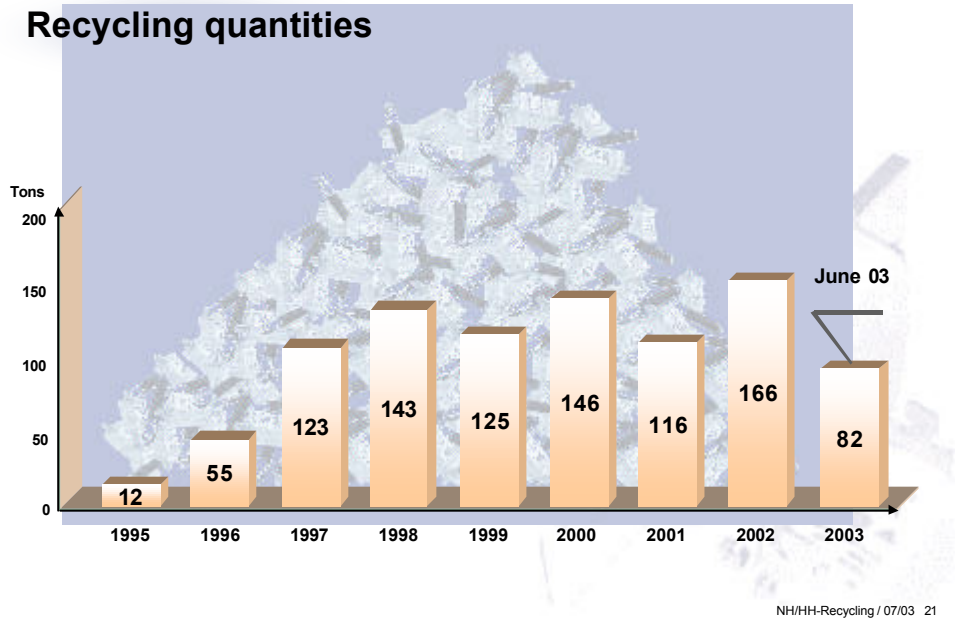

NH/HH-Recycling

Verein zur Förderung des umweltgerechten Recycling von abgeschalteten NH/HH-Sicherungseinsätzen e.V.

DEVELOPMENT OF LEGISLATION IN THE AREA OF ENVIRONMENTAL PROTECTION IN EUROPE AND EFFECTS TO BE EXPECTED ONTO THE FUSE INDUSTRY

Gerd Fink

Association for the promotion of environmentally compatible recycling of disused LV HRC/HV HRC fuse links
Regensburg, Germany, Tel. +49 (0941) 790-2587, Fax. +49 (0941) 790-2766,
mailto:gerd.fink@siemens.com

Abstract: Environmental protection is a particular challenge for the increasing European community. In addition to the presentation of the corresponding legislation to be expected until 2006 respectively 2008 in Europe, possible influences of the legal regulation on manufacturing, transportation and distribution of fuse links are outlined. As far as available, replacements of materials and alternative procedures will be indicated.

Environmental protection is a particular challenge for the increasing European Community.
In future, there will be three basic essentials, which are the taking back and recycling, the restriction of substances and in the near future, the eco-design requirements.

The WEEE – Directive, it stands for “Waste of electrical and electronic equipment” which will come into force in August 2004 is the core of a taking back and recycling system. The countries have to install a collection and take back system free of charge for consumers that ensures the return of the electronic equipment from August 2005.
The producers have to warrant financing of disposal take care for correct recycling and recovery of waste. In this case, the European legislation is the minimum requirement for national legislation and it concerns also “... other monitoring and control instruments used in industrial installations (e.g. in control panels)”. (Cat. 9).
The “Restriction of use of certain hazardous substances in electrical and electronic equipment,” (RoHS) will come into force in August 2004, valid in July 2006. There are no national differences or exemptions with material restrictions. Today, the equipment category 9 “monitoring and control instruments” is exempted from RoHS, but the reviews every 4 years may lead to the cancellation of all exemptions. The expected limits are (07/2003), e.g. 0,1 wt.% for Pb, Hg and 0,01 wt.% for Cd.
The third column has to guarantee the design and production in an environmentally more efficient way. The Eco-design requirements for energy using products (EuP) are estimated 2008 for coming into force. The first offical draft of the European Community is in preparation.

What effects have all these arising requirements on the Fuse Industry and what has to be done? First of all, the critical substances in fuses have to be recorded already, today! What kind of substances which are probably included in fuses are concerned? Well known are Pb, Cr(VI), Cd, Halogenides, - the polyprominated biphenyls (PBB) and polyprominated diphenylethers (PBDE). For the most of these substances mentioned before are technical solutions existing or in development. The producers have to qualify and to use them. In the next step, when the critical substances are identified, the producers should design roadmaps for the substitution to non-hazardous substances. And what is the matter with a “Taking back and recycling system” the WEEE asked for? A system like this is already existing in Europe for fuse links. The different countries or manufacturers can easily copy the principle of this system , which is well known in Germany as “Association for the promotion of environmentally-compatible recycling of disused LV HRC/HV HRC fuse links.”

The manufacturers in Great Britain started also with a system like this and colleagues from The Netherlands are really interested and are collecting fuses. In a pilot phase the NH/HH – System, as we call it in Germany can be accommodated and extended to all European countries.
For the future, we all have to design and produce our fuse-product in an environmentally more efficient way regarding the known EuP-principles for new design and production.
So we can save our environment – it is the only one we all have got.

PARTIAL DISCHARGE (PD) BEHAVIOR OF HIGH VOLTAGE FUSES WITH MODIFIED FILLER

J. Gärtner[(1)], M. Krins[(2)], E. Gockenbach[(1)], H. Borsi[(1)]

Institute of Electric Power Systems - Division of High Voltage Engineering (Schering-Institute)[(1)], University of Hannover, Callinstraße 25A, D-30167 Hannover, Germany, gaertner@rrzn.uni-hannover.de
Siemens AG[(2)], Power Transmission and Distribution, High Voltage, Nonnendammallee 104, D-13629 Berlin, Germany, matthias.krins@siemens.com

Abstract: In conventional current-limiting hv-fuses granular quartz is used as arc quenching filler. The gas filled pore space between the filler's grains tends to favor PD generation. These PD have been analyzed by means of a phase resolved PD analysis (PRPDA) at different testing conditions (voltage, current, pressure, temperature, gas). A reduction of the PD may be achieved by eliminating the pore space of the filler or by electrical field grading. Pore space was eliminated by filling it with quartz powder, field grading was achieved by enhancing the dielectric properties of the pore's environment (i.e. the sand). Among the presented modifications clogging with quartz powder is most favorable, since its high impact on PD, low costs and negligible changes to the production process of the fuses. In addition a strong decay of the switching overvoltage was revealed during AC switching tests at critical current I_2 of fuses filled with modified filler.

Keywords: current limiting high voltage fuse, partial discharge behavior, corona, switching overvoltage

1. Introduction

Asset management is a major concern in cost efficient power delivery [1]. Beside others it involves condition-based maintenance, which relates to online monitoring of different quantities, one of them being PD [2]. Since switchgear assemblies – in which fuses are integrated [3, 4] – tend to decrease in size [5], the PD behavior of fuses becomes a growing concern.

PD in the form of *corona* concerns usage of fuses since the early days, because a degeneration of the fusible elements [6] takes place. Modern current-limiting fuses are corona resistant, but a certain quantity of PD still remains, which does not affect the fuses' characteristics [7]. However it may tamper online monitoring of PD in devices connected to the fuse.

In a previous paper [7] descriptions of some aspects of the PD behavior of hv-fuses are already presented as concepts for PD elimination modifications of the fuse housing and environment are shown. Now, we will focus on a description of the fuses' PD behavior by means of sophisticated PD measurement techniques and reduction of PD using filler modifications.

Filler modification is a difficult task, since it directly affects the "heart" of the fuse: the arc-quenching medium. A large number of papers and patents [e.g. 8-19] deal with such modifications, but most of the fuses in use are still filled with ordinary granular quartz. The arc-quenching medium is crucial for the current-limiting behavior of the fuses [e.g. 20-23], because it strongly cools down the arc which appears when the fuse switches. Until switching, the filler also influences the thermal equilibrium of the fuse, which is important for its time-current characteristic (see [24] for an enumeration and discussion of different investigations). After switching, the fuse has to resist the recovery voltage, which consist of a steady-state part [25], maybe 1.5 times higher than the rated phase-to-ground voltage [26] and a transient part being massively affected by the fuse itself. The fuses' performance depends not only on the filler's physical and chemical properties, but also on the method used for application [27, 28].

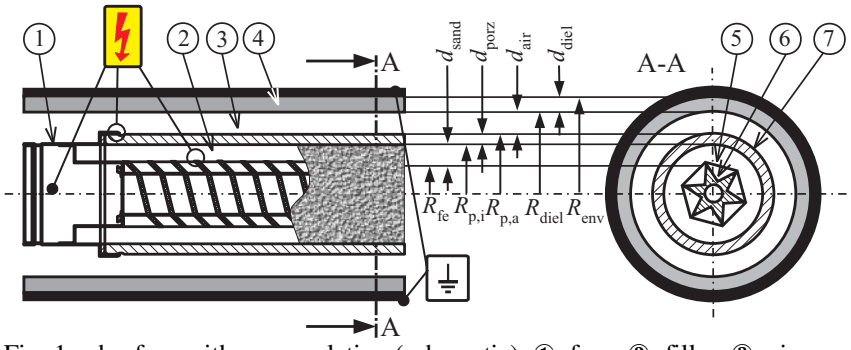

Fig. 1: hv-fuse with encapsulation (schematic): ①: fuse, ②: filler, ③: air gap, ④: dielectric, ⑤: fusible elements, ⑥: fuse's core, ⑦: porcelain tube.

2. Partial discharges: genesis and measurement

It is known from high-voltage engineering, that in cavities inside insulating materials electrical discharges evolve, due to local excess of the electrical breakdown field strength of the medium, which fills the cavities' volume.

If we suppose the fuse being a cylindrical capacitor, neglecting the helical arrangement of

the fusible elements (⑤ in Fig. 1), the electrical field strength can be calculated by the well known formula for cylindrical capacitors with "stacked dielectrics" [29].

$$\left|\vec{E}_{\text{sand}}\right| = \frac{1}{r \cdot \varepsilon_{\text{sand}}} \cdot \frac{U}{\frac{1}{\varepsilon_{\text{air}}} \cdot \ln(R_{\text{diel}}/R_{\text{p,a}}) + K} \qquad (1)$$

with

$R_{\text{fe}} < r < R_{\text{p,i}}$, radius of interest

$$K = \frac{1}{\varepsilon_{\text{sand}}} \cdot \ln(R_{\text{p,i}}/R_{\text{fe}}) + \frac{1}{\varepsilon_{\text{porz}}} \cdot \ln(R_{\text{p,a}}/R_{\text{p,i}}) + \frac{1}{\varepsilon_{\text{diel}}} \cdot \ln(R_{\text{env}}/R_{\text{diel}})$$

ε = dielectric constantl

R_{fe} = medium radius of fusible elements

$R_{\text{p,i}}, R_{\text{p,a}}$ = inner, outer radius of porcelain tube

R_{diel} = inner radius of dielectric

R_{env} = radius of grounded environment

U = applied voltage .

Obviously, if d_{air} is eliminated ($R_{\text{diel}} = R_{\text{p,a}}$), the el. field becomes maximal for fixed r. This is the reason, why PD may become a future concern, since switchgear assemblies are decreasing in size. Otherwise, this is the simplest technique for PD elimination, since increasing d_{air} decreases the el. field strength. These calculations can only serve as a rough overview, since neglecting the helical arrangement of the fusible elements and their shape leads to underestimation of the real field strength by factor 10-100. An FEM-model reveals a factor of 28, when fusible wire elements with a diameter of 0.15 mm and a length of 600 cm are considered. The calculated field strength at the fusible elements' surface is 13.7 kV/mm for an 6/12 kV, 630 kVA prototype current-limiter, d_{air} being zero, d_{diel} = 10 mm, $R_{\text{p,a}}$ = 27.5 mm.

PD measurement and analysis

The well-known PD equivalent circuit [30] shown in Fig. 2 can be explained as follows: The dielectric with void is divided into 3 capacitors: one for the "sane" part (C_1), one for the void (C_2) and one for the dielectric above and under the void (C_3). If an AC voltage is applied, all capacitors will charge, until the void's breakdown voltage is reached. C_2 will discharge resulting in a voltage drop. C_2 will then be recharged by the "sane" dielectric C_1 and capacitors outside (e.g. C_c, but also capacitors in the environment i_{env}), until the breakdown voltage is reached again. This may repeat for several times per cycle. PD pulses can be detected through measurement of the charging current of the dielectric himself (serial coupling, i_A) or the current of C_c (parallel coupling, i_m). Since the exact values of the capacitors are unknown (except C_c), the integration of i_m never leads to the exact value of the dispersed charge, but to the so-called *apparent charge* q_a.

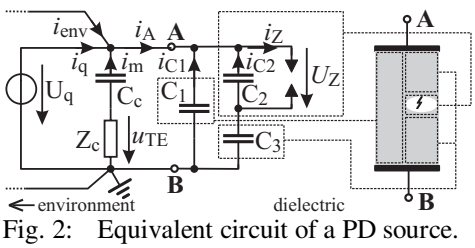

Fig. 2: Equivalent circuit of a PD source.

Since impulses can be detected outside the dielectric through C_c, they may also be detected by other "capacitors", such as cables connected to switchgears. Depending on the magnitude of the PD pulses and the damping until they arrive at the cable, sensitive PD measurement may no longer be possible or special techniques [31] must be applied.

If PD impulses are detected in a dielectric, it appeals to know their cause or source. This knowledge can be gained by analysis of different impulse parameters, like their height, length, shape, time of occurrence etc. One of the widely used analysis methods is phase resolved partial discharge analysis (PRPDA) [33, 34], where different PD

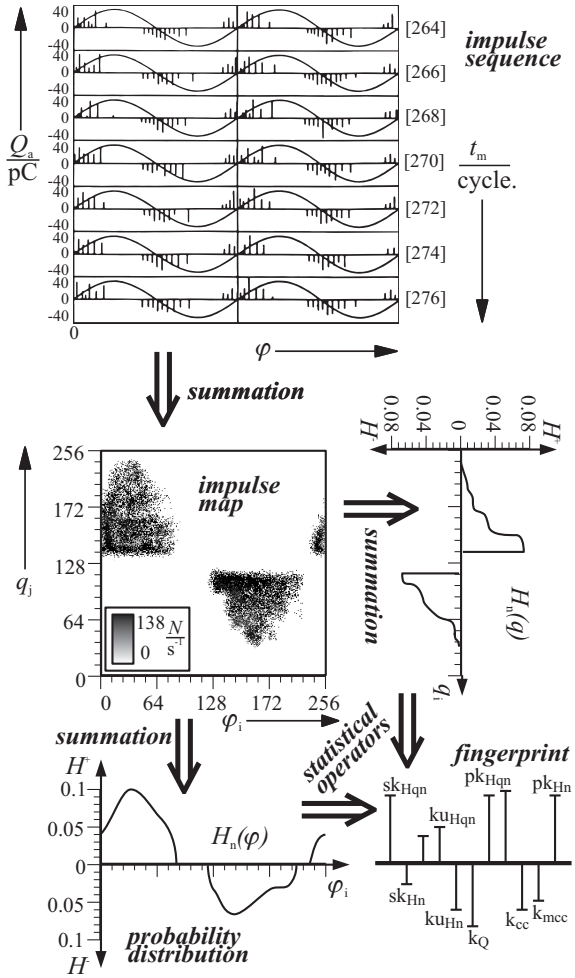

Fig. 3: Scheme of PRPD analysis (meas. data from [32]).

parameters are analyzed with respect to the phase of the supply voltage.

If an AC voltage is supplied to a dielectric with internal faults, PD may occur as shown in Fig. 3. As can be seen, the impulses occur at distinct phases of the AC voltage, with a certain resemblance from cycle to cycle. PRPD-detectors now sum up the amount of impulses in distinct phase windows for a distinct time. This gives a histogram of the amount of impulses vs. phase of test voltage. Eventually, the PRPD-detector is also able to classify the impulses by their apparent charge, so a two-dimensional distribution called *impulse map* **M** (Fig. 3) can be formed. In this map each pixel (m(i,j)) represents the amount of impulses occurring at phase φ(i), with an apparent charge of q(j). Under special conditions, experts are able to distinguish different PD sources by looking to the image of **M**, but there are also mathematical and statistical tools available for extraction of features that could be used for classification [35, 36]. PRPD-method gets nowadays completed by impulse sequence analysis [37].

Statistical and mathematical analysis of **M**

If the marginal distributions of **M** are calculated (Fig. 3), two important distributions are obtained, one being the impulse distribution vs. phase of occurrence $H_n(\varphi)$, the other the impulse distribution vs. apparent charge $H_n(q)$. If the map is multiplied by the calibration vector of the measurement device, the charge map **Q** results, which leads to distributions of the charge ($H_q(\varphi)$, $H_q(q)$). Dividing $H_q(\varphi)$ by $H_n(\varphi)$ leads to the mean impulse height $H_{qn}(\varphi)$. If this is still insufficient, **Q** can be multiplied by the vector of the test voltage giving **E**, the energy map and corresponding distributions. All these distributions may be interpreted as discrete probability functions and treated with statistical tools like formation of momentums (1st momentum being the mean μ, 2nd the divergence σ, 3rd the skewness *sk* and 4th the kurtosis *ku*), Weibull analysis etc., or mathematical tools as correlation analysis (giving cross-correlation factors k_c and k_{mcc}), peak detection (pk_{Hqn}, pk_{Hn}), point of inertia analysis, transformations (fourier, wavelet) and so on. These analyses are carried out not only for whole maps (**N**, **Q**, **E**), but also for their parts (pos. / neg. pulses $\mathbf{X}^+$ / $\mathbf{X}^-$ or pos. / neg. half-waves of voltage $\mathbf{X}_\cap$ / $\mathbf{X}_\cup$). The result is a set of characteristic features called *fingerprint*, which aims to identify a PD source [34].

3. Specimens, test-setup and measurement techniques

Most of the PD measurements were carried out with the test vessel described in [7], using commercial 10/20 kV, 40 A fuses. For easy exchange of the filler, some of the fuses were fitted with a screwable cab, equipped with sealing joints. One fuse was perforated at the ends to allow application of different gases.

Filler

As base filler commercially available sand (H31 from Quartzwerke, Germany) was used. The filler modifications comprised the addition of

- 10 %, 20 % and 30 % of quartz powder as pore filler,
- 200 ml of $[SiO_2]_x$ as solidifying pore filler,
- up to 10 % of SiC for stress relieving,
- 10 % of TiO_2 to enhance the dielectric properties of the sand,
- up to 1.3 ml of water (H_2O) for stress relieving.

The modified filler was prepared in a rotating drum. Rotation was stopped, when the mixture was visible homogeneous. In case of quartz powder a special technique was used to suppress segregation of the bi-dispersive grain size fractions.

The filler was applied to the fuses on a vibrating device, until the fuses were completely filled and no more visible settling was achieved.

In case of $[SiO_2]_x$ and H_2O, the indigents were supplied to the filler after mounting the fuses and application of the base filler. The specimens were tempered at 150° C for 48 hrs.

Test setup for PD measurements

In addition to the test setup used in [7], a potential free current transformer was inserted, allowing a current to be driven through the fuse, while simultaneous measuring the PD.

The fuses were introduced to the test vessel and the test voltage was applied for 40 min. Eventually current in different amounts (10, 20, 30 and 40 A) were also applied to the fuses.

With voltage applied to the fuse under test, the PD detector was programmed to record impulses over the whole test duration in periods of 1 min. This allows the observation of the temporal PD behavior. The PD-detector consisted of an *ICM-Device* from *Power Diagnostix*, Aachen, Germany, able to record maps of size 256x256 (i.e. 256 windows of charge as well as phase). The recorded maps where read into a program and statistical as well mathematical operations carried out using a *Sun E10k*, equipped with 56 CPUs, 32 GB RAM and 1 TB of storage.

Specimens for switching tests

For switching tests specimens were used consisting of a prototype fuse with characteristic values of 6/12 kV and 630 kVA. The prototypes were

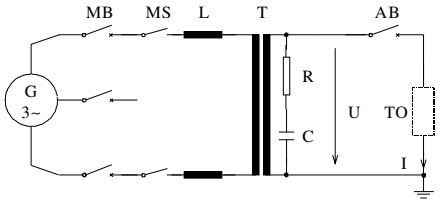

Fig. 4: Test circuit for I_2-test.

equipped with three band type fusible elements of 600 mm length in parallel, bearing equidistant hole-constrictions in their middle. Filler with quartz powder in different amounts was used.

Setup for switching tests

The setup for the switching tests consisted of a single-phase direct test circuit (Fig. 4). A synchronous generator fed via a master-breaker and a making switch the primary side of a transformer. On its secondary side the fuses were mounted in series with an auxiliary breaker. The latter was used to determine the parameters of the prospective transient recovery voltage (TRV) and the prospective current in preliminary setting tests. During the tests with the fuses (TO) the AB was closed. The inductance L was tuned for a prospective current of I_2 = 5.6 kA, R and C were adjusted to form a TRV with a peak value of u_c = 22 kV and a rate of rise of 0.11 kV/µs as is required by [25]. The making switch served to realize the desired making angle of 10°, while the master-breaker was used to de-energize the test circuit after the test. The power-frequency recovery voltage was adapted to 10.4 kV by the help of the transformer and was applied to the fuses for at least 60 s after arc extinction.

4. Results

PD analysis

Fig. 5 shows a typical distribution of impulses rate vs. apparent charge for an unmodified fuse at the beginning of the test. As can be seen, the positive impulses are slightly preferred. Bipolar logarithmic scaling is used, i.e. two decades per polarity of the PD pulses. The peak at ±6 nC is caused by the

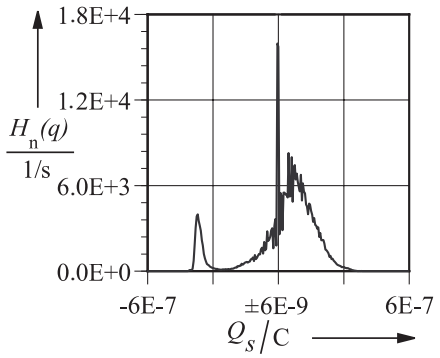

Fig. 5: $H_n(q)$ for unmodified fuses at 20 kV.

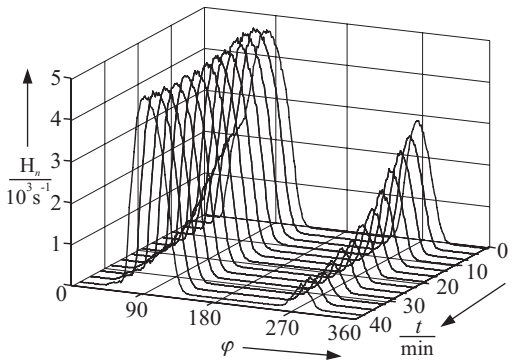

Fig. 6: $H_n(\varphi)$ distribution over time, at 20 kV, 10 A.

measurement device and discriminated in further data analysis.

If such diagrams are stacked for consecutive measurement intervals, a 3D-view of the PD history results, as shown in Fig. 6 for the impulse rate vs. phase of occurrence $H_n(\varphi)$. Here the strong decay of PD impulses rate over the time becomes obvious, in particular for impulses in the negative half-wave.

Fig. 7 shows PRPD-fingerprints of unmodified fuses at 20 kV, 0 and 40 A, being calculated at 0, 20 and 40 min. of the test duration. The fingerprints resemble to the fault classification "narrow cavity in solid material" and "multiple point-plane

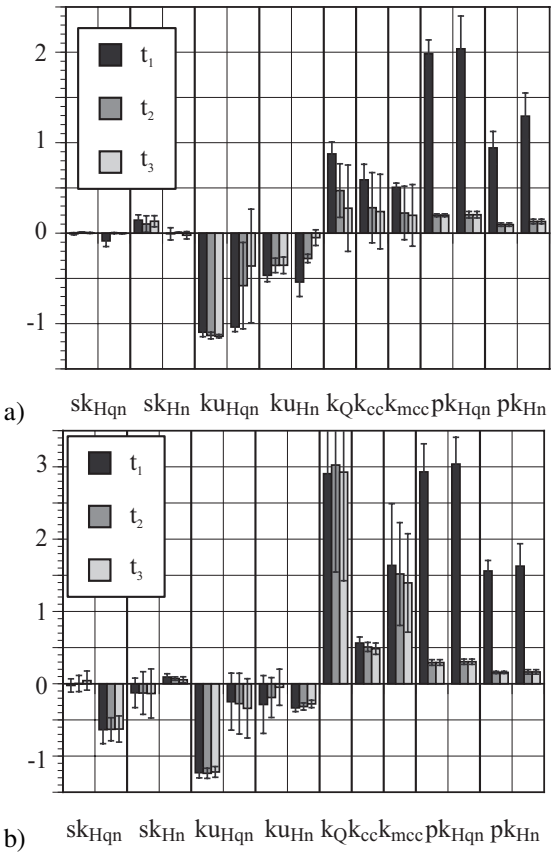

Fig. 7: PRPD-fingerprint of fuses at 20 kV and a) 0 A and b) 40 A. t_1 = 0, t_2 = 20, t_3 = 40 min.

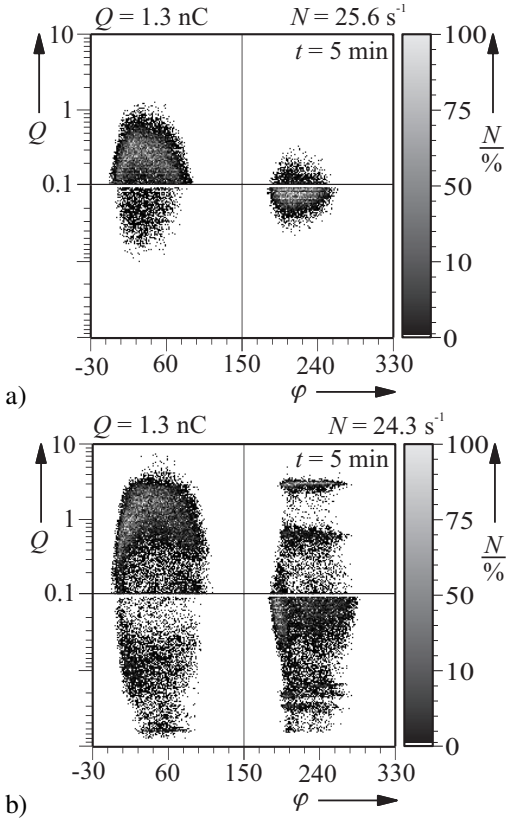

Fig. 8: PD Maps for different gaseous filler components: a) air, b) pure N_2.

configuration in air" [34], but matching is not absolute. Especially the cross-correlation factor k_Q, which compares the distributions of charge in the positive and negative half-waves, shows strong deviations. As noticeable from the error-bars, the data manifests a strong variation. This is inherent to all the measurements carried out and caused by the complex structure of the filler.

The gaseous component of the filler also affects the PD activity (Fig. 8): In air, a lower level of apparent charge compared to N_2 is found. Also a strong decay of PD activity over the time (e.g. Fig. 6, 9) can be observed. This indices the formation of ozone (O_3) in samples with air, which reduces electrical field strength due to its dipole character and

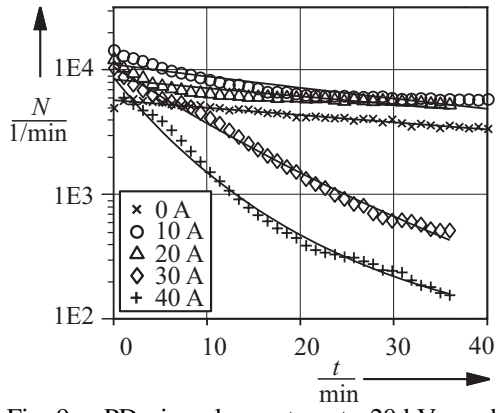

Fig. 9: PD impulse rate at 20 kV and different currents, unmodified filler.

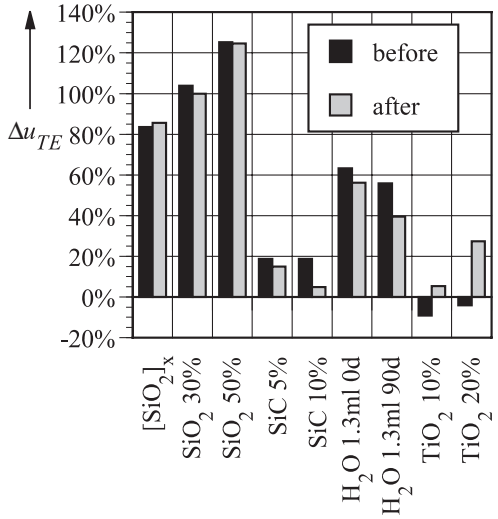

Fig. 10: PD performance of different fillers, before and after 40 min.

therefore decreases PD activity. In case of pure N_2 no O_3 can be formed and no decay in PD activity happens. Comparing the total sum of apparent charge for pos. and neg. half-wave, in N_2 a nearby equal distribution is found, whereas in air a large difference was observed.

The biggest impact on the PD behavior was found, when current was applied to the fuse. Fig. 9 shows the drastic decay in PD activity for different current values. The decay is more pronounced for higher currents, which is explainable by thermal expansion of the filler's components (i.e. pressure rise in the gas, tighter contact between the grains) and the higher intrinsic conductivity of SiO_2.

The influence of pore filler on the PD inception voltage u_{TE} becomes obvious in Fig. 10, where the

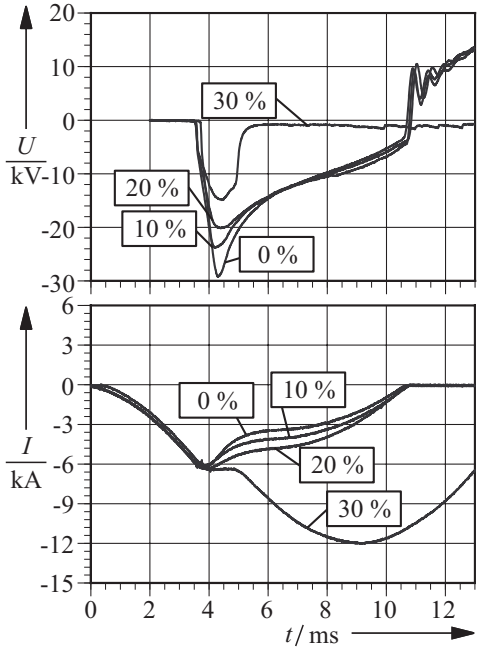

Fig. 11: I_2-test on fuses with different pore filler amount.

difference in PD inception voltage Δu_{TE} (compared to unmodified filler) is shown. The best performance is achieved with $[SiO_2]_x$ and quartz powder (SiO_2 in Fig. 10), followed by addition of water (H_2O). The latter shows decreasing performance when measured again after 90 days (H_2O 90d), because water is integrated in the crystal lattice. Worst performance was observed with SiC and TiO_2.

Switching tests

Fig. 11 summarizes the I_2-switching behavior of fuses with pore filler. The percentage shows the weight content of the pore filler. Most impressive is the reduction of the switching overvoltage u_{sw}, which decreases from about 30 kV at 0 % pore filler to approx. 14 kV at 30 % pore filler. This is in accordance with [23], where a decrease of the electrical field strength in the arcing channel for smaller sized filler grains was found, but contradicts findings in [10, 16], where a more compact filler leads to higher u_{sw}.

Evaluating the Joule integrals (Fig. 12), no distinguishable differences can be found in the pre-arcing interval. However, the decrease in u_{sw} is attended with higher I^2t-values in the arcing interval: The I^2t-values increase with higher pore filler degree. This is in contrast to [10, 11, 12, 38], where filler with higher compactness or smaller medium particle size is suspected to give lower I^2t-values, but agrees with findings for fuses with small grained filler [9, 13].

Because of the elevated I^2t-values, the fuse has to deal with higher switching energies, therefore production-level fuses have to be carefully designed. At 30 %, the fuses were not able to switch, leading to excessive high values of the arcing Joule-integral.

The misbehavior of the fuse filled with 30 % of pore filler may be explained by the excessive Joule-energy consumed while switching: If Fig. 11 is considered, the current remains nearly constant after ignition of the arc, instead of decreasing as for the fuses with other amounts of filler. After 5 ms, the

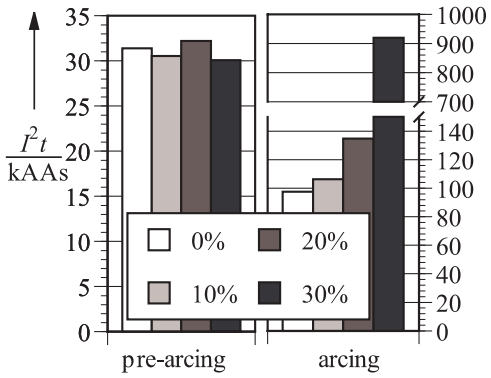

Fig. 12: I^2t-values of fuses with different amount of pore filler in the pre-arcing and arcing interval.

Fig. 13: Fulgurite of a fuse with 30 % of pore filler after I_2-test.

current increases to the prospective current and the arcing voltage drops to about 500 V, resulting in an overload of the fuse. After the test, only parts of the fuse could be retrieved. The fuses' core showed no clear distinguishable fulgurite. Instead a crumbly, foamy and pumiceous mass was found (Fig. 13), somewhat similar to fulgurites found in fuses with very fine grained filler [23]. This led to the assumption, that the constrictions of the fusible elements – maybe distinct or several windings of the helical filaments too – were short-circuited in the moment of arcing, resulting in an unabridged arc, which could not be cleared.

The short-circuiting of the constrictions and fusible elements windings may be explained by the consistency of the filler. At 30 % pore filler content, the percolation point is reached and the smaller grains of the pore filler embed the larger grains, resulting in a higher mechanical elasticity of the filler, therefore degradation of mechanical stiffness [39]. If arcing occurs, the filler cannot resist the pressure rise in the arc channel [40] and yields away, leading to an unabridged arc.

5. Conclusion

Filler modifications can impede PD generation, but also influence the switching behavior of the fuse. The PD reduction was achieved with different fillers, quartz powder giving the best results.

The PD behavior of fuses was analyzed by use of PRPDA. Fuses manifest a strong decay in PD activity when current is applied. There is also a decay of PD activity over the time, which can be explained by generation of ozone inside the fuse.

The use of bi-dispersive filler not only obstructs PD generation, but also reduces the peak of the

switching overvoltage. This decrease is combined with an increase of arcing energy, which must be considered in the fuse design. A certain level of pore filler addition cannot be exceeded, since the fuses loose their ability to extinct the current.

The concept of bi-dispersive filler has to be investigated further by additional measurements like complete IEC282 type test (I_1, I_3), long-time tests and determination of the time-current curve, whereas it is known from [41], that time-current characteristic is slightly slower for finer grains.

References

[1] Sturm M, "Systeme zur zukünftigen Energieoptimierung und –vermarktung I". *Scriptum*, Univ. Hannover, 2003.

[2] Peier D; Temmen K: "Beurteilung der Degradation von Isolierungen mittels Teilentladungsmessung". *Elektrie* 53(1999), No. 9-10, pp. 314-9, 1999

[3] Erlenhof A; Grote J; Heiß W; Müller HJ; Siebel KH; Wittek L: "Platzsparender und berührungssicherer Kurzschlußschutz von Transformatoren und Mittelspannungs-Netzstationen". *Elektrizitätswirtschaft*, Vol. 84 (1985), No. 10, pp. 356-70, 1985.

[4] Dirks R: "Die HH-Sicherung als Herausforderung an den Schaltanlagen-Konstrukteur". *Elektrizitätswirtschaft*, Vol. 87 (1988), No. 16/17, pp. 781-2, 1988

[5] Walz RD; Büscher A; Primus IF: "Die neue ökonomische 24-kV-Schaltstation, schlüsselfertig am Kranhaken". *Elektrizitätswirtschaft*, Vol. 97 (1998), No. 4, pp. 26-34, 1998.

[6] Läpple H: "Die neue Hochspannungs-Hochleistungssicherung (HH-Sicherung) der SSW". *Siemenszeitschrift*, Vol. 11, No. 2, pp. 65-70, 1931.

[7] Gärtner J; Gockenbach E; Borsi H: "Influences of hv-fuses on Partial Discharge Measurement of Electrical Equipment". *ICEFA* Turin 1999, pp. 77-82.

[8] Paukert J: "Search for new extinguishing media for LV fuses". *ICEFA* Eindhoven 1987, pp. 44-9.

[9] Turner HW; Turner C: "Phenomena occurring during the extinction of arcs in fuses". *Int. Symp. on switching Arc Phenomena*, Lodz, 1973, pp. 253-6.

[10] Namitokov KK; Frenkel ZM: "Influence of Quartz-Filler Density on Arc Processes in Fuse". *Electrotekhnika* Vol. 54 No. 8, pp. 36-7, 1983.

[11] Lipski T: "Behaviour of stone-sand fuses in short-circuit conditions". *Proc. 10th Int. Conf. on Gas discharges and their Application*, Swansea, 1992, pp. 204-7.

[12] Lipski T; Pikon M: "A Comparison of Current Interruption by Sand SiO_2 and Sand SiO_2/Gas SF_6 Fuses". *ICEFA* Ilmenau 1995, pp. 176-9.

[13] Ossowicki J: "Influence of quartz-filler granulation on breaking D.C. Overloads by Means of Strip Fuses". *Int. Symp. on switching Arc Phenomena*, Lodz, 1973, pp. 262-4.

[14] Shea JJ; Crooks WR; Smith JDB: "Gas Evolving Materials for Improved Low Current Interruption in High Voltage Current Limiting Fuses". *IEEE Trans. on Power Del*., Vol. 10, No. 1, pp. 258-65, 1995.

[15] König D; Trott J; Müller HJ; Müller B: "Switching Performance of High-Voltage Fuse-Elements in Different Solid and Gaseous Filling Media". *ICEFA* Eindhoven 1987, pp. 50-6.

[16] Ilyina NA; Zhemerov GG; Zaika EI; Shklovsky IG: "The Basic Principles to Engineer a High Quality's Fuses for Power Semiconductor Convertors". *ICEFA* Turin 1999, pp. 315-8

[17] Saqib MA; Stokes AD: "Characteristics of Fuse Arcing in Different Fillers". *ICEFA* Turin 1999, pp. 275-8.

[18] Bussière W: "Influence of sand granulometry on electrical characteristics, temperature and electron density during high-voltage fuse arc extinction". *J. Phys. D: Appl. Phys.* 34 (2001), pp. 925–35, 2001.

[19] Kaltenborn U; Rocks J; Skryten PK: "Löschmedium zum Löschen von Lichtbögen". *Patent application* EP 1 162 640 A1, European Patent Office, Munich, 2001.

[20] Kroemer H: "Der Lichtbogen an Schmelzleitern in Sand". *Arch. f. Elektrotechnik*, Vol. 36, Iss. 8, Berlin 1942, pp. 455-70.

[21] Johann H: "Die Lenkung des Schaltvorgangs in Hochspannungs-Sicherungen mit körnigem Löschmittel". *VDE-Fachberichte*, 18(1954), Wuppertal, 1954, pp. 34-8.

[22] Vermij L: "Electrical behaviour of fuse elements". *PhD*. TH Eindhoven, 1969.

[23] Huhn P: "Über das Verhalten eines durch Drahtexplosion eingeleiteten Lichtbogens in körnigem Medium". *PhD*. TU Hannover, 1971.

[24] Egert D: "Ein Beitrag zur mathematischen Modellierung der physikalischen Vorgänge in Hochspannungs-Hochleistungs-Sicherungen". *PhD*. TH Illmenau, 1990

[25] DIN EN 60282-1: "Hochspannungssicherungen, Teil 1: Strombegrenzende Sicherungen (IEC 60282-1:1984 + A1:1996)". VDE-Verlag GmbH Berlin, 1998.

[26] Wright A, Newberry PG: "Electric Fuses". Peter Peregrinus Ltd. 1982.

[27] Chen S: "Research on the Technique of Filling Quartz Sand in Fuse". *ICEFA* Eindhoven 1987, pp. 93-8.

[28] Ehrhardt A: "Schaltverhalten von Sicherungen bei kleinen Überströmen unter besonderer Berücksichtigung des Wiederzündens". *PhD*. TU Ilmenau, 1999.

[29] Wolf I: "Grundlagen und Anwendungen der Maxwellschen Theorie I". *B.I. Hochschultaschenbücher*, Vol. 818, Wissenschaftsverlag, Mannheim, 1968.

[30] Kreuger FH: "Partial Discharge Detection in High-Voltage Equipment". Butterworths, London, 1989.

[31] Schichler U: "Erfassung von Teilentladungen an polymerisolierten Kabeln bei der Vor-Ort-Prüfung und im Netzbetrieb". *PhD*. Univ. Hannover 1996

[32] Suwarno: "A comparison between void and electrical treeing discharges in polyethylene". *Proc. of The 6th Int. Conf on Properties and Applications of Diel. Materials,* Xi'an, China, pp. 493-6, 2000.

[33] Okamoto T; Tanaka T: "Novel Partial Discharge Measurement Computer-Aided Measurement System". *IEEE Trans. on El. Ins*, Vol. E1-21, pp. 1015-9, 1986.

[34] Gulski E.: "Computer-Aided Recognition of PD Using Statistical Tools". *PhD*. TU Delft, 1991

[35] Bartnikas R: "Partial Discharges". *IEEE Trans. Diel. and Ins.*, Vol. 9, No. 5, pp. 763-808, 2002.

[36] van Brunt RJ: "Stochastic properties of partial-discharge phenomena". *IEEE Trans. on El. Ins.* Vol. 26, No. 5, pp. 902-48, 1991.

[37] Hoof M: " Impulsfolgen-Analyse: Ein neues Verfahren in der Teilentladungsdiagnose". *PhD*. UG Siegen, 1997

[38] Lee S; Kim IS; Han SO: "The Test Method to Aquire the Optimal Parameter for CL-Fuse". *ICEFA* Turin 1999, pp. 265-70.

[39] Yin H: "Acoustic Velocity and Attenuation of Rocks: Isotropy, Intrinsic Anisotropy, and Stress Induced Anisotropy". *PhD*. Stanford Univ. 1992.

[40] Jakubluk K; Lipski T: "Dynamics of fulgurite formation during arcing in hrc fuses". *J. Phys. D: Appl. Phys.* 26(1993), pp. 424-430, 1993.

[41] Trott J: "Untersuchungen zur Lichtbogenlöschung in Hochspannungs-Hybridsicherungen". *PhD*. Darmstadt 1988

Acknowledgments

The authors like to thank EFEN Elektrotechnische Fabrik GmbH, Eltville, Germany, for the manufacturing of the test fuses, SIEMENS AG, Berlin, Germany for carrying out the switching test, and Dipl.-Ing. R. Jochem who did most of the PD measurements.

ACTION OF THE SAND IN ULTRA-FAST FUSES. PROBLEMATIC

Jean-Louis Gelet[1] **and Jean-Michel Missiaen**[2]

[1] FERRAZ-SHAWMUT
Rue Vaucanson - 69720 Saint Bonnet de Mure – France
Tél. : 33 (0) 4 72 22 66 30 - Fax : 33 (0) 4 72 22 66 14
jean.louis.gelet@fr.ferrazshawmut.com

[2] Laboratoire de Thermodynamique et de Physico-Chimie Métallurgiques (UMR 5614 CNRS-INPG/UJF)
Domaine Universitaire , BP 75 - 38402 St Martin d'Hères - France
Tél. : 33 (0) 4 76 82 66 76 - Fax : 33 (0) 4 76 82 67 44
missiaen@ltpcm.inpg.fr

Abstract: *FERRAZ-SHAWMUT intends to improve his knowledge about design and manufacturing of fuses. One very crucial point is the relationship between sand and the behaviour of the electrical arc during fuse-operation. In the past many tests have been carried out, in which the parameters of the manufacturing-process were adjusted or modified, and afterwards arcing parameters were measured. It was very difficult to draw out evidence of correlation.*
One idea is to characterize not only the manufacturing-process but its results. How are the sand grains arranged, specially around the fuse-element and even more specially around the necks where the arc is initiated. The knowledge of the arrangement of sand-grains will be necessary for any understanding and physical modelling of electrical arc as phenomenon involving materials.
FERRAZ-SHAWMUT, Ecole des Mines de Saint-Etienne and LTPCM-Grenoble are collaborating in that way.

Keywords: *(e.g. electric fuse, ignition arc, current limitation, over voltage)*

1. Introduction

Since at least 1666 and the fundamental discovery of inertia by Isaac Newton, scientists know that it is not possible to pass from a physical state nr 1 to a state nr 2 within a null time. Concerning fuses, it means that when occurs the blowing, the current will decrease within a few time. In other words, fuse becomes a variable resistance, which value increases from a very low value to infinity. The physical principle of this variable resistance is nothing more than an electrical arc.

Another way for watching to the operation of the fuse is to consider that electrical energy $\frac{1}{2}Li^2$ inside the circuit must be absorbed. Then the arc is nothing more than a machine transforming rapidly electrical energy to thermal energy. The materials around arc are heated and play as a storage-tank. After the electrical current reaches zero, the heat can be dispatched into the surroundings.

Sand is in charge to absorb a large quantity of this energy, thanks to its high melting temperature and melting energy.

Sand is also in charge, thanks to its porosity to control the flow of highly energized materials (hot liquid, gazes and plasmas) and hence to control the arc-voltage.

2. Problematic

Further to these qualitative considerations, the job of the engineer is to give values to the physics.

In that way, many studies have been carried out from theoretical and experimental points of view [1 to 10]. There is today an evident tendency to propose as ROCHETTE [9-10] and CLAIN [10], a model of the electrical arc where the sand is a porous material through which runs a gaseous flow in addition with a thermal flux. The porous material is considered as homogeneous. In fact, this is not true and we can suspect that electrical arc will be deterred by the location and the size of the first grain it will meet. Vivier [11] did the demonstration that even when all the fuse-manufacturing parameters are controlled and repeated, a variability of the arc-voltage as soon as within arc-ignition, could be observed. His observations were specially significant because he used simple fuses, with only one row of necks in a large sand core. Indeed, in case of many rows in series and in parallel, the variability is erased because of statistical effects.

The problem is to explain how could the grains-arrangement deter the arc-ignition. Hence, it appears that it is necessary to describe the grains-arrangement.

3. Characterizations of the sands:

Particular materials are very common on the surface of the earth and used in many industrial and human activities. Without any order, we can quote as examples : sands (of course), seeds (corn, rice, beans, nuts), medical powders, washing powders, wood-sawdust, concrets, etc… Nevertheless, scientists have not yet found the models in order to describe their behaviour and even more, they have not yet a good understanding of their behaviour.

When we try to characterize powders or sands, a triple question is asked :

- do you want to characterize the grains (their shape, their size, their material…) ?
- do you want to characterize the sand as a continuous material (quasi-solid when it is motionless and quasi-liquid when it is moving)?
- do you want to characterize the arrangement of the grains within a quasi-solid state ?

3.1. Characterization of the grains :

Sand grains can be characterized by their material(s), including the purity of this material and eventually the presence of two or several materials.

They can be also characterized by the size, or better by the size-distribution of the grains.

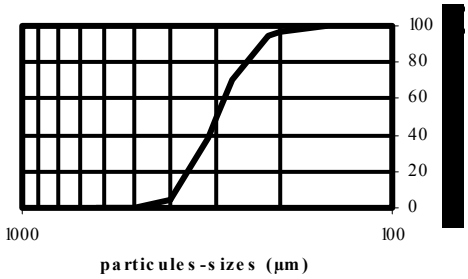

Fig.1 : usual cumulative distribution-curve for sand

The document API - Recommended Practice 58 gives a chart allowing to class grains versus two parameters so called sphericity and rondicity :

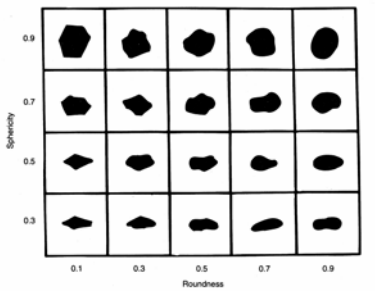

Fig.2 : chart of rondicities and sphericities according to API 58.

3.2. Characterization of sand as continuous material :

Two series of parameters could be used in order to characterize sands as continuous materials. Some of these parameters consider sands as quasi-solids :

- permeability (measurement of the velocity of a gaseous or liquid flow through a porous material),
- measurement of the shear-stress (Jenike-cell).

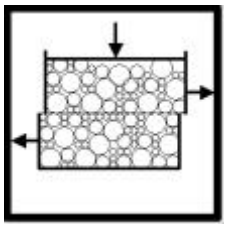

Fig.3 : Principle of Jenike-cell : a two-parts-box is filled with powder. Then it is submitted to shearing-strains.

Other parameters consider sands as quasi-liquid :

- flow-rate and angle of repose.

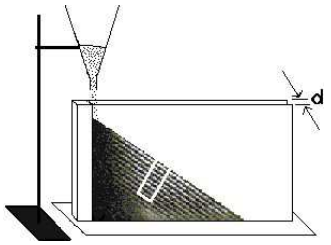

Fig.4 : measurement of flow-rate and angle of repose.

3.3. Characterization of the arrangement of the grains within a quasi-solid state :

New developments in picture-analysis allow to better characterize the arrangements of granular materials. We can quote the works carried out by SERRA [11-12] and JL CHERMANT *et all*. [13-14-15]. FERRAZ-SHAWMUT also carried out studies with help from high-school laboratories [16-17-18].

The method of characterization consists in three steps :

1. preparation of the sample,
2. SEM-micrographs and picture-treatment,
3. mathematical analysis.

3.3.1. Preparation of the sample :

Sand-cores are compacted in containers (in fact ceramic fuse-bodies) and then agglomerated with water-glass according to the usual industrial manufacturing-process. As made, sand cores present a porosity and their cohesion is not sufficient for any further mechanical operation. It is the reason why, the core is impregnated with a epoxy resin. Impregnation allows the core to be cut and polished without risk of breaking. Note that, for the time being, no fuse element are added to sand-core.

3.3.2. SEM-micrographs and picture-treatment :

The samples are observed by back scattering electrons microscopy. In comparison with optical microscopy, this method allows to improve the contrast between the two phases, i.e. silica and resin.

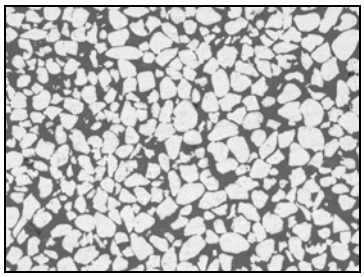

Fig.5 : SEM-micrograph.

Afterward, the quality of the picture is not sufficient to proceed to mathematical analysis. The first SEM-picture has to be transformed into a binary picture, with only black or white spots.

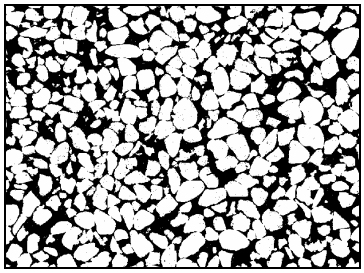

Fig.6 : binary picture.

And then, grains have to be separated from each others. Filtering and thresholding of the binary picture are necessary to get a workable picture from the point of view of mathematical analysis. An algorithm for automatically partition of phases has been used. Unfortunately a final “manual” operation cannot be avoided.

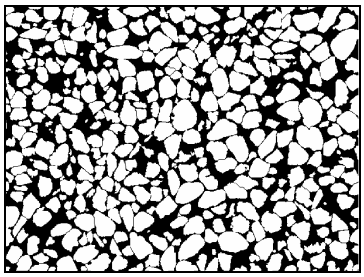

Fig.7 : pictures with separated grains.

3.3.3. Mathematical analysis:

Anybody could believe that the distribution of the grain-sizes will be homogeneous inside a container. But, with a minimum of consideration, it will appear that from the bottom to the top of the container, maybe will occur some segregation between big and large particles. In fact, reality is out of this evidence and we can observe clusters or lines of particles of comparable sizes.

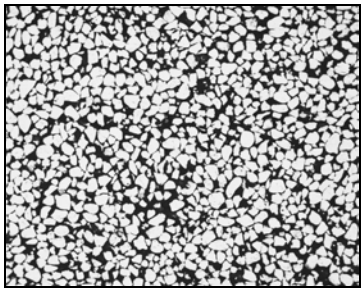

Fig.8 : SEM-micrograph showing clusters of big grains and clusters of little ones.

Hence, it is very interesting to go further from the simple compacity for characterizing the grain-arrangement. What is generally proposed is to consider following parameters :

- length between intercepts (intercepts are counted along a line, each time that the line goes inside a grain).

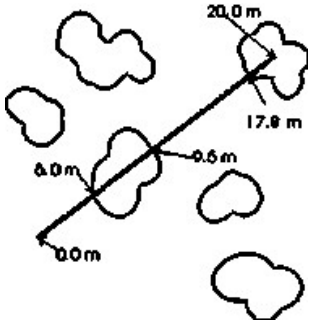

Fig.9 : Definition of intercept. Along the line, we meet two inputs in the grains, i.e. two intercept. Distance between these two intercepts will be considered.

- surface-ratio of the grains to the total area,
- quantity of objects per surface-unit.

Just considering the length of intercepts (or the surface-ratio, or the number of objects) is not sufficient, even if statistical calculations such as mean value, standard-deviation or distribution-curve are done.

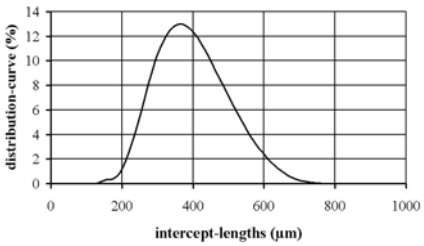

Fig.10 : usual distribution-curve for intercept-lengths.

Solution is to carry out a standard-deviation-analysis. It consists in calculating the value of the parameter on sub-areas, all sub-areas constituting a partition of the total one. All the values measured on the sub-areas are used for calculating a mean and a standard-deviation. By making variations of the size of the sub-areas, we get the curve of the standard-deviation versus the size of the sub-areas.

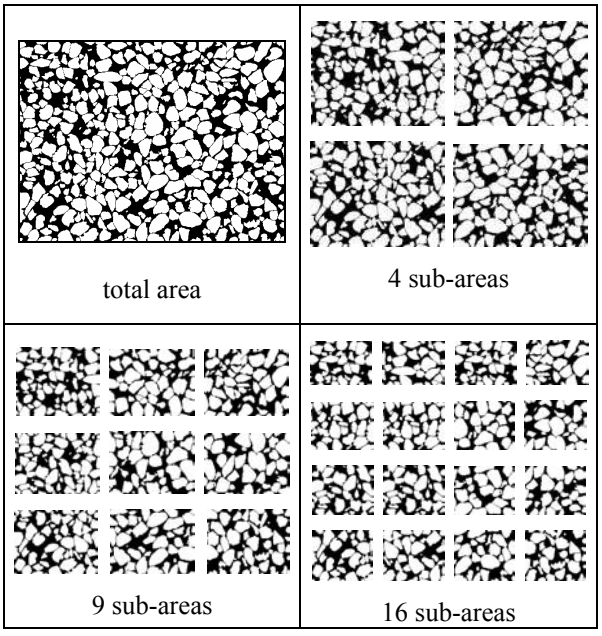

Fig. 11 : Principle of the successive sharing of the total area to sub-areas.

Standard-deviations (or variances) are then plotted versus the size of the sub-areas. That gives curves which are characteristic of the arrangement of the grains within the sample.

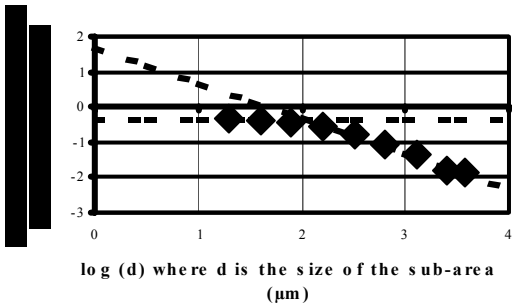

Fig. 12 : Curve of the standard-deviation-analysis for surface-area.

3.3.4. Comments:

Let us consider the parameter "surface area". See fig. 12.

For low sizes of sub-areas, standard-deviation doesn't depend on the size of sub-area. It just depends on the global porosity of the sample.

For bigger sizes of sub-areas, it is possible to demonstrate that standard-deviation is as the inverse of the size.

The curve is composed with two linear parts. Crossing of the two lines is a characteristic point called the "range of the curve".

Let us now have a look to the same analysis-curve for intercept-lengths.

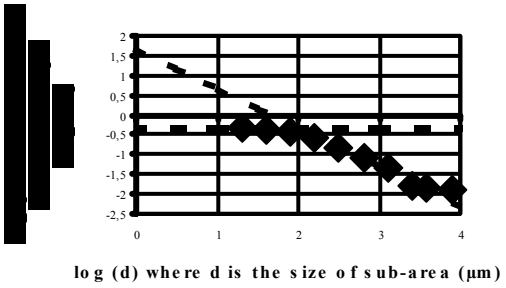

Fig. 13 : Curve of the standard deviation-analysis for intercept-lengths.

Evidence is that we find again some identical lines, but for the very largest sub-area sizes, a new flat stage appears.

The interpretation of this is that the parameter "surface-area" is constant over the all global surface, but the parameter "intercept-length" may vary from one region to the other one of the global area. It is a "measure" of the clusters of big and little grains.

4. Conclusions

FERRAZ-SHAWMUT is continuously tending to improve the quality and the performances of its products. For example, many adjustments of the sanding process are carried out in order to get the better and the more reliable electric characteristics. The problem is that between input-parameters, i.e. manufacturing-parameters and output-parameters, i.e. results of electrical tests, there is a lack of possible observations.

Standard-deviation analysis is a way to observe the arrangement of the grains. Of course this is still a heavy method, but it can be, with a minimum of improvements, very helpful for a better understanding of the operation-phenomena and for any modelling.

References

[1] Saqib M.A., Stokes A.D., Seebacher P.J. "Pressure inside the arc channel of high-voltage fuse" *ICEFA* Torino 1999.

[2] Saqib M.A., Stokes A.D., James B.W., Falconer I.S. "Arc temperature measurement in a high-voltage fuse" *ICEFA* Torino 1999.

[3] Lipski T., "Generation and propagation of the pressure due to the fuse-element disintegration in H.B.C. fuses" *Proc. of the Conf. on Gas Discharges and their Applications - Oxford, IEEE Conf. Pub, pp 87-90,* 1985.

[4] Wolny A., "Effect of fuse element confinement on the rate of rise of fuse arc ignition voltage" *ICEFA* Torino 1999.

[5] Gnanalingam S., Wilkins R. "Digital simulation of fuse breaking tests" *IEEE proc. Vol. 127, nr 6, pp 434-440* 1980.

[6] Bussière W., Bezborodko P., Pellet R. "Spectroscopy study of cutting electrical arc in H.B.C. fuse" *ICEFA* Torino 1999.

[7] Bussière W., "Influence of sand granulometry on electrical characteristics, temperature and electron density during high-voltage fuse arc extinction*" J. Phys. D:Appl.physs. ,34, p 925-935,* 2001.

[8] Murin-Borel V., Lieutier M., Parizet M.J. "Electric field and pressure measurements in high voltage fuses" *ICEFA* Torino 1999.

[9] Rochette D., Clain S. "Numerical simulation of Darcy and Forchheimer force distribution in a H.B.C. fuse" *Transport in Porous Media, 53, pp 25-37,* 2003.

[10] Rochette D. "Modélisation et simulation de la décharge d'un arc électrique dans un fusible moyenne tension", *Thèse de Doctorat en Physique, Université Blaise Pascal Clermont-Fd,* 2002.

[11] Vivier G., "Relations entre la microstructure des blocs agglomérés et les propriétés électriques des fusibles", *Thèse de Doctorat, INSA Lyon,* 2000.

[11] Serra J., "Images Analysis and Mathematical Morphology" *Academic Press* 1982.

[12] Serra J. "Image Analysis and Mathematical Morphology vol.2 : theoretical advance", *Academic Press* 1988.

[13] Coster M., Chermant J.L. "Précis d'analyse d'images" *Les presses du CNRS* 1985.

[14] Boitier G., Chermant J.L., Chermant L., Doireau F. Vicens, J. "Morphologie par analyse d'images de composites à fibres longues : principes et résultats", *in La Revue de Métallurgie*, Dec. 1977.

[15] Coster M., Chermant J.L. "Image analysis and ceramics" *in La Revue de Métallurgie* Feb. 2000.

[16] Gelet J.L., Missiaen J.M. "Le rôle du sable dans les fusibles ultra-rapides » *Congrès Matériaux SF2M Tours* 2002.

[17] Acevedo D., Missiaen J.M., Gelet J.L. "Caractérisation d'agglomérés de sable pour fusibles de puissance" *Proc. De la poudre au matériau massif Albi* 2003.

[18] Roueche E., Thomas G., Perier-Camby L., Seris E., "fragmentation de grains de sable. Suivi par émission acoustique et bilan de population" *Proc. De la poudre au matériau massif Albi* 2003.

THERMAL FATIGUE DAMAGE OF ULTRA-FAST FUSES

Jean-Louis Gelet[(1)]

[(1)] FERRAZ-SHAWMUT
Rue Vaucanson
69720 Saint Bonnet de Mure – France

Tél. : 33 (0) 4 72 22 66 30
Fax : 33 (0) 4 72 22 66 14
jean.louis.gelet@fr.ferrazshawmut.com

Abstract: *In ultra-fast fuses, current-density can reach values as high as several hundred of A/mm². This induces an important heating and consequently stresses in the more fragile area of the conducting element, i.e. the notches. As the fuse is often submitted to cyclic loads, ageing of the notches occurs and then the fuse opens. FERRAZ-SHAWMUT is for a long time aware of this phenomenon and since years has carried out many tests on his fuses. Rules does exist in order to choose the right fuse for a given application [1]. But, keeping in mind the permanent will of better service to his customers, FERRAZ-SHAWMUT is now working for improving the calculation of the life-time of the fuses in case of long durations (typically ten to thirty years).*
As it is not possible to wait for years, an accelerated tests-method has been settled in additional with pure mechanical tests, allowing to reach millions of cycles. Analysis of the tests-results shows that ageing of fuses is a combination of both fatigue and creep. Furthermore, validation of the accelerated tests is assured by SEM-observations.

Keywords: electric fuse, cyclic load, fatigue, creep

1. Definition of the problem

For the protection of power-semi-conductors, specific ranges of fuses are designed, following IEC standard 269-4. The fundamental specificity of these fuses is to be able to operate very rapidly in case of short-circuits in the field. That means that for a given rated-current, these fuses are required to have a minimal conducting area; or, on another hand, for a given I²t, to carry a maximal current.

But carrying a maximal current doesn't go without any risks. The biggest of them is the occurrence of some metallurgical fatigue phenomenon. Indeed, by Joule-effect, the current-conduction induces a heating of the conductors, specially at the notches of fuse-elements. Then, the temperature would cause some dilatation of the metal. But, as this dilatation is interfered with sand around the notches, stresses are developed. Note that stresses are generated all along the element, but they are amplified on the restrictions of the necks.

When fuses are used in a cyclic way, the alternation of stressed and relaxed states leads to ageing by fatigue phenomenon.

The problem with power-semi-conductor-fuses is to find the better compromise between I²t and ageing. For a long time, FERRAZ-SHAWMUT is aware of this phenomenon and thanks to many tests, could develop the method allowing to correctly choose a fuse.

Nowadays requirements from customers concern figures for very long life-durations, up to thirty years, and statistical considerations giving evaluation of tolerances around mean values.

This requires new tests-programs. It is very understandable that testing fuses for excessive long times is not possible and that accelerated tests are to be thought.

One idea is to heat only the notches, which are actually the only part of the fuses subject to ageing. Even though the nearest environment of the notches is kept as in fuses, it is possible to drastically reduce the thermal time-constant of the test-sample and then to reach high numbers of cycles, comparable with long life-durations.

2. Tests

2.1. Principle of the tests

A single fuse-element is supporting the current. This element is placed on an aluminium cooling-water-box. Electrical insulation between fuse-element and water-box is done by an insulating tape. In spite of this, there is a good thermal conductivity between

the fuse-element and the cooling-box. Notches are surrounded by sand. The sand is held inside a fuse-ceramic-body.

In addition, the drop-voltage between each side of the raw of notches is permanently measured. It allows to get the mean temperature of the notches from the variation of resistivity of the fuse-element-metal versus temperature. See Fig.1.

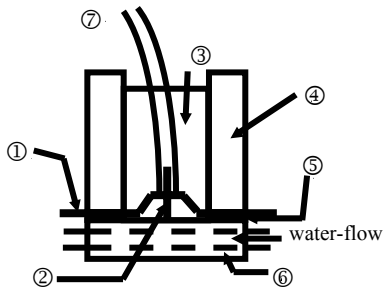

Fig.1 : Principle of the tests :①fuse-element; ②notches; ③sand; ④ceramic body; ⑤ insulating tape; ⑥water-box for cooling; ⑦drop-voltage measurement.

It has been checked that ON/OFF cycles such short as 10 sec/10 sec will allow to get significant temperature-rise during the ON-phase and a cooling to sufficiently low temperature during OFF-phase. For example and depending on the current, the mean temperature of the notches can reach 200÷300°C during ON-phase and decreases to 25÷40°C during OFF-phase.

Large interest of this accelerated test is demonstrated if we take care that same temperature-rises as for 1 hour ON/1 hour OFF-cycles is got within 10 + 10 seconds. In other words, number of cycles is multiplied by 360 within the same time. Thirty years will be reduced to 1 month.

2.2. Tests-results

These accelerated tests bring several levels of results.

2.2.1. Increase of temperature at the end of fuse-life :

Thanks to the temperature-measurements, it appears that the fatigue phenomenon doesn't occur suddenly. The increase of the resistance begins to be significant when a half to a third of the life-duration is still remaining.

When tests are carried out on complete semi-conductor-fuses, with many rows in series and in parallel, the death of the fuses is very sudden, as only a few percents of the life-duration is still remaining.

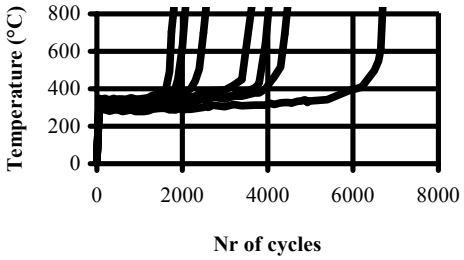

Fig.2 : Measurement of temperature through the drop voltage allows to show that the damage increases first slowly and then is accelerated at the end of life-time.

2.2.2. Numbers of cycles versus current

Numbers of cycles have been plotted versus test-current. Afterwards, statistical treatment of the results gives the mean value

$$\log(N) = -23.\log(I) + \text{cste} \quad (1)$$

and the tolerance for the life-duration.

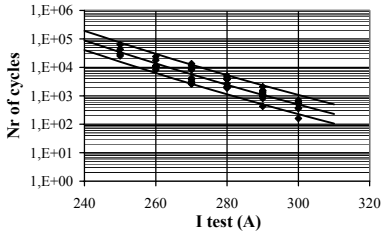

Fig.3 : Numbers of cycles are plotted versus the test-current, here with log-lin scale. Mean curve and 90%-tolerance-curves are also plotted.

2.2.3. Numbers of cycles versus temperature

Numbers of cycles have been plotted versus maximal temperature at the end of 10s/10 sec. cycle. Afterwards, statistical treatment of the results gives the mean value :

$$\log(N) = -8.\log(\theta\text{maxi}) + \text{cste} \quad (2)$$

and the tolerance (for instance at 90%) for the life-duration.

In addition with thermal models giving the temperature of the notches during cyclic use, they will allow to determine the numbers of cycles a fuse will withstand in the field.

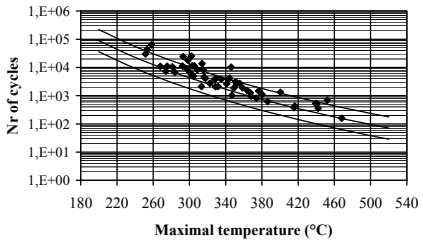

Fig.4 : Numbers of cycles are plotted versus the maximal recorded temperature, here with log-lin scale. Mean curve and 90%-tolerance-curves are also plotted.

2.2.4. Numbers of cycles versus temperature-increase

Statistical treatment of the results gives the mean value

$$\log(N) = -5.5.\log(\Delta\theta) + \text{cste} \qquad (3)$$

and the tolerance (for instance at 90%) for the life-duration.

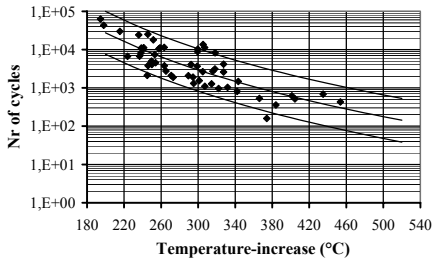

Fig.5 : Numbers of cycles are plotted versus the recorded temperature-increase, here with log-lin scale. Mean curve and 90%-tolerance-curves are also plotted.

3. Validation

3.1. From theory of fatigue

In the 60's, COFFIN [2-3] and MANSON [4] carried many works on fatigue-phenomenon. One of their more interesting results is that the life-duration of the materials depends on the level ε of the strains according to the expression :

$$\log(N) = a.\log(\varepsilon) + \text{cste} \qquad (4)$$

According as strains are plastic or elastic, these authors announced following values for coefficient a:

for plastic strains, a varies from –1.4 to –2,
for elastic strains, a varies from -6 to –10.

These results came mainly from tests carried out on steels and stainless steels. FERRAZ-SHAWMUT did tests on pure silver, as used for manufacturing fuse-elements.

Mechanical bending tests have been carried out on a rotating machine. They led to the following values for the coefficient a :

for plastic strains, a varies from –2.5 to –3,
for elastic strains, a varies from -6 to –8.

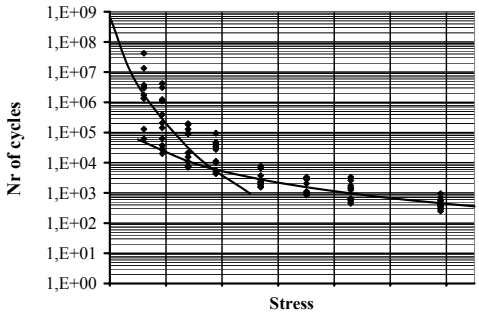

Fig.6 : Numbers of mechanical cycles are plotted versus the stress, here with log-lin scale. Two kinds of behaviour are observed according to the level of stresses.

3.1.2. Extension of the model to thermal fatigue

LEMAITRE and CHABOCHE [5] have first introduced the idea that thermal fatigue was a combination of mechanical fatigue and creep. After them, MANSON [6-7], HALFORD [7-8] and HIRSCHBERG [8] proposed four typical four typical cycles :

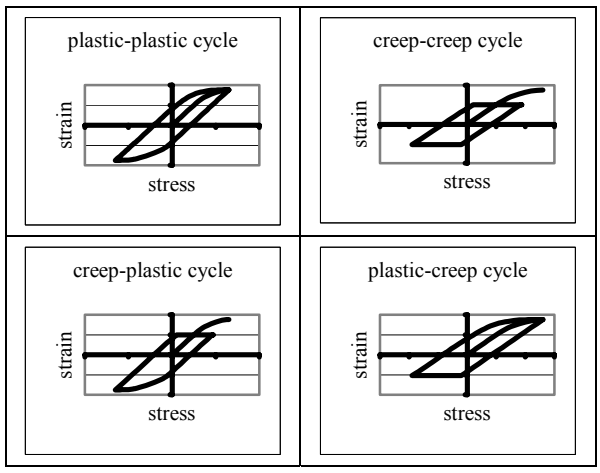

Fig. 7: Four typical cycles combining plastic strain and creep.

For each one of these typical cycle, a law gives the number of cycles versus the strain :

$$\log(N_{ij}) = -\gamma_{ij}.\log(\varepsilon_{ij}) + cste \qquad (5)$$

where the indexes i and j represent c or p, for plastic and creep,

ε_{ij} is the part of the total strain corresponding to the typical cycle ij.

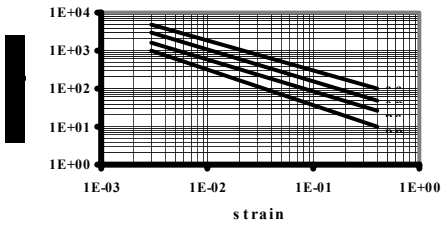

Fig. 8: For each one of the typical "plastic-creep" cycles, it is possible to estimate one ageing-law.

The total strain is the summation of the different strains of each typical cycle :

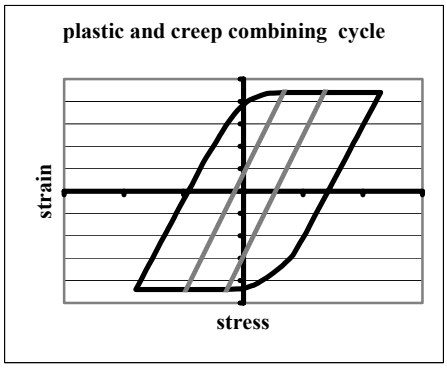

Fig. 9: Example of combination of 3 typical cycles.

The number of cycles for the total strain is assumed to follow a law as :

$$\frac{1}{N_{total}} = \sum \frac{\varepsilon_{ij}}{\varepsilon_{total}} x \frac{1}{N_{ij}} \qquad (6)$$

$$\varepsilon_{total} = \varepsilon_{pp} + \varepsilon_{pc} + \varepsilon_{cp} + \varepsilon_{cc} \qquad (7)$$

As presented previously, FERRAZ-SHAWMUT carried out accelerated tests. Different relationships have been found, according to what parameter was considered as stress :

$$\log(N) = -23.\log(I) + cste \qquad (1)$$

$$\log(N) = -8.\log(\theta maxi) + cste \qquad (2)$$

$$\log(N) = -5.5.\log(\Delta\theta) + cste \qquad (3)$$

Note that there is a good coherence between expressions including current and maximal temperature. Indeed, it is possible to approach that temperature is as the 3rd power of the current :

$$\theta = \theta_0 + (1+\alpha.\theta)Ri^2 \approx Ri^3 \qquad (8)$$

Furthermore, we could make the assumption that stresses or strains are directly proportional to the temperature θ or to the temperature-increase Δθ. Indeed, as θ is due to the sand-interfered thermal expansion, we could write :

$$\varepsilon = \frac{\Delta l}{l} = \frac{1}{l}.\lambda.\Delta\theta \qquad (9)$$

were :

l is the concerned length of material,

Δl is the linear expansion of the material due to temperature,

λ is linear-expansion-coefficient of the material,

$\Delta\theta$ is the temperature-increase.

If this assumption was true, we would have to find out the same coefficients a as for mechanical-tests on pure silver. As we don't, that means that actual strain might be a combination of both fatigue and creep phenomena.

3.3.2. From SEM-observations

We did SEM observations on fuse-elements after ageing by different ways (usual electrical cycle, accelerated tests, mechanical tests). The main pieces of information concern:

Slip-bands : traces observed on the surface of the samples. They correspond to a displacements at crystallographic plans inside the metal-grain. Slip-bands may be at the origin of a crack.

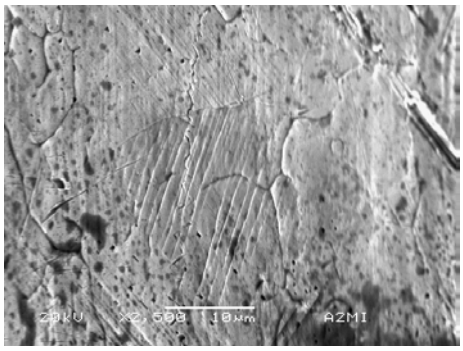

Fig. 10 : Slip-bands on a fuse-element after rupture. 450 electric cycles 1h ON/1 h OFF.

Fatigue lines : traces observed on the crack-area. They correspond to the incremental successive steps of the propagation of the cracks.

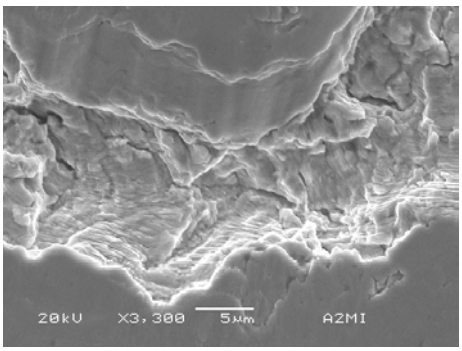

Fig. 11: Fatigue-lines on a sample after rupture. 39000 mechanical bending-tests cycles.

Grain-decohesion : observed at both surface and crack-area. They correspond to the opening of cracks between metal-grain (intergranular cracking).

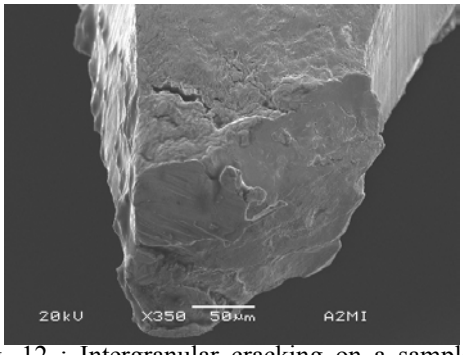

Fig. 12 : Intergranular cracking on a sample after rupture. 1200 mechanical bending-tests cycles.

Transgranular cracking : observed at both surface and crack-area. They correspond to the opening of cracks through one metal-grain.

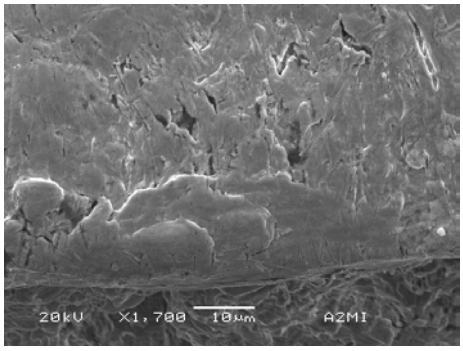

Fig. 13 : Transgranular cracking on a sample after rupture. 39000 mechanical bending-tests cycles.

3.2.2. Comparison of the observations:

The following table 1 summarizes what kind of indications have been got, depending on the kind of the test and the level of solicitation. In addition to this chart, some comments may be done :

- fatigue lines always occur,
- slip-bands have been clearly observed in case of plastic strains. Some indications have been observed in case of elastic strains, but for the time being, it has been difficult to settle if there were actually slip-bands,
- in case of plastic strain, cracks are transgranular and intergranular ; in case of elastic strains, only transgranular cracks have been observed.

tests	Nr of cycles	slip-bands	fatigue-lines	grain-crack	strain
mechanical	$2.2.10^6$	no		transgranular	elastic
mechanical	180.10^3	no	yes	transgranular	elastic
mechanical	39.10^3	yes	yes	trans & inter	transition e/p
mechanical	$1.2.10^3$	yes far from crack	yes	trans & inter	plastic
accelerated	$>25.10^3$		yes	trans & inter	transition e/p
accelerated	$>1.2.10^3$		yes	trans & inter	plastic
electric 1hON/1hOFF	540	yes far from crack	yes	trans & inter	plastic

Table 1 : Summary of the SEM-observations.

4. Conclusions:

A set of conclusions have been drawn out of this study :

a) ageing of the necks of the fuse-element occur slowly, in contradiction with what is observed on complete fuses.
b) mechanical tests show that up to 10^4 cycles, strains on pure silver are plastic,
c) mechanical tests show that over 10^5 cycles, strains are elastic,
d) electrical tests (usual and accelerated) led to ageing by both plastic strain and creep.
e) the knowledge of the partition between plastic strains and creep will be necessary in order to reach a good ageing-model.

Nevertheless, it seems that these conclusions could be appreciated by additional tests :

- accelerated tests up to 500.10^3 to 10^6 cycles in order to clearly check the sharing between elastic and plastic behaviours,
- accelerated tests with different ON-times in order to underline the effect of creep,
- continuous-creep tests in order to know actual withstanding of pure silver versus this kind of solicitations and to compare the crack-aspect to the ones got under cyclic loads.

References

[1] FERRAZ-SHAWMUT– leaflet NT59.
[2] Coffin L.F. : "Internal stresses and fatigue in metals". *Elsevier,* New-York 1959.
[3] Coffin L.F. :"Fatigue" *Corporate Research and Development, GE Company, Schenectady,* New-York 1972
[4] Manson S.S. "Fatigue, a complex subject, some simple approximations". *Experimental Mechanics* 1965.
[5] Lemaître J., Chaboche J.L. : "Method of metal characterization for creep and low cycle fatigue prediction in structures." *1st symposium on Mechanical Behaviour of Metals,* Kyoto 1973.
[6] Manson S.S. "Thermal stress and low Cycle fatigue" *McGraw Hill* 1966.
[7] Manson S.S., Halford G. "*Int. Conf. Thermal and High Strain fatigue*" London 1967.
[8] Hirschberg M.H., Halford A.J. "Strain range partitioning. Atool for characterizing high temperature low cycle fatigue" *NASA* 1975

Intelligent fuse for M.V. distribution systems: a current need.

Juan Carlos Gómez
Rio Cuarto National University, Engineering School,
Power Electric System Protection Institute
Ruta 36, Km. 601, Río Cuarto, Córdoba
ARGENTINA
Phone: +54 358 4676175, Fax: +54 358 4676171
Email: jcgomez@ing.unrc.edu.ar

Abstract:
The widespread application of fuses is based upon its low cost, high reliability that roots in their simplicity, and on the application of well-known physical principles. From its invention (roughly by 1880), the main improvements have been aimed to use of better materials, to extend the application range, and towards the development of faster and cheaper construction techniques. Many parallel and series combinations of similar or different fuse links were also described in the literature. The phrase "New fuse design or type for specific applications …" has been groundlessly expressed many times. No critical changes towards adding intelligence to the traditional fuse have been lately produced. During more than 120 years of fuse application several improvements have been published at conferences and magazines, but just a few of them have been really available and of stable market position. A literature survey of the main fuse intelligence adding and innovations from their beginnings is here described and discussed. Current needs, especially for medium voltage fuses applied to distribution systems having embedded generation are also presented. Directionality and discrimination between phase-to-earth and phase-to-phase faults are today fuse capability needs, describing some ideas about the ways to reach them. Medium voltage fuse technology urgently need of new breed and fresh blood, otherwise their future application would be very uncertain, which unfortunately have been broadly revealed in the past. Distribution system is still a field where fuses are strongly suited thus any effort towards increasing its presence would be worthwhile.

Keywords: electric fuse, distributed generation, discrimination, intelligence

I. INTRODUCTION

Unfortunately, we, fuse researchers are seeing as day by day fuses are relegated to smaller and smaller niches, such as semiconductor protection, and medium voltage motor applications. Such exclusion is perhaps caused by the lack of new fuse designs able to adapt to the quickly changing electrical system needs.

Lately, big movement has been done towards the improvement of motor protection fuses, but the distribution system fuse has been practically left aside except for the breaking capacity widened towards the low current area [1].

In many application fields, especially on low and medium voltage distribution applications, fuse competitor devices have incorporated a big deal of improvements and enhancements, specially giving flexibility and adaptability. Two characteristics of which the traditional fuse lacks.

The very high cost of fuse developments, primarily due to the high short-circuit testing charges, trends to slow down the introduction of new fuse designs.

Today due to this fuse flexibility lack, fuses are in risk to be banned of any distribution circuit having distributed generation (DG).

The cited flexibility can be also called as intelligence, understanding for intelligent fuse the protection device that is able to make decisions, for instance doing opening and reclosing operations, discriminating direction and detecting phase currents from earth currents.

II. BACKGROUND AND HISTORY OF FUSE IMPROVEMENTS

The today widespread application of distribution fuses is based upon its low cost, high reliability that roots mainly on their simplicity, and on the application of well-known physical principles.

From fuse beginnings, first scientific reference by Sir. Edward Nairne during 1773 and first official US fuse patent granted to Thomas Edison by 1880, the main improvements have been aimed to use of better materials, to extend the current and voltage application ranges, and towards the development of faster and cheaper construction techniques [2, 3].

Between the transcendental fuse improvements the M-effect incorporation by Metcalf during 1939 need to be mentioned [4].

After that early improvements many changes into the original fuse design have been presented, all of them in order to extend the low current interruption capability having different acceptation or success degrees.

Among them can be mentioned:

- Utilization of non-traditional fuse element metals, as for instance Aluminum or Cadmium [5, 6].
- Use of bounded silica sand [6].
- Use of two dissimilar bounded or unbounded metals [7, 8].
- Current limiting and expulsion elements put together inside a single fuse body [9, 10].
- Paralleled combination of high-voltage expulsion fuse and Z_nO varistors [11].
- Hybrid fuse using SF_6 or vacuum fuse in series with traditional high current part [1, 12].
- Repetition fuse and self-healing or permanent fuse using high-pressure sodium and mercury as fuse elements, idea lately extended to the application of polymeric compounds [13, 14].

During more than 120 years of fuse application many improvements have been published at conferences and magazines, but just a few of them have been really available and of stable market position.

The phrase “New fuse design or type for specific applications …” has been groundlessly expressed many times. No critical changes towards adding intelligence to the traditional fuse have been lately produced.

A literature survey of the main fuse intelligence adding and innovations from fuse design beginnings intending to analyze the presented DG problem was done. From this survey, just two suitable original ideas had come out, the application of chemical charges and the use of saturable transformers.

The two ideas can be summarized as follows.

a) Application of chemical charges:

The idea was originally presented for Muth & Zimmermann by 1938 [15], based upon the fuse blowing due to the ignition of a chemical charge caused by a externally controlled heater, being the device described as the combination of the accuracy of a relay with the cheapness of the fuse. Afterwards the same idea was pursued and developed, especially on the ignition control system, introducing in the market by 1963 the device called “limiter”, which have been since in the

market [16]. The same concept was further developed and applied to the Automatic Seccionalizer, coming out by the eighties [17]. By the same decade many other designs using this principle were presented, especially developed for medium voltage distribution systems, having dissimilar market success [18, 19]. One of them, called Electronic Power Fuse loaded with up-to-date or last generation electronics has got a relatively good foot in the market, in spite of its still high cost [20]. By 1990 a technical paper was produced, presenting a new design applying this concept to low voltage dc systems, called Smart Fuse [21]. No more than five years ago, the limitations of the application of this chemically charged device for the expansion of distribution systems were emphasized giving recommendations about how to avoid frequent misapplications [22].

b) Use of saturable transformers

During the seventies an interesting idea was proposed, related to the availability in a single fuse cutout of a double fuse time-current-characteristic. This double TCC was obtained by using a current transformer which working zone included the saturated and non-saturated areas, changing the two paths current sharing depending on the overcurrent level. The mentioned design was proposed for the solution of coordination problems between the main feeder and branch protections. Initially the current transformer was located by the detachable fuse link, being lately attached to the fix cutout part [23].

III. PROPOSED FUSE

One of the today most important needs is the availability of medium voltage fuses especially designed for being applied to distribution systems having embedded generation, where particular requirements shall be considered. Figure 1 shows a typical system having embedded distributed generation. In Fig. 1 the Sensitive Equipment and faulted branch locations are shown in Distributed Generation and main supply sides respectively.

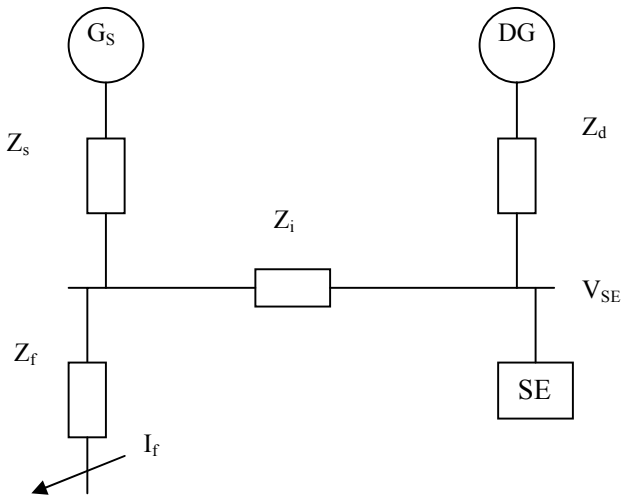

Fig. 1, Typical distribution system having DG

Currently there is a big movement in the field of distribution generation having DG mainly due to the present Power Quality strict requirement, being voltage sag presence one of the biggest issue [24].

From the voltage sag point of view, is really very important to keep the DG connected and feeding the system during fault events, due to its capability to backup the system voltage, increasing the possibility that the sensitive equipment would remain operative. In the other hand there is a serious risk of keeping part of the system working under “islanding” conditions. Besides there are serious difficulties on getting selective coordination for all the possible operating conditions, having the fault energy coming from either the main supply or from the DG, being the DG presence in the system decision of the DG owner and not of the main utility.

The solution for the listed drawbacks can be done by using complex and expensive

protection schemes, due to many of the needed task are out of the traditional fuse reach. Among the intelligence that the fuse today needs to have, the most important ones are directionality and discrimination if ground is included in the fault path.

Besides the solution must have a cost enough low as to keep the complex fuse as an attractive possibility if compared with the competitors.

Both ideas have been combined in a design that analytical studies shown to be very auspicious. As the design is in its way to start the patenting process, no further details can be provided here.

IV. CONCLUSIONS

Medium voltage distribution fuse technology urgently need of new breed and fresh blood, otherwise their future application would be very uncertain, which unfortunately have been broadly revealed in the past. Distribution system is still a field where fuses are strongly suited thus any effort towards sustaining and increasing its presence would be worthwhile. The joint application of the well-known chemical charges and saturated transformer technologies allows the production of a fuse able to operate following two dissimilar TCC depending on the direction of the current passing through the fuse construction.

REFERENCES

1- Konig, D., Brechtken, D., High Voltage Hybrid Fuse, 2nd Inter. Conference on Elect. Contacts, Arcs, Apparatus and Applications, pp. 122-126, 1993.

2- Nairne, E., Electrical Experiments by Mr. Edward Nairne, Phil. Transactions, Royal Society (London), 1774.

3- McEwan, P., Mr Edward Nairne FRS – Discoverer of the electric fuse ?. Perspektywy Rozwoju Technik Przerywania Pradu, ISSN 1225-5766, Gdansk, 1996.

4- Metcalf, A., A new fuse phenomenon, Beama Journal, Vol. 44, pp. 109-12 and 151-152, 1939.

5- Westrom, A., Crooks, W.R., Narancic, V., Current limiting fuses – a comparative evaluation, 9° IEEE Power Engineering Society, Minneapolis, 1981.

6- Leach, J. G., New application flexibility for Medium-Voltage Current-Limiting fuses, IEEE Trans. on Industry Applications, Vol. IA21, No 4, pp. 1075-1080, 1985.

7- Narancic, V., Braunovic, M., Westrom, A., The composite fuse – a new technology for current limiting fuses, 7° IEEE Power Engineering Society, pp 462-470, 1979.

8- Gómez, J., Tourn, D., McEwan, P.; Investigation of the pre-arcing behavior of dissimilar uniform double element, filled fuse, using finite element CAD techniques, Fourth International Conference on Electric Fuses and their Applications, Nottingham, pp. 65-67, 1991.

9- Rosen, P., Full-range fusing – a new concept in system protection, Electrical Review, V. 213, No 4, pp. 33-34, 1983.

10- Miura, H., Takaoka, N., Tanahashi, Y., Ono, Y., Kito, Y., New dual-element current limiting power fuse with full protection capability against any fault current, IEEE Trans. on Power Apparatus and Systems, Vol, PAS-98, No 6, pp.1885-1894, 1979.

11- Wolny, A., Stokes, A.D., Kacprzak, B., High-voltage fuse behavior with varistor commutation, IEE Proc. Gener. Transm. Distr., Vol. 141, n° 1, pp. 3337, 1994.

12- Bucher, T., Encapsulated current-limiting fuses: grounded-front design, IEEE Trans. on Power Apparatus and Systems, Vol. PAS-101, No 7, pp.1975-1978, 1982.

13- Itoh, T., at al, Design considerations on the ppf for a control center, IEEE Trans. on Power Apparatus and Systems, Vol. PAS-92, No 2, pp. 1292-1297, 1973.
14- Gundlach, H., A self-restoring current-limiting device, 3° International Symp. On Switching Arc Phenomena, Poland, pp. 287-292, 1977.
15- Muth, H., Zimmermann, K., Steuerbare Sicherungen im Maschennetzbetrieb, ETZ, vol. 59, pp. 1257-1261, 1938.
16- Bruckner, P., A new type of switching device with extremely short breaking times, ETZ-A, pp. 33, 1958.
17- Rosen, P., Golden, F., A single-phase automatic sectionalizer, IEEE Power Engineering Society, California, 1986.
18- Pflanz, H., Clark, T., Albani, O., The development of the current limiting protector (CLP), IEEE Trans. on Power Apparatus and Systems, Vol. PAS-100, No 7, pp. 3609-3616, 1981,
19- Ranjan, R., Design, Development and Application of Smart Fuses – Part 1, IEEE Trans. on Industry Applications, Vol. 30, No 1, pp.164-169, 1994.
20- Glenn, D., Cook, C., A new fault-interrupting device for improved medium-voltage system and equipment protection, IEEE Industry Applications Society, Chicago, 1984.
21- Martin, D., Smart fuses enter with a small bang, Electrical Review (UK), May, pp. 7, 1990.
22- Das, J., Limitations of fault-current limiters for expansion of electrical distribution systems, IEEE Trans. on Industry Applications, Vol. 33, No 4, pp. 1073-1082, 1997.
23- Aubrey, D., New 11 kV expulsion fuses for overhead lines, Electrical Times, August 1, 1974.
24- Gómez, J. C., Morcos, M. M.; Coordinating Overcurrent Protection and Voltage Sag in Distributed Generation Systems, IEEE Power Engineering Review (Feature Article), Vol. 22, n° 2, Feb. 2002, pp. 16-19.

Thermal Modeling of High Voltage H. R. C. Fuses and Simulation of Tripping Characteristic

G. Hoffmann[(1)] and **U. Kaltenborn**[(2)]

ABB Switzerland Ltd, Corporate Research[(1,2)], Segelhof 1, CH-5405 Baden-Dättwil, Switzerland,
guido.hoffmann@ch.abb.com[(1)], uwe.kaltenborn@ch.abb.com[(2)]

Abstract: The operation of a fuse is always a thermal process. To know the thermal behavior of a fuse is important for an optimized design as well as for the right choice of the fuse rating for each application. A model for a fuse based on the Thermal Network Methodology was developed, including terminals, electrical connections, and a fuse canister. In this model, the thermal behavior of a h.r.c. fuse is only dependent on the design of the fusing element, the material parameters, and the ambient conditions. The elements of the thermal network are based only on the geometry and the material properties of the different components. The simulated temperatures were compared with measured temperatures at defined positions of the fuse. By introducing the thermal capacitance as an additional material parameter, a time-dependent dynamic simulation becomes possible. It was shown that such a dynamic model allows a highly accurate simulation of the tripping characteristic of high voltage h.r.c. fuses.

Keywords: high voltage fuse, h.r.c. fuse, thermal simulation, thermal network

1. Introduction

The physical processes in a fuse are always initiated by the thermal behavior of the fuse in the specific application. In the electrical grid a fuse, or better the fuse element, is a defined reduction of the electrical conductor cross-section. This means an increase of the electrical resistance. Each resistance is corresponding to a certain electrical loss. Due to the fact that the impedance of a conventional fuse is very low, most of the electrical losses in fuses appear as thermal losses.

These thermal losses of the fuse element have to be forced away from the fuse element. This will happen along the fuse element and radial through the arc extinguishing medium and the housing. If the thermal losses produced in the fuse element and the heat flow away from the fuse element reaches equilibrium, the temperature of the fuse element will stay stabile. As soon as the equilibrium is distorted in such a way that the heat flow away from the fuse element is less than the thermal losses, a thermal run away occurs. Due to the temperature dependency of the electrical resistance of metals, the resistance will increase with the temperature and therefore increase the thermal losses. This deadly spiral will continue until the melting point of the fuse element is reached and the fuse will trip.

To understand and to optimize the operating mechanisms of h.r.c. fuse links, the thermal behavior of the fuse itself and their application is of major interest. Having the opportunity to simulate the thermal processes at the fuse element dependent on the fuse design enables new features for the optimization of h.r.c. fuses. On the other hand, new fuse designs can be evaluated for their thermal behavior. By introducing a dynamic model including thermal capacitances, also the tripping characteristic can be simulated. This will have a great impact to the development and test costs of new fuses.

Extending the model with thermal models for the specific applications enables the user of h.r.c. fuses to choose the right ratings and to evaluate critical load cycles and to identify potential overload capacities for a dynamic grid loading.

2. Fundamentals of the thermal network method

The thermal network method is based on the analogy between the electrical and thermal flow field [1-2], (Table 1).

Table 1: Analogy between electrical and thermal flow field

Electrical Parameter			**Thermal Parameter**		
Potential difference	$\Delta\varphi$	V	Temperature difference	$\Delta\vartheta$	K
Electrical current	I	A	Heat flow	P	W
Electrical resistance	R_{el}	Ω	Thermal resistance	R_{th}	K/W
Electrical capacity	C	As/V	Heat capacity	C_W	Ws/K

Due to this analogy heat transport processes in electrical devices can be described with thermal networks, which consists of heat sources, thermal resistances, and heat capacities.

As the thermal resistances, the heat capacities and heat sources are temperature-dependent the

resulting thermal network is nonlinear. The networks will iterative calculated by using the nodal point procedure known from electrical network calculations. That means thermal networks can be solved with common network analysis programs like PSpice or SIMplorer [2-3].

3. Structure of the thermal networks

For every individually device like the h.r.c fuse itself, the fuse mounting, the fuse canister for ring main unit installations or the connecting cables, separate thermal networks were designed. These networks are comparable with modules, which can be easily connected together by defined nodes.

In thermal networks the heat sources like the fuse wires, the contacts, and the conducting parts of the fuse mounting will be simulated as electrical resistors, which are temperature- and current-dependent. The heat conduction in the fuse in radial direction to the surface of the ceramic tube or in axial direction to end caps as well as the convection to the ambient air and the radiation to ambient (free air) or to an opposite surface (canister) were modelled with corresponding thermal resistors in the network.

All necessary simulation parameters for the network elements (resistors for heat conduction, radiation and convection and heat capacity) result from the geometry and the different material properties of the fuse.

For the creation of the thermal networks the fuse as well as the fuse canister will be discredited into different parts, i.e. the fuse into end caps and several slices of the middle part (tube).

The modelling of the fuse with the thermal network method will be shown with simplified networks on following examples:

- Simulation of the fuse wire
- From the fuse wire to outer surface
- End caps and fuse terminal
- Canister

The thermal networks were created with the SCHEMATICS-GUI and solved with the PSpice-solver[1]. The elements for the thermal processes where used from a thermal library available from THETA[2], and own extensions.

3.1. Simulation of the fuse wire

The heat source in a fuse is the conducting fuse wire. In case of common medium voltage fuses this fuse wire is made of silver. For different nominal current ratings you will find a different number and different dimensions of fuse wires wounded around a ceramic star-shaped stick in the fuse.

Normally a single fuse wire consists of a silver band with several constrictions for the arc extinction in case of short-circuit-currents. These constrictions can have different shapes, for the present model the constriction has semicircular punched areas on both sides.

Every flow of current through a silver wire will produce power losses:

$$P = kI^2 R(\vartheta) \tag{1}$$

The power losses depends on the current displacement factor k, the squared current I^2 and the electrical resistance $R(\vartheta)$. This temperature-dependent resistance can be calculated by

$$R(\vartheta) = \frac{\rho_{20} l}{A}\begin{bmatrix} 1 + \alpha_T(\vartheta - 20°C) + \beta_T(\vartheta - 20°C)^2 \\ + \gamma_T(\vartheta - 20°C)^3 + \delta_T(\vartheta - 20°C)^4 \end{bmatrix} \tag{2}$$

with:

$$\rho_{20} = 0.017961 \frac{\Omega mm^2}{m}$$

$$\alpha_T = 9.623 \cdot 10^{-4} \frac{1}{K}; \quad \beta_T = 1.277 \cdot 10^{-5} \frac{1}{K^2}$$

$$\gamma_T = -1.908 \cdot 10^{-8} \frac{1}{K^3}; \; \delta_T = 1.013 \cdot 10^{-11} \frac{1}{K^4}$$

where ρ_{20} is the resistivity of the silver wire at 20°C and α_T, β_T, γ_T, and δ_T are the thermal coefficients describing the temperature dependency.

Normally only α_T will be used for a linear increase of the resistivity with the temperature. Because the heat source element in the thermal library is programmed to use the four coefficients the resistivity curve was fitted in this way.

This also increases the simulation accuracy in the range of higher temperatures where the resistivity doesn't follow the linear increase of only one coefficient. The high temperature range is especially important for simulation of the pre-arcing time because there the accuracy up to the melting point of the silver wire is needed.

To simulate the heat source, i.e. for the dimensioning of the melting wire, it is necessary to consider the geometry of the fuse wire, especially the constrictions of the fuse wires, which has to be implemented into the calculations.

There are different possibilities like FEM simulations to calculate the electrical resistance of the constriction, but [4] describes an easy to use empirical method for the calculation of the

1 OrCAD PSpice and Schematics Version 9
2 Ingenieurbüro Theta (Dresden/Germany)

resistance-change of a fuse wire with one or more constrictions.

The parameter of the constriction coefficient E will be introduced, which is independent from dimension and the material of the fuse wire. The constriction coefficient could be applied to all sections of wires with a particular geometric base. It is a function of the base figure.

Wire sections with a number of constrictions for the limitation of high current arcs and with a shape of circles (Fig. 1) can be calculated with [4]:

$$E = \frac{\pi}{2}\left(\sqrt{\frac{r}{e}} \cdot arctan\sqrt{\frac{r}{e}} - \frac{r}{b}\right) \qquad (3)$$

where r is the radius of the semi-circular holes in the fuse wire, e is half of the constriction width, and b is half of the fuse wire width.

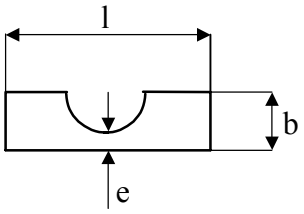

Fig. 1: Section of a fuse band with a constriction

Now the resistance of melting wire with changed cross section can be calculated as follows:

- Melting band with one constriction

$$R_1 = \left(1 + E\frac{b}{l}\right)R_0 \qquad (4)$$

- Melting band with n constrictions:

$$R_1 = \left[1 + \left(E_1 + E_2 + ... + E_n\right)\frac{b}{l}\right]R_0 \qquad (5)$$

R_1 is the resistance of a wire section with one or more constrictions and R_0 is the resistance of a wire section without constrictions. Both wire sections have the same length.

The relation R_1/R_0 is a factor for the increase of the resistance by the constrictions.

For the simulation of the heat source, the fuse wire was disassembled into 2 parts.

- a homogeneous part (plane wire without constrictions) of the fuse wire with a constant cross section.
- a second part of the fuse wire with all constrictions

From the relation of the lengths of these two different parts of the fuse wire the same relation of the electrical resistances can be calculated.

With these both resistances two heat sources can be created. Because there is the possibility to add a current displacement factor in the heat source element this is an easy way to regulate the influence of the constrictions. For the homogeneous part of the melting wire the current displacement factor is 1. For the part of the fuse wire with constrictions it will be larger than 1 depending on the geometry and can be calculated with the above equations (4), (Fig. 2).

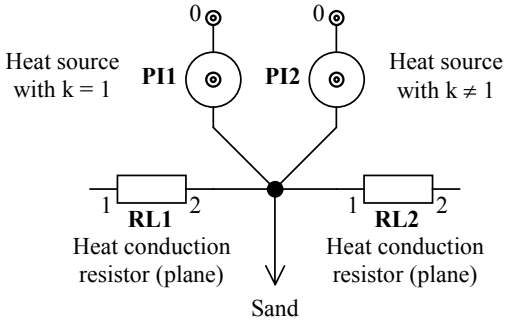

Fig. 2: Simulation of the melting wire with two different heat sources

It is of course also possible to use only one heat source for the fuse wire instead of two. This one heat source will generate the same amount of energy and will lead to the same simulation results.

3.2. From the fuse wire to outer surface

For the simulation the fuse will be cut into several slices of the same thickness. Fig. 3 shows for one slice the radial heat transfer with the radial heat conduction in the fuse sand, the radial heat conduction in the ceramic tube, and the heat radiation and convection at the surface of the fuse. The slices will connect axial with thermal conduction resistors. The connection point is situated in the middle of a coaxial section for the fuse sand and the ceramic tube. There is also the connection point for the heat capacity.

The parameters of the elements (heat capacity, plane/coaxial heat conduction resistor, heat radiation/convection resistor) result only from the geometry and the material properties of the fuse.

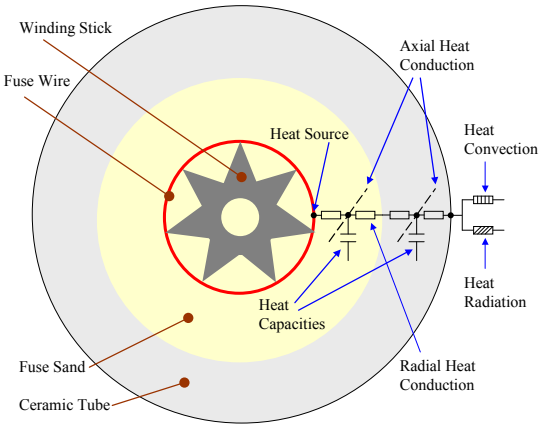

Fig. 3: Heat transfer from the heat source (fuse wire) to the surface of the fuse

This sub-network was reused, because the material properties for the calculation of the heat capacities and the geometric dimensions of the heat conduction resistors of the fuse sand and the winding stick are the same in every slice of the fuse.

Only the thermal conductivity of the fuse sand must be defined for the sub-network because it is not constant. The thermal conductivity of the fuse sand is dependent on the temperature, so it will be vary from the melting wire to the inner side of the ceramic tube as well as from the middle of the fuse to the end caps.

3.3. End caps and fuse terminal

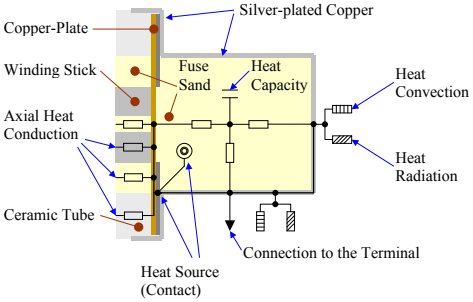

Fig. 4: Schematic thermal network of the fuse end cap with a heat source (wire-cap contact)

Fig. 4 shows only a rough schematic circuit of the fuse caps. The real structure of the thermal network in the simulation is considerably more detailed. The axial heat conduction of the fuse sand, the winding stick and the ceramic tube consists of several thermal elements. For each part there are two plane heat conduction resistors, two coaxial heat conduction resistors and a heat capacity. The copperplate has two heat conduction resistors and a heat capacity; the contact to the heat source has also two heat conduction resistors.

The silver-plated copper cap was cut into four sections. All sections are connected together with heat conduction resistors and have their own heat convection and heat radiation resistors according to the surfaces. One of these sections contains the connection to the terminal. Of course the contact surface of this connection is not an operative surface for heat transfer by convection or radiation.

Also this part was created as a reusable sub-network. Only one parameter, the thermal conductivity of the fuse sand, can differ between both sides and will be defined externally.

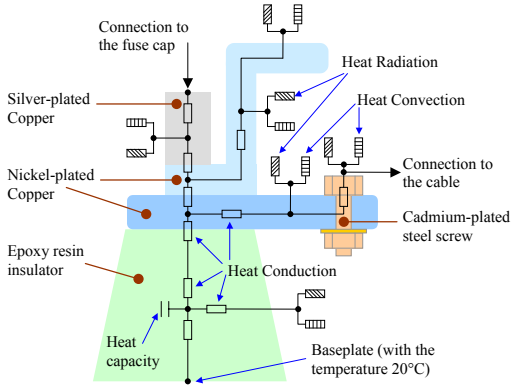

Fig. 5: Schematic thermal network of the terminal

Fig. 5 shows a simplified schematic thermal network of the terminal. The metal parts (nickel-plated copper) of the terminal have a lot of different surfaces, e.g. vertical and horizontal surfaces for heat release upward and downward. Therefore it was necessary to cut the metal parts of the terminal into sections with different kinds of surfaces.

The emission coefficients of the different surfaces (silver-plated copper, nickel-plated copper, cadmium-plated steel and epoxy resin) as well as the thermal conductivity and the specific heat capacity were measured or taken from literature [1-5-6-7]. The emission coefficients of the cadmium-plated screw and the silver-plated copper were measured with an infrared camera. Therefore samples of both plated materials were heated and the temperature was measured with a thermocouple as reference and the infrared camera system. The emissivity in the camera was adjusted up the point where the reference temperature was reached.

The temperature of the base plate at the bottom of the insulator was assumed to be the same as the ambient temperature.

3.4. Fuse Canister

The previously developed thermal network model of the fuse was extended by a separate model of the fuse canister It can be easily applied to other rated fuses or be implemented in larger models like a complete switch-gear (Fig. 6).

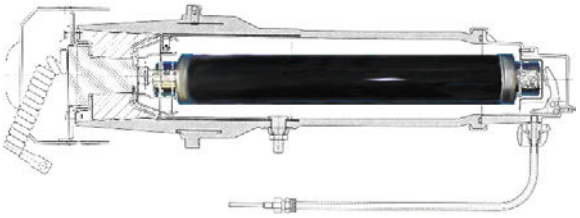

Fig. 6: Fuse in canister (schematic)

The canister was split into 6 main sections based on the geometry (Fig. 7). Each of the 6 main sections is separated into a number of sub-sections, which were connected to the model of the fuse.

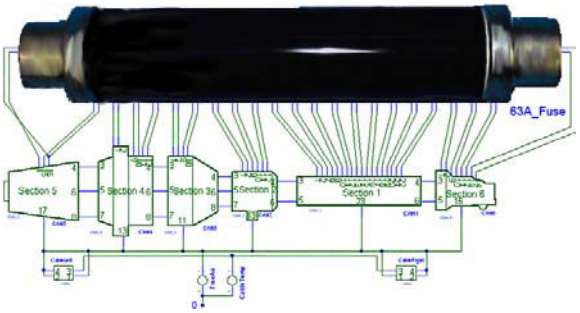

Fig. 7: Schematic of different canister parts in the thermal network

The heat transfer between the fuse and the canister and the radiation and convection outside the canister was taken into account.

For comparison with the measurements it was assumed in the simulation that the canister is placed in free air and not in a switchgear.

4. Results of the simulation

The values of the measured temperatures are averages of three experimental runs with self-assembled fuses and two experimental runs with a serial fuse. The self-assembled fuses were prepared with thermocouples on the wire, the winding stick, the inner ceramic tube, the contacts, and the surface of the fuse. The fuse from the serial production was prepared with thermocouples on the surface of the fuse, the terminal, and the connections to the cables. For comparison all measured values were normalized with the ambient temperature to 20°C.

4.1. Static simulation results at steady state

According to IEC 60282-1, the steady state of the temperature values is defined as the point where the temperature rise is less than 1 K during one hour. All temperature-rise tests ran over five hours and fulfilled the criterion for steady state.

For the free air steady state comparison all measurements and simulation results are related to the nominal current of the fuse (normal operating conditions). For the comparison of the simulated and measured temperatures of the fuse in the canister the de-rated current was used.

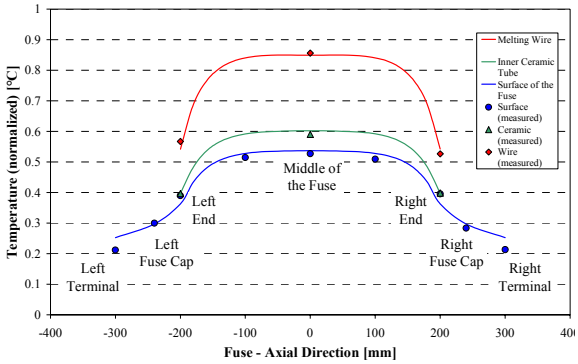

Fig. 8: Steady state axial temperature distribution of the fuse with terminals (free air)

The simulated temperatures match very well with the measured values (Fig. 8). Smaller deviations can be seen for the terminals. Here the networks for the cable and the terminal networks are not so detailed discretized compared to the fuse, due to the fact that the main interest was on a good model with high accuracy of the fuse.

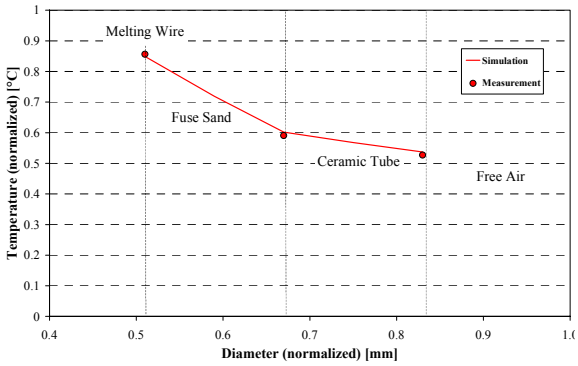

Fig. 9: Radial temperature distribution at the middle of the fuse

Especially at the middle section of the fuse, where the hottest region is located, a very good consistency of the measured and simulated

temperatures (Fig. 9) was reached. This high accuracy is necessary to gain acceptable results for the dynamic simulation of the pre-arcing time.

The same simulations up to the steady state point were made for the fuse mounted in a fuse canister. The corresponding de-rated current was used; like the current in switchgears for transformer protection (Fig. 10).

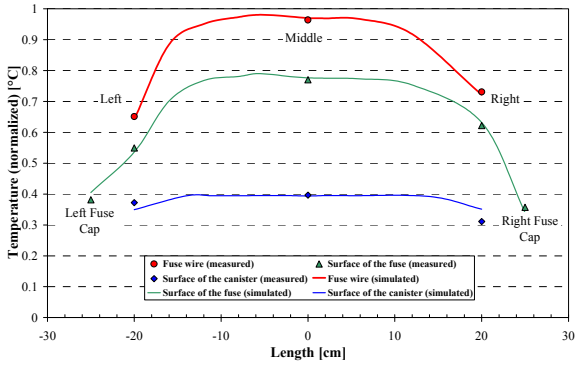

Fig. 10: Steady state axial temperature distribution of the fuse in the canister

The static simulations of the fuse in the canister showed also a very good accordance between simulated and measured data, especially again in the middle of the fuse/canister (Fig. 11).

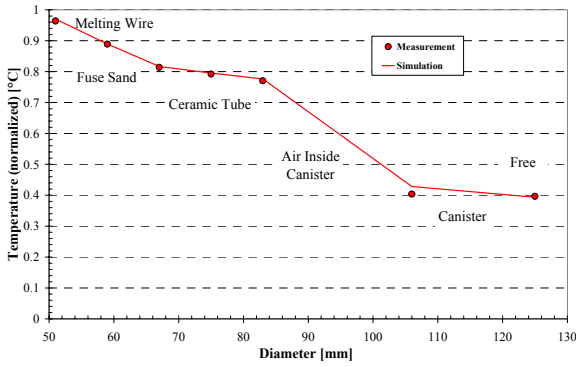

Fig. 11: Steady state radial temperature distribution at the middle of the fuse

This model of a fuse-canister combination can be further used as a separate part for the simulation of complete switchgears.

4.2. Dynamic simulation results

By adding heat capacity elements, which are only dependent on the volume, the density and the specific heat capacity of the material, to the existing static models the thermal networks become dynamic and can be simulated time dependent.

This feature opens a lot of different opportunities of simulations shown in the next examples.

The heating up of the fuse at nominal conditions can be simulated (Fig. 12). Influences on the steady-state-temperature and -time like material or fuse wire changes; changes on the contacts etc. can be easily estimated.

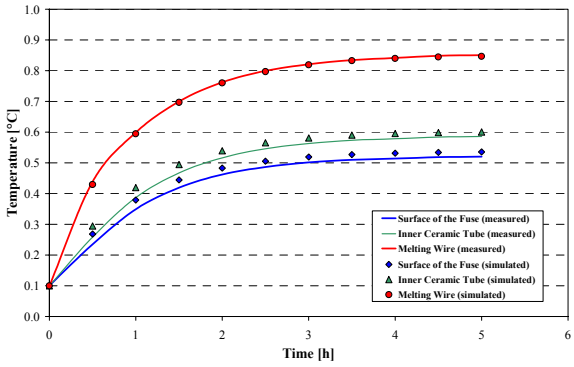

Fig. 12: Dynamic behaviour at the middle of the fuse (free air)

Another option is the simulation of the pre-arcing-time of the fuse; the time up to the melting temperature of the silver fuse wire (Fig. 13).

The current can be an over-current with a typical hot spot region in the middle of the fuse as well as a short circuit current with adiabatic heat up of all constrictions.

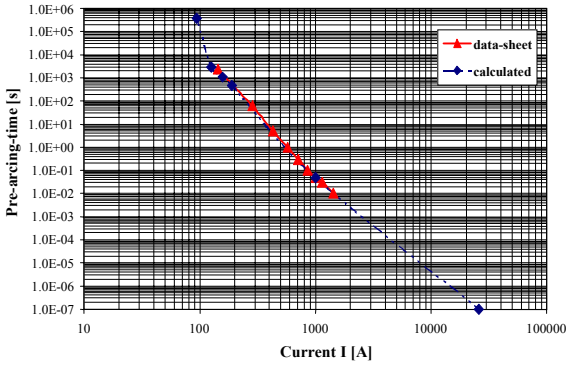

Fig. 13: Dynamic behaviour – pre-arcing time

Especially for higher over-currents and short-circuit currents a very good consistency with data sheet values was reached.

The M-effect, provoked by a low melting metal or alloy on the silver fuse wire, which starts a diffusion process at low over-currents and leads to a thermal runaway and tripping of the fuse, was not taken into account in this simulation. That means that the I-t-characteristic in this region of lower over-currents will not be exact simulated.

A third example is the dynamic simulation of the complete fuse-canister combination under the aspect of the dependent reaction of the different components on load peaks.

Fig. 14 shows the dynamic behavior of the fuse-canister combination for a defined typical load curve over a day. There the maximum current is related to the de-rated current of the fuse-canister combination for a transformer application.

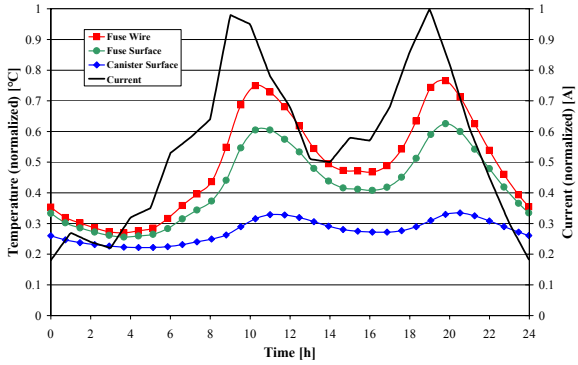

Fig. 14: Dynamic behaviour of a fuse and canister for a typical daily load curve

By expanding this thermal network of a fuse-canister combination to a complete switchgear-model, it becomes possible to estimate the overload capacity of the system.

Especially the demands for short time overloading of the system can be fulfilled if the load curve over the day and the ambient conditions are known. The temperature distribution and time characteristic can be calculated. Dependent on the difference to the maximum allowed temperatures a prediction about the overload capacity and reserves of the system can be made.

5. Conclusion

A dynamic electro-thermal simulation based on the thermal network methodology was evaluated for a h.r.c fuse used in free air or in combination with a fuse canister for switchgears. From the fuse itself and additional parts like the free air mounting or the fuse-canister, structured models were developed to simulate different combinations and larger systems like complete switchgears.

Static simulations of the fuse were done with a very high accuracy. The static simulation was extended to a complete model of a fuse in a canister for switchgear applications. By including thermal capacitances in these models a dynamic simulations became possible. The dynamic model was verified with a simulation of the heating-up time up to steady state conditions and with a simulation of the pre-arcing time of a standard fuse.

It was shown that the described thermal network simulation shows a high potential for a variety of different applications:

- Development support
- Identifying user risks
- Evaluating the right de-rating current
- Evaluating overload capacity without destructive failure of the fuse

References

[1] Böhme H.: “Mittelspannungstechnik”. Verlag Technik 1992.

[2] Kessler A.: “Zur Theorie des Wärmequellennetzes”. *Archiv für Elektrotechnik*, Vol 49, No 2, 1964, pp. 109-123.

[3] Schenk M., Löbl H.: “Strombelastbarkeit und Erwärmung der Geräte in Netzstationen“. *Elektrizitätswirtschaft*, Vol 99, No.15, 2000, pp.23-31.

[4] Johann H.: “Elektrische Schmelzsicherungen für Niederspannung: Vorgänge, Eigenschaften, technischer Einsatz”. Springer-Verlag 1982.

[5] Verein Deutscher Ingenieure (Ed.): “VDI-Wärmeatlas: Berechnungsblätter für den Wärmeübergang”. 8th rev. Edition, Springer-Verlag 1997.

[6] Smithells C. J.: “Metals Reference Book”. 5th Ed. London & Boston: Butterworths, 1976.

[7] CRC Handbook of Chemistry and Physics. 78th Ed. Boca Raton; New York: CRC Press, 1998.

HEATING OF FUSE-ELEMENTS IN TRANSIENT AND STEADY-STATE

K. Jakubiuk, W. Aftyka

Gdańsk University of Technology
Gdańsk, Poland
kjakub@ely.pg.gda.pl, waftyka@ely.pg.gda.pl

Abstract: Results of numerical calculations of fuse-element heating in transient and steady-state, performed in FLUX 2D software. The calculations take into account the heating of the whole fuse-element. Temperature in the fuse-element was chosen for analysis. Following the examinations performed, it was noted that during calculation of pre-arcing parameters, it is necessary to take heat conduction in the fuse-element into consideration, as well as the variable (as a function of temperature). In steady-state, the current density boundary value was determined, above which the fuse-element temperature begins to rise rapidly. Assumptions for the model and results of numerical calculations are given.

Keywords: electric fuse, heating, numerical modelling

1. Introduction

Heating of fuse-elements has been well examined by experimental methods [2]. However, experimentally, it is difficult to determine the temperature values and distribution inside the fuse. This difficulty can easily be overcome using a simulation method, which provides the information we want in a very short time [1,4]. However, the simulation method is not perfect. The main disadvantage of simulation methods are difficulties in determining the material, electrical and thermal properties, and especially their relation to temperature. The purpose of the paper is to check what errors are made during calculations of some of the fuse parameters using simplified relations given in literature, eg. [2]. In the paper, a simulation method was chosen for examination of fuse heating in transient and steady-state. Since this subject matter is very broad, the scope of research in this paper has been narrowed down to examining the distribution of temperature in the fuse-element. The scope of research includes also the determination of the effect of various simplifications, used mainly in analytical calculations to obtain a distribution of temperatures and to determine the effect of the shape and number of fuse-element constrictions on the heating process in transient and steady-state. Calculations were performed in FLUX 2D software [5]. The FLUX 2D package allows for analysis of coupled electromagnetic and thermal fields in transient. Steady-state were examined in such a way that the transient was analysed until the distributions of both fields became steady. The 2D package, used to examine fuse, allows for examination of axially symmetrical shaped fuse. Calculations in FLUX software are made in the finite element method in space and the method of finite differences as a function of time [5].

2. The model of the fuse-element and fuse

The source of heat in a fuse-element is Joule heat produced in the fuse-element. The fuse assumed for analysis (Fig. 1a) is axially symmetrical. Within the accepted symmetry, fuse-elements were assumed to have the shape of a wire (Fig. 1b) and of a cylindrical tube (Fig. 1c). Both fuse-element shapes had the same cross section area in the non-constricted part.

Tubular fuse-elements, though rarely used in fuses [2], allow to model the amount of heat given up from the fuse-element surface to the surroundings, by changing the tube diameter. Tube-shaped fuse-elements are equivalent to fuse-elements in the form of metal foil of various thicknesses and widths - but with the same cross-section area. The assumed constrictions in fuse-elements with two different shapes and various dimensions (Fig. 2) model various amounts of heat given off and taken away along the fuse-element.

Various simplifications of the model, consisting in consideration or neglection of heat exchange between various areas of the fuse, can be introduced through appropriate boundary conditions or by assigning appropriate values to thermal conduction coefficients λ_k for the k-th area of the fuse [3]. In transient, the following boundary conditions were modelled in this way:

a) no heat is carried off - adiabatic heating ($\lambda_1 = \lambda_2 = 0$),
b) heat is carried off along the fuse-element to the contacts ($\lambda_2 = 0$),

c) heat is carried off to the contacts and to the surroundings.

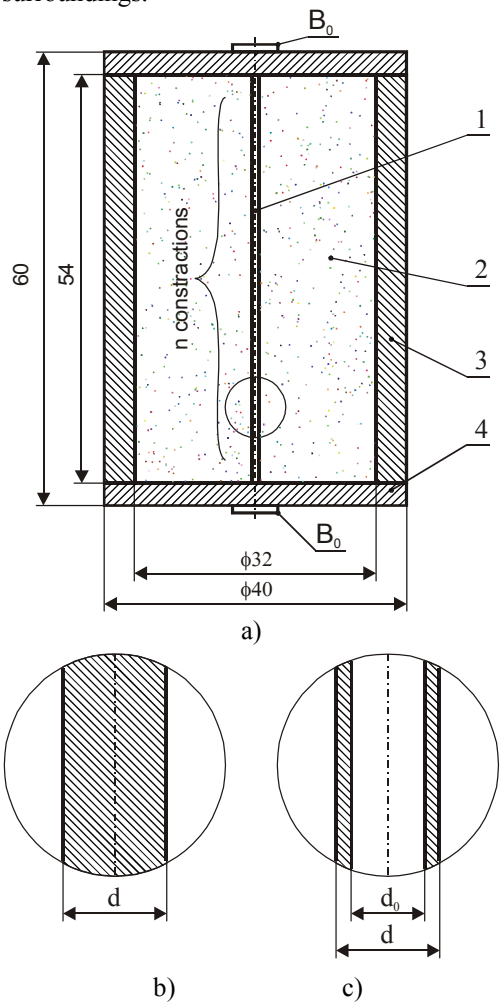

Fig. 1. Fuse assumed for analysis
a) fuse cross section, b) wire fuse-element (cross-section area - 0.75 mm^2), c) tubular fuse-element (cross-section area - 0.75 mm^2)
1 – fuse-element, 2 – sand, 3 – isolation tube, B_o – current feed surface

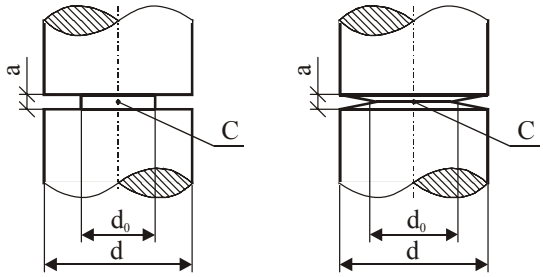

Fig. 2. The examined shapes of constrictions in a wire-shaped fuse-element
a) rectangular, b) triangular
denotation of a rectangular constriction: „r-0.2" for a=0.2d and „r-1" for a=d
denotation of a triangular constriction: „t-0.2" for a=0.2d and „t-1" for a=d

In steady-state, we can, of course, consider only variant b) or c). Heat transfer from the fuse-element takes place through thermal conduction, while from the fuse casing to the surrounding air – by convection [3], according to the formula

$$q_k = \alpha_c (T_{3p} - T_o) \qquad (1)$$

where: α_c – coefficient of heat loss, T_{3p} – temperature of the fuse surface, T_o – temperature of the surroundings.

Giving up heat from the contacts was modelled in such a way that a constant temperature was assumed at part of the contact area – marked in Fig. 1 by the symbol B_o. In both transient and steady-state, heating was examined until the moment when the maximum temperature in the fuse-element reached melting point. During heating to a higher temperature, fuse-element disintegration may take place and then the manner of its heating will change [1].

2. Fuse-element heating in transient

2.1. The model of fuse-element heating

In order to examine the fuse-element heating process in transient, it was assumed that current densitiy at the ends of the fuse-element is homogeneous, and increases in a linear manner as a function of time, in accordance with the formula

$$j = At \qquad (2)$$

where: A – rise steepness of current density increase, t – time.

An approximately linear character of current escalation, especially during the initial phase, occurs most frequently in short-circuit currents and is convenient for comparison of fuse-element heating in various conditions. For fuse-element cross-section dimensions occurring in practice, we can neglect the skin effect in calculations of the current density distribution in the fuse-element (the depth of penetration of the electromagnetic field is greater than the cross-section dimensions of the fuse-element) and assume that at any moment, the quasistatic distribution of potential φ(t) in the fuse-element is described by the formula [1]

$$\nabla \cdot (\sigma \nabla \varphi) = 0\,, \qquad \mathbf{j} = \sigma \nabla \varphi \qquad (3)$$

where: **j** – the vector of current density, $\sigma = \sigma(r,z,T)$ – conductivity dependent on co-ordinates and temperature in accordance with the formula

$$\sigma(r,z,T) = \frac{\sigma_o}{1 + \alpha\,[T(r,z,t) - T_o]} \qquad (4)$$

Distribution of temperature in the fuse-element is described by the equation of thermal conductivity

$$\rho c_p \frac{\partial T}{\partial t} = \lambda \nabla^2 T + \frac{j^2}{\sigma} \qquad (5)$$

where: ρ - density of the medium, c_p – specific heat, λ – thermal conductivity, j – module of current density.

In the remaining areas of the fuse, the temperature distribution is described by the formulae (5), which omit the last component (there is no heat source). If in formula (5) we omit the second component on the right, the heating will have an adiabatic character. Distributions of temperature in particular areas of the fuse are connected by appropriate boundary conditions. For current density, a homogeneous distribution at the ends of the fuse-element was assumed as a boundary condition, described by relation (2). In particular areas of the fuse-element, the assumed material data and coefficients [1] are given in table 1.

Table 1. Material data and coefficients

Parameter	Designation of material – Fig. 1			
	1	2	3	4
λ, W/(m·K)	396	1,2	1	396
c_p, J/(kg·K)	386	80	800	386
ρ, kg/m^3	8930	1500	2400	8930
α_c, W/(m^2·K)	-	-	10	-
σ_0, S/m	5,98·10^7	-	-	5,98·10^7
α, 1/K	0,0039	-	-	0,0039

2.2. Calculation results

In the process of fuse-element heating in transient, an important parameter is time until melting point (T_m). In order to determine the effect of various factors on fuse-element heating, the results obtained were compared with the results obtained for adiabatic heating. The results were compared for identical values of parameter A (2) at point C of the fuse-element constriction (Fig.2). Calculations were performed for parameters of the fuse-element given in table 1.

Fig. 3 presents an example of temperature distribution at the instant when $T_{max}=T_m$ in the area of fuse-element constriction r-0.2 (Fig. 2) for various values of parameter A and various conditions of heat transfer from the fuse-element.

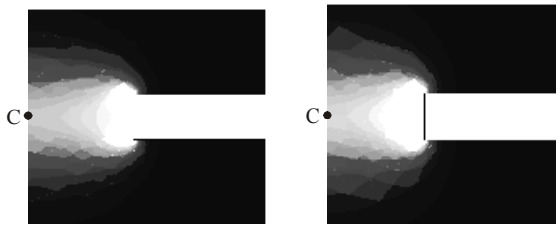

a) b)

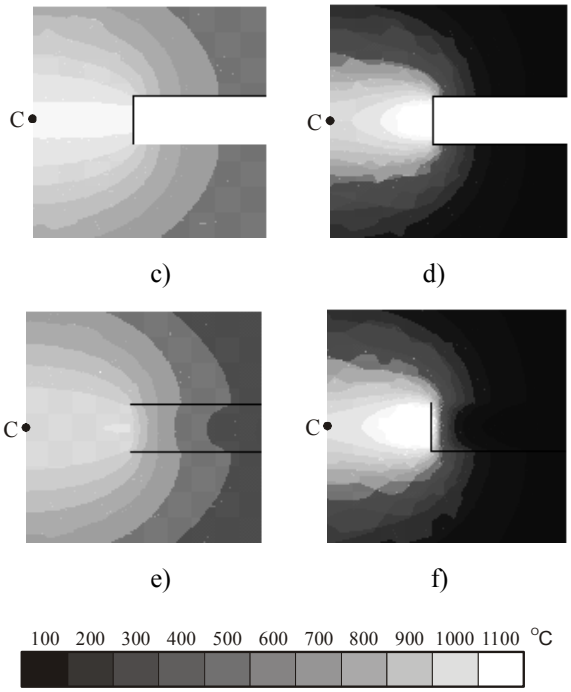

c) d) e) f)

Fig. 3. Temperature distribution in the fuse-element in the constriction area r-0.2 for A=10 kA/(mm^2·ms) (a,b,c) and A=1000 kA/(mm^2·ms) (d,e,f) during adiabatic heating (a,d) heat being carried off along the fuse-element (b,e), and heat being carried off along the fuse-element and into the surroundings (c,f)

Fig. 4÷7 present results of simulation of temperature, time until melting point (T_m) and pre-arcing Joule integral (I^2t_p) as a function of various parameters of the fuse-element and parameter A (2).

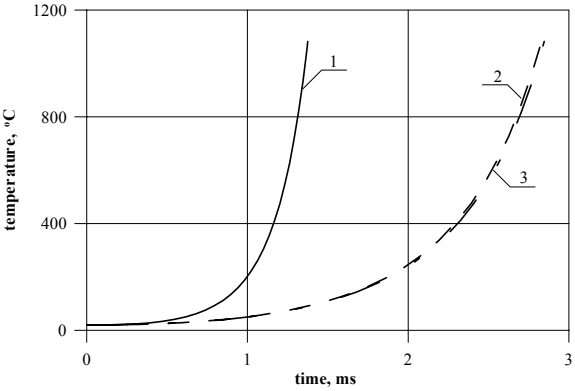

Fig. 4a. Trace of temperature at point C as a function of time, constriction 1:5, shape r-0.2, A=10 kA/(mm^2·ms)
1 – adiabatic heating, 2 – heat carried off only to the contacts, 3 – heat carried off to contacts and to surroundings

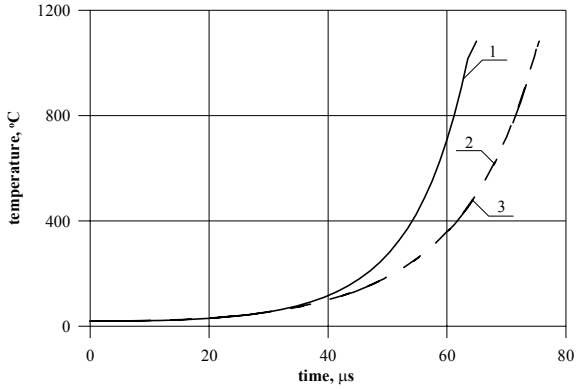

Fig. 4b. Trace of temperature at point C as a function of time, constriction 1:5, shape r-0.2, A=1000 kA/(mm^2·ms);
1 – adiabatic heating, 2 – heat carried off only to the contacts, 3 – heat carried off to contacts and to surroundings

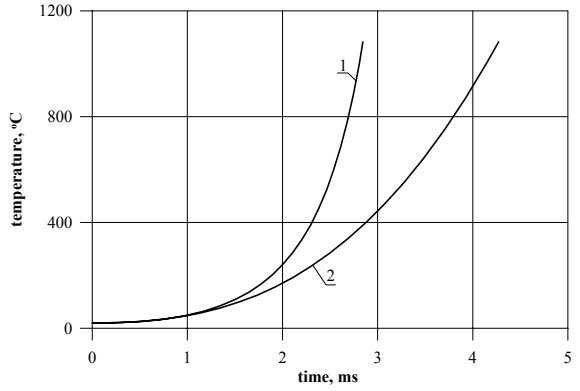

a)

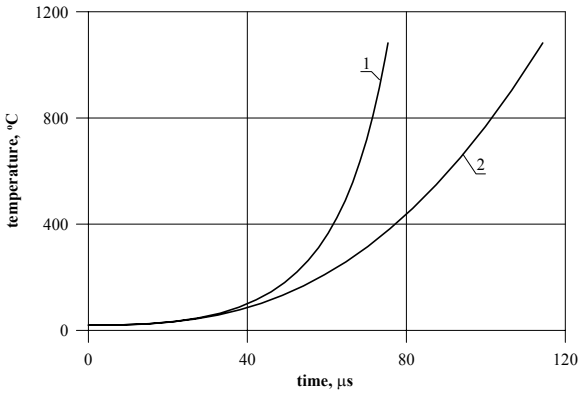

b)

Fig. 5. Trace of temperature at point C as a function of time for constriction 1:5, shape r-0.2:
a) A=10 kA/(mm^2·ms), b) A=1000 kA/(mm^2·ms)
1 – $\sigma=\sigma(r,z,T)$=var, 2 – $\sigma=\sigma_o$=const.

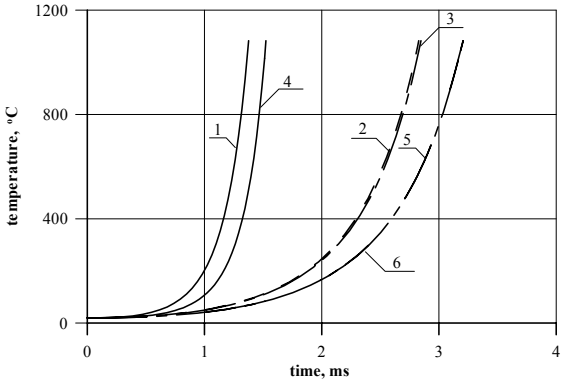

Fig. 6. Trace of temperature at point C as a function of time for: constriction 1:5, A=10 kA/(mm^2·ms)
1 – adiabatic heating – r-0.2, 2 – heat carried off only to the contacts – r-0.2, 3 – heat carried off to contacts and to surroundings – r-0.2, 4 – adiabatic heating – t-0.2, 5 – heat carried off only to the contacts – t-0.2, 6 – heat carried off to contacts and to surroundings – t-0.2

Heating of the fuse-element constriction (Fig. 4) depends largely on the value of parameter A and on the conditions of heat transfer from the fuse-element. In transient, heat transfer to sand, compared with heat transfer along the fuse-element, is practically insignificant. As could be expected, the effect heat transfer along the fuse-element is the greater, the smaller the value of A is.

Accounting for variable conductivity as a function of temperature (Fig. 5) has a serious effect on fuse-element heating calculations. Assumption of constant conductivity, independently of the value of parameter A, causes considerable extension of time until melting point, and so, an increase of I^2t_p.

During calculations of fuse-element heating tor an element with several constrictions (in transient), for various parameters, mutual interaction between constrictions in the heating process was not noted. The effect of constriction shape on its heating is shown in Fig. 6. This effect is not significant and plays a more important role during adiabatic heating. The constriction length influences the amount of heat given off in the constriction, while the shape effects the current density in the constriction. In Fig. 6 the different traces result from different current density distribution in both cases. As the value of parameter A grows, the differences between the traces decrease. Comparative, relative results of temperature calculation, time until melting point T_m and I^2t_p as a function of parameter A for various conditions are presented in Fig. 7. All the calculated magnitudes are related to the same magnitudes calculated for adiabatic heating. Variable conductivity as a function of temperature has been taken into account.

It ensues from Fig. 7a, that at small values of A, time until T_m is considerably longer when heat is carried away from the fuse-element, than during

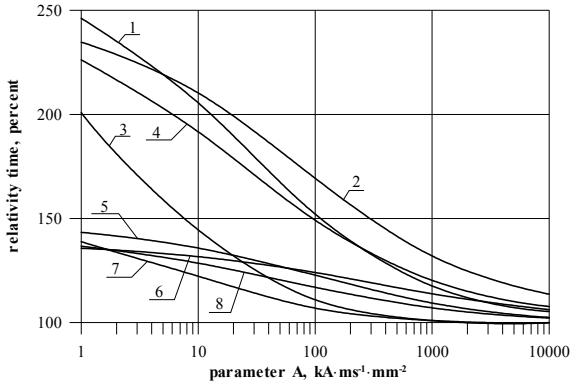

a)

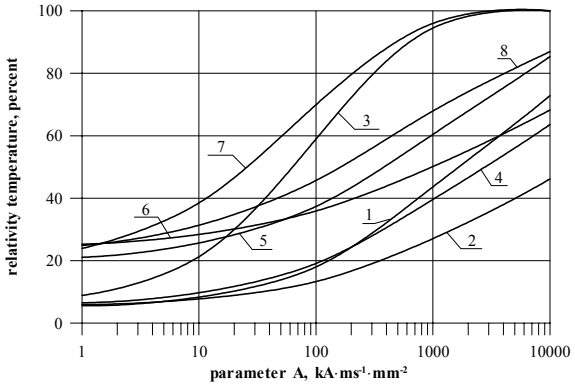

b)

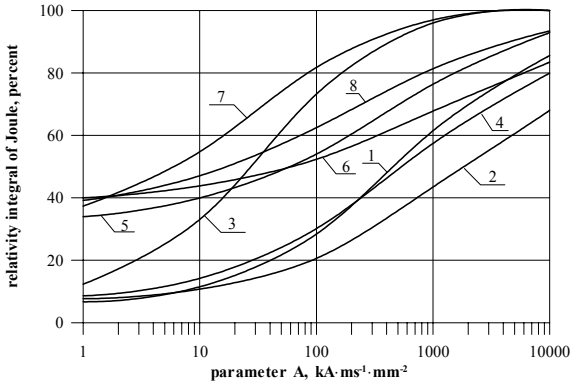

c)

Fig. 7. Dependencies between relative values: time until T_m at point C - a) temperatures at point C at the instant of reaching T_m during adiabatic heating - b) and I^2t_p - c) when heat is carried off to the contacts and to the surroundings, related to the same magnitudes during adiabatic heating, and parameter A
1 – constriction 1:5, shape r-0.2; 2 – constriction 1:5, shape t-0.2; 3 – constriction 1:5, shape r-1; 4 – constriction 1:5, shape t-1; 5 – constriction 1:2, shape r-0.2; 6 – constriction 1:2, shape t-0.2; 7 – constriction 1:2, shape r-1; 8 – constriction 1:2, shape t-1

adiabatic heating (for A=10 kA/(mm^2·ms) relative time is from 105 to 210%). Relative time is greater for larger fuse-element constrictions and for triangular constriction shape, which results from a nonhomogeneous current density distribution. For values of parameter A > 1000 kA/(mm^2·ms) we can assume that heating until T_m is practically adiabatic.

The relations presented in Fig. 7b indicate what relative temperature (relative to T_m) is reached at point C at the instant when T_m is achieved during adiabatic heating. The lowest temperature occurs at point C, at low value of A, large constriction (1:5) and with a triangular shape of the constriction, while the highest temperature occurs for high value of A, small constriction - 1:2 and rectangular shape of the constriction. Such dependencies of relative temperature result mainly from the conditions in which heat is carried off, and from current density distribution in the constriction. At small values of parameter A, especially in a large constriction of little length, a large amount of heat has enough time to be carried off from the constriction into the surroundings. For greater values of A, the amount of heat carried off into the surroundings is smaller. With a triangular constriction, the current density distribution is more nonhomogeneous in the constriction area and this is why the temperature at point C is lower than in the case of a rectangular constriction.

The dependency between relative value I^2t_p and parameter A is similar to the dependency between relative temperatures (Fig. 7c). The values of I^2t_p have been related to I^2t_p during adiabatic heating calculated to the moment when T_m is reached at point C. Qualitatively, these dependencies are almost identical, but they differ quantitatively. Quantitative differences result from the fact that, at a given value of A, the relative temperature depends both on duration of heating and on changes of conductivity (4) during this time, while the Joule'a integral depends only on the duration of heating. Therefore, relative values of I^2t_p are greater than the relative values of temperature in the same conditions.

It ensues from the traces shown in Fig. 7 that calculations of pre-arcing time, pre-arcing Joule integral and temperature distribution in the fuse-element in transient state should be performed, taking into account the process of heat transfer from the fuse-element and variable conductivity [3]. Calculations made using simplified relations lead to considerable errors, especially for small values of parameter A.

3. Heating of the fuse-element in steady-state

3.1. The model of fuse-element heating

The fuse-element heating process in steady-state is described by formula (5), in which the component

on the left equals zero. However, due to the fact that, the *Steady thermal* module of the FLUX software package lacks the possibility to account for the dependence between conductivity and temperature [5], steady-state in the fuse-element was analysed in such a way, that calculations were performed for the transient until temperature distributions in the fuse-element steadied. It was assumed that current density at the ends of the fuse-element is homogeneous and has an exponential trace, in accordance with the formula

$$j = J_o[1 - \exp(-\frac{t}{T_o})] \qquad (6)$$

Current density J_o (6) may express direct current density, as well as the effective value of a current changing periodically as a function of time. In the second case, the current change period should be considerably shorter than the time constant T_o. With this assumption, for alternating current, temperature changes connected with current change period are not accounted for.

3.2. Calculation results

In the process of fuse-element heating in steady-state, temperature distribution depends on many parameters. In the paper, the effect of current density J_o (6), fuse-element dimensions and the degree and number of constrictions on temperature distribution in the fuse-element was examined. The effect of the constriction shape was not examined. The effect of the number of constrictions on temperature was investigated. In steady-state, a very important role is played by the manner in which heat is carried off from the fuse-element. It was assumed that heat transfer from the fuse-element takes place through convection – from the surface (excluding the contact faces from which heat is carries away by means of thermal conductivity) B_o (Fig. 1). The effect of various parameters of heat transfer from the fuse on the temperature distribution in the fuse-element was not examined.

Selected results of calculations of the temperature in the constriction located in the mid-length of the element are presented in Fig. 8÷11.

It results from Fig. 9÷11 that for a given fuse-element, there exists a certain boundary current density value, above which the temperature of the constrictions, and therefore the temperature of the entire fuse-element, begins to increase rapidly. $J_{og} \approx 100$ A/mm^2 can be assumed as the current density boundary value for the given fuse-element. The value of J_{og} allows us to determine eg. sustained boundary current for a given fuse [2].

From Fig. 9, it ensues that failing to account for variable conductivity in calculations leads to large errors, especially for current densities $J_o > J_{og}$.

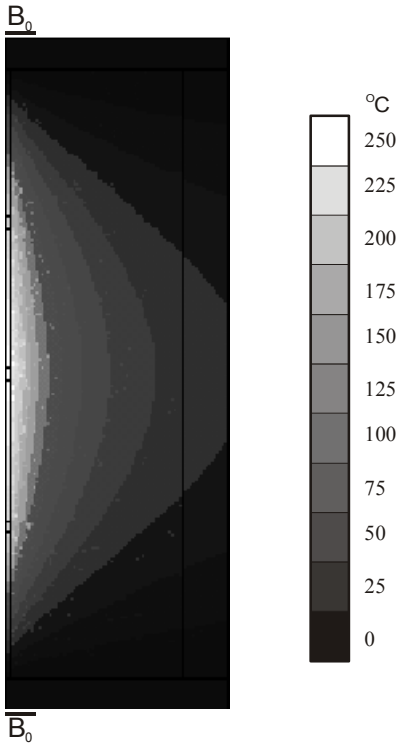

Fig. 8. Distribution of temperature in the fuse in steady-state for J_o=100 A/mm^2 (wire element, n=3, constriction 1:5)

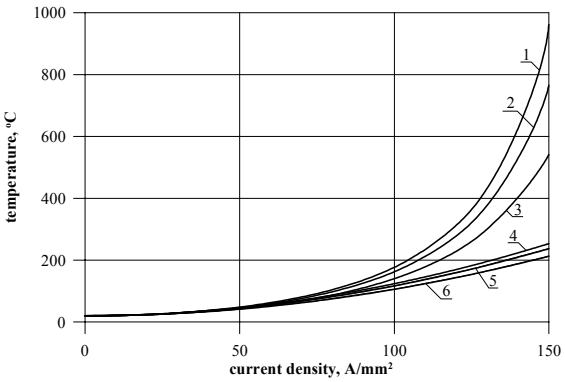

Fig. 9. The relation between temperature in the fuse-element constriction 1:5 as a function of current density J_o for n=1 and:
$\sigma=\sigma(r,z,T)$=var: 1 – wire fuse-element, 2 – tubular fuse-element with 0.2 mm thickness, 3 – tubular fuse-element with 0.1 mm thickness;
$\sigma=\sigma_o$=const.: 4 – wire fuse-element, 5 – tubular fuse-element with 0.2 mm thickness, 6 – tubular fuse-element with 0.1 mm thickness

If the condition $J_o > J_{og}$ is met in a given fuse, heat transfer from the fuse-element to the sand medium plays an important role (Fig. 10 and 11). The temperature of the fuse-element with a larger surface area (tubular element) builds up more rapidly than in a fuse-element with a small surface area (wire-element).

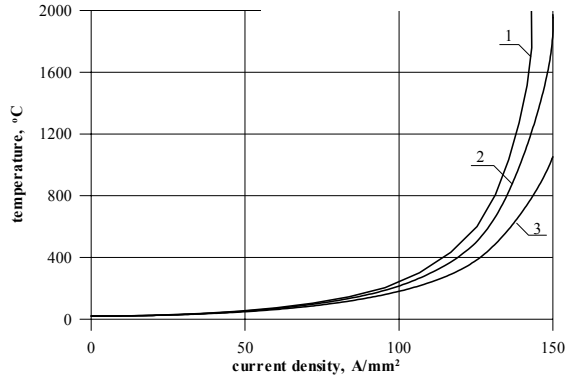

Fig. 10. The relation between temperature in the 1:5 constriction as a function of current density J_o for: n=3 and $\sigma=\sigma(r,z,T)$=var
1 – wire element, 2 – tubular fuse-element with 0.2 mm thickness, 3 – tubular fuse-element with 0.1 mm thickness

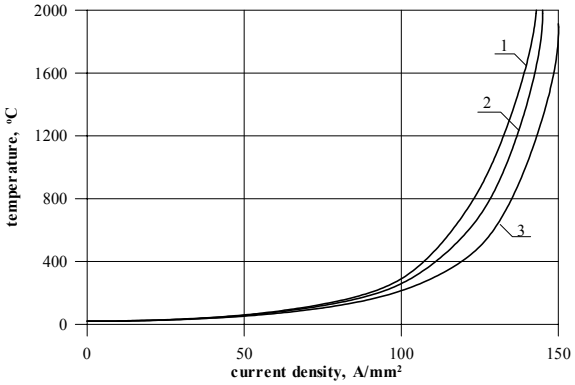

Fig. 11. Relation between temperature in the fuse-element constriction 1:5, as a function of current density J_o for: n=5 and $\sigma=\sigma(r,z,T)$=var
1 – wire element, 2 – tubular fuse-element with 0.2 mm thickness, 3 – tubular fuse-element with 0.1 mm thickness

If the $J_o > J_{og}$ is met, the number of constrictions in the fuse (Fig. 9 ÷ 11), has a significant effect on the temperature in the constrictions.

The time necessary to achieve steady-state of temperature in the examined fuse-element can be assumed as equal to 10 minutes.

4. Summary and conclusions

The following conclusions result from the considerations and calculations performed:

a) regarding fuse-element heating in transient:

- calculations should take into account the variable conductivity of the fuse-element as a function of temperature. Otherwise, serious errors are made;
- at low current densities, heat transfer from the constrictions to the unconstricted parts of the fuse-element should be taken into account;
- the degree of constriction plays a significant role;
- the shape of the constriction plays a small role resulting from nonhomogeneous distribution of current density in the constriction. Greater nonhomogeneity occurs in short constrictions;
- transfer of heat from the fuse-element to the surrounding sand does not play a significant role.

b) regarding fuse-element heating in steady-state:

- there exists a boundary value for current density in the fuse-element, above which its temperature will begin to rise rapidly;
- calculations should account for variable conductivity as a function of temperature. Otherwise, serious errors can be made;
- the temperature of the fuse-element, especially at current densities greater than the boundary density, is affected by the number of constrictions.

Acknowledgement

Authors have a pleasure to acknowledge that described investigations were carried out in the frame of project no 8 T10A 05821 sponsored by the Polish Committee of Scientific Research.

References

[1] Jakubiuk K.: Electrical explosion and implosion of conductors. Technical University of Gdańsk Publishing 2000.

[2] Lipski T.: Bezpieczniki niskonapięciowe. Warszawa. WNT 1968 (in Polish).

[3] Sasu M., Oarga G.: Simulation of the heat transfer phenomena in variables section fusible elements in non-adiabatic regime. Springer-Verlag 1992.

[4] Zhang Juan, Ma Zhiying: Mathematical model of two dimensional temperature field and its application in high-voltage current-limiting fuse-link. Power System Technology. Vol. 19, No 12, Dec 1995.

[5] Flux 2D. User's guide. Version 7.30.

FUSE PROTECTION OF TRANSFORMER POLE SUBSTATION IN POLAND

Józef Ossowicki[(1)], Remigiusz Joeck[(2)]

Instytut Elektrotechniki Oddział w Gdańsku[(1)], 80-557 Gdańsk, ul. Narwicka 1
ENERGA SA[(2)], 80-557 Gdańsk, ul. Marynarki Pol. 130, remigiusz.joeck@energa.pl

Abstract: The transformers protection in pole substations MV/LV 15/0,4 kV or 20/0,4 kV, is closely connected with the protection of complete substation. In Poland, on the MV side mainly expulsion fuses are used but on the LV side are used current limiting fuses with t-I characteristic gG or gF. It was proved that transformers rated up to 400 kVA could be effectively and inexpensively protected by fuses against results of overloads and short-circuits.

Keywords: protection, transformer pole substation, expulsion fuses, overload, short-circuits, t-I characteristic

1. Introduction

Correct protection of transformer pole substation MV/LV against overloads and short-circuits, has an essential influence on consumers supply continuity and safety of people or animals situated close to the substations. In Poland MV pole substations with typical rated voltage of 15/0,4 kV or 20/0,4 kV are mainly situated on the terrains of: agriculture, small industrial plants or other consumers. They are built as free–standing constructions with solutions depending on local conditions. Many years of domestic maintenance experiences proved [4] that the cheapest as well as effective transformer protection in these substations on the MV and LV side against results of overloads and short-circuits, are properly selected fuses [1, 3, 8, 10, 11]. In Poland for 40 years for protection of three-phase transformers rated up to 400 kVA on the 15 kV or 20 kV side, where prospective short-circuit current does not exceed 3,15 kA [4, 8, 19], were used domestic expulsion fuses (fig. 1A). For protection of larger transformers or in case of larger short-circuit currents there are used limiting fuses (fig. 1B).

Voltage, rated current and breaking capacity of a fuse are selected according to the basic rules, taking into consideration permissible transformer overloads. The permissible operation overload is essential in the case of distribution transformers. It was accepted that distribution oil transformer overloads with current 1,5 I_{nT} and 1,3 I_{nT} should not lasted longer than adequately 2 and 10 h [5]. Due to the fact that the transformer has thermal time-constant larger than series connected conductors and apparatus, all circuit elements [5] should have the rated current larger than transformer e.g. $I_n \geq 1{,}25 I_{nT.}$ This rule applies also secondary transformer circuit.

At the beginning of the 70-ties there was a tendency in Western Europe, especially in France to simplify transformer pole substation by eliminating protections on the MV side. Many fuses were removed what was explained that they operate due to not justified reasons. It was soon apparent that the fuses lack of was the reason of many transformers faults which were dangerous for surrounding. There were stated cases of oil leaks and even oil ignition which is an unacceptable ecological danger for the environment.

Considering different ways of transformer pole substation protection, the transformers faults statistics should be observed. Statistics from different countries could differ a lot, because they concern transformers produced, installed, protected and

supervised according to the rules of specific technical education. Polish observations of 6 000 distribution transformers from period 1990 – 1992, proved that every year 1% of them are damaged, c.a. 2/3 faults are internal short-circuit of HV windings, from these windings to core or oil tank, and also between HV winding and LV winding [5]. (Undoubtedly, the newest domestic transformers have several times lower fault rates). Similar German observation [1] of 600 000 oil distribution transformers, proved that average fault rate was ten times lower because every year 0,1% transformers were damaged. Despite a small fault amount in the latest years, due to the ecological requirements, there is an observed noticeable comeback to protection of transformer pole substations by fuses. It was proved by experimental testing [2] carried out on single-phase transformer substations models, rated 50 and 100 kVA. The testing aim was an explanation of MV fuses operation without reasons especially during atmospheric discharges. The good example could be the co-operation between French power engineers and SIBA company where the new fuse construction was developed [20]. It enables easy fuse links replacement by hot stick from the ground level (without pole climbing).

On the contrary to West Europe experiences, in Poland almost for 10 years there is a tendency to eliminate MV fuses in pole substations which are rated lower than 400 kVA [6, 12]. It is a result of too many unjustified reasons of expulsion fuse operations, caused probably by information lack in catalogues how to select properly these fuses considering operation co-ordination with fuses on the LV side. For example in the catalogue [19] there are presented recommended expulsion fuse nominal currents for transformer protection on the rated voltage of 15 kV. The maximum nominal currents of fuses with gG characteristic which can be used on the 0,4 kV side there were not mentioned.

2. Fuse selection in transformer pole substations

In Poland are used three variants of transformer substation protection by fuses (fig. 1).

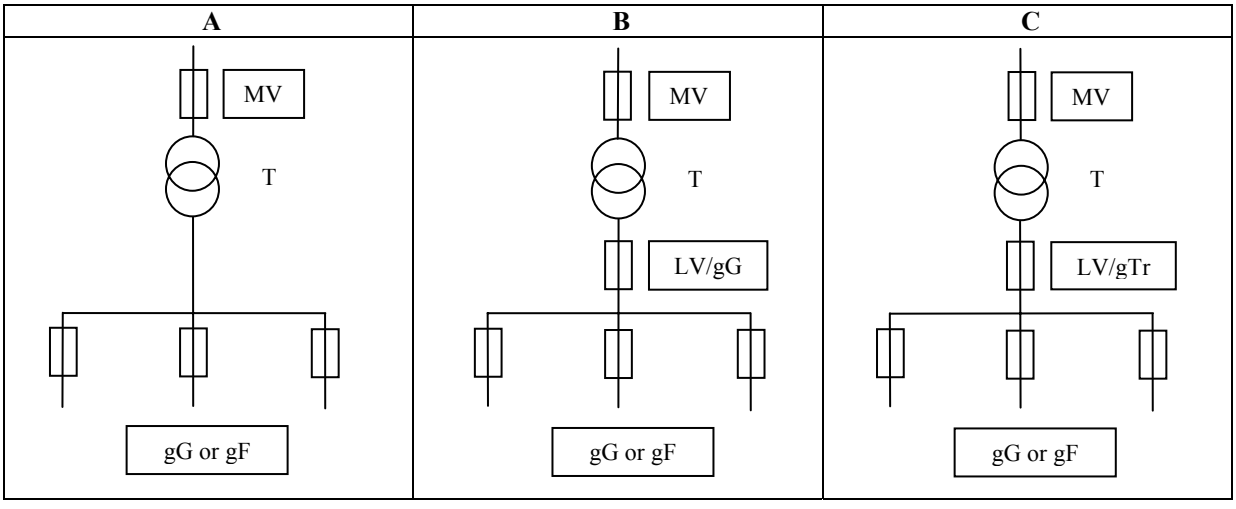

Fig. 1. Protection methods of transformer pole substations MV/LV

The protection method should be selected according to nominal transformer power and prospective short-circuit current on the MV side.

- **A** – On the MV side are used expulsion fuses when nominal transformer power is not larger than 400 kVA and prospective short-circuit current does not exceed 3,15 kA (unless the expulsion fuses producer proves that his fuses can be used for protection of transformers with larger nominal power or in network with larger prospective short-circuit current).
- **B** – On the MV side are used classic current limiting fuses when prospective short-circuit current is larger than 3,15 kA or when nominal transformer power exceeds 400 kVA.
- **C** – Is used when nominal transformer power is larger than 630 kVA and does not exceed 1000 kVA.

Typical transformer pole substation (fig. 2) consists of a transformer (T) with nominal power not exceeding 250 kVA supplied from MV network usually through expulsion fuses (1), and surge arresters (not shown on the fig. 2).

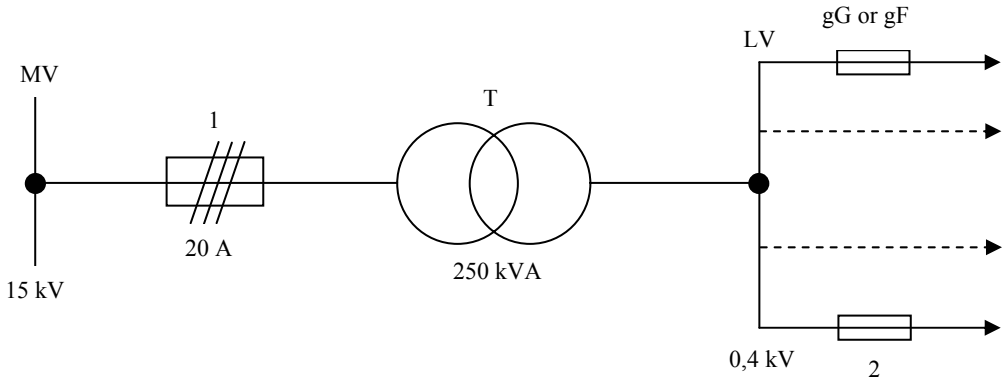

Fig. 2. Typical diagram of transformer pole substation (overvoltage protection is not shown)

In the new products offered among other producers by ZRE Gdańsk [18] one of MV fuse base insulator is also a surge arrester. On the transformers secondary side, in the LV part, particular outgoing feeders are protected by fuses (2) with t-I characteristic gG or fast gF in case of rural network when shock prevention is required.

3. Protection on the MV side

The tasks of MV fuses in transformer pole substation are:

- protection of the substation part between fuses connections and transformer clamps against results of short-circuits,
- transformer protection against: oil tank fault, oil leak and possible its ignition due to the short-circuit inside transformer caused by e.g. insulation breakdown,
- cut-off of two and three-phase short-circuits when they appears on the secondary transformer side, on the substation part between bushings and fuse entrance clamps or fuse load switches on the particular outgoing feeders (fig. 2).

Fuses for transformers protection should have big enough operation current $I_{f0,1}$ with prearcing time of

0,1 s regarding making current holding and selectivity with protections on the secondary side. Relative value (with reference to nominal current of fuse-link I_n should fulfil the condition (1) [16]

$$\frac{I_{f0,1}}{I_n} \geq 7 \cdot \left(\frac{I_n}{100} \right)^{0,25} \quad (1)$$

Fuses should have relatively small prearcing current I_{f10} in time 10 s due to detection of turn to turn short-circuit on the secondary transformer side and selectivity with preceding protections, so the condition (2) [16] should be fulfilled

$$\frac{I_{f10}}{I_n} \leq 6 \quad (2)$$

MV fuses should be selected according to the following:

- Their nominal short-circuit breaking capacity declared by producer should be not lower than prospective short-circuit current in the installation place.
- They should not operate during transformer switching on in any phase time. It is a convention [5, 8] that prearcing time at current 12 $I_{nT} \geq 0,1$ s ; and at current 25 $I_{nT} \geq 0,01$s. In their catalogues fuse producers usually describe type and values of fuse nominal currents which should be used for transformers protection.
- Their t-I characteristic in prearcing time (starting from overload to short-circuit in whole range) should run above t-I characteristic of LV fuse cut-off for the biggest nominal current of fuse situated in LV switchgear (fig. 3). Usually it is accepted that it is the close current to nominal transformer current I_{nT}.
- They should operate in a period shorter than 1 s, if two or three-phase short-circuit on the secondary transformer side in the substation part between bushings and LV fuses clamps appear (fig. 2);
- The maximum value of Joule integral I^2t of MV fuse cut-off should not exceed $10^6 A^2s$. This condition is caused by durability of transformer tank to bursting when internal short-circuit occurs in the transformer [10].

Requirements mentioned above are easily met in domestic expulsion fuses [4, 17, 19].

On the Fig. 3, continuous lines present prearcing t-I characteristics of expulsion fuses for rated voltage of 15 kV (have been produced in Poland for many years). Dashed lines show the characteristics (calculated to the 15 kV side) of maximum fuse disconnection time (characteristic gG) permitted by Polish Standard [14]. Fuses from many producers are in use in Poland. Their t-I characteristics sometimes differ a lot but all of them should be placed in required band shown in Polish Standard [14]. Due to their variety maximum characteristics of permissible disconnection times should be chosen in the selectivity analysis. The greatest approach between these characteristics, occurs when short circuit current on the 0,4 kV side calculated to the 15 kV side is ca. $2,5I_n$ of expulsion fuse.

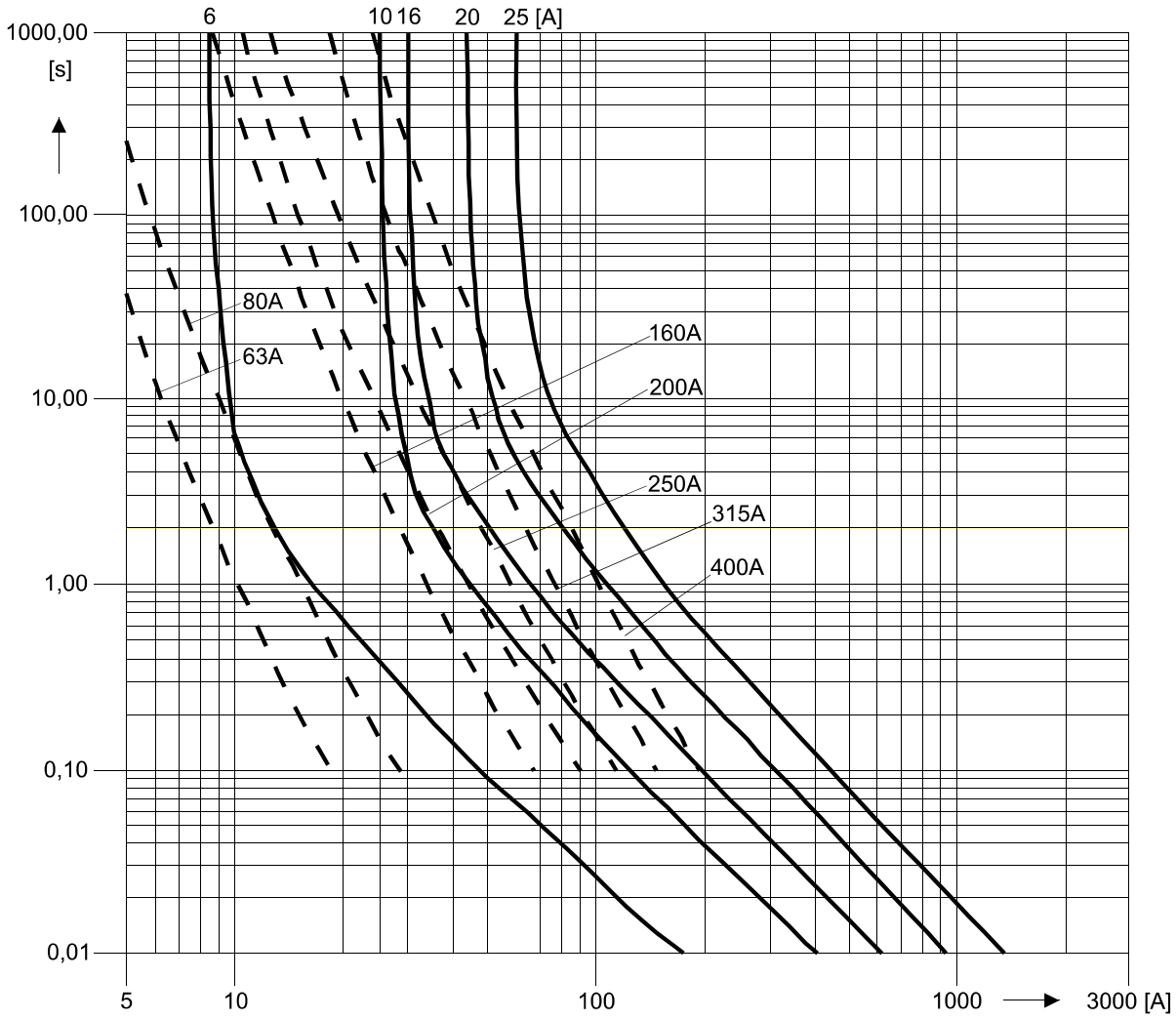

Fig. 3. Example of t-I characteristics of: prearcing domestic expulsion15 kV fuses (continuous lines); gG fuse disconnection calculated to the 15 kV side (dashed lines). Explanations in the text …

In Table 1 it is shown an example of properly selected domestic expulsion fuses which protect the transformers rated 63 ÷ 400 kVA. On the 0,4 kV side there are used fuses with gG characteristic.

Table 1. Example of fuse selection in transformer pole substations 15/0,4 kV

Transformer rated power [kVA]	Nominal voltage 15 kV		Nominal voltage 0,4 kV	
	Transformer rated current [A]	Fuse rated current [A]	Transformer rated current [A]	Fuse rated*) current [A]
63	2,43	6	91,0	63
100	3,85	10	144,5	125
160	6,20	16	231,0	200
250	9,60	20	361,0	315
400	15,40	25	578,0	400

*) It is the largest rated current of gG fuse-link which assures selective fuse operations.

4. Protection on the LV side

- Fuse selection and protection method of transformer pole substation on the LV side depends mainly on nominal transformer power, less on fuse type or prospective short-circuit current on the MV side.
- To protect transformers rated up to 400 kVA against results of overloads and short-circuits, properly selected fuses on outgoing feeders in LV switchgear (fig. 1A) should be satisfied, because in opinion of experienced people there is a low probability of exceeding permissible transformer overloads by current 1,3 I_{nT} during 10 h and current 1,5 I_{nT} during 2 h.
- To protect transformers larger than 400 kVA should be used a protection on the entrance to the LV switchgear. For this purpose fuses with transformer characteristic gTr are the most suitable [17] (fig. 1C). Their advantages are that they enable full using of permissible transformer overload [9] and better limit short-circuit current than fuses with gG characteristic.

5. Conclusions

- Many years of maintenance experiences in West Europe concerning use of classic limiting fuses and Polish experiences in use MV expulsion fuses, point at that the cheapest and also most effective way of transformer protection and other parts of substation, against results of overload and short-circuit are properly selected fuses.
- For transformer protection on the MV side with nominal power not exceeding 400 kVA, when prospective short-circuit currents do not exceed 3,15 kA, domestic expulsion fuses are recommended [18].
- Transformers larger than 400 kVA should be protected by classic short-circuit current limiting fuses when prospective short-circuit current exceeds 3,15 kA on the MV side.
- The mistakes in maintenance can be avoided if expulsion fuse links are marked by transformer nominal power and not by nominal current, according to the standard DIN/VDE [17] for LV fuse links with gTr characteristic.
- The MV fuses task is to protect transformers against results of internal short-circuit (oil tank damage, oil leak and possible its ignition due to short-circuit occurred inside the transformer) and cut-off of two and three-phase short-circuit when it appears on the primary or secondary side in the substation part between transformer clamps and fuses.
- Due to the introduction of a new standard PN-IEC 60282-2 [14], some technical parameters of domestic expulsion fuses (especially for rated current of 6A) should be corrected and catalogues completed with necessary technical data, especially Joule integral I^2t in prearcing time and during cut-off is what is needed for designers and users for proper fuses application.

6. References

[1] Hampel W. ; Hartmann E.; Karlscheur W.;Tenberge W.: „Schutz von Verteilungstransformatoren“, Elektrizitätswirschaft, Jg. 91 (1992), Heft 25 z. 1660-1663

[2] Hamel A.; Paquette M.; St-Jean G.: “Nuisance Fuse Operation on MV Transformers During Storms”, IEEE Transactions on Power Delivery, Vol. 5, No. 4, November 1990

[3] Hartmann E.: „Verhalten und Schutz von Verteilungstransformatoren“, CIRED 89

[4] Kacprzak B.; Hyrczak A.: “Service experience of new high-voltage expulsion fuses at rural outdoor networks”, CIRED 1989, s. 76-79

[5] Lipski T.; Musiał E.: „Bezpieczniki topikowe i ich zastosowania”, Rozdz.8.4.

Podręcznik przygotowany do druku
[6] Michniewski R.: „Eksploatacja stacji transformatorowych 15/0,4 kV słupowych uproszczonych w ZE Toruń S.A.”, Biul. Infor. PTPiREE, nr 2/96
[7] Ossowicki J.; Sibilski H.: „Zabezpieczenia rozdzielnic pierścieniowych średniego napięcia”, WE 2000, nr 9
[8] Ossowicki J.: „Nowoczesne zabezpieczenia transformatorów rozdzielczych”, Przedsiębiorstwo ENERGO- EKO- TECH Poznań - Kiekrz paźdz. 2000
[9] Ossowicki J.: „Bezpieczniki topikowe o charakterystyce gTr w stacjach transformatorowych”, Biul. Infor. PTPiREE nr 3/2002
[10] Planzlaff K.P., Schemmann B.: „Prűfung des Verhaltens bei inneren Fehlern im Transformatorenraum bei nicht begehbaren Ortsnetzstationen“, Elektrizitätswirtschafft, Jg. 89(1990) Heft 16/17
[11] Popeck C.A., Lewis W.A. and Allen G. D.: “The Application of Current Limiting to Distribution Circuit Protection”, USA 1977
[12] „STANDARDY TECHNICZNE OBOWIĄZUJĄCE DLA URZĄDZEŃ SN i nN EKSPLOATOWANYCH W ENERDZE GDAŃSKIEJ KOMPANII ENERGETYCZNEJ”, S.A. Gdańsk styczeń 2002
[13] PN-92/E-06110: „Bezpieczniki topikowe wysokiego napięcia. Bezpieczniki ograniczające prąd”
[14] PN-HD 630.2.1. S5: 2003 (U) „Bezpieczniki topikowe niskonapięciowe. Część 2-1: Wymagania dodatkowe dotyczące bezpieczników przeznaczonych do wymiany przez osoby wykwalifikowane (przeznaczone głównie do stosowania w przemyśle). Sekcja od I do V: Przykłady typowych znormalizowanych bezpieczników”
[15] PN-IEC 60282-2: „Bezpieczniki topikowe wysokonapięciowe. Bezpieczniki gazo-wydmuchowe”, listopad 1999
[16] IEC Publ. 787: “Application guide for the selection of fuse-links of high voltage fuses for transformer circuit applications”, 1983
[17] DIN/VDE 0636-201/A10 z października 1997.: „Niederspannungssicherungen (NH-System) Teil 2: Zusätzliche Anforderungen an Sicherungen zum Gebrauch durch Elektrofachkräfte bzw. elektrotechnisch unterwiesene Personen (Sicherungen überwiegend für den industriellen Gebrauch). Hauptabschnitte I bis V“
[18] Katalog firmy ZRE Gdańsk: „Wysokonapięciowy zespół zabezpieczający typu WZZ”
[19] Katalog firmy ZRE Gdańsk: „Wkładka bezpiecznikowa gazowydmuchowa napowietrzna typu WBGN”
[20] Katalog firmy SIBA: „HH –Sicherungseinsätze HH 1- 03/00“

NEW PRINCIPLES FOR A SAFE INTERRUPTION OF LOW CURRENTS IN HIGH-VOLTAGE HIGH-RUPTURING CAPACITY FUSES

Uwe Kaltenborn[(1)], Guido Hoffmann[(2)]

ABB Switzerland[(1,2)], Corporate Research, CH-5405 Baden, Switzerland
uwe.kaltenborn@ch.abb.com[(1)], guido.hoffmann@ch.abb.com[(2)]

Abstract: Based on the definition of IEC 60282-1, backup-fuses have to interrupt currents higher than the minimal breaking current. Full-range fuses have to interrupt all currents, which are able to melt the fusing element. Severe circumstances like reduced heat-transfer or external heating might trip the fuse when the actual operating current is below the minimum breaking current or the melting current. In consequence the fuse can explode. Therefore the use of fuses in severe environments with high operating temperatures like fuse canisters and cubicles for electrical switchgears can dramatically aggravate a high risk of failure. Utilizing novel concepts like high-energy materials will enable a defined temperature-dependent tripping of the fuse. Combining this technology with a novel enhanced arc quenching material will lead to an interruption of very low and critical over-currents also in fuse canisters and cubicles under severe thermal conditions.

Keywords: h.r.c. fuse, low over-currents, arc-quenching, interruption, arc-initiation

1 Introduction

Electrical high rupturing current fuses have to act as protection devices in medium voltage distribution grids. The main task is to protect critical equipment to failure currents. There are two types of failure currents: short circuit currents and over-currents. Short circuit currents have to be handled so fast that the fuse operation limits the maximum current. The current limitation of the short circuit currents will be handled by a fuse element with serial constrictions. In case of a short-circuit current all serial constrictions will melt off at nearly the same time. Due to the high number of foot-points of the serial arcs, the resulting arc-voltage is high enough to quench the arc and to interrupt the current. This technology is well proven and accepted.

The handling of over currents is much more critical. Here a complete other physical effect has to be taken into account. Due to the thermal behavior of the fuse, the fuse element will melt at the hottest point. Now the arc starts to burn and will be extended along the fuse element. To interrupt such an arc, the plasma has to be cooled to increase the electrical resistance of the arc and therewith to drive the arc-voltage above the recovery voltage. The cooling of the arc body appears by dissipating the heat of the arc into the fuse sand utilizing the melt enthalpy of the sand. A major problem occurs if the plasma of the arc is stable burning but do not reach the necessary temperature to melt the quartz sand at around 1700 °C, than the arc will not be interrupted. Due to the pressure build up inside the fuse, the fuse body will explode.

Such critical events can happen due to several reasons:

- The over current is smaller than the minimum breaking current.
- A reduced heat transfer away from the fuse leads to a tripping by overheating the fuse at currents below the minimum breaking current.
- Due to an external heat source the fuse will be heated until melting of the fuse-element at currents below the minimum breaking current.

In case of the reduced heat transfer and the overheating by an external heat source, the critical currents can be below the rated current. For a safe handling of such critical situations, new concepts were developed. By implementing High Energy Materials (HEM) a purely temperature dependent triggering of the fuse could be reached. Combining this effect with new arc quenching materials, able to cool low current arcs, an enhanced protection range towards low currents could be shown for h.r.c. fuses.

2 Temperature Depending Tripping of a Fuse

A fuse in a circuit corresponds to a significant reduction of the cross section of the electric conductor. Reducing the cross section leads to an increase of the resistance (1) and of the power dissipation (2):

$$R(\vartheta) = k\frac{\rho(\vartheta)\cdot \ell}{A} \tag{1}$$

$$P = U \cdot I = kI^2R(\vartheta) \tag{2}$$

The main part of the losses will be released as thermal losses, because of the small inductance of the fuse. In the case of an over-current, the thermal losses will depend on the square root of the current.

To melt the silver wire, a temperature of 960 °C is needed.

If the fuse has the ability to interrupt every current that is melting the fuse wire, the fuse is called a full range fuse. Common principles of full-range fuses operate with two serial fuse wires of different materials, a heating chamber or a large number of small parallel wires.

Another opportunity is the use of a thermal limiting striker. Here the external overheating of the fuse will release the striker, which can than trigger a load-break switch for a safe interruption of the current. In such a case the fuse itself does not operate as a fuse.

3 Influencing the Tripping Temperature of a Fuse

There is one technology since more than 70 years in place, which allows a reduction of the pre-arcing time of a fuse at low over currents: the so-called M-effect after A. W. Metcalf [1]. To initiate a tripping of a fuse at lower temperatures, a piece of thin is placed on the silver based fuse element. Thin and silver are two materials able to diffuse into the other material. This diffusion leads to an Silver-Thin alloy of Ag_3Sn, which melts at 232°C. As each diffusion process is dependent on activation energy and time, the temperature of the fuse wire will be heavily influences the time of diffusion and therewith also the tripping time of the fuse as seen in Fig. 1.

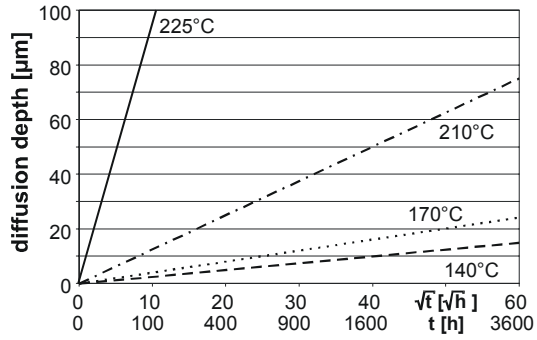

Fig. 1: Diffusion-depth over time of a silver-tin-system depending on the temperature [2]

Due to the slow diffusion speed of the M-spot at temperatures in the range of 200 to 250 °C, a method of tripping a fuse without any delay at lower temperatures would increase the triggering sensitivity of a fuse at low current switching.

3.1 High Energy Materials

Another way to influence directly the tripping of the fuse-element is the application of so-called High-Energy Materials (HEM). Such materials are able to release a high amount of thermal energy at temperatures up to 3000 K due to an exothermic chemical reaction. Such reactions can be initiated by reaching a defined temperature in the range of around 70 °C up to 250 °C. Applying such materials directly to the fuse element enables a nearly instantaneous tripping by reaching the critical temperature of the HEM.

All HEM are based on the following reaction principle (3 - 5):

$$\text{Propellant} + \text{Oxidizer} \xrightarrow{70°C - 250°C} \text{Initial Reaction} \quad (3)$$

$$\text{Heat Producer} + \text{Oxidizer} \xrightarrow{\text{Initial Reaction}} \text{Melting Heat} \quad (4)$$

$$\text{Propellant} + \text{Heat Producer} + \text{Oxidizer} \longrightarrow \text{Melting} \quad (5)$$

The HEM can be divided by the most critical component, the propellant. There are two major groups of material, the so-called thermites and the stable nitric compounds. For the heat producer as well as for the oxidizer several chemical structures are known. In the most cases these heat producers and oxidizers can be used for both propellants. The major differences will be the burning temperature and the reaction velocity.

3.2 Thermite Based HEM

In cooperation with RUAG Munition (former Swiss Munition Enterprise Thun) several thermite based HEM were tested. A special metal/metal-oxide reaction is used, wherein the metal-oxide exists in a meta-stable condition. For this heat producing reaction, locally temperatures higher than 2000 K were measured. The initial reaction is described in formula (6):

$$\left\{Me^a + Me^aO_y\right\} + O_x \rightarrow 2Me^aO_x + \tfrac{y}{2}O_2 + Q(kJ) \quad (6)$$

To feed this reaction, originally oxygen from the environment was used. The materials for instance are used in applications like compact single use heaters to prepare food. In a fuse the amount of oxygen is insufficient to feed this reaction, due to the fact of the compact filling with sand. Therefore an additional oxidizer was implemented. This reaction is starting at low temperatures and produces temperatures high enough to trigger a second fast burning metal/metal-oxide reaction (7).

$$Me^b + Me^cO_z \rightarrow Me^bO_y + Me^c + Q(kJ) \quad (7)$$

The thermite based HEM are dissolved in an organic binder and therefore are liquefied. This liquid was applied by painting it onto the fuse element. Hardening of the HEM occurred by heating the fuse element up to temperatures around 50°C. The binder evaporates and the material is fixed.

3.3 Stabilized Nitric Compounds

Several organo-nitric compounds show a good thermal stability up to temperatures above 200°C. Two of these materials are Guanidine Nitrate ($CH_6N_4O_3$) (8) with a melting point of 216°C and

Guanidine Acetate ($CH_5N_3CH_3COOH$) (9) with a melting point of 226°C.

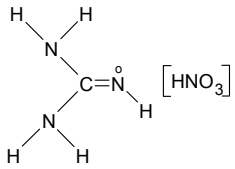

Guanidine Nitrate (8)

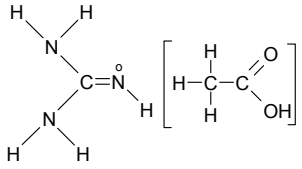

Guanidine-Acetate (9)

Mixtures of these materials with common oxidizers like nitrates, chlorides or peroxides, showed no degradation for temperatures below 190°C. The reaction of these mixtures can reach temperatures up to 1500°C. To generate more heat, added magnesium shows a further increase of the released amount of heat. The reactions for a complete oxidation of Guanidine Nitrate and Guanidine Acetate is shown in (10) and (11).

$$CH_6N_4O_3 + 5O_2 \longrightarrow CO_2 + 4NO_2 + 3H_2O \quad (10)$$

$$4(CH_5N_3CH_3COOH) + 29O_2 \longrightarrow 12CO_2 + 12NO_2 + 18H_2O \quad (11)$$

The propellant / oxidizer ratio has a major influence to the reaction speed. To guarantee a complete reaction, the propellant / oxidizer ratio should be less than 1. On the other hand, the burning velocity of the mixtures has to be tuned in such a way that the sonic velocity is not reached. Otherwise the mixture will be rated as an explosive material with several safety indications.

3.4 Influence of the HEM on the Pre-Arcing Time of a Fuse

Applying the HEM to a fuse element leads to the situation that the tripping of the fuse element is purely dependent from the thermal situation inside the fuse. After igniting the HEM, a high amount of heat will be released, which melts the fuse elements. By comparing a conventional fuse element including a M-spot with the same fuse element having a HEM applied, a significant reduction of the pre-arcing could be measured. Fig. 2 shows the relation between the pre-arcing time and the applied current. The current is based on the melting current of the fuse element with M-spot.

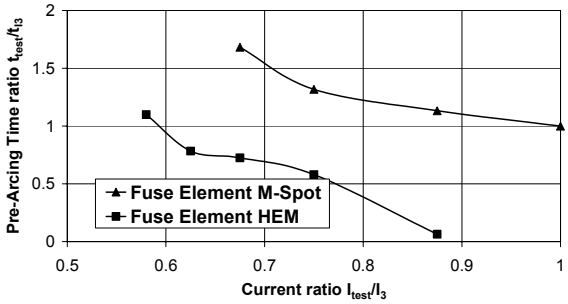

Fig. 2: Pre-arcing time versus test current of a standard fuse element with M-spot and a standard fuse element with HEM, all values related to the values of the minimal breaking current (I3 in accordance with TD 3 IEC 60282-1) of the M-Spot element

4 Arc-Quenching

After realizing a clear defined temperature dependent tripping of the fuse-element, the resulting arc must be interrupted. There are several principles available. Due to drawbacks for the known concepts, a new concept was developed and tested.

4.1 Known Principles

- Improved cooling of the arc by reduced particle size:
  Due to the fact that the melting energy of the sand is decreasing with a decreased particle size, a much more reduced particle size as used today will increase the cooling of the arc. The drawback of such a solution is the reduced ability of the sand to adsorb the metal vapor from the evaporated fuse wire after interrupting the current. Due to the hot metal gas, the dielectric recovery of the arc channel will be not sufficient to withstand the recovery voltage. A re-ignition might occur.
- Improved cooling of the arc by adding electronegative substances:
  Adding materials to the fuse sand, which are generating electronegative gases when they are heated, will also cool the arc. The electronegative gases will adsorb electrons from the arc-plasma. Such a material is PTFE, also known as Teflon®. At higher temperatures flour-gases will be generated. Beside the ecological aspect also a technical drawback has to be considered. Due to the significant difference of the specific density of quartz sand and PTFE a decomposition of both components is very likely and the availability of PTFE to the arc is not guarantied.
- Applying cooling media to the fuse wire:
  Utilizing the thermal energy to initiate a chemical reaction will also lead to a cooling effect at the arc. One example is the use of Aluminiumtrihydrate ($Al(OH)_3$). Here the energy will be used to feed the reaction of Aluminiumtrihydrate to alumina. This

will be done in two steps of oxidation: the Boehmite reaction (12) and the Alumina reaction (13) [3, 4].

$$2Al(OH)_3 + Q(kJ) \longrightarrow 2AlOOH + 2H_2O \quad (12)$$

$$2AlOOH + Q(kJ) \longrightarrow Al_2O_3 + H_2O \quad (13)$$

This reaction is mainly used as a flame retardant in filled polymers. The operating temperature for these applications is limited to maximum 150°C. For the use in fuses the maximum hot spot temperatures at the constrictions has to be taken into account, as temperatures above 170°C can be easily reached. That means that the cooling medium has to withstand such temperatures without degrading. In case of Aluminiumtrihydrate the degradation process starts between 150 and 175°C (Fig. 3). Therefore an application of such material has severe restrictions.

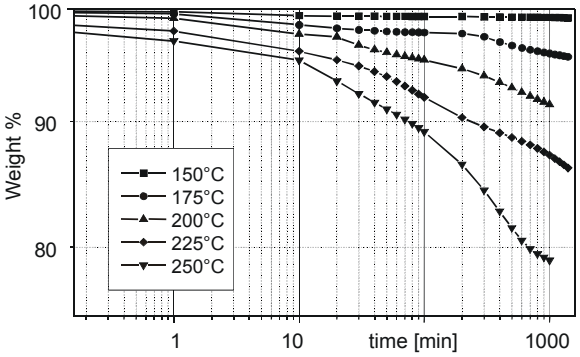

Fig. 3: Weight loss of Aluminiumtrihydrate ($Al(OH)_3$) over time dependent on the temperature

- Fast extension of the arc length:
  Another opportunity to revoke energy from the arc is the fast increase of the arc length. Applying a high number of parallel fuse elements with reduced cross-section might do this. In such a case the following restrictions has to be taken into account. If the number of parallel wires is to high, the commutation time of the arc will unacceptably increase. Another effect is the reduced distance between the wires. Due to the level of the recovery voltage a minimum insulation distance between the wires is necessary. Beside these technical issues also a production problem will occur. The resulting reduced cross-section of the single wire will make it impossible to handle such thin wires with traditional wire designs. New concepts like substrate power fuses are enablers for new design strategies dealing with a high number of parallel wires [5].

4.2 Novel Types of Arc Quenching Materials

The thermally defined tripping of a fuse has one major drawback. The energy of the burning arc will be insufficient to reach the temperature necessary to melt the extinguishing medium, the sand. By melting the sand, the energy for this process is taken away from the arc, which lead to a reduced temperature of the arc plasma. If the temperature of the plasma is low enough, the plasma channel will be quenched until implosion and the current is than interrupted. The whole effect depends on the interaction between the arc-plasma temperature and the molten volume of extinguishing medium. The volume of molten arc quenching material is than corresponding with the amount of energy taken away from the arc.

To enhance the arc-quenching effect, three possible effects can be utilized:

- Particle size:
  A reduced particle size is equivalent to an increased particle surface and therefore a reduced differential volume is needed to adsorb the same amount of energy.
- Melting point:
  A lower melting point would give the opportunity to increase the molten volume and to utilize the necessary higher energy uptake.
- Enthalpy of fusion:
  Utilizing materials with a higher fusion enthalpy will result in a higher adsorption of the arc-energy in a smaller volume of molten material.

Preferable a combination of all three opportunities should be realized. Table 1 is showing a comparison of three materials, useable as arc quenching materials. Beside the well-known quartz-sand as a reference, alumina and boric acid were chosen.

Table 1: Melting point and fusion enthalpy of different materials used as filler in AQM [6]

	SiO_2	Al_2O_3	BH_3O_3
melting point m_p [°C]	1713	2054	170
enthalpy of fusion ΔH [kJ/mol]	8.51	111.4	22.3

Alumina shows the major advantage with the high value for the enthalpy of fusion and the availability of a broad variation of commercial available grain sizes, down to nano-powders. Both effects are well compensating the higher melting point.

Boric Acid shows a reduced melting point in conjunction with a higher enthalpy of fusion. A major drawback for this material is the fact that the particle size is not controllable. Due to small difference between operating temperature and melting point, a solidification of the boric acid powder will happen.

For a real fuse-design the interruption capability of an arc-quenching material is important, but also effects like dielectric recovery after current interrup-

tion, thermal conductivity and costs are important. Considering all these boundary conditions, a direct placement of the needed amount of arc-quenching material to the potential arcing area would be the most efficient solution. For an industrial production process, this is nearly impossible. A potential solution was found by embedding the arc-quenching material into a matrix-material.

As the processing of an inorganic matrix material is rather complicated, an organic matrix material would be preferable. All carbo-organic materials might be excellent useable for an efficient low-cost process, nevertheless due to the high temperatures near the arc, those materials will be oxidized to gases and highly electrically conductive carbon black, which is than limiting the dielectric withstand voltage after the current interruption.

Utilizing silicone-based polymers a work-around for the drawback of the carbo-organic materials was found. Beside the easy to handle production process an increased dielectric and thermal behavior was measured.

4.3 Current Interruption Behavior of New Arc Quenching Materials

To evaluate the arc-quenching capability, all tests were based on one standard fuse design. As a reference a standard fuse filled with quartz-sand was used. The new materials were applied directly to the fuse wire. To compare the results, the ratio of the minimal applicable testing current for a safe interruption was related to the baseline of the rated current of the used fuse design (14).

$$C = \frac{I_{test}}{I_{rated}} \tag{14}$$

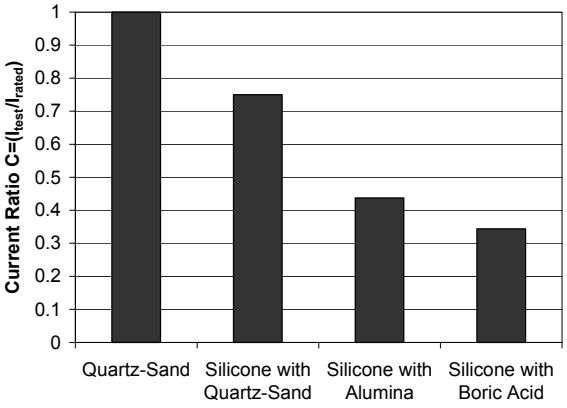

Fig. 4: Related ratio of minimal breaking current and rated current dependent on the applied arc-quenching material

In result of the tests of the minimal breaking current (TD3 in accordance to IEC 60282-1) a certain reduction of the minimal breaking current based on the current ratio (14) was measured. Also quartz-sand in a silicone matrix showed a better performance as pure fuse sand. Alumina and boric acid performed significantly better (Fig. 4).

Additional experiments were performed with ultra-fine alumina to show the influence of the particle size. Using ultra-fine alumina with particles sizes near the nano-range, lead to a further reduction of the minimal breaking current (Fig. 5).

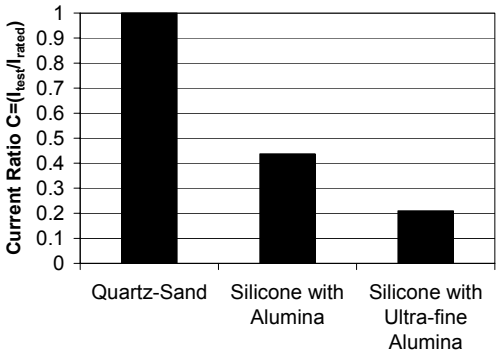

Fig. 5: Related ratio of minimal breaking current and rated current dependent on the grain size of the alumina used for the arc-quenching material

4.4 Dielectric Behavior of the New Arc Quenching Material

For the fuse-design the dielectric behavior of the arc-quenching materials is very important as well. This was measured in a needle-plan configuration as seen in Fig. 6.

Fig. 6: Needle-Plan arrangement for the measurement of the breakdown strength of the arc quenching materials

The needle-plan setup was chosen to gain an additional safety margin compared to the real design inside a fuse. There we have the sharp edges of the fuse-element as the electrodes, which is more a needle-needle arrangement with a slightly reduced inhomogeneity of the electric field compared to a needle-plan arrangement. Mainly two materials were compared: fuse sand and alumina filled silicone. The needle was adapted to the electrode in such a way that the distance was exactly 1 cm. To realize repeatable measurements, the sand was compacted inside a PTFE-ring. In opposition to that the alumina filled silicone sampled were produced with vacuum casting including the electrode setup. For each material 10

measurements with an a. c. voltage-rise test (ΔU=1 kV/s) were performed. The average breakdown values indicated that for a strongly inhomogeneous setup quartz-sand shows twice the dielectric strength than atmospheric air, and alumina filled silicone nearly 9 times (Table 2, Fig. 7, Fig. 8).

Table 2: Average a. c. breakdown field strength of arc-quenching materials and atmospheric air

Material	Air	Quartz	Alumina filled Silicone
E [kV/cm]	~ 5	10	43.4
σ [kV/cm]	-	0.6	7

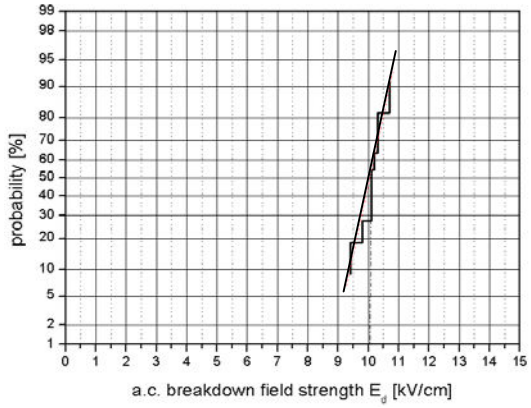

Fig. 7: Probability of the a. c. breakdown field strength of quartz sand in a needle-plan arrangement

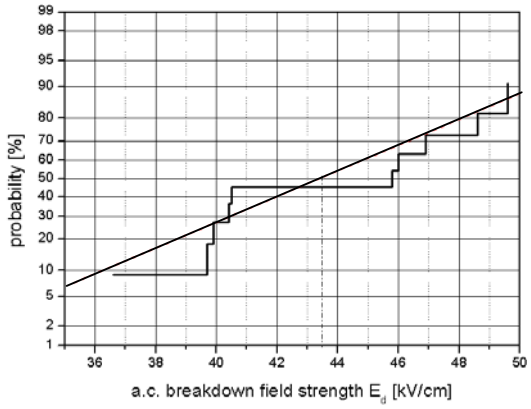

Fig. 8: Probability of the a. c. breakdown field strength of alumina filled silicone in a needle-plan arrangement

4.5 Thermal Conductivity of Arc Quenching Materials

Another important issue for the fuse-design is the thermal behavior of the arc-quenching material. The thermal conductivity and capacitance of the arc quenching material heavily influence the thermal equilibrium of the fuse link and therefore the current rating of the fuse.

The thermal conductivity was measured for quartz-sand and alumina filled silicone (Fig. 9). Due to the better conductivity of alumina compared to quartz sand, the expected result was obtained. The temperature dependency with the negative slope of alumina filled silicone is clearly dedicated to the behavior of the silicone matrix. Finally it can be concluded that the thermal behavior of the alumina filled silicone is better than for quartz-sand over the measured temperature range, which includes the nominal operating range.

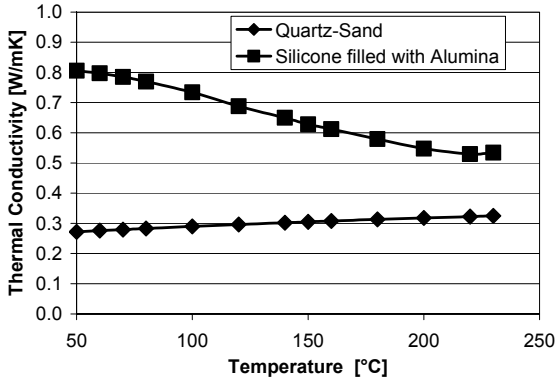

Fig. 9: Thermal conductivity of arc quenching materials dependent on the temperature

The thermal capacitance of the arc quenching material has a direct influence on the dynamic thermal behavior of the fuse-link and therewith to current-time characteristic of a fuse. A high thermal capacitance is decreasing the temperature rise at the fuse element. The measurements of the thermal capacitance (Fig. 10) were done with the Differential Scanning Calorimetry (DSC), using a temperature stabilized measuring chamber.

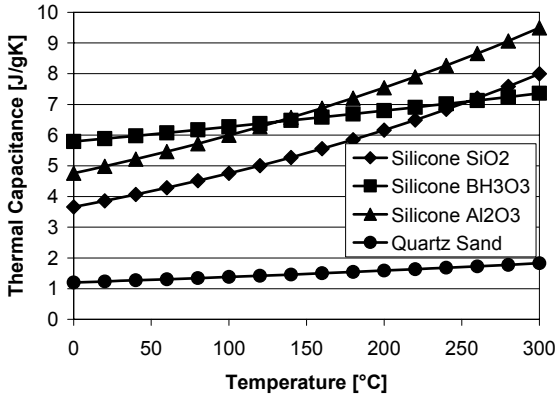

Fig. 10: Thermal capacitance of arc-quenching materials dependent on the temperature

All silicone based materials showed a significant higher thermal capacitance than the original quartz sand, whereas the alumina-filled silicone outperformed the other materials. The thermal capacitance is increasing with the temperature for all materials.

4.6 Mechanical Implications

Due to the stiffness of the silicone matrix of the new arc-quenching materials, the increased mechanical stresses have to be taken into account. Using the Finite Element Solver ABAQUS, the displacement stresses in a standard fuse, utilizing a star-shaped winding stick and fuse-elements with constrictions, were simulated. The potential stress and the deformation of the fuse element are shown in Fig. 11.

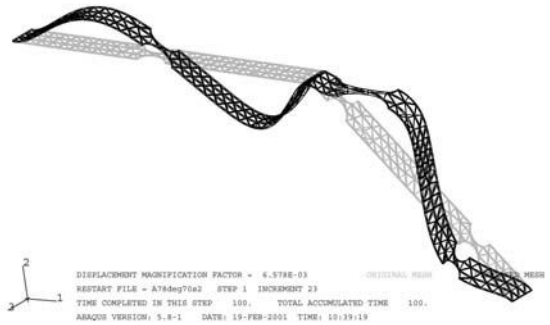

Fig. 11: FEM-simulation of the displacement of a fuse-element in a standard h.r.c. fuse (only the virgin and the stressed fuse-element shown)

Based on the simulation results (Fig. 12) a significant increase of the displacement stresses by a minimum factor of 10 was found. Two main reasons for the increased stressed were identified and simulated (Fig. 13, Fig. 14): the thickness of the arc-quenching material and the number of ribs of the winding stick.

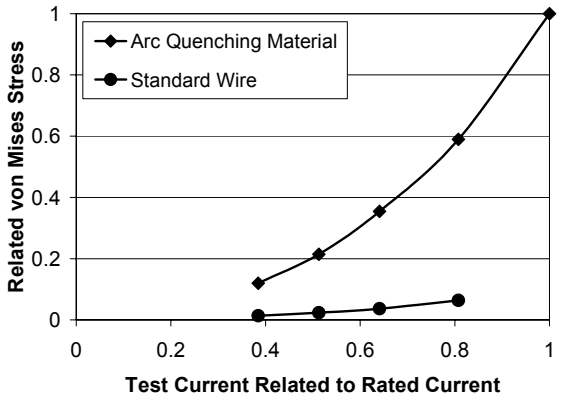

Fig. 12: Related von Mises Stress versus the related test current for a fuse-element with and without arc-quenching material (alumina filled silicone)

Due to the in-compressibility of the silicone matrix of the arc-quenching materials, a higher thickness of the applied material will lead to a higher mechanical stress (Fig. 13). A reduction of the thickness from 3 mm to one mm leads to stress reduction off 25 %.

Another topic is the number of ribs. As the ribs of the winding stick are the mechanical carrier of the wounded shape of the fuse-elements, they are also the cause for mechanical stresses (Fig. 14). By changing the numbers of ribs from 6 to 7, only a moderate increase was found by the simulation. Increasing the number of ribs to 8 led to a significant increase of the mechanical stresses. The explanation for this effect is the increased number of constrictions located directly on or near a rib, which might be specific for the chosen type of fuse-element.

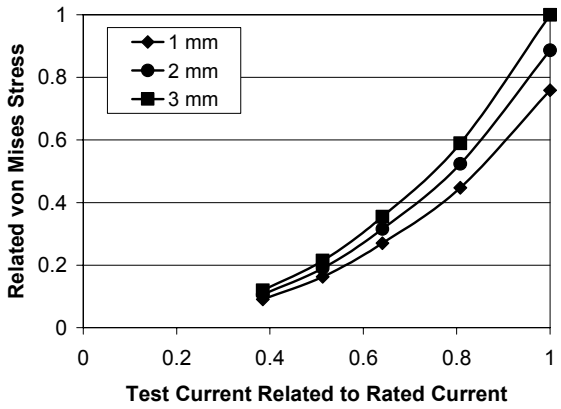

Fig. 13: Related von Mises Stress versus the related test current for fuse-elements with arc-quenching material (alumina filled silicone) of different thickness

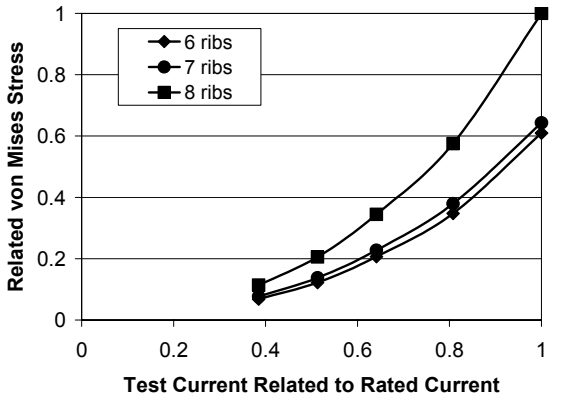

Fig. 14: Related von Mises Stress versus the related test current for fuse-elements with arc-quenching material (alumina filled silicone) dependent on the number of ribs of the winding stick

5 Combined Application of High Energy Materials and Novel Arc Quenching Materials

It was shown that the handling of low over-currents could be improved by applying HEM for a thermally defined tripping and new arc-quenching materials. To realize such a functionality in a fuse, both effects have to be implemented without interfer-

ences. Therefore fuse-elements covered with HEM and alumina filled arc-quenching material was produced and the minimum breaking current was tested. In result (Fig. 15 and Fig. 16) no interference of both technologies could be found. Combining both methods did not influence the pre-arcing time, as well as the minimum breaking current.

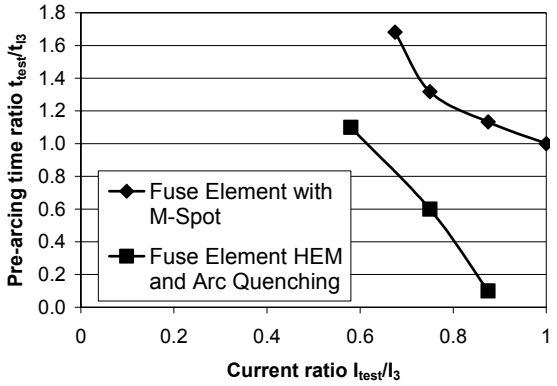

Fig. 15: Pre-arcing time versus test current of a standard fuse element with M-spot and a standard fuse element with HEM and arc quenching materials, all values related to the values of the minimal breaking current (I3 in accordance with TD 3 IEC 60282-1) of the M-Spot element

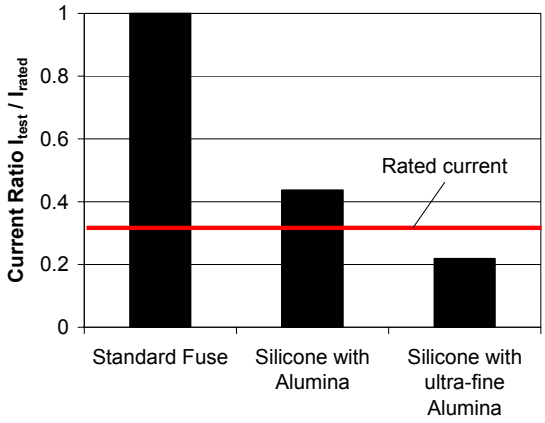

Fig. 16: Related ratio of minimal breaking current and rated current for fuses with HEM and different Arc quenching material

6 Conclusions

The interruption of low over-currents of a h.r.c. fuse was divided into two physical processes: the thermally induced tripping and the interruption of the arc. Due to the application of new materials improvements for both processes were found.

For the thermally induced tripping of a fuse, the M-spot is a well-known technology. By applying so called High-Energy Materials (HEM) based on thermites or stabilized nitric compounds, the tripping temperature and the melting time of conventional h.r.c. fuse elements could be reduced. This results in a reduced pre-arcing time. Due to the possibility of fine-tuning the behavior of the HEM, the pre-arcing I-t characteristic can by customized.

Interrupting the initiated arc is always related to the energy adsorption by the arc-quenching medium. It was again shown that new materials could improve the performance of a fuse. Inorganic fillers based on minerals, showed a better energy adsorption than conventional fuse sand. Applying these powder-like materials to a silicone-based matrix allows a direct placement of the materials to the fuse-element. The positive effect of different fillers and different grain sizes were shown. Especially arc-quenching materials based on alumina filled silicones showed a very good performance. The minimal breaking current could be reduced to values below the melting current of the fuses. This effect is very helpful for full-range fuse applications, or for fuses applied to severe thermal environments like fuse-canisters and switchgears. There the fuse is able to operate without a derating, as long as the melting temperature of the fuse element is not reached.

Beside the dielectric and the thermal behavior of the new arc-quenching materials, also the higher mechanical stresses at the fuse elements due to the new materials were simulated and discussed.

Finally successful tests with fuse elements incorporating HEM and the new arc-quenching material were performed. An interference of the two approaches was not found.

Literature

[1] Metcalf, A.W.: A New Fuse Phenomenon", BEAMA Journal 1939

[2] Daalder, J. E.; Kulsetas, J.; Rondeel, W. G. J.: "Ageing in Fuses with M-effect", 4th Conference on Switching Arc Phenomena, pp. 295-299, Lodz, Poland, 1981

[3] Seim, R.: "Minerale", 1st edition, Neumann Verlag, Leipzig, 1981

[4] Salmang, Scholze: "Keramik, Teil 2: Keramische Werkstoffe", 6th edition, Springer-Verlag, 1983

[5] Wilniewczyc, M.; Hoffmann, G.; Kaltenborn, U.: „Application of Thick Film Substrate Technology in High Voltage HRC Fuses"; ICEFA 2003, Gdansk, Poland 2003

[6] Lide, D. R. (ed.): "CRC Handbook of Cemistry and Physics", 78th edition, CRC Press, New York, 1998

THE IMPACT OF HV FUSE DESIGN AND APPLICATION ON THE DEVELOPMENT OF INTERNATIONAL STANDARDS

John G. Leach

Hi-Tech Fuses, Inc., Hickory, NC, USA, jgleach@hi-techfuses.com

Abstract: All fuse types that presently exist were once used in a new application for the first time. The process whereby such a new fuse and application becomes sufficiently recognized that its special requirements are covered in standards, both national and international, is both complex and somewhat arbitrary. The objective of this paper is to discuss this process as it relates to certain fuse designs and to explain why differences often exist between national and international (IEC) standards.

Keywords: (high voltage fuse, electric fuse, fuse standards, IEC)

1. Introduction

For a particular fuse application, there are three main requirement areas that should be considered, and so warrant inclusion in a standard. The first area involves the ability of the fuse to function under normal conditions. When there are no fault or overload conditions present, it must be able to carry current without any deterioration that might impair its ability to later perform an interrupting function. In addition, as a device that produces heat, it must not cause thermal damage to other equipment, and when the whole fuse includes insulating supporting means, it must meet appropriate dielectric requirements. Physical requirements (size, suitability for liquid immersion, etc.) also fall into this area. The second area relates to the ability of the fuse to be able to successfully interrupt all fault current conditions that it is required to interrupt (that is for the fuse to perform its primary intended function). The third area relates to the ability of a fuse to coordinate correctly with other protective devices in the system. Standards address these areas with testing requirements and application advice. The ability of a fuse to meet requirements in all of these areas must be considered when determining the suitability of a particular fuse design for an application.

The sets of circumstances that lead to fuses being developed to meet a particular market need are quite varied. At one extreme is the situation where an existing design is used for a new application that requires no testing and perhaps only a minor mechanical change to the fuse. An example of this may be a fuse requiring different mounting hardware. If this does not affect the fuse operation, and the conditions of the application do not demand more capability from the fuse, no additional tests are necessary. At the other extreme is the situation where a new fuse design is needed because no existing design is suitable. The new requirements may be physical (e.g. smaller in length or diameter), electrical (e.g. fault currents having higher TRV values, X/R, or circuit voltage), or environmental (e.g. higher ambient temperature, use in an enclosure, or immersion in fluid). Circumstances such as these would obviously require extensive testing to demonstrate the capability of the new design.

Between these two extremes are conditions that may require only limited additional testing, perhaps where an existing design is used in a new application. Additional tests could be very simple, for example thermal tests to establish a new fuse current rating, or complex, for example the need for capacitive current interrupting tests on a fuse to be used for capacitor protection that has previously only been tested with inductive currents.

If one has a completely new application, it is easy to see why not all of the tests needed to ensure a fuse will be suitable are in an established fuse standard. However, when a new fuse is developed for an existing, established, application, it would be easy to suppose that that all of the necessary testing to qualify the design does appear in the relevant fuse standards. Unfortunately, this is not necessarily true, and to understand why requires a knowledge of what standards are, and how they are developed. In most cases, tests have been added to standards based on field problems, or problems discovered in the development of a basic fuse type. As a result, one can say that, in general, existing standards were written for specific designs of fuses, and for specific applications. However, this normally requires several manufacturers to suggest changes. Suppose a manufacturer discovers that their fuse design needs a particular test to ensure its suitability for an application. This may not be reflected in the standard, either because they do not propose such a test for inclusion (perhaps thinking it unique to their design) or because a proposal from them was not accepted by the standards making body.

Presently, there tends to be two major "schools" of thought concerning the writing and maintaining of standards. The first holds that only the simplest tests, that everyone can agree applies to all fuses, should be included in standards. The premise for this approach is that, since testing just “to the standard” does not

and can never relieve a designer of the responsibilities of thoroughly understanding his or her product, and hence carrying out the appropriate testing, an elaborate standard is unnecessary. This could be considered the "old school" approach, and, since the premise is undoubtedly correct, is valid in a situation where all manufacturers and users are very knowledgeable. Members of the second "school" acknowledge that standards can never contain all of the testing necessary for a manufacturer to know that their design is good. However, they hold that, since users tend to be less knowledgeable today (and in many parts of the world enrolment in electrical power degrees has declined significantly in recent years), it is appropriate that standards contain more application information and more comprehensive testing requirements, to cover known areas of concern. The content of any particular national or international standard tends to lie between these two extremes, reflecting the view of the majority of those involved with its development. Generally, users tend to fall more into the second "school", and manufacturers are somewhat split between them.

The object of this paper is to give illustrations of how fuse developments and applications have produced changes in International Electrotechnical Commission (IEC) standards, based on input from certain national standards. However, it will also illustrate why some proposed changes have not been reflected in IEC and so why national and international standards are not always in agreement.

2. The standard development process

The basic process whereby standards are developed may be illustrated by an entertaining (and possibly apocryphal) story from the earliest days of current-limiting fuses. It is said that as maximum fault currents rose, CL fuses were unable to successfully interrupt the higher currents. A standard was therefore developed to require fuses to be tested to determine their maximum interrupting (breaking) current (now also called I_1 or Test Duty 1). At high currents, failure generally tends to be of a bursting nature. This is because the higher the prospective current, the higher is the current at melting. This produces greater shockwaves from material vaporization, and energy absorption by the fuse occurs over a shorter time. It was therefore easy to see why a fuse might experience problems at higher currents, and solutions included making the fuse body and end caps stronger. When failures continued to be experienced, even though the maximum interrupting rating of the fuse had not been exceeded, it was discovered that current-limiting fuses were also sensitive at a lower value of current where absorbed (arc) energy was actually higher. This was the now well-known (although perhaps not well understood) I_2, or TD2, test condition. For some designs, this condition was more severe than the I_1 condition. At the time, this was not intuitively obvious, despite the fact that it is relatively simple to calculate that the system stored energy at fuse melting (most of which must be absorbed by the fuse) actually increases as fault currents decrease, at least until just before the fuse no longer current limits. However, since for many designs the stored arc energy represents less than half of the actual arc energy, the point on the voltage waveform when a fuse begins to arc makes a big difference to the additional energy supplied from the source during arcing. This increases the current that produces maximum arc energy to a value higher than that producing maximum stored energy. Higher arc energy produces larger diameter fulgurites (the fulgurite is the insulating glassy material produced when an element arcs and melts quartz sand filler material). Again speaking generally, failures in the maximum arc energy region tend to be of a thermal nature, or for spirally wound elements, of a turn-to-turn bridging nature. The point here is that while, in retrospect, it is relatively easy to predict what should be realized about the behaviour of a new fuse design, at the time it is much less obvious. This has proven the case in many other fuse developments; it has required service experience (and sometimes service failures) to understand the complexities of what, to too many people, is considered a relatively simple device, the fuse.

The above illustration of the standards making process points to the main reason why national and international standards differ. When a group gathers to produce or update a standard, the primary driving force is their own experience with the fuse designs with which they are familiar. The worldwide production of High-Voltage fuses, while representing a substantial industry in terms of units and economic value, is never the less quite small when compared to many other parts of the electrical industry. As a result, not many countries have indigenous fuse design and manufacturing operations. It is therefore not unusual for only a few countries to send experts to participate in the development of IEC fuse standards, even though much wider fuse usage exists in countries that are not represented. Furthermore, participation has been declining. For example, in the last ten years, there have been four meetings of the IEC High-voltage Fuse subcommittee SC32A with two of them in the last five years. Although 21 countries sent representatives to one or more of these meetings, only six were represented at both of the last two meetings! Most of the actual work is done in the influential working group/maintenance team meetings (those responsible for actually writing the text submitted for national committee voting). In the last five years, there have been six of these meetings, but only seven countries have been represented. With a small number of experts, it is often difficult for

consensus positions to be established when new ideas are introduced, because practices are indeed different in different parts of the world. As a result, IEC standards tend to represent the minimum requirements for the majority of fuse types. However, this "lowest common denominator" approach may not represent an adequate test requirement for all fuse types and applications. With increasing "globalisation", there comes a desire to use a common standard everywhere, but even IEC itself, with its recent rulings on "Global Relevance", recognizes that a "one size fits all" approach does not necessarily represent the best possible solution everywhere. In fact, although the use of a single common standard has many obvious advantages, in a significant number of applications it can be at best, unhelpful, while at worst, it may lead to fuses being used in applications for which they are unsuited and potentially hazardous.

In section 3, this paper seeks to illustrate how certain fuse design and application developments have led to changes in some national standards. Sometimes these changes have resulted in changes to IEC standards, while in other cases they have yet to be accepted internationally. For applications having requirements not presently covered by IEC standards, particular care must be taken if fuses are selected that have only been tested to IEC. Because the author is most familiar with IEEE and IEC standards, the comparisons made in this paper will be between these documents. Obviously, many other national standards reflect regional concerns, and may have relevance outside their immediate area of influence.

3. Differences in standards

3.1 Introduction

IEEE high-voltage fuse standards are developed, primarily, by representatives from the USA and Canada. However, the IEEE, as an international body, welcomes participation from any member. The IEEE fuse standards therefore tend to represent, not only practice in the USA, but also practice throughout the world where North American-style electrical distribution systems are used. After development, however, recognition as an American National Standard is obtained from ANSI (American National Standards Institute Inc.). The IEC and IEEE standards to be compared are listed in "References".

3.2 Publishing format

The most obvious difference between IEC and IEEE standards is the form in which they are published. While of no technical consequence, a brief explanation of the format differences is in order. IEC has two main fuse test standards, IEC 60282-1 [1] for current-limiting fuses and IEC60282-2 [2] for expulsion fuses. IEEE incorporates both fuse types into one testing standard, C37.41 [3]. However, this one standard is used in conjunction with other standards. C37.40 [4] covers Standard Service Conditions and Definitions, while C37.48 [5] and C37.48.1 [6] contain application information. Individual types of fuses have their own specification documents that contain information such as preferred values of current, voltage, and interrupting rating, arc voltage limits, etc. In addition, fuses are classed as either power or distribution class, depending upon the typical location where they are to be used. Power class tends to be used closer to a substation and is characterized by higher values of X/R for example. Specification documents are C37.42 [7] for expulsion type distribution class fuses and cutouts, C37.46 [8] for power class fuses (expulsion and current-limiting) and C37.47 [9] for distribution class current-limiting fuses.

3.3 Voltage rating

After format, possibly the most obvious difference between IEEE and IEC standards is in the voltage used to test fuses. In both IEEE and IEC standards, actual fuse interrupting tests are performed in single-phase circuits. However, for current-limiting fuses, IEC tests assume that all current-limiting fuses are intended for use in grounded wye three-phase circuits, while IEEE standards assume that many fuse types are intended for single-phase operation. This difference in approach can be traced to the fact that, at least at one time, most European fuses were used in three-phase circuits while many North American type fuses were used in single-phase circuits. IEC standard 60282-1 therefore requires that the high current tests (I_1 and I_2) be performed at only 87% of the rated voltage of the fuses. As specified in the application section of the standard, if a fuse is to be used in a single-phase circuit, or in a delta system, the rated voltage of the fuse should be at least 115% of the maximum applied voltage. In the case of IEEE standards, all distribution class fuses are tested with a voltage equal to the rated voltage of the fuse. For power class fuses, only the I_1 test is performed at 87 percent of the rated voltage of the fuse (at the full rated maximum interrupting current) and then the test is repeated at 87 percent of the rated maximum interrupting current, but at the full rated maximum voltage. A power fuse is therefore suitable for single-phase use providing the available fault current does not exceed 87% of its rated interrupting current. Many current-limiting fuse designs combine these two tests, using 100 percent of both rated maximum voltage and rated interrupting current as is done for distribution class fuses. Expulsion fuses tested to IEC are allowed the same option (two sets of I_1 tests) if the fuse is only to be used in three-phase circuits, otherwise they are tested at full voltage.

Although these testing differences are quite confusing, in the past this has not been a problem. IEC standards have two columns of preferred

standard voltages, series I and series II. The first is noted as being based on practice in Europe, and the second on practice in the U.S.A and Canada. Because most fuses tested to IEC have used the European voltages, which are generally higher than the North American values, the nearest higher voltage rating European fuse will normally have been tested to as high or higher voltage than a North American fuse. For example, compare preferred series II voltages of 8.3kV and 15.5kV with series I voltages of 12kV and 17.5kV. Even though I_1 and I_2 tests for current-limiting fuses would be performed at 10.44kV and 15.2kV for the European fuses, these values exceed, or are very close, to standard North American voltages.

A serious problem could arise, however, if a manufacturer were to test a fuse using the IEC standard, but picking a North American preferred voltage (series II) and using 87% of this voltage as the I_1 and I_2 test voltages. In this case, a misunderstanding on the part of the user could lead to service failures. For example, it is common to use an 8.3kV North American fuse (tested to IEEE) on a single-phase circuit based on 12.47kV or 13.2kV grounded wye three-phase circuits. The maximum permitted line-to-neutral voltages on these two circuits equals 7.62kV and 8.07kV respectively. If an 8.3kV fuse were tested to IEC, a single fuse would only have been shown to be capable of interrupting 7.2kV, and so may experience difficulty with a 6% or 12% over-voltage in the two circuits, respectively. A similar situation exists with many other standard North American system voltages. This is because the standard North American fuse voltages were chosen to correspond to standard system voltages assuming that the fuses would be tested using North American testing practices. This is not an unreasonable assumption! Here is a case where, in an attempt to make a European standard into an International standard, the melding together of two different philosophies may lead to incorrect application if the user does not fully understand the subtleties of the IEC standard, and does not read the "fine print"!

3.4 Extended recovery (maintained) voltage

3.4.1 Introduction

During fuse interrupting performance tests, recovery voltage is maintained across the fuse for a minimum specified period after current interruption. This is to show that current flow will not be re-established, and that the fuse will be able to withstand system voltage for an extended period. Obviously, this duration must be sufficient to achieve its aim without being any longer than necessary (due to the high cost of test time). All fuse standards have a specified duration that depends on the type of fuse and the type of test. For example, IEEE standards for current-limiting fuses have durations of one minute for the I_1 test and 10 minutes for the I_2 and I_3 tests (I_3 being essentially the lowest current at which a fuse must demonstrate interruption capability). In IEC standards, current-limiting fuses have durations of only 15 seconds for the I_1 test and one minute for the I_2 and I_3 tests. For non-dropout expulsion type fuses (fuses that remain connected in the circuit after operation) both IEC and IEEE require 10 minutes for test currents higher than 20% of the rated interrupting current and one minute for the two required lower current tests. Dropout fuses require only 0.5 seconds or the dropout time, whichever is greater. The IEC expulsion fuse standard has the same values as the IEEE standard because it was revised in the mid 1990s to essentially lineup with IEEE C37.41. However there is clearly a substantial difference between the IEC and IEEE standards for current-limiting fuses. It could be argued that, if the longer duration is necessary for a valid test, the testing of some fuse designs to IEC standards would seem to be inadequate, or alternatively, manufacturers testing to IEEE are wasting a lot of money! To understand why this difference exists, and what steps have recently been taken to narrow the gap, requires first a study as to why, over 30 years ago, the IEEE standard was changed from the values still used by IEC.

3.4.2 Changes to the IEEE fuse standards

Specified recovery voltage durations were first established in an era when virtually all current-limiting fuses used ceramic or glass bodies, ceramic cores, silver elements, quartz sand, and copper or brass end caps. Generally, these fuses were what would now be classed as backup fuses. With this type of design, electrical breakdown tends to occur immediately after interruption, or not at all. Therefore, providing the fuse body did not burst due to thermal stress (usually within about one minute), a brief recovery voltage period was enough to show that a fuse would not then fail by dielectric breakdown. This was valid even if the fuse body temperature continued to rise for some time after current interruption as heat was gradually transferred from the fulgurite through the filler material. Most early fuse designs contained virtually no components that could thermally deteriorate over time.

In the USA, there was a quicker adoption of different fuse construction materials than in Europe. This was caused by factors that included the high cost of ceramics, the desire for more compact fuses, and a requirement to be able to interrupt lower currents (general-purpose and full-range fuses). Application differences encouraged the development of different fuse types. For example, a lower domestic utilization voltage (110V rather than the 240V in Europe) and greater distances between customers led to the widespread use of small transformers containing current-limiting fuses. Typical materials used for current-limiting fuses in the USA have included glass-reinforced epoxy fuse

bodies, mica-based materials, gas evolving materials, and plastics for cores, and, to assist in current interruption, silicone rubber and various filler additives. While many of the newer designs performed very well, during the 1960's a series of service problems were experienced in North America with several common types of current-limiting fuses from a variety of manufacturers. Most of these fuses were characterized as having components made from materials that included organic matter (that is materials incorporating the element carbon in their chemical structure) and/or gas evolving materials in which one of the gasses included water vapor. After extensive testing it was determined that a possible failure mode of this type of fuse was re-establishment of current flow some period of time after an apparently successful current interruption. That is to say, failure was occurring after the end of the brief specified duration of recovery voltage that had been used to certify the designs. Although several different failure modes were discovered (see 3.4.3), in all cases the obvious solution was to increase the specified duration. This allowed time for fuse components to begin to cool, and for any component deterioration caused by heat flow to occur, before voltage was removed from the fuse. The recovery voltage duration had to be a compromise between assuring that appropriate "deterioration" had occurred while minimizing the testing cost and inconvenience. For the reasons outlined in 3.4.3, durations of 10 minutes were chosen for Test Duties 2 and 3. In the current-limiting region, failure phenomena were linked primarily to high component temperatures. Because I_2 generally produces more heat than I_1, a value of only 1 minute was chosen for Test Duty 1. These changes to the IEEE recovery voltage duration were adopted in 1969. Experience has confirmed that fuses tested this way do not then breakdown after an operation in normal service.

3.4.3 Choice of recovery voltage duration

Several potential failure mechanisms were identified. One appears to be the production of carbon from organic materials in the fuse body (with no other organic material in the fuse). This carbon is not produced until a particular body temperature is reached, and the time for this to occur depends on the fuse design. The most critical factors would appear to include the heat generated in the fulgurite (arc energy), the distance between the fulgurite and the fuse body, the thermal conductivity of the filler material, and of course the breakdown temperature of the organic material. Tests have shown that peak body temperatures typically occur between about 1 and 4 minutes after current interruption. Testing experience has shown that the majority of breakdown failures from this mechanism occur during the first 5 minutes of recovery voltage, although a small number of failures have been reported between 5 and 10 minutes [10]. A recovery voltage duration of 10 minutes therefore appears to be appropriate, incorporating some safety margin. IEEE and IEC standards for expulsion fuses permit the 10 minute recovery voltage period to be terminated if the leakage current through the fuse is monitored, and has been below 1mA for at least two minutes. However, this technique is not suitable for current-limiting fuses (and is therefore not permitted). For the type of failure mechanism described above, leakage current is typically very low for most of the period before breakdown. This is because the decomposition process is not initiated by heat from any leakage current, but rather from thermal conduction within the fuse. When failure does occur, the leakage current usually increases for less than a few seconds before complete breakdown occurs. This failure phenomenon is most common with I_2 tests, but could occur for I_3 tests where extensive arcing occurs, and/or where fuse melting time is very long, particularly if element temperatures are not limited by the use of low melting point materials (e.g. "M" effect).

The physics of this failure mechanism appears not to have been investigated and explained. Observation suggests that although the carbon must come from the fuse body, the final conductive path is not usually along the body, but rather along the fulgurite surface. One mechanism that has been postulated by the author is that breakdown of the body material, at temperatures between about 250ºC and 400ºC, produces a gas containing carbon atoms. Since the temperature of the fulgurite is much hotter, (quartz sand melts at approximately 1700ºC) a gas could further breakdown depositing carbon atoms on the fulgurite or the sand immediately adjacent to the fulgurite, ultimately producing a conductive path. This would appear to be an interesting phenomenon, worthy of study by a laboratory possessing the appropriate equipment.

Another failure mode that has been observed involves fuses that generate water vapor to assist current interruption. The water (often contaminated by decomposition products of the binders used to construct the gas-evolving materials) is deposited on the inside surface of the body. "Treeing" has been observed on this surface, ultimately leading to a steady increase in leakage current until failure. This has normally occurred within 10 minutes of fuse current interruption. The phenomenon has been observed for both I_2 and I_3 tests on fuses. Fuses using gas-evolving materials are usually classed as general-purpose or full-range.

A third observed failure mode occurs within fuse cores, even when the material from which they are made is inorganic. Inorganically bonded mica makes a very effective core material, since it can be punched very precisely. However, mica contains molecular water that is released at quite high

temperatures. Some forms of mica product therefore have a temperature limit above which the release of water molecules causes the core to "puff up" (analogous to "popping" pop corn). It was discovered that the creation of what was, in effect, a hollow core could result in electrical breakdown in high stress areas of the core in certain designs. Since the failures occurred in the 1 to 10 minute time frame, they were discovered by development testing using the IEEE fuse standard and appropriate remedial action was possible. Obviously, if a core includes organic material, this could lead to problems if carbon was produced in a location and quantity that could lead to a breakdown. Such problems have been discovered by the extended recovery voltage test.

Based on the long and successful experience with the extended recovery voltage duration testing of IEEE standards, in the year 2000 the USA requested that such testing be included in IEC 60282-1 (it was already included in IEC60282-2). At the same time, elevated temperature testing for fuses in enclosures (discussed in 3.5) was also proposed. The USA felt that it was important for International Standards to reflect the concerns of the North American market, not just because we are members of the world community, but also because the same basic types of fuses and applications common in North America are in use in other countries around the world. It is certainly possible to postulate that "North American" type fuses, produced outside North America but intended for the same applications as fuses tested to IEEE standards, might only be tested to IEC standards. This could lead to equipment failures if the IEC recovery voltage duration was insufficient to show up a deficiency in the design. The USA's proposals to IEC became very controversial. A small number of European countries vigorously opposed them, although other countries, both inside and outside Europe were more favorably disposed to the suggestions. The positions taken by IEC participants tended to reflect their experience with designs that were most common in their country (or that they themselves manufactured). One basic argument against the proposals was that if certain existing designs were not experiencing field problems, it is an unreasonable burden to increase testing on all fuses because other designs and applications exist that do need more rigorous testing. Of course, this is a powerful argument against ever making changes to standards, and is only valid if certification requirements are such that all existing designs must be re-tested to a new standard. This issue points to a fundamental difference in philosophy between European and North American practices, and partially explains why, in the past few decades, the USA has embraced changes to standards so much more readily than Europe. It also explains why IEEE and IEC standards that were once so similar are now so different. This is discussed in 3.4.5.

3.4.5 Certification procedures

In the USA, two types of certification are common for high-voltage fuses. The first, limited primarily to industrial applications, and mostly to motor starter fuses, is UL recognition. Underwriters Laboratories Inc. conduct a thorough evaluation of a product, including observing all short-circuit testing and production testing before recognizing the product. UL examination is ongoing during the product's life. This is a long, rigorous, and expensive process. Electric Utilities do not use UL recognition (which applies mostly to higher volume low-voltage products). The other type of certification, used for all other HV fuses and applications, is "self-certification". In this, the fuse manufacturer performs testing, either at an independent laboratory or in their own facilities, and issues their own certificate of compliance. In Europe, the most common form of certification is to employ a "third party", usually a test laboratory such as KEMA. This tends to be more expensive than self-certification, although less costly than UL recognition. In addition, European customers are more likely to require re-certification to the latest standard. This is not the practice in the USA, where established designs are not re-certified unless required by a customer (which is uncommon unless problems have been experienced). Re-certification can obviously be an expensive proposition.

3.4.6 IEC proposal for extended recovery voltage

After many years of IEC debate in the maintenance team (MT3) and sub-committee (SC32A) responsible for IEC 60282-1, a compromise position has been reached. At the time of writing, a Committee Draft Vote (CDV) is in preparation for submission to the National Committees in mid-2003. The proposal is to change the recovery voltage duration **only** for fuses that contain critical amounts of organic material, and are therefore classed as "organic". The duration is increased to 10 minutes for backup, general-purpose, and full-range type fuses at TD2, and for general-purpose and full-range type fuses at TD3. To address the concern regarding re-certification, the fuse manufacturer is allowed to decide whether their product should be classed as "organic". Therefore, if a fuse contains organic or other material that could lead to breakdown after current interruption, the design is classed as organic and it would receive the more rigorous tests. However, if the fuse contains no organic material, or if it contains organic material but in such quantity or location that the manufacturer feels that the fuse is not likely to be subject to deterioration and breakdown, then it would not be classed as organic, and would receive only the usual testing. It is anticipated that a manufacturer would conduct sufficient testing during the development phase of a

new design to determine whether the longer duration tests are necessary for the certification testing.

3.5 Elevated temperature testing

3.5.1 Introduction

Traditionally, standard service conditions for IEEE and IEC standards included an ambient temperature no higher than 40 ºC. In North America, the use of fuses in enclosures that subjected them to elevated surrounding temperatures or restricted cooling became common in the 1960's. Fuses are often used in transformers, where they are subjected to very significantly elevated surrounding temperatures. This practice was later followed in many other countries that used similar types of distribution systems. Other fuses, in both Europe and elsewhere, are used in switchgear subjected to solar radiation and high outdoor temperatures, or contained in "pods" or canisters that severely restrict heat loss from the fuse. Although thermal conditions for these applications are less severe than the transformer applications, service problems were experienced with fuses in many types of enclosures all over the world, usually due to misapplication. Clearly, changes in fuse standards to recognize these expanded service conditions became necessary.

3.5.2 IEC Response

In the early 1990's IEC responded to just the application aspects of current-limiting fuses in enclosures in what is now informative Annex F of IEC 60282-1 ("Determination of derating when the temperature surrounding the fuse exceeds 40 ºC"). The object was to determine the correct rated current for a fuse in an enclosure, so that it would not overheat, and so generate excessively high surrounding temperatures. It was felt that in this way no problems would occur (e.g. causing a backup fuse to melt at a current it could not interrupt). However, while this approach may be adequate for an inorganic backup fuse, in the USA it was felt that general-purpose and full-range fuses are often intended to be able to interrupt fault/overload currents. These currents may cause the fuse's surrounding temperatures to be higher than 40ºC before the fuse is required to interrupt. Even with a backup fuse, while it may not be intended to interrupt an overload current, overloading that produces high surrounding temperatures may also lead to insulation breakdown and a high fault current that the fuse has to clear. In IEEE standards it was felt that addressing only fuse derating was inadequate for their typical applications.

3.5.3 IEEE response

In response to problems in the USA and Canada, IEEE standards developed new application information and testing for "fuses in enclosures". This was first published for current-limiting fuses in 1980 and for expulsion fuses in 1991. Concerns over the effect of enclosure and/or elevated temperature on fuse performance were addressed in four main areas. The first area was that of the effect of changes in heat loss on the melting characteristics and current rating of the fuse, and was addressed with application information. The second area was that of elevated fuse component temperatures after current interruption, where the concerns were similar to those discussed in section 3.4. The third area involved the effect on general-purpose and full-range fuses, where long time melting currents could be reduced, possibly to values less than a fuse could successfully interrupt. These two areas were addressed with additional current interrupting tests. The fourth area involved sealing liquid submersible fuses to prevent leaks at elevated temperatures. This was addressed by thermo-cycling tests.

The concept of "rated maximum application temperature" (RMAT) was introduced. This is the highest surrounding fluid temperature, specified by the fuse manufacturer, for which a fuse is rated as suitable for use. It is the temperature at which additional interrupting tests are performed, and in the case of a sealed fuse, the maximum thermo-cycle temperature. Fuse tests at I_2 and I_3 are therefore specified at this elevated temperature, in addition to the usual tests at room temperature. In the case of a general-purpose fuse, a new (lower) I_3 current has to be used, one that causes melting in not less than one hour under the high temperature and/or restrictive cooling conditions. In the case of a full-range fuse, the I_3 current test is done only at the RMAT, but with the current to be interrupted determined as being lower than the lowest current that could melt the fuse at its RMAT. Testing is normally performed in an oven but if a particular enclosure subjects the fuse to more severe conditions, then the tests should be in that enclosure. The combination of fuse and enclosure is defined as a "fuse enclosure package" (FEP) and it is the responsibility of the FEP manufacturer to test the fuse in their enclosure, or to ensure appropriate tests have been performed.

It was found that, for most fuse designs, breakdown failures caused by elevated body temperatures at I_2 tended to be more common during this testing. The reason is that the final temperatures of the body and other components tend to be higher when the fuse starts off hot. This occurs despite the arc energy being slightly lower due to a reduction in melt I^2t. Because failures were found to be temperature driven, elevated temperature I_1 testing was considered unnecessary. It was found that the 10 minute recovery voltage duration was effective at catching these thermally induced breakdowns, although when the fuse is in a close fitting enclosure, the greater thermal mass of the fuse and container

tended to push the fuse breakdown time closer to ten minutes than those occurring in open air.

3.5.2 IEC Proposal

As with the extended recovery voltage duration, the USA felt that the absence of any elevated temperature testing in IEC meant that a large number of worldwide applications were not being adequately covered by an "international" standard. The USA therefore proposed additional "fuses in enclosure" testing for current-limiting fuses, based on the IEEE standards. As discussed earlier, the US proposal met with a lot of opposition from Europe. Since certain European designs used primarily inorganic materials, some felt that any elevated temperature testing was unnecessary, except in the case of full-range fuses. Here, it was recognized that elevated temperatures would reduce the lowest current that a fuse had to interrupt, increasing test severity. However, this had already been addressed in the 1997 edition of IEC 60282-1. The IEEE elevated temperature full-range fuse TD3 testing had been incorporated into IEC for those fuses intended for use in a surrounding temperature over 40 ºC. This was in addition to a more simple room temperature test for full-range fuses intended for use under 40 ºC. Again, after much discussion, a compromise proposal is being introduced into the CDV. At the time of writing, it is proposed that additional testing only apply to "organic" fuses. Again, organic is to be determined by the fuse manufacturer, based on whether they feel such additional testing is necessary. Additional I_2 testing is to be specified at the fuse's RMAT for backup, general-purpose and full-range fuses. However, a further compromise was demanded by some countries. This was that the additional testing only applies to fuses in applications where the fuse itself is not the primary source of heating for the enclosure. Therefore, applications such as fuses in transformers, or switchgear subject to solar radiation, would require the additional testing. However, other applications, such as with the fuse in a "pod", canister, or indoor switchgear, would not be covered, even though such applications affect heat loss from the fuse both before and after current interruption.

TD3 testing of general-purpose fuses is not included, as some felt that users would not expect a general-purpose fuse in an enclosure to still be able to interrupt a (reduced) current that caused melting in one hour. In other words, a general-purpose fuse may not be a general-purpose fuse over 40 ºC. This is to be addressed in an application note. There is an attempt to include I_3 testing of back-up fuses where the melting time is over 100s. The logic here is that extended melting times could result in high body temperatures and elevated surrounding temperatures could lead to even higher body temperatures, but whether this will be included is not yet known.

4. Conclusions

The preceding sections give a few examples of how experiences in new applications, and with new designs of fuses, can result in changes to, and expansions of, national standards, specifically IEEE standards. However, as has been shown, this does not mean that they will automatically be reflected in an international standard. This can happen even if many manufacturers and users require and accept such changes, and the circumstances that have led to such changes exist in more than one country or geographical area. Instead, many factors including differences in philosophy regarding certification testing, the familiarity of a country's representatives with differing fuse types, and even which countries are actively involved in IEC activities, all have an influence on what testing is deemed to be appropriate for inclusion in an international standard. Clearly, it is not possible, or proper, to put everyone's concerns into an IEC standard. However what this means is that users must be very cautious when specifying fuses for a particular application. It may be necessary to consider more than just whether a manufacturer possesses a certificate of compliance with the IEC "lowest common denominator" standard.

5. References

[1] IEC 60282-1 ed5 (2002-01), High Voltage Fuses – Part 1, Current-Limiting Fuses

[2] IEC 60282-2 ED 2.1-1997, High Voltage Fuses – Part 2, Expulsion Fuses

[3] IEEE Std C37.41™-2000, IEEE Standard Design Tests for High-Voltage Fuses, Distribution Enclosed Single-Pole Air Switches, Fuse Disconnecting Switches, and Accessories (ANSI)

[4] IEEE Std C37.40™-1993, IEEE Standard Service Conditions and Definitions for High-Voltage Fuses, Distribution Enclosed Single-Pole Air Switches, Fuse Disconnecting Switches, and Accessories (ANSI)

[5] IEEE Std C37.48™-1997, IEEE Guide for Application, Operation, and Maintenance of High-Voltage Fuses, Distribution Enclosed Single-Pole Air Switches, Fuse Disconnecting Switches, and Accessories (ANSI).

[6] IEEE Std C37.48.1™-2002, IEEE Guide for the Operation, Classification, Application, and Coordination of Current-limiting Fuses with Rated Voltages 1-38kV (ANSI).

[7] ANSI/IEEE Std C37.42™-1996, American National Standard Specifications for High Voltage Expulsion Type Distribution Class Fuses, Cutouts, Fuse Disconnecting Switches and Fuse Links

[8] ANSI/IEEE Std C37.46™-2000, American National Standard for High Voltage Expulsion and Current-Limiting Type Distribution Class Fuses and Fuse Disconnecting Switches.

[9] ANSI/IEEE Std C37.47™-2000, American National Standard for High Voltage Current-Limiting Type Distribution Class Fuses and Fuse Disconnecting Switches

[10] Zawadzki, J., Powertech Labs Inc., Surrey B.C., Canada, "Private communication with USA Technical Advisory Group to IEC SC32A", August 2002

Note that [7], [8], and [9] were developed and published by the National Electrical Manufacturers Association before having ownership and maintenance transferred to IEEE in late 2002.

Effect of contactless hybrid current limiter on voltage dips in power system

Piotr Leśniewski[(1)], **Borys Semenowicz**[(2)] and **Roman Partyka**[(3)]

Gdansk University of Technology[(1,2,3)], Wlasna Strzecha 18A Str. 80-952 Gdansk,
plesn@ely.pg.gda.pl [(1)], bsemen@ely.pg.gda.pl [(2)], rpartyk@ely.pg.gda.pl [(3)]

Abstract: The paper presents the operation of a hybrid contactless short-circuit current limiter on the basis of computer simulation. Special attention was paid to the possibility of the quality improvement of the delivered electrical energy, through the limitation of the duration of voltage dips in the power grid owing to the application of a hybrid circuit breaker. The calculations were performed using the PSPICE and MATLAB software.

Keywords: electric fuse, contactless hybrid current limiter, simulations, current limitation, voltage dips

1. Introduction

In power distribution systems the power quality is of increasing importance as the low voltage consumers use microelectronic components for control and operation, which are sensitive to voltage dips and power supply interruptions. Voltage dips can be defined as follows: a voltage dip is a sudden voltage reduction ranging from 10% to 90% of the nominal voltage and with a short circuit duration from 10 ms up to one minute [1]. In the US a short-duration reduction (up to a few seconds) in the voltage amplitude is termed a voltage sag [2].

Typically, voltage dips are due to short circuit faults in the power system. The time of disturbance elimination by classical contact circuit breakers is of several dozens milliseconds. It is too long to limit fault currents, and to reduce the duration of the voltage dip. Effective limitation of voltage dips can be achieved, among other means, by the application of hybrid circuit breakers [2,3], whose idea consists in the compensation of flaws of the contact circuit breaker with a semiconductor switch in parallel intercepting the current during the process of interruption. Such limiters may be characterized by high speed of operation (below 1 ms) and the ability to conduct considerable currents during normal operation, if special drives are applied.

One of the first hybrid circuit breakers put in the practice was that designed by Collard and Pellichero [4]. Later on Żyborski [5] and Bartosik [6] significantly developed their idea. A modified approach was presented by Wolny [7,8] who applied a special ultra short fuse in the place of the contact switch. This way the need for a fast electrodynamic drive was eliminated, which allowed to considerably reducing dimensions and costs of the hybrid current limiter. The new device is called the contactless hybrid current limiter (CHCL).

The paper presents the possibility of elimination of voltage dips in power distribution systems, using a contactless hybrid current limiter. The analysis was performed using computer simulation for the operation of assumed models of current limiters.

Below, an analysis of effects of the arc ignition model applied on the calculation results is presented. Ultra-short fuse arc models based on a modified black-box arc model, as well as models offered by commercial software packages were used. Results of the simulation carried out with the application of the PSPICE and MATLAB were compared with experiments on a real contactless hybrid current limiter

2. Design of the analyzed CHCL

In Fig. 1 the structure of the analyzed CHCL is presented. It consists of the following basic elements: the ultra short fuse (USF) shunted by the semiconductor device (SD), controlled by a special control system (CS), and the metal oxide varistor (MOV) absorbing the magnetic field energy of the switched-off circuit. The triggering impulses are controlled by the voltage across the USF.

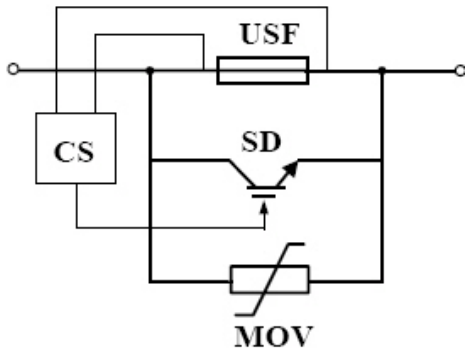

Fig. 1: The model of a DC CHCL [7]

An ultra short fuse as a part of the CHCL assembly is characterised by the following properties:

- short fuse element: a few millimetres in length;
- very fast t – I characteristic;
- very high current density in working conditions;
- marginal power losses in normal conditions.

In Fig. 2 the voltage and current traces of the CHCL operation are shown. The experiments were carried out in the oscillatory LC circuit at the frequency of 480 Hz and the prospective short-circuit current of 1.2 kA. The used frequency higher then 50 Hz increased the rate of current rise, important for the operation of current limitation devices.

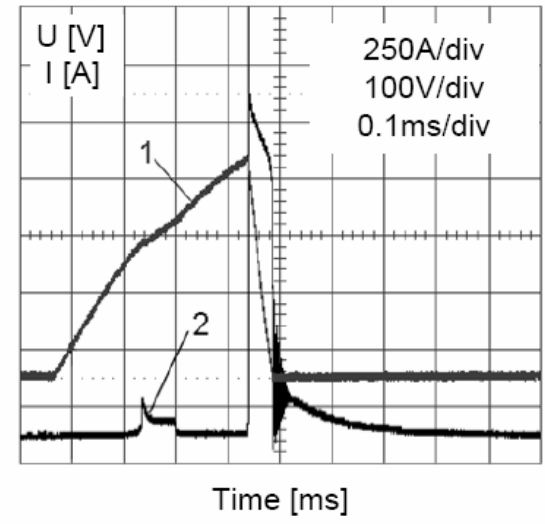

Fig. 2: Current and voltage records of the CHCL operation
1 - the current, 2 - the voltage

3. The hybrid switch calculation model

Mathematical modelling is a powerful tool in the analysis of operation of hybrid switches, allowing for a better identification of requirements concerning the switch components and the effect of circuit parameters, as well as the switch behaviour in critical conditions. However, it is important to properly select the simulation models. Since it is impossible to create a model taking under account all the possible phenomena playing a role in the current limitation process, certain simplifications are very often introduced, or commercial software packages offering simplified models are used. In simulations of the operation of a CHCL, the selection of the ultra short fuse arc model is a difficult and important issue, since due to the prevailing axial cooling no existing arc model can be directly applied.

The calculations were performed using the PSPICE and MATLAB software. The process of current commutation between the fuse and the IGBT was modelled with the MATLAB, while the process of current transfer from the IGBT to the varistor was modelled with the PSPICE software.

In Fig. 3 a diagram of the CHCL used for simulations is shown. 30-nH inductance of current commutation loop was assumed, as well as 50-μΩ resistance. The mutual inductance was neglected.

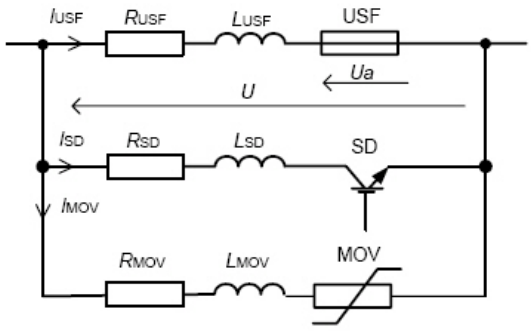

Fig. 3: The modelled circuit of current commutation loop

3.1 The ultra-short fuse model

In hybrid circuit breaker the arc voltage is the driving force of the arc-to-SD current transfer. Therefore the arc model must be carefully selected.

In regard to the PSPICE simulations, the arc model was founded on a voltage-controlled switch modified by the application of a nonlinear resistance connected in parallel to the opening contacts. A varistor with the threshold voltage of 20 V was used, as the nonlinear element.

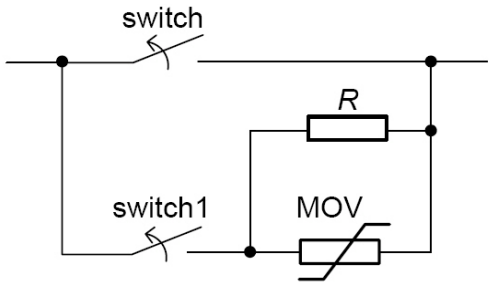

Fig. 4: The USF model (PSPICE)

The simulation results for the assumed model are presented in Fig. 5.

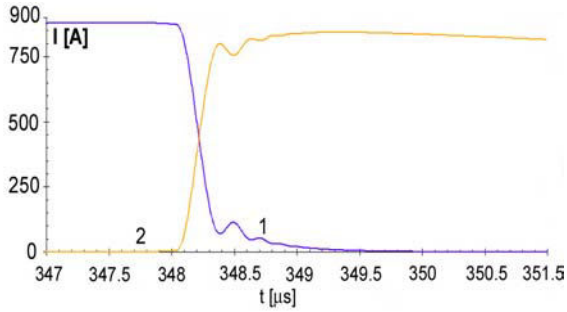

Fig. 5: The simulated IGBT – MOV current transfer
1 – the IGBT current, 2 – the MOV current

With regard to the MATLAB a ready-to-use model based on the Cassie's concept is offered [9]. This model is described by the following relationship:

$$\frac{1}{g}\frac{dg}{dt} = \frac{d\ln g}{dt} = \frac{1}{\tau}\left(\frac{u^2}{U^2{}_c - 1}\right) \qquad (1)$$

where: g – the conductance of arc, u – the voltage across the arc, i – the current through the arc, τ – the arc time constant, U_c – the constant arc voltage.

The independent parameters (τ, U_c, g(0), a_t (s)) have to be selected and set manually.

In order to model the process of disintegration of the fuse element and the fuse arc ignition, initially the following fuse model was applied:

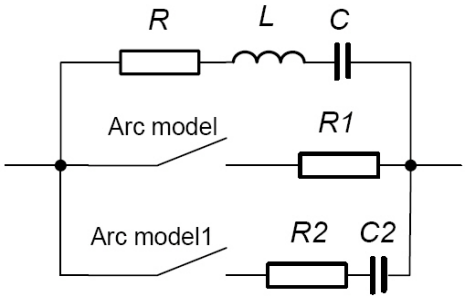

Fig. 6: The USF model (MATLAB)

However such a rough model did not work properly. Hence modification had to be introduced consisted in the addition of energy-absorbing elements connected in parallel to the arc. The resistance and capacitance were used. Dozens of experiments have proven, that such a model operates in a satisfactory manner providing reliable results for the current transfer between elements of the CHCL. The simulation results are presented in Fig. 7.

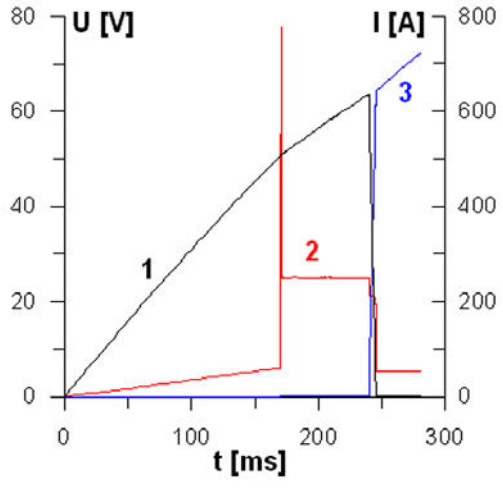

Fig.7: The simulated USF – IGBT current transfer
1 – the USF current, 2 – the USF voltage, 3 – the IGBT current

The results of simulations are presented in Fig. 8. The calculations were carried out in the oscillatory LC circuit at the frequency of 480 Hz and the prospective short-circuit current of 1.2 kA

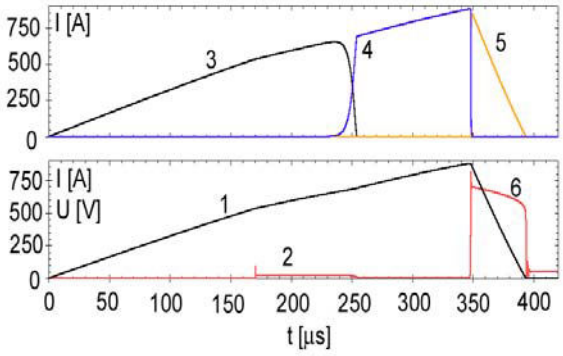

Fig. 8 : The simulation of CHCL operation (PSPICE)
1 – the short-circuit current, 2 – the USF voltage, 3 – the USF current, 4 – the IGBT current, 5 - the MOV current, 6 – the MOV voltage

Satisfactory agreement between the results obtained with the simulation (Fig. 8) and measurements (Fig. 2) allows for an extension of the application of the model used e.g. for the analysis of the CHCL operation in circuits and conditions, say, in an AC circuit at the frequency of 50 Hz.

3.2. Models of semiconductor devices

Commercial programs offer a large selection of models of the semiconductor devices available on the market. The list is amended every time when a new device is developed. Different approaches of model selection are adopted in the MATLAB and the PSPICE. In the former case, parameters of a generic model of the device are modified in accordance to the actual catalogue data. In the case of the PSPICE ready-to-use models are only available.

4. Effect of CHCL on quality of energy

Today voltage dips are the most important power quality problems. Each year they disturb production, resulting in large economical losses, especially in the case of electronic devices (computer equipment, PLC programmable controllers) which are very sensitive to voltage changes. The voltage dips are characterised by two parameters:

- duration Δt and
- depth ΔU.

Voltage dips are due to short circuit faults in power distribution systems and other high overcurrents producing significant voltage drops across impedances of the system's elements. The magnitude of a voltage dip is mainly determined by the faulted line impedance and the connection method of the transformer windings [10]. The short-circuit fault reduces the voltage almost to zero exclusively at the fault position. Both Δt and ΔU

depend on the speed of CB operation. The CHCL being fast reduces the extend of voltage dips.

To eliminate short circuits contact switches are commonly used. Their operation time is of the order of tens of milliseconds. A long duration voltage dips can not be tolerated in the power grid due to the susceptibility of the electronic devices used. The regulations proposed by the CBMA (Computer Business Manufacturer Association) [11], define a band characteristic presenting the acceptable limits of the voltage changes in both directions, i.e. the dips ΔU and overvoltages as a function of , the disturbance duration Δt. With regard to the voltage dips the acceptable Δt is of several ms. This characteristic was modified in 1996 and now it is known as the ITIC (Information Technology Industry Council) characteristic [11]. A classical switch cannot ensure such a short time of elimination of a short circuit fault.

On the substitution of fast semiconductor or hybrid switches for contact circuit breakers the duration of voltage dips can be significantly reduced [2,3]. In LV networks CHCL can be applied. However, in the latter case features of IGBT define current limitation capacity of the whole assembly. Due to the relatively low current switching ability of the transistor, at present, the CHCL can be applied in circuits with rated currents of maximum several hundreds amperes.

In Fig. 9 the modelled power system has been presented, in which the simulations of a short-circuit fault interruption by means of a classical contact CB vs. CHCL were performed. Line – erth short circuit at A was assumed. The values of parameters used in the simulations are given in Table 1.

Table 1. The parameters of the modelled network used in simulations

Element	Symol	Value
System impedance	Z_{sc}	54Ω
Step-down transformer	MV/LV	630kVA 16.75kV/400V D1/Yg
Step-down transformer	HV/MV	6.3MVA 115kV/16.5kV Yg/D11
Cable line impedance	Z_c, Z_{c1}	Length: 10km 0.74Ω
Load impedance	Z_l	0.58Ω power factor: cosφ = 0.86

The numerical experiment was performed with the MATLAB software.

When the voltage on the faulted line goes to zero at the fault location, the voltage at the substation and on the parallel feeders depend on the distance of the fault from the substation.

In Fig. 10, 11, 12 clearing of a short circuit fault in the power system by contact CB is presented. The assumed fault clearing time corresponding to the voltage dip is Δt =51ms.

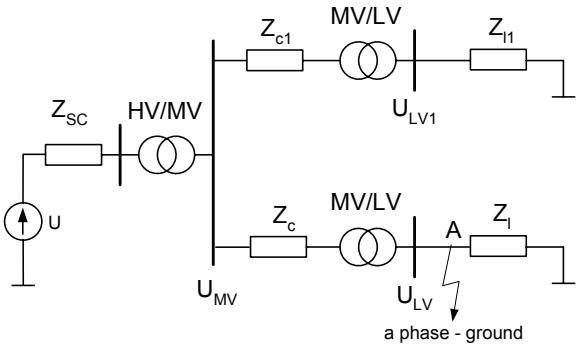

Fig. 9 : The modelled power-system grid
U – the voltage source, Z_{SC} – the system impedance, HV/WV, MV/LV –the transformer, Z_l, Z_{l1} – the load impedance, Z_c, Z_{C1} – the cable line impedance

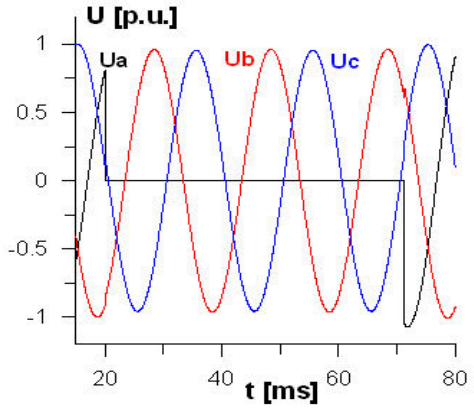

Fig. 10: The simulated U_{LV} voltage traces at the fault location when the short-circuit fault is cleared with a contact CB
Ua, Ub, Uc – the voltages on the busbars U_{LV}

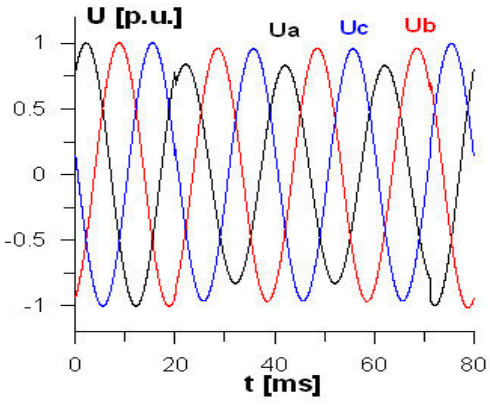

Fig. 11: The simulated U_{LV1} voltage traces of the nearest switchgear, when the short circuit is cleared with a contact CB
Ua, Ub, Uc – the voltages on the busbars U_{LV1}

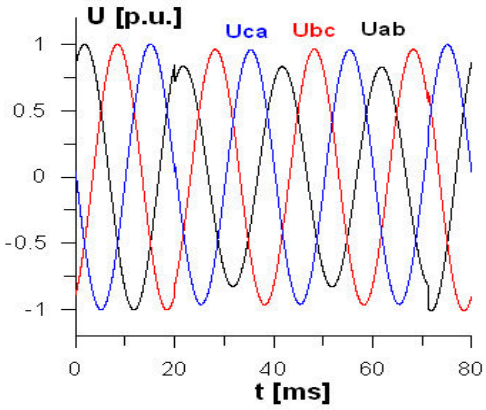

Fig. 12: The simulated U_{MV} voltage traces when the fault is cleared with a contact CB
Uab, Ubc, Uca – the voltages on the busbars U_{MV}

In Fig. 13,14,15 similar simulated voltage traces of the interruption of the short circuit current are presented when a hybrid circuit breaker with the switching off time $\Delta t = 2$ ms was used.

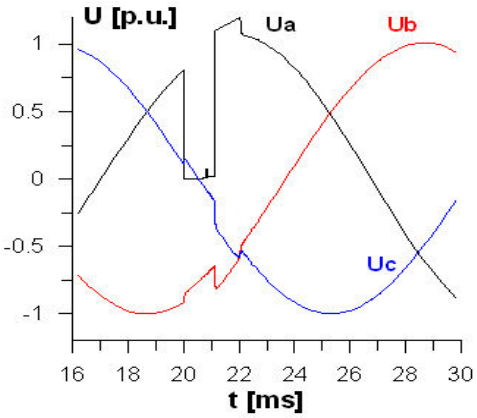

Fig. 13: The simulated U_{LV} voltage traces when the fault was cleared with the CHCL
Ua, Ub, Uc – the voltages on the busbars U_{LV}

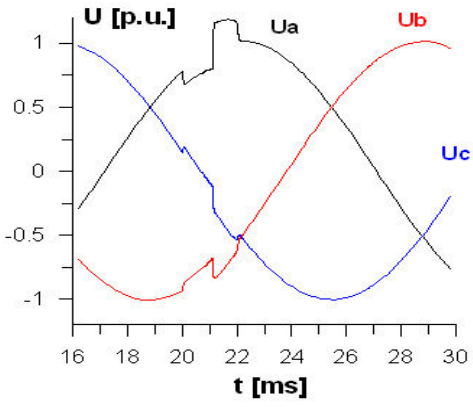

Fig. 14: The simulated U_{LV1} voltage traces when the fault was cleared with the CHCL.
Ua, Ub, Uc – the voltages on the busbars U_{LV1}

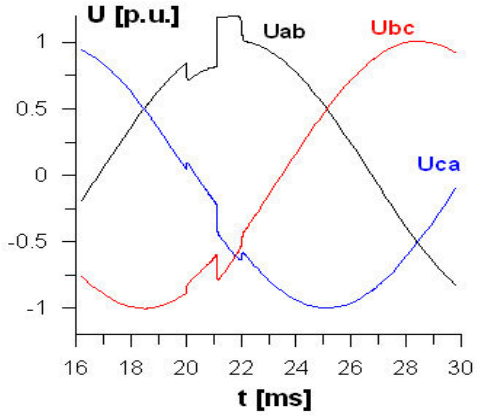

Fig. 15: The simulated U_{MV} voltage traces when the fault was cleared with the CHCL
Uab, Ubc, Uca – the voltages on the busbars U_{MV}

Owing to the application of the hybrid CB the time of power supply disturbance was significantly reduced. Since this time does not exceed several ms, the disturbance cannot be called „voltage dip" any more, if the definition by [1] is taken under consideration.

5. Effect of the IGBT control on the operation of a hybrid circuit breaker

In the operation of a hybrid circuit breaker an important problem is the proper control of the semiconductor device [13]. Delayed turn-off causes an increase in the cut-off current, while in the case of an early turn-off, there is the possibility that the gap in the molten fuse element will be too short and will not withstand the recovery voltage. Durations of the fuse element melting and the increase in the recovery dielectric strength are associated with the cut-off current, while the recovery voltage, which must be withstood by the limiter, depends on the actual state of the power system. Any delay in the cut-off process is detrimental, as it increases the limited current, fault clearing time and the energy allowed through by the hybrid circuit breaker.

Selection of the optimal making and cut-off moment of the semiconductor device is of great significance for the quality of the power supply. The shorter the duration of the short circuit fault, the sorter the duration of the voltage disturbance in the power system will be. However, selection of very short turn-on and let-through times of the IGBT will cause the arc reignition, and this way an increase in the duration of disturbance in the power delivery and the possibility of current limiter damage.

A considerable limitation of the disturbance duration is achieved using a hybrid circuit breaker. In this case, the time necessary to eliminate a disturbance depends, to a great degree, on the IGBT control delay.

However, the selection of the optimum current let-through time of the semiconductor device is a very complex issue. It should be as short as possible from the point of view of the quality of the supplied power. On the other hand, taking into consideration the current transfer requirements it must be long enough to allow for the disintegration of the fuse element and the recovery of dielectric strength of the fuse, in order to prevent the reignition.

6. Summary

The proposed model of CHCL enables simulation of the short circuit current interruption. The difference between calculation results and measurements are quite modest.

The CHCL model used for simulation of a short-circuit current interruption in an example network confirms the expected effect of voltage dips reduction by the hybrid current limiter.

Since CHCL operation depends on current in a similar manner as a classic fuse, the level of voltage dips changes as short circuit conditions in contradiction to other hybrid current limiters.

Pre-arcing time depends of the fuse element dimensions. However the arcing and SD operation times are linked to the fuse element decomposition and the recovery of voltage strength. In advantageous conditions the time needed to eliminate the short circuit by this switch is in the order of several hundred μs.

Appropriate control of the semiconductor device plays an important role in the CHCL operation. The fuse-element burn-back time and the gap deionisation have to be taken under consideration.

Acknowledgements

The research on contactless current limiting device has been carried out in the frames of the research project No: 8 T10A 058 21 financed by the Committee of Scientific Research in Poland.

References

[1] Brauner G., Hennerbicher Ch.: "Voltage dips and sensitivity of consumers in low voltage networks". CIRED, 18-21 June 2001.

[2] Żyborski, J. Holc A.: "Energy quality improvement by ultra rapid L.V. fault current limiting and interrupting". 10-th International Symposium on "Short Circuit in Power Systems", Lodz, 28-29 October 2002, Conf. Proc., pp.243-248.

[3] Behrens P., Cieleit A., Ginzburg M., Stachorra E.K: "Fault current limiters for distribution networks – state of the art and development projects". Electrical Power Quality and Utilisation, Tom 8, Zeszyt 1/2, 2002r, pp. 29-32.

[4] Collart P., Pellichero S.: "A new high speed DC circuit breaker: the D.H.R". Colloquium Organized by Professional Group P6 and P2, London, 1989.

[5] Czucha J., Pikoń M., Żyborski J.: "Ultra rapid IGBT current limiting interrupting device of very high breaking capacity". 8th International Symposium on Short-Circuit Current in Power System, Brussels 1998, pp.219-222.

[6] Batrosik M., Wójcik F.: "Arcess DC hybrid circuit breaker". SAP&ETEP-97, Lodz 1997.

[7] Wolny A., Semenowicz B.: "Hybrid contactless short-circuit current limitation". 10-th International Symposium on "Short Circuit in Power Systems", Lodz, 28-29 October 2002, Conf. Proc., pp.221-225.

[8] Wolny A., Semenowicz B., Leśniewski P: "Features of a short fuse, as a main current path of a contactless hybrid current limiter". 10-th International Symposium on "Short Circuit in Power Systems", Lodz, 28-29 October 2002, Conf. Proc., pp.227-230.

[9] Schavemaker P.H.: "Arc model blockset for use with MATLAB Simulink and Power System Blokset – User's guide". Delft University of Technology, 2001.

[10] M.F. McGranaghan, Mueller D.R., Samotyj M.J.: "Voltage sags in industrial systems". IEEE Trans. Industry Applications, vol. 29, no. 2, March/April 1993, pp.379-403.

[11] http://www.dorrough.com/What_s_New/PLM-120/PowerMonTM/CBEMA_Curve/cbema_curve.html (Current May 2003).

[12] http://www.itic.org/technical/iticurv.pdf (Current May 2003)

[13] Leśniewski P., Semenowicz B., Gohra K.: "Influence of circuit parameters on the process of current transfer in the hybrid circuit breaker". XIII-th Symposium on Electrical Apparatus and Technologies SIELA 2003, 29-30 May, 2003, Conf. Proc. Vol. I,

21st CENTURY GUIDANCE USING INTERNATIONAL STANDARDS

Gordon Newbery

Cooper Bussmann, Burton-on-the-Wolds,
Leicestershire, LE12 5TH, UK gordonn@bussmann.co.uk.

Abstract: The paper highlights the considerable amount of application guidance, which can be found within the International Electrotechnical Committee, IEC, Fuse Publications. Although there are some "stand-alone" Application Guides either on fuse systems or specific topics, additional information can be found within the Fuse Standards including Annexes. Salient information is brought together with respect to low voltage, miniature and high voltage fuses, and it shows many common principles in all three areas. The paper thus gives a framework for further reading to assist in the understanding of the use of fuses in modern installation applications.

Keywords: electric fuse, application guide, fuse standard.

1. Introduction

Fuses [1] have been used for over 100 years and can be considered as mature products, with the exception of modern developments such as "chip fuses", fuses for the protection of power semiconductors and full range high voltage fuses. Significant progress has been made on International Standardisation on fuse performance and restricting dimensional variants. The vital "SECURE" role of fuses in circuit protection, their performance and application are not generally covered in technical educational establishments and "taken for granted". This presents problems for the new generation of electrical technicians, installers, planners and specifiers.

The main task of IEC Standards is to formulate test requirements to cover a wide variety of needs. Having achieved this, the fuse Standards are now mostly finalised rather than subject to radical new revision. However, recently attention has been focussed on "Application Guides" and information to assist the user. In addition, within the IEC Fuse Standards, particularly in the Annexes, there is a lot of useful information relating the standardised test requirements to practical applications.

Such information is often overlooked and this paper will highlight and bring together such information and steer the user to useful application information. Although the information in the paper will relate to specific Standards or Guides, in many cases the same principles can be applied to other fuses. The paper will cover fuses in the following areas:

- Low Voltage fuse types.
- Semiconductor Protection fuse types
- Miniature fuse types
- High Voltage fuse types
- Temperature Rise considerations

2. Low Voltage Fuses

2.1 Scope

IEC 60269 Standards are applicable to fuses incorporating enclosed current-limiting fuse-links with rated breaking capacities of not less than 6kA, intended for protecting power frequency a.c. circuits of nominal voltages not exceeding 1,000V or d.c. circuits of nominal voltages not exceeding 1,500V.

IEC 60269-1: General
IEC 60269-2: Supplementary requirements for fuses for use by authorised persons
IEC 60269-2-1: Examples of standardised fuses
IEC 60269-3: Supplementary requirements for fuses for use by un-skilled persons
IEC 60269-3-1: Examples of standardised fuses.
IEC 60269-4: Supplementary requirements for fuse-links for the protection of semiconductor devices.
IEC 60269-4-1: Examples of standardised fuse-links.

Fuse-links for the protection of semiconductor devices are covered in Section 3.

2.2 IEC 60269-1

2.2.1 I^2t Calculations (Annex B)

For 50Hz a.c. symmetrical circuits, it is not possible to obtain a pre-arcing time of 0.01 seconds due to the heating and cooling of the element during the first half cycle [2]. However, pre-arcing I^2t values may be found useful in the short-time region and are specified in Table 6 of IEC 60269-1. Annex B gives a method of determining these values from test points more easily obtained and for smaller current ratings in a homogeneous series.

A future amendment Annex B3 is in the final stages of preparation, showing how to estimate the operating I^2t at reduced voltage.

The operating I^2t values can be estimated at lower voltages than those measured during tests 1 and 2 of Table 12a, using the following formula:

$$\text{Operating } I^2t \text{ at reduced voltage } V_r = \left\{\frac{\text{Operating } I^2t \text{ at test voltage } V_t}{\text{prearcing } I^2t}\right\}^{V_r/V_t} \times \text{prearcing } I^2t$$

The experts on the IEC fuse committee refer to this as the "Henry Turner Formula" in memory of one of the pioneers in fuse technology.

2.2.2 Ambient Temperature and Surroundings (Annex D)

This gives some general guidance for example:-

An increase in ambient temperature will produce a similar temperature rise and therefore a predictable increase in actual temperature of the fuse. If this exceeds any specified limits, then a de-rating will be required.

The effect on fusing and non-fusing current will be minimal.

The installation conditions such as enclosure, mounting surface, adjacent heat generating devices and cross-section and insulation conductors, can affect the operating conditions.

2.3 Application Guide, IEC 61818TR

2.3.1 General

By the time this ICEFA Conference is held, this Technical Report should have been published. It gives information on the application of fuses, which are not always covered, as well as important facts, which are sometimes difficult to locate in Standards. The guide also makes reference to other IEC Standards and publications.

2.3.2 Benefits

This section summarises the important benefits of current-limiting cartridge fuse-links. Most of these benefits are well documented. However, the following are considered to be of topical interest.

- Safe, Silent Operation – no emission of gas, flames, arcs or other materials when clearing the highest levels of short circuit currents. In addition, the speed of operation at high short circuit currents, significantly limits the arc flash hazard at the fault location. The award winning paper [3] in the previous ICEFA Conference covered the subject of Arc Flash Hazard. This is becoming of increasing concern, particularly in the USA.
- Improved Power Supply Quality – current-limiting fuses interrupt high fault currents in a few milliseconds, minimising dips in system supply voltage. This is important for sensitive electronic equipment and components.
- The ability of the fuse to handle very high fault current allows for easy and inexpensive system expansion without the need to upgrade protection.

2.3.3 Fuse Combination-Units

It is important to differentiate between the various types of fuse combination-units, see Table 1 and note the modern terminology, replaces "isolator" by "disconnector".

Table 1. Definitions and symbols of fuse-combination-units

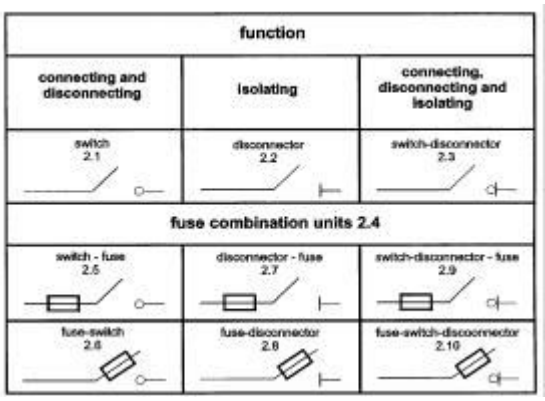

2.3.4 Fuse Selection and Markings

Types of low voltage fuses are designated by two letters, as shown in Table 2.

Table 2. Fuse application

Type	Application (characteristic)	Breaking Range
gG	General purpose mainly for conductor protection	Full range
gM	Motor circuit protection	Full range
gN	North American general purpose for conductor protection	Full range
gD	North American general purpose time delay	Full range
gR, gS	Semiconductor protection	Full range
gU	Wedge tightening fuse for Utilities	Full range
gL, gF, gI, gII	Former type of fuse for conductor protection (replaced by gG type)	Full range
aM	Short circuit protection of motor circuits	Partial range (back-up)
aR	Semiconductor protection	Partial range (back-up)

- The first letter describes the breaking ranges:
  a - partial range : all currents between the lowest current indicated on its operating time – current characteristic and its rated breaking capacity.
  g - full range : all current which cause the melting of the fuse element up to its rated breaking capacity.
- The second letter describes the application (characteristics or utilisation category).

This information is "buried" within the Standards and is difficult to locate.

2.3.5 Wiring Regulations

The guide highlights the principles of conductor protection both in accordance with IEC 60364-5-52 and the National Electric Code in the USA, thus covering most global market requirements.

The subject of protection by automatic disconnection of supply in IEC 60364-4-41 is illustrated covering TN, TT and IT systems. Examples are given showing the calculation of the "fault loop impedance".

2.3.6 Power Factor Correction Capacitors

A useful section is included on a subject not widely found on low voltage fuses. This recommends a fuse-link value of 1.6 to 1.8 times the rated current of the capacitor unit or capacitor bank and takes into account the following:

- Inrush currents must not melt or deteriorate the fuse element.
- Potential over-currents must not lead to premature operation of the fuse-links.

2.3.7 d.c. Applications

Guidance is given on this subject, which is generally poorly documented. This shows the d.c. voltage rating is dependent on the time constant and that the operating times can vary considerably with the time constant.

2.4 Fuses and Contactors/Motor Starters

2.4.1 General

This is an important application area for fuses. In view of their high current limiting properties, maximum utilisation of contactors/motor starters can be achieved by fuses compared with other circuit interrupting devices. In 1996, IEC 611459 was published, this was produced by IEC low voltage working group with input from a contactor/motor starter expert. The principles of co-ordination are also summarised in IEC 61818TR (2.3)

2.4.2 IEC 60947-4-1

IEC 611459 outlines the tests specified at three levels of prospective current.

I_c crossover current (intersection of the mean time/current characteristic of the fuse and overload relay of the starter)
I_r Intermediate fault current
I_q Rated conditional short circuit current.

The criteria for co-ordinating these three currents are described in detail and the publication then illustrates co-ordination methods to give type 2 co-ordination for I_q and I_r.

2.4.3 Survey of Type Testing

A survey is presented of the rated currents, I^2t values and cut-off currents of fuses correctly chosen according to the ratings of the starters they protect, based on the results of successful type testing throughout the world. The studies revealed that there is no major difficulty in achieving satisfactory co-ordination at the most exacting of the levels with modern contactors.

Examples of typical fuse-link ratings used for motor starter protection are shown in table 3 for an average motor-starting duty of a motor full-load current of 28A. This illustrates how the type of fuse-link can influence the optimum current rating.

Table 3. Fuse types and ratings

Fuse Type	Origin	Suitable Rating
gG	General purpose IEC fuse	63A
gM	Motor circuit fuse	32M63
aM	Back-up fuse	32A
gN	North American general purpose fuse	70A
gD	North American time-delay fuse	40A

3. Semiconductor Protection

3.1 General

Fuse-links for the protection of semiconductor devices were introduced in commercial numbers some 40 years ago and still evolving to meet the developments in semiconductors and their applications. Manufacturers specialising in the fuse-links, supply comprehensive information and

there have been many papers written on the subject at previous ICEFA conferences.

Within the IEC Standards there are two useful references for the application of fuse-links for semiconductor devices.

- Appendices of IEC 60269-4
- IEC 60146

3.2 Appendices of IEC 60269-4

3.2.1 Object

The object of this guide is to explain the performance to be expected from the fuse-links in terms of their ratings and in terms of the characteristics of the circuits of which they form a part, in such a manner that this may form the basis of the selection of the fuse-links.

In essence it relates the standardised test conditions to practical situations. Appendix A covers the following:-

- Current carrying capabilities
- Voltage characteristics
- Power dissipation characteristics
- Time current characteristics
- Breaking Capacity
- Commutation

Attention is drawn to the effects of "cyclic" loading or repetitive duty currents. For both rated and overload currents under such conditions fuse-links should not be operated too close to their time-current characteristics. The concept of a conventional overload curve is introduced, see Fig. 1. (X and Y are points of verified overload capability)

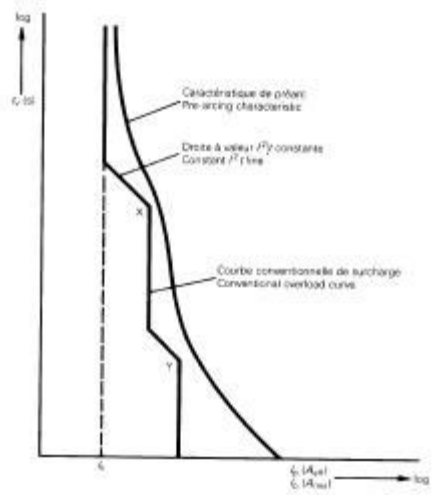

Figure 1: Conventional overload curve

In practice manufacturers supply multiplying coefficients for common cyclic duties to simplify the assessment in practical application.

Appendix A also draws attention to the effects of frequency and d.c. conditions, which can significantly influence the performance.

Appendix B gives a survey or checklist of 17 items on information to be supplied by the manufacturer in his literature (catalogue).

3.3 IEC 60146

This application guide covers the protection of semiconductor converters against over currents by fuses.

The object of the guide is to advise on the specific fuse features and on the specific converter features, which are to be observed to ensure correct application of semiconductor fuses in converters and to give specific recommendations for trouble free operation of converters protected by fuses.

The guide is limited to commutated converters in single way and double way connections for non-regenerative and regenerative loads. It covers the voltage capacity required for fuses in the above connections, for example in a regenerative load in a three-phase double-way connection for a conduction through (shoot through) or firing fault in practice the rated a.c. voltage of the fuse should be greater than

$$U_{ac} + \frac{U_{dc}}{\sqrt{2}}$$

In addition, the fuse should be capable of clearing U_{dc} with the time constant of the fault circuit.

4. Miniature Fuses

4.1 Scope

IEC 60127 Standards relate to miniature fuses for the protection of electrical appliances, electronic equipment and component parts, thereof normally intended to be used indoors.

IEC 60127-1	:	General
IEC 60127-2	:	Cartridge fuse-links
IEC 60127-3	:	Sub miniature fuse-links
IEC 60127-4	:	Universal modular fuse-links, UMF.
IEC 60127-5	:	Guide for quality assessment
IEC 60127-6	:	Fuse-holders
IEC 60127-10	:	User guide

A miniature fuse-link is an enclosed fuse-link of breaking capacity not exceeding 2kA and which has at least one of it's principal dimensions not

exceeding 10mm. (Principle dimensions are length, width, height and diameter).

Cartridge fuse-links to IEC 60269-2 are nominally 5 x 20 mm or 6.3 x 32 mm and up to 250V a.c.

The case (body) of a sub-miniature fuse-link has no principle dimensions exceeding 10 mm. The standardised terminations are either radial or axial leads.

Universal modular fuse-links are adapted for direct electrical connection to printed circuit boards or other conductive substrates, incorporating features designed to provide a degree of interchangeability where necessary, the fuse-links can be through hole or surface mount. Standardised products specify the terminal spacing.

IEC 60127-5 is a guide for quality assessment of miniature fuse-links. It gives a guide for tests for assessing the quality of miniature fuse-links, other than type tests, for the case where there is no complete agreement between the user and the manufacturer on what such tests should be. It provides guidelines and limits generally acceptable for quality control purposes by large scale users and manufacturers of miniature fuse-links, typically of lot sizes of 10,000 or more.

IEC 60127-6 covers fuse-holders up to 16A, accepting cartridge fuse-links according to IEC 60127-2 and sub miniature fuse-links according to IEC 60127-3. It covers a wide variety of unexposed or exposed fuse-holders, for example:-

- Types of mounting
- Methods of fastening
- Methods of insertion of fuse carrier into fuse base
- Types of terminals
- Protection against electric shock

4.2 User Guide

This user guide, IEC 60127-10, was published in January 2002. The object is to introduce the user to the important properties of miniature fuse-links and fuse-holders and to give some guidance in applying them.

The properties of miniature fuses are highlighted:-

- Protecting upstream, isolating downstream and diagnosing fault location
- Wide range of fuse-links and holders
- Lower cost and small dimensions
- Wide range of tamper-proof and reproducible characteristics
- Discrimination (selectivity)
- Safe and reliable

Attention is drawn that the characteristics of fuses conforming to other Standards, such as CSA – C22.2 No. 248.14 or UL 248-14, could be quite different from the IEC 60127 characteristics. Additionally, these other Standards may not specify the same characteristic definitions or precise time gates. Accordingly, the definitions of speed of operation, FF, F, M, T, TT are left to the individual fuse manufacturers and can vary widely.

Unlike power systems it is often difficult to calculate the maximum potential fault current of a circuit/application. Often it is an assumed theoretical value, assigned by a safety agency. In some cases, the suitability of a fuse's breaking capacity is determined by testing the fuse in the end product, under short circuit conditions.

The guide has tables of standardised fuse-links in IEC 60127-2, 3 and 4, giving salient properties for ease of reference.

Some good general guidance is provided on fuse selection and is usually dictated by three basic categories of criteria:

a) Electrical requirements of the application, including I^2t and d.c. requirements.
b) Conformance to published safety standards.
c) Mechanical properties/physical size.

Attention is drawn to the selection of the thermal rating of the fuse holder. It is based on the maximum power acceptance of the fuse holder, taking into account the local thermal conditions. The maximum **sustained** dissipation of the fuse-link shall be less than, or equal to, the admissible power dissipation of the fuse holder.

The guide advises that consideration should be given when fuse-links are used at extra low voltages, i.e. the range of 10V, especially for fuse-links of low rated current, see Fig. 2.

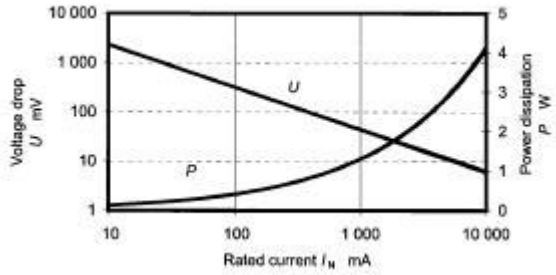

Fig. 2: Power dissipation P and voltage drop U according to rated current I_n.

Due to the non-linear increase of the voltage drop when the fuse element approaches melting point, care must be taken to ensure that there is sufficient voltage available to cause the fuse-link to operate when an electrical fault occurs.

5. High Voltage Fuses

5.1 Scope

High Voltage fuses covers all types of fuses designed for use outdoors, or indoors on alternating current systems of 50Hz and 60Hz and of rated voltages exceeding 1,000V:-

IEC 60282-1 : Current Limiting Fuses
IEC 60282-2 : Expulsion Fuses

In addition, there are three publications which have been produced and maintained by the IEC High Voltage Fuse Committee:-

IEC 60549 : External protection of shunt capacitors
IEC 60644 : Motor circuit applications
IEC 60787 : Transformer circuit applications

5.2 Current Limiting Fuses

The 2002 edition of IEC 60282-1 was editorially changed, so the clause numbers aligned with the switchgear Standards, thus making it more user friendly.

Application Guides are given in Clause 8 and presents suggestions on application, operation and maintenance as an aid in obtaining satisfactory performance with high voltage, current-limiting fuses

It cautions that high voltage fuses should be handled with at least the same degree of care as any other precision made item of equipment (such as a relay). In addition, if during internal installation and service, fuses are subjected to severe mechanical stresses, then special tests may be agreed by the user and manufacturer of the fuses and the switchgear. For switch fuse combinations, see IEC 60420.

A section includes the selection of the rated current of the fuse-link, although as will be seen in 5.4, 5.5 and 5.6, the chosen rated current for the fuse-link in applications are generally dictated by transient phenomena in the circuit related to switching, such equipment as transformers, motors or capacitors.

However, fuse-links are inherently and invariably mounted in more adverse thermal conditions than the standardised test arrangements, for example, in enclosed fuse "pods". A typical de-rating can be 25% of the rated current, so in such applications the service current carrying capability of the fuse-link has to be assessed.

The selection of the rated voltage should be selected with regard to:-

- **Three Phase Solidly Earthed Neutral Systems** the highest line-to-line voltage
- **Single Phase Systems** 115% of the highest single phase system voltage
- **Three Phase Isolated Neutral Systems** testing is necessary at higher than the 0.87 times the voltage rating of the fuse, as specified in the Standard
- **Capacitive currents** in phase-to-earth faults

With regard to operation, special care should be taken to see that the fuse-link is securely locked in the service position. It is also advisable to remove and insert fuses when in an off-load or de-energised condition.

Section 8.3.4 covers selection according to class: backup, general purpose or full range and minimum breaking current.

The Standard has a number of "normative" and "informative" annexes. The "informative" annexes are:

Annex B: Reasons which led to the choice of TRV (transient recovery voltage) values for test duties 1, 2 and 3.
Annex C: Preferred arrangements for temperature rise tests of oil-tight fuse-links in switchgear.
Annex D: Types and dimensions of current limiting fuse-links specified in existing National Standards.
Annex F: Determination of de-rating when the temperature surrounding the fuse exceeds 40^{o}C. This gives a worked example that is worthy of examination and could well apply to low voltage installations.

5.3 Expulsion Fuses

Application Guides are given in Clause 11 of IEC 60282-2 and presents suggestions on the application, operation and maintenance as an aid in obtaining satisfactory performance with expulsion and similar fuses.

The reader is reminded that drop-out fuse carriers that remain in the open position for prolonged periods of time, may accumulate water and pollution in their internal parts, which may result in the degradation of their operational properties.

Fuses should be mounted in the position specified by the manufacturer and precautions taken for the high noise level and emission of hot gasses.
Like current limiting fuses, the current rating of expulsion fuses are generally dictated by transient current phenomena in the circuits they are protecting.

There are three classes of fuses based on the protection of the associated transformers, capacitor banks and feeder circuits.

Class A: Remotely placed from major substations.
Class B: Close proximity to major substations.
Class C: Close proximity to major substations without parallel-connected loads.

Some National Standards include additional requirements, including special applications including:

- Spark production tests
- Robustness
- Forces required to open and close drop-out fuses
- Current surge withstand tests.

- The standard includes three "informative" annexes.

Annex A: Reasons for the selection of breaking test values
Annex B: Typical fuse-link dimensions
Annex C: Operating rods

5.4 Transformer Circuit Applications

The most common application for high voltage fuses is for transformer circuits. The object of the Application Guide IEC 60787 is to satisfy criteria for co-ordination with other circuit components and to give guidance with particular reference to their time/current characteristics and ratings. The guide covers current limiting fuses to IEC 60282-1 and not expulsion fuses to IEC 60282-2.

The characteristics relating to the protection of a HV/LV transformer circuit is shown in Fig. 3.

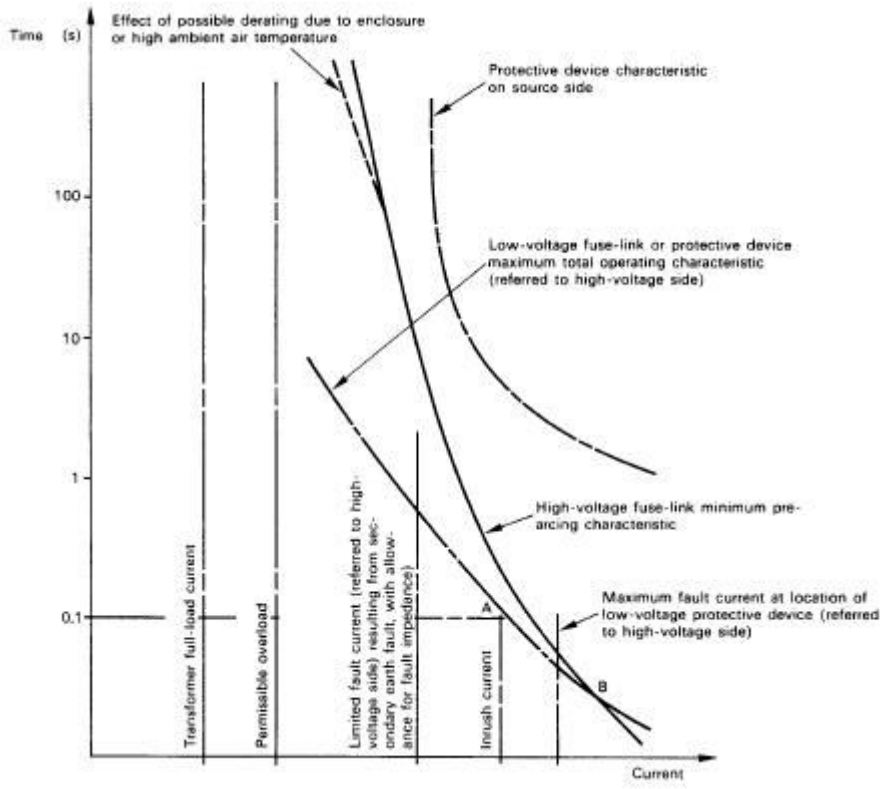

Fig. 3: Factors to be considered which are discussed in the guide.

The two major factors which determine the fuse-link rating are:-

- Transformer in-rush withstand current. Fuse-links require relatively high operating current in the 0.1 second region. For practical purposes this may be taken from 10 to 12 times the highest continuous current associated with the actual transformer size for duration of 0.1 seconds.

- Transformer permissible overloading

This can be up to 150% for a few hours and although the fuse-link current rating chosen for in-rush withstand is usually much higher than the full load current of the transformer, it has to be greater than the permissible overloading under abnormal

service conditions. Such service conditions must also cover fuse-links mounted in an enclosure and for high ambient temperature. For example in some cases the fuse-link can be de-rated up to 25% (see 5.2).

5.5 Motor Circuit Applications

IEC 60644 gives additional pulse withstand tests and also guidance on selection.

In the case of motor circuits, the requirements are somewhat different to those in transformer circuits and special motor circuit fuse-links are marketed. These requirements include:

- Relatively high operating current (slow operation) in the 10 second region to withstand the motor starting current .
- Relatively low operating current (fast operation) in the region below 0.1 seconds to give short circuit protection to associated switchgear devices, cables and motors and their terminal boxes

The additional pulse withstand tests first introduces the 'K' factor. The 'K' factor defines an overload characteristic to which the fuse-link may be repeatedly subjected under specified motor starting conditions and other specified motor operating overloads, without deterioration.

The overload characteristic is obtained by multiplying the current on the pre-arcing characteristic by 'K' (less than unity).

This is very similar to the concept of overload characteristics for the protection of semiconductor devices (see Section 3.2.1).

Two sequences of withstand tests are specified and both are based on the pre-arcing current at 10 seconds.

5.6 External Protection of Capacitors

IEC 60549 is a Standard covering fuses which are intended to clear either faults inside a capacitor unit to permit continued operation of the remaining parts of the bank in which the unit is connected (unit fuses) or faults on the whole capacitor bank to isolate the bank 'on the system' (line fuses).

The Standard advises that the rated current of the fuse shall be at least 1.43 times the rated current of the capacitor. This takes into account harmonic currents and capacitor tolerance, but does not take into account the effects of charging in-rush currents, which may require a further increase in current rating of the fuse.

The tests in the standard cover:

- Capacitive breaking current
- Discharge (endurance and withstand)

6. Temperature Rise

IEC 60943 is a technical report covering guidance concerning the permissible temperature rise for parts of electrical equipment, in particular for terminals and was prepared by the Fuse Committee. It is more of a "classical" reference document covering the temperature rise in electrical assemblies, generally and not specifically to fuses The report is split into two sections:

- Theory
- Applications

and these are supported by additional information in the annexes.

The report is intended to supply: General data on the structure of electric contacts and the calculation of their ohmic resistance.

- The basic ageing mechanisms of contacts.
- The calculation of the temperature rise of contacts and connection terminals.
- The maximum "permissible" temperature and temperature rise for various components, in particular the contacts, the connection terminals and the conductors connected to them.
- The general procedure to be followed by Product Committees for specifying the permissible temperature and temperature rise.

7. Conclusions

The paper describes how the guidance given in the International Fuse Standards will assist the user to ensure that the SECURE over-current protection of electrical circuits is sustained into the twenty-first century. Please remember SECURE protection is:-

S Safe
E Economical
C Current-limiting
U Universal
R Reliable
E Effective

References

[1] Wright A., Newbery P.G. "Electric Fuses". Peter Peregrinus Ltd. 1995.

[2] Leach J.G., Newbery P.G. and Wright A., "Analysis of high-rupturing-capacity fuse-link pre-arcing phenomena by a finite-difference method" PROC.IEE, Vol. 120, No. 9, September 1973.

[3] Saporita V.J., "Using current-limiting fuses to reduce hazards due to electrical arc-flashes" ICEFA Turin 1999, p.163.

THERMAL SIMULATIONS OF FAST FUSES FOR POWER SEMICONDUCTOR DEVICES PROTECTION

Adrian Pleşca

"Gh. Asachi" Technical University, Blvd.D.Mangeron 51-53, Iaşi, Romania
aplesca@ee.tuiasi.ro

Abstract: One of the most important problem as regard fuses operating and especially fast fuses operating is their thermal behaviour during steady-state or transient operating conditions. That because a good corelation between fast fuses and power semiconductors to be protected means also besides electrical parameters corelation and an adequate thermal behaviour from both sides.
This paper takes into account the thermal aspects of fast fuses within transient operating conditions, and the analysis is done using a FEM method to simulate the complex thermal behaviour. There are shown the thermal field into different parts of fuse body and also the temperature distribution at a momentary time.

Keywords: fast fuses, power semiconductors, thermal simulations

1. Introduction

Power electronics is often said to have brought in the second electronics revolution. The first electronics revolution made the modern microelectronics integrated circuits available. At the root of the both revolutions was the historic invention of the transistor by Bardeen, Brattain and Shockley in 1948. During the recent years, we have seen widespread application of power electronics in industrial, commercial, residential aerospace and military applications. As the size and cost of power electronics decrease along with the improvement of performance and reliability, power electronics applications will spread practically everywhere.

Power semiconductor device is the heart of modern power electronics because it is indeed the most complex, delicate and "fragile" element in a converter.

It can observe a continuously expansion of power electronics and converters which include power semiconductors into a lot of applications, but also results important conclusions as regards special operating conditions, such as: using a lot of components in parallel branches, intermittent load currents, failure currents which can reach hundreds of kA, special climatic and mechanical stresses. All these unfavorable operating conditions lead to special protection means for power converters and their components, especially to overcurrents.

The power semiconductor devices working into steady state or transitory operating conditions, lead to heating of device because of power dissipation. For a good operating and to avoid thermal run away, it is necessary to assure the heating evacuation from semiconductor structure. The thermal equilibrium condition, which means the same values for generated energy and evacuated energy from semiconductor device, is reached at a silicon temperature structure below 125^0C. Over this temperature there is an important degradation of specific proprieties of power semiconductor.

These devices have very limited overload capacities and, as they were expensive, the fuse manufactures attempted to produce fuses which are more sensitive to overloads and which would operate more quickly than their conventional designs.

2. Fuses for power semiconductors

Fuses are among the best known of electrical devices because most of us have quite large numbers of them in our homes and, unless we are extremely fortunate, we are made aware of their presence from time to time when one must be replaced because it has blown, or to use the official term, operated. They are basically simple and relatively cheap devices, although their behavior is somewhat more complex than may be generally realized.

The underlying principle associated with fuses is that a relatively short piece of conducting material, with cross-sectional area insufficient to carry currents quite as high as those which may be permitted to flow in the protected circuit, is sacrificed, when necessary, to prevent healthy parts of the circuit being damaged and to limit the damage to faulty sections or items to the lowest possible level.

Fuses incorporate one or more current-carrying elements, depending on their current ratings, and melting of these, followed by arcing, occurs when excessive overcurrents flow through them. They can be designed to safely interrupt the very highest fault currents that may be encountered in service, and, because of the rapidity of their operation in these circumstances, they limit the energy dissipated during fault periods. This enables the fuses to be of relatively small overall dimensions and may also lead

to economies in the cost and size of the protected equipment.

Because of the above advantageous features, fuses have been and are used in a wide variety of applications, and it appears that the demand for them will continue at a high level in the future. They were undoubtedly incorporated in the earliest electric circuits in which the source power and value of the equipment were significant.

From power semiconductor overcurrent protection point of view a special fuses were made, so called fast fuses.

Taking into account the thermal phenomena complexity, especially for transitory operating conditions, as regards fast fuses heating; it was done a thermal field simulation for a fast fuse with rated current, 100A, using FLUX2D software. The current test was by 300A and the thermal field is shown at time t = 26.04s. Because of simmetry, the simulation was done only for a half of fuse, the thermal field being the same on the other half of fuse. The environment temperature was 20^0C.

The next pictures show the thermal field at the whole fuse, main component parts, and also the temperature distribution along the component parts.

- whole fuse body

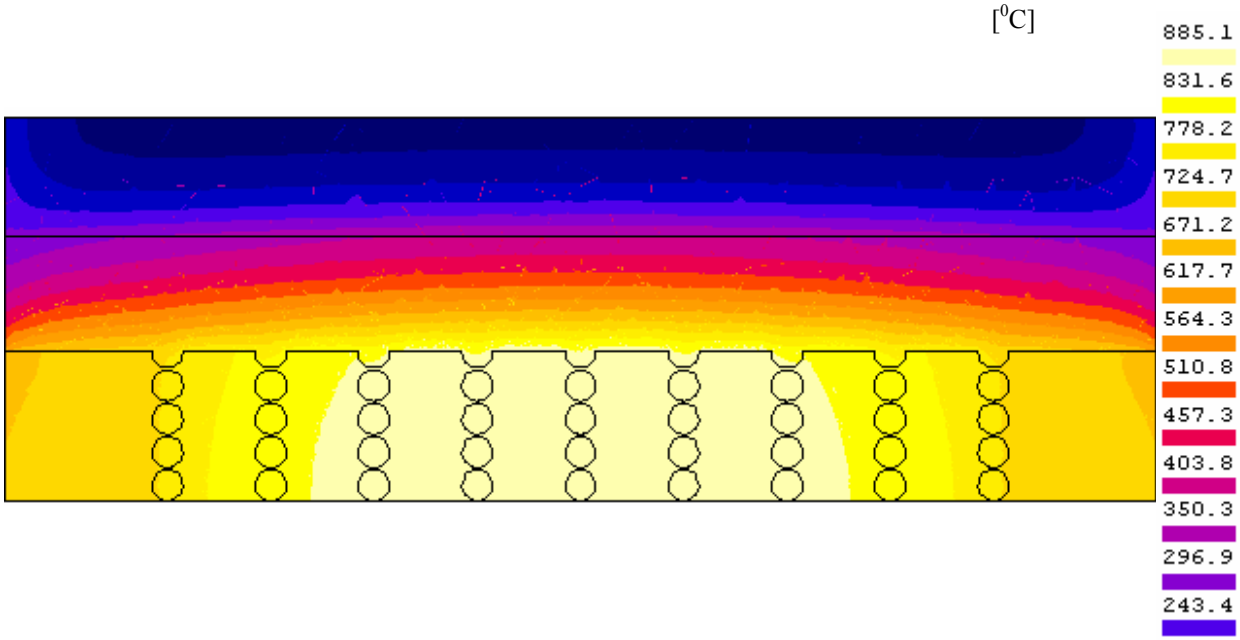

Fig.1 Thermal field in whole fuse body at t = 26.04 seconds

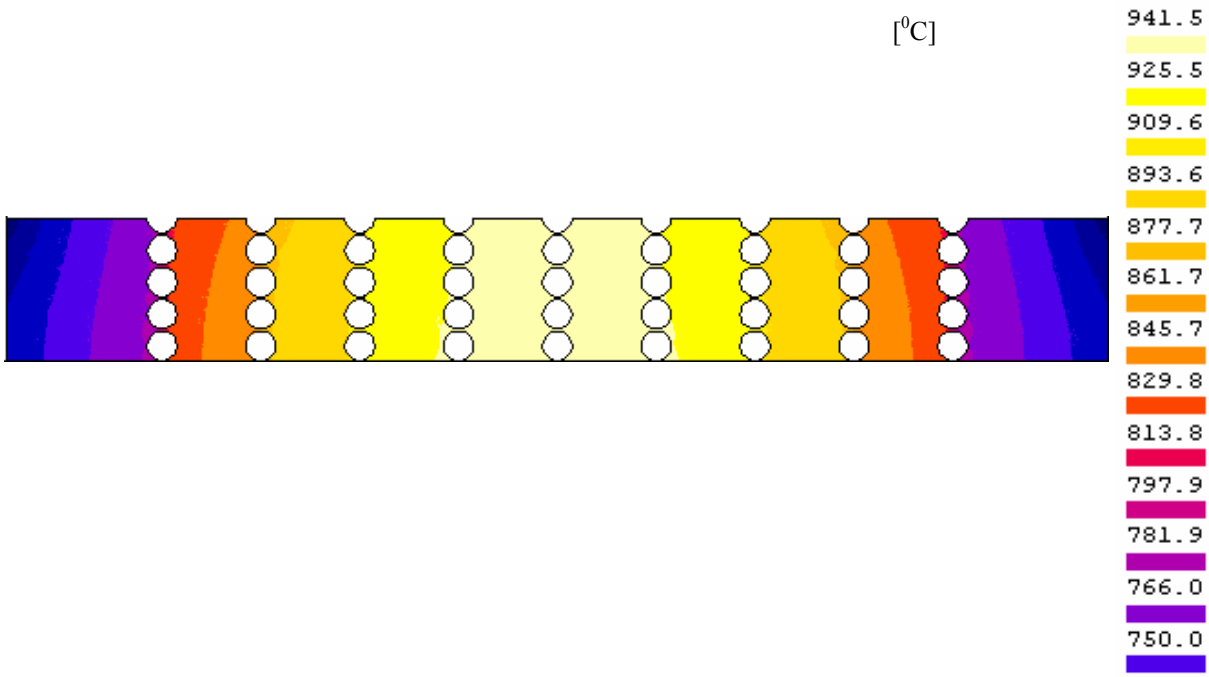

- fuse-link

Fig.2 Thermal field along fuse-link at moment t = 28.75 seconds

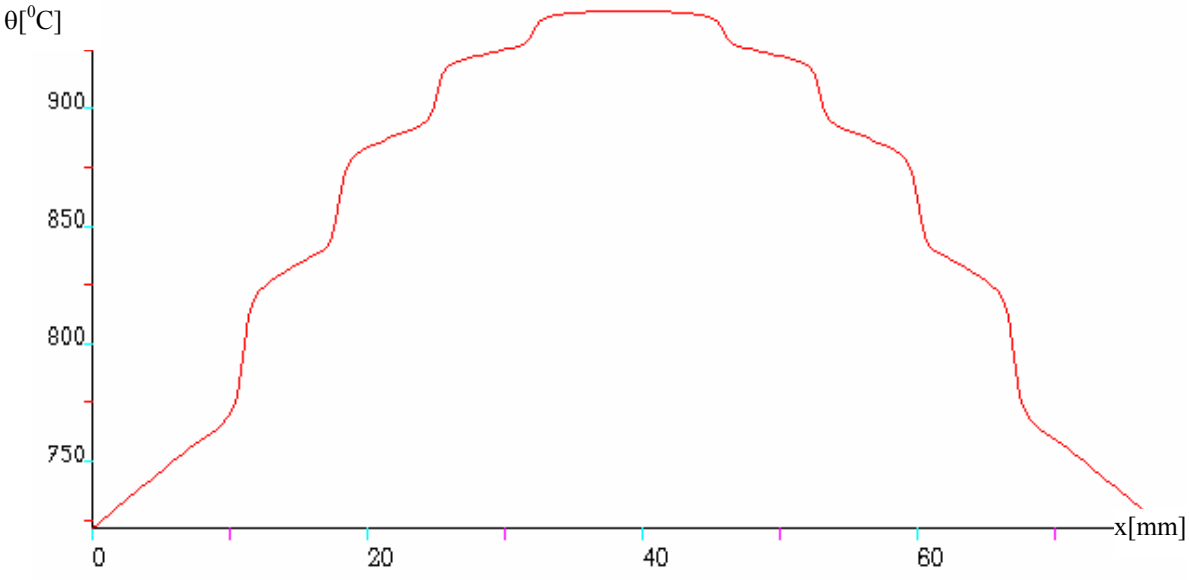

Fig.3 Temperature distribution along fuse-link at moment t = 28.75 seconds

- silica sand

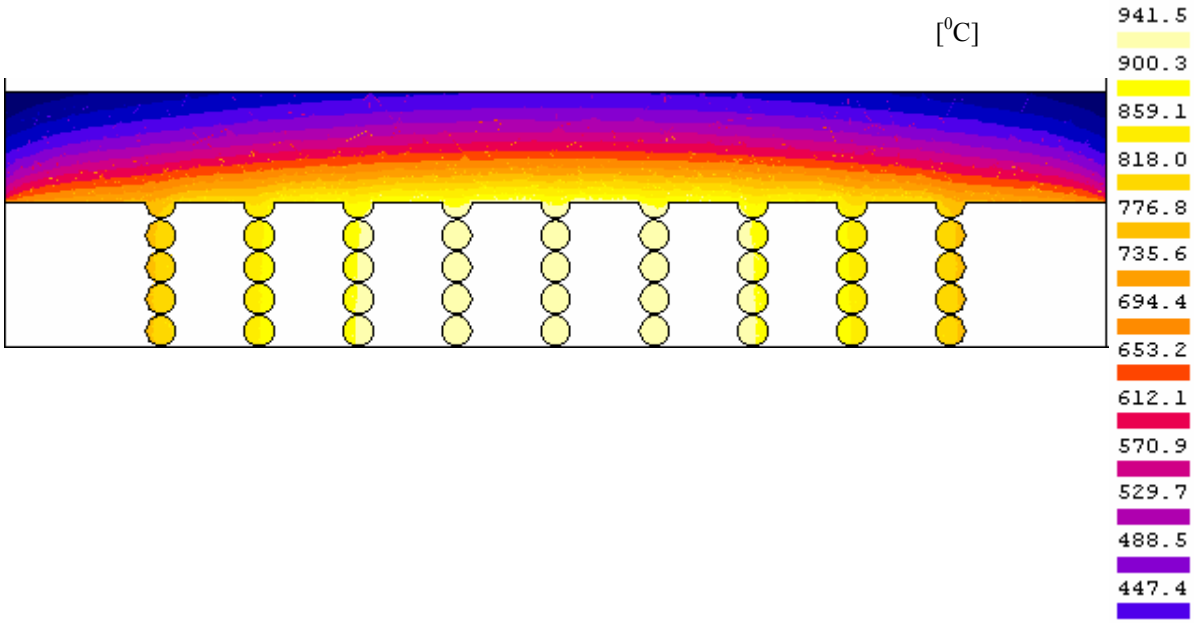

Fig.4 Thermal field into silica sand at moment t = 28.75 seconds

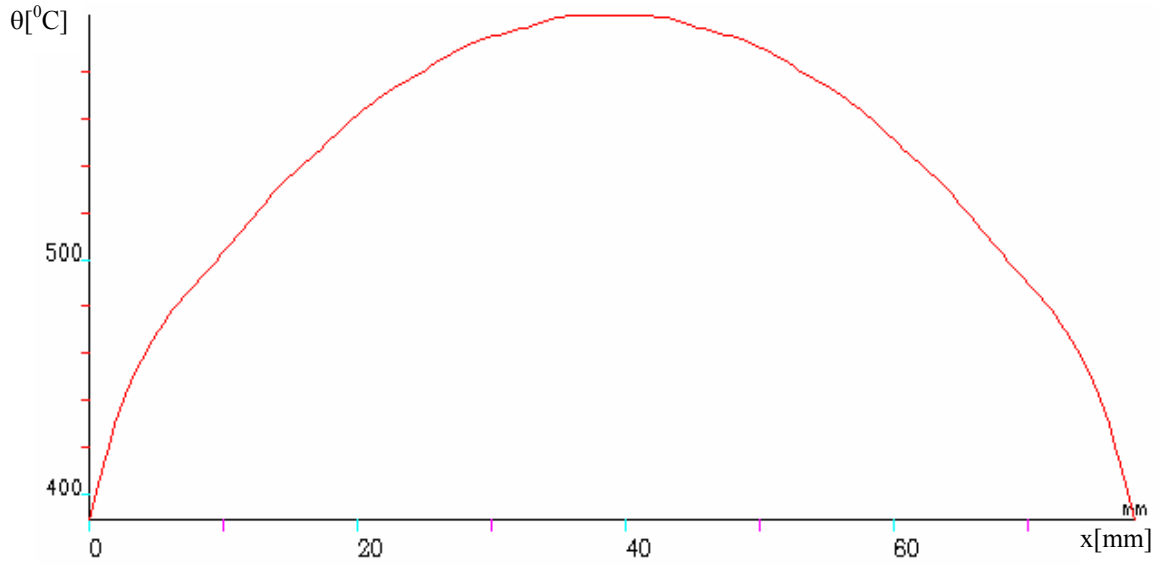

Fig.5 Temperature distribution along silica sand at moment t = 28.75 seconds

- ceramic body

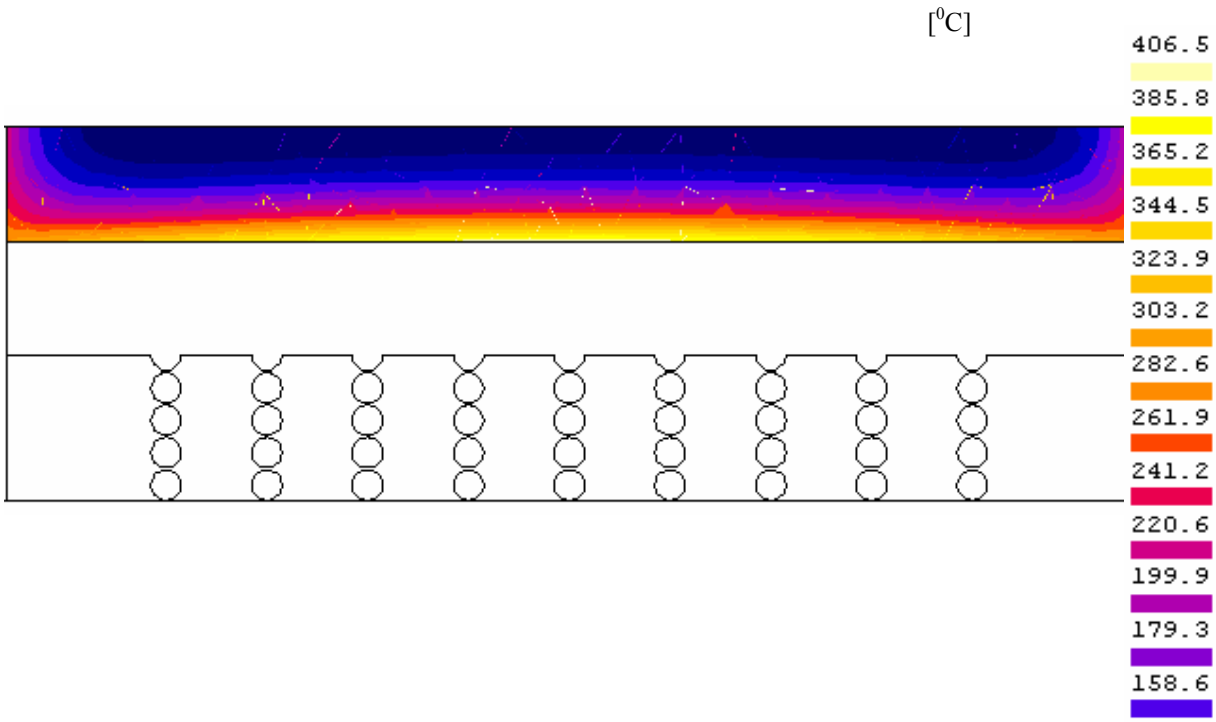

Fig.6 Thermal field into ceramic body at moment t = 28.75 seconds

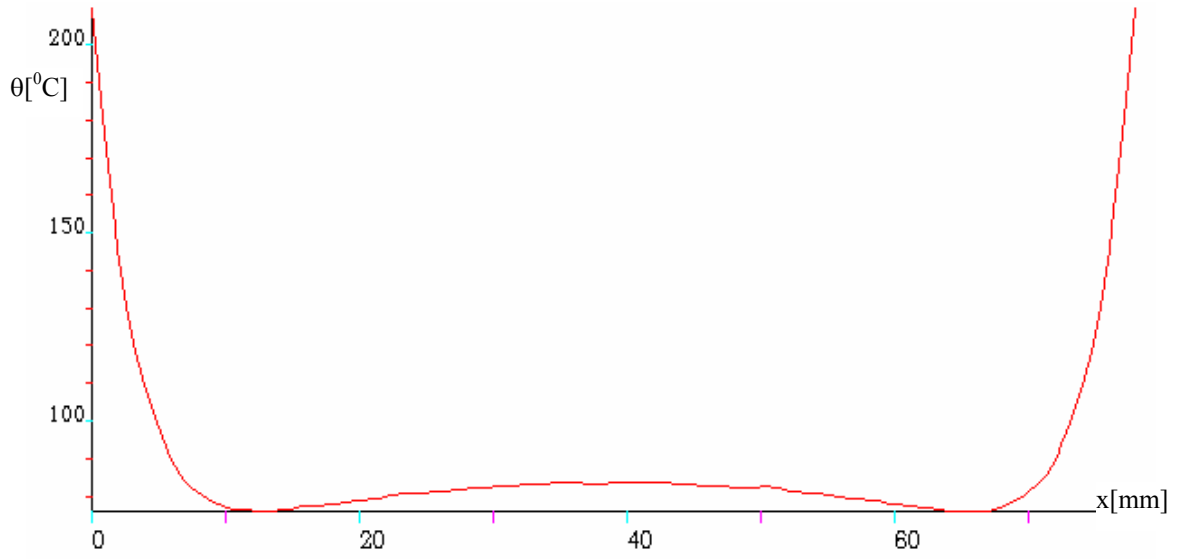

Fig.7 Temperature distribution along ceramic body at moment t = 28.75 seconds

3. Conclusions

Further on, are presented the main conclusions of this simulation study as regards thermal field and temperature distribution at fuses for power semiconductors protection.

- because of very complex thermal phenomenon the analysis of fast fuses thermal field can be done using the simulation software FLUX2D, in this way it can be calculated the temperature of fuse anywhere at any time moment;
- in any cases that were analysed it can observe a maximum temperature in the middle of component part and the minimum values at the ends;
- in the case of temperature distribution along the fuse-link it can observ the notches influence because of the specific fuse-link geometry;
- temperature distribution along ceramic body underline the influence of contacts, and so the maximum temperature values are at the ends because of higher thermal conductivity, 60.6[W/m^{0}C], and only 1.5[W/m^{0}C], for ceramic fuse body;
- using the simulation software it can improve the fast fuse designing that implies a better protection for power semiconductors and also new solutions.

References

[1] Adam M., Baraboi A., Pancu C. and Pleşca A., "Thermal stresses of fuses and protected semiconductor devices", *Sixth International Conference on Electric Fuses and their Applications, ICEFA*, Torino, Italy, pp.319-322, 1999.

[2] Pleşca A., Leonte P. and Licău M., "Electrothermic field and the influence of filled material upon fuses behaviour", *International Conference on Fundamentals of Electrotechnics and Circuit Theory, IC-SPETO*, Tom I, Gliwice-Ustroń, Poland, pp.155-158, 2001.

[3] Wright, A., Newbery, P.G.: "Electric Fuses", 2nd edition, Published by The Institution of Electrical Engineers, London, United Kingdom, 1995.

[4] Pleşca A.: "Overcurrent protection systems for power semiconductor installations", *PhD Thesis*, Iaşi, Romania, 2001.

MATHEMATICAL MODEL USING MACROSCOPIC AND MICROSCOPIC SCALES OF AN ELECTRICAL ARC DISCHARGE THROUGH A POROUS MEDIUM IN HBC FUSES

Rochette David[(1)], Clain Stéphane[(2)] and Bussière William[(3)]

LAEPT CNRS UMR 6069 [(1,3)], Phys. Bât. 5 – 24, Av. des Landais – F63177 AUBIERE CEDEX FRANCE,
david.ROCHETTE@laept.univ-bpclermont.fr [(1)], william.BUSSIERE@laept.univ-bpclermont.fr[(3)]
LMA CNRS UMR 6620 [(2)], 24, Av. des Landais – F63177 AUBIERE CEDEX FRANCE,
stephane.CLAIN@math.univ-bpclermont.fr [(2)]

Abstract: We introduce a model to describe the mechanical interaction and the energy transfer mechanisms from arc column toward to porous medium occurring in the HBC fuse. The model is built on a macroscopic and microscopic approach in order to evaluate more accurately the thermal evolution of the solid phase and the vaporization and condensation processes of the silica sand. We consider a thermal model at the scale of a sand grain to determine the temperature evolution of the plasma and the sand grains and the mass transfer between the two phases. The gas flow is based on the compressible homogenized Euler equations with two species (air and silica vapours) coupled with a porous media model taking into account the mechanical interaction and the porosity variation. The governing equations are discretized following a finite volume scheme coupled with a fractional step technique. We obtain a realist evaluation of the pressure and the temperature as well as the vaporization and condensation areas in the fuse.

Keywords: H.B.C. fuse, porous media, heat transfer, Darcy's and Forchheimer's laws, macro/micro scales, finite volume.

1. Introduction

The process in the HBC fuse involves a compressible gas flow from low to high speed through a porous medium, the presence of important exchanges of energy by heat transfer between arc plasma and silica sand, the creation and the condensation of gaseous material. To describe the evolution of physical parameters such that the velocity, pressure and temperature of the gas, we use the homogenized Euler equations taking into account the presence of a porous medium since the morphology of silica grains influences the arc behaviour [1, 2]. The mechanical interaction between gas and silica sand is governed by the Darcy law which represents the viscous friction and the Forchheimer law which represents the inertial and turbulence friction. A large part of the energy contained in the arc plasma is transmitted to the porous medium. To describe the interfacial heat transfer and the mass transfer, we use a pore description named microscopic modelling of the heat transfer [3]. Our modelling consists in representing a sand grain and a pore by a simplified two-dimensional geometry. From the energy point of view, we assimilate the porous medium as a succession of gas and material layers of thickness R representative of the grain size [4]. We impose that the ratio between the solid and the fluid layer is equal to the porosity. We therefore obtain a two-dimensional model where (Ox) is the principal convection axe of the previous one-dimensional problem and (Oy) is the pore axe to represent the thermal distribution in the grain sand. For any position in the fuse, the porous medium is described following the vertical axe by $\overline{T}(x,y,t)$ on the interval [0, (1-ϕ)R] where R is the characteristic scale of a grain and ϕ is the medium porosity. The volume occupied at the micro scale by the gas and the solid phases are respectively Ω_g =[(1-ϕ)R,R] and Ω_s =[0, (1-ϕ)R]. We assume each volume as one as shown in figure 1.

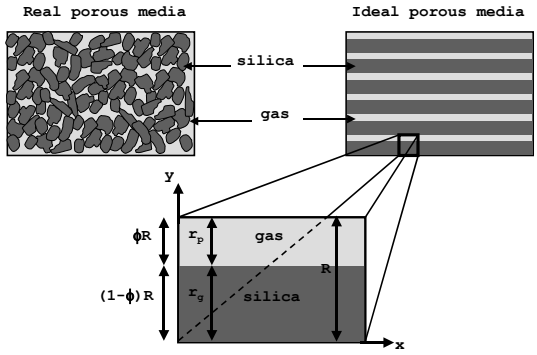

Fig. 1: Microscopic schematic description of a silica grain and a pore.

In section 2, we introduce the mathematical model compounded of a microscopic thermal 2D model and a macroscopic gas flow 1D model. Section 3 is devoted to numerical methods to obtain an approximated solution, we use a finite volume scheme based on a fractional step technique. In section 4, the geometry of the problem is given and

in the last section some numerical results are presented.

2. Mathematical model

2.1. Solid-gas total energy model

The major idea is to introduce the conservation energy equation both for the gas and the solid. We use the total energy form due to the pressure variation. Let us denote by $\overline{E}(x,y,t)$ the total energy density, $\overline{T}(x,y,t)$ the gas or solid temperature, $\overline{u}(x,y,t)$ and $\overline{v}(x,y,t)$ the gas velocity in x-direction and y-direction respectively, we then have:

$$\frac{\partial \overline{E}}{\partial t}+\frac{\partial\left[\overline{u}\left(\overline{E}+\overline{P}\right)\right]}{\partial x}+\frac{\partial\left[\overline{v}\left(\overline{E}+\overline{P}\right)\right]}{\partial y} -\frac{\partial}{\partial x}\left(k_x(\overline{T})\frac{\partial \overline{T}}{\partial x}\right)-\frac{\partial}{\partial y}\left(k_y(\overline{T})\frac{\partial \overline{T}}{\partial y}\right)=S \qquad (1)$$

where $k_x(\overline{T})$ and $k_y(\overline{T})$ are the thermal conductivities, P is the pressure and S represents the total power density injected during fuse operation.
We introduce a new assumption: due to the weak thickness of the gas pore, the gas turbulence effects involve that the temperature, energy, pressure and density of the gas are invariant following y-direction. In the solid phase, only the dissipation effects exist since the convection is null and the pressure is constant. Consequently, in the solid part, the total energy equation is rewritten in the form:

$$\frac{\partial \overline{H}}{\partial t}-\frac{\partial}{\partial x}\left(k_x(\overline{T})\frac{\partial \overline{T}}{\partial x}\right)-\frac{\partial}{\partial y}\left(k_y(\overline{T})\frac{\partial \overline{T}}{\partial y}\right)=S \qquad (2)$$

where $\overline{H}$ denote the total enthalpy.
In the gas phase, Eq. (1) becomes:

$$\frac{\partial \overline{E}}{\partial t}+\frac{\partial\left[\overline{u}\left(\overline{E}+\overline{P}\right)\right]}{\partial x}-\frac{\partial}{\partial x}\left(k_x(\overline{T})\frac{\partial \overline{T}}{\partial x}\right)-\frac{\partial}{\partial y}\left(k_y(\overline{T})\frac{\partial \overline{T}}{\partial y}\right)=S \qquad (3)$$

Let us a small time interval Δt, the splitting operator technique yields that Eq. (3) can be approximated by solving successively a one-dimensional convection equation

$$\frac{\partial \overline{E}}{\partial t}+\frac{\partial\left[\overline{u}\left(\overline{E}+\overline{P}\right)\right]}{\partial x}=0$$

and the two-dimensional conduction equation:

$$\frac{\partial \overline{H}}{\partial t}-\frac{\partial}{\partial x}\left(k_x(\overline{T})\frac{\partial \overline{T}}{\partial x}\right)-\frac{\partial}{\partial y}\left(k_y(\overline{T})\frac{\partial \overline{T}}{\partial y}\right)=S$$

on the small time interval.

Since we assume a gas temperature invariant following (0y), we get that the one-dimensional total energy satisfied $E(x,t)=\overline{E}(x,y,t)$ and thus $T(x,t)=\overline{T}(x,y,t)$, therefore $\partial\overline{T}/\partial y=0$ in the gas domain. The heat transfer between the two phases allows to evaluate the mass transfer by vaporization or condensation [4].

2.2. Gas flow model

The one-dimensional governing equations for a single phase fluid flow in an isotropic, homogeneous porous medium based on the compressible flow Euler equations [5] can be written in the following form:

$$\frac{\partial(\rho_{si}\phi)}{\partial t}+\frac{\partial(\rho_{si}\phi u)}{\partial x}=r \qquad (4)$$

$$\frac{\partial(\rho_a\phi)}{\partial t}+\frac{\partial(\rho_a\phi u)}{\partial x}=0 \qquad (5)$$

$$\frac{\partial(\rho\phi u)}{\partial t}+\frac{\partial(\rho\phi u^2+\phi P)}{\partial x}=P\frac{\partial\phi}{\partial x}-\phi^2\frac{\mu}{k}u-\phi^3\beta\rho|u|u \qquad (6)$$

$$\frac{\partial(E\phi)}{\partial t}+\frac{\partial\left[(E+P)\phi u\right]}{\partial x}=Pu\frac{\partial\phi}{\partial x} \qquad (7)$$

$$\frac{\partial\phi}{\partial t}=-\frac{\vec{v}_{abl}.\vec{n}}{R} \qquad (8)$$

where ρ_{si}, ρ_a and ρ are respectively the silica vapours, air and gas density and v_{abl} is the ablation velocity of the solid.
In Eq. (4), the quantity r represents the material source or loss due to the vaporization or condensation of the silica sand. In Eq. (6), the expression $\phi^2\frac{\mu}{k}u$ represents the viscous friction between fluid and grains silica sand where μ is the dynamic viscosity, k is the medium permeability and the term $\phi^3\beta\rho|u|u$ is the Forchheimer flow resistance where β is the Forchheimer coefficient.
In addition to close the system, we use the ideal gas equation of state:

$$p=(\gamma-1)\rho e \text{ with } \gamma>1,$$

where γ is the ratio of specific heat and e is the specific internal energy.

3. Numerical method

The numerical method is based on a fractional step technique [6]. Assume that we know approximations ρ_{si}^n, ρ_a^n, u^n, E^n, ϕ^n and T_g^n for the gas and $\overline{T}^n$, $\overline{H}^n$ for the solid at time t^n and let Δt be a small time interval.

- We first compute an approximation $\rho_{si}^{n+1/3}$, $\rho_a^{n+1/3}$, $u^{n+1/3}$, $E^{n+1/3}$, $\phi^{n+1/3}$ and $T_g^{n+1/3}$ solving Eqs. (4) - (7) without the source term using a two orders finite volume method.
- Secondly, we compute an approximation $\rho_{si}^{n+2/3}$, $\rho_a^{n+2/3}$, $u^{n+2/3}$, $E^{n+2/3}$, $\phi^{n+2/3}$ and $T_g^{n+2/3}$ adding the source term via an ordinary differential equation.
- The main point is to define $\overline{H}^{n+2/3}$ in the gas using $E^{n+2/3}$ and $u^{n+2/3}$ to take into account the convection effect. In the solid, we take $\overline{H}^{n+2/3} = \overline{H}^n$. We then solve the heat equation in the whole domain to obtain $\overline{H}^{n+1}$ using a finite volume method.
- At the moment $\overline{H}^{n+1}$ is not homogeneous in the gas phase due to the diffusion process. Therefore, we compute a new E^{n+1} using an average of $\overline{H}^{n+1}$ following y-direction in the gas and $u^{n+2/3}$ to take the heat transfer into account.
- We finally obtain all the variables at time t^{n+1}.

3.1. The heat equation resolution

To obtain a numerical approximation of the heat transfer, we use a finite volume scheme [4]. We introduce a bidimensional mesh compounded of rectangular cells. The computation is built on an implicit finite volume scheme. Indeed an explicit scheme leads to very small time step to satisfy the stability condition and yields to non reasonable computation time. The implicit formulation is given by:

$$\rho_l c_v \overline{T}_i^{n+1} = \rho_l c_v \overline{T}_i^n + \frac{\Delta t}{\Delta x}\left(F_1^{n+1} - F_3^{n+1}\right) + \frac{\Delta t}{\Delta y}\left(F_2^{n+1} - F_4^{n+1}\right) \quad (9)$$

where F_1, F_2, F_3 and F_4 represent the numerical fluxes at the cell interfaces using a centred difference scheme. The equation is rewritten in the matricial form:

$$A.\overline{T}^{n+1} = B(\overline{T}^n)$$

where A is a symmetric matrix for a rectangular mesh. We obtain $\overline{T}^{n+1}$ solving the linear system Eq. (9) by a conjugated gradient method.

3.2. The convection model resolution

In order to obtain an approximate solution of the gas flow model in porous media, we use a fractional step technique [6]: on the one hand we solve separately during a small time step Δt the homogeneous conservative system, and on the other hand the right-hand side terms. Let U^n (conservative variable) be an approximation of U (t^n) at time t^n. In order to obtain an approximation of U (t^{n+1}) at time $t^{n+1}=t^n+\Delta t$, we first determine an approximate solution of the homogeneous problem using the finite volume scheme of the form:

$$\tilde{U}_i^{n+1} = U_i^n - \frac{\Delta t}{\Delta x}\left(F_{i+1/2}^n - F_{i-1/2}^n\right) \quad (10)$$

where $F_{i+1/2}^n$ and $F_{i-1/2}^n$ represent respectively the numerical fluxes calculated at the interface cells $x = x_{i+1/2}$ and $x = x_{i-1/2}$ using Roe method. Assumed now that $\tilde{U}^{n+1}$ is the approximated solution value at $t=t^{n+1}$ of the previous homogeneous problem, we solve the ordinary differential equation. Numerically, we add the right hand side contribution using a fourth-order explicit Runge-Kutta method.

4. The fuse domain geometry

The Fig. 2 represents the fuse domain used for the 1D 2D coupled models. The x-direction represents the gas flow direction for a fuse of length L=20 mm and the y-direction represents a sand grain and the pore for evaluate the thermal exchanges. During the pre-arc period, the energy is injected in the solid and when the electrical arc is initiated, the energy is injected in the arc plasma.

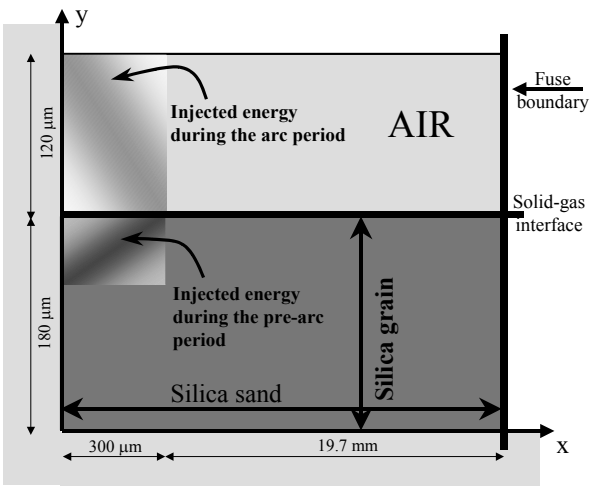

Fig. 2: Geometry of the fuse domain following x-direction and microscopic description of a silica grain following y-direction.

5. Numerical results and discussion

We present a simulation of an electrical arc discharge through a porous medium using realistic physical parameters for the silica sand. At the initial time, the system is at rest, the gas presents in the silica sand interstices is at atmospheric pressure and ambient temperature. Computations have been performed using the C++ finite volume library OFELI [7].
We present the plasma pressure evolution during the fuse operation and the mechanical granular pressure measured by piezoelectric pressure transducer at two positions (9 mm and 17 mm) in Fig. 3.

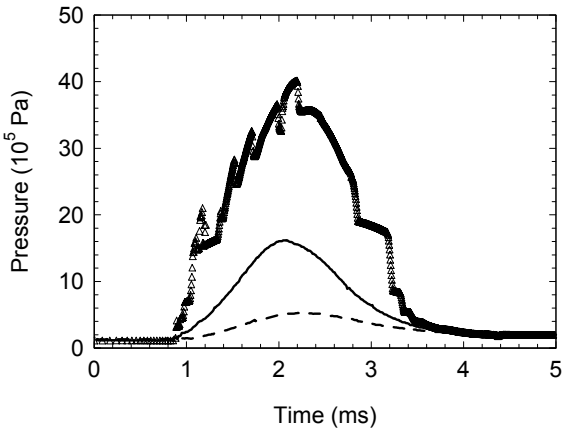

Fig. 3: Evolution of the plasma pressure versus time (Δ). The solid and the dash lines represent respectively the granular pressure measured at 9 and 17 mm of the arc column.

The plasma pressure increases up gradually to the maximum value which falls nearly on the same time of the maximum electric power. We note that the three profiles have the same evolution, during the discharge the arc plasma induces a stress effect on the peripheral grains.

The Fig. 4 represents a comparison of the plasma temperature evolution during the fuse operation between the numerical simulation and the spectroscopy [8].

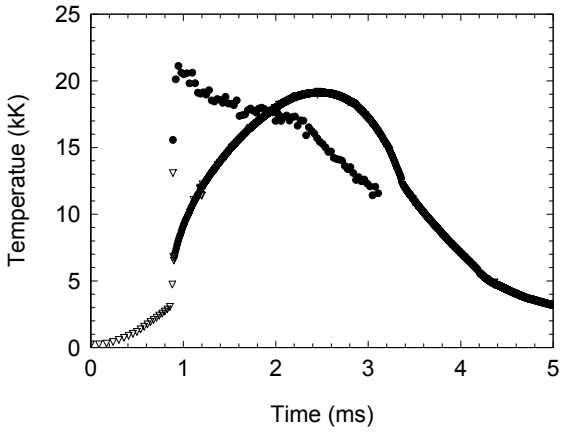

Fig. 4: Evolution of the plasma temperature versus time. The (∇) and (•) represent respectively the numerical simulation and the spectroscopy.

We note that two maximums are the same order around 20000 K, but we have a difference on the profile evolution. Several explications can be formulated: the modelling represents the phenomenon following only one direction, the pre-arc period corresponding to the joule heating of the silver fuse element is approximated by a heating of the silica grains. Moreover the spectroscopy method integrates a 3D phenomenon.

The Fig. 5 and Fig. 6 represent respectively the gas pressure and the gas temperature evolution during the maximum of the injected energy (t=2.3 ms) in the fuse domain. The phenomenon influences only the first 6-8 mm. The silica sand has absorbed the mechanical shock wave and the energy generated by the discharge. We can suppose that the 4-6 mm area is the preponderant area where takes place the fulgurite.

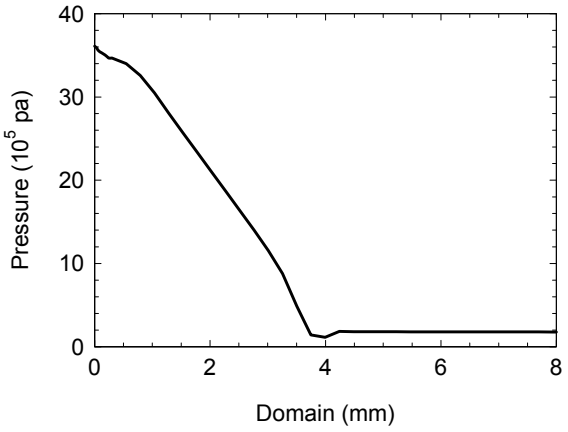

Fig. 5: Evolution of the gas pressure versus fuse domain at time t=2.3 ms.

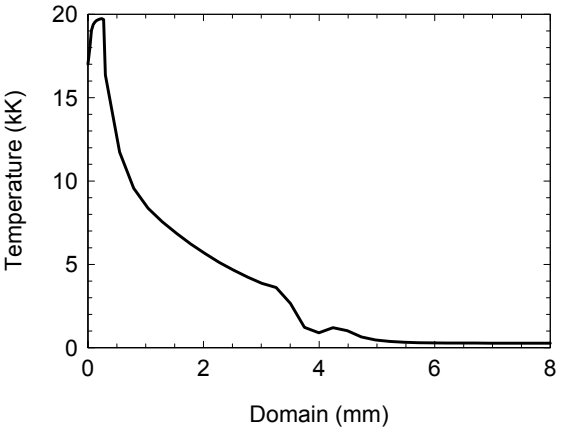

Fig. 6: Evolution of the gas temperature versus fuse domain at time t=2.3 ms.

The Fig. 7 represents the thermal mapping of the silica sand at time t=2.3 ms. The plasma pressure is evaluated around 20000 K.

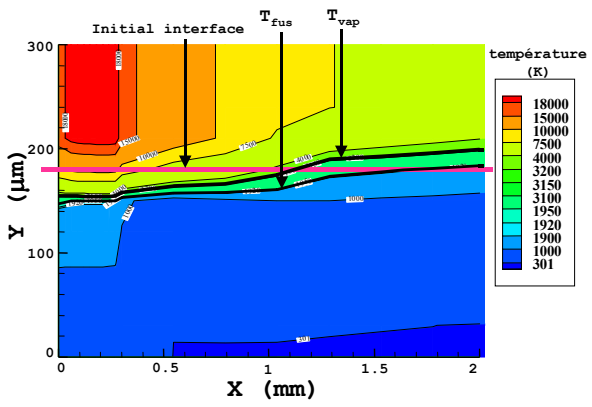

Fig. 7: Evolution of the solid and gas temperature versus fuse domain during the arc period t=2.3 ms.

The first silica grains are partially vaporized and in a area farer, the silica vapour are recondensed at the contact with cold silica grains in comparing the vaporization isothermal with the initial solid-gas interface. Moreover, we note a liquid area evaluated by the vaporization and fusion isothermal.

In Fig. 8, we compare a fulgurite with the porosity evolution of the fuse domain. The porosity allows to show the evolution of the porous medium. The fulgurite is a combination of molten and vaporized fuse element metal and silica sand. In the first millimeters the porosity increases corresponding at the vaporization process and farer the porosity decreases corresponding to the silica sand vapour recondensed. We note that the areas of vaporization and recondensation are in according with the experimental fulgurite.

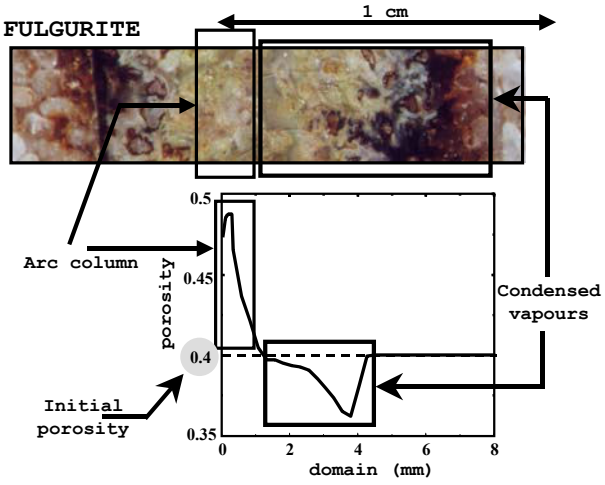

Fig. 8: Comparison of the fulgurite and the porosity evolution of the silica sand.

4. Conclusion

A compressible gas flow model in porous media using a microscopic description of the heat transfer between the plasma and the silica sand was developed. The convection model based on the homogenized equations at two species in porous media takes into account the mechanical interaction due to the porous medium and the thermal model based on the total energy conservation allows to evaluate the heat and mass transfer between the two phases.

The numerical simulation with realistic physical parameters for the silica sand used in industrial fuses gives a description of the pressure, temperature evolution during the fuse operation. We have observed that the high plasma pressure 40×10^5 Pa is maintained due to the conjunction of a high temperature, the gas produced by vaporization and

the Forchheimer force. The model allows to evaluate the vaporized and recondensed areas in the fuse domain.
Future works will consist in realizing a more complete model in adding the silver species and the pre-arc period corresponding to the Joule heating of the silver element.

Acknowledgements

We thank, both for their financial support and their help through many discussions, M. S. Melquiond and X. Godechot from Alstom, M. Vérité from E.D.F, M. T. Rambaud and J.L. Gelet from Ferraz-Shawmut, and M. C. Fiévet and F. Gentils from Schneider Electric.

References

[1] Saquib M.A., Stokes A.D., "Characteristics of fuse arcing in different fillers". *ICEFA* Turin 1999, p. 275.

[2] Bussière W., "Influence of sand granulometry on electrical characteristics, temperature and electron density during high-voltage fuse arc extinction", J. Phys. D: Appl.Phys., 34, pp 925-935, 2001.

[3] Bouddour A., Auriault J. L., Mhamdi-Aloui M., Bloch J. F., "Heat and mass transfer in wet porous media in presence evaporation-condensation", Int. J. Heat Mass Transfer, Vol 41, No 15, 2263-77, 1998.

[4] Rochette D, "Modélisation et simulation de la décharge d'arc electrique dans un fusible moyenne tension", Ph.D Thesis (in french), Blaise Pascal University.

[5] Jiang P.X., Ren Z.P., "Numerical investigation of forced convection heat transfer in porous media using a thermal non-equilibrium model", International Journal of Heat and Fluid Flow, 22, 102-110, 2001.

[6] Toro E.F., "Riemann Solvers and Numerical Methods for Fluid Dynamics", Springer-Verlag, Berlin.

[7] Touzani R., Object Finit Element Library OFELI, Copyright © 1998-2001.

[8] Bussière W., "Mesure des grandeurs (T, N_e, P) au sein du plasma d'arc des fusibles en moyenne tension », Ph.D Thesis (in french), Blaise Pascal University.

Dielectric strength of the ultra-short fuse

Borys Semenowicz[(1)], Roman Partyka[(1)]

Gdansk University of Technology[(1)], Własna Strzecha 18A Str. 80-952 Gdansk,
bsemen@ely.pg.gda.pl [(1)], rpartyk@ely.pg.gda.pl [(2)]

Abstract: The assembly of a very short fuse and the semiconductor switch connected in parallel costitute fast acting, contactless hybrid current limiter whose characteristics strongly depend on features of the short fuse. Both static voltage withstand and the recovery of dielectric strength of the short fuse co-operating with the semiconductor device are discussed. The dielectric strength of the gap between fuse contacts defines the length of the fuse element, and the recovery time dictates the time of current interception by the semiconductor device. It has been shown that the fuse element length of about 1 mm is sufficient for LV current limiters and an optimum time of current interception by the semiconductor device exists.

Keywords: short electric fuse, short gap dielectric strength, fuse recovery voltage, hybrid current limiter

1. Introduction

Hybrid short circuit current breaking and limiting devices were first proposed several years ago by Collart and Pellichero [1]. They were relatively slow due to the inertia of the operating mechanism. Czucha and Żyborski [2] sped up the operation by the application of a switch, whose contacts were simply bent by an impulse of strong magnetic field. Recently, Wolny [3,4] developed the idea of a fuse substitution for the contact switch in the hybrid assembly, to avoid problems with the operating mechanism and to reduce costs and dimensions of the current limiter by removal of the expensive equipment indispensable for generation of strong magnetic field.

The latter hybrid assembly has been called contactless hybrid current limiter (CHCL). There are the fuse features, which decide CHCL characteristics. After the fuse element has been completely decomposed, the static voltage strength of the gap between fuse electrodes, defines the permissible length of the fuse element, and consequently the intensity of axial cooling effect. The gap between fuse electrodes must not be shorter than that withstanding the required testing voltage after the decomposition of the fuse element.

The time of current interception by the semiconductor device is connected with the recovery process of the fuse dielectric strength. This time affects the level of current limitation. The longer the semiconductor device passes the current through, the higher the cut off current is.

Two factors influence the semiconductor let through time: the speed of the fuse element decomposition after the arc ignition, and the deionisation of the created gap. The former defines the optimum turn-on time of the parallel semiconductor device, starting the current transfer, and the latter – the moment of turn-off of the semiconductor device transferring the current to the energy absorber (MOV) forcing the current to zero. Below, both factors are discussed.

2. Fuse static withstood voltage

A short fuse is also applied in the main circuit of the two-path fuse. In CHCL and in the former case the practical lengths of fuse elements are comparable, as the axial heat conduction cooling effect in both cases must be dominant. Nevertheless, the shapes of electrodes differ, as in the two-path fuse a dielectric barrier has to be inserted into the gap to enhance the arcing voltage and dielectric strength. It is easier to model electric field in the short fuse designed for CHCL.

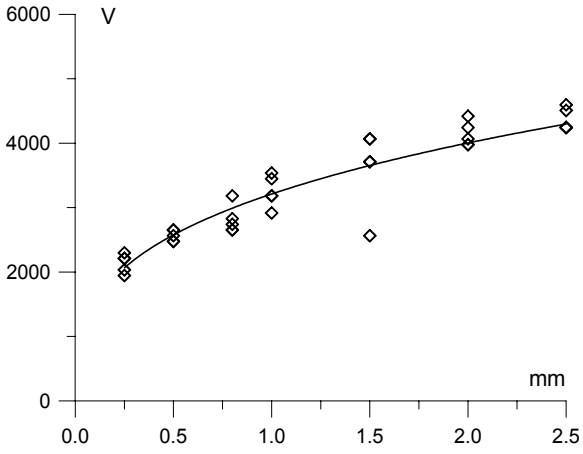

Fig. 1 Dielectric strength of the air gap between copper flat electrodes with sharp edges, vs. distance, modelling a short fuse for two-path fuse assembly [5]

Extensive, research on the dielectric strength of a short fuse for the two-path fuse assembly was carried

out by Sztenc [5]. He used air and compressed gases and changed the fuse gap in the range of 0.25÷2.5 mm. His model consisted in flat electrodes with sharp edges perpendicularly joined with flat bus-bars. Based on private connections selected results of his measurements are shown in Fig. 1. It is noticeable that in the air the withstood voltage rises slower than proportionally as the fuse gap, and a 1-mm gap is sufficient for LV applications.

Results of tests carried out at compressed air show an exponential dielectric strength increase as the pressure, Fig. 2 [5].

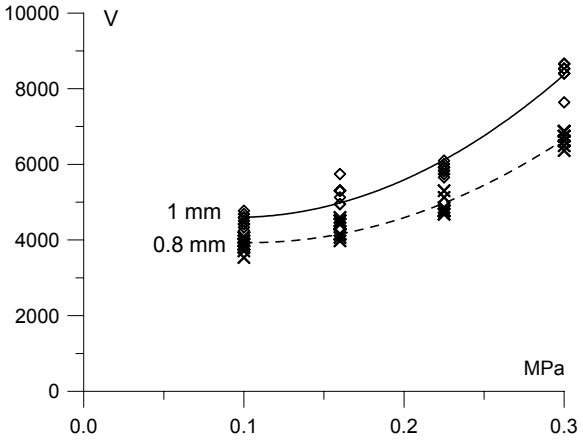

Fig. 2 Dielectric strength of the air gap between copper flat electrodes with sharp edges vs. pressure, modelling a short fuse for two-path fuse assembly [5]

The tests by Sztenc [5] were carried out with a set of clean electrodes. No marks of erosion caused by the arc were considered. To find out how far his results differ from those expected for a short fuse designed for CHCL operating in practical conditions, the authors performed additional tests. The short fuse with 0.5-mm strip fuse element after the operation withstood 1.8 kV. This is slightly less than Sztenc measured [5]. However, such dielectric strength can be considered sufficient for LV applications, in which energy absorbing varistor for current limitation is used.

3. Short fuse dielectric strength recovery

In CHCL the operating fuse is shunted by the semiconductor device connected in parallel, intercepting the current. The fuse-to-semiconductor current transfer, and next the semiconductor-to-energy absorber (MOV) one are controllable. It is important to avoid the latter operation before the fuse recovers its full dielectric strength. In Fig. 3 typical current and voltage profiles of CHCL operation are shown. The time T1 is the fuse arcing time, and T2 is the time of semiconductor state on. T2 has to be long enough to ensure the required fuse dielectric strength. On the other hand, its extension negatively affects the current limitation ability of CHCL. Therefore, T2 should be selected precisely.

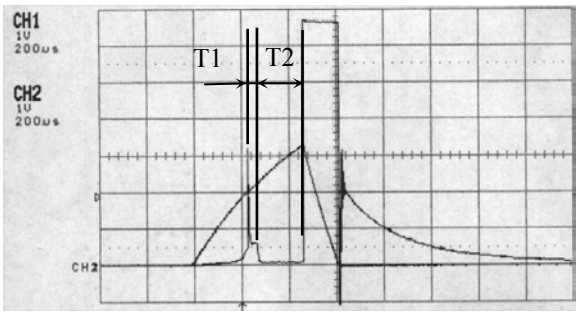

Fig. 3. Voltage and current profiles for CHCL operation: T1 – the arcing time, T2 – the semiconductor time on

The process of recovery proceeds under a very low voltage of a few volts associated with the semiconductor U_F. It can be faster than that in the case when the post-arc plasma is stressed by the rising recovery voltage delaying the discussed process.

A very important factor affecting the rate of strength recovery is the volume and the degree of ionisation of the post-arc gap, which depends on the current and arcing time. Therefore the experiments on the identification of the dielectric strength should consider the relationship between T1 and T2.

3.1 Conditions of experiments

Experiments were carried out in an oscillatory set-up and the typical CHCL assembly shown in Fig. 4. IGBT was used as the semiconductor device intercepting the current from the fuse. It was turned on and off by the controller 1, producing a pulse, lasting from 1µs to 100 ms. The controller operation could also be delayed in relation to the instant of the fuse arc ignition in the range of 1µs to 100 ms. The arc ignition was discriminated at the voltage level of +24 V.

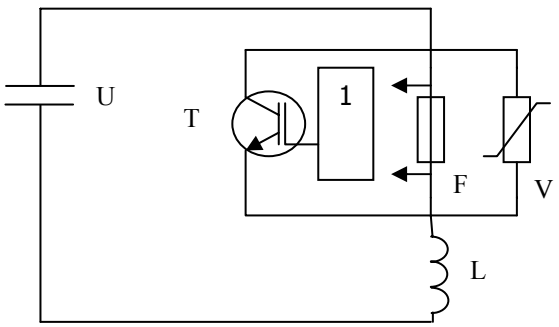

Fig. 4 Experimental set-up for identification of the short fuse dielectric strength recovery: F – the tested fuse, L – the reactor, T – IGBT, U – the

energy source (capacitor bank), V – energy absorber (MOV), 1 – IGBT controller

In order to facilitate exact measurements of the gap between contacts, the 0.1-mm ∅ copper fuse element was stretched between two askew cylindrical electrodes, Fig. 5. Such arrangement also reduced the effect of edges, which were moved away from the closest points, connected with the fuse element.

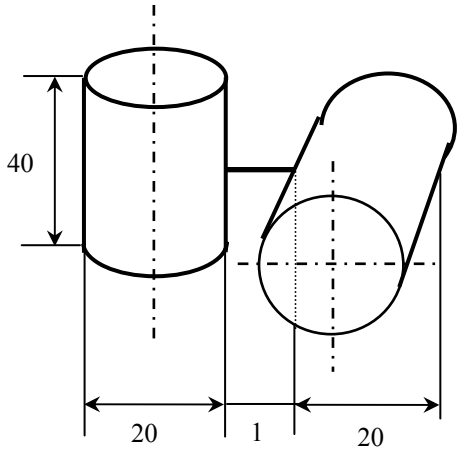

Fig. 5 Arrangement of electrodes for testing of dielectric strength recovery

3.2 Testing procedure

The test-circuit reactor was set in such a way that the capacitor bank of 2 mF charged up to 100 V produced the prospective test current of about 2 kA at the frequency of 480 Hz. High frequency ensured the rate of current rise higher than that at 50 Hz, almost by a factor of 10. Changing the time corresponding to the state on of the semiconductor device (T2) at a given constant arcing time (T1) the border conditions between successful and unsuccessful current interruption were identified. The record of successful interruption is shown in Fig. 3, and the failure is presented in Fig. 6. The arcing time T1 was changed in the range of 1μs÷50 μs.

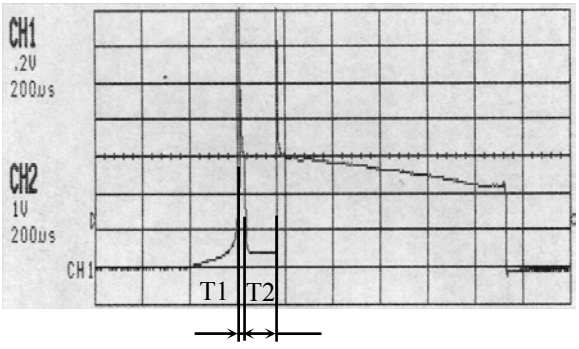

Fig. 6 Unsuccessful operation of current breaking with CHCL: T2 is too short

The voltage to be withstood by the short fuse was forced by the energy absorber, whose threshold voltage acquired 1 kV.

The relationship between the shortest permissible time on of IGBT and the arcing time is presented in Fig. 7.

4. Results of experiments

The experiments provide important information that an optimum arcing time T1 exists. For the relatively thin fuse element, used in experiments, it only amounts 15 μs. Both increase and reduction of T1 lead to the prolongation of recovery time of the fuse dielectric strength T2, corresponding to the recorded boundary time of IGBT on.

It was assumed that such a course of the recovery characteristic of the short fuse dielectric strength depended on two factors: the fuse element decomposition time and the temporal process of the arc ignition between electrodes.

No doubt, creation of a stable arc column needs time. Initially the arc plasma is cool and its volume is modest. With time the plasma extends and ionisation degree rises. The longer the process lasts, the more difficult and time-consuming deionisation. There is additional factor magnifying that process. The fault current rises as time. The longer the arcing time, the higher the arc current is. This has to affect the recovery time of the fuse dielectric strength.

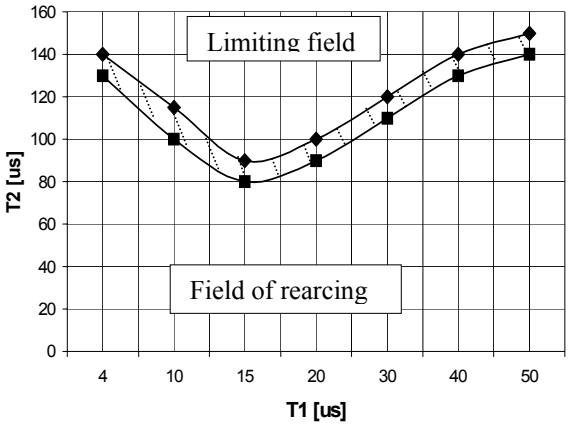

Fig. 7 The relationship between the shortest permissible IGBT time on and the arcing time of the short fuse

To estimate the possible influence of the fuse element decomposition on the recovery time of the fuse dielectric strength the energy dissipated in the fuse has been compared with the energy required for the fuse element decomposition. These energies have been calculated based on the recorded current and arc voltage traces, and the mass of the fuse element.

The deposited energy for the minimum T2 (T1=15μs) amounted to 0.22 J, while the fuse ele-

ment decomposition requires 0.0067 J. In accordance to the actual knowledge, approximately 30% of the fuse element decomposition energy is sufficient to destroy the fuse element of a classical fuse. Supposed, this rule is also true for a short fuse, one can recon that the minimum time of the dielectric strength recovery is observed when the arcing time is strictly associated with the full decomposition of the fuse element.

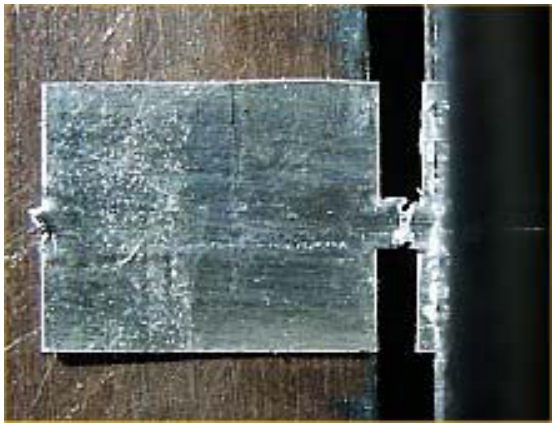

Fig. 8 The silver-strip fuse element after 1-μs arcing

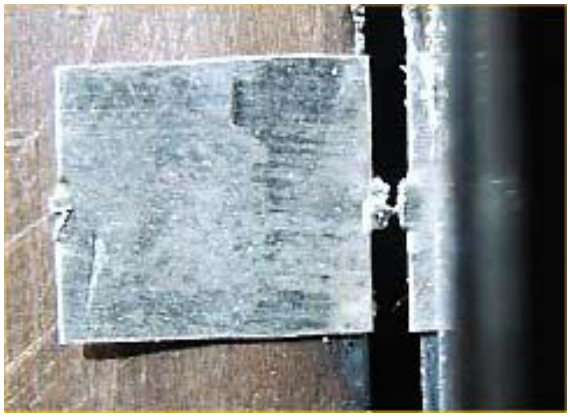

Fig. 9 The silver-strip fuse element after 2-μs arcing

Fig.10 The silver-strip fuse element after 4-μs arcing

In order to estimate the speed of the fuse element decomposition a few photographs of fuse elements were taken during the process of their disintegration. The fuse was shunted at a selected instant. In Fig. 8, 9 and 10 the silver-strip fuse elements are shown after 1 μs, 2 μs and 4 μs of arcing.

5. Conclusions

The fuse element of a short fuse for CHCL can be as short as 1 mm, since a 1-mm air-gap created after the fuse operation withstands more than 3 kV.

The relationship between the short fuse dielectric strength and the separation of electrodes is approximately a cube-root function.

The recovery of the short fuse dielectric strength depends on the rate of the fuse element decomposition and the time on of the semiconductor device shunting the fuse.

There is the optimum arcing time regarding the recovery of short-fuse dielectric strength. It is approximately equal to the time needed for the fuse element decomposition.

Acknowledgements

The research on contactless short-circuit current limiting devices has been carried out in frames of the current research project No: 8 T10A 058 21
supported by the Committee of Scientific Research in Poland.

References

[1] Collart, P., S. Pellichero: “A new high speed DC circuit breaker: the D.H.R”. Colloquium Organized by Professional Group P6 and P2, London, 1989.

[2] Czucha, J., M. Pikoń, J. Żyborski: ”Ultra rapid IGBT current limiting interrupting device of very high breaking capacity”. 8th International Symposium on Short-Circuit Current in Power System, Brussels 1998, pp. 219 –222.

[3] Wolny, A., B. Semenowicz: “Hybrid contactless short-circuit current limitation”. Int. Symposium on Short-Circuit Currents in Power Systems, Łódź (Polska) 2002 r., s. 221-225

[4] Semenowicz, B, P. Leśniewski, and K. Gohra, ”Operation of an ultra-short fuse shunted by a semiconductor device: simulation and experiments”. XIII-th Symposium on Electrical Apparatus and Technologies SIELA 2003, 29-30 May, 2003, Conf. Proc. Vol. I,

[5] Sztenc, K.: ”Two-pass fuse with variety of insulations gases”. MSc thesis, Gdańsk University of Technology, Gdansk 2001.

Protection against fault arcs in low voltage distribution boards

J.G.J. Sloot [(1)] and R.J. Ritsma [(2)]

Eindhoven University of Technology [(1)], Netherlands, j.g.j.sloot@tue.nl

Prof. Damstra Laboratory [(2)], Eaton Electric NV, Netherlands, r.ritsma@holec.nl

Abstract:
Modern low voltage distribution systems often are installed without main protection equipment on the low voltage side of distribution transformers; it is relied on the relay or fuse on the high voltage side of the transformers. This article demonstrates that such philosophy can result in long lasting voltage dips and failing protection. Practical cases of arc faults in main low voltage distribution installations are discussed, as well as laboratory experiments.

Keywords: electric fuse, fault arc, low voltage installations, voltage dips

1. Introduction

In the Netherlands, medium voltage grids typically deliver power to groups of customers by means of Ring Main Units (RMU) like Figure 1, around 10 kV/400V transformers. This is a well-proven concept with switch disconnectors and fuses on both sides of the distribution transformer. For transformers above 630 kVA, circuit breakers can be preferred above fuses at locations D and E, because of the limited nominal current ranges of fuses.

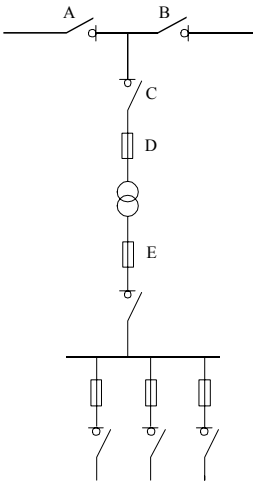

Fig. 1: Conventional set-up for a RMU.

In practice it is more often observed however, that the main low voltage protection (location E in Figure 1) is just kept away, leaving the protection of the distribution board completely to the fuse or circuit breaker on the high voltage side. This decision is probably motivated by efforts to reduce costs of equipment, and may be selectivity arguments.

Such philosophy can be acceptable as long as only the protection of conductors against conducting short circuit currents is required. However, in the case where an open arc is initiated in the low voltage distribution board, the protection on the high voltage side is mostly too slow to offer relevant protection against arcing effects.

In such situations explosive conditions have to be expected within the low voltage compartment of a ring main unit or a metal enclosed assembly on the low voltage side for an industrial application.

Even more dangerous situations can occur for industrial installations where the low voltage distribution is constructed with plastic insulation against the wall of a factory hall, because such locations are accessible to factory workers, walking alongside. Figure 2 shows the appearance of such a distribution [1], which is possible without short circuit protection between transformer and the main distribution installation.

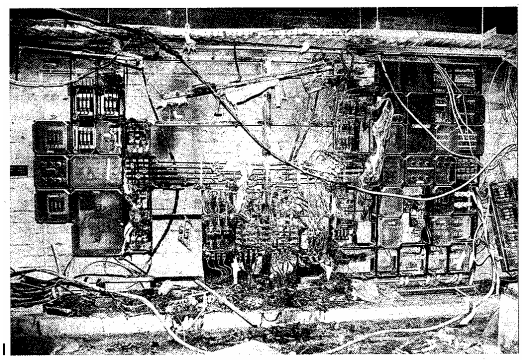

Fig. 2: Burned out Low Voltage Distribution Board after an arc fault.

Also when a circuit breaker is installed as a main protection of the low voltage board, arcing effects are

hardly limited when due to selectivity matters, the tripping delay is commonly set at the maximum delay value (e.g. 0,5 sec).

2. Recent accidents with fault arcs in the low voltage distributions

Some recent accidents can be mentioned for Dutch low voltage distributions without main low voltage protection. Figure 3 shows the basic set-up of such a configuration.

An industrial customer used two 10 kV connections with a coupling possibility between the low voltage distributions. Only the high voltage sides of the transformers were equipped with a power circuit breaker (A) or fuse. Circuit breaker A hat settings $I_{>}$ = 300 A, $t_{>}$ = 5 min and $I_{>>}$ = 600 A, $t_{>>}$ = 0.3 sec. On the low voltage side a switch disconnector (B) was installed. (Sometimes installation drawings are confusing when switch disconnectors are wrongly presented like power circuit breakers with a cross!).

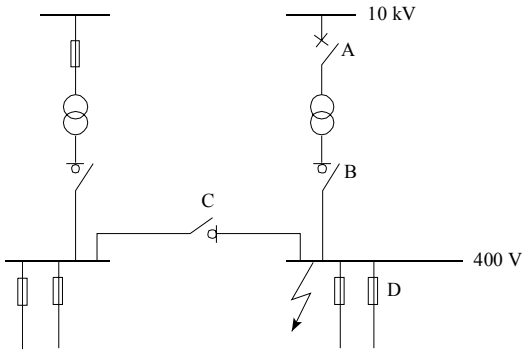

Fig. 3: Industrial installation with internal arcing

From this industrial installation a disturbance was reported recently.

When electricians arrived at the location, they noticed that the lighting on the terrain (fed by fuse D in figure 3) showed an irregular behaviour, lasting for at least more than ten minutes. From the main low voltage distribution big bangs were heard, while smoke was noticed. It was decided not to enter the distribution room but to send an alarm to the fire brigade, after which the fire was extinguished with CO_2.

Now the main distribution was inspected. The rail system was heavily damaged, complete copper parts were disappeared. Especially near to grounded parts of the installation holes were formed, apparently because of fault arc effects.
An arc had apparently moved along the complete rail system, under influence of magnetic forces (Figure 4).

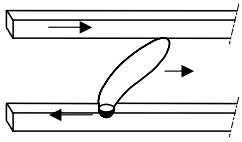

Fig. 4: Moving arc between rail system

The fault was finally interrupted by the circuit breaker on the high voltage side. The fault currents at the high voltage side were registrated as slightly above 600A in the phases, while on the low voltage side the phase currents were about 15 kA. (Theoretically higher values up to 20 kA were expected from calculations based on the available short circuit power and the short circuit impedance of the transformer.) Considering the enormous destruction, it was concluded that the situation had lasted for many minutes, despite the settings of the protection. It is not unthinkable that the low voltage arcs reached such considerable lengths, that they resulted in a limiting effect on the current, preventing the high voltage relay to come into action. Further the arcs could have shown a temporarily extinguishing and restriking behaviour (the irregular functioning lighting installation, as mentioned in the above, was connected behind location D in Figure 3).

This assumption was based on open arc experiments in our laboratory, with phase voltage 303 V, where the setting of the test was 48 kA, and cos Φ = 0.13, while the measurement during the arcing test showed 35 kA and cos Φ = 0.55. The initial arc length was about 25 mm, but flashovers to grounded parts must have caused greater arc lengths.

Table 1 Current limitation effect by arcing

	Vphase [V]	Current [kA]	cosΦ
setting 1	303	48	0.13
measurement 1	303	35	0.55
setting 2	303	86	0.18
measurement 2	303	67	0.64

As a further practical example, recent Dutch arcing accident will be mentioned. The 630kVA transformer was protected by high voltage 50A fuses. At the low voltage side only a switch-disconnector was fitted as incomer of the metal enclosed assembly.So here again: no short circuit protection at the low voltage side of the transformer. At the low voltage site a theoretically short circuit current of 19 kA could be expected, based on the transformer and the short circuit power of the grid. Due to unclear reasons an internal arc was initiated in the metal enclosed assembly. The assembly was completely

destroyed; it took more than half an hour before the voltage was interrupted *manually*!

3. Comparison with former arc fault tests

Former arc fault tests [2] in the Kema laboratories, Arnhem, showed the minimal effect of high voltage protection against low voltage arc faults. Figure 5 shows the basic set-up for the tests.

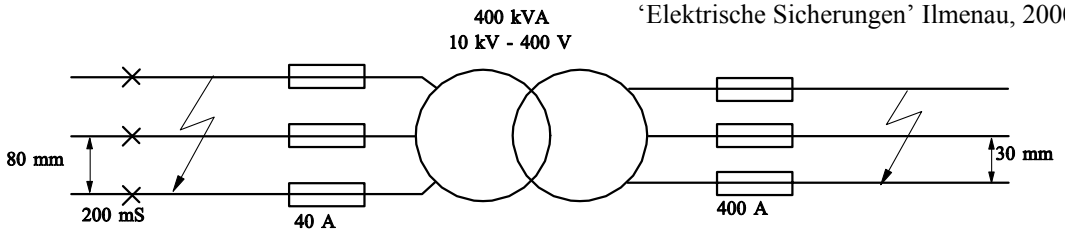

Fig. 5: Test set-up with fault arcs on both sides of a distribution transformer.

On the low voltage side of the transformer, 17 kA fault arcs were initiated. Arcing effects were minimal when low voltage fuses (400 A) were installed. The noise and visual effect increased enormously when during a next test, the low voltage fuses were removed, leaving the task of the interruption to the high voltage fuses (40A). Conditions became shocking when both low and high voltage fuses were removed, after which a high voltage circuit breaker with setting 200 ms performed the current interruption of the low voltage arcing fault. (Also the arcing effect on the high voltage side was investigated, but will not be discussed here).

4. Conclusion and recommendations

From recent field experiences and former laboratory experiments it can be concluded that for an acceptable protection against low voltage arc faults, low voltage fuses should be installed directly at the low voltage side of the distribution transformer, whenever the nominal current range allows such application. For transformers above 630 kVA a low voltage circuit breaker can be chosen as an alternative. In this case it shall be taken into account that the tripping delay of the circuitbreaker for short circuit shall be as short as possible.

Although one is generally afraid for selectivity problems in practice, arcing protection should be considered as an even more severe problem. Morover with a well designed installation shorter delay times than the maximum setting for short circuit currents to garantee selectivity are certainly possible. Whenever the high voltage side can be protected by fuses, these also have the preference above a breaker, from the standpoint of protection against arc faults. A more general overvieuw of of arc fault effects and available protection methods like fast earthing and/or circuit breakers operated by sensors, was presented elsewhere [3].

Literature

[1] Moeller product brochure, Germany.

[2] Pettinga, J.A.J.: “Protection against fault arcs” (in Dutch), Energietechniek 7/8, 1993, pp. 535-538.

[3] Sloot, J.G.J.: “Current limiting fuses and other protection for reducing hazards”. 1st Workshop ‘Elektrische Sicherungen’ Ilmenau, 2000.

ELECTRIC ARCING BURN HAZARDS

A. D. Stokes[(1)] and D. K. Sweeting [(2)]

University of Sydney[(1)], Australia 2006, stokes@ee.usyd.edu.au
Sweeting Consultants[(2)], PO Box 389 Newport 2106, david@sweeting.com.au [(2)]

Abstract: The paper presents recent results in the area of high power testing aimed at improving the safety of electrical staff working on live equipment. The driver for this work is the American Standard on such exposure hazards, which has the potential for international adoption and, in the authors' opinion, does not provide a suitable methodology for assessing the hazard. A selection of results will be presented, obtained in a high-power-system supplied commercial test laboratory, using the latest CCD based high-speed video recording methods. Results are reported for 415V currents in the range 1,000 to 70,000 prospective rms amperes and for tests at 5,000V in the range 1,000 to 27,000A. The nature and evolution of the three-phase open-air arc will be shown with results on practical switchboards. The impact of conventional protective devices such as HRC fuses is included together with some disturbing results for circuit breaker protected systems. The presentation will include CD based video sequences, which will emphasise the violent impact of these explosive events.

For an electronic copy of this paper with colour images simply email to one of the authors.

Keywords: (Arc hazards, burns, high-power testing, high speed videography, personal protective equipment.)

1. Introduction

Modern electric fuses are marvellous devices for protecting life and equipment from the potential power of uncontrolled electricity. Since the coming of electricity in the 1870s, they have been in the front line of electrical defence. Indeed, it is fair to say that without the virtually fail-safe protection of the electric fuse there would be no modern electrical industry. Electricity would be regarded as far too dangerous for widespread use.

A second line of defence for people working on live electrical apparatus is PPE, personal protective equipment, formalised in the USA by NFPA 70E, [15]. During the past few years, there has been a positive explosion in the application of fire resistant clothing for electrical workers, largely driven by the IEEE Society for Petroleum and Chemical Engineering, culminating in the issue of IEEE 1584, [34] which aims to provide "*techniques for designers and facility operators to apply in determining the arc-flash hazard distance and the incident energy to which employees could be exposed during their work on or near electrical equipment*".

A huge amount of work has been done to permit the calculation of actual arcing conditions in the face of interaction with a wide variety of fuse and other switching equipment. The guide "*presents methods for the calculation of arc-flash incident energy and arc-flash boundaries in three-phase ac systems to which workers may be exposed. It covers the analysis process from field data collection to final results, presents the equations needed to find incident energy and the flash-protection boundary, and discusses software solution alternatives. Applications cover an empirically derived model including enclosed equipment and open lines for voltages from 208 V to 15 kV, and a theoretically derived model applicable for any voltage. Included with the standard are programs with embedded equations, which may be used to determine incident energy and the arc-flash-protection boundary"*.

The basic premise of the standard is that the burn hazard due to electric arcs is one of radiative heating and that all of the arc dissipation is converted to radiation. It will be shown here that radiative heating is a significant component of the arc load, but convective heating due to the plasma cloud is far more important. As a consequence IEEE Standard 1584 grossly overestimates the hazard for high voltage exposures but severely underestimates the heat load for exposure voltages below 1000V.

Section 5.1 of IEEE 1584, dealing with arc models states a "*theoretically derived model, based upon Lee's paper [B19], is applicable for three-phase systems in open air substations, and open air transmission and distribution systems. This model is intended for applications where faults will escalate to three-phase faults. Where this is not possible or likely, this model will give a conservative result*".

The paper referred to, Lee, 1982, [9] makes no reference to the rich literature on electric arcs, beginning with Davey, 1802 [1] and including such important whole books as [2] to [8], all predating the Lee paper by more than 15 years. From the description given in IEEE 1584 it is clear that the Lee paper is regarded as the starting point for understanding the behaviour of electric arcs. However Lee, [9] states, (p248), that "*the maximum arc wattage is ... 0.5 times the maximum kVA bolted fault capability of the system at that point. ...There will be lower arc energies than this but there is no way to predict them.*" These grossly presumptuous statements have no references to support them and

ignore the wealth of previous research referred to in the texts, [2], and [6] to [8] that suggest arc voltages of the order of 5 to 10 volts per centimetre of arc length for virtually all arcs in open air. Lee further states that the arc "*shape is not important, only that it has the required area. For simplicity we will consider it is a sphere and will have a diameter that gives the specific surface area"*. In table 2 Lee gives results for his calculation of sphere diameter as a function of arc power. As an example, for a three phase arcing exposure of 5000V, 20,000A the Lee prediction forecasts a plasma diameter of 170 mm. The diameter is not considered to be a function of arc duration, only arc power! The authors' test results for this condition, for an arc duration of 0.5 seconds, described later, show a brilliant plasma cloud some 3000 mm long and around 1500 mm tall in the plane of the camera. Similarly the calorimetric data reported later do not support the idea that radiant heating is the main hazard. The heat load for objects within the cloud is much higher (> 3 times) than just due to radiation alone.

Deficiencies in the Lee paper would be of little consequence if corrected, some 20 years after publication, but this has not been done with IEEE 1584. The standard clearly promulgates the Lee proposition that radiation is the key source of arc hazard and in doing so continues to ignore the rich subsequent literature on this topic. For example Jones, 1988, in his book "*High pressure arcs in industrial devices*", [12] provides some 55 pages of review of the literature on arc radiation and cites some 86 references. None of this is mentioned in IEEE 1584.

Whilst radiation is clearly a very complex topic it is widely recognised, [12], that only some 10 to 20% of total arc power actually escapes as radiation. Most arc power is delivered to, and stored in the plasma cloud as high temperature plasma enthalpy. In low voltage situations the plasma cloud has the potential to deliver much more serious injuries to exposed workers than those predicted by the simplistic and faulty approach adopted in IEEE 1584, which, for its own references on arc hazards has drawn almost exclusively on literature from the petroleum and chemical industry, [9] to [11], [14], and [16] to [32].

2. Data supporting IEEE 1584

The standard IEEE 1584 is unusual in a number of ways. It is accompanied by a substantial number of spreadsheet data including the results of some 313 short-circuit tests designed to reinforce the conclusions reached. The data includes such parameters as:

- Open circuit voltage phase-phase (kV)
- Bolted (prospective) fault current (kA)
- X/R ratio
- Electrode material SS, AL, CH, CS
- Gap between electrodes (mm)
- Gap electrodes to box (mm)
- Distance from arc to calorimeters (mm)
- Arc duration (msec)
- Box width + height/2 (mm)
- Box depth (mm)
- Number of phases
- Electrode configuration (parallel or inline)
- Arc current (kA)
- Arc voltage line-line (kV)
- Arc energy (kJ)

This wealth of data has made it possible to identify those aspects of the arc modelling that have resulted in faulty hazard prediction. Also helpful are the large number of references given.

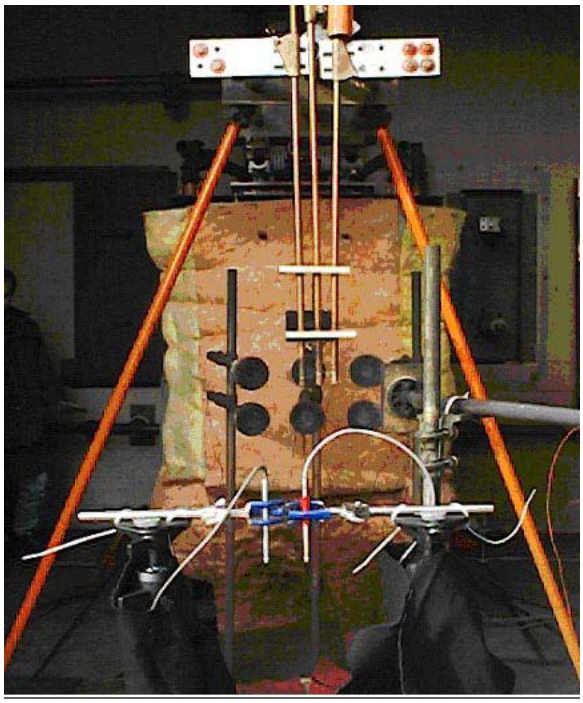

Figure 1 Geometry used for IEEE 1584 open arcs

Figure 1 has been taken from Doughty et al [24] and shows an arrangement of three parallel electrodes running from top centre in a vertically downwards direction. The calorimeter holders are the circular objects seen in centre view. With such an arrangement the arc is forced in a downward direction and none of the calorimeters intercept arc plasma heat load. This is the key weakness of the modelling approach and appears to have been a common feature of all 313 arc tests carried out to support the IEEE 1584 standard.

3. Arc Modelling

The arc modelling tests carried out here preceded the publication of IEEE 1584 and were sponsored by a

large user of bulk electricity which had become concerned about possible errors in the impending standard based on the publication record being cited in precursor documents.

Because of the complexity of the arcing process the authors have modelled arcs of the kind that may create significant hazards using only experimental methods. An insulated test structure was arranged using precisely machined Australian hardwoods to lock a series of heavy duty electrodes into parallel configurations with the option of electrode separations from 25 to 150mm, figure 2. The electrodes projected some 300 mm from the support structure. This value was chosen as a compromise between a sufficient distance to minimise insulation charring due to radiant arc heating (not entirely successful) and a small enough distance to minimise electrode movement due to magnetic forces (achieved). The top most electrode was aligned at a shallow angle to the others and used only for single phase testing with gaps as small as 5 mm.

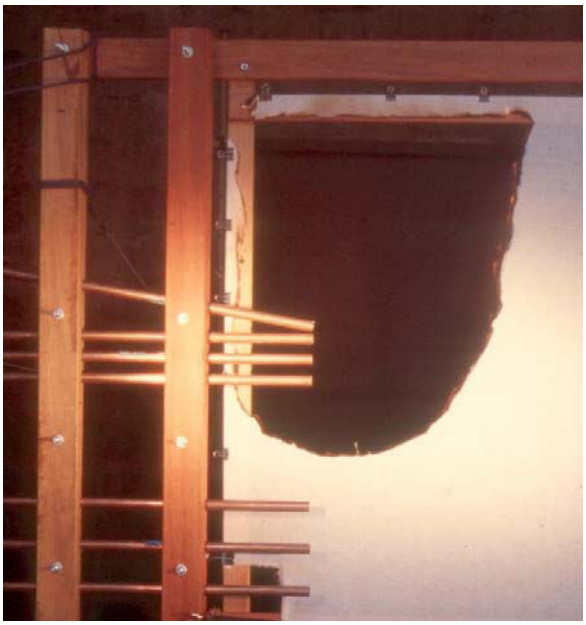

Figure 2 Arc hazard setup.

Electrodes of high conductivity copper and structural grade aluminium of 25.4 mm diameter were used for all tests. For some of the tests, including that shown in figure 2, a light gauze was fastened immediately adjacent to the plane of the electrodes as a sensitive indicator of the burning reach of the plasma cloud. All tests were monitored using high speed videography at 1000 frames per second focussed on the arc core, and both normal video and still photography for overall records. The total of all files created by the imaging and analysis process exceeds 1,800,000,000 bytes.

For single phase open air arcs at a supply voltage of 415V self interruption always occurred in < 10 ms.

For three phase open air arcs at a supply voltage of 415V self interruption always occurred in < 40 ms.

Stokes and Oppenlander [13] gave, in terms of absolute current values:

$$Power = (20 + 5.34 \times z) \times Current^{1.12} \text{ watts} \quad (1)$$

for a rather large data set with single-phase arcs having **opposing** electrodes and z as the arc gap in centimetres. For the present three phase arcs with **parallel** electrodes at a separation of some 45mm the empirical relation:

$$Power = 362 \times Current\_rms^{1.12} \text{ watts} \quad (2)$$

was found to give the best empirical fit to the present data allowing for rms and absolute three-phase current differences in the quoted data Equation (2) underestimates the mid range of current power data by some 10% at currents of the order of 4000A. No significant influence of electrode separation was observed for reasons that will be detailed later.

For electrode gaps much larger than a few hundred millimetres it may be appropriate to increase the arc power by an added voltage drop at approximately 2 volts per centimetre of arc gap as follows:

$$Power = 25 \times (20 + 2 \times z) \times Current\_rms^{1.1} \text{ watts} \quad (3)$$

Figure 3 shows condensed detail of current and voltage waveforms for a 20,800A rms test. Full data sets are available and consist of many MB of such densely packed data as to be impossible to fully present here in complete form. However they all show the following features:

- The arc voltage grows during the first 30 ms indicating that it takes that long for the overall arc paths to fully develop. This is confirmed in the high speed video images discussed later.
- The arc voltage fluctuates around a mean value that is approximately sinusoidal with time. This is due essentially to the time varying arc geometry and does not imply a linear current-voltage relationship
- For three-phase tests at different currents the fitted sinusoidal voltage has an amplitude that varies approximately as

$$RMS\_Voltage \propto RMS\_Current^{0.12} \quad (4)$$

- For tests at the same nominal current but with different arc duration the dissipated energy varies with arc power times arc duration.

4. Arc Photography

4.1 Conventional videography

All tests were recorded using conventional videography using rapid response CCD cameras.

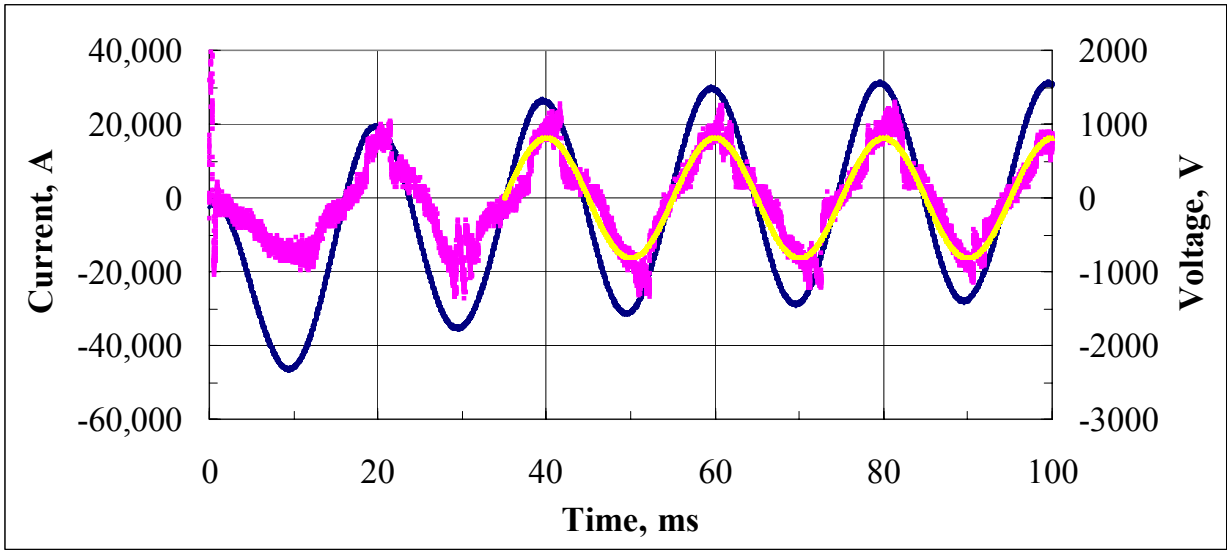

Figure 3 Current and voltage waveforms for the first 100ms of test 8047_010, 20,800A rms, .5000V

Even so the huge range of arc brightness was such that complete image saturation was always obtained during the main arcing phase.

Figure 4 Test 8047_010, 20,800A, 0.109 seconds.

For short duration arcs, typically 100ms and less, the cameras recovered within some 40 ms, and useful images of the dying, but still brilliant plasma cloud were obtained. For longer arc durations camera recovery was many times slower so that only the final stages of plasma cooling were captured. At the higher currents the records show powerfully driven convective flows. These have been assembled as MPEG files some of which will be shown during the conference meeting. Figure 4 shows the extent of the plasma cloud for a three phase arc of 20,800A rms and duration of 0.109 seconds. In the movie sequence, to be shown during the conference, the plasma cloud can be seen to be driven from left to right at an average speed of some 8 m/s. A very substantial cloud of arc "dust" was created that shows very clearly the continuing convectively driven flow.

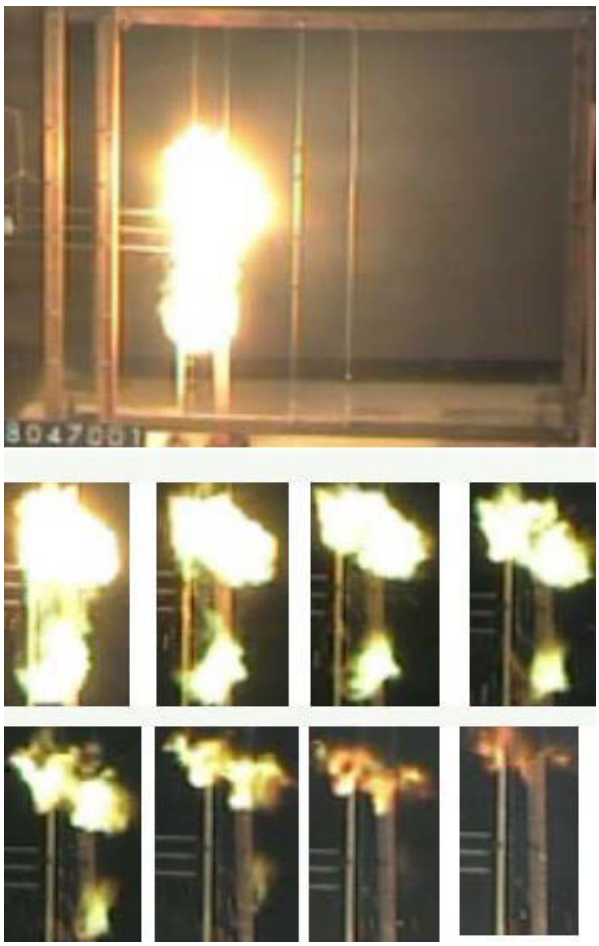

Figure 5 Test 8047_001, 991A, 0.11s. Top view is a general image at 40ms after arc interruption. The others are compact views at successive 40ms intervals.

Figure 5 shows the dying phases for a 991A rms arc of 0.1 seconds duration. The plasma cloud fades to invisible after some 300ms.
At these low currents there is minimal convective flow and the main movement is a gently rising cloud that cools to below visibility generally over a period of some half a second.

Calorimeter heat load measurements support the expectation that arc burn hazards within the plasma cloud are many times (>3) higher than those in off axis positions where only radiant heating is possible.

4.2 High Speed Videography

High speed black and white video records have been taken using a Redlake Motion Pro CCD based camera running at 1000 frames per second and recording for up to several seconds. These have subsequently been edited using Adobe Premiere 6.5 into MPG files and with a Redlake viewing utility to create sequences of individual JPG files.

Figure 6 gives current – voltage waveform detail and figure 7 shows the final frames, each separated by 1ms from the next, prior to disconnection for an arc of 20,800A rms with electrode separation of 50mm.

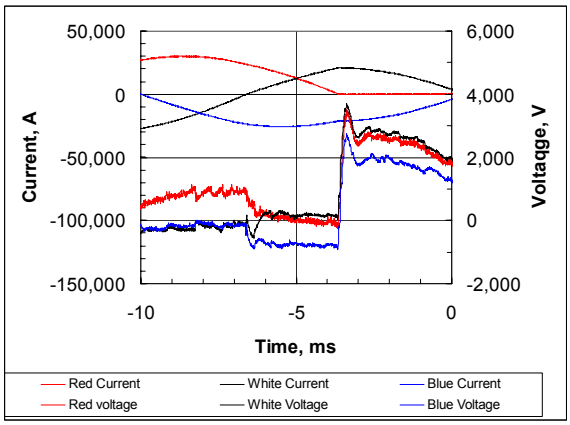

Figure 6 Current and voltage waveform detail for the last 10 ms of arcing for the 20,800A rms arc shown in figure 7.

The first frame of figure 7 shows three arc flares with their origins at the electrode tips which are separated by 50 mm. When the flares pass currents of opposite sign, the arc columns repel each other. When of the same polarity, they attract each other. This sequence can be clearly seen in all of the arc records and cycles in keeping with the evolution of the currents. In figure 7 the top arc has been interrupted in the second last frame and the two remaining arcs, being of opposite polarity repel each other. Notice that these effects are always directed away from the arc power-source and so create a magnetically driven flow from left to right. In the arc plane from top to bottom these same effects act to spread arc plasma in the vertical plane of figure 7.

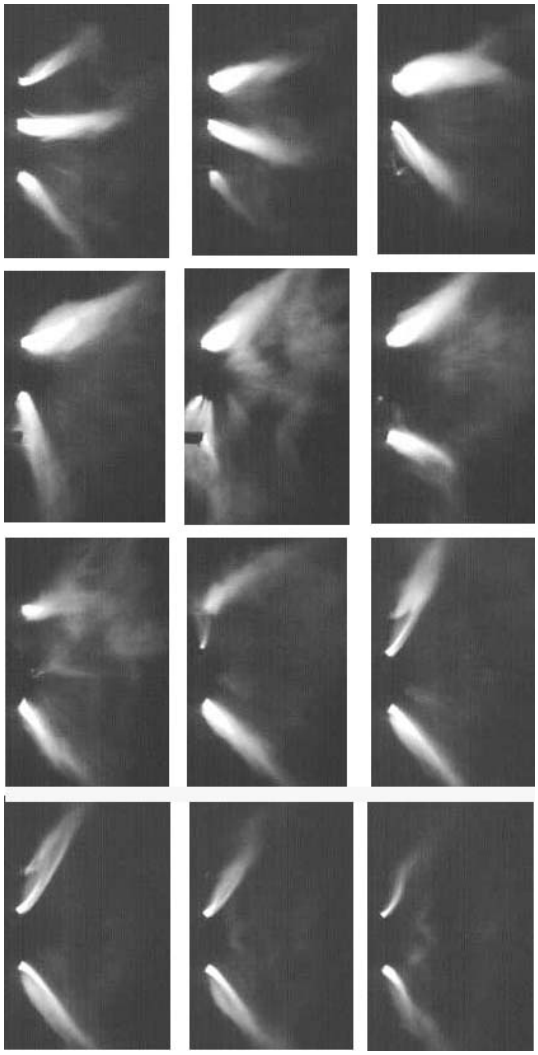

Figure 7 High speed images for test 8047_012, 20.800A rms - just prior to interruption.

Note that far more detail can be seen in the moving images of these records a selection of which will be presented during the conference proceedings.

4.3 Image analysis

Stokes and Oppenlander [13] used high speed film methods to record arc detail with opposed electrodes. These techniques while excellent for colour image visualisation are notoriously difficult when seeking quantitative photometric detail. The Motion Pro CCD based camera has a very nearly linear response which requires absolute calibration for a very limited range of photometric values.

Advantage has been taken here of this feature to provide estimates of the absolute luminosity of the arc development as a function of time and the decay time constant of various features as the arcing process continues. These have been given in terms of the standard luminous variable, the lux, figure 8. As a reference, a bright summer day will have a midday ground level illumination of the order of

20,000 lux. The brightest measurement in the arc column shown in figure 8 is some three orders of magnitude brighter than bright sunlight. This data tracks the brightness of a plasma element from its creation in the plasma flare to its eventual disappearance as the element moves through the arc space. The data has been obtained by detailed examination of individual high speed images using Adobe Photoshop methods to quantify the photometric values. Data marked 'Photoshop' have been measured directly from the images while data marked 'Lux' were calculated from the brightest part of the image, assuming an exponential decay with fitted time constants. These luminous decay time constants are shown in figure 9.

It will be apparent from the results given in figure 9 and from the arc flare images of figure 7 that the brightest parts of the arc have a very short lifetime, typically less than a millisecond.

It is well known that arcs burning on non-refractory electrodes such as copper and aluminium have interfaces with the electrode tips that produce highly concentrated cathode and anode 'spots' from which are driven powerful convective plasma flow, or jets, Maecker, in [8].

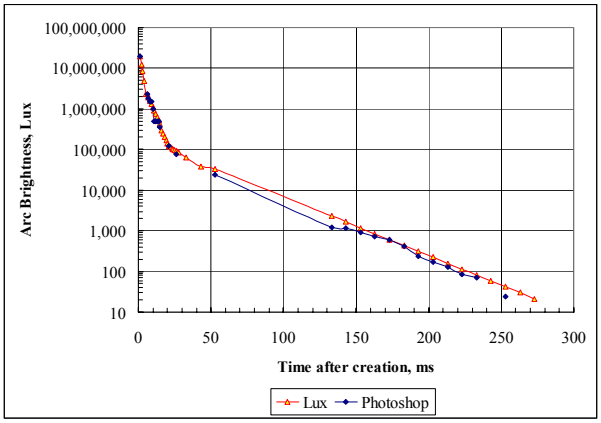

Figure 8 Photometric data for test 7977_007, arc current 20,000A rms.

As the plasma flow carries away arc heated gases they cool rapidly at first but then far more slowly as the plasma cloud brightness reaches values closer to a high temperature combustion flame, corresponding with the images shown in figures 4 and 5.

Lux data are based on a luminous parameter which depends on the colour of the radiant power. At the peak sensitivity of the eye there are 680 lumens/radiant-watt. Using this value a calculation has been made of the equivalent radiant power and, from the Stefan-Boltzmann law, the corresponding peak plasma temperature. For an effective emissivity of 0.15 the plasma temperatures calculated are shown in figure 10. For effective emissivities of 0.1 and 0.05 the peak plasma temperatures would be 15,100K and 18,000K respectively. Both values are regarded as too high for an open air unconstricted arc.

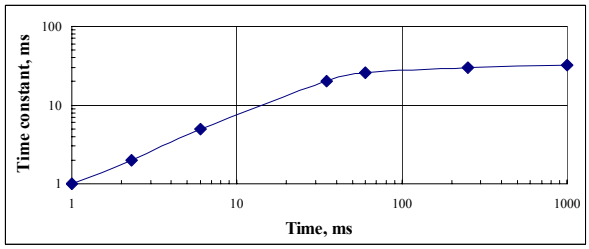

Figure 9 Luminous decay time constant as a function of time after plasma element creation.

Conversely if one takes an emissivity of 1.0, the value required by the assumptions of the standard IEEE 1584 the corresponding peak temperature would be less than 9000K. Maecker, in [8] has shown that even for a confined 5mm diameter nitrogen arc such a temperature would be reached with an arc current of less than 20A compared with the 20,000A used for the test from which the results in figures 6 to 10 were obtained.

4.4.2 Arc Plasma

The surrounding plasma cloud, even though brilliant to the eye and much larger in total volume than the key radiating zone, has a lifetime of less than a second and contributes very little to the total radiant power loss. It does however contain the majority of the arc energy and, from calorimetric measurements, is likely to produce the most severe burn injuries.

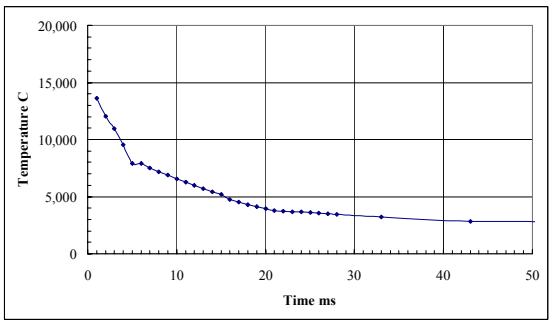

Figure 10 Plasma temperatures as a function of time after creation.

The authors do not say that burns produced alone by radiant heating are not important. They are! However, radiant heating is only a small fraction of the heat balance for almost all electric arcs, even those designed for illumination purposes, [12]. Rather, most arc dissipation, especially for open air arcs is consumed by the creation of a very substantial and extremely hot plasma cloud (~ 3000K).

4.4.3 Consequential Physical Damage

Electric power engineers have known of the damage that is caused by such plasma clouds for over 50 years. Arcs can burn in confined spaces, such as switch boards, switch rooms and gas insulated spaces. A most important consideration is the explosive air pressure rise that can result. For many years switchboards and switch rooms have been explicitly vented so as to direct arc plasma away from doors and access panels to protect workers from severe mechanical impact damage. GIS enclosures have been explicitly designed to withstand the maximum pressure rise that might result from a credible arcing fault. If arcs produced only radiant heating almost none of this design complication would be necessary!

The video evidence referred to above should provide convincing and quantitative confirmation of the importance of such bulk air heating and lay to rest the fiction, [9], that arcs are small spherical objects that only radiate their electrically dissipated power!

4.4.4 Arc Reignition

At every current zero, the arc must reignite and form a new cathode on the other electrode. Intuitively one would expect that if the arc does reignite it will do so through the shortest available path. For the tests at 5000V, reignition was always observed, but not by the shortest available path. The sequence of high speed video images shows clearly that reignition will follow the much longer conducting path of the current channel just before current zero even if more than an additional 100mm over the shortest possible path.

In high voltage circuits, the arc restrikes rapidly and the current normally continues to flow until the protection operates. The actual fault current is also generally a close approximation of the prospective fault current, unless current limiting devices such as HV fuses are present.

It was noted above that an empirical observation from the current-voltage records obtained here was clear self extinction for low voltage (240 and 415V) three phase arcs even for electrode spacings as little as 5mm and prospective currents as high as 70,000A rms. There are two underlying physical principles that have a bearing on this process.

The first is the 'de-ion' phenomena, [4] and [6] which occurs whenever the current passes through zero and is a principle used in almost all low voltage circuit breakers. For non-refractory electrodes including copper and aluminium a space charge region develops around the new cathode that requires a 'glow to arc' transition involving sheath voltages of the order of 300V before a low voltage arc cathode can be formed. If the recovery voltage does not rise rapidly enough to this value, no new arc can form and the current will be interrupted.

The second influence, on low voltage systems, is the influence of the arc voltage on both the amplitude and phase angle of the fault current. The arc voltage is higher than would be predicted from electrode spacing, due to the long arcing path lengths which can be seen in figure 7 and often exceed 300mm in total length regardless of the actual electrode separation (even if as small as 5 mm). Typical arc voltages of several hundreds of volts are involved and these act to reduce the actual arcing current, sometimes to less than half the prospective value.

The arc voltage also brings the current more in phase with the system voltage, so reducing the recovery voltage available to reignite the arc at current zero.

In low voltage systems, with small creepage paths across the insulation between phases and earth, the insulation degraded by the arcing process has been observed to breakdown under normal voltage stress. In low voltage circuits, these processes have been observed to produce repeated pulses of self-interrupted arcing followed by delayed flashovers.

5. Conference Images

During the conference a series of video sequences, will be shown that graphically illustrate, and expand upon the points made in this paper.

6. Discussion and Conclusions

Whilst the results given here are sufficient to demonstrate the fundamental weakness of IEEE 1584 the authors are keenly aware that much more experimental work will be required to properly quantify the full range and extent of burn hazards to which electrical workers may be exposed and the accurate description of such hazards by equations such as (1) to (4) which must, presently, be regarded as first approximations.

For example, during the conference proceedings it will be shown that low voltage system protection can be required to operate with repeated pulses of current, which are significantly smaller than the prospective fault current with considerable delays between the pulses.

The authors observe that digital relays are available that reset rapidly when the current returns below the reset level. These relays can completely miss faults of the kind described above unless an individual episode of arcing lasts long enough to cause a trip. Special care is therefore required in selecting digital relays with algorithms that can tolerate this form of fault current for low voltage systems.

Mechanical disc relays can wind back during the current pauses and fail to trip when the effective integral of the fault current and duration should have resulted in a trip. This became apparent in separate tests, which were not part of the present series.

A sequence will be shown where brief, self interrupted, arcing periods were followed by longer dormant intervals. The particular test sequence to be shown continued for some 16 seconds. Relay tests with the recorded current confirmed that the protection would not trip. The test was manually disconnected but not before the entire local area of the switchboard frame had reached incandescence. In the working situation which this test was aimed at understanding, an electrical worker lost his life.

Fuses have not yet been tested with this form of current, but the authors anticipate the melting time of HRC fuse elements will not be increased to the same extent as relays. On low voltage systems, the fuse arc in series with the fault arc should decrease the time between fusing and clearing. It is not anticipated high voltage fuses will see this form of pulsating current.

7. References

[1] H. Davy, Journal of the Royal Institution, 1802

[2] H. Ayrton, "The Electric Arc," The Electrician Series, D. Van Nostrand Company, Inc., New York, 1902

[3] J. S. Townsend: "Electricity in Gases," Oxford University Press, New York, 1914

[4] J. Slepian: "Conduction of Electricity in Gases," Westinghouse Electric and Manufacturing Co., 1933

[5] E. L. E. Wheatcroft: "Gaseous Electrical Conductors," Oxford University Press, New York, 1938

[6] J. D. Cobine: "Gaseous Conductors" Dover, 1958

[7] J. M. Somerville: "The Electric Arc" Methuen, 1959

[8] S. C. Haydon "Discharge and Plasma Physics" University of New England Press, 1964

[9] Lee, R., "The other electrical hazard: electrical arc blast burns," IEEE Transactions on Industry Applications, vol 1A-18. no. 3, p. 246, ,May/June ,1982

[10] R. H. Lee, "The shattering effect of lightning-pressure from heating of air by stroke current," IEEE Transactions on Industry Applications, vol. IA-22, pp. 416–419, 1986

[11] Lee, R. and Dunki-Jacobs, J. R., "Pressures developed by arcs," IEEE Transactions on Industry Applications, vol 1A-23, pp. 760–764, 1987

[12] G. R. Jones "High pressure arcs in industrial devices", Cambridge University Press, ,1988

[13] A. D. Stokes and W. T. Openlander "The Electric Arc in Open Air" Journal of Physics D, 1991

[14] Jamil, S., Jones, R. A., McClung, L. B., "Arc and flash burn hazards at various levels of an electrical system," Petroleum and Chemical Industry Conference, Industry Applications Society 42nd Annual, Denver, CO, pp. 317–325, ,Sept. ,1995

[15] Standard for Electrical Safety Requirements for Employee Workplaces, NFPA 70E, , 1995

[16] M. Capelli-Schellpfeffer, M. Toner, R. C. Lee, and R. D. Astumian, "Advances in the evaluation and treatment of electrical and thermal injury emergencies," IEEE Transactions on Industry Applications, vol. 31, pp. 1147–1152, ,Sept./Oct. ,1995

[17] Deaton, R. and Gostic, J. M., "Installation and operational considerations of arc resistant switchgear," Petroleum and Chemical Industry Conference, Industry Applications Society 43rd Annual, Philadelphia, PA, pp. 307–313, ,Sept. ,1996

[18] Heberlein, G. E., Jr., Higgins, J. A., and Epperly, R. A., "Report on enclosure internal arcing tests," IEEE Industry Applications Magazine, vol. 2, no. 3, pp. 35–42, ,May/June ,1996

[19] Neal, T. E., Bingham, A. H., and Doughty, R. L., "Protective clothing guidelines for electric arc exposure," Petroleum and Chemical Industry Conference, Industry Applications Society 43rd Annual, Philadelphia, PA, pp. 281–298, ,Sept. ,1996

[20] M. Capelli-Schellpfeffer, R. C. Lee, M. Toner, and K. R. Diller, "Correlation between electrical accident parameters and ssustained injury," presented at the 43rd Annual IEEE Petroleum and Chemical Industry Technical Conference, Philadelphia, PA, Paper PCIC-96-35., 1996

[21] T. E. Neal, A. H. Bingham, and R. L. Doughty, "Protective clothing guidelines for electric arc exposure," presented at the 43rd Annual IEEE Petroleum and Chemical Industry Technical Conference, Philadelphia, PA, Paper PCIC-96-34., 1996

[22] R. Deaton and J. M. Gostic, "Installation and operational considerations of arc-resistant switchgear," presented at the 43rd Annual IEEE Petroleum and Chemical Industry Technical Conference, Philadelphia, PA, Paper PCIC-96-36, 1996

[23] G. E. Heberlein, J. A. Higgins, and R. A. Epperly, "Report on enclosure internal arc tests," IEEE Industry Applications Magazine., vol. 2, pp. 35–42, Jan./Feb., 1996

[24] Doughty, R. L., Neal, T. E., Dear, T. A., and Bingham, A. H.,"Testing update on protective clothing and equipment for electric arc exposure," Petroleum and Chemical Industry Conference, Industry Applications Society 44th Annual, Banff, Alta., Canada, pp. 323–336, Sept. ,1997

[25] Jones, R. A., Liggett, D. P., Capelli-Schellpfeffer, M., Macalady, T., Saunders, L. F., Downey, R. E., McClung, L. B., Smith, A., Jamil, S., and Saporita, V. J., "Staged tests increase awareness of arc-flash hazards in electrical equipment," Petroleum and Chemical Industry Conference, Industry Applications Society 44th Annual, Banff, Alta., Canada, pp. 313–322, Sept., 1997

[26] Jones, R. A., Liggett, D. P., Capelli-Schellpfeffer, M., Macalady, T., Saunders, L. F., Downey, R. E., McClung, L. B., Smith, A., Jamil, S., and Saporita, V. J., Video plus CD ROM, "Arc flash hazards in electrical equipment," Prepared during laboratory testing in support of "Staged tests increase awareness of arc-flash hazards in electrical equipment," Petroleum and Chemical Industry Conference, Industry Applications Society 44th Annual, Banff, Alta., Canada, pp. 313–322, Sept. ,1997

[27] S. Jamil, R. A. Jones, and L. B. McClung, "Arc and flash burn hazards at various levels of an electrical system," IEEE Transactions on Industry Applications, vol. 33, pp. 359–366, Mar./Apr., 1997

[28] Doughty, R. L., Neal, T. E., Macalady, T., Saporita, V., and Borgwald, K., "The use of low voltage current limiting fuses to reduce arc flash energy," Petroleum and Chemical Industry Conference, Industry Applications Society 46th Annual, San Diego, CA, pp. 371–380, Sept., 1999

[29] Doughty, R. L., Neal, T. E., and Floyd, H. L., "Predicting incident energy to better manage the electric arc hazard on 600-V power distribution systems," IEEE Transactions on Industry Applications, vol. 36, no. 1, pp. 257–269, Jan./Feb., 2000

[30] SFPE Engineering Guide to Predicting First and Second Degree Skin Burns, Society of Fire Protection Engineers Task Group on Engineering Practices, 2000

[31] Crnko, T. and Dyrnes, S., "Arcing fault hazards and safety suggestions for design and maintenance," IEEE Industry Applications Magazine, vol. 7, no. 3, pp. 23–32, May/June, 2001

[32] Porcaro, C. R. and Porcaro, P., "Windows-based rapid and precise electrical power systems calculations," Petroleum and Chemical Industry Conference, Industry Applications Society 48th Annual, Toronto, Ont., Canada, pp. 119–138, ,Sept. ,2001

[33] Gregory, G. D., Lyttle, I., and Wellman, C. M., "Arc flash energy limitations using low-voltage circuit breakers," Petroleum and Chemical Industry Conference, Industry Applications Society 49th Annual, New Orleans, LA, ,Sept. ,2002

[34] IEEE Standard 1584, "Guide for Performing Arc-Flash Hazard Calculations", sponsored by the Petroleum and Chemical Industry Committee, September 2002

INFLUENCE OF LOAD CURRENT ON THE OPERATING CHARACTERISTIC OF FUSES

L. Cinnirella (°), G. Farina (°), C. Ruffino(°), A. Sironi(*), M. Tartaglia(°°)
(°) Istituto Elettrotecnico Nazionale G. Ferraris, Torino, Italy
(*) AEM S.p.A., Milano, Italy
(°°) Dipartimento Ingegneria Elettrica Industriale, Politecnico di Torino, Italy

Abstract*:* Aim of the paper is to determine the influence of the initial thermal conditions of the fuse element on the operating time and the let trough energy of fuses. An experimental investigation on two types of fuses has been performed starting from different thermal steady state conditions and in particular the cases of no load current and fuse rated currents are compared by evaluating pre-arcing and time-current characteristics for fuses rated 125 and 250 A. The effects of making angle for different prospective currents on operating characteristics are evaluated and final comments are given on possible influence on the selectivity of the intervention in case of fault.

I. INTRODUCTION

Operating characteristics of low voltage fuses are usually determined by laboratory tests starting with the fuse element at ambient temperature. In practice complex loading cycles can vary over a wide range [1] when the over current begins. Aim of the paper is to evaluate the influence of the initial thermal conditions of the fuse element on the operating time and let trough energy of the fuses, that are expected lower than the value obtained with a test without load current. In fact, as it was shown in [2], pre-arcing Joule integral is influenced by test current amplitude and making angle which modify the heating process of the fuse element and its behaviour. A significant influence is also expected by initial thermal conditions that means initial loading current.

To this end an experimental investigation has been performed on two different types of fuses (125 and 250 A rated currents) starting with thermal steady state conditions obtained by loading the fuse with its rated current and without current before the beginning of the short-circuit.

The test circuit has been arranged in order:

- to get a known preliminary heating (that means a initial known load current);
- to maintain initial thermal state;
- to state a short circuit condition by a suitable making angle.

It is essential to avoid absence of current trough the fuse during the transition from the rated load current to the one of fault in order to ensure repetitive test conditions, because the thermal behaviour of fuse elements quickly modifies when the current flowing changes. The case of an electrical distribution system will be analysed. Fuses usually employed in substations, with rated current of 125 and 250 A, are investigated in order to verify the effects on the operating characteristic and the influence on the selectivity of the intervention in case of fault. The power distribution system, used by AEM in Milan (Italy) and in 14 smaller towns of the surrounding area, can be split into typical radial structures which includes one transformer supplying some primary lines with secondary branches for users protected by fuses.

The test circuit is detailed in section II and the experimental results are discussed in section III. The practical consequences of the present investigation on fuse behaviour and on protection selectivity are discussed. Section IV gives final conclusions.

II. EXPERIMENTAL ANALYSIS

II.1 Test Circuit

The test circuit is represented in Fig. 1. The fuse under test is loaded by its initial load current (the rated current in our cases) until the steady state condition is reached. This is done by means of a low voltage transformer. A measure of the fuse temperature by a thermocouple placed on the fuse body verifies that the steady state condition is actually achieved. After this initial fuse heating the supply circuit is commutated from the low voltage source (less than 12 V at 50 Hz) to the test voltage (420 V at 50 Hz) by opening the contactor C_1 and immediately closing the contactor C_2.

In these conditions the fuse continues to be loaded by its rated current. The current amplitude is controlled both by the impedance Z (adjusted for the short circuit current) and by a resistor R_2 suitable to obtain the rated current of the fuse in the circuit.

After a time of about 20 seconds, sufficient to recover the thermal steady state conditions of the fuse, altered by the commutation operation, the resistor R_2 is short-circuited by an electronic device which makes the short circuit current. The making instant of the short circuit test, from which the fuse interruption behaviour depends [2], is varied at each test in order to verify the behaviour of the fuse in all closing conditions. By means of a data acquisition system the test current and the supply voltage are recorded and the main test quantities are evaluated.

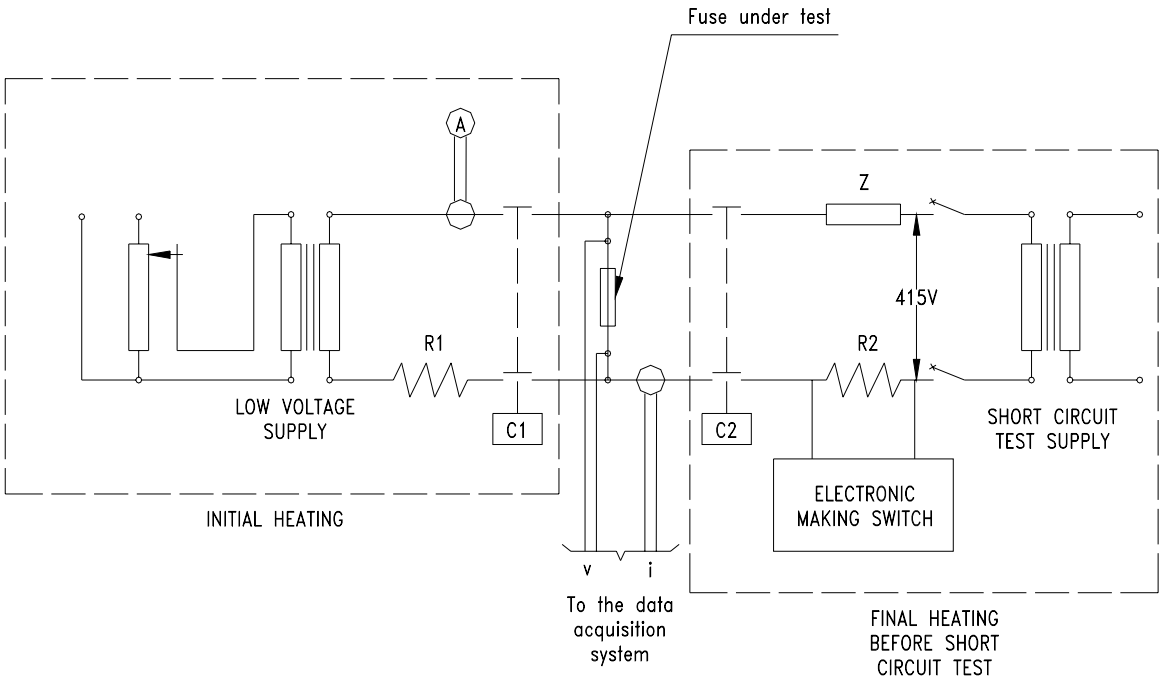

Fig. 1 Test circuit

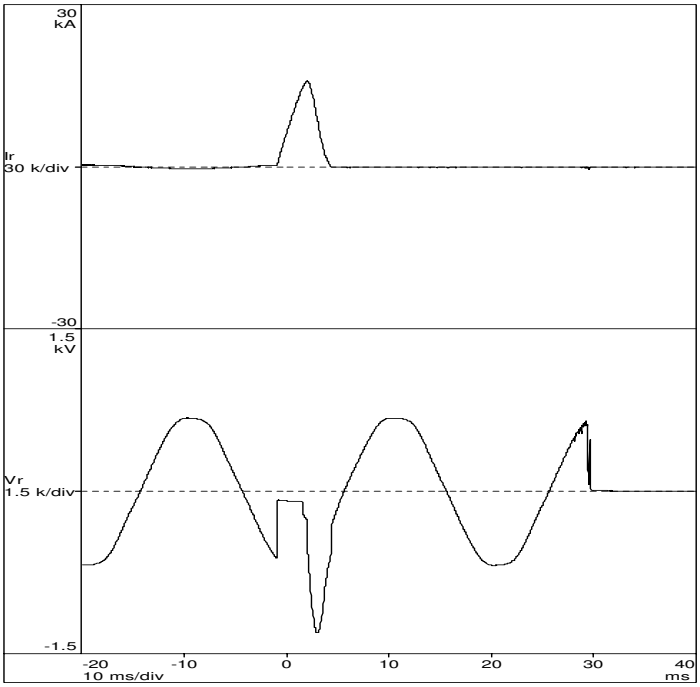

Max peak current	15,92 kA
Prearc time	2,48 ms
Total duration	5,30 ms
I^2i prearc	193,0 kA^2s
I^2total	506,3 kA^2s

Fig. 2 Currents and voltages on a hot 250 A fuse tested at 15 kA.

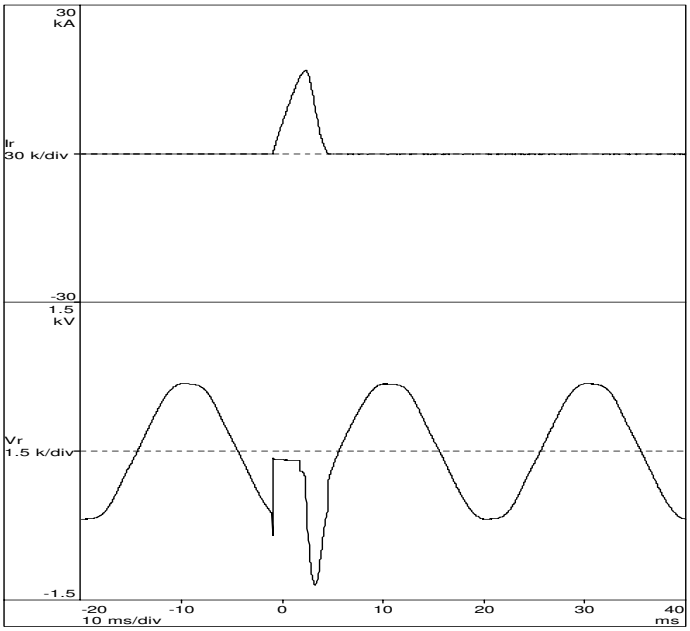

Max peak current	16,94 kA
Prearc time	2,66 ms
Total duration	5,52 ms
I²i prearc	277,9 kA²s
I²total	608,2 kA²s

Fig. 3 Currents and voltages on a cold 250 A fuse tested at 15 kA.

The tests have been repeated also without the pre-heating of the fuse before the short-circuit test. In these cases the contactor C_2 is always kept closed and the resistor R_2 is excluded from the test circuit.

II.2 Test conditions

The analysis has been applied to fuse types most frequently used by AEM in the distribution network of Milan. In particular two values of rated currents are considered: 250 A and 125 A. Usually fuses having 250 A protect main low voltage distribution lines and these lines frequently supply secondary lines with 125 A fuses at their starting points. The fault current examined have been 5, 10 e 15 kA with a power factor equal to 0,2.

The initial load conditions compared are the case of rated current and the one of no load . The fuse behaviour is analysed by recording test current and voltage and evaluating pre-arcing, total Joule integrals and arc energy.

III. RESULTS

Some typical test results are reported in Fig. 2 and 3. In particular Fig. 2 shows fuse voltage and currents for the 250 A fuse tested at 15 kA with initial load current equal to the fuse rated current; approximately 1 h is needed to reach the thermal steady state.

Fig. 3 includes plots of current and voltage of a fuse tested at 15 kA when the short circuit test starts without initial load and with the fuse at ambient temperature.

The recorded voltage is the supply one.

Of course some differences are found in waveforms of currents and voltages because of the effects of initial load on the pre-arcing and total Joule integral. As well known and justified in [2] pre-arcing and total Joule integral are influenced by making angle which modifies current waveform and this effect is more evident in the cases of relatively low short circuit currents.

This phenomenon, during the pre-arcing time, seems due mainly to the thermal conduction along fuse element and fuse terminals, being very low the heat transferred to the sand for short time as those we are considering. Therefore the initial load modifies the initial thermal state of fuse elements and it causes a reduction of pre-arcing Joule integral. As a consequence of the different starting instant of the arc, also arcing and consequently total Joule integrals change.

The results are reported in the following figures 4, 5, 6, 7, 8 and 9 which report the results obtained for the two sizes of fuses with 3 values of short circuit current.

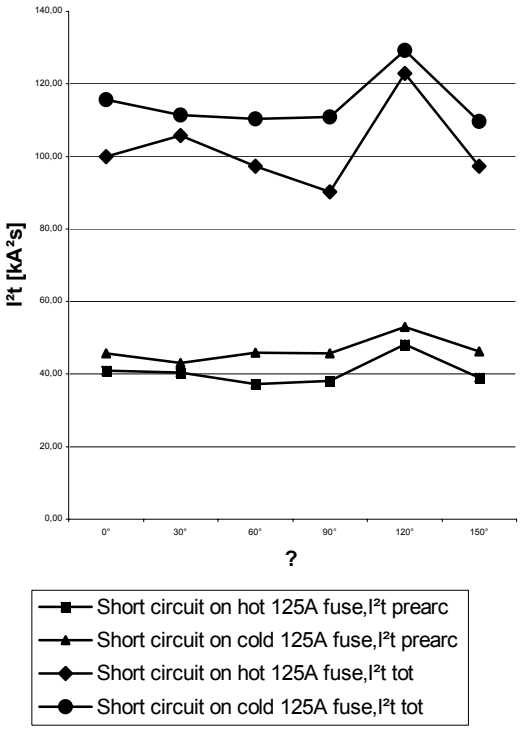

Fig. 4 Joule integrals for a 125 A fuse at 5 kA

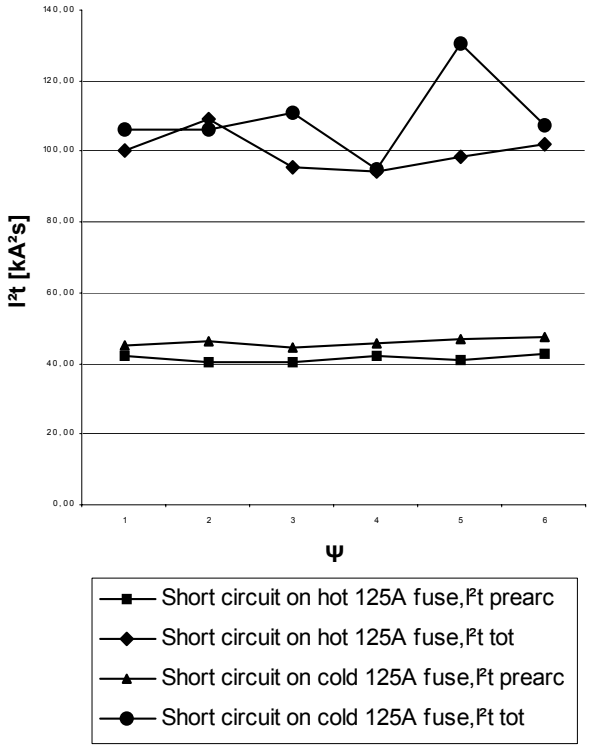

Fig. 5 Joule integrals for a 125 A fuse at 10 kA

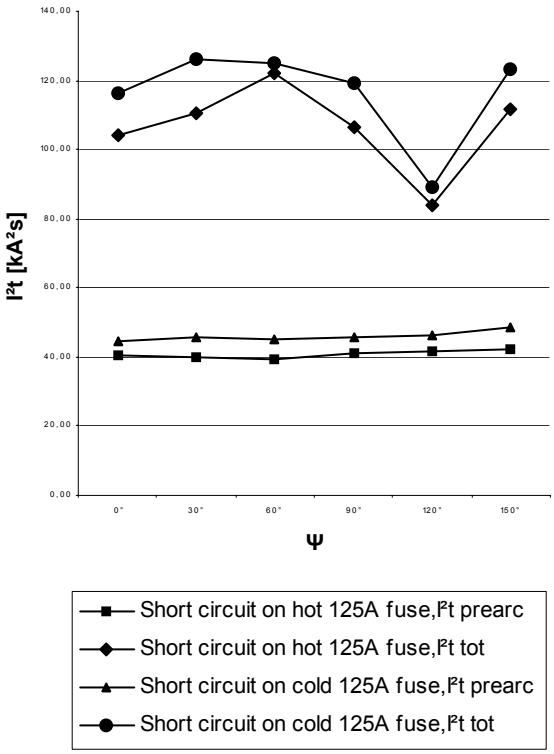

Fig. 6 Joule integrals for a 125 A fuse at 15 kA

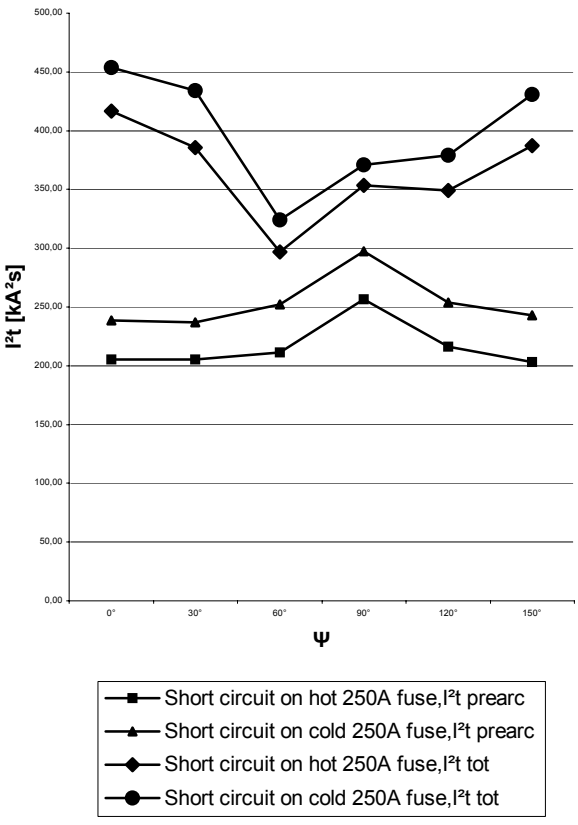

Fig. 7 Joule integrals for a 250 A fuse at 5 kA

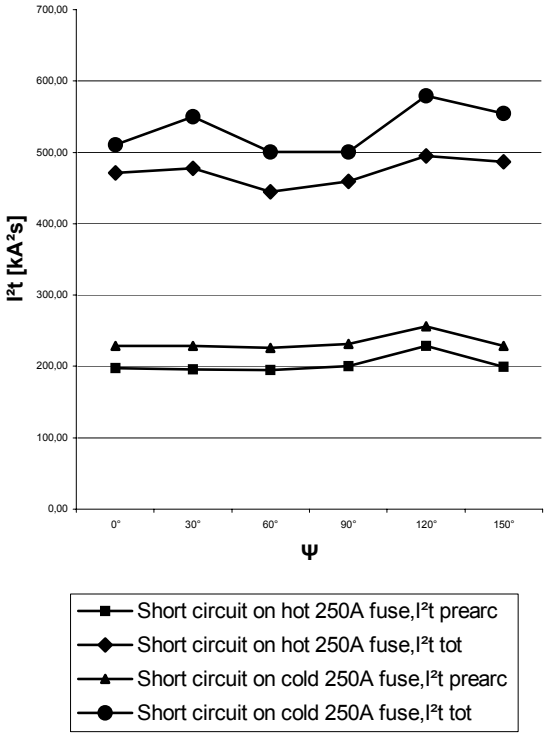

Fig. 8 Joule integrals for a 250 A fuse at 10 kA

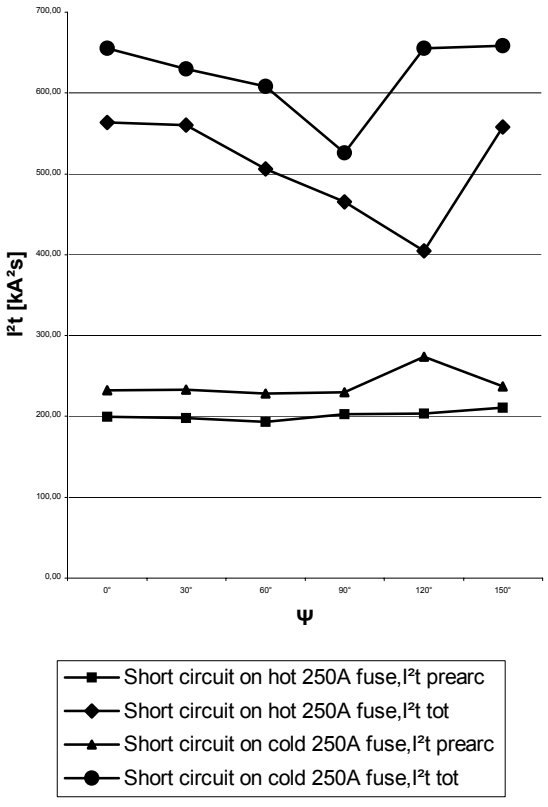

Fig. 9 Joule integrals for a 250 A fuse at 15 kA

The experimental results point out the differences on the operating characteristics due to the initial thermal state of the fuse. These differences consist in a reduction of the Joule integral with an initial load which are found in the order of 10% for all tests.

IV. CONCLUSIONS

In this paper the effects on an initial load current on the operating characteristics of fuses have been experimentally investigated. As expected the effects of an initial load give a reduction of pre-arcing and total Joule integral. However these reductions seem to be relatively weak because their amplitude (about 10%) lays within the uncertainty of an industrial product. Moreover, the effect is a reduction of specific energy let-through in the protected circuit that means a reduction of circuit thermal and mechanical stresses. In conclusion, for the limited selection of fuse analyzed, one can use the operating characteristics obtained on fuses without any initial load current and the results are approximated according a small security factor because of the actual values found when an initial condition is considered.

REFERENCES

[1] R. Wilkins, H.C.Cline, "*Assessment of complex loading cycles and estimation of fuse*-life", VI ICEFA Conference, Torino, 20-22 September 1999, pp. 141-144.

[2] O. Bottauscio, G. Crotti, G. Farina, "*Non adiabatic process in fuse elements with heavy current faults*", IV ICEFA Conference, Nottingham, 23-25 September 1991, pp.151-155.

[3] IEC Standard 60269-1 (1998-12) "*Low voltage fuses – Part 1: General requirements*".

[4] IEC Standard 60909 (1992-09) "*Short-circuit current calculations in three-phase ac systems*".

CURRENT DIVERSION AROUND A FRAGMENTING WIRE DURING THE VOLTAGE SPIKE ASSOCIATED WITH EXPLODING WIRES

Michael J Taylor

QinetiQ, Gun Propulsion Technology, Bldg H7, Fort Halstead, Sevenoaks, Kent, TN14 7BP, United Kingdom. mjtaylor4@qinetiq.com

Abstract

This paper explores the physical processes that occur during the electrical explosion of fuse wires, particularly the voltage spike that occurs shortly after the wire melts in high-inductance circuits. The observations show that the physics is similar for a range of experimental parameters, discussed in detail. It would appear that the wire heats up and melts homogeneously. Following this, radiant plasma (with a brightness temperature of around 16 000 K in higher powered tests) is observed to form in a spot-like fashion along the length of the wire. The spots develop longitudinally along the wire length, merging to form a continuous plasma column. A dramatic increase in the electrical resistance of the exploding wire accompanies the plasma development, giving rise to the voltage spike. The rise in resistance is found directly proportional to the total length of the plasma column. X-radiography shows that, shrouded by the plasma, condensed wire fragments, with lengths of several centimetres, remain. This, and other evidence, indicates that current is diverted around the seemingly lower resistance fragments, preferring the plasma (flashover). An hypothesis is given to explain this phenomena.

Keywords: Exploding fuse wires, current diversion, flashover, copper vapour electrical conductivity

1. Introduction

The electrical explosion of metallic conductors (fuse wires) has been studied at QinetiQ for the purposes of understanding the generation of metallic plasma for the UK MoD electrothermal-chemical (ETC) gun programme. An understanding of the physical processes occurring during the electrical explosion is essential to allow predictive modelling of plasma generator operation.

Fuse wires studied were typically copper, with diameters of 0.5 to 1.0 mm and length in excess of 100 mm. In this work, one module was used of a ten module, 500 kJ, 800 μF crow-barred capacitor based pulse forming network [1] with circuit inductance ranging from 26 μH to 800 μH. Charge voltages varied but all were less than 22 kV. The relatively high circuit inductance typically gave discharge durations from 2 to 10 ms. Peak currents were between around 10 and 36 kA. Current rise rates were between 20 and 200 MA s^{-1}, which is low, compared to many other exploding wire studies. The inductance also ensures that current continually flows with no current 'dwell' much debated in earlier exploding wire work where circuit inductance was far lower [2]. The crow-bar diode fitted within the module ensures there is no current reversal.

2. Application

The idea of using electrical energy for gun propulsion is almost as old as the discovery of the electromagnetic force. In 1844, the newly invented electric gun "SIVA" (The Destroyer) was claimed by a Mr Benningfield to be able to fire a continuous stream of balls at a rate of more than 2000 min^{-1} and kill at a distance greater than a mile [3]. Nothing much is known about the device or how it operated, but the concept is suggested used electrical energy to provide the propulsive force for driving projectiles in military applications.

Today, work is still progressing on a number of electric gun designs. The work reported within this paper was undertaken by QinetiQ on behalf of the UK MoD's effort for the ETC gun. The ETC gun utilises dense, non-ideal plasma for ignition and combustion control of otherwise conventional weapons [4]. The plasma propellant interaction is beneficial in terms of propellant ignition and combustion control [5, 6, 7, 8, 9]. The exploding wire studies described in this paper were undertaken in the context of developing capillary plasma generators (CPGs) for the ETC gun [10]. CPGs are typically polyethylene tubes in excess of 100 mm in length and 5 mm diameter, with a copper rear electrode and annular front electrode connected via a copper wire ranging in diameter form 0.5 to 1 mm [11]. It is the

metallic plasma, venting from the CPG, which is used for interaction with the energetic propellant.

Key to CPG development has been the generation of a computer model to simulate CPG operation [12]. The multi-species Eulerian hydrodynamics code currently supports a '1.5 dimensional' (1.5D) modular model called EDENET. This model has radial and axial components, which are executed separately but output from one component can be used as input to the other component. The physics of CPGs is strongly two dimensional (2D), with the physical properties having gradients both in the axial and radial direction. However, a fully 2D model would be expensive in computer processing time; the 1.5D approach allows simulations to be completed in a few hours on a conventional desk top personal computer. Each main model comprises a number of sub-models or sub-routines responsible for different sub-systems within the CPG, including an exploding wire sub-routine. The equation of state for copper utilised by the model is Cu_3 from the SESAME database (Los Alamos National Laboratory, USA). These are supplemented with transport data (electrical conductivity) from experimentally validated [13] work by Desjarlais [14]. The exploding wire studies discussed within this paper are similar to those used to initiate plasma within a CPG, and CPG operation will depend upon the mode of wire vaporisation. The predicted mass and energy flux venting from the device will be strongly influenced by initial plasma conditions following the wire explosion phase.

Much effort has gone into the study of the plasma venting from the CPG. A tentative experimental energy budget has been made for the CPG and venting plasma [11]. The main finding from this and other studies [15] was that radiation is prevented from interacting with the CPG components or propellant by an optically thick condensing vapour boundary layer. The thermal characteristics of this boundary layer are thought to play a central role in the electrothermal ignition of energetic materials in ETC experiments. The electrical properties of this boundary layer are also thought to play an important role in the wire explosion process. This is discussed in detail later.

The next three sections describe the electrical characteristics, and photographic and x-radiographic investigations into the wire explosion event.

3. Wire explosion studies – (i) electrical study

The wire explosion studies reported within this paper were conducted in an open air environment. Work has also been performed with confined wires and wires exploded within a pressurised environment (several tens of megapascals). The confinement and/or pressurisation is found to alter the properties of the plasma, but the initial wire explosion process, the subject of this paper, is largely unaffected.

Wires are contained between two copper electrodes in a semi-balanced field assembly to reduce the non-axial magnetic field produced by the supply cables, thus reducing the off-axis Lorentz forces on the current carrying material during the wire explosion process. Figure 1 shows a schematic of the assembly. The wires were attached in a number of different ways, including using tape to suspend the wires 2 mm from the electrodes. No significant difference in the mode of wire explosion was measured for any attachment method. Generally, the experimental copper wires were run through axial holes incorporated in the electrode design.

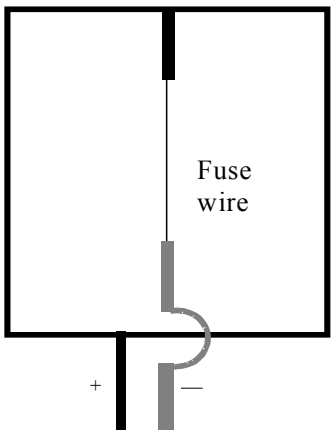

Fig. 1: Schematic of the semi-balanced field assembly used for open air exploding wire studies

Time resolved measurement of voltage across the wire was made using a calibrated 3000:1 voltage divider. Crocodile clips attached the terminals of the voltage divider directly to the wire ends in the case where the wire ran through the electrodes. These wire ends were found largely unaffected after the discharge, with the crocodile clips still firmly attached. Time resolved current flowing through the wire was deduced from measurement of the rate of change of current. This was achieved by use of a calibrated Rogowski coil around the electrical supply cables. From the time resolved voltage and current, the load resistance, discharged energy and power were deduced.

Figures 2 - 4 show the electrical data during ET165 Test 21: a 1 mm diameter, 175 mm long copper wire explosion in air, using the semi-balanced field assembly. The wire mass was 1.2 g. This was a relatively low powered test, utilising a single module fitted with the 800 μH inductor. Recorded peak current was around 10 kA and peak voltage was around 16 kV. Peak power was around 15 MW with total energy discharged being around 15 kJ. Peak rate of rise of current for this test was around 20 MA s^{-1}.

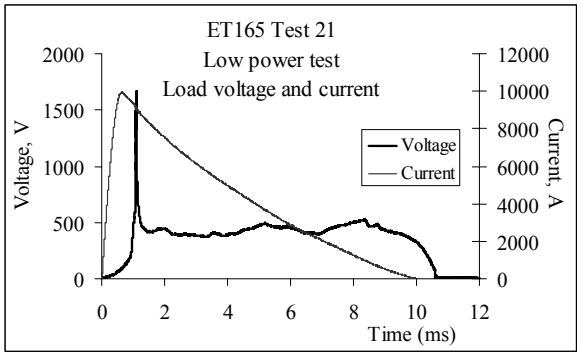

Fig. 2: Load voltage and current for low powered exploding wire in air test

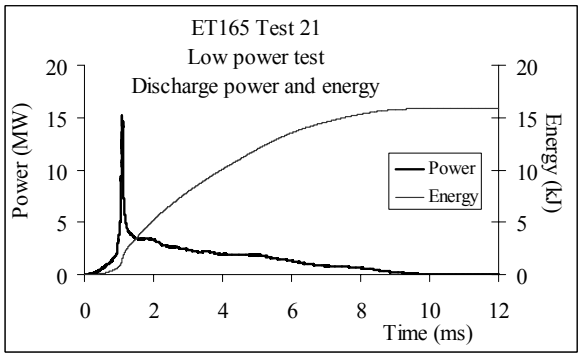

Fig. 3: Discharge power and energy for low powered exploding wire in air test

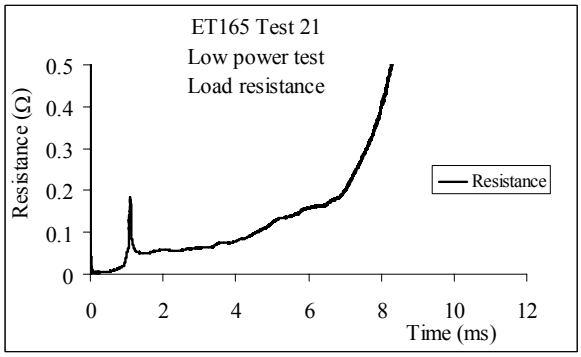

Fig. 4: Load resistance for low powered exploding wire in air test

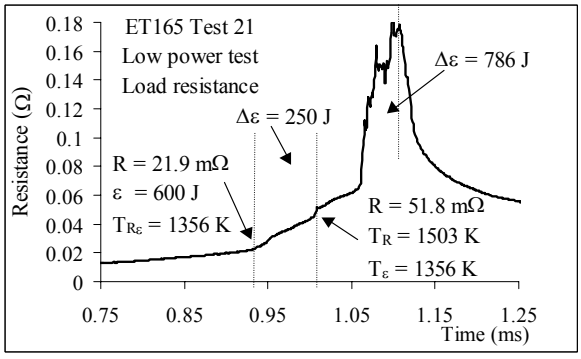

Fig. 5: Load resistance for low powered exploding wire in air test - detail of resistance spike

Several features, identifiable from Figures 2 – 5, are common to all the tests undertaken during these as well as many other similar exploding wire tests and are insensitive to the discharge power or experimental conditions (i.e. confinement or pressurisation). Initially, the resistance rise is smooth indicating an initial smooth heating period. Then, after two small discontinuities in the rate of rise in resistance, a sudden rise occurs. This can be seen shortly after 1 ms in this particular test. With the load current remaining reasonably constant during this period (more so for the high powered tests), this sharp rise in resistance causes a rise in load voltage and thus a rise in discharge power. Following this, the load resistance decreases, giving the characteristic resistance *spike*, and levels out at a plateau value, here, of around 50 mΩ. The plateau value is found to be sensitive to experimental conditions and can be maintained with the discharge of additional capacitor modules. However, as the available supply of power reduces, the load resistance increases towards open circuit conditions.

The most interesting feature is the resistance spike. This has been known about for many years. In earlier exploding wire work where circuit inductance was far lower [2], the current ceased to flow and a much debated current 'dwell' occurred. During this dwell, the current (and power) was found to reduce to very low values before resuming after a short period. The increase in resistance leading to either the dwell or the voltage spike is associated with the formation of a plasma discharge (flashover). The formation of plasma during these tests is discussed in detail later.

Figure 5 shows a detail of the resistance *spike* period. In this example, the first small discontinuity in the rate of change of resistance starts at 0.935 ms. At this moment, the value of resistance, R is 21.9 mΩ and discharged energy, ε is 600 J. The wire temperature is calculated both from the resistivity, T_R and energy, T_ε and is informative in understanding the relevance of this discontinuity. Assuming uniform heating, both the resistance [16] and energy indicate the wire to be at the melting point of 1356 K. Additionally, the wire is in the solid phase, showing that this feature is associated with the start of wire melt. This agrees with other findings that the onset of melting can be identified to a reasonable degree of accuracy on the resistance trace as a small ramp as the solid to liquid phase change occurs [17].

The resistance increases until at 1.013 ms when a second small discontinuity in the rate of change of resistance occurs. 250 J of additional electrical energy, Δε was discharged after the start of melt during this period. This is exactly the amount of energy required to melt the wire. However, the resistance is higher than might be expected from the molten wire at this temperature [18], and indicates that the wire temperature, T_R is more than 1500 K.

However, this temperature is based upon the assumption of homogenous heating, which may no longer be valid and/or the wire may no longer be continuous. Both explanations are supported from evidence discussed in the next sections.

The resistance spike occurs shortly after the second small discontinuity in the rate of change of resistance. The spike could be mistaken for wire vaporisation, but consideration of the energy shows this not to be so. The additional energy following the end of melt until the peak in resistance is 786 J. Assuming no heat loss and no bulk heating of the wire, this is enough to vaporise a maximum mass of 0.13 g of copper, around 10% of the total. Hence, 90% or so of the wire must still be in the solid phase close to the boiling point. High rates of radiative energy loss during this period indicate that the amount of vaporisation will be less than this.

4. Wire explosion studies – (ii) photographic study

Visual images captured by a digital gated 'Ultranac' fast framing camera of an unconfined exploding wire in air show that a radiant discharge (flashover) occurs. This is first observed at the electrodes and wire centre, and then at random locations along the wire in a spot fashion, as shown diagrammatically in Figure 6. Here, the plasma is represented by negative images acquired from an actual wire explosion, but the wire location (discussed in more detail below) is shown for indication only as the wire location cannot be seen on the photographic images. Homogenous heating of the wire no longer applies once flashover begins.

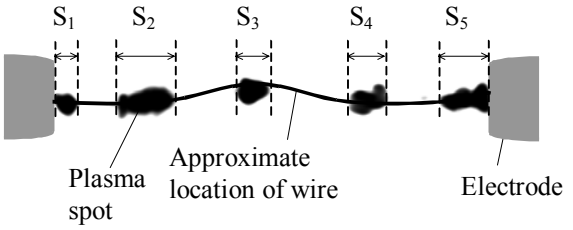

Fig. 6: Negative image of wire in air recorded prior to resistance peak in the visible with exposure time of 100 ns

The radiant emittance of the molten portion of the wire is low in comparison with the bright spots developing in the images. Spectra recorded from such spots [19] reveal that the radiant parts are from copper plasma, with a brightness and colour temperature of around 16 000 K for higher powered tests. The entire wire appears to be covered in radiant plasma at peak resistance.

The development of the plasma spots has been studied using photographic images. The development in the radial direction of the spots is characterised by a sudden expansion to between 5 and 12 mm, often followed by a pause and then a slower expansion to many tens of millimetres. Individual spots develop apparently in a random fashion, although this can be controlled to a certain extent with small nicks in the wire. For high powered discharges, the initial rate of expansion was greater than 1200 m s^{-1} followed by a slower expansion of around 400 m s^{-1}. For low power discharges, the expansion was dramatically slower (around 14 m s^{-1}) and the length of the pause considerable, although the spot diameter at the pause was similar. The pause at this spot diameter is thought to be due to a balance between spot temperature (resistivity), current and wire resistance.

With the axial development of individual spots, they tend to expand and coalesce at high velocities. The total length of the plasma (here called the shroud length) can be measured from the photographic images. This is shown in Figure 6 as the sum of the individual lengths of S_1 to S_5. The edges of the plasma spot boundaries are poorly defined, but the digital images allow an edge to be objectively determined within one pixel of error. Integrated axial expansion in this example was 13 km s^{-1}.

From measurement of the shroud length, it is evident that there is a strong relationship between this and the resistance of the wire/plasma system. Figure 7 shows the normalised shroud length along with the resistance (spike region) for a high powered test. Figure 8 shows that the relationship between the resistance and the coverage of the wire is linear (with an r^2 value of 0.9922).

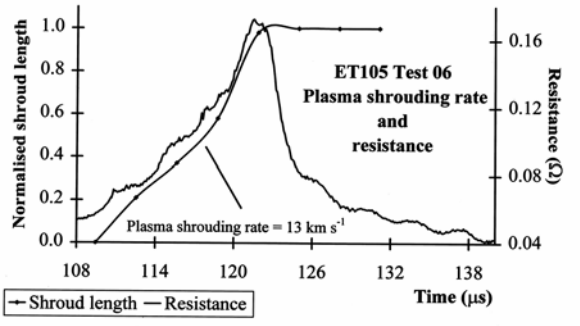

Fig. 7: Plasma shroud length versus resistance of exploding wire in air (high powered test)

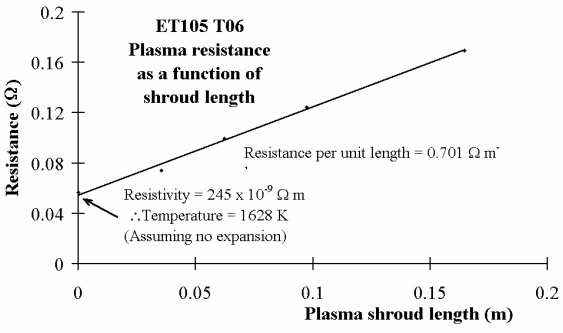

Fig. 8: Plasma shroud length versus resistance of exploding wire in air (low powered test)

The implication of the relationship between resistance and shroud length is that the rise in resistance of the wire/plasma system is associated with the plasma rather than with the unshrouded condensed portions of the wire. The temperature of the wire immediately prior to shrouding (of around 1628 K, given by the intercept in Figure 8 and assuming uniform heating), indicates that the wire temperature is below the boiling point (2840 K). Presumably, the unshrouded wire temperature does not increase much more, as this would lead to a non-linear relationship with shroud length.

The relationship shown in Figure 8 has been repeated for many tests, with a wide range of discharge powers. With the higher powered tests, the resistance and power profiles are very similar due to the current being reasonably constant for this period of the discharge. It could be argued from the results for the higher powered tests alone that it is the power (or indeed the voltage) that is proportional to the shroud length. For the low powered tests, the discharge power and resistance have very different profiles as the current changes over the 'wire explosion' period. The graphs of shroud length versus resistance derived from low powered tests indicate that the linearity between the two is maintained. No such relationship with power (or voltage) is maintained for these low powered tests.

Photographic evidence, together with the electrical considerations, suggests that at the peak in resistance the wire is largely in the condensed phase with plasma shrouding it. It is presumed from the linear relationship with shroud length and resistance that the electrical current is largely being conducted through this plasma. If it were not, then the linear relationship between resistance and shroud length, as well as the energy transfer processes required for the maintenance of the plasma temperature, would both need to be explained.

5. Wire explosion studies – (iii) x-radiographic study

To confirm the low condensed mass loss predicted during the wire explosion process from electrical considerations, and to gain further insight into the development of the condensed exploding wire material beneath the plasma sheath, pulsed x-radiological studies were performed. For these exploding 150 mm long, 1 mm diameter wire tests, around 14 kJ of energy was discharged in 0.7 ms, with a peak power of around 120 MW. The fast framing camera was again used to compare individual x-radiographs with photographs. Figure 9 shows six photograph and x-radiograph 'montages' and a further two photographs highlighting intermediate plasma development. The first image is a montage but not simultaneous, with the x-radiographs being captured a few microseconds prior to the photograph. The two images that follow are enhanced digital images taken 1 μs apart with an exposure time of 100 ns. The following five images are montages made from simultaneous x-radiographic and photographic images.

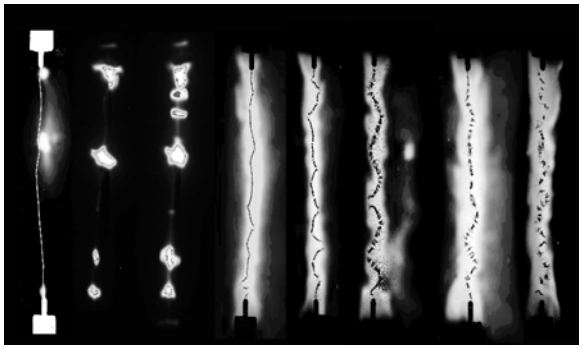

Fig. 9: Photographic and x-radiographic 'montages'

The x-radiographic work [20] indicates that condensed fragments of the wire, several centimetres long, exist for a period after the peak in resistance. This fragmentation is similar to that reported throughout earlier exploding wire studies [2] as well as more recent literature [21, 22]. Two fragmentation processes seem to be occurring: a coarse process that occurs before the peak in resistance, and a finer process that seems to occur after peak resistance. The resolution in these images for condensed copper has been determined to be around 100 μm, suggesting that the second process may have been underway before the peak in resistance if the initial breaks were less than 100 μm wide.

The coarse process fragments the wire into pieces several centimetres long. The origin of the breaks in the (initially undamaged) wire has been shown [20] to be associated with kinks established during the buckling of the wire. Measurement of the individual wire lengths shows that buckling is consistent with thermal expansion. It was originally thought that the longitudinal confinement of the wire by the electrodes was responsible. However, recent work [23] has shown that freely suspended wires also suffer similar buckling, demonstrating that the wire's own inertia is sufficient confinement. Excess heating at the kink locations leads to premature vaporisation at these sites. Further heating of these locations is thought to be radiative once covered in plasma; it has been shown [20] that the kink locations are coincident with the formation of plasma spots. The fine process fragments the wire into a random and increasing number of smaller pieces.

Other workers in this field often make no distinction between the coarse and fine structures. It has been suggested that thermally-induced stress or other wave phenomena cause the fragmentation, possibly while the wire is still in the solid phase [22, 24, 25]. Nasilowski first showed that it is possible for

the wire to fragment whilst still in the solid phase [26], repeated by Graneaue [21] and others, although the experimental conditions were somewhat different. Examination of the recovered wire showed little evidence of melting. Molokov and Allen [22] reports that, for current densities in the range 10^8 – 10^9 A m^{-2}, solid phase fragmentation due to thermal stress waves is likely to occur. Lukyanov and Molokov [27] go as far as to predict the number of fragments expected by this process. Current densities reported here are somewhat higher at peak current, but pass through the range quoted above while the wire is still solid. Whether there is sufficient time for solid phase fragmentation to occur is debatable. Work at QinetiQ is ongoing to determine if solid phase disintegration of the wire is occurring under these conditions by interrupting the current through the wire during mid-explosion.

Shvetsov *et al* [28], among others [2], suggest that the fine structure may be due to 'magnetohydrodynamic (MHD) instabilities of the necking type' [28]. Here, the current flowing through the molten wire acts to cause the metal to flow into a series of globules and necks [26], or reinforces a similar pre-existing structure [28]. Once established, material flows from the necks to the globules, giving the fine structure appearance shown in Figure 9.

Close inspection of the x-radiographs pre-peak resistance (Figure 10) shows no indication of necking associated with the MHD effect. Further, the finer structure first occurs at the kink location, once plasma spot development is well underway. What appears to be vapour bubbles (appearing as 'smoke-rings' [29] on the x-radiograph) can be seen. It is feasible that micro-fractures occurring in the solid phase seed the vapour sites, by introducing local thermal gradients within the solid wire.

However, a striated appearance is expected with simple boiling without the need for invoking solid phase micro-fractures, as the forming vapour bubble is free to expand radially but constrained longitudinally. The fine structure is being formed at the inner side of the kink as shown in Figure 10. The plasma might be expected to be hotter in the inside of the kink, causing that side of the wire to boil first. Several of the fragments show curvature at their ends, presumably caused by localised pressure developed during the vaporisation.

Another important finding from images such as those shown in Figure 9, is that condensed material remains essentially at the same location until it has all evaporated away. This indicates that the Lorentz forces associated with the buckled wire are insufficient to drive the condensed fragments from their axial position, adding weight to the argument that very little current is being conducted through the fragments. Lack of Lorentz forces is also cited in reference [29] and x-radiographic images clearly show it not to have any significant effect in reference [28]. Further, the confinement of the wire in a capillary [20] appears to make little difference to the physical mechanisms of the exploding wire.

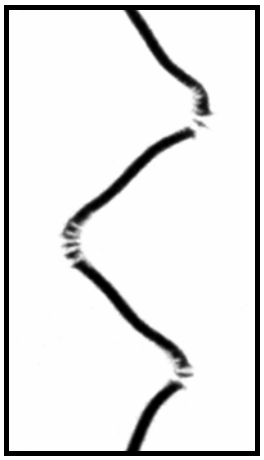

Fig. 10: Exploding wire in air magnified x-radiological image

6. Hypothesis for the diversion of current around condensed wire fragments

It has been argued above that current is being diverted around the condensed fragments of an electrically exploding wire (flashover) through the seemingly higher resistance plasma. This phenomenon is also reported on work conducted for the electric armour programme [29], for aircraft radome lightning segmented divertor strips [24, 30] and segmented strip ETC igniters [31]. Arguments are presented in [29] and [31] that the effect is essentially geometrical, limited to an aspect ratio of gaps and fragments of about unity. In the work described here, the fragment length is at least ten times that of the gap length. A physical mechanism that explains current diversion is still needed for these aspect ratios and the following argument attempts to provide one.

It is stated in [24] that the electrical conductivity of the metal vapour under exploding wire conditions was the most difficult part of the process to model. Recently published work by Desjarlais [14] has provided experimentally validated [13] electrical conductivity data in the liquid vapour transition region that may help to provide a solution to the current diversion. (The conductivity of liquid copper at atmospheric pressure as calculated from Desjarlais work is in excellent agreement with respect to that from Dyos [18]).

Copper vapour is a very poor conductor relative to the cool plasma and is often referred to as the 'insulation phase'. It is proposed that there might exist an electrically insulating vapour boundary layer that naturally forms as a result of thermal gradients at

the plasma/condensed wire fragment interface, assuming that there are no discontinuities in temperature at the interface. This idea is used to explore the current diversion phenomenon.

A simplified model of a copper fragment surrounded by a plasma has a condensed copper fragment of length, l_c diameter, d_c and temperature, T_c sited within a copper plasma column of length, l_p diameter, d_p and uniform temperature, T_p. A vapour boundary layer of thickness, t and at uniform temperature, T_v surrounds the fragment. Current is initially passing into the problem through the plasma due to an applied potential. It then has the option of continuing to conduct through the plasma, or pass through the copper vapour boundary into the condensed fragment. It would then conduct through the condensed fragment and re-enter the plasma by re-passing through the vapour boundary. The relative resistance of the plasma column and that of the vapour boundary together with the condensed fragment will determine the relative current density within the plasma and fragment. This problem is shown schematically in Figure 11. Apart from the application of the vapour boundary layer, the model is thus far similar to Powell's [31].

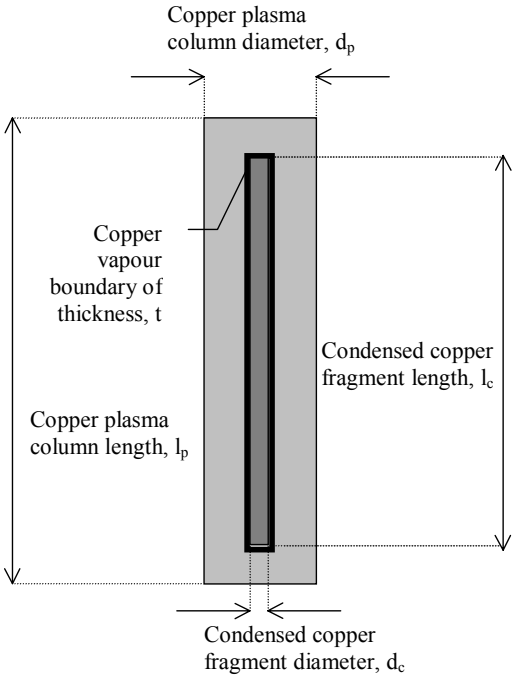

Fig. 11: Schematic of a plasma-shrouded exploding condensed wire fragment

Powell continued to solve the magnetic diffusion equation, restricted to a limited set of geometrical arrangements in an attempt to understand the experimentally demonstrable current diversion. Here, current diversion has been explained by use of a simple resistor network treatment without recourse to specific geometries, by putting the copper plasma in parallel with a copper vapour boundary layer and the condensed copper fragment. The approach was to impose a value of resistance upon the vapour boundary layer to compel current to favour the route through the plasma. The thickness of the vapour layer, t would be the only variable for a given temperature, T_v that would allow the boundary resistance to be adjusted. The thickness would then be obtainable from the relationship between this imposed resistance and the vapour conductivity given by Desjarlais at T_v.

It was necessary to establish what complexity was required to model the current density through the vapour boundary along the length of the wire. It seemed obvious that the current passing through the vapour would not be uniform along the length, l_c but would be concentrated at the two ends. Simply treating the entire vapour boundary as two resistors (with cross sectional area $\pi d_c l_c/2$) would be unlikely to give a realistic solution for the vapour thickness. A process of mesh refinement was therefore applied to try to find an acceptable degree of complexity. This was achieved by modelling the plasma column and condensed fragment as an increasing number of series resistors. Each plasma and condensed copper resistor was connected together by a resistor representing the vapour. The values of each resistor representing plasma and condensed copper was calculated, with a total fragment length, l_c taken to be 50 mm, and diameter, d_c of 1 mm, and a plasma column diameter, d_p of 6 mm. There is no limit to the number of such fragments, shown in figure 12, which could be in series. However, in this case with a wire length of around 150 mm, there would be three such segments. A plasma temperature, T_p of 10 000 K, vapour temperature, T_v of 2850 K and condensed copper temperature, T_c at 2840 K was assumed. The values of the resistors representing the vapour were varied until sufficiently little total current was flowing through the condensed fragment at the mid-point $l_c/2$ to be deemed as negligible with regard to the lack of experimentally observed effects (such as the Lorentz force). A circuit simulation package was used to determine the current at each point within the resistor network for each case as complexity increased. It was found that by dividing the plasma and condensed copper columns into first two, then four, eight, twelve and finally sixteen parts showed that increasing complexity reduced the thickness of vapour required by smaller increments, and that further complexity would little alter the value further.

Figure 12 shows a schematic circuit diagram of an example problem. Resistors R1 – R16 represent the plasma; R17 – R33 represent the vapour boundary and R34 – R49 represent the condensed wire fragment. The values of the resistance for each section of the sixteen part problem, which give around 95 % of the total current flowing through the plasma at the mid-point, $l_p/2$ (i.e. between resistors R8 and R9 in figure 13) were for the plasma,

(R1 – R16) taken as 19 mΩ; for the condensed fragments, (R34 – R49) were 2.47 mΩ and those for the vapour boundary, R_v (R17 – R33) were 12 Ω. Under these conditions and with an arbitrary voltage of 300 V, the values of current in the plasma, I_p between R8 and R9 was 971 A, and the current in the condensed fragment, I_c between R40 and R41 was 56 A. The value of the vapour conductivity, (R17 - R33) using the Desjarlais conductivity of copper vapour at a temperature of 2850 K was 3.83 Ω^{-1} m^{-1}. This gave a boundary layer thickness of around 30 μm, thought to be a reasonable order of magnitude for such a simple model. There was a maximum of 12.4 A flowing through the first (and last) sections of the boundary layers (R17 and R33). This diminished to 1.5 A through the centre sections (R24 and R26).

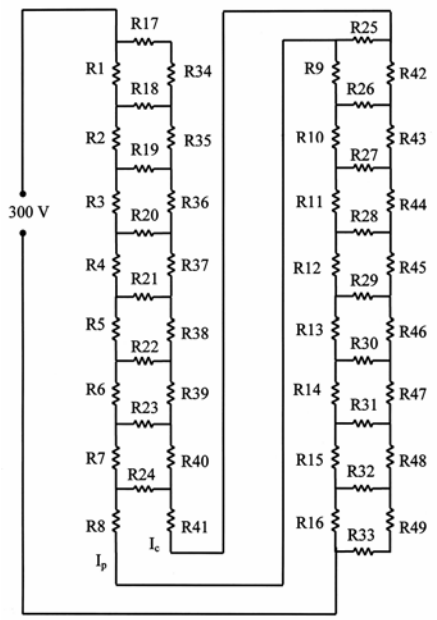

Figure 12: Schematic circuit diagram of a plasma-shrouded exploding condensed wire fragment

Maximum current densities based upon the arbitrary voltage of 300 V are for the plasma 34 MA m^{-2}, for the condensed fragment 71 MA m^{-2} and for the boundary layer 1.3 MA m^{-2}. Sensitivity analysis has shown this model to be insensitive to the condensed-phase temperature (conductivity), but highly sensitive to the plasma-phase temperature (conductivity), with a less thick vapour barrier being required for hotter plasma. This finding of plasma temperature sensitivity may go some way to explaining why the wire blow is so similar for a wide range of electrical discharge power levels: a thicker boundary layer is required for a less energetic event due to the cooler plasma. A thicker boundary layer would naturally form with lower plasma temperatures. Changing the voltage across the model from the arbitrary 300 V does alter the magnitude of the current density but not, of course, the ratio of the currents I_p to I_c.

A more complete model [32], taking into account radial resistance of the plasma, has shown the boundary layer thickness to be nearer 1 μm.

7. Summary and conclusions

This work has outlined experimental efforts to further understand the wire explosion process. The aim of the work was to provide data for the development and validation of computer codes that model the operation of capillary plasma generators for the electrothermal-chemical gun for the UK MoD. As such, much progress has been made and the code is capable of predictive operation within a range of discharge parameters.

Electrical, photographic and x-radiographic evidence has been used to build up this understanding over the course of several years and hundreds of tests, although much understanding is still required.

The main conclusion from this work is that a plasma sheath develops over the condensed (liquid) remnants of an exploding wire (flashover). The plasma is metallic in nature and originates from vapour issuing from small breaks along the wire length. The current is diverted from the wire and through the seemingly higher resistance plasma during the development of the sheath. This causes a steep rise in load resistance and the characteristic voltage spike seen in many exploding wire tests. The rate of rise in resistance is directly proportional to the length of plasma sheath. Peak resistance is defined when the entire wire length is shrouded. Further heating of the wire is thought to be mainly radiative. Attempts have been previously made to explain the counter-intuitive current diversion. These relied on the geometry of the fragmenting wire/plasma system and were not applicable to the fragmentation here. Hence, an alternative explanation has been put forward that relies on the properties of an hypothetical thermal vapour boundary layer existing between the condensed wire and plasma. This layer has a high resistivity and effectively increases the resistance of the wire fragments. The thickness of the boundary layer required to maintain the majority of the current through the plasma is found to be around one micron.

Acknowledgement

[1] B. Augsburger et al, "DRA 500 kJ Multi-module Capacity Bank", *IEEE Transactions on Magnetics* **31**, 1, January 1995

[2] Exploding Wires volumes 1-4, edited W G Chace and H K Moore (New York: Plenum) 1959 - 1968

[3] I. R. McNab., "Early Electric Gun Research", *IEEE Transactions on Magnetics*, **35**, 1, January 1999
[4] M. J. Taylor, "Plasma Propellant Interactions in an Electrothermal-Chemical Gun", PhD Thesis, September 2002 http://www.qinetiq.com/technologies/military/plasma_propellant.html
[5] G. P. Wren, W. F. Oberle, N. Sinha, A Hosangadi and S. M. Dash, "U.S. Army Activities in Multidimensional Modelling of Electrothermal-Chemical Guns," *IEEE Transactions on Magnetics* **29**, 1, pp 63-636, January 1993
[6] C. R. Woodley and S. R. Fuller, "The Effect of Plasmas on the Combustion Rates of Solid Propellants", The International Autumn Seminar on Propellants, Explosives and Pyrotechnics, Shenzen, China, October 1997
[7] G. L. Katulka et al, "Experimental Characterisation of Plasma Effects on Energetic Materials for Electrothermal-Chemical Launch Applications," *IEEE Transactions on Magnetics* **35**, 1, pp 197-199, January 1999
[8] C. R. Woodley and S. J. Billett, "Modelling of Enhanced Gas Generation Rates in a 155 mm ETC gun," IEEE Transactions on Magnetics **37**, 1, pp 207-210, January 2001
[9] M. J. Taylor and C. R. Woodley, "Variation in Enhanced Gas Generation Rates in Electrothermal-Chemical Closed Chamber Studies" 19th International Symposium of Ballistics, Interlaken, Switzerland, May 2000
[10] D. C. Haugh and M. A. Firth "UK Electric Gun National Overview", *IEEE Transactions on Magnetics*, **37**, 1, pp 33-36, January 2001
[11] M. J. Taylor, "Measurement of the Properties of Plasma from ETC Capillary Plasma Generators", *IEEE Transactions on Magnetics,* **37**,1, pp 194-198, January 2001
[12] D. C. Swift, 1998 Hydrocode Modelling of Plasma Capillaries *APS Plasma Physics Meeting, New Orleans*
[13] A. W. DeSilva and J. D. Katsouros, " Electrical Conductivity Measurement in Dense Metal Plasmas: Comparisons of Several Metals", *Journal de Physique IV,* **10**: (P5) 2000, pp 209-214
[14] M. P. Desjarlais, "Practical Improvements to The Lee-More Conductivity Near The Metal-Insulator Transition", *Contributions To Plasma Physics* **41,** 2-3, 2001, pp 267-270
[15] M. J. Taylor, "Ignition of Propellant by Metallic Vapour Deposition for an ETC Gun System", *Propellants, Explosives, Pyrotechnics* **26**, pp 137 – 143, August 2001
[16] Resistivity data for copper extrapolated from CRC Handbook, 79th Edition
[17] M. M. Martynyuk,, "Transition of Liquid Metals into Vapor in the Process of Pulse Heating by Current", *Int. J. Thermophysics*, **14**, 3, 1993 pp 457-470
[18] G. T. Dyos and T. Farrell , "Electrical Resistivity Handbook" (London: Peter Peregrinus), 1992
[19] M. J. Taylor, "Spectral Acquisition and Calibration Techniques for the Measurement of Radiative Flux Incident upon Propellant", *Propellants, Explosives, Pyrotechnics* **28**, 1, 2003, pp 18-25
[20] M. J. Taylor, "Formation of Plasma Around Wire Fragments Created by Electrically Exploded Copper Wire", *J. Phys D: App Phys*, **35**, 7, 2002, pp 700-709
[21] P. Graneau, "Wire Explosions", *Phys. Lett.* **120A** 77-9, 1987
[22] S. Molokov and J. E. Allen, "The Fragmentation of Wires Carrying Electric Current", *J. Phys. D: Appl. Phys.* **30,** 1997, pp 3131-3141
[23] M. J. Taylor and R. J. Gardner, "X-ray of Thicker Exploding Wires", *Unpublished QinetiQ report,* 2001
[24] M. L. Coffman, " The First Picosecond in an Exploding Wire", Exploding Wires volume 3*,* edited W G Chace and H K Moore (New York: Plenum), 1964, pp 89-102
[25] Y. Me-Bar and R .Harel, "Electrical Explosions of Segmented Wires", *J. App. Phys.* **79,** 4 ,1996, pp 1864-1868
[26] J. Nasilowski, "Unduloids and Striated Disintegration of Wires", Exploding Wires volume 3, edited W G Chace and H K Moore (New York: Plenum), 1964, pp 295-313
[27] A. Lukyanov and S. Molokov, "Flexural Vibrations Induced in Thin Metal Wires Carrying High Currents", *J. Phys. D: Appl. Phys*. **34**, 2001, pp 1543-1552.
[28] G. A. Shvetsov, A. D. Matrosov, S. V. Fedorov, A. V. Babkin and S. V. Ladov, "Quest of Possibilities for Controlling the Shaped-charge Effect by Electromagnetic Action", *4th All Electric Combat Vehicle Conference, Noordwijkerhout, Netherlands,* 7th – 9th January, 2002
[29] C. E. Hollandsworth, J. D. Powell, J. Keele and C. R. Hummer, " Electrical Conduction in Exploded Segmented Wires", *J. App. Phys.* **84,** 9, 1998, pp 4992-5000
[30] Drumm, "Investigations into Segmented Divertor Strips" *23rd ICPL, Firenze (Italy) 23- 27 September 1996*
[31] J. D. Powell and L. D. Thornhill, "Current Distribution and Plasma Properties in Injectors for Electrothermal-Chemical Launch", *IEEE Transactions on Magnetics*, **37**, 1, 2001, pp 183-187
[32] J. Dunnett, Fluid Gravity Engineering, St Andrews, Scotland. Personal Communication, September 2002

HIGH VOLTAGE VACUUM TYPE FULL-RANGE CURRENT LIMITING FUSE

Wang Jimei
Xi'an Jiaotong University
Xi'an P.R. China

Ma Zhicheng
Xi'an Fusegear Factory
Xi'an P.R. China

Abstract: Actually it is a high voltage vacuum fuse coupled with a full range current limiting fuse in tandem used to protect electric power system. The fuse configuration, basic principle, speedy expansion of electric power capacity in China it is in urgent need to develop a fuse of this kind.

Keywords:

1 Introduction

Presently, no high voltage vacuum type full range current limiting fuse is available in our domestic market for protection of electric power system in case of short circuit and over-load current. However, the full range current limiting fuse plays a functional role in close coordination with the intelligent power system currently.

The application of full range current limiting fuse for electric power system protection has been popularized in the world. It is obvious that the back-up fuses arc still being used in China. It will become obsolete and then gradually eliminated.

2 Configuration and basic principle of high voltage vacuum type full-range current limiting fuse

Figure 1 shows the cross-sectional profile of the fuse which is composed of a vacuum fuse element I fully immersed in epoxy resin and a current limiting fuse 2 wholly embedded in silica sand medium within an insulated envelop, both of them are coupled in tandem.

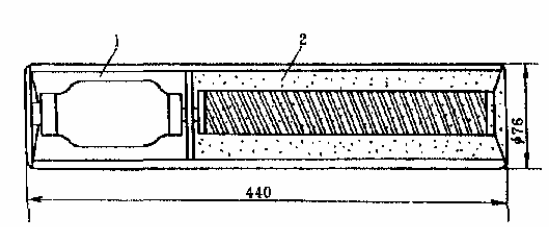

Fig. 1. Configuration of high voltage vacuum type full range current limiting fuse

2.1 Vacuum fuse part

The main construction of vacuum fuse part is as a vacuum interrupter shown in Fig.2. the vacuum Fuse consists of glass envelope l, glass shielding 2, conducting rods 3 and 5, input terminal 4, output terminal 6 and fuse element 7. The envelope should be vacuumized to 10^{-3}Pa. The shielding is made of glass to prevent from metallic vapour spraying lo the glass envelope during the course of current breaking as vaporized metallic particles condensed on the internal surface of the envelope readily form a conductor between the input and output terminals.

The conducting rods and input/output terminals are made of OHNC copper material. The material of fuse clement may be selected to satisfy design requirements, as shown in Table 1.

Table 1 Physical characteristics of fuse materials used in vacuum fuse

Material	Symbol	Density	Melting point °C	Heat conductivity W/m°K	Resistivity $10^{-8}\Omega$m
Cadmium	Cd	8.65	321	92	7.4
Copper	Cu	8.96	1084	398	1.69
Iron	Fe	7.86	1536	80	9.71
Gold	Au	19.32	1063	315	2.4

A fuse element is commonly used with a current density ranged from 100 to 160 A/mm^2. In our designed fuse, for instance, a copper strap of 4 x 0 1 mm^2 in cross-area is selected for rated current 63A fuse, the current density of which will be approximately 63/4x0.1 = 160A/mm^2. Both length and area of the fuse element are used to define the rated current and the ampere-second characteristics as in our designed where the rated voltage and current are 12kV and 63A respectively. The geometrical dimensions of the fuse element arc show n in Fig.3

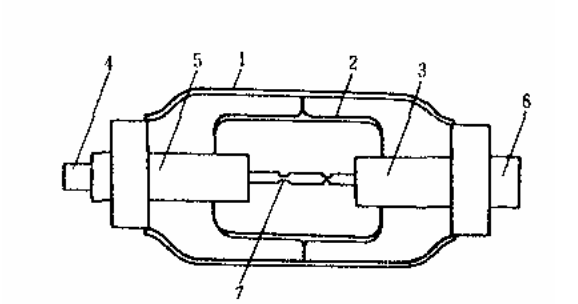

Fig.2. Schematic diagram of vacuum fuse

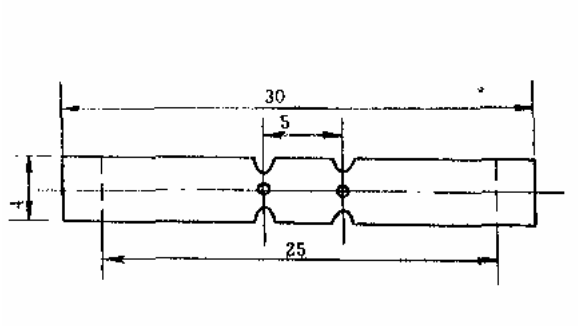

Fig.3. Geometrical dimensions of fuse element

2.2 Current limiting fuse part

As show n in Fig.4, Insulating envelope made of high strength glass fibre with resin polymerized, quartz sand 2 of 98% in purity, terminal cup 3 made of silver plated copper, fuse element 4 of 99.99% silver with cross-area 2.54x0.145 mm^2 and length 640mm wound on an asterisk ceramic supporter. The profile of fuse element is shown in Fig.5. At the end of terminal cup, an acting indicator or a striking pin to show whether the fuse has been operated or its switchgear mechanism has been acted.

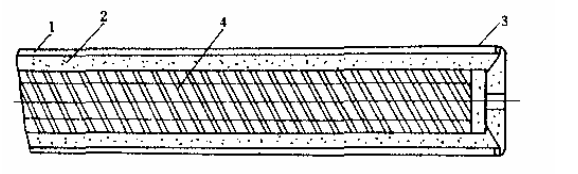

Fig.4. Configuration of current limiting fuse

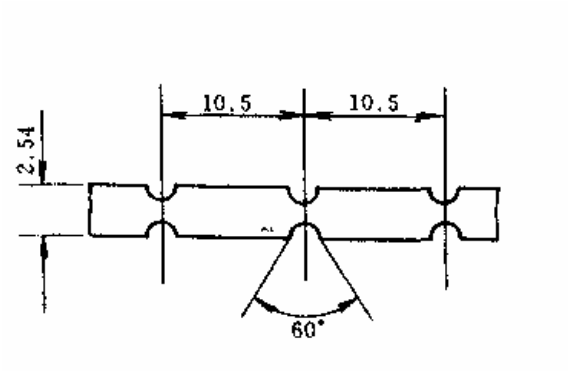

Fig.5. Profile of full range current limiting fuse element

3 Characteristic tests and measured results

The following characteristic tests and analyses were conducted on our designed sample of high voltage vacuum fuse coupled with current limiting fuse in tandem.

3.1 Test and result analysis conducted on vacuum fuse

In Fig.6 it shows the circuit diagram for pre-arc time vs prospective current curve test (i.e. ampere-second characteristics test) of the vacuum fuse, in which source supply switch Km, voltage regulator T of large capacity, stabilizing resistor R, short circuit switch Ks, ammeter A or oscillograph to be instead, in case the test current being two times greater than rated current of vacuum fuse sample to be tested
The measured results of pre-arc time vs prospective current of the tested vacuum fuse arc shown in Fig 7. It can be seen that the curve at small over-current varied quite steeply, that means to say the fuse has high sensitivity and reliability for protective function.

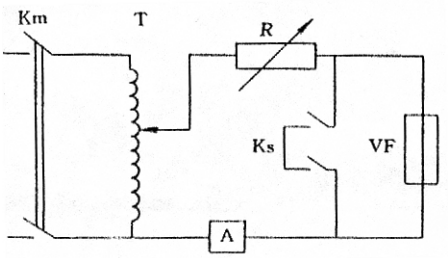

Fig.6. Circuit diagram for vacuum fuse pre-arc time vs prospective current curve test

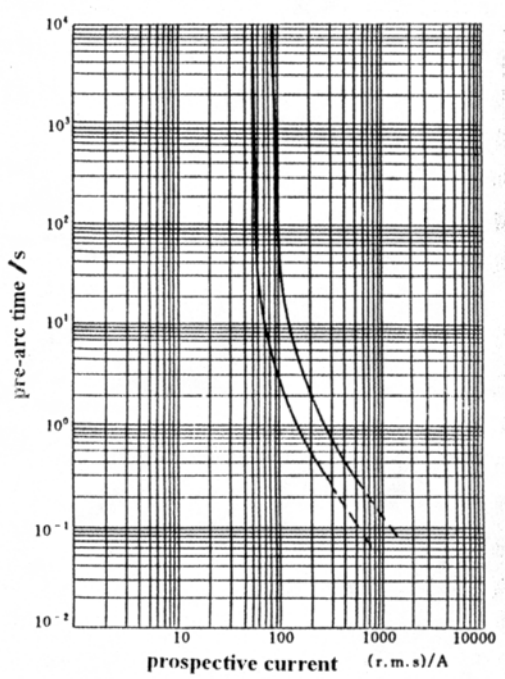

Fig.7. Characteristic curve of pre-arc time vs prospective current curve of vacuum fuse

3.2 Test and result analysis conducted on current limiting fuse

The circuit diagram of pre-arc time vs prospective current curve (i.e. ampere-second characteristics test) for the current limiting fuse is exactly same as that shown in Fig.6. The measured results are shown in Fig.8, from which it is observed that when over current in the current limiting fuse was as about 4 times less as the rated value (the dotted line Fig.8), the fuse has no capability to interrupt the short circuit current.

3.3 Determination of intersecting point

Based on the results measured above, it can be observed that the rated current of 50A or 60A current limiting fuse is not competent lo interrupt the circuit current less than 200A or 500A respectively. When a high voltage vacuum fuse is coupled with a current limiting fuse in tandem (i.e. the curves in Fig 7 and Fig.8 overlapped one another), two intersecting points are found at 280A and 420A respectively as shown in Fig.9, thus forming two continuous characteristic curves through these two points. Obviously, the vacuum fuse displays its capability to interrupt minimum over-current lo maximum short-circuit current, thus forming a full range fuse.

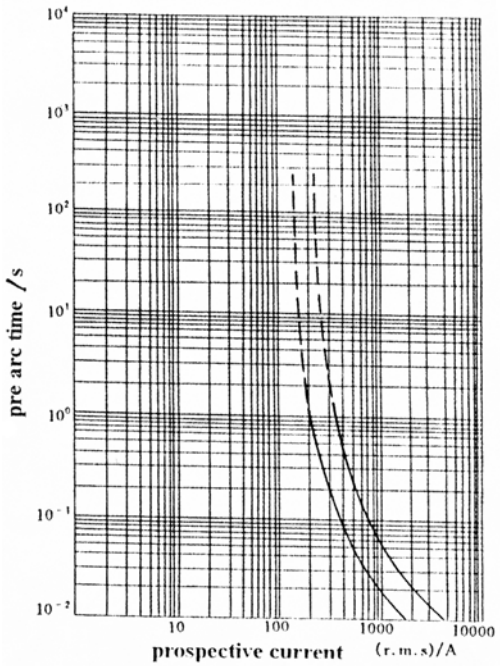

Fig.8. Characteristic curve of pre-arc time vs prospective current of current limiting fuse

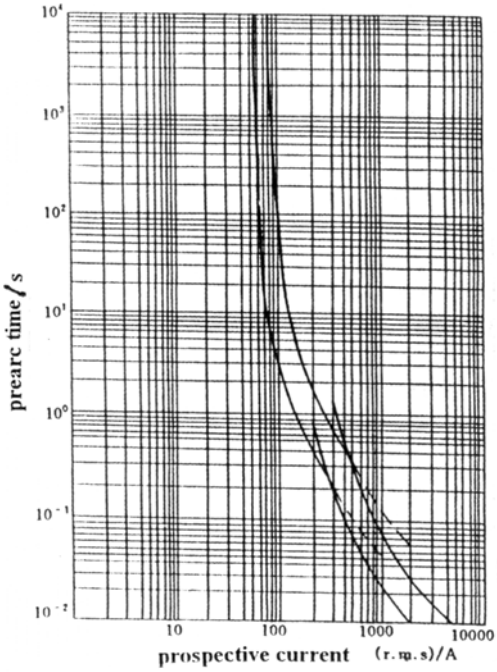

Fig.9. Characteristic curve of full range performance fuse

4 Conclusion

Despite of the fact that Gdansk Technical University of Poland and Xi'an Jiaotung University of China have conducted on research and development of a fuse of this kind in 1998, no high voltage vacuum type full range current limiting fuse is available at home and abroad currently. It is quite necessary to develop this kind of fuse in order to meet speedy

expansion of electric power system capacity. Fortunately Hangzhou Baoda Electric Co,Lid of Zhejiaug province, P.R.. China has developed the fuse and undertaken the business in the production of it for power system protection.

References

[l] Wang jimci, High voltage alternating current fuse , Xi'an Jiaotung University Publishing House ,Xi'an. China, Sept.2000
[2] National Standard B I5166.1-I5166.5 High Voltage Fuse. Feb.l, 1995.

THE CONTRIBUTION OF CURRENT-LIMITING FUSES TO POWER QUALITY IMPROVEMENT

R. Wilkins and **J.C. Chenu**

Ferraz Shawmut, 1 rue Novel, Villeurbanne, F-69626, France
bobwilkins@clara.co.uk , jean.claude.chenu@fr.ferrazshawmut.com

Abstract: Voltage sags caused by power-system faults can cause serious problems for computer systems, adjustable-speed drives and other industrial and domestic equipment. The effect of a voltage sag depends on its magnitude and duration. The use of current-limiting fuses for system protection reduces the duration of voltage sags, without producing excessive overvoltages, thus improving power quality.

Keywords: power quality, current-limiting fuses

1. Introduction

Ideally an electric utility should provide an a.c. supply with a voltage of constant magnitude and frequency and a perfect sinusoidal waveshape. The term "power quality" is essentially voltage quality [1], and the ITIC curve shown in Fig. 1 is widely used to define the maximum voltage deviations which are acceptable, as a function of time. Note that the shorter the time, the greater the voltage deviations which are allowed.

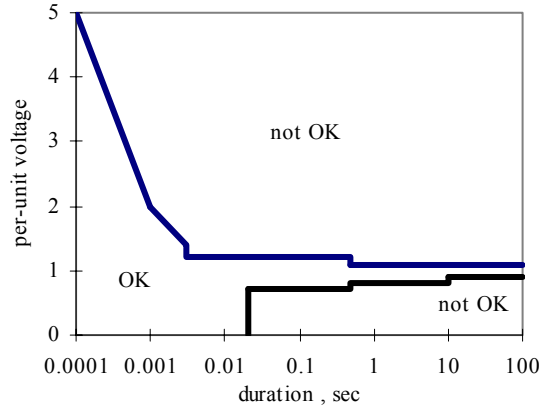

Fig.1 ITIC curve

The ITIC (Information Technology Industry Council, formerly CBEMA) curve was originally developed for mainframe computer systems, and strictly applies only to 120V equipment subject to very specific types of voltage deviations. Similar curves can be found for other types of equipment such as UPSs [2], but in the absence of an alternative the ITIC curve has become a *de facto* standard for all types of equipment and power systems.

Voltage sags (or dips) are mostly caused by motor starting, magnetizing inrush currents, or short-circuit faults, (which give the most severe sags [3]). If an event occurs which causes a voltage/time point to fall below the lower curve in Fig. 1, it is presumed that malfunction of parallel-connected equipment such as computers, adjustable-speed drives and control systems can occur. The sensitivity of this type of equipment and the associated cost of downtime has been a major factor in the increasing importance of power quality studies in recent years. It has also led to the development of equipment such as uninterruptible power supplies, dynamic voltage restorers, constant-voltage transformers and static transfer switches to mitigate the effects of voltage sags.

The upper curve in Fig. 1 represents overvoltage limits, dictated by malfunctions such as operation of overvoltage trips, insulation failure and over-stressing. Sustained overvoltages (voltage swell) of +10% are allowable for times greater than 0.5s. Short-duration transients are usually caused by capacitor switching or lightning. There is some uncertainty about the short-time overvoltage curve. In the field many overvoltage spikes above the withstand curve which caused no problems have been observed [4]. There is also debate about how the curve should be interpreted for short-duration non-sinusoidal voltages and how the per-unit magnitude should be defined [1].

2. Current-limiting protection

The ITIC curve shows that for a bolted short-circuit fault (zero voltage) the fault must be cleared in less than 0.02s. This requires fast-acting protection, and in [4] it was pointed out that current-limiting fuses can meet this requirement at low cost, except in very rare cases where the supply system is weak and the short-circuit current is too low to cause the fuse to operate in current-limiting mode [4,9].

When a current-limiting fuse clears a short-circuit fault there is a system voltage sag during the fuse prearcing time followed by a voltage rise during the arcing time, and there was some initial concern

that the high arc voltage generated by the fuse could be higher than permitted by the ITIC curve. However, calculations for a typical UL class J fuse showed that the highest peak arc voltages remained within ITIC limits [4].

This has been confirmed by field tests on a radial 7.2 kV residential system subjected to single-phase short-circuit faults at various locations [5,8]. Measured voltage dips lasted only for about 2ms and the maximum voltage rises were about 1.7 p.u., both within the ITIC limits. ATP simulations using a resistance-time fuse model gave similar results.

It was also concluded in [5] that current-limiting fuses mitigated the voltage sag better than expulsion fuses, and caused less disturbance to parallel-connected loads, because the fuse arc voltage supports the system voltage, promoting recovery. In addition the current-limiting fuses provided their expected limitation of peak current and I^2t.

3. Example

The system shown in Fig. 2 will be used to illustrate in detail the voltage sags, voltage rises, effects on parallel loads, and limitation of energy provided by current-limiting and non-current-limiting protection.

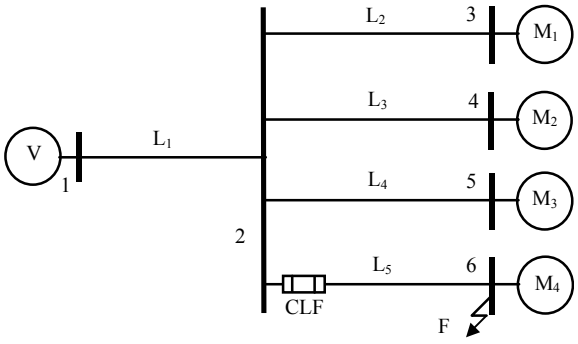

Fig.2 Motor control centre

The system of Fig. 2 has been discussed previously [6]. In this paper we will look at the behaviour in more detail. It represents a typical motor control centre with 2 smaller motors (M_1 and M_2) and 2 larger motors (M_3 and M_4). For a fault at bus 6, (on the terminals of M_4), bus 2 is the "point of common coupling" (PCC), as far as the other parallel-connected motor loads are concerned.

3.1 With current-limiting fuse protection

Fig. A.1 shows the system transients over a 0.1s period surrounding a 3-phase-to-ground short-circuit fault at bus 6, with M_1 and M_3 initially lightly loaded and M_2 and M_4 fully loaded, when protected by current-limiting fuses rated at 150% of the motor full-load current. The fault is cleared by operation of the 3 fuses in line 5. These results were computed using the method described in [7], which uses standard fuse models and takes into account 3-phase effects in the operation of the fuses as well as motor electrical and mechanical transients.

When the fault occurs the voltage at the point of common coupling (bus 2) sags to a low level, but only for a few milliseconds, until the fuses melt. In the cases shown the melting times are 9.2,5.2 and 3.3ms, so the sag duration is well within the ITIC undervoltage curve shown in Fig.1. After the fuses switch to the arcing mode the bus voltage is raised due to the appearance of the fuse arc voltages, and the fault currents in the three phases are forced to zero. The highest peak current in line 5 is 13.7 p.u.

The waveshape of the voltage transients produced during fuse operation is non-standard as far as the ITIC curve is concerned, but if we approximate them as half-sine waves of medium frequency they correspond to r.m.s. values of 1.45, 1.53 and 1.34 per-unit with durations of 2.5, 3.4 and 1.34 milliseconds. These points are close to the upper ITIC curve, but do not pose any significant problem.

After the current has been interrupted the voltages at the PCC recover to their normal values very quickly.

The raising of the bus voltage during the fuse arcing phase aids the re-acceleration of the parallel-connected motors. In effect the high resistance of the fuses in the arcing mode diverts the supply current into the parallel paths.

If the fault had been at the terminals of one of the smaller motors, M_1 or M_2, clearance of the fault by the corresponding (smaller) fuses would be faster still, with even less disturbance to the system..

3.2 With non-current-limiting protection

Fig. A.2 shows the computed interruption transients for the system of Fig. 2 if the current-limiting fuses are replaced by non-current-limiting devices which produce negligible arc voltage and which take about 2½ cycles to clear the fault. The high peak after the first quarter-cycle is composed of the fault current from the source via line 1 plus contributions from all the parallel-connected motors. There is no current limitation, which gives higher thermal and electromagnetic stresses on the circuit components. The peak network current is 21 p.u. while the I^2t let through after the fault is cleared is

almost 10 times higher than if the circuit were protected by the fuses.

In this case the voltages at bus 2 sag to about 0.15-0.22 per-unit for 41-46 milliseconds, which is well in the lower region of unacceptable power quality shown in Fig. 1. However bus 2 voltage remains depressed even after the fault has been cleared. It increases slowly from about 0.6 per-unit and remains below the ITIC curve for a considerable time. The reason for this is that the speed of the parallel-connected motors drops significantly during the long-duration voltage sag. After the fault is removed all the parallel motors re-accelerate, drawing a high current from the supply, which causes the duration of the voltage sag at bus 2 to be further extended.

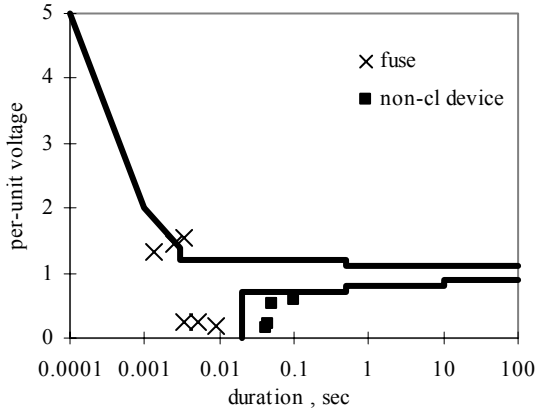

Fig. 3 Sags and peaks for the system of Fig. 2

Fig. 3 shows how these results relate to the ITIC curve. For each data point an approximate r.m.s. value of voltage has been plotted for the corresponding time duration. With current-limiting fuses the voltage sags are within ITIC limits, but with non-current-limiting protection this is not the case.

4. Conclusion

Current-limiting fuses provide protection against disruptive heating and electromagnetic effects, but also make an important contribution to the improvement of power quality. They achieve this by operating within one half-cycle, to limit the duration of voltage sags, and without producing unacceptably high voltages.

The resulting short duration of the disturbance to the system avoids further depression of voltages due to motor re-acceleration and other load effects.

Using fuses to improve the power quality of a power system is also a very inexpensive option. For systems where the cost of installing dynamic voltage restorers and similar types of equipment cannot be justified, high-speed protection by current-limiting fuses is very economical way of mitigating the effects of voltage sags.

In low and medium voltage industrial, commercial and residential network, current-limiting fuses have been improving power quality for more than 60 years, long before power quality became an important issue.

5. References

[1] R.C. Dugan, M.F. Mcgranahan and H.W.Beaty "Electrical Power Systems Quality", McGraw Hill 1996.

[2] Uninterruptible power systems (UPS) - Part 3: Method of specifying the performance and test requirements. IEC 62040-3, 1999-03.

[3] M.H.J. Bollen. "Voltage sags in Three-Phase Systems" *IEEE Power Engineering Review*, Sept 2001, pp 8-11.

[4] R. Wilkins and M.H.J. Bollen. "The role of current-limiting fuses in power quality improvement" *3rd International Conference on Power Quality*, Amsterdam, 24-27 October 1994.

[5] Lj.A Kojovic, S.P. Hassler, K.L. Leix, C.W. Williams and E.E. Baker. "Comparative analysis of expulsion and current-limiting fuse operation in distribution systems for improved power quality and protection" *IEEE Transactions on Power Delivery*, July 1998. pp 863 - 869.

[6] R. Wilkins and H.C.Cline. "Current-limiting Fuses Improve Power Quality". *Power Quality Assurance Magazine*, September 1999.

[7] R. Wilkins, A.J. McDonald and M. Castillo. "Computation of short-circuit transients in industrial networks protected by current-limiting fuses". *8th International Symposium on Short-Circuit Currents in Power Systems*, Brussels, 8-10 October 1998.

[8] Lj.A Kojovic, S.P. Hassler, H.Singh and C.W. Williams. "Current-limiting Fuses Improve Power Quality" *IEEE Transmission and Distribution Conference and Exposition 2001* IEEE/PES, vol 1, pp 281-286.

[9] J.C. Gomez and M.M. Morcos. "Coordinating Overcurrent Protection and Voltage Sags in Distributed Generation Systems. *IEEE Power Engineering Review*, Feb 2002, pp 16-19.

6. Appendix

Figs A.1 and A.2 on the following pages show the transient responses computed for Fig. 2.

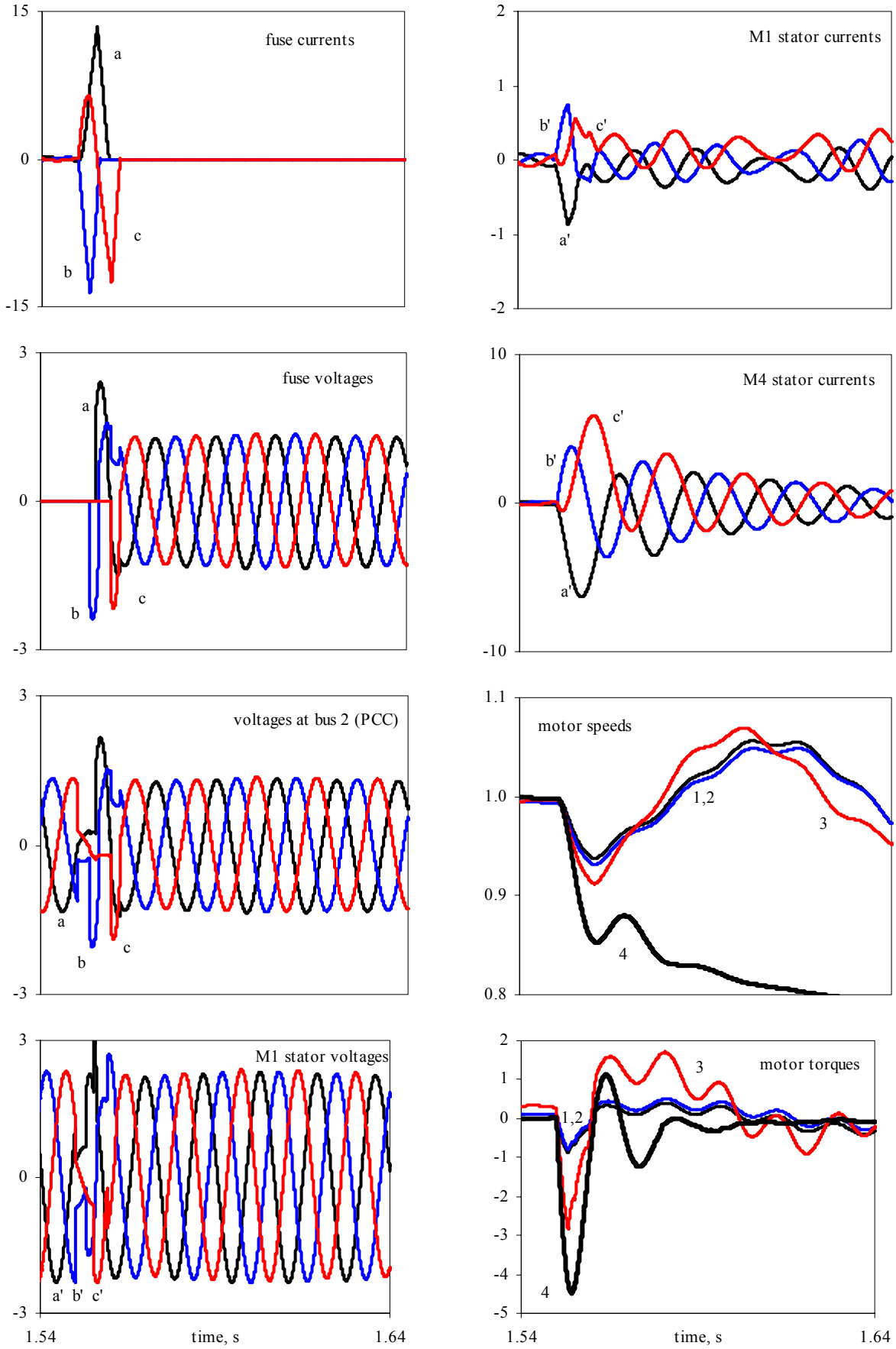

Fig. A.1 Transients with C-L protection

(all y-axis values are per-unit)

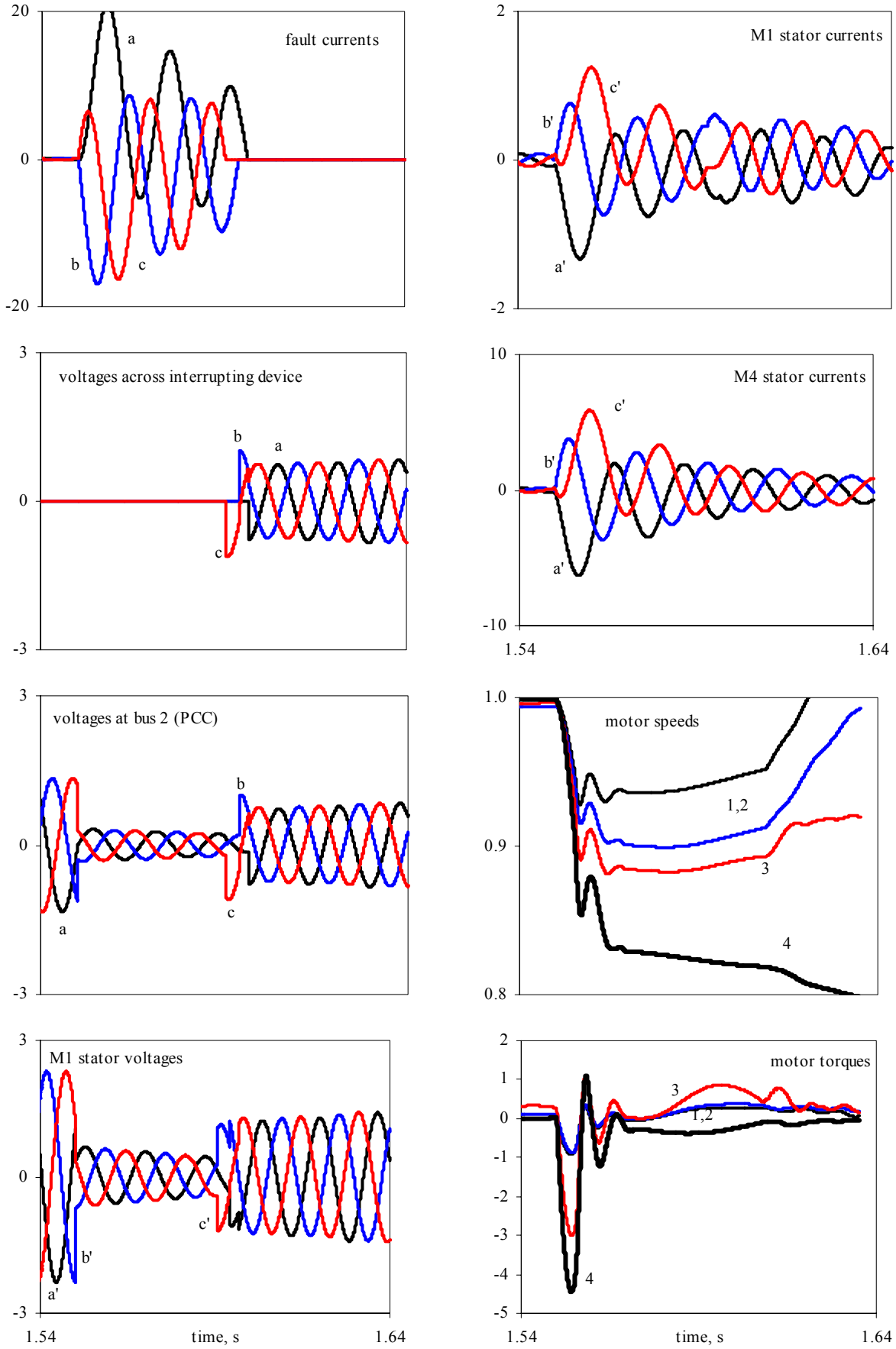

Fig. A.2 Transients with non-C-L protection

(all y-axis values are per-unit)

TIME-DOMAIN ANALYSIS OF 3-PHASE ARC FLASH HAZARD

R. Wilkins, M. Allison and **M. Lang**

Ferraz Shawmut, 374 Merrimac St, Newburyport, MA 01950, USA
bobwilkins@clara.co.uk , malcolm.allison@ferrazshawmut.com , mike.lang@ferrazshawmut.com

Abstract: Conventional arc flash hazard calculators use simple formulae to calculate the flash protection boundary and the incident energy density. A new method is described which models the circuit response and the operation of current-limiting fuses in the time domain, and the radiation-focusing effect of the equipment enclosure. The fault arcs are represented by a semi-empirical *v/i* model.

Keywords: arc flash hazard, current-limiting fuses

1. Introduction

The 2002 edition of the NEC requires equipment, on which work may be required to be done when energized, to be labelled, warning of arc flash hazard [1-3]. The 2003 edition of NFPA 70E requires a flash hazard analysis to be done before a person can work near to energized equipment, and to determine the type of protective clothing needed [2].

There are several different methods in use at present to calculate the flash boundary distance and incident energy upon a worker [2,4-7], and the new IEEE standard 1584 proposes a formula based on a statistical fit to test data obtained in several high-power test laboratories in North America [8].

In this paper a time-domain analysis method is presented, which can be used as an arc flash calculator, and which also allows current-limitation by fuses and other effects to be studied.

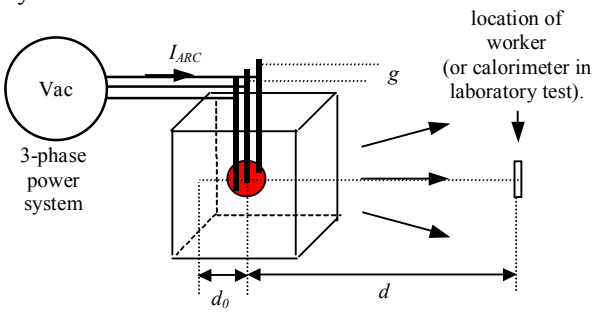

Fig. 1: Arc flash in an open box

Fig. 1 shows a schematic representation of an arc flash hazard incident. In laboratory tests the arcs are initiated by fine trigger fuse wires. High-current arcs which are not restricted move, due to magnetic forces, so as to increase the area of the circuit loop. For the geometry shown this causes the arcs to be driven downwards and to burn at the electrode-busbar tips, to form what is commonly referred to as a 3-phase "arcing fireball".

However the behaviour of the 3-phase free-burning arcing fault in equipment is chaotic, involving rapid and irregular changes in arc geometry due to thermal buoyancy and electromagnetic forces, arc extinction, plasma jets, sudden shortening due to restriking and reconnection across electrodes or plasma parts, and many other effects.

2. Time domain model

The given quantities are the network data (voltage, bolted-fault current, frequency, X/R ratio) and the equipment dimensions (bus electrode gap and location, box dimensions). It is required to calculate the arcing current (so that the operating time of protective devices can be found), and then the incident energy density E_i due to thermal radiation at a distance d from the arcing fireball.

Most conventional arc flash hazard calculators use a least-squares best-fit to the test data to give simple formulae for I_{ARC} and E_i in terms of the input data. Although the fault arc behaviour is difficult to model, the behaviour of the other parts of the system (electrical circuit, current-limiting fuse, thermal radiation) are well-known. These parts can be modelled accurately in the time-domain, reducing the area of uncertainty to that of the arcing fireball itself.

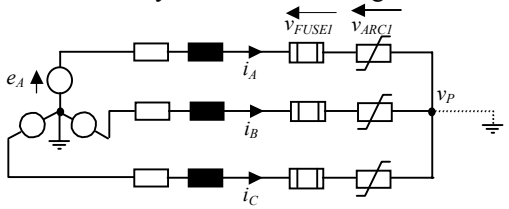

Fig. 2: Circuit model

Fig. 2 shows the circuit model, which includes a set of 3 current-limiting fuses in series with the arcing fault. The arcing fault is initially modelled as a set of fine trigger fuse wires with a fixed melting I^2t, and then the subsequent arcing fireball is modelled as a star-connected set of non-linear resistances. For ungrounded faults the sum of the phase currents is zero, which enables the potential v_P to be calculated. The transient circuit current can then be found by numerical solution of the circuit differential equations :

$$\begin{aligned}\frac{di_A}{dt} &= \frac{e_A - Ri_A - v_{FUSE1} - v_{ARC1} - v_P}{L} \\ \frac{di_B}{dt} &= \frac{e_B - Ri_B - v_{FUSE2} - v_{ARC2} - v_P}{L} \\ \frac{di_C}{dt} &= \frac{e_C - Ri_C - v_{FUSE3} - v_{ARC3} - v_P}{L}\end{aligned} \qquad (1)$$

$v_P = 0$ if the star point is grounded, otherwise

(a) if all fuses are intact

$$v_P = -(v_{FUSE1} + v_{FUSE2} + v_{FUSE3} + v_{ARC1} + v_{ARC2} + v_{ARC3})/3$$

(b) after 1st fuse has cleared (say in phase *a*)

$$v_P = (e_B + e_C - v_{FUSE2} - v_{FUSE3} - v_{ARC2} - v_{ARC3})/2$$

Cyclically similar expressions may be written if phase *b* or phase *c* clears first [9]. If a back-up breaker is used rather than fuses, the fuse voltages are all set to zero.

3. Fault arc characteristics

The single-phase high-current arc in air has a rising *V-I* characteristic which can be represented as

$$V_{ARC} = V_E + k\, I_{ARC}{}^X g^Y \qquad (2)$$

Measurements by Fisher [10] using currents up to 41.6kA and arcing gaps *g* from 25-100mm found that $X \approx 0.15$ and $Y \approx 0.5$. Ignatko [11] studied arcs from 5-150kA with gaps from 5-200mm. He measured the electrode-fall voltage (V_E) with Langmuir probes (23.5V for copper electrodes), and the actual arc length (which is greater than the gap distance) was measured photographically, to obtain the column gradient. Ignatko's data also fits the form of equation (2), with similar *X* and *Y* to Fisher's.

Stokes and Oppenlander [12] found $X \approx 0.12$ and $Y \approx 1.0$ for horizontal and vertical gaps of 5-500mm with currents up to 20kA. Their photographs revealed the complex variations in arc geometry in detail. Paukert [13] reviewed data from seven different laboratories and found approximate average values of $X \approx 0.2$ and $Y \approx 0.47$.

Given the very variable nature of the fault arc the data in the literature shows a remarkable agreement. The arc voltage shows a weakly rising dependence on current, with $X \approx 0.12$-0.2. In some cases it is not clear whether published data refers to instantaneous current or true r.m.s. current, but the trend is the same. The dependence on *g* is more variable, probably as a result of the use of differing electrode geometries.

For the 3-phase case, the behaviour of the arcing fireball is different and not well known, but as a first step (as originally suggested by Fisher) it can be represented as 3 separate star-connected single-phase arcs, each of which can be modelled by an equation of the same form as (2), but the values of *k, X* and *Y* have not been measured directly.

The unknown 3-phase values of *X* and *Y* were determined using the following procedure. First the value of a constant arc voltage was found which gave a true r.m.s. arcing current which agreed exactly with the values measured in the IEEE tests. This was done by repeatedly solving (1) for each test shot, computing the true r.m.s. current over the last cycle before the circuit opened, and iteratively adjusting V_{ARC} to obtain agreement. Then *X* and *Y* were determined by multiple regression (304 test shots were used in the analysis). This gave $X = 0.173$ and $Y = 0.222$, values which are consistent with expectations from data on the single-phase arc.

Then it was assumed that the same *X* and *Y* can be used to relate the instantaneous arc voltage and current (*v* and *i*), giving a nonlinear transient arc model of the form

$$v_{ARC} = V_E + K\, i_{ARC}{}^{0.173} g^{0.222} \qquad (3)$$

Finally the value of *K* was found by a second iterative fitting to the measured arcing current. However *K* was not constant, but a relatively strong function of the line-to-line test voltage V_{LL}. ($K = 1.827 V_{LL}{}^{-0.377}$ with V_{LL} in kV). This dependency is not easy to explain, but can also be found in Schau and Schade [14] and the IEEE formula. It is probably connected with the assumption that the arc is quasi-static, and possibly that the effects of arc extinction and restriking around voltage zero are not modelled. There was also a box effect; *K* must be multiplied by 0.797 for tests in a box.

Using this model together with the circuit equations (1), the circuit currents, voltages, power

and energy can be computed. Typical results are shown in Figs. 3a-3d for an ungrounded arcing fault.

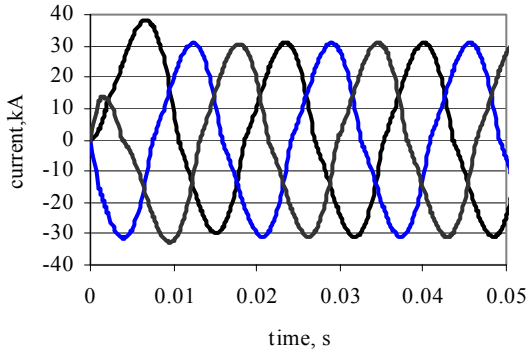

Fig. 3a: Computed current transients

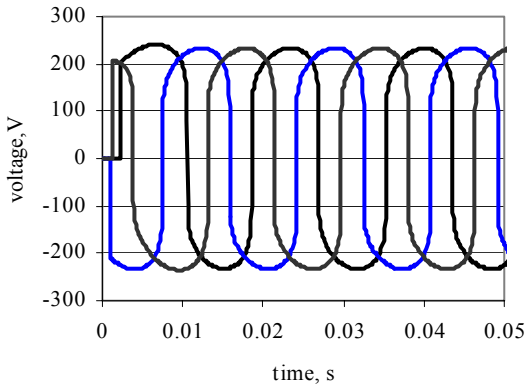

Fig. 3b: Computed arc voltage transients

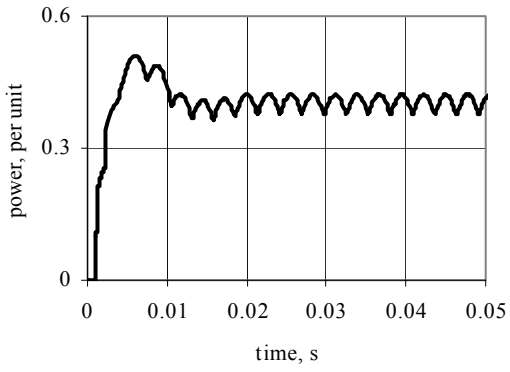

Fig. 3c: Instantaneous 3-phase power

The waveshapes are similar to published data [5,14]. The current stabilises quite quickly because of the damping effect of the fault arc resistance. The delay in appearance of the arc voltage is the fusion time of the fine trigger wires in each phase. Fig. 3c shows the instantaneous power as a fraction of the bolted-fault VA. In the example shown this ratio is close to the worst-case value of 0.5. The build-up of arc energy in Fig. 3d is almost linear, but with a delay of a few milliseconds after the fault begins.

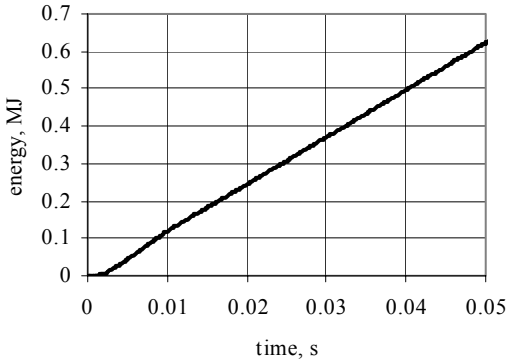

Fig. 3d: Total arc energy

These solutions were obtained using 4th order Runge-Kutta integration of the equations, with automatic adjustment of the time step to achieve a preset accuracy. However the resistance of the arc model (3) tends to infinity as the current nears zero, giving a very low circuit time-constant, which causes the time step to be reduced to a very small value, and the solution "grinds to a halt". The method of solving this problem is given in section 8.

Gammon and Matthews [15] calculated arcing currents for 1-phase arcing faults using a similar time-domain method (Runge-Kutta integration, using both Fisher's and Stokes and Oppenlander's model). They assumed that the arc extinguishes at each current zero and then reignites in the next half-cycle when the gap voltage reaches a fixed breakdown level (dielectric reignition), whereas the model described here shows a continuous variation of current through the zero-crossing period. Dielectric reignition occurs for a 1-phase arc where the power input to the arc drops to zero when the current reaches zero. However for a 3-phase arcing fireball the situation is less clear. Although the current in one phase may reach zero the power input to the fireball continues via the other two phases.

3.1 Calculation of arcing current

Using the model the r.m.s. arcing current (geometric mean value for the 3 phases over the last cycle before circuit opening) was computed and compared with the measured values given in [8]. The results are shown in Fig. 4a, and the values predicted by the IEEE formula are shown in Fig 4b.

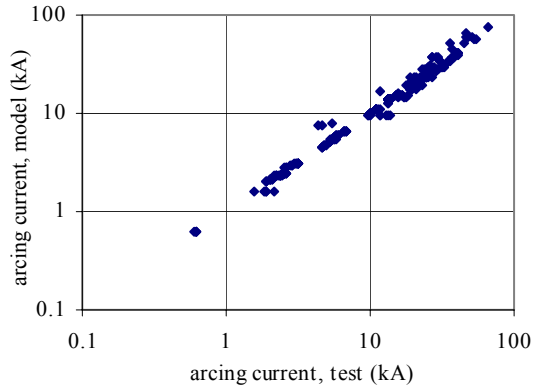

Fig. 4a: Comparison of predicted and measured arcing current (time-domain model).

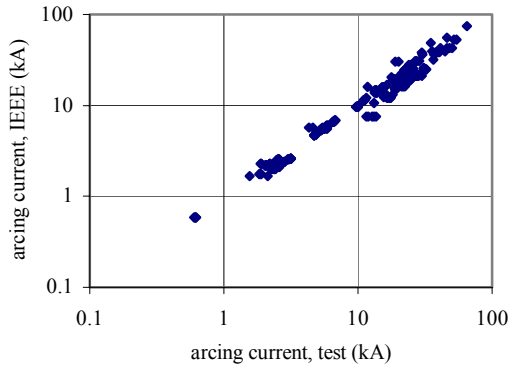

Fig. 4b: Comparison of predicted and measured arcing current (IEEE 1584 model).

The time-domain model gives a slightly better correlation (r^2=0.989) than the IEEE formula (r^2=0.978). The computed value of total arc energy also agreed well with the test values (r^2=0.955).

Fuses were not used for the tests shown in Fig. 4, the circuit being cleared by a back-up breaker. The data covers voltages from 208V to 13.8kV, bolted fault currents from 700A to 106kA, arcing gaps from 7.1mm to 152mm, and various box dimensions, as well as tests in the open (304 tests in all).

4. Calculation of incident energy density

In [8] it is assumed that the incident energy density falls with distance from the arcing fireball according to $(1/d^x)$ where x is a "distance exponent". For a spherical fireball in the open with a total energy W_{ARC} the direct radiated energy density at a distance d is $\beta W_{ARC}/(4\pi d^2)$ where β is the fraction of the total arc energy which is emitted as radiant heat. The distance exponent in this case is 2.

For tests in an open box, the focusing effect of the box changes the situation, as shown in Fig. 5.

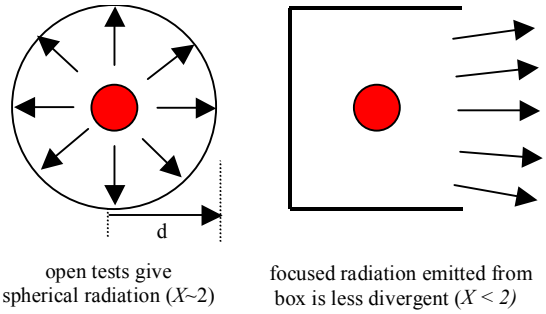

Fig. 5: Box focusing effect

For open box tests, as d gets smaller, the distance exponent falls, eventually towards zero, when the radiant heat appears as a plane wave. The same effect can occur as the box dimensions change. Reflections of heat from the back and sides of the box can make the arc and the box appear as one much larger heat source, reducing the effective distance exponent.

4.1 Tests in the open

Fitting to the IEEE test data using multiple regression gave the following model :

$$E_{max} = 0.1026\ E_S^{0.958}\ g^{0.284}\ V_{LL}^{-0.532} \quad (4)$$

E_{max} = mean maximum energy density at a distance d, (cal/cm^2)
E_S = spherical component of energy density = $W_{ARC}/(4\pi\ d^2)$
W_{ARC} = total computed arc energy , J

Fig. 6 shows a good correlation (r^2 = 0.949) between the predictions of (4) and the test values.

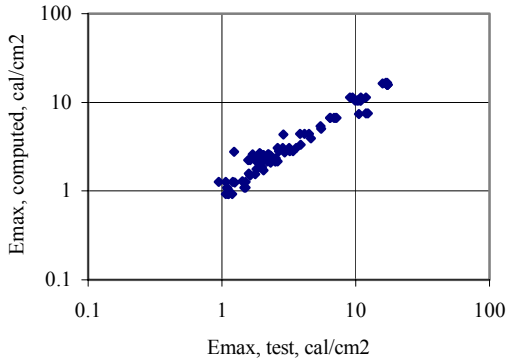

Fig. 6: Predicted incident energy, all open tests

4.2 Tests in a box with one side open

Rather than using distance exponents, it is possible to calculate the focusing effect of the box directly, using **radiative view factors** [16]. The view factor *Fij* between 2 surfaces *i* and *j* is defined as the fraction of the radiated energy leaving surface *i* which strikes surface *j*.

Radiated energy from the arc strikes the back and sides of the box and is then reflected out towards the calorimeters. It is necessary to take multiple reflections into account, as these are not negligible. The inner surfaces behave as **diffuse absorbers and reflectors** with a reflectivity α. Incident radiation is reflected equally in all directions, as illustrated in Fig.7.

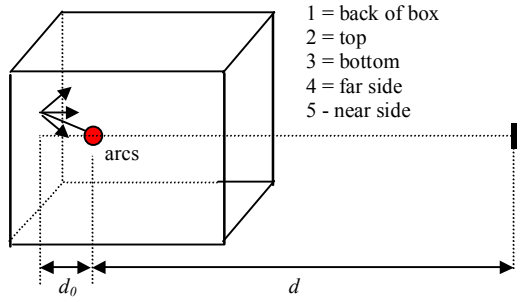

Fig. 7: Box geometry for calculation of reflections

The arcing fireball is treated as a spherical source of heat. For a single reflection the fraction of the arc energy which strikes side *k* is $F_{SK}.(\beta\, W_{ARC})$. F_{SK} is the view factor from a spherical heat source to a rectangular plate, and is an easily calculated geometrical function [16]. If the diffuse reflectivity is α, the fraction of the reflected energy which strikes the calorimeter is then $\alpha.F_{SK}.F_{KC}\,(\beta.W_{ARC})$, where F_{KC} is the view factor between side *k* and the calorimeter. Using the reciprocity principle [16] $A_C F_{CK} = A_K F_{KC}$, where A_K is the area of side *k* and A_C is the area of the calorimeter. So the energy striking the calorimeter is $\alpha.F_{SK}.F_{CK}\,(A_C/A_K)\,(\beta W_{ARC})$. This then gives the incident energy density at the calorimeter due to a single reflection as

$$E_1 = \alpha.F_{SK}.(F_{CK}/A_K)\,(\beta W_{ARC})$$

where F_{CK} is the view factor from the calorimeter to the side *k*.

Multiple reflections are treated similarly. For a triple reflection, say from the arc to the back of the box (side 1), then to the far side (4), then to the bottom (3), the energy arriving at the calorimeter is

$$E_3 = \alpha^3.F_{S1}.F_{14}.F_{43}.\,(F_{C4}/A_4)\,(\beta.W_{ARC})$$

and the total reflected energy $F_R(\alpha).W_{ARC}$ is obtained by summing all the contributions from all the reflections. For a 5-sided box the number of possible reflections off *N* surfaces is *5!/(5-N)!* a total of 325 paths, as shown below.

No of reflections	No of paths
1 (i.e. single)	5
2	20
3	60
4	120
5	120

Although there are a large number of quadruple and quintuple reflection paths, their contribution to the total energy is small because of the multiplying factor α^4 or α^5, and the reflectivity α must be less than 1. Using this method the effect of the box can be taken into account simply by adding the total reflected energy density to the spherical component (which strikes the calorimeter directly without any reflections). Eqn (4) is then modified to

$$E_{\max} = 0.1026\{E_S + F_R(\alpha)W_{ARC}\}^{0.958} g^{0.284} V_{LL}^{-0.532} \quad (5)$$

The only unknown is the reflectivity α. By varying α and computing the correlation between the predictions of (5) and the test data, the optimum value of α was found to be 0.56. This corresponds well with values to be expected from graybody diffuse reflectors. In a typical case direct spherical radiation accounts for about 50% of the incident energy while the paths with 5 reflections contribute only 0.1%. Multiple reflections of higher order than this can be neglected.

Fig. 8a shows a comparison between the incident energy density predicted by (5) and the measured mean maximum values for the entire IEEE data set.

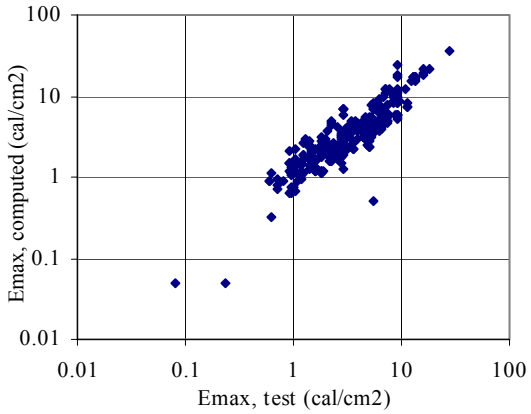

Fig. 8a: Computed vs. measured incident energy

Fig. 8b gives a similar comparison for the IEEE formula.

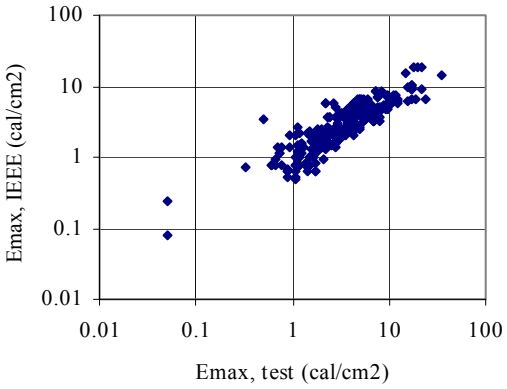

Fig. 8b: IEEE formula prediction compared with test

The time-domain computer model gives a significantly better correlation ($r^2 = 0.856$) than the IEEE formula ($r^2 = 0.775$). While the chief cause of variability is the chaotic behaviour of the fault arc, it is also clear that variations in reflectivity of the inner box surfaces will make a significant difference to the results.

5. Effect of current-limiting fuses

The model used is based on that described in [17], with some enhancements.

5.1 Prearcing model

The melting time is found by computing the evolution of the true r.m.s. current in each phase, and switching to the arcing state when the fuse's melting-time/current characteristic is crossed, as shown in Fig. 9.

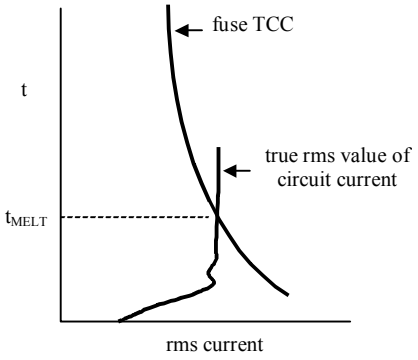

Fig.9: Computation of melting time

The fuse TCC is stored as a table which is dynamically fitted with cubic spline functions, and interpolation is used (as with all the models), to find the exact crossing point. For times shorter than the lowest tabulated value, the adiabatic melt I^2t is used.

The true r.m.s. (virtual) current in each phase is computed as $[\int i^2 dt / t]^{0.5}$

5.2 Arcing models

These are as given in [17] and model arc ignition in the notches, burnback, fusion of the sand, arc merging, and final arc extinction. Each arc is modelled as a simple cylindrical channel. For each fuse design, details of the element construction and materials are needed, and the resulting models give very good agreement with oscillograms obtained from fuse type testing.

Figs. 10a-10c show the results of typical calculations for the interruption of a 50kA ungrounded arcing fault in a 600V 60Hz 3-phase system by an 800A class L fuses, closing at zero degrees of phase *a*. The other data used to obtain these results was :

p.f. = 0.1 g = 32 mm
d_0 = 102 mm d = 457.2 mm
and the box size was 508 x 508 x 508 mm.

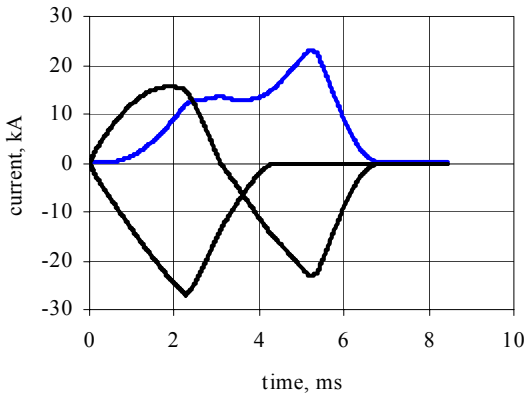

Fig.10a: Currents for arcing fault with fuses

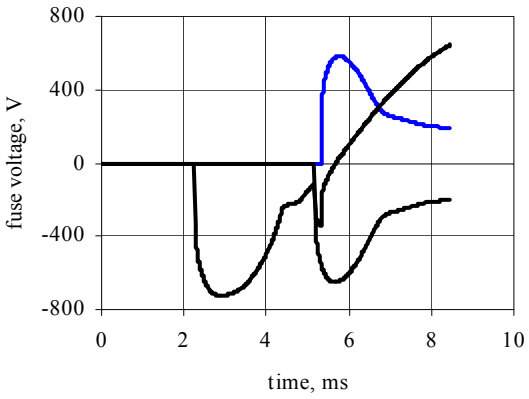

Fig. 10b: Fuse arc voltages

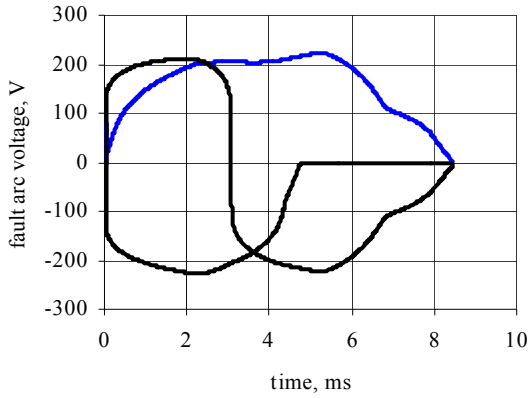

Fig. 10c: Arcing fault voltages

In the case shown the fuse in phase *c* melts first and limits the current. The appearance of the phase *c* fuse arc voltage changes the rates-of rise of current in the other two phases. The phase *b* and phase *a* fuses melt just before the phase *c* fuse clears, and then the *b* and *a* fuses clear together against the line-to-line voltage.

5.3 Point-on-wave effects

The possible sequences of events during clearing are very complicated, involving fuse melting and clearing in each phase, merging of arcs between notches, and interaction between the phases (if the fault is ungrounded). If a fuse just fails to melt within a particular half-cycle, the melting time jumps to a subsequent half-cycle. In Figs. 10 all 3 fuses opened, but in many cases only 2 fuses operate.

The results are also affected by the point-on-wave at which the arcing fault begins. For 3-phase systems, all possible outcomes are covered if the closing angle θ (with respect to the voltage of phase *a*) is varied in the range $0 \le \theta \le 60°$.

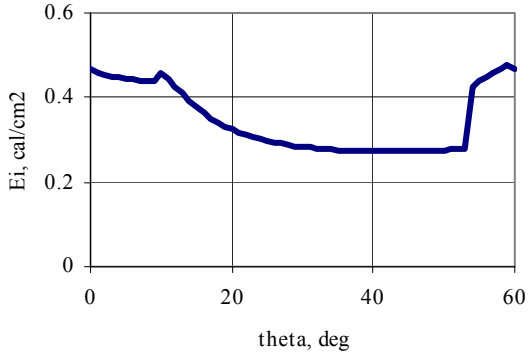

Fig. 11a: 3x1200A class L fuses @ 100kA

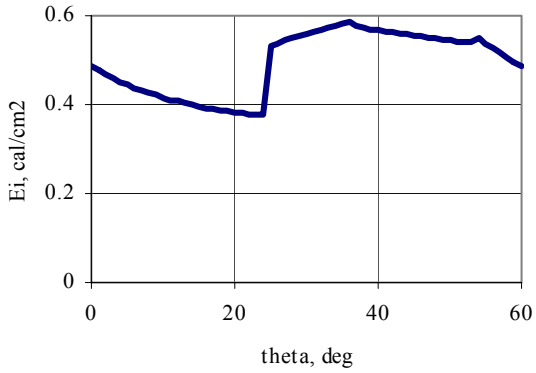

Fig. 11b: 3x1200A class L fuses @ 44.7kA

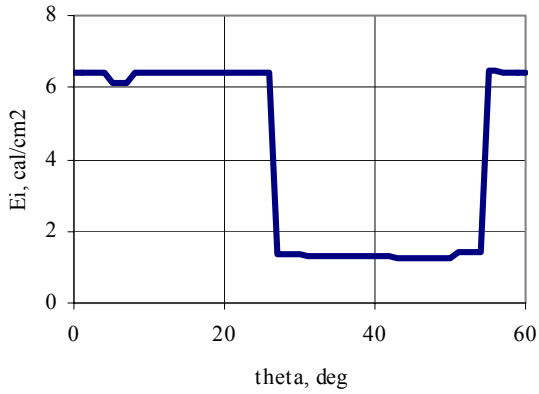

Fig. 11c: 3x1200A class L fuses @ 18.25 kA

Figs. 11a - 11c show the variation of arc flash energy density E_i with closing angle for three levels of bolted fault current. There are many discontinuities, associated with different sequences of fuse operation. Near the threshold current (Fig. 11c), the jumps in E_i are very large.

Fig. 12 shows the computed critical closing angle (i.e. that which produces the highest value of E_i) for a 1600A class L fuse, as a function of available bolted fault current.

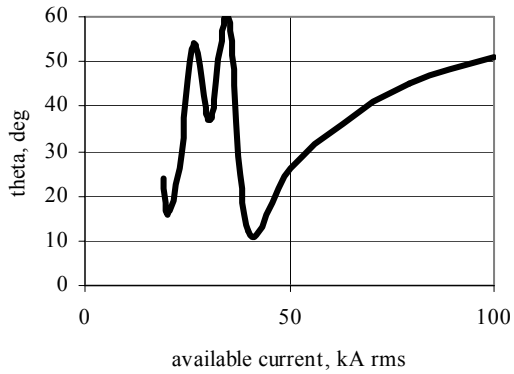

Fig. 12: Critical closing angle, 1600A class L fuses

Below the threshold (about 20kA for Fig. 12) the results are not significantly affected by closing angle. Within the threshold region (20-40kA for Fig. 12) the critical angle oscillates wildly as the available current is changed. Above the threshold (in the current-limiting region) the curve becomes smooth but does not always increase as shown. For some fuses a discontinuity followed by a decrease can be observed.

After examining point-on-wave effects for several different fuse designs, and considering the additional variations which will be found in practice, due to the chaotic fault arc behaviour, it is concluded that it is not possible to recommend a worst-case closing angle for arc-flash testing, in a similar way to that which is used for type testing of current-limiting fuses. The best recommendation appears to be to use random closing, but with several tests, to obtain a range of arc flash energy values.

5.4 Arc flash characteristic

For a given set of data (equipment type and circuit parameters) it is useful to plot the arc flash energy density as a function of available current. Fig. 13 shows a typical characteristic computed for a set of 3 1200A class L fuses. The upper curve is the maximum value (worst closing angle) and the lower curve is the minimum value (best closing angle).

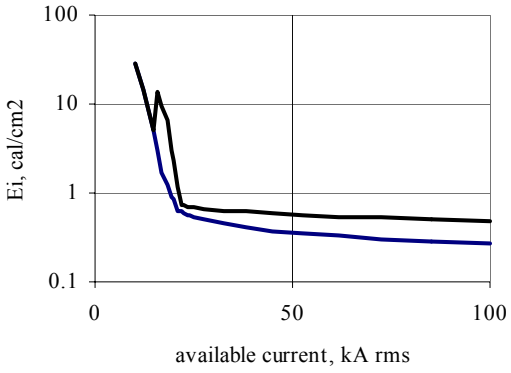

Fig. 13: Arc flash characteristic

Fig. 13 is similar to published test data [18] for 1200A class L fuses, although for slightly different test conditions. It shows that this fuse can limit the arc flash energy density to a level well below the critical value for a 2nd-degree burn (1.2 cal/cm^2), but only if the available bolted-fault current is high enough to cause operation in the current-limiting mode.

For these calculations it was assumed that the fault arcs were represented by (3) with unchanged values of *k, X* and *Y*. However, some changes may be needed, because Stokes and Oppenlander [12] showed that for time durations of a few milliseconds, the arc does not move far from its starting location, so the fault arc geometry for very short times will be different from that which develops over a period of several cycles, giving a possibly significant change in fault arc voltage and incident energy.

6. Conclusions

A time-domain model of arc flash hazard has been developed. The ordinary differential equations for the 3-phase circuit and any current-limiting fuses are solved by 4th-order RK integration with automatic control of the time step.

The arcing fault fireball is represented as a star-connected set of non-linear resistors, and the their characteristics have been determined by least-squares fitting to the published IEEE dataset. The resulting arc characteristics are similar to those which have previously been measured for high-current single-phase arcs in air.

For arcing faults in an open box, the focusing effect of the box is taken into account using radiation view factors to allow for multiple reflections of radiant heat.

The final model calculates the incident energy density due to the arc flash at a distance *d* for tests in the open or in a box of arbitrary dimensions, with a given electrical power system and interbus electrode gap. It gives good correlation with the IEEE 1584 test data and can also be used to study point-on-wave and other effects.

Furthermore the model has the potential for further improvement if a better model of the arcing fireball can be developed.

7. References

[1] National Electric Code, 2002 Edition. National Fire Protection Association. NFPA 70.

[2] Standard for Electrical Safety Requirements for Employee Workplaces, NFPA 70E, 2003 Edition. National Fire Protection Association.

[3] Jones, R.A, and 9 other members of an IEEE-PCIC working group. "Staged Tests Increase Awareness of Arc-Flash Hazards in Electrical Equipment". IEEE Petroleum and Chemical Industry Conference Record, Sept 1997, pp 313-332.

[4] Lee, R.H. "The Other Electrical Hazard: Electric Arc Blast Burns". IEEE Transactions on Industry Applications, vol IA-18. No 3, May-June 1982, pp 246-251.

[5] Neal, T.E., Bingham, A.H. and Doughty, R.L. "Protective Clothing Guidelines for Electric Arc Exposure". IEEE

Transactions on Industry Applications, vol 33, No 4, July/August 1997, pp 1043-1054.

[6] Doughty, R.L., Neal, T.E., and Floyd II, H.L. "Predicting Incident Energy to better manage the Electric Arc Hazard on 600V distribution systems". Proc.IEEE PCIC, Sept 1998, pp 329-346.

[7] Doughty, R.L., Neal, T.E., Dear, T.A. and Bingham, A.H. "Testing Update on Protective Clothing and Equipment for Electric Arc Exposure", IEEE Industry Applications Magazine, Jan-Feb 1999, pp 37-49.

[8] IEEE Guide for Performing Arc-Flash Hazard Calculations. IEEE Standard 1584, IEEE, September 2002.

[9] Wilkins, R. "3-phase operation of current-limiting power fuses", 3rd Int Conf on Electric Fuses and their Applications, Eindhoven, 1987, pp 137-141.

[10] Fisher, L.E. "Resistance of low-voltage arcs". IEEE Transactions on Industry and General Applications, vol IGA-6, No 6, Nov-Dec 1970, pp 607-616.

[11] Ignatko, V.P. "Electric characteristics of AC open heavy-current arcs". 3rd International Symposium on Switching Arc Phenomena, TU Lodz, Poland, 1977, pp 98-102.

[12] Stokes, A.D. and Oppenlander, W.T. "Electric arcs in open air". J. Phys. D: Appl. Phys. vol 24, 1991, pp26-35.

[13] Paukert, J. "The arc voltage and the resistance of LV fault arcs". 7th International Symposium on Switching Arc Phenomena, TU Lodz, Poland, 1993, pp 49-51.

[14] Schau, H. and Stade, D. "Requirements to be met by protection and switching devices from the arcing protection point of view". Proceeding of 5th International Conference on Electric Fuses and their Applications, Technical University of Ilmenau, Germany, Sept 1995, pp 15-22.

[15] Gammon, T. and Matthews, J. "Instantaneous arcing-fault models developed for building system analysis". IEEE Transactions on Industry Applications, vol 37, No 1, 2001, pp197-203.

[16] Ozisik, M.N. "Heat Transfer", McGraw-Hill, 1985.

[17] Wilkins, R. "Standard Fuse Model for System Short-Circuit Studies." 8th International Symposium on Switching Arc Phenomena, TU Lodz, Poland, 1997, pp 163-166.

[18] Doughty, R.L., Neal, T.E., Macalady, T.L., and Saporita, V. "The use of Low-Voltage Current-Limiting Fuses to Reduce Arc Flash Energy." IEEE Transaction on Industry Applications, vol 36, no 6, November-December 2000, pp 1741-1749.

8. Appendix

The numerical problem associated with the infinite fault arc resistance as the current passes through zero can be solved by connecting a fictitious high-value shunt resistor in parallel with the fault arc as shown below.

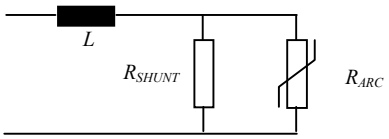

Before solution R_{SHUNT} is set to *L/1.0E-6* which ensures that the series time constant never falls below 1μs, whatever the value of R_{ARC}. This produces a smooth and rapid progression of the solution through the current zero. Furthermore the value of R_{SHUNT} is so high that it makes a negligible difference to the r.m.s. arcing current, I^2t and energy. However there is a penalty to pay for this. During the solution it is essential to calculate how the total circuit current divides between the two parallel resistors, to avoid numerical instability, and so that the arc voltage can be calculated. This is not trivial, as R_{ARC} is non-linear. However it can be done simple and quickly using the Newton-Raphson method. Without this computational device the model and solution method described in section 2 could not be implemented.

Application of Thick-Film Substrate Technology in High Voltage HRC Fuses

M. Wilniewczyc[(1)], **G. Hoffmann**[(2)] and **U. Kaltenborn**[(3)]

ABB Sp. z o.o.[(1)], ul. Zeganska 1, PL-04-713 Warszawa, Poland, mariusz.wilniewczyc@pl.abb.com
ABB Schweiz AG, Corporate Research[(2,3)], Segelhof 1, CH-5405 Baden-Dättwil, Switzerland,
guido.hoffmann@ch.abb.com[(2)], uwe.kaltenborn@ch.abb.com[(3)]

Abstract: High voltage HRC fuses manufactured today typically comprise wire or strip fuse-elements wound round a non-conductive support element (star-core). This paper presents a unique design of a high voltage HRC fuse, utilising thick-film substrate technology. In contrast to conventional wire or strip designs, and a known design of HV fuses utilising thick-film technology, wherein helical fuse-elements are supported on a glass tube [4], the design presented in this paper embodies fuse-elements of a unique design screen-printed on to flat non-conductive substrates. The design of the fuse-elements, arrangement of the fuse-elements on the supporting substrates and, finally, the layout of the substrates inside the fuse housing of standard dimensions contribute to generating adequate arc voltage and achieving high rupturing capacity sufficient for high voltage applications.

Keywords: (high voltage fuse, HRC fuse, substrate fuse)

1. Introduction

This paper presents a unique design of an HV substrate fuse. The design was developed and successfully tested in accordance with the IEC 282-1 standard on full-size prototypes. From HV test results it is evident that thick-film substrate technology is applicable for HV fuses. The main advantages of the fuse design presented in this paper are: high resistance to vibrations, highly accurate and reproducible film deposition technology and, hence, low scatter of I:t characteristics and other parameters, very low switching voltage. Due to the exceptional design the manufacturing process can be substantially automated.

2. Design of the HV substrate fuse

2.1 Materials and deposition technology

Various techniques exist for laying down conductive fuse-elements on to non-conductive substrates; starting with every kind of thin-film deposition technique (sputtering using glow discharge technology), vapour deposition (gas-phase chemical process) or electroplating (liquid-phase chemical formation); at the other end of the spectrum there is thick-film technology with the screen-printing process. To achieve small power losses, which are directly related to the resistance of the printed metal layer, printing thick-film conductive layers is necessary. The various film deposition technologies carry different price tags and, hence, only some of the available techniques could be used for an economically viable HV fuse design. Consequently, thick-film screen-printing was chosen as the conductive film deposition method. This printing method is mature, easily obtainable and inexpensive [1-2].

As for the substrate material, different material classes like ceramics, glasses or glass-ceramics are available [5]. The following substrate materials were investigated: alumina, aluminium nitrite, beryllia, Robax, Borosilicate glass and other special glasses.

The preferred conductive layer material is silver paste, due to its good solderability, good adhesion and good electrical and thermal properties. Depending on the substrate material and firing conditions different silver pastes were used. The recommended firing profile varies slightly for the different pastes used. The common phase is a drying step at approx. 120°C and a peak temperature between 400°C and 800°C (depending on the type of paste used). The peak time is 15 minutes. Firing of all samples was carried out in a box furnace.

The accuracy of the printed silver layer structure is one of the most important issues. The quality of the constrictions (e.g. width tolerance) depends on the quality of the printing mask and on the physical properties of the silver paste and substrate material used. The main concern is the surface tension of the paste. To obtain adequate printed geometry the paste should show good wetting behaviour during the printing process. The substrate material has a significant influence on the quality of the printed layer as, depending on the substrate's surface free energy, the printed layer demonstrates better or worse wetting properties. After the firing process is complete the printed layer must have good adhesion to the substrate [3].

A number of different substrate fuse samples were produced using a semi-automatic screen printer. After printing the quality of the printed film was verified using high-magnification video, SEM and optical laser techniques, Fig. 1 and Fig. 2.

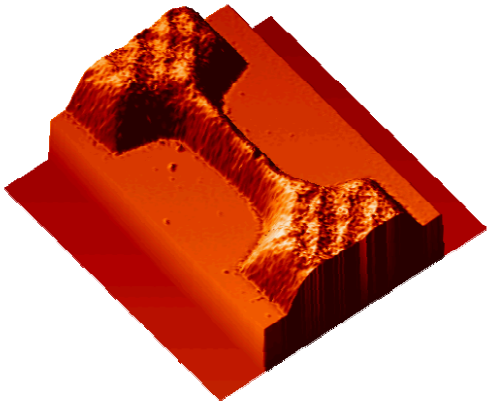

Fig. 1: Screen-printing: 3D SEM image of fuse-element constriction.

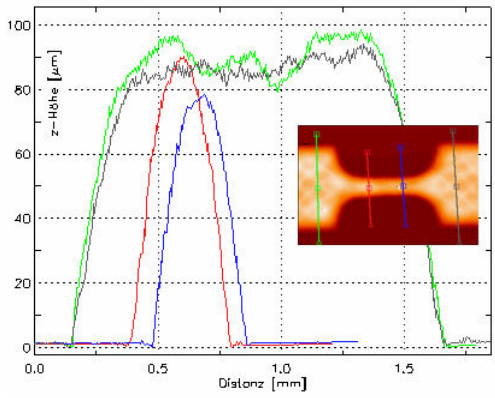

Fig. 2: Screen-printing: profile of the printed layer.

To obtain comparable results for different substrate thicknesses the table height of the screen printer is adjusted. By doing so the distance from the sieve to the substrate is kept constant. When changing the printing paste, which also requires a new sieve or at least thorough cleaning of the previously used sieve, critical printing parameters such as mesh size, squeegee speed, pressure etc. are adjusted for the specific physical properties of the paste (e.g. different viscosity).

2.2 Fuse-element design

The fuse embodies a number of substrates with thick-film fuse-elements screen-printed on to them. To accommodate the required fuse-element length on the available length of the substrate - which is limited by the standard length of fuse housing - the fuse-element zigzags between the two connection areas located at shorter ends of the substrate, Fig. 3.

Fig. 3: Fuse-element and substrate geometry.

A number of constrictions are located along the length of the fuse-element to facilitate multiple arc ignitions and to generate sufficient arc voltage to interrupt the fault current. The constrictions are normally located in the vertices of the zigzag. One or more constrictions may also be located in the straight segments linking the vertices, Fig. 4.

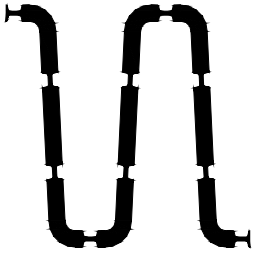

Fig. 4: Location of constrictions along fuse-element length.

The amplitude of the zigzag, its shape, location and number of constrictions differ depending on the required voltage rating, an example of fuse-element design rated at 7 kV is shown in Fig. 5.

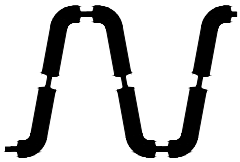

Fig. 5: Example of fuse-element design rated at 7 kV.

In order to ensure sufficient dielectric clearance after interruption is complete the number of zigzags, the cycle and amplitude of an individual zigzag and the angle between the straight segments linking the vertices are selected for a given voltage rating. The geometry and cycle of the zigzag are also so selected as to ensure that the arc can only develop along the fuse-element length. Excessive reduction in the cycle of the zigzag would result in individual arcs merging in an uncontrollable fashion thus shortening the total arc length and, consequently, in an unacceptable reduction in total arc voltage. This in most cases would lead to unsuccessful interruption and possible fuse explosion. On the other hand the cycle cannot be freely expanded due to standardised - and limited - fuse dimensions. Finding the golden optimum proved to be one the most important issues.

The fuse-element may be laid on one side of the substrate (referred to henceforth as ‘single sided’ printing or substrate) or both sides of the substrate

(referred to henceforth as ‘double sided’ printing or substrate) – the latter permits doubling of the number of parallel fuse-elements (hence nearly twofold increase in the nominal current rating and improvement of switching characteristics) without increasing the cost of the substrates and space used. For the highest current ratings double sided printing is practically the only feasible solution.

2.3 Arrangement of substrates in fuse housing

Depending on the required fuse current rating one or more substrates - hence one or more parallel fuse-elements - may be arranged inside the housing. Current ratings for which up to 6 parallel fuse-elements are sufficient are realised using 3 double sided substrates positioned in a ‘triangular arrangement’ (the substrates are so arranged that their cross-section resembles an equilateral triangle), Fig. 6.

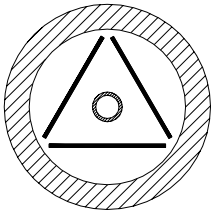

Fig. 6: Triangular arrangement of substrates.

Current ratings for which more than six parallel fuse-elements are needed are realised using from 4 to 8 single- or double sided substrates (hence from 8 to 16 parallel fuse-elements) positioned in a ‘star-shaped arrangement’ (the substrates are so arranged that their cross-section resembles a star), Fig. 7. Conventional striker wire is situated inside the insulating tube located along the symmetry axis of the fuse.

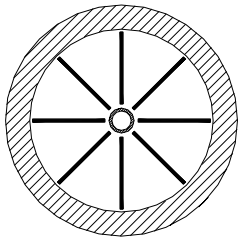

Fig. 7: Star-shaped arrangement of substrates.

2.4 Test results

2.4.1 Electro-mechanical cycling tests

Long-term stability of the printed silver layer laid on the substrate was examined. Fatigue, for example de-bonding of the metal layer from the substrate, would cause unacceptable changes in the tripping and interruption behaviour of the fuse, which might lead to a malfunction [5]. During the firing process, all organic solvents are completely oxidised. At higher temperatures special glass-particles embedded in the silver paste melt and create a liquid phase between the conductive layer and the substrate. After the firing process is complete interfacial adhesion between the conductive layer and the substrate is provided by the glass layer.

It is known that different substrates show different adhesion properties to glass and metal layers. Good adhesion between the conductive layer and the substrate must be ensured during the entire lifetime of the fuse, during which the fuse is normally subjected to long periods of electro-thermal cycling. Consequently, to ensure long-term stability of the fuse electro-mechanical cycling tests were performed in a climatic chamber on several different substrate materials. The temperature profile used for the test is shown in Fig. 8.

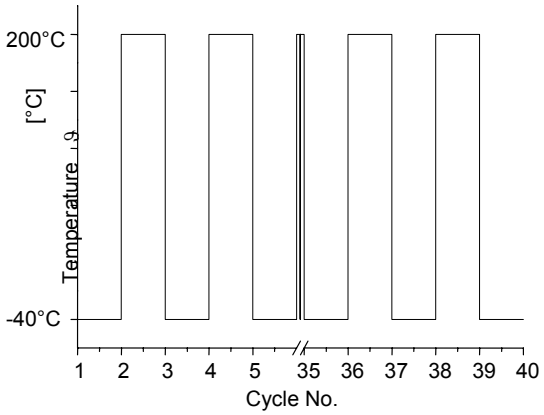

Fig. 8: Thermal cycling profile in a climate chamber.

All samples survived the harsh test without failure. No film de-bonding or breakdown of the substrate or conductive layer was observed. Initially this was very surprising for the aluminium-nitrite substrate, as this material needs special glasses for good adhesion at standard firing process. The reason for such an unexpected - but positive - result might be the slightly decreased cooling rate after firing during the batch process compared to a continuous process. The slower glass cooling process probably helped to reduce the internal and interfacial stresses and, hence, created good conditions for strong adhesion.

The disadvantage of the above test is that the conditions of thermal cycling in the climate chamber are not completely comparable with real electro-mechanical cycling conditions found in service. In the climate chamber the temperature of the whole

fuse-element and the substrate is increased in an almost uniform manner. In the real world the fuse-element is the heat source, in particular the constrictions, which results in non-uniform temperature distribution in the fuse-elements and the substrate. Due to different mechanical properties of the conductive film and the non-conductive substrate both materials are subjected to high internal stresses. Thermal expansion coefficient and modulus of elasticity have the greatest effect on the magnitude of the stress [5].

To identify any potential problems related to long-term stability of the fuse under real operating conditions and to compare the behaviour of different substrate materials under current cycling conditions additional tests were performed. Loading current was set to the nominal (rated) current of the substrate fuses used, Fig. 9.

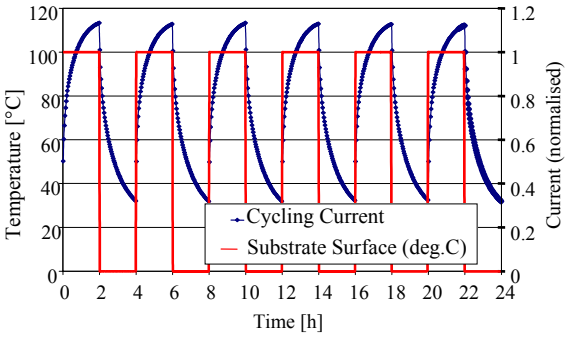

Fig. 9: Cycling current and temperature profiles.

Both the ON and OFF times were set to 2 hours. Voltage across fuse terminals and temperatures in the geometrical centre of each sample were measured and recorded using computerised data acquisition system. The electro-mechanical current cycling test ran over a period of four weeks. All tested fuse samples successfully passed the test: no perceptible change in measured temperature or resistance was observed.

2.4.2 Dielectric tests

The dielectric behaviour of a fuse is one of the key issues. Although capability to interrupt a fault current is the main functionality of the fuse, its capability to withstand recovery and nominal voltage of the electrical system are essential. The dielectric strength of the fuse is related to the dielectric strength of an individual zigzag. For the purpose of the dielectric strength test the worst case condition was simulated, with no arc-quenching material present in the fuse. Initially one notch per each parallel fuse-element was tripped, and afterwards PD-inception voltage was measured in an HV-circuit, Fig. 10.

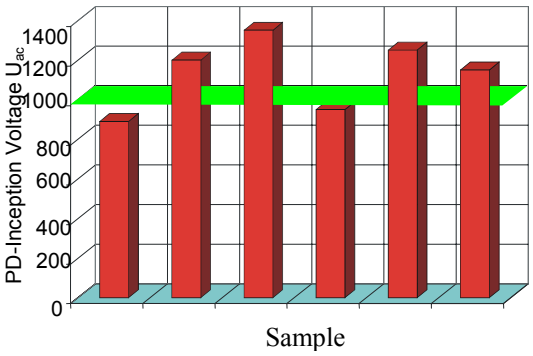

Fig. 10: PD-inception voltage for tripped substrate fuses without arc-quenching material.

The average PD-inception voltage was found to be approximately 1000 V. It can be concluded that the dielectric strength of the design is adequate. If necessary, dielectric strength could be increased further by application of special arc-quenching materials.

2.4.3 Current interruption

HV short-circuit and overcurrent tests (TD1, TD2 and TD3 test duties) were carried out on full-scale prototypes of the substrate fuse design presented in this paper. The fuses successfully passed short-circuit and overcurrent tests. Fig. 11 shows fulgurite formed at progressive stages of current interruption at 7 kV TRV.

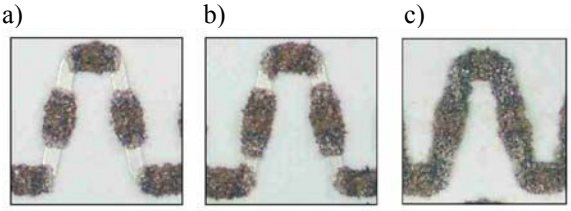

Fig. 11: Fulgurite formed at progressive stages of current interruption (a, b, c).

Fig. 12 shows fulgurite formed on a different fuse-element design printed on borosilicate glass after successful short-circuit current interruption at 12 kV TRV.

Fig. 12: Fulgurite formed after successful short-circuit current interruption at 12 kV TRV.

Typical current and voltage traces recorded during short-circuit interruption are shown in Fig. 13.

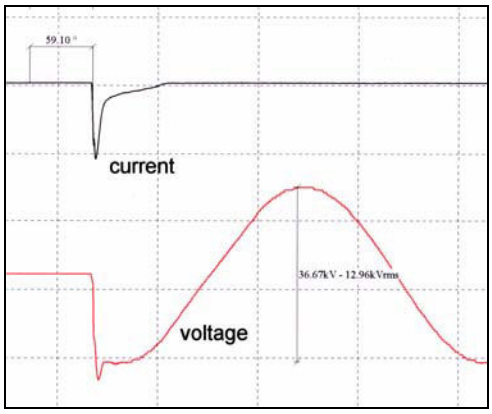

Fig. 13: Current and voltage traces recorded during short-circuit interruption.

It is noteworthy that during interruption the fuse generates very low switching voltages. This characteristic makes the design and technology particularly suitable for HV fuses for the protection of power electronic devices.

3. Conclusions

The paper presents a novel design of an HV substrate fuse. From the electro-mechanical current cycling tests performed to verify long-term behaviour of the new design it is clear that the design and materials show negligible degradation – no cracking, film de-bonding from the substrate or perceptible change in fuse-element resistance could be observed. The design was successfully tested on full-size prototypes under HV conditions, which ultimately proves that thick-film screen-printing technology is suitable for commercial HV fuse-protection applications.

References

[1] Schuegraf Klaus K.: "Handbook of thin-film deposition processes and techniques: principles, methods, equipment, and applications". Noyes Publications 1988.

[2] Pitt Keith E.G.: "Thick Film Component Technology". Mackintosh Publication Ltd 1981.

[3] Eustathopoulos N., Nicholas M.G., Drevet B.: "Wettability at High Temperatures". Pergamon Press 1999

[4] "HOLEC FULLRAN Full-Range fuses for ring main units in medium voltage distribution and industrial networks", Publication 3.11.1

[5] Wilniewczyc, M.: "Electro-Mechanical analysis of Thin-Film Substrate Fuses Using Finite Element Methodology", PhD thesis, 1999

Acknowledgements

The Authors thank ABB Ltd. for supporting the research project undertaken between ABB Corporate Research / Switzerland and ABB Sp. z o.o. / Poland.

A NEW METHOD OF CURRENT LIMITATION

Andrzej Wolny

Gdańsk University of Technology, Faculty of Electrical and Control Engineering
Ul. Własna Strzecha 18A, 80-952 Gdańsk, Poland, awolny@ely.pg.gda.pl

Abstract: A new idea of a hybrid contactless current limiter and its applications are discussed. On the substitution of a special ultra-short fuse for a contact switch in the hybrid current limiter a new device has been obtained, suitable for fast short-circuit fault clearing. The fuse role is only to operate at faulty conditions, forcing current transfer into a parallel semiconductor switch. Then the current is interrupted at an appropriate instant. In the practice no current breaking capacity of the fuse is required, since the voltage across terminals dictated by the semiconductor is less that that needed for arc ignition. Therefore an extremely short, axially cooled fuse element suffices, which enables the application of extremely high current densities in normal conditions. Consequently, fast, very high current limiters are easy to build. They can be helpful in the reduction of voltage dips.

Keywords: hybrid circuit breaker, current limitation, electric fuse, voltage dip

1. Introduction

Electric fuses are cheap, fast operating and reliable current breaking devices, and some of them can effectively limit short circuit currents. Regretfully, the latter feature depends on the generation of high arcing voltage, exceeding that of the power system. For HBC fuses such condition requires the application of a relatively long fuse elements. The longer the fuse element the worse the cooling conditions are, which means that long and massive fuse elements have to be used. Consequently, the arc extinction becomes difficult, and high-rated fuses, say for rated currents higher than 1000 A are not easy to build.

Therefore, a time ago the idea was developed, to apply two separate fuse elements [1]. One of them would start the fuse operation, and the other one – would be responsible for current interruption. This way two-paths fuses were invented, consisting of a very short, main-path fuse element with reduced cross-sectional area due to the effective axial cooling, and an auxiliary, long, low current HBC fuse connected in parallel with that main-path one. However, current transfer between parallel current paths requires the arcing voltage of approximately 100÷200 V in the main path to cover the inductive voltage drop along the commutation loop and that across the HBC fuse. This condition is difficult to fulfil, if a really short main fuse element is to be applied. Hence, auxiliary methods have to be used, such as the mechanical arc extension, complicating design of the two-path fuse, and slowing down its operation. At present, moderate ratings are merely available.

The trend of power quality improvement defines new requirements for the permissible voltage dips and current limitation conditions. In the case of high current installations there is a selection of current limitation devices available, but no one of them seems to be optimum. Neither fuses nor hybrid circuit breakers, combining the advantageous features of the contact and semiconductor switches can be considered flawless. Especially the latter depending on characteristics of the operating mechanism looks slow and bulky. However, a combination of a two-path fuse and a hybrid current limiter gives a new device, which can be called contactless hybrid current limiter (CHCL). It is relatively small, reliable, operates almost as fast as a fuse and is easy to build for quite high currents. One can expect that it should be significantly cheaper then other high current limiting devices.

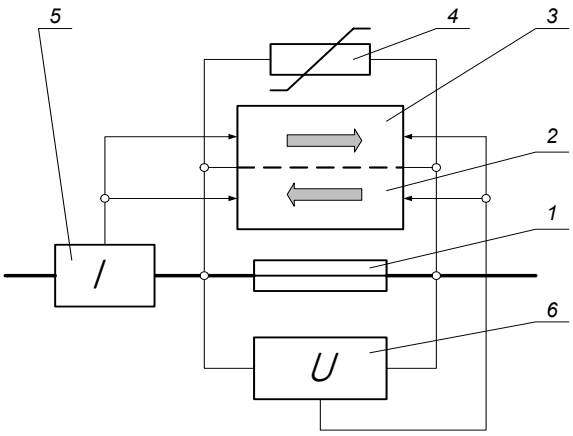

Fig.1 Contactless hybrid current limiter (CHCL): 1 – fuse, 2,3 – two-direction semiconductor switch, 4 – energy absorber, 5 – current sensor, 6 – voltage sensor

The idea of CHCL is presented on the example in Fig. 1. It is worth noting that here the branches of the two-directional semiconductor switch (2 and 3) are connected in parallel. However, in some cases, e.g. on the application of IGBT the connection in series is required.

2. Basic features of CHCL

If a fuse substitutes for the contact switch of a hybrid circuit breaker the conditions of operation of such CB change drastically. First of all, the current interruption process starts automatically on melting of the fuse element. This is a fast action and no intervention of any control system is required. No delay owing to the operating mechanism takes place. However, this also means that there is no way to control the circuit opening.

The CHCL minimum *t-I* characteristics entirely depend on the fuse.

On the other hand the current limitation and breaking conditions are closely connected with the semiconductor switching device. Hence, no current higher than that permissible for the transistor can be let through.

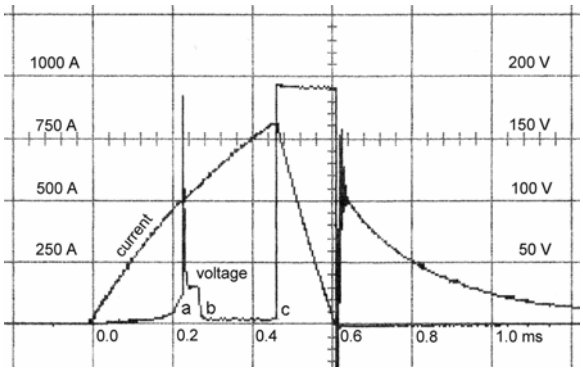

Fig. 2 CHCL operation: a – fuse arc ignition, b – transistor on, c – transistor off

However, it is worth noting that the current limitation level must rise as the recovery time of the fuse dielectric strength (time between points b÷c), Fig 2. This means that selection of a transistor, fixing the maximum permissible current through, is equivalent to a rough definition of features of the short fuse.

Say, the available transistor can turn 4 kA off, and the CHCL is expected to interrupt 100-kA prospective current rising at the rate of 40 A/μs. Then the short fuse must operate and recover dielectric strength in 100 μs.

3. Ultra-short fuse

Up-to-date semiconductor devices are fast and easy to control. There is no problem in their accurate turning on and off. Therefore it is the fuse applied in the CHCL that is responsible for basic features of the whole assembly.

3.1 Fuse element length

Since the fuse does not need to display any current breaking capacity, no arc quenching chamber or filler is required. The recovery of the fuse dielectric strength, after the fuse operation, proceeds fast under extremely low voltage (a few volts) enforced by the transistor turned on. After having turned the transistor off, the fuse dielectric strength is not affected by any parallel low-resistance elements, like polluted chamber walls. Therefore the gap between the fuse contacts can be significanntly reduced, which in turn permits application of very short fuse elements.

The short fuse element just connects massive electrodes, which must be separated in such a way that the gap created after the fuse element disintegration withstands the voltage enforced by the energy absorbing varistor connected in parallel. This means that a gap of 1÷2 mm in open air may be sufficient for LV applications, if almost uniform electric field is ensured. Experiments show that a 1-mm gap between electrodes with quite sharp edges withstands about 2 kV [2]. Filling the fuse with a compressed gas or applying vacuum, a similar gap can withstand much higher voltages. Thus, for both LV and HV applications extremely short fuse element can be used, which ensures its very effective axial cooling.

3.2 Fuse element cross section

Even very thin fuse elements, can carry relatively high load currents, when they are short enough. For instance it was tested that a 1 mm long, silver fuse element with the cross-sectional area as small as 0,07 mm^2, needed at least 180 A to melt [3], which is equivalent to $j \sim 2.5$ kA/mm^2. In this case the ratio $l/\sqrt{S}$ of the fuse element length l and the side $\sqrt{S}$ of the square calculated from the fuse element cross-sectional area S amounted to 3.8. When $l/\sqrt{S}$ reduces, the axial cooling improves, and a higher fuse element current density is allowed. Consequently, a short fuse element with $S \sim 1$ mm^2 may be sufficient to carry several-kA working currents.

3.3 *t-I* characteristics

In contrast to classical fuses very strong axial heat conduction affects the course of fuse *t-I* characteristics, even at very high prospective currents [4] slowing down the fuse operation in the whole range of interest, Fig. 3.

To show the difference between classical and ultra short fuses two lines **a** and **b** corresponding to the Meyer's (1) and the Preece's (2) rules for a long copper fuse element with $S = 0.108$ mm^2 are drawn. These lines constitute asymptotes of *t-I* characteristic for a simple, long fuse element in free air cooled by convection at low overcurrents or heated adiabatically, without energy exchange at high short circuit currents.

$$\int_0^t i^2 dt = K_M S^2 \qquad \text{(Meyer)} \qquad (1)$$

$$I_{melt} = k_m d^n \qquad \text{(Preece)} \qquad (2)$$

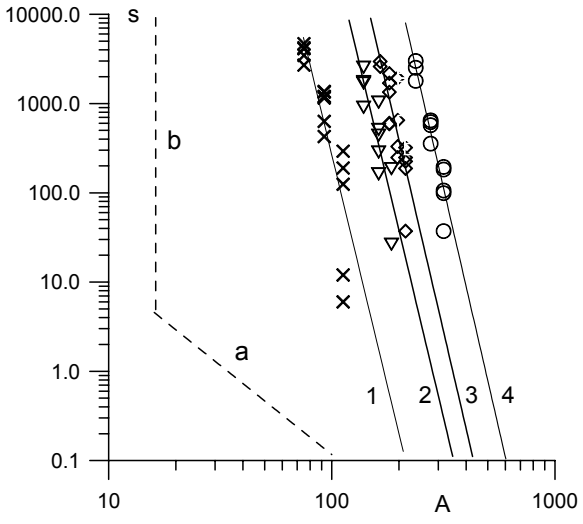

Fig. 3 Short fuse *t-I* characteristics for a variety of fuse element thickness and materials:
1 - Al 200 μm, 2 - Cu 108 μm, 3 - Ag 91 μm, 4 - Ag 124 μm, a – Meyer, b – Preece [4]

Looking at the experimental *t-I* profiles presented in Fig. 3 one can notice that all of them incline in the same manner, which means that the relationship between the temperature increase $\Delta\vartheta$ and the current density j for various fuse element materials and cross sections only differ by a coefficient.

When cooling by heat axial conduction preveils, in quasi static conditions, the power deposited in the fuse element $P_{el} = P_{cond}$, which means that for constant heat sink temperature and a fuse element unit length:

$$\frac{\rho_0 (1+\alpha_\rho \Delta\vartheta)}{S} (j S)^2 = 2\lambda_0 (1+\alpha_\lambda \Delta\vartheta) S \Delta\vartheta \quad (3)$$

and consequently

$$\Delta\vartheta = \frac{\rho_0 (1+\alpha_\rho \Delta\vartheta)}{2\lambda_0 (1+\alpha_\lambda \Delta\vartheta)} j^2 \quad (4)$$

The temperature increase $\Delta\vartheta$ is independent of the fuse element cross-sectional area, or its shape at a given current density.

Both the electrical and heat conductivities influence $\Delta\vartheta$ in the same manner: inversly proportional. This relationship is true for quasi static conditions, i.e. for a few kA/mm^2, or moderate overcurrents. At very high fault currents the effect of the axial heat conduction reduces, and that of the heat absorption by the fuse element rises pushing the *t-I* characteristic closer and closer to the Meyer's line. Neither in such a case the cross-sectional area of the fuse element affects *t-I* profiles for a given current density j^2.

To avoid extremely thin fuse elements for low-rated fuses, special alloys may be more practical than commonly used silver and copper.

The time needed for the fuse element decomposition is always very short, even at relatively low overcurrents. The distribution of temperature shown in Fig. 4 demonstrates that only a very short segment of the fuse element can melt and break. Next the burn-back of remaining fuse element stumps, as short as 0.5÷1-mm takes little time. Recorded times of the fuse element decomposition only acquired a few microseconds.

3.4 Fuse characteristics shaping

It is worth noticing that the fuse element connection with terminals (electrodes) significantly affects the temperature distribution. The broken line visible in Fig. 4 marks the temperature of the fuse element at the points of connection. It is quite high. By selection of an adequate solder, the metallurgic effect can be achieved, facilitating the *t-I* curve shaping. The length of the connection and physical features of solder may also affect these characteristics at short circuit currents.

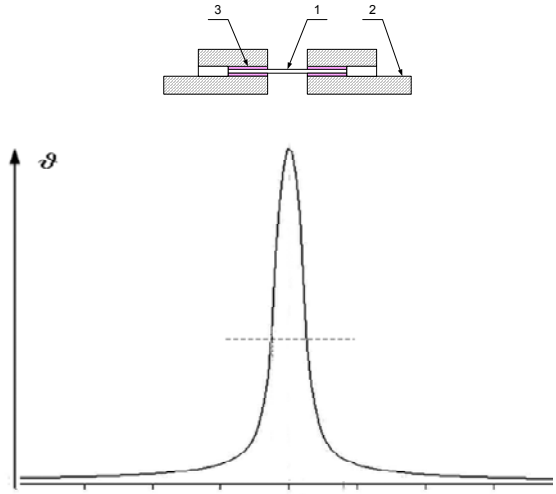

Fig. 4. Temperature distribution along the short fuse:
1 – the fuse element, 2 – terminal, 3 – solder, 2-mm horizontal division

3.5 Arcing voltage

The domination of axial cooling affects the arcing voltage, which behaves similarly to that of the arc burning between plates of a chute. It is very stable and amounts to approximately 25 V for the fuse element length of 1 mm, Fig. 5. This is in agreement with the rule stating that the cooling effect proportional to the arc cross-sectional area produces a constant arcing voltage. Its value is sufficient for the enforcement of fuse-to-semiconductor device current transfer. It is worth mentioning, that much higher arc ignition voltage, Fig. 2, can facilitate fast current transfer in contrast to classical contact switches used in hybrid current limiters.

As the discussed ultra short fuse is not equipped with any arc quenching means, the recovery of dielectric strength is only ensured by the recombination and diffusion. Both of them proceed quite slowly.

Luckily, the recovery time depends on the transferred current, and not on the fault prospective current, or limited current, as the plasma remained to deionise is associated with the former. Comparing ultra short fuse and a simple contact switch, one can come to the conclusion that no essential difference in their recovery processes can be expected, as the mass of the fuse element is extremely small and in some cases may be even compared to a contact bridge. The only important feature is the presence of remnants of the fuse element, when the arcing time is too short, which may substantially reduce the voltage withstood. This means that the parallel semiconductor switch must be controlled precisely to ensure optimum conditions of current limitation.

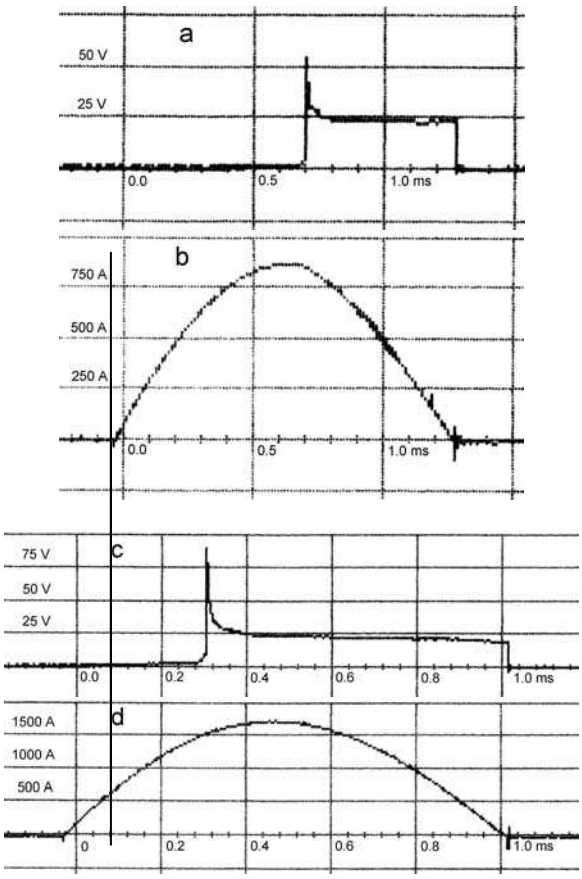

Fig. 5 Current and arcing voltage traces of an ultra short fuse for two different prospective currents: the silver fuse element, 1 mm long with the cross-sectional area of 0,07 mm^2

The power losses ΔP at working currents depend on the fuse element volume V for the assumed current density j.

$$\Delta P = \rho\,(1+\alpha_\rho \Delta\vartheta) V \cdot j^2 \qquad (5)$$

For a copper fuse element, 1 mm long, 0.5 mm in diameter, at j = 2.5 kA/mm^2 the power losses acquire 50 W. It is not much, if one considers that such a fuse is designed for approximately 1-kA rated current.

General features of the ultra short fuse have a lot in common with the comparable ones of the contact bridge.

3. Design of CHCL

Application of a very short fuse element facilitates design of a compact fuse, with external dimensions smaller than those of a semiconductor diode for comparable rated current, owing to less power losses. One can estimate, the fuse only dissipates about 10% of the diode power losses.

Hence the fuse can be made in a pill form with relatively massive contacts. It is worth mentioning that the bulk of heat generated in the fuse can be dissipated by adjacent terminals or even radiators, which help reducing contacts dimensions. Thus, the depositable fuse may be extremely small and cheap. It is demonstrated on the example in Fig. 6.

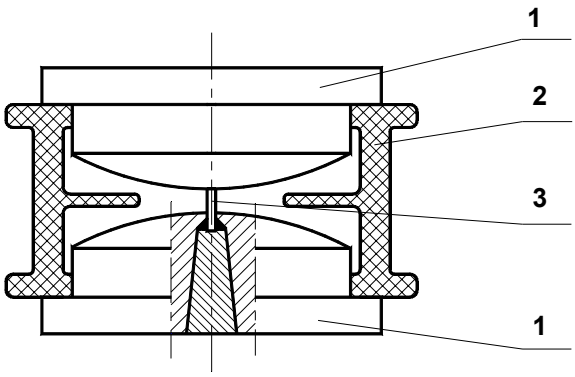

Fig. 6 Example design of an ultra-short fuse

Other parts of the CHCL are multi-use and durable. Transistors only pass the current through over, say, 100 μs. So they do not need radiators. The control unit must only be fed during the operation. Hence, a battery will do. Example design of CHCL is shown in Fig. 7.

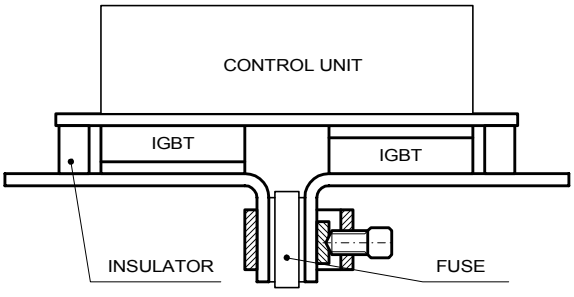

Fig. 7 Example design of CHCL

4. Application

CHCL is a compact, 1-phase, very fast-operating LV current limiter, easy to build for high working currents, above the limit of classical fuse applications. The high voltage design is possible, however economically it is less attractive. CHCL looks like one-shot device, however the only depositable part is a small fuse, cheap and easy to replace. The current limiter features depend in a great extend on that fuse.

Such characteristic indicates the possible fields of CHCL applications. It is perfect for back up or life protection in high current circuits, especially in marine and industrial power systems. It may protect high current rectifiers and convertors.

Owing to its fast *t-I* characteristics CHCL is well suited rather to short circuit current limitation and interruption than overcurrent protection.

5. Conclusions

On substitution of an ultra short fuse for the contact switch in the hybrid current limiter a new current limiting device, CHCL, is developed with special characteristics.

The short fuse is fully responsible for *t-I* characteristic, while the current interruption capacity depends on the semiconductor device in parallel to the fuse.

The short fuse offers fast *t-I* characteristics due to effective axial cooling by means of heat conduction.

CHCL is well suited for current limitation. Its characteristics of overcurrent interruption are difficult to form; however some possibilities exist.

The fuse element can be as short as 1 mm for both LV and HV applications if only adequate gas filling and pressure will be adopted.

The limited current is higher then the fuse element melting current due to the required time for the recovery of the fuse dielectric strength. The latter depends on the fuse arcing time.

The relationship between the recovery time of the fuse dielectric strength and the fuse arcing time shows a minimum associated with the fuse element decomposition and arc plasma temperature and volume.

Acknowledgements

The research on contactless short-circuit current limiting devices has been carried out in frames of the current research project No: 8 T10A 058 21 supported by the Committee of Scientific Research in Poland.

References

[1] Krasuski, B., W. Związek and E. Szymański: "Working conditions of two-path fuse", Int. Symposium on Switching Arc Phenomena, Łódź (Poland) 1985, p. 368.

[2] Semenowicz, B., R. Partyka: "Dielectric strength of the ultra-short fuse", Int. Conf. on Electric Fuses and their Application, Gdańsk 2003 (accepted)

[3] Wolny, A., B. Semenowicz: "Hybrid contactless current limitation". Int. Symposium on Short-Circuit Currents in Power Systems. Łódź (Poland) 2002, p. 221.

[4] Sinkiewicz, T.: "Short fuse t-I chracteristic" (in Polish), MSc thesis, Gdańsk University of Technology, Gdańsk 2003.

HIGH VOLTAGE PROTECTIVE ASSEMBLY

B. Kacprzak[(1)], R. Partyka[(2),] J. Żyborski[(3)], K. Dopke[(4),] H. Bednarski[(5)]

Technical University of Gdańsk, High Voltage and Electrical Apparatus,
Wlasna Strzecha Str. 18A, Gdańsk 80-952, Poland [(1,2,3)]
E-mail: rpartyk@ely.pg.gda.pl [(2)], zyborski@ely.pg.gda.pl[(3)]

ZRE GDANSK Company Ltd, Gdańsk 80-719, Poland[(4,5)]
Litewska Str. 14A, E-mail: krzysztof.dopke@zregdansk.pl[(4)]

***Abstract**:* This paper describes a new high voltage protective assembly, which comprises both fuse protection and overvoltage protection for overhead transformer- distribution stations. The metal-oxide surge arrester without gaps performs two functions: it limits overvoltages at transformer input and supports the carrier of gas expulsion fuse. That way one of the two support insulators per each pole can be substituted by the surge arrester. The high voltage protective assembly is advantageous for technical reasons and for significant economic savings.

Keywords: electric fuse, current limitation, overvoltage protection

1. Introduction

The protection of overhead transformer-distribution stations is put in practice by the use of H.V. fuses and surge arresters. Expulsion fuses and metal- oxide surge arresters without gaps are commonly used to this purpose [1, 2, 3, 4]. A set of three- pole H.V. fuses usually forms a separate electrical apparatus, comprising three single fuse bases installed on six support insulators. The surge arresters are installed on another base, separately, nearby the H.V. fuses.

The surge arrester without gaps, owing to its design, can perform not only the function of overvoltage protection. It can be used as a support insulator also. The surge arrester can be installed in vertical, horizontal or in any intermediate position. Thus, the three support insulators from 3- pole fuse protection set can be replaced by surge arresters type AZB. This solution is applied in the High Voltage Protective Assembly type WZZ, which incorporates both expulsion fuses and metal- oxide surge arresters without gaps, AZB type. A detail description and results of the tests performed on the High Voltage Protective Assembly type WZZ will be presented in the next section.

2. High voltage protective assembly

2.1. General

The High Voltage Protective Assembly type WZZ, Fig. 1, is applied to the protection of overhead transformer-distribution stations against the effects of overcurrents (short circuits, heavy overloads), lightning surges and switching overvoltages in AC networks. There are three options of the High Voltage Assembly, for rated voltages: 12, 17.5 and 24 kV respectively.

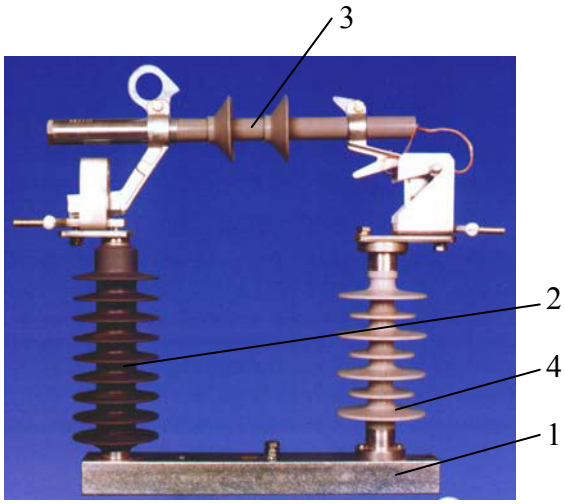

Fig. 1: High voltage protective assembly WZZ, rated voltage 17.5 kV
1- Base, 2- Surge arrester AZB, 3- Fuse carrier OWBG, 4- Support insulator

The WZZ Protective Assembly, Fig. 1, incorporates a base (1), expulsion fuse and metal-oxide surge arrester without gaps AZB (2), which is installed as a substitute of one of the two support (standoff) insulators (4) for each fuse-carrier. Two kinds of fuse carriers (3), type WGBNp and OWBG, can be applied in the WZZ Protective Assembly (see Sec. 2.2). The OWBG fuse carrier has an enhanced short circuit current breaking capacity in comparison to WGBNp. The second support insulator (4) of the fuse –carrier performs the function of insulation to earth for the WZZ protective assembly.

2.2. Gas expulsion fuse carrier

There are produced two types of gas expulsion fuse carriers, coded WGBNp and OWBG respectively, Fig. 2. The main difference between the two fuse carries is in the way and direction of gas expulsion. The WGBNp fuse carrier is open at both ends so gas expulsion is possible from the upper and lower outlet. The OWBG fuse carrier is closed at the upper end by a gas reservoir what results in an intensive gas expulsion in lower direction only. That is why the fuse carrier OWBG has an increased breaking capacity in comparison to the fuse carrier type WGBNp, Table 1. The design of both fuse carriers is similar, so the description will be given for the type OWBG only.

The fuse carrier type OWBG is made up of an insulating liner of high electrical and mechanical strength, with an ablative auxiliary tube, which is glued to the inside of the liner, a conducting ferrule of the upper gas-reservoir with a nut and bolt electrode. The lower contact of the fuse -link carrier with the terminal of flexible tail electrode is permanently fastened on the tube. The upper terminal is fixed to the upper ferrule with an adjustment of the

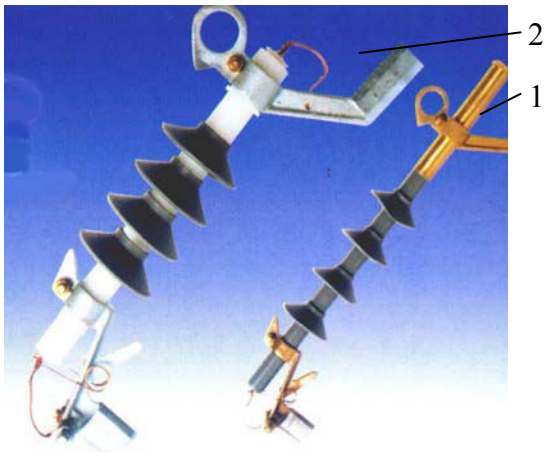

Fig. 2: Fuse link carrier for WZZ protective assembly
1- Fuse carrier OWBG-17.5, 2- Fuse carrier WGBNp-17.5

contacts distance of the carrier to the relevant dimensions of the fuse base. There in lower contact is set a spring which drives the flexible tail.

The fuse - link comprises a fuse -element that is coated with ablative material, a flexible tail and clamping sleeve, Fig. 3.

Table 1. Ratings of fuse carriers

Voltage		12 kV	17.5 kV	24 kV
Conventional thermal current of fuse- carrier	WBGNP	25 A	25 A	25 A
	OWBG	40 A	40 A	
Breaking current	WBGNP	3.15 kA	3.15 kA	3.15 kA
	OWBG	8 kA	5 kA	
Fuse-link currents	WBGNP	4÷25 A	4÷25 A	4÷25 A
	OWBG	4÷40 A	4÷40 A	
Frequency		50 Hz		

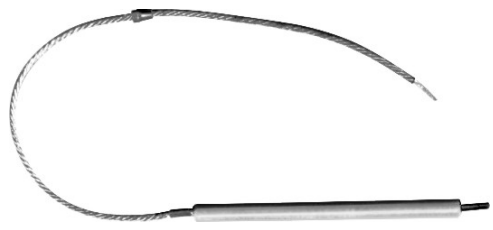

Fig. 3: Fuse link for WZZ protective assembly

2.3. Surge arrester

AZB type surge arrester without gaps, Fig. 4, is made of zinc- oxide varistor. The varistor pellets are connected in series and housed in a glass- epoxy

Fig. 4: Metal- oxide surge arrester without gaps type AZB

tube, which is closed at both ends by metal ferrules with connection terminals of the arrester. The set is sheathed with silicon elastomer, forming a tight, cylindrical housing with protective fins. The material and the creepage distance provide adequate insulating properties.

The arrester's end-of-life is indicated by a black insulating ring which is placed between the two protective fins of the surge arrester. When the arrester fails, the power arc is ignited along the surface of the ZnO varistor block. During arc creeping the black ring is sectioned then ejected to the ground indicating arrester's end-of-line.

The main advantages of surge arresters type AZB are:

- stability of protective characteristics,
- suitability to the installation in vertical or horizontal position,
- mechanical robustness, e.g. against vandalism
- long creepage distance,
- suitability to the application as the support insulator,
- in the case of short circuit current flow through the surge arrester there is no danger of fragmentation (explosion) of arrester housing.

The surge arrester meets the requirements for the IEC Zone III-Class outdoor use. The properties of AZB type surge arresters, confirmed by the Power Engineering Institute in Warsaw, are given in Table 2. They conform with standards: PN-IEC 99-4: 1993 and IEC-600099-4: 1998.

Table 2. Ratings of surge arresters type AZB

Continuous operating voltage (kV)	2.55 ÷ 34.0
Rated discharge current 8/20 μs	10 kA
Maximum discharge current 4/10 μs	100 kA
Short- circuit strength (0.2 s)	20 kA
Energy absorbing capacity	3.7 kJ/kV
Class of line discharge	1
Surge current withstand capacity of 2000 μs duration	230 A

2.4 Support insulator

The support outdoor insulator type C04 – 145, Fig. 5, is made up of a round glass-epoxy rod that is covered by a silicon sleeve with anti-rain protective fins. Aluminum ferrules are mounted at both ends of the insulator. The main field of application of composite insulators C04 – 145 is high voltage overhead electrical equipment:

- fuse-bases type PBNUs-24,
- high voltage protective assemblies type WZZ,
- transmission lines and switchgear,
- disconnectors and mechanical switches.

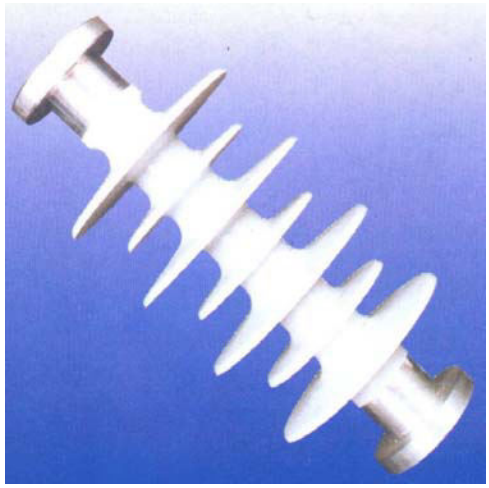

Fig. 5: Support outdoor insulator type C04 – 145

3. Tests

The High Voltage Protective Assembly Type WZZ - 12, WZZ - 17.5 and WZZ – 24 passed the type tests performed by The Institute of High Voltage, Gdansk University of Technology and The Power Engineering Institute in Warsaw. The tests have confirmed the ratings of fuse carriers given in Table 1. Exemplary oscillograms from the breaking capacity tests, for rated voltage 12.0 and 17.5 kV, are shown in Fig. 7 and Fig. 8, for the fuse carriers OWBGw6-12 and OWBG2-17.5 respectively.

4. IMMUNITY TO FUSE MALFUNCTION DURING STORMS

Nuisance fuse operation during thunderstorms may appear [5]. It is due to the interaction between surge arresters, transformer and fuse. If a lightning stroke is of long duration, the short- duration high current pulse is followed by a long duration low current pulse. An average amplitude of that low current pulse is 100 A, and its duration may be many miliseconds. Under these circumstances, the voltage across the transformer primary is not the sinusoidal AC line voltage but is much higher and constant, due to operation of surge arrester voltage under low current pulse. The transformer core becomes saturated then and the winding inductance dramatically drops. Resulting abnormal

magnetizing current can melt the fuse and cause nuisance operation.

Fuse malfunction as described in the reference [1] has not been observed in wide application on site of the WZZ protective assembly.

5. AVANTAGES OF WZZ ASSEMBLY

The High Voltage Protective Assembly type WZZ is advantageous for the following features: stable protective characteristics:

- large energy absorption capacity
- pollution-proof
- mechanical robustness
- low mass
- simplified construction of pole transformer.

6. APPLICATION EXAMPLE

An example of application of the High Voltage Protective Assembly type WZZ to the protection of an overhead transformer- distribution station is shown on site in Fig. 6.

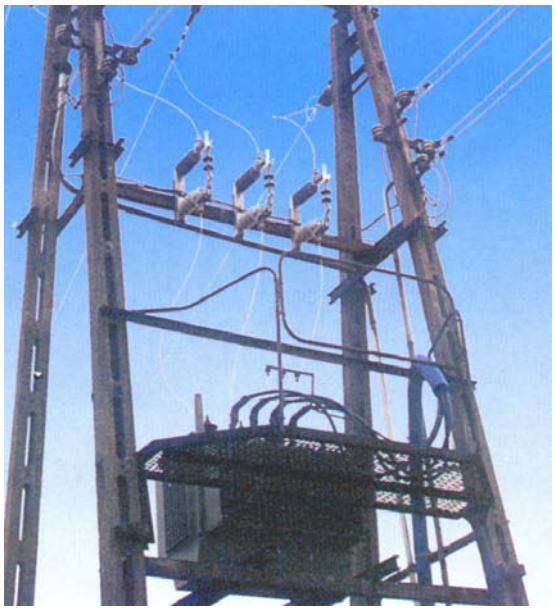

Fig. 6 Combined short circuit current and overvoltage protection of an overhead transformer- distribution station using the High Voltage Protective Assembly type WZZ 17.5

CONCLUSIONS

The High Voltage Protective Assembly type WZZ is a novelty in the field of the protection of overhead transformer- distribution stations. Owing to the performance of two functions by one assembly that is short circuit protection and surge protection, the WZZ is advantageous for technical reasons and significant economic effects.

ACKNOWLEDGEMENTS

The High Voltage Protective Assembly WZZ was worked out in frames of the joint research-application project No: 8T10A 02796 C/2868, which was run by Technical University of Gdansk, High Voltage and Electrical Apparatus and ZRE GDANSK Company Ltd, and was financed by the Committee of Scientific Research in Poland in the years 1996 – 1998.

REFERENCES

[1] Wolny A., Stockes A.D., Kacprzak B.: „High voltage fuse behaviour with varistor commutation", Proc. IEE, Gen. Transm., Distrib., vol. 141, No. 1, p. 33-37, 1994.

[2] Wolny A., Stockes A.D.: „ Varistor assisted fuse current breaking". Int. Symposium on Switching Arc Phenomena, Lodz, Poland, p. 245-248., 1993.

[3] Wolny A.: New protection means: varistor assisted fuse. Proc. ICECAAA, Xi'an, China, p. 524-528, 1997..

[4] Wolny A.: What can fuses offer to survive the next century. 6th International Conference on Electric Fuses and their Applications, Torino, Italy, p. 1-9, 1999.

[5] Hamel A., St-Jean G, Paquette M.: "Nuisance fuse operation on MV transformers during storms", IEEE Transactions on Power Delivery, Vol. 5, p. 1866-1874, 1990.

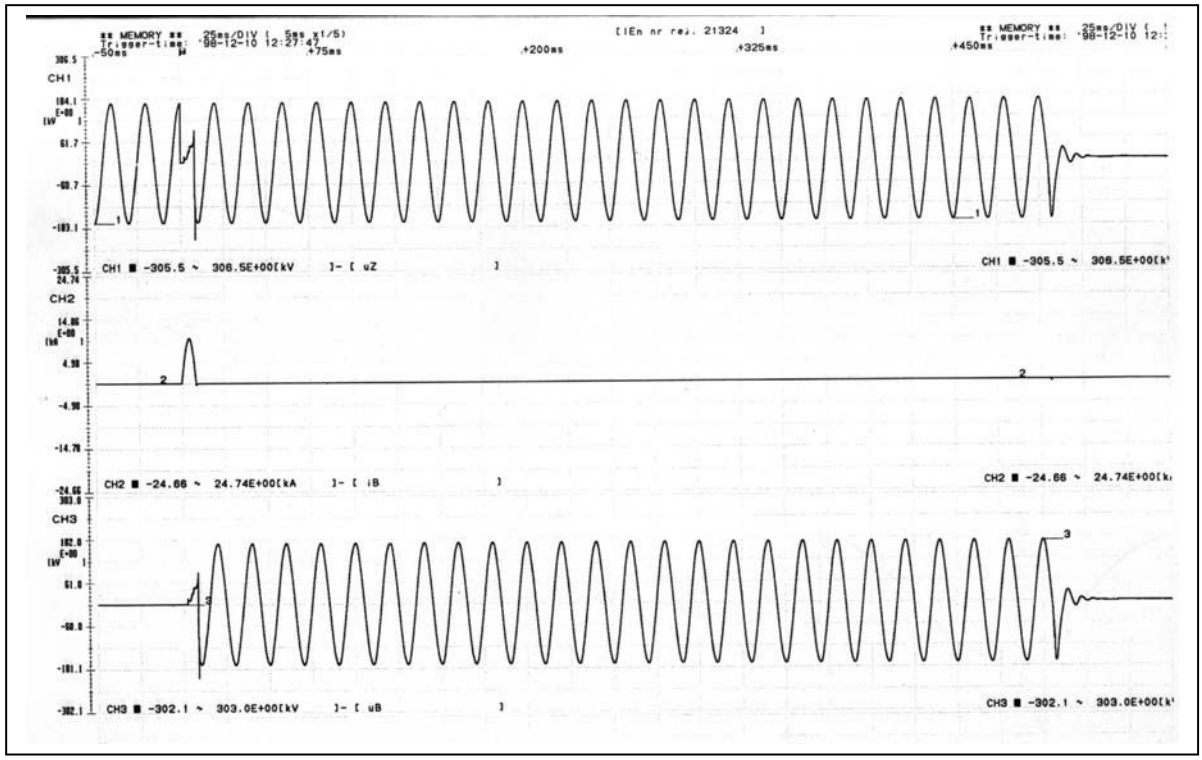

Fig. 7 Breaking capacity test of WZZw-12 High Voltage Protective Assembly, with fuse base PBGw 1-12, fuse carrier OWBGw6-12 and fuse link 40A.

Test voltage 12 kV, prospective short circuit current 8.27 kA, making angle 90º, arcing time 8.3 mS.

Breaking capacity test of I_1 current performed by The Institute of Power Engineering in Warsaw, Distribution Equipment Laboratory, by the courtesy of The Laboratory.

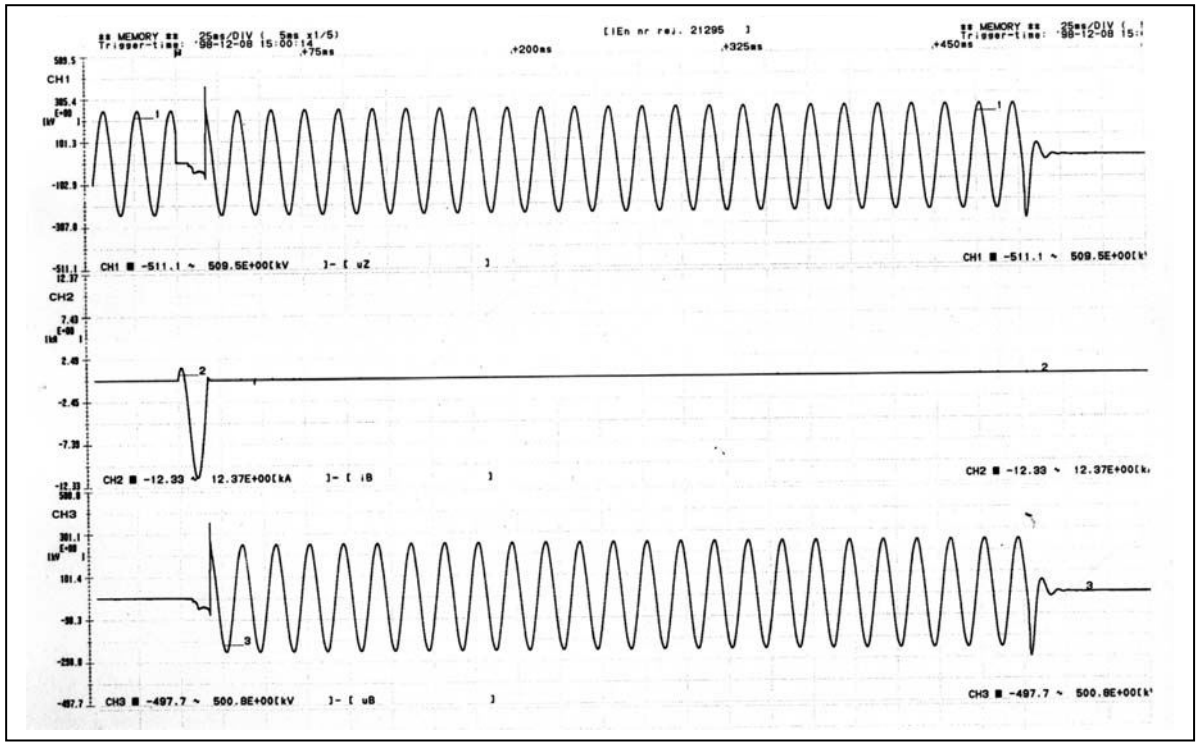

Fig. 8 Breaking capacity test of WZZ-17.5 High Voltage Protective Assembly, with fuse base PBG1-17.5, fuse carrier OWBG2-17.5 and fuse link 40A.

Test voltage 17.8 kV, prospective short circuit current 5.03 kA, making angle 142º, arcing time 17.8 ms.

Breaking capacity test of I_1 current performed by The Institute of Power Engineering in Warsaw, Distribution Equipment Laboratory, by the courtesy of The Laboratory.